XXXIX Congresso Brasileiro de Aplicações de Vácuo na Indústria e na Ciência

08 a 11 de outubro de 2018 - Joinville - SC

CADERNO DE RESUMOS XXXIX CBrAVIC

PATROCÍNIO

Agilent Technologies

HMINI

mks
Technology for Productivity

AVACO
TECNOLOGIA EM VÁCUO

EDWARDS
WWW.EDWARDSVACUUM.COM

Leybold

ULVAC
ULVAC Technologies, Inc.

Conexões TUPY
Sua marca de confiança.

Inergiae
Conversores Estáticos

Anton Paar

FCA BRASIL
SOLUÇÕES EM VÁCUO

supplier

THORLABS
Entrega em 2 semanas no Brasil

ORGANIZAÇÃO

UDESC
UNIVERSIDADE
DO ESTADO DE
SANTA CATARINA

UNIVERSIDADE FEDERAL
DE SANTA CATARINA

INSTITUTO FEDERAL
Santa Catarina

Sociedade Brasileira de Vácuo

ÁGORA TECH PARK

AJECI
Associação Joinvilense de Engenheiros Civis

APOIO

CNPq
Conselho Nacional de Desenvolvimento Científico e Tecnológico

CREA-SC
Conselho Regional de Engenharia, Arquitetura e Agronomia de Santa Catarina

IUVSTA

döhler
Completa o seu vida

Comissão organizadora local:

Luís César Fontana (UDESC)
Abel André Cândido Recco (UDESC)
Daniela Becker (UDESC)
Jacimar Nahorny (UDESC)
Julio César Sagás (UDESC)
Joel Stryhalski (IFSC)
Diego Alexandre Duarte (UFSC)
Ricardo Antonio De Simone Zanon (UDESC)
Ivani Teresinha Lawall (UDESC)
Luiz Clement (UDESC)
Carlos Roberto Grandini (UNESP)
Jaison Vieira da Maia (IFSC)
Alexandre Werner Arins (IFSC)
Rafael Gallina Delatorre (UFSC)
Viviane Lillian Soethe (UFSC)
Wagner Maurício Pachekoski (UFSC)
Alexandre Mikowski (UFSC)
Gabriel Benedet Dutra (UFSC)
Giorgio Ernesto Testoni (UniSociesc)
Henrique de Souza Medeiros (Católica/SC)
Carla Dalmolin (UDESC)
Francine Rafaeli Kasulke (NITEC-UDESC)
Patrícia Becker (AJECI e UDESC)

Diretoria da SBV- sbvdiretoria@gmail.com

Presidente: Prof. Alvaro José Damião (IEAv)
1ª Vice Presidente: Prof.ª Maria Lucia Pereira da Silva (USP/FATEC)
2º Vice Presidente: Prof. Francisco Tadeu Degasperi (FATEC)
1º Secretário: Luciano Rugério Silva (Inertsolutions)
1º Tesoureiro: Prof. Marcos Massi (Universidade Mackenzie)
2º Tesoureiro: Profa. Nazir Monteiro dos Santos (INPE)
Diretor Científico: Prof. Carlos Roberto Grandini (UNESP)
Diretor Cultural: Prof. Antonio Renato Bigansolli (UFRRJ)

Comitê Científico

Abel André Cândido Recco (UDESC)
Adriano Gonçalves dos Reis (UNESP - SJC)
Aleandro Ribeiro Marquesi (ITA)
Alexandre Mikowski (UFSC)
Alexandre Werner Arins (IFSC)
Álvaro José Damião (IEAv)
Angelo Gobbi (LNNano)
Argemiro Soares da Silva Sobrinho (ITA)
Carla Dalmolin (UDESC)
Carlos Roberto Grandini (UNESP- Bauru)
Claudia Renata (UESC)
Clodomiro Alves Júnior (UFERSA)
Cristiane Stegemann (ITA)
Daniela Becker (UDESC)
Danieli Aparecida Pereira Reis (UNIFESP-SJC)
Dante Ferreira Franceschini Filho (UFF)
Dianclen do Rosário Irala (Católica-SC)
Diego Alexandre Duarte (UFSC)
Douglas Marcel Gonçalves Leite (ITA)
Deborah Cristina Ribeiro dos Santos (FATEC)
Elidiane Cipriano Rangel (UNESP – Sorocaba)
Evaldo José Corat (INPE)
Francisco Tadeu Degasperi (FATEC)
Gabriel Benedet Dutra (UFSC)
Gelson B. de Souza (UEPG)
Francisco Tadeu Degasperi (CEETEPS - FATEC SP)
Gilberto Petraconi Filho (ITA)
Giorgio Ernesto Testoni (UniSociesc)
Graziela da Silva Savonov (INPE)
Henrique de Souza Medeiros (Católica-SC)
Homero Santiago Maciel (ITA)
Jacimar Nahorny (UDESC)
Joel Stryhalski (IFSC)
Julio César Sagás (UDESC)
Konstantin G. Kostov (UNESP-Guaratinguetá)
Leandro Leite Tezani (CEITEC)
Leide Lili G. Silva Kostov (FATEC)
Lívia Elisabeth Brandão (UFLA)
Luis César Fontana (UDESC)
Marcelo Gomes (ITA)
Márcio Mafra (UTFPR)
Marco Antonio Ramirez Ramos (UNIVAP/SP)
Maria Lúcia Pereira da Silva (USP)
Maria Margareth da Silva (ITA)
Mariana Amorim Fraga (Universidade Brasil)
Mário Ueda (INPE)
Maurício Antonio Algatti (UNESP)
Milton Eiji Kayama (UNESP)
Milton José Cinelli (UDESC)
Moisés Parucker (UNIFEI)
Nazir Monteiro dos Santos (INPE)
Nilson Cristino Cruz (UNESP – Sorocaba)
Paulo César Borges (UTFPR)
Pedro Augusto de Paula Nascente (UFSCar)
Rafael Gallina Delatorre (UFSC)
Rodrigo Sávio Pessoa (Universidade Brasil)
Rogério Moraes Oliveira (INPE)
Rogério Pinto Mota (UNESP – Guaratinguetá)
Sérgio Henrique Pezzin (UDESC)
Silmara Kabayama (UNIFEI)
Silvio Brunatto (UFPR)
Viviane Lílian Soethe (UFSC)
Vladimir Jesus Trava-Airoldi (INPE)
Wagner Pachecovski (UFSC)
Walman Benicio de Castro (UFCG)
Wisley Falco Sales (UFU)

Comitê Acadêmico

UDESC

Júlia Karnopp
Teresa Tromm Steffen
Thais Macedo Vieira
Lucas Kunicki
Paula Fin
Aline Medeiros Morais
Douglas Washington da Silva
Rafael Fróis
Renan Augusto da Cunha
Beatriz Gevaerd
Elisa Segundo
Letícia Trezecik Silvano
Marco Aurélio Nespolo Vomstein
Camila Presendo Pinto
Letícia Maria Scolaro
Gabriel Cardoso Grime
Sarah Helem Tschá

UFSC

Matheus Gonçalves
Letícia Silva
Rodrigo Santiago
Isabelle Quintiliano
Gabriella Xavier
Laura dos Santos
Rodrigues da Silva
André Concer da Silva
Elizabeth Trindade
Daniel Vanin
Nicolas Fanchin
Marcus Schroeder
Daniela Librelato

Católica de Santa Catarina

Gustavo Franco
Samuel Strelow
Joel Luiz da Rosa

XXXIX Congresso Brasileiro de Aplicações de Vácuo na Indústria e na Ciência

08 a 11 de outubro de 2018 - Joinville - SC

PALESTRAS
XXXIX CBrAVIC

SBV historical review

Alvaro José Damião
Instituto de Estudos Avançados, Departamento de Ciência e Tecnologia Aeroespacial, São José dos Campos, Brasil

The Brazilian Vacuum Society (SBV) is a nonprofit organization. It was founded on May 17, 1978 at a meeting of scientists, professors, engineers and technicians held at the Instituto Militar de Engenharia (IME), Rio de Janeiro. In 1984 the headquarters was moved to UNICAMP University, in Campinas, São Paulo.

The SBV is an active community, bringing together Universities, Research Institutes and Industries covering several areas of the knowledge which involves vacuum technology. Nowadays, the number of participants is about 500. The SBV organizes its annual Vacuum Congress (Congresso Brasileiro de Aplicações de Vácuo na Indústria e na Ciência – CBRAVIC) and Vacuum Courses in a period preceding the Congress. The main point in this meeting is to provide an opportunity for the students to present their papers, discuss them in an academic environment and have a direct interaction with the invited speaker. CBRAVIC extends over a three day period and typically includes 10 invited plenary presentations and 200 contributed papers on original research and development. In addition, it is traditional that in the days before and after the congress the SBV offers some courses on Basic and Advanced Vacuum Technology and on related topics such as Surfaces and Interfaces, Thin Films, Characterization Techniques, Metrology, Solar Cells, Plasma Applications and Atomic and Molecular Physics.

Workshops on Liquid Crystal, Plasma Science, Diamond and Related Materials and Nanostructured Materials have been supported by the SBV with both domestic and international participation. Also, the SBV supports the Brazilian Journal of Vacuum Application (Revista Brasileira de Aplicações de Vácuo), which is a periodical on Vacuum Science and Technology. It has been edited for 39 years, without interruption. It is issued three times per year and is supported by national and international referees and members of the editorial board. A great effort is focused on expanding the Brazilian Vacuum Society activities to the South American regions. Articles can be submitted in English, Portuguese and Spanish. The SBV recognizes the extreme effort being made by some researchers and engineers in order to keep our society looking to the future. Accordingly, in 1992 it was introduced the grade of Honorary Membership, and Prof. Dr. Ross Alan Douglas from UNICAMP University was the first to be honored with this permanent position in 1995. During the year 2000, as part of the annual congress, the SBV introduced an innovation in terms of cultural incentives to general scientific information, including some short and instructive courses to the "high school teacher communities" expounding the history of vacuum science and technology, its applications, and its influence on people's every-day life. It remains until today and it was attended by more than 350 students and teachers at last CBRAVIC edition. The Brazilian Vacuum Society Administration (elected by all members for two years with permission to be re-electing once more) is composed of: the President, first and second Vice President, first and second Secretary, first and second Treasurer, Cultural Director, Scientific Director, and two Board Councillors. The SBV also nominates two Councilors and Divisional representatives for all scientific areas of the IUVSTA. Finally, the major purpose of the Brazilian Vacuum Society is to:

- disseminate the application and theory of vacuum science and technology to the developed communities throughout our country, including all Universities, Research Institutes and Industries,

- facilitate cooperation among different scientific and technological communities, by organizing congresses, workshops and courses involving many areas of the knowledge which is related to vacuum technology,
- keep together, in permanent contact, the academic activities in Universities and the practical activities in Industry, and
- represent the Brazilian Scientific and Technological Communities on Vacuum and Related Areas within IUVSTA.

Modelling
A tool for better understanding of reactive sputtering processes

Soren Berg
The Angstrom Laboratory, Uppsala University, Sweden
soren.berg@angstrom.uu.se

Sputtering is a widely used thin film deposition technique. Pure metal films can be deposited over large area substrates at high deposition rates. During processing in inert gas like Ar only the power to the target, the Ar pressure and deposition time need to be considered to obtain the desired film thickness. Co-sputtering from several targets can be used to deposit alloy films. DC magnetron (DCM) sputtering is probably the dominating sputtering technique. Sputtering from insulating targets can not be carried out by DCM sputtering. Costly RF-equipment has to be used for such sputtering processes. RF sputtering is not suitable for large area targets. A common alternative to RF sputtering is therefore to deposit insulating oxide films by reactive DCM sputtering. Unfortunately reactive DCM sputtering processes are not as easy to control as the inert Ar sputtering process. Adding oxygen to the Ar plasma influences the target conditions significantly and may result in an uncontrolled avalanche-like transition from high to low deposition rate. In the high rate mode primarily pure target metal atoms are sputter eroded. In the low rate mode a thin oxide layer (poisoned layer) are formed at the target surface having substantially lower sputter erosion rate than the rate from the pure non-poisoned metal target. Experience has shown that the desired processing point to get as high deposition rate as possible accompanied by depositing a fully stoichiometric oxide film happens to be critically close to where the process avalanches from high to the low sputtering rate. The critical processing parameter is primarily the supply of the reactive gas. As an extra complication the critical point for avalanche from high to low rate is not at the same position as when returning back from low to high rate. The process exhibits a hysteresis. There are no stable processing conditions inside the hysteresis region. Establishing an understanding of how different processing parameters influence the overall processing behaviour is requested in order to obtain stable processing conditions.

The Thin Film Group at Uppsala university in Sweden has presented a simple and easy to use analytical model for reactive sputtering processes. In the litterature it is referred to as the ”*Berg model*”. With this model it is quite easy to predict the influence of individual parameters on the overall processing behaviour. Despite the simple assumptions this model has turned out to predict the general shapes of a wide veriety of processing conditions. Having access to a reliable model offers the possibility to predict behavior as well as search for optimal processing conditions. It is also possible to investigate if a process may be modified as to eliminate the hysteresis and thereby obtain much simpler processing control.

It should be pointed out that the original Berg model can not be applied to processes where gases like e.g hydrocarbons are used. Here the gas molecule in the plasma may decompose into solid carbon and be deposited as free carbon at the substrate without reacting with the sputtered metal and form carbide. The deposited film may consist of unreacted metal, some carbide as well as some free carbon. A model for such a system has to consider the more complex particle fluxes from target to the substrate. We will briefly outline how this may be treated. Results from this new modified model will also be presented.

Titanium alloys for biomedical applications: past, present and future

Carlos Roberto Grandini, FBSE [1,2]*

[1] *UNESP - Univ Estadual Paulista, Lab. Anelasticidade e Biomateriais, 17.033-360, Bauru, SP, Brazil*

[2] *IBTN/Br - Institute of Biomaterials, Tribocorrosion and Nanomedicine – Brazilian Branch, 17.033-360, Bauru, SP, Brazil*

carlos.r.grandini@unesp.br

Metals are currently used for medical devices and over 70% of medical implants consist of metals, of which, over 90% are orthopedic implants [1]. Despite the large number of metallic medical devices in use today, they are predominantly made up of only a few metals. Metallic alloys such as titanium continue to be one of the most important components used in orthopaedic implant devices due to favorable properties of high mechanical strength, rigidity, fracture toughness and their reliable mechanical performance as replacement for hard tissues [2]. The most widely used titanium alloy for biomedical applications is the Ti-6Al-4V, however, previous studies showed that vanadium cause allergic reactions in human tissue and aluminum has been associated with neurological disorders [3].

Beta-Ti alloys containing completely biocompatible elements are exceptionally prospective materials for manufacturing of bioimplants. These biomaterials have the ability to introduce the most important property of biochemical compatibility which is low elastic modulus [4]. However, most of researches on metal are surface modification of titanium materials [5], while magnesium alloys and titanium alloys are still studied. According to the rise of regenerative medicine, the demand of research on metals is decreasing. On the other hand, many researchers made the effort to substitute metals to polymers or ceramics in medical devices, but still metals occupy a large share. Nowadays, low modulus β-type Ti-based alloys are still being developed. Meanwhile, porous Ti-based alloys are being developed as an alternative orthopedic implant material, as they can provide good biological fixation through bone tissue ingrowths into the porous network [6].

In this presentation, we would like to discuss the evolution, evaluation and development of the modulus of elasticity as an effective factor on the performance of beta alloys and prospective of them in the medical field. The first section focuses on the fundamental requirements titanium biomaterial should fulfill and its market and application prospects. This section is followed by discussing basic phases, alloying elements and mechanical properties of low modulus β-type Ti-based alloys. Thermal treatment, grain size, texture and properties in Ti-based alloys and their limitations are discussed in the third section. Finally, the fourth section reviews the influence of microstructural configurations on mechanical properties of porous Ti-based alloys and all known methods for fabricating porous Ti-based alloys. Recent information about biomedical titanium alloy development and 3D printing will be supplied. This section also reviews prospects and challenges of porous Ti-based alloys, emphasizing their current status, future opportunities and obstacles for expanded applications. Overall, efforts have been made to reveal the latest scenario of bulk and porous Ti-based materials for biomedical applications

References

[1] J.A. Helsen and H.J. Breme, "*Metals as Biomaterials*", Wiley, USA, 1998.

[2] Y. Li et al., Materials, **7**, 1709-1800 (2014).

[3] M. Geetha et al., Prog. Mat. Sci., **54**, 397-425 (2009).

[4] M. Niinomi; M. Nakai and J. Hieda, Acta Biomaterialia, **8,** 3888-3903 (2012).

[5] L. Wang and L.-C. Zhang, "*Development and Application of Biomedical Titanium Alloys",* Bentham Science Publishers, UK, 2018.

[6] K. Palka and R. Pokrowiecki, Adv. Engin. Mat., 20, 1700648 (2018).

Acknowledgments

The author would like to tanks the Brazilian Agencies CAPES, CNPq and FAPESP for financial support.

Applications of plasma in physical and chemical processes

Nito A Debacher
Departamento de Química – UFSC, Florianópolis, SC, Brasil
nito.debacher@ufsc.br

In this contribution our recent studies by atmospheric pressure thermal plasma and non-thermal plasma of dielectric barrier discharges (DBDs) are presented with particularly focus on: degradation of greenhouse gases, syngas and black carbon production; polymer surfaces modification; nanoparticles and carbon nanotubes production and modification; and wastewater treatment. Syngas and black carbon are produced by thermal plasma from a mixture of methane (CH_4) and carbon dioxide (CO_2). Polymer surfaces are functionalized by non-thermal plasma activating halogen species and replaced by amine groups of chemical interest. Polymer surfaces are also modified from hydrophobic to hydrophilic and make it suitable for cell attachment and proliferation for biomedical purposes. Hydrophilic carbon nanotubes are produced from black carbon by non-thermal plasma discharge over the water surface. Wastewater are treated by non-thermal plasma discharge which lead to chemical activation through the production of various reactive chemical species (e.g. OH, H, O, H_2O_2, H_2, O_2, O_3) that can break down and remove persistent organic pollutants (POPs) present in the aqueous phase. The results obtained under different plasma discharge regimes will be reported and discussed.

I.G., De Souza, N.A., Debacher. Molecular conversion processing of greenhouse gases of global warming effect and conversion units employing a solid particle trap (2011), Patent US7964169, US12445910.

L., Cottet, L. O., de Brito Benetoli, N. A., Debacher. Producing carbon nanotubes and carbon nanostructures involves treating cold plasma and carbon sources in liquid medium. (2015), Patent BR102013026766-A2, BR10026766.

T., Felix; J.S.Trigueiro; N.Bundaleski; O.M.N.D.Teodoro; S.Sério; N.A.Debacher. Functionalization of polymer surfaces by medium frequency non-thermal plasma. Appl. Sur. Sci. 428, (2018), 730-738.

B.M., Cadorin, V.D. Tralli, E. Ceriani, L.O de Brito Benetoli, E. Marotta, N.A Debacher, C. Paradisi. Treatment of methyl orange by nitrogen non-thermal plasma in a corona reactor: The role of reactive nitrogen species. J. Haz. Mat., 300, (2015), 754-764,

M., Fouodjouo, S. Laminsi, G.Y. Kamgang, M.T. Mengue, N.A. Debacher. Non-thermal plasma induced total mineralization of glyphosate in water in the presence of iron II ions. J. Braz. Chem. Soc., 26 (3), (2015), 411-419.

ESS vacuum system status

Marcelo Juni Ferreira
European Spallation Source – ERIC, Specialized Technical Service, Vacuum Section, Lund, Sweden
marcelo.ferreira@esss.se

The European Spallation Source (ESS) is a multi-disciplinary research infrastructure neutron source facility based on a 2GeV-5MW linear accelerator. The goal of ESS is to be the brightest neutron facility and to enable novel science in many fields such as biology research, environmental technologies and fundamental physics. The facility includes Super-conductive Radio-frequency cavities (SRF) to accelerator a proton beam to produce neutron by spallation process on a helium-cooled tungsten wheel, possibility to host 42 neutron instruments and a supercomputing data management and software development center.
The ESS vacuum section has the overall responsibility for all technical vacuum systems used on the Accelerator, Target and Neutron Scattering Instruments (NSS). The team has the responsibility to provide internally or to the in-kind partners, guidance, on-going support and oversight during design, fabrication, installation, commissioning and operation. This allows an integrated approach to be adopted to ensure the implementation of a cost effective vacuum program from the initial design through procurement and operation. The implementation of that will allow to ensure the standardize of vacuum designs for e.g. vacuum chambers, vacuum instrumentation, vacuum insulation on cryo-line, and any other equipment exposed to a technical vacuum environment.
It will be given an overview of the ESS Vacuum System status, on the accelerator, the ion source and Low Energy Beam Transport (LEBT) description with some early result from the operation, status of vacuum control system, on the Target last updates on the monolith vessel details, including the Proton Beam Window (PBW) and an overview of the NSS instruments early design. A short introduction about ESS Vacuum Laboratory and activities will be presented.

On the formation and diagnostics of nanoparticles in process plasmas

H. Kersten, Z. Marvi, E. von Wahl, A. Hinz, O. Polonskyi, T. Trottenberg
Group PlasmaTechnology, IEAP, University Kiel, Leibnizstr.19, 24098 Kiel, Germany
kersten@physik.uni.-kiel.de

The main sources of nanoparticle (NP) generation during plasma surface processing and the formation of nano-composite materials are (i) the formation of large molecules, mesoscopic clusters and particles in the plasma bulk by chemically reactive gases, and (ii) the formation and incorporation of particles at surfaces (target, substrate) by means of plasma-wall interaction. The plasma process promotes the particle formation by excitation, dissociation, reaction and charging of the involved species in the gas phase.
Different stages of particle growth in the gas phase can be observed by various plasma diagnostics as mass spectrometry, photo-detachment, IR absorption, microwave cavity measurements, Mie scattering and self-excited electron resonance spectroscopy (SEERS). Common diagnostics of particle formation also use the observation and analysis of harmonics and other discharge characteristics [1]. In particular, the early stages of the particle growth are not well investigated since they are often experimentally inaccessible by these methods.
One of the most important challenges concerning particle transport and extraction is the description of the force balance which is coupled with the ion and electron currents onto the dust particle surface in electric fields along the plasma presheath and sheath.
Since gravity for nanoparticles is negligible compared to other forces in the gas discharge the particles can be dispersed and confined in the entire plasma volume. Due to the collection of charge carriers (electrons and ions) onto the growing nanoparticles the plasma parameters are affected in a characteristic manner. For example, typical variations of bias voltage, electron temperature, electron density and other discharge parameters are observed during a growth cycle [2,3,4]. The oscillating dust cloud, in turn, induces spatial variations of the plasma potential. As important parameters we monitored the self-bias voltage at the powered electrode, gas pressure and the shape of the dust particle cloud by laser light scattering and CCD video imaging.
The experiments were performed in an asymmetric, capacitively coupled rf-discharge in acetylene, where multiple growth cycles can occur, and novel collection methods have been tested in order to get a better insight into the early stages of particle growth.
Making use of the correlations between the particle growth cycles and the observed quantities of the dusty plasma discharge it was possible to monitor each growth process in-situ. This allows for collection of particles at any desired stage of the growth cycle. Size distributions of the nanoparticles at the different stages of the growth cycle as well as the deposition patterns were determined ex-situ by scanning electron microscopy (SEM). The observations correlations can be used for the prediction of the NP growth.

[1] Schauer, J.C. et.al., 2004, *Plasma Sources Sci. Technol.*, 13, 636.
[2] Hinz, A., von Wahl, E., Faupel, F., Strunskus, T., Kersten, H., 2015, *J. Phys. D: Appl. Phys.*, 48, 055203.
[3] Wegner, T., Hinz, A., Faupel, F., Strunskus, T., Kersten, H., Meichsner, J., 2016, *Appl. Phys. Lett*., 108, 063108.
[4] Hundt, M., Sadler, P., Levchenko, I., Wolter, M., Kersten, H., Ostrikov, K., 2011, *J. App. Phys.*, 109,
123305.

Everything Starts in A Vacuum! How will Quantum-Based Vacuum Metrology Shape the Future of Technology?

Jay H. Hendricks
Thermodynamic Metrology Group, National Institute of Standards and Technology – NIST, USA
jay.hendricks@nist.gov

New methods of pressure and vacuum realization that are based on quantum calculations are currently under development. This is exciting in that it fits with the current SI-redefinition paradigm, that if a new technique relies upon a quantum property, measurement, calculation, or invariant of nature, then this technique can have served as a primary standard. Standards built this way are then directly tractable to the SI and will not itself require re-calibration. For the Pascal, a Fixed Length Optical Cavity (FLOC) and methods the enable the FLOC to be primary, including a Variable Length Optical Cavity (VLOC) will be discussed. These new methods operate by measuring the gas pressure though the interaction of light with the atomic or molecular properties of the gas and have enabled a new quantum-based pressure standard. Development of these new standards will enable the elimination of mercury manometers, a standard that has been in use for four centuries. The talk will cover the current status of the effort by National Metrology Institutes to re-define standards through the use of quantum based measurements and will connect current NIST this efforts to the coming SI-Redefinition. The talk will also briefly update activates to develop a Cold Atom Vacuum Standard (CAVS) which will enable a quantum-based vacuum standard capable of measuring extreme vacuum (XHV). Evangelista Torricelli invented the mercury pump in 1643, and while he did not realize it at the time, started a new field of vacuum technology which lead to the explosion of technology that lead to the modern national vacuum societies of today!

Plasma as technological alternative for the sustainable development of semi-arid

Clodomiro Alves Junior
Laboratório de plasma aplicado na agricultura, saúde e meio ambiente – UFERSA, Mossoró, RN, Brazil
clodomiro.jr@hotmail.com

The Semi-Arid Federal Rural University has an economically strategic geographical position, responsible for 95% of the marine salt national production, greater national oil and natural gas production on land, besides an important exporter of tropical fruits, as well as its potential in wind energy and solar. However, due to the fragility of the semi-arid region, it is imperative that its development be rational and sustainable. Plasma can be an important energy source in technological solutions for environmental sustainability. In this sense, the Laboratory of plasma applied to agriculture, health and environment - Labplasma is developing several researches in order to add scientific, technological, economic and environmental value to regional products and processes. In the present work the results of these surveys are presented. Plasma applied on the surface of a liquid solution, for example, changes its physical-chemical properties like pH and electrical conductivity, changing the solubility limit of the compounds. This fact can be used to selectively precipitate seawater salts. On the other hand, reactive species of oxygen and / or nitrogen based plasma, called RONS, are capable of producing oxidative damage or rupture of the cell membrane of microorganism, as well as the reduction in its replicative capacity, caused by UV radiation. This is the axis of research that we are developing at UFERSA for sanitation and conservation of post-harvest fruits. Also, dormancy, which consists of germination resistance of some seeds, can be broken by plasma treatment. Hydrophilic functional groups are formed on the surface of these seeds, increasing their imbibition and, consequently, the germination rate. Other interesting examples of research, taking the plasma as an energy source, will be discussed in the present work.

The vacuum system of the Sirius light source

Rafael M. Seraphim
Laboratório Nacional de Luz Síncrotron – LNLS, C.P. 6192, 13083-970 Campinas-SP, Brasil
rafael.seraphim@lnls.br

Sirius is a 3 GeV 4th generation light source under construction by the Brazilian Synchrotron Light Laboratory (LNLS). Sirius will be the second machine of this generation around the world and will have the lowest emittance, 0.25 nm.rad, in its energy class. It will generate a high-brilliance radiation over a billion times higher than the UVX, LNLS current light source. Sirius will be the largest and most complex scientific facility ever built in Brazil and will open new research opportunities for the Brazilian and Latin American scientists.

The vacuum system of the Sirius machine demands cutting-edge technologies and aggressive design concepts to meet the machine requirements. The Sirius accelerators will have more than 1 km of ultrahigh vacuum chambers. The storage ring, which is the main accelerator of the Sirius machine and represents about 0.51 km, is based on 20 cells of a highly compact magnet lattice – 5 bend achromat (5BA). This lattice concept leaves very little space for installing the vacuum components. Therefore, narrow vacuum chambers capable of absorbing unused synchrotron radiation are needed. In this way, most of the vacuum chambers are being made of copper and have narrow copper cooling pipes attached to their outer side. Due to the small vacuum conductance of the chambers, on account of their narrow cross section, vacuum pumping is based on distributed concept and then non-evaporable getter (NEG) coating, a technology developed by CERN, is being extensively used, with more than 95% of the chambers being coated. Together with MAX IV, a Sweden light source under commissioning, Sirius will be the first synchrotron light sources that will have the vacuum system mainly pumped by NEG coating technology.

In this talk, it will be presented an overview of the Sirius light source with an emphasis on the vacuum system.

XXXIX Congresso Brasileiro de Aplicações de Vácuo na Indústria e na Ciência

08 a 11 de outubro de 2018 - Joinville - SC

PALESTRAS TÉCNICO-COMERCIAIS XXXIX CBrAVIC

AUTOMATIC FEEDBACK CONTROL IN REACTIVE HIPIMS BY MEASURING THE PULSE PEAK CURRENT AND ADJUSTING THE PULSE FREQUENCY

T. Shimizu[1]*, M.M. Villamayor[2], J. Keraudy[3], Rafael Sánchez[4]
[1]*Tokyo Metropolitan University*
[2]*Linköping University*
[3]*Linköping University*
[4]*Ionautics AB*

1. Introduction

Reactive magnetron sputtering is a physical vapor deposition technique, which is applied to grow compound films such as nitrides, oxides, and carbides. An inherent feature in reactive magnetron sputtering is process instability due to the complex relation between the fluxes of reactive gas and sputtered metal from the cathode [1]. High reactive gas fluxes induce compound formation on the cathode (target), which is referred to as target poisoning. Since the sputtering efficiency of the compound material is typically lower than that of the corresponding metal target, poisoning usually causes a significant decrease in flux of metal from the cathode [1]. Therefore, to obtain stoichiometric compound films with relatively high deposition rates, the process generally has to be maintained in the transition region between the metallic and the compound mode, where instability due to hysteresis is commonly observed [2]. The objective of the present study is therefore to explore the feasibility of a peak target current regulation technology.

In reactive HiPIMS to stabilize the transition zone during reactive deposition over a wide range of experimental conditions. As a simple and cost effective approach to stabilize the discharge current at a given set point, the present study implements a feedback control system by automatic regulation of the pulse frequency. To this purpose, we first monitor waveforms of the real-time pulse current to study the process characteristics during reactive HiPIMS of Hf in different Ar/N2 gas mixtures and for different pulse frequencies. Based on this characterization, the possibility of stabilizing the reactive HiPIMS process by the discharge current characteristics under the control of the pulse frequency is investigated. Finally Hf– N films were grown under peak current, Ipk, regulation and their stoichiometric properties, deposition rates and crystal structures were evaluated and compared to that of conventional reactive HiPIMS without I_{pk} regulation.

2. Experimental

Experiments were performed in an ultra-high vacuum stainless-steel chamber with a base pressure below 10^{-6} Pa. A Hf (99.9 % purity) disk with a diameter of 76.2 mm and a thickness of 6.35 mm was used as sputtering target. Ar gas with a purity of 99.9997% was introduced into the chamber through a mass flow controller and the Ar flow rate was adjusted between 26–28 sccm to maintain a constant partial pressure of 0.4 Pa. N_2 gas (99.9995% in purity) was introduced into the chamber and the N_2 flow rate was varied from 2.0 to 4.0 sccm to grow films in the transition, and the compound sputtering modes. The average sputtering power delivered to the target was varied in the range from 100 to 200 W depending on the discharge current for a constant applied voltage of 450 V. Unipolar pulses with a length of 25 μ s and a frequency in the range from 450 to 1200 Hz were supplied by a HiPSTER 1 pulsing unit (Ionautics AB) fed by an MDX 1 K DC power supply (Advanced Energy). The HiPSTER unit was modified to realize PID-regulation of the frequency based on the internally recorded I_{pk} value. The discharge current and voltage time characteristics were recorded by the HiPSTER 1 and monitored on a Tektronix TDS 520 C digital oscilloscope directly connected to the pulsing unit.

3. Results and Discussions

The Ar partial pressure was kept constant at 0.4 Pa in all experiments and the N_2 flow was increased from 1.5 to 4 sccm in a controlled manner. A constant pulse voltage of 450 V was applied at the generator output. The pulse conditions were fixed to a duration of 25 μs and a frequency of 600 Hz. The average target power varied in the range of 100 to 140 W due to the change in pulse current. Figure 1 shows how the discharge current waveforms change: (a) with and (b) without the pulse frequency control. As can be seen from the variation of the waveforms in figure 1 (b), the peak current, I_{pk}, value starts to rise at 2.1 sccm and it increases almost linearly from 2.1 to 3.5 sccm when running in conventional reactive HiPIMS mode. However, by controlling the pulse frequency to keep the I_{pk} value constant, figure 1 (a), almost the same current waveforms were obtained for different N_2 gas flows. For example, for a N_2 gas flow of 3.5 sccm, the discharge current curve peaking at 74 A in figure 1 (b) could be reduced and actively stabilized to the set peak value of 50 A (figure 1 (a)) by altering the frequency from the previously set value of 600 to 1150 Hz. By this frequency increase, the average power increased from 135 to 270 W leading to an increased sputtering of the compound layer. The reactive Hf HiPIMS process in Ar/N_2 mixtures can be stabilized by

*Corresponding author: simizu-tetuhide@tmu.ac.jp

regulating the frequency to maintain a constant peak value of the current in the pulse, the Ipk . This is likely to work for all process conditions where there is a simple relation between Ipk and the reactive gas content in the process chamber. The applicability of the I_{pk} regulation by the above described feedback control loop on the actual film growth of HfN was evaluated by comparing the film properties of Hf– N films deposited at various N2 gas flows of 2.0, 2.4, 2.8, 3.2, and 3.6 sccm with and without I_{pk} regulation. Both processes were operated at constant pulsing conditions (450 V and 25 μ s pulse width). The trends of the variation of current waveforms with increasing gas flow and the controllability of the peak target current by pulse frequency. The films deposited with I_{pk} regulation demonstrate a rapid increase of deposition rate with increasing N2 flow, while the deposition rate without regulation decreases as a consequence of target poisoning. The result for regulation is clearly due to the relatively higher applied average target power by increasing the pulse frequency for the higher N2 low conditions. The films deposited with I_{pk} regulation exhibited a much broader process window. In this case, all deposited films at different N2 flow rates (2.0– 3.6 sccm) had visually the same golden colour of the stoichiometric composition while without I_{pk} regulation variations of the colour by altering the N2 flow were clearly observed.

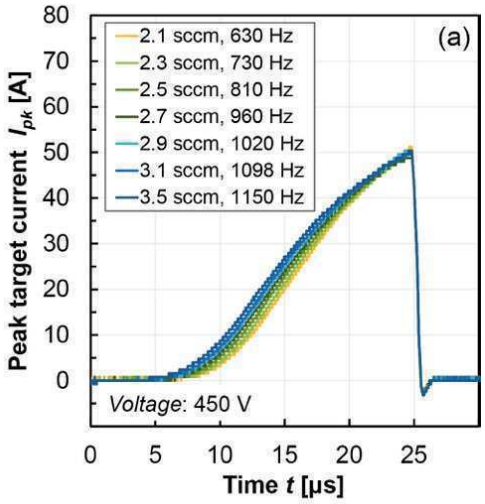

Fig. 1. *Shows a HiPIMS pulse discharge with pulse frequency control where the peak current is keeping constant at different gas flows.*

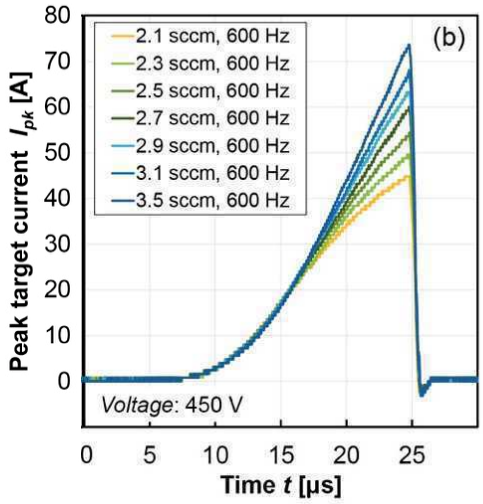

Fig. 2. *Figure Shows a HiPIMS Pulse discharge without pulse frequency control at different gas flows the peak current vary*

4. References

[1] Berg S and Nyberg T 2005 Thin Solid Films 47 215.
[2] Sproul W D, Christie D J and Carter D C 2005 Thin Solid Films 491 1
[3] Gudmundsson J T, Brenning N, Lundin D and Helmersson U 2012 J. Vac. Sci. Technol. A 30 030801
[4] Kouznetsov V, Mac.k K, Schneider J M, Helmersson U and Petrov I 1999 Surf. Coat. Technol. 122 290
[5] Helmersson U, Lattemann M, Bohlmark J, Ehiasarian A P and Gudmundsson J T 2006 Thin Solid Films 513 1
[6] Wallin E and Helmersson U 2008 Thin Solid Films 516 6398
[7] Aiempanakit M, Larsson P, Sarakinos K, Jensen J, Kubart T and Helmersson U 2011 Thin Solid Films 519 7779
[8] Audronis M, Bellido-Gonzalez V and Daniel B 2010 Surf. Coat. Technol. 204 2159
[9] Vlček J, Rezek J, Houška J, Čerstvý R and Bugyi R 2013 Surf. Coat. Technol. 236 550
[10] Sittinger V, Ruske F, Werner W, Jacobs C, Szyszka B and Christie D J 2008 Thin Solid Films 516 5847

*Corresponding author: simizu-tetuhide@tmu.ac.jp

XXXIX Congresso Brasileiro de Aplicações de Vácuo na Indústria e na Ciência
08 a 11 de outubro de 2018 - Joinville - SC

APRESENTAÇÕES ORAIS XXXIX CBrAVIC

Apresentações orais do XXXIX CBrAVIC

ID	TÍTULO
#3	**CHARACTERIZATION OF ALUMINA LAYERS PRODUCED BY ELETROLYTIC PLASMA AT DIFERENT CURRENT DENSITIES** *D. C. R. Santos, G. S. Reis, R. R. Lucas*
#11	**DESIGN OF ATMOSPHERIC PRESSURE PLASMA JETS FOR UNIFORM MODIFICATION OF SMALL 3D OBJECTS** *Konstantin G. Kostov, Taina S. M. Mui, Rogerio P. Mota, Fellype de Nasimento*
#12	**PLASMA ACTIVATION OF POLYAMIDE FABRIC SURFACE BY HYBRID CORONA-DIELECTRIC BARRIER DISCHARGE** *G. Petraconi, F. Gasi, E. Bittencourt, A.H.R Castro, F.S. Miranda, A. M. Essiptchouk, L. Nascimento, R. S. Pessoa, A. Petraconi*
#14	**PROPERTIES OF DLC FILMS DEPOSITED BY PIII&D INSIDE TITANIUM ALLOY TUBE OF SMALL DIAMETER** *N.M. Santos, M. Ueda, S.F.M. Mariano*
#17	**MEASUREMENT OF THE BREAKDOWN VOLTAGE ON THE SURFACE OF THE ALUMINIZED POLYIMIDE FILM TREATED BY PIII** *A. R. Marcondes, R. M. Oliveira, J. O. Rossi, M. Ueda*
#18	**COMPARISON OF DCMS AND HiPIMS OPERATING REGIMES FOR DEPOSITION OF PURE AND NITROGEN-DOPED TITANIUM DIOXIDE THIN FILMS** *C. Stegemann, D. A. Duarte, A. S. Silva Sobrinho, D. M. G. Leite, M. Massi*
#21	**CHARACTERIZATION OF ITON THIN FILMS GROWN BY EVAPORATION AND PECVD** *M. Sparvoli, V. Pederzini, R. K. Onmori, I. Y. Abe, A. T. Lopes*
#24	**BARRIER PROPERTIES OF HIGH PERFORMANCE PMMA-SILICA PROTECTIVE COATINGS** *Andressa Trentin, Andressa de L. Gasparini, Flávio A. Faria, Samarah V. Harb, Fábio C. dos Santos, Celso V. Santilli, Peter Hammer*
#25	**AUTOMATED CRYSTALLOGRAPHIC ORIENTATION MAPPING OF TI-NB COATINGS SPUTTER-DEPOSITED ON AISI 316L STAINLESS** *E.D. Gonzalez, A.L. Gobbi, C.R.M. Afonso, P.A.P. Nascente*
#51	**EFFECT OF PLASMA PARAMETERS ON CARBON NANOTUBE FUNCTIONALIZATION BY MALEIC ANHYDRIDE** *Teresa Tromm Steffen, Luis César Fontana Daniela Becker*
#58	**MAGNETIC PROPERTIES OF Gd/GdN SUPERLATTICES** *Francisco Alfaro, Julio César Sagás, Luís César Fontana*
#63	**SYNTHESIS AND CHARACTERIZATION OF NICKEL/ALUMINA CATALYTIC MONOLITH** *Maíra O. Palm, Mauro E. S. Júnior, Leonardo Cardoso, Diego A. Duarte, Rafael de C. Catapan*
#88	**TRIGGERING VARIATIONS IN PHASE STABILITY BY TUNING THE PULSE FREQUENCY IN PULSED-DC MAGNETRON SPUTTERING OF A STAINLESS STEEL TARGET** *Marcus V. F. Schroeder, Abel A. C. Recco, Carlos M. Garzón*
#99	**ALL-OPTICAL ELECTRICAL CONDUCTOR TEMPERATURE CHARACTERIZATION USING A FIBER BRAGG GRATING** *Milton José Cinelli, Gabriel Bolacell, Stenio Aristilde, Cristiano M. B. Cordeiro, Mauro Rosa*

#100	**INCREASING THE PLASMA CURRENT THROUGH IMPROVEMENT OF SECONDARY ELECTRONS EMISSION IN CCP-PLASMAS BY USING A NEW ASYMETRIC BIPOLAR PLASMA POWER SUPPLY (ABiPPS)** *Juliano Sadi Scholtz, Alessandro Luiz Batschauer, Marcello Mezaroba, Luis César Fontana*
#104	**BIODIESEL PRODUCTION THROUGH THE PLASMA TECHNOLOGY** *M. M. Machado, C. R. S. de Carvalho Pinto, A. L.V. Cubas, R. A. V. Montalván, E. H. S. Moecke, C. R. Oliveira Junior, J. M. K. Gelsleichter, K. S. Barcelos, J. A. Bork*
#115	**EFFECTS OF PARTIAL SUBSTITUTION OF CARBON BY NITROGEN ON MICROSTRUCTURE AND HARDNESS OF AISI 420 STEEL** *Felipe Augusto de Aguiar Possoli, Euclides Alexandre Bernardelli, Julio Cesar Klein das Neves, Paulo César Borges*
#127	**AISI 420 PATTERNING BY LOW-TEMPERATURE PLASMA NITRIDING** *F. I. Zanetti, I. G. Zanella, W. L. Alexandre, R. P. Cardoso, S. F. Brunatto*
#128	**USING A THREE-ELECTRODE DC REACTOR FOR ATMOSPHERIC PRESSURE PLASMA-ASSISTED NITRIDING: INITIAL RESULTS** *G.S. Kobayashi, F.A. Zaias, R.P. Cardoso*

CHARACTERIZATION OF ALUMINA LAYERS PRODUCED BY ELETROLYTIC PLASMA AT DIFERENT CURRENT DENSITIES

Santos, D. C., R.*, Reis, G. S., and Lucas, R. R.
Laboratório de Plasma Eletrolítico (LaPE), Fatec de Pindamonhangaba, CEETEPS/SP.

1. Introduction

Plasma Electrolytic Oxidation (PEO) is an innovative technology applied for the modification of metallic surfaces, mainly light metal alloys, such as aluminium, titanium, magnesium, and zirconium. This electrolytic process, unlike the conventional anodization, is performed under high voltage, and this later is responsible for plasma breakdown inside the electrolytic solution [1]. The plasma introduces thermochemical reactions that alters the properties of the growth layers. When the work electrode is aluminium, that oxide layer is alumina (Al_2O_3), and its properties depends on experimental parameters, such as voltage, current, temperature, time and electrolyte, among others [2]. This work shows the effect of electric current and process time adjusted for PEO of 5052 aluminium alloy. In order to do that, an alkaline solution was prepared with borax ($Na_2B_4O_7$).

2. Experimental

Small coupons of 5052 aluminium alloy were treated by PEO, in a solution prepared with distilled water and borax (10 g/l). The electrolytic system used in that processes was fed by DC high power supply (20 kW), operating in galvanostatic mode, which allowed the treatments at constant currents of 0.5, 1.0, 1.5, 2.0 and 2.5 A. The treatments were performed at different times of 6 and 10 min. The growth rate of alumina layers was determined by mass measures, achieved before and after each process, using an analytical balance (E = ± 0.1 mg). The crystallinity and the morphology of PEO alumina were evaluated by X-ray diffraction (XRD) and Scan Electronic Microscopy (SEM), respectively.

3. Results and Discussions

Fig. 1 shows that 10 min-PEO promoted significant mass deposition compared to 6 min-PEO, mainly increasing the current density. This later causes the elevation of process temperature, which favor the growth of the layers, but the process time is important to predominance of kinetic reactions for alumina formation. XRD analysis shows the PEO-layers are composed by γ- Al_2O_3 and α- Al_2O_3, but this later is promoted by current density elevation, and appears in greater amount at 10-min PEO process. The PEO layer morphology is like corals, as depicted in Fig. 2. Theirs size and roughness depend on the process time, but significantly alterations occur as current density is increased at longer PEO process.

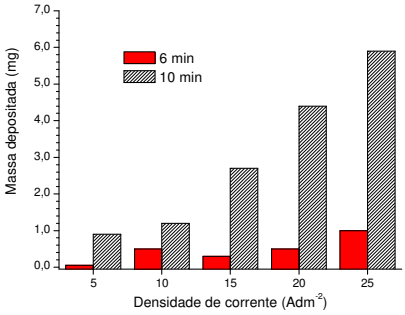

Fig. 1. *PEO-layer mass as function of current density and process time.*

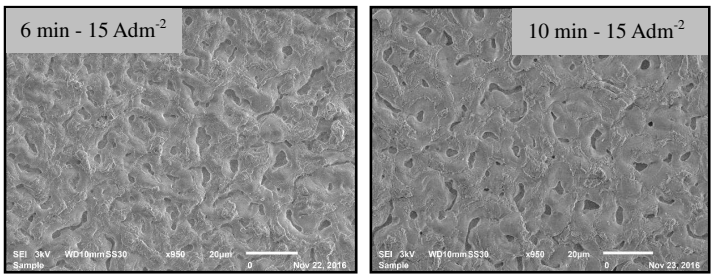

Fig. 2. *MEV morphology of PEO-layers grown in borax electrolyte, composed by O (~60%) and Al (~40%).*

4. References

[1] Li, Q., Liang, J., Wang, Q. **Plasma Electrolytic Oxidation Coatings on Lightweight Metals**. In Modern Surface Engineering Treatments. Edited by Mahmood Aliofkhazraei. InTech 2013. Available at https://www.intechopen.com/books/modern-surface-engineering-treatments.

[2] A. Akbar *et al.* Surface modification of aluminum alloy 6060 through plasma electrolytic oxidation. **International Journal of Engineering Works**, Kambohwell Publisher Enterprises, 2017, 4(6), p. 114-123.

Acknowledgments

The authors thank to FAPESP for financial support, UNESP-Sorocaba for MEV images, and INPE – S. J. Campos for XRD analysis.

*Corresponding author: deborah.santos@fatec.sp.gov.br

DESIGN OF ATMOSPHERIC PRESSURE PLASMA JETS FOR UNIFORM MODIFICATION OF SMALL 3D OBJECTS

Konstantin G. Kostov[1]*, Taina S. M. Mui[1], Rogerio P. Mota[1] and Fellype de Nasimento[2]
[1]*São Paulo State University – UNESP, Campus in Guaratinguetá – FEG, CEP 12516-410, SP, Brazil*
[2]*State University of Campinas – UNICAMP, IFGW, Campinas, CEP 13083-970, SP, Brazil*

1. Introduction

In the last decade atmospheric pressure plasma jets (APPJs) have been extensively studied because their operation does not require expensive vacuum vessels and pumping systems thus allowing compact and low-cost plasma sources that can be readily employed in on-line material processing and biomedicine [1, 2]. In such devices electric discharge is ignited in a noble gas that flows through a thin dielectric tube and the resulting plasma is ejected into the surrounding air. APPJs can generate up to several cm-long plasma plumes that are easily adapted to treat irregular 3D objects. However in the most excitation schemes and working gases the plasma plume diameter is usually on the order of 1-2 mm thus limiting the modified area to few cm^2. Moreover, the surface modification is usually not uniformly distributed [3]. In this work we report on an APPJ terminating with a conical horn-like nozzle that is specially developed for uniform surface modification and for treatment of 3D objects.

2. Experimental

Fig. 1 depicts a schematic drawing of the plasma jet configuration employed in this work. It consists of a pin electrode centered inside a Pyrex glass funnel. The device was installed vertically with the funnel exit pointing downward. Polyethylene Terephthalate (PET) samples with diameter larger than the horn diameter were fixed on a glass table with a grounded metal electrode beneath it. The device was operated in Ar flow and three funnels with different exit diameters were employed with the purpose to extend the treatment area. Also, for bigger horn diameters the discharge power density is reduced and the gas temperature can be kept low enough to treat thermosensitive objects.

3. Results and Discussions

PET surface modification along the sample radius was assessed by a series of water contact angle and XPS measurements performed. Surface roughness was evaluated by AFM measurements. The results show that depending on jet operating conditions, such as jet-sample distance, horn diameter and gas flow rate, uniform surface modification over the entire area covered by the horn can be achieved. Treatments in vertical samples that fit inside the conical horn were conducted and the surface modification along the sample height was also uniform.

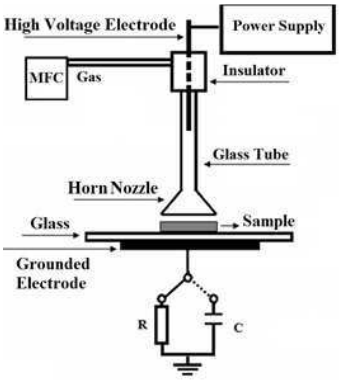

Fig. 1. *Experimental setup.*

Fig. 2. *Photo of a plasma jet with vertical sample*

4. References

[1] S. Reuter, Th. von Woedtke and K.-D. Weltmann, J. Phys. D: Appl. Phys., **51**, 233001 (2018).
[2] F. Fanelli and F. Fracassi, Surf. Coatings Technol., **322,** 174-201 (2017).
[3] I. Onyshchenko, N. De Geyter and R. Morent, Plasma Process. Polym., **14**, 1600200 (2017).

Acknowledgments
This research was funded by FAPESP under grant 2015/21989-6

*Corresponding author: kostov@feg.unesp.br

PLASMA ACTIVATION OF POLYAMIDE FABRIC SURFACE BY HYBRID CORONA-DIELECTRIC BARRIER DISCHARGE

Petraconi, G[1], Gasi, F[2], Bittencourt, E[1], Castro, AHR[1], Miranda, FS[1] and Essiptchouk, AM[3], Nascimento, L[1], Pessoa, RS[1]* and Petraconi, A[1].
[1]*Instituto Tecnológico de Aeronáutica-ITA*
[2]*Universidade Federal do ABC-UFABC*
[3]*Universidade Estadual Paulista-UNESP*

1. Introduction

The modification of fabric surface with cold plasma treatment is becoming more common due to economic and environmental advantages. For polymer materials, cold plasma is used to improve surface properties, such as wettability, surface adherence and printing capacity, through interaction of reactive species with the surface [1] [2]. The main goal of this paper was to evaluate the effect of plasma treatment (hybrid corona-DBD) on knitted fabrics (polyamide 6.6 with elastomer). The effectiveness of the modifications was assessed by a comparative contact angle between samples, as well as the dyeing properties.

2. Experimental

A knitted fabric composed of 92% polyamide 6 (PA 6.6) and 8% elastomer was used for this research. The polyamide fabric was subjected to air plasma treatment under atmospheric pressure, with a power of 57 W (exposure time from 0 to 2000ms). The plasma equipment used was "PLASMA LABO", produced by the textile machinery manufacturer Arioli.

3. Results and Discussions

Figure 1 shows the decay curve with the purpose of evaluating variations of the contact angle versus time (t). After application of the plasma discharge with a power of 57 W, the sample remained in a conditioned environment without vacuum preservation in order to measure the decay effect. Figure 2 shows an increase in the transmittance of groups corresponding to C-H, N-H and N-O. The increase in the transmittance of these groups provides a greater dyeing affinity, thus improving dye efficiency.

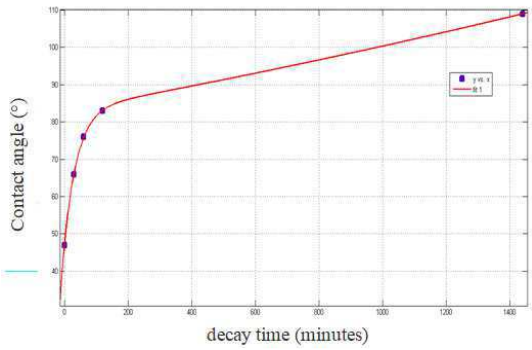

Fig. 1. *Contact angle decay curve versus time*

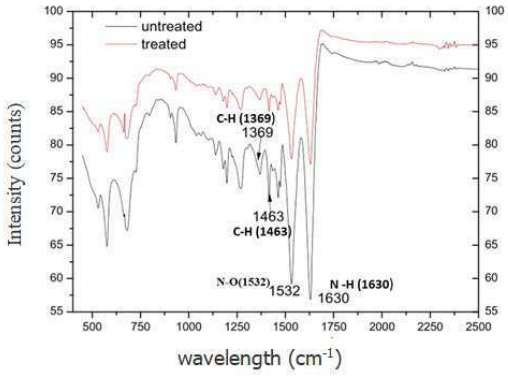

Fig. 2. *Infrared Spectrum*

In order to evaluate the color change, a spectrophotometer was used with the purpose of quantifying the color strength in duplicated measurements. By using the plasma treatment, a better fixation of dye was observed. Dyeing with a basic and acid dye caused the dyeability to increase for both power plasma compared with the untreated sample. This analysis was based on color strength and solidity tests.

4. References

[1] F. Caiazzo, P. Canonico, R. Nigro, V. Tagliaferri, Electrode discharge for plasma surface treatment of polymeric materials, Journal of Materials Processing Technology. 58 (1996) 96–99. doi:10.1016/0924-0136(95)02112-4.
[2] R. Morent, N. De Geyter, J. Verschuren, K. De Clerck, P. Kiekens, C. Leys, Non-thermal plasma treatment of textiles, 3427–3449. doi:10.1016/j.surfcoat.2007.12.027.

*Corresponding author: rspessoa@ita.br

Acknowledgments
We acknowledge the financial support of FAPESP, CNPq and CAPES.

*Corresponding author: rspessoa@ita.br

PROPERTIES OF DLC FILMS DEPOSITED BY PIII&D INSIDE TITANIUM ALLOY TUBE OF SMALL DIAMETER

N.M. Santos*, M. Ueda and S.F.M. Mariano
National Institute for Space Research, São José dos Campos, SP, Brazil

1. Introduction

Diamond-like carbon (DLC) films have interesting properties for technological applications, such as high hardness, wear resistance, low friction coefficient and biocompatibility [1]. Using DLC films as protective coatings can increase the lifetime of the tubes used in propulsion of spacecrafts and thermal control systems of satellites and inhibit the permeation of corrosive species from the fuels and the cooling fluids through the film-metal interface. The properties of the films deposited by Plasma Immersion Ion Implantation and Deposition (PIII&D) system generally depend on the deposition conditions, which determine their microstructure, especially the respective proportions of sp^3 and sp^2 carbon site [2, 3]. Therefore, the objectives of this work were the production of DLC films inside metal tubes to increase the useful lifetime in the applications of the aerospace, oil and gas sectors, taking advantage of the plasma ejected from the interior of the tube for the coating of flat samples and to investigate the properties of these films.

2. Experimental

The films were prepared in a stainless steel cylindrical vessel with a volume of 20 liters, by PIII&D system using acetylene plasma, by driving Hollow Cathode (HC) discharges inside the tube attached to the top part of the chamber. The tube used was titanium alloy (Ti6Al4V), with 15 cm length and small internal diameter of 1.1 cm, with one side closed configuration. Polished samples of Ti6Al4V (TAV), and pieces of p-type silicon, were fixed along the inner tube wall for subsequent analysis of the DLC coatings. The material expelled by the HC driven tube was deposited in a commercial Si-wafer disc target, placed 7 cm from the tube exit. Prior to each deposition, the tubes were further cleaned in argon plasma for 10 min (4kV, 15A, 20μs, 500Hz). Acetylene plasma was generated by the application of pulses of 2kV, 15A, 20μs, 500 Hz rate, reaching temperatures of about 1000ºC quickly. Deposition time varied from 30 to 240 minutes. Chemical structure of DLC films were analyzed by Raman Spectroscopy and the film thicknesses were measured by Field Emission Gun – Secondary Electron Microscopy (FEG/SEM/EDS), and the topography was evaluated from surface images.

3. Results and Discussions

The ID/IG value indicated the existence of monocrystalline graphite on the film. The internal wall of the tube was completely covered by DLC films, as well as the samples placed inside the tube. The DLC deposition on these samples also revealed to be of quite a good quality, totally adhered, with thickness between 2 to 25 μm. It was found that the plasma ejected from the tube has also good properties, such as high density, stability of the discharge, uniform plasma and with high rates of implantation and deposition. Finally, it can be used for coating planar components with success.

4. References

[1] S.F.M. Mariano, M. Ueda, R.M. Oliveira, E.J.D.M. Pillaca,; **N.M. Santos,** Magnetic-field enhanced plasma immersion ion implantation and deposition (PIII&D) of diamond-like carbon films inside tubes. Surface & Coatings Technology. v. 312, p. 47-54, 2017.
[2] Y. Lifshitz, "Diamond-like carbon present status", Diamond and Related Materials, v.8, p. 1659-1676, 1999.
[3]J. Robertson, Diamond-like amorphous carbon. Materials Science and Engineering R v. 37, p. 129-281 (Reports: A review journal), 2002.

Acknowledgments

The authors thank the CNPq for financial support.

*Corresponding author: nazirmonteiro@gmail.com

MEASUREMENT OF THE BREAKDOWN VOLTAGE ON THE SURFACE OF THE ALUMINIZED POLYIMIDE FILM TREATED BY PLASMA IMMERSION ION IMPLANTATION

Marcondes, A.R.[1]*, Oliveira, R. M.[1], Rossi, J.O. [1] and Ueda, M. [1]
[1]*National Institute of Space Research, São José dos Campos – São Paulo – Brazil*

1. Introduction

Passive thermal control systems used in satellites utilize aluminized polyimide film (Kapton™) as the outermost layer. In contact with the harsh space environment, polyimide film suffers multiple types of degradation. At Low Earth Orbit (LEO) (up to 1,000 km) a significant degradation of the Kapton is the electrostatic discharge (ESD) that may occur due to the charge accumulation on the surface of the film. The main source of charge build-up is the low dense plasma present at LEO. So, it is desirable to improve the dielectric breakdown voltage on the surface of the Kapton in order to reduce the probability of ESD occurrence which, in its turn, could keep the internal parts and components of the satellite safer against electrical damages.

2. Experimental

Kapton film type HN (1 mil in thickness) has been treated by plasma immersion ion implantation of nitrogen (PIII) [1]. The treated film and the pristine aluminized Kapton, as well as the untreated Kapton film without aluminum have had their surface breakdown voltage measured at several pressure conditions. The distances between the two electrodes set up to apply the voltage on the film surface were kept approximately the same and the small variation in the electrodes distance from one set of measures to another was considered by expressing the breakdown voltage as a function of the product of the pressure (*p*) by the electrodes distance (*d*). So, the curves obtained can be considered as Paschen curves.

3. Results and Discussions

The curves of breakdown voltage as function of the product *pd* are shown in Figure 1 for: (a) air, when no film was present between the electrodes; (b) film of pristine Kapton without aluminum; (c) film of pristine aluminized Kapton, and (d) film of aluminized Kapton treated by PIII. As one can see the surface breakdown voltage of the aluminized Kapton treated by PIII in the region of low pressure (pd < 10^{-3} Torr.cm) is higher than the breakdown voltage of the pristine aluminized Kapton and in these cases the breakdown voltages seems to be approximately constant which may allow extrapolating the values to the pressures found at LEO which can be as low as 10^{-11} Torr. This result indicates that the treatment of Kapton by PIII of nitrogen can be advantageous to reduce the risk of ESD phenomenon in the film of Kapton used in LEO.

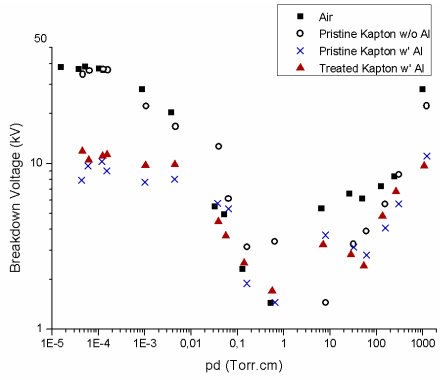

Fig. 1. *Breakdown voltage of the air, pristine Kapton without aluminum, pristine aluminized Kapton and aluminized Kapton treated by PIII of nitrogen as function of the product of the pressure (p) by the distance (d) between the two electrodes used to apply the voltage on the surface of the film*

4. References

[1] MARCONDES, André Ricardo; UEDA, Mario; ROSSI, José Oswaldo. Effect of nitrogen plasma immersion ion implantation on surface electrical breakdown strength of the aluminized polyimide. **Revista Brasileira de Aplicações de Vácuo**, v. 36, n. 3, p. 122-130, 2018.

Acknowledgments

We would like to thanks to the Brazilian Ministry of Science, Technology, Innovation and Communication that has supported this work.

COMPARISON OF DCMS AND HiPIMS OPERATING REGIMES FOR DEPOSITION OF PURE AND NITROGEN-DOPED TITANIUM DIOXIDE THIN FILMS

C.Stegemann[1*], D.A. Duarte[2], A.S.S. Sobrinho[1], D.M.G. Leite[1], and M. Massi[3]
[1]*Technological Institute of Aeronautics, Plasmas and Processes Laboratory, São José dos Campos, SP, Brazil.*
[2]*Federal University of Santa Catarina, Joinville Center of Technology, Joinville, SC, Brazil.*
[3]*Mackenzie Presbyterian University, School of Engineering-PPGEMN, São Paulo, SP, Brazil.*

1. Introduction

The flow of reactive gas inserted into the gas mixture present in the process chamber during the deposition period is directly related with the final characteristics of the obtained films. In addition to reacting with deposited atoms on the surface of the substrate, the reactive gas atoms also react with atoms of the target surface, which modifies the deposition yield changing deposition rate, secondary electron generation and stoichiometry of the films [1]. The formation of a layer on the target surface is result from the reaction of the deposition material with reactive gases and occurs concurrently with an increase in pressure in the process chamber due to the fact that the reactive gas is not being fully consumed in the deposition. This effect is called target poisoning and it depends on the reactivity of the target material as well as on the energy of the particles that reach it [2], and this mode allows the deposition of stoichiometric composite films [3]. Hysteresis effect occurs when there are variation of the discharge parameters with the insertion or removal of reactive gas. The stabilization of the transition zone between the two modes brings advantages to the deposition of the films with certain desired characteristics, and this stabilization can be done, among other ways, by the pumping increase on the process chamber during the discharge, reduction of the area of the target or, for some metal oxides, nitrogen insertion into the gas mixture [4].

2. Experimental

The films of TiO_2 and N-TiO_2 were deposited in crystalline silicon using the sputtering technique by direct current magnetron sputtering (DCMS) and by high power impulse magnetron sputtering (HiPIMS), without heating the substrate. All the depositions were performed by sputtering of a titanium target, with a power of 300W, pressure of 5 mTorr, target-substrate distance of 11 cm and time of deposition of 120 minutes. TiO2 films were grown in an atmosphere with 10.4 sccm of Ar and 3.5 sccm O_2, and N-TiO_2 by 10.4 sccm of Ar, 0.6 sccm of O_2 and 10 sccm of N_2. For HiPIMS depositions were employed the frequency of 250 Hz and action time of 150 ms [5].

3. Results and Discussions

From the variation of the total pressure with the insertion or removal of oxygen we can observe that the different experimental parameters used for the depositions showed changes of behavior between the insertion or removal of gas, configuring the hysteresis regime, in higher or lower proportion. The oxygen fluxes are related to the best data in terms of the films characteristics for optical applications obtained by the group previously [6], such that for the growth of TiO_2 films the flow of 3.5 sccm was used, as Fig.1, and for N-TiO_2 the flow of 0.6 sccm, as Fig. 2.

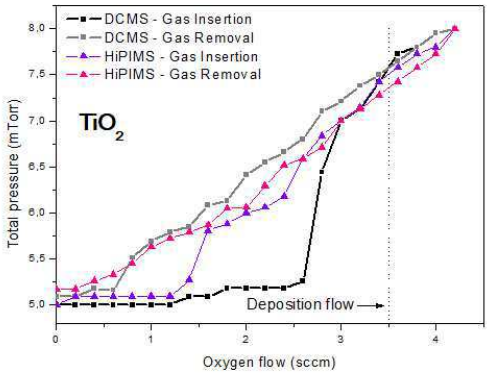

Fig. 1. *Pressure configuration with the insertion and removal of reactive gas for TiO_2 films deposition.*

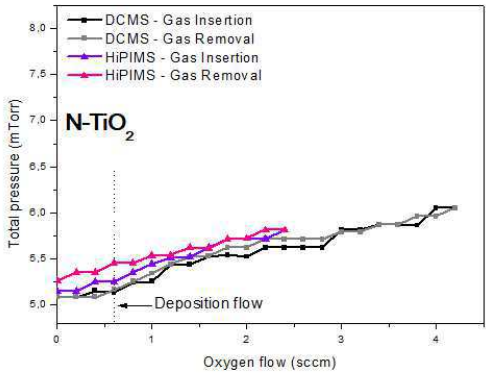

Fig. 2. *Pressure configuration with the insertion and removal of reactive gas for N-TiO_2 films deposition.*

The region in which there was a change between the operating points, metallic and oxide, is characterized by a transition point which is evidenced by the abrupt increase of the pressure due to the increase of the gas flow inserted in the chamber. In Fig. 1, this transition point corresponds to the fluxes of 2.6 sccm for DCMS and 1.4 sccm for HiPIMS, and from this we have that both films were deposited in the operating oxide mode.

*Corresponding author: cristianestegemann@yahoo.com.br

The hysteresis region decreases for deposition of deposited TiO_2 films by HiPIMS compared to those grown by DCMS. The mechanism that provides this decrease, or even the disappearance of the hysteresis in some cases, was the decrease in formation of composite layers on the oxide target because of the rarefaction of gas during the time interval in which the pulse is switched on [9]. In addition, even though the oxygen is quite reactive, the oxidation reaction decreases during pulse time off [8], and finally, the target erosion rate ends up being higher due to the higher voltage values at which the HiPIMS discharge reaches [4].

From Fig. 2, referring to the deposition of doped films, we can observe that it was not possible to separate the transition points between the modes of metallic operation and oxide. In addition, there is no significant variation between insertion or removal of the gas flow, regardless of whether the discharge is DCMS or HiPIMS, characterizing a hysteresis-free discharge. Nitrogen insertion is an alternative to decrease hysteresis known in the literature [4], however, the insertion of more reactive gas in the chamber favour the appearance of the cathodic arc discharge regime, and for this reason, it was not possible to make the study with the flow above 2.4 sccm for the HiPIMS operating regime.

In general, the rate of sputtering is reduced when there is poisoning, since in addition to the normal target erosion process, there was chemisorption or even implantation of particles in the target. The deposition rate for TiO_2 films was 1.5 nm/min in DCMS mode and 0.5 nm/min in HiPIMS mode. For N-TiO_2 films in DCMS mode the rate was 3.0 nm/min and 1.5 nm/min for HiPIMS. The major difference between the two modes of operation of the discharge, DCMS and HiPIMS, was that the HiPIMS plasma presents secondary electron emission values much higher than DCMS, such that it was the mechanism for its energy supply [9]. However, the emission of secondary electrons is dynamic during this kind of discharge, since the composition and the intensity of the ion flow vary during the pulse [1], [10]. Due to the characteristics of the HiPIMS discharge, in addition to noble gas ions reacting by to remove atoms from the target, the reactive gas and the target atoms can also be ionized and act in the process etching the deposited film in the substrate, consequently reducing the rate of deposition, a process known in the literature as self-sputtering.

4. References

[1] A. Anders, “Tutorial: Reactive high power impulse magnetron sputtering (R-HiPIMS),” *J. Appl. Phys.*, vol. 121, no. 17, p. 171101, May 2017.

[2] D. Depla and R. De Gryse, “Target poisoning during reactive magnetron sputtering : Part I : the influence of ion implantation,” *Surf. Coat. Technol.*, vol. 281, 2003.

[3] S. Berg and T. Nyberg, “Fundamental understanding and modeling of reactive sputtering processes,” *Thin Solid Films*, vol. 476, no. 2, pp. 215–230, Apr. 2005.

[4] M. Aiempanakit, T. Kubart, P. Larsson, K. Sarakinos, J. Jensen, and U. Helmersson, “Hysteresis and process stability in reactive high power impulse magnetron sputtering of metal oxides,” *Thin Solid Films*, vol. 519, no. 22, pp. 7779–7784, 2011.

[5] C. Stegemann, R. S. Moraes, D. A. Duarte, and M. Massi, “Thermal annealing effect on nitrogen-doped TiO2 thin films grown by high power impulse magnetron sputtering plasma power source,” *Thin Solid Films*, vol. 625, pp. 49–55, Mar. 2017.

[6] D. A. Duarte, M. Massi, and A. S. da S. Sobrinho, “Development of Dye-Sensitized Solar Cells with Sputtered N-Doped TiO2 Thin Films: From Modeling the Growth Mechanism of the Films to Fabrication of the Solar Cells,” *Int. J. Photoenergy*, vol. 2014, pp. 1–13, 2014.

[7] A. Anders, “High power impulse magnetron sputtering and related discharges: Scalable plasma sources for plasma-based ion implantation and deposition,” *Surf. Coatings Technol.*, vol. 204, no. 18–19, pp. 2864–2868, Jun. 2010.

[8] E. Wallin and U. Helmersson, “Hysteresis-free reactive high power impulse magnetron sputtering,” *Thin Solid Films*, vol. 516, no. 18, pp. 6398–6401, Jul. 2008.

[9] A. Anders, “Discharge physics of high power impulse magnetron sputtering,” *Surf. Coatings Technol.*, vol. 205, no. SUPPL. 2, pp. S1–S9, 2011.

[10] D. Depla, X. Y. Li, S. Mahieu, and R. De Gryse, “Determination of the effective electron emission yields of compound materials,” *J. Phys. D. Appl. Phys.*, vol. 41, no. 20, p. 202003, Oct. 2008.

Acknowledgments

The authors thank the financial support of FAPESP (Grant 2011/50773-0), CNPq (Grant 555.686/2010-8) and CAPES (Grant 88881.122156/2016-01).

*Corresponding author: cristianestegemann@yahoo.com.br

CHARACTERIZATION OF ITON THIN FILMS GROWN BY EVAPORATION AND PECVD

M Sparvoli [1]*, V Pederzini [1], R K Onmori [2], I Y Abe [2] and A T Lopes [2]
[1]*Universidade Federal do ABC, Centro de Matemática, Computação e Cognição, Santo André, São Paulo, Brasil, marinsparvoli@yahoo.com.br*
[2]*Universidade de São Paulo, São Paulo, Brasil*

1. Introduction

Indium Tin Oxide (ITO) is a degenerate semiconductor material with high band gap, transparent in the visible range of the solar spectrum and belonging to transparent conductive oxide (TCO) class. Because its properties, this thin film is used as transparent electrode in a wide variety of applications. This material is an n-type semiconductor and its high conductivity is due to both oxygen vacancies and tin, which acts as donor. Moreover, due to its wide band gap, 3.5 – 4.0 eV, it exhibits high optical transmittance [1-4]. Recently it was obtained a new oxide type that combines ITO and nitrogen: the indium-tin-oxynitride (ITON). The incorporation of nitrogen into the film could improve further the optical and structural properties of the ITON films and thus making ITON film an ideal transparent and conducting material for opto-electronic applications.

2. Experimental

Deposition of oxide and oxynitride thin films is generally performed in plasma-containing systems like sputtering and pulsed-laser deposition systems. In this work, ITO films were fabricated by evaporation and nitrogen was incorporated by PECVD (plasma-enhanced chemical vapor deposition) technique at temperature range of 140 - 320 °C, forming ITON films. The substrate was p-type silicon wafer with 0.5 mm thickness.

3. Results and Discussions

Transparent and uniform ITON films with fine grain size in the range of 50 to 200 nm have been fabricated using the evaporation method.

The spectral response, quantum efficiency and responsivity were estimated for samples annealed with four different temperatures in PECVD process. By studying these electrical properties is possible to reach conclusions about the application of these materials in sensors in the infrared region as well as solar cells. Quantum efficiency describes the response of the sensor to different wavelengths of the electromagnetic spectrum.

The ITO as evaporated is opaque and with a brown color because it probably presents vacancies where lacked oxygen. When the material has undergone the annealing process with nitrogen or oxygen, these elements were incorporated, modifying their characteristics.

4. References

[1] H. Stroescu, M. Anastasescu, S. Preda. Thin Solid Film, unpublished.
[2] E.Aperathitis, M. Modreanu, M.Bender, V.Cimalla, G.Ecke, M. Androulidaki, N.Pelekanos, "Optical characterization of indium-tin-oxynitride fabricated by RF-sputtering", Thin Solid Films, v. 450, p. 101–104, 2004.
[3] M. Himmerlich, M. Koufaki, Ch. Mauder, G. Ecke, V. Cimalla, J. A. Schaefer, "Surface composition and electronic properties of indium tin oxide and oxynitride films", Surface Science, v. 601, p. 4082–4086, 2007.
[4] E. Aperathitis, M. Bender, V. Cimalla, G. Ecke, M. Modreanu, "Properties of rf-sputtered indium–tin-oxynitride thin films", Journal of applied physics, p. 1258-1266, 2003.

Acknowledgments

The authors would like to thank to the Laboratório de Sistemas Integráveis da Universidade de São Paulo by measurements, to Mr. Adir J. Moreira for technical support, Fapesp and CNPq for financial support.

*Corresponding author: marinsparvoli@yahoo.com.br

BARRIER PROPERTIES OF HIGH PERFORMANCE PMMA-SILICA PROTECTIVE COATINGS

Andressa Trentin[1], Andressa de L. Gasparini[1], Flávio A. Faria[1], Samarah V. Harb[1], Fábio C. dos Santos[1], Celso V. Santilli[1], Peter Hammer[1*]

[1]*São Paulo State University (Unesp), Institute of Chemistry, 14800-060, Araraquara-SP, Brazil*

1. Introduction

Organic-inorganic hybrids, applied as anticorrosive coatings on carbon steel, have been prepared by the sol-gel process from the radical polymerization of methyl methacrylate (MMA) and 3-(trimethoxysilyl) propyl methacrylate (MPTS), using the thermal initiator benzoyl peroxide (BPO), followed by the hydrolytic condensation of tetraethoxysilane (TEOS) and MPTS.

2. Experimental

To investigate the influence of the synthesis conditions on the structural properties, the PMMA-silica hybrids have been prepared at different synthesis temperatures of the organic precursor (80 - 100 °C) and by varying the BPO to MMA molar ratio (0.01 – 0.1). The structural characteristics of less than 10 μm thick coatings, deposited on carbon steel by dip-coating were correlated with their anticorrosive barrier properties, studied by electrochemical impedance spectroscopy.

3. Results and Discussions

Raman and X-ray photoelectron spectroscopy results showed that a higher quantity of BPO increases the polymerization degree of the organic phase, while the structural effect of the synthesis temperature is less pronounced. At optimized preparation conditions (80 °C, BPO/MMA = 0.05) the hybrid coatings presented significantly improved thermal stability, with an increment of 40 °C determined by thermogravimetric analysis, and an excellent anticorrosive performance of 20 GΩ cm^2 in a saline medium (3.5% NaCl), remaining essentially unchanged after more than 20 months of immersion. The long durability has been related to synergism between the both phases forming a dense capacitive diffusion barrier. A binary dielectric layer approach based on the Young model [1,2], describing a slowly propagating water uptake zone and an unaffected adjacent inner layer, has been applied to explain the impedance profiles recorded during long-term exposure of the coatings.

References

[1] L. Young, Academic Press, New York, 1961.

[2] A.S. Nguyen, M. Musiani, M.E. Orazem, N. Pébère, B. Tribollet, V. Vivier, Electrochim. Acta 179 (2015) 452-459.

* Corresponding author: peter.hammer@unesp.br

AUTOMATED CRYSTALLOGRAPHIC ORIENTATION MAPPING OF TI-NB COATINGS SPUTTER-DEPOSITED ON AISI 316L STAINLESS STEEL

E.D. Gonzalez[1], A.L. Gobbi[2], C.R.M. Afonso[1,3] and P.A.P. Nascente[1,3*]

[1]*Federal University of São Carlos, Graduation Program in Materials Science and Engineering, 13565-905, São Carlos, SP, Brazil.*

[2]*Brazilian Center for Research in Energy and Materials, Brazilian Nanotechnology National Laboratory, 13083-970, Campinas, SP, Brazil.*

[3]*Federal University of São Carlos, Department Materials Engineering, 13565-905, São Carlos, SP, Brazil.*

1. Introduction

AISI stainless steel (SS) and Co alloys are employed for manufacturing orthopedic implants due to their reasonably adequate bulk properties. Commercially pure (CP) Ti and its alloys have better biocompatibility and corrosion resistance, but are also considerably more expensive, than SS and Co alloys [1]. During the processing of the Ti-based alloys, α'-Ti (hexagonal close packed – HCP), α"-Ti (orthorrombic), and β-Ti (body-centered cubic – BCC) metastable phases may be formed, and these phases have characteristics that approximate the conditions of the human bone, such as a low elastic modulus. Adding Nb to Ti causes a decrease in the elastic modulus, and Nb has been found to be a non-allergenic and non-toxic alloying element [2].

An interesting option to overcome the costly use of bulk Ti-Nb alloy would be to coat an implant with a Ti-Nb thin film having adequate composition and thickness so that the coating would enhance the implant material biocompatibility. Our group has proposed the use of Ti-Nb-Zr [3, 4] and Ti-Nb [5, 6] alloy thin films deposited by magnetron sputtering as surface coatings for SS. In this work, Ti-Nb coatings were deposited on AISI 316L SS by magnetron sputtering and then were characterized by scanning and transmission electron microscopy (STEM) coupled with energy-dispersive X-ray spectroscopy (EDS) and transmission electron microscopy (TEM) coupled with automatic crystal orientation mapping (ACOM).

2. Experimental

The Ti-Nb coatings were deposited on SS substrates by co-sputtering pure Ti and Nb targets. The magnetron sputtering system was an AJA Orion 8 Phase II J, and the deposition conditions were: base pressure of 1.0×10^{-5} Pa, working pressure of .67 Pa, argon flux of 20 sccm, cathode power of 30 W, substrate bias voltage of 30 V, and substrate temperature of 200°C. The substrates were cut in the form of 15 mm diameter disks from an AISI 316L SS sheet (1 mm thick) with composition (in wt%) of 0.022 C, 0.53 Si, 0.93 Mn, 0.024 P, 0.0042 S, 16.5 Cr, 9.53 Ni, 1.945 Mo, 0.2935 Cu, and 71.95 Fe. The targets were Ti and Nb disks (50.8 mm diameter and 3 mm thick) with a purity of 99.95 %. The target-sample distance was 20 cm. It was applied a DC power of 300 W to the Ti target, and power values of 70,80,100, and 140 W to the Nb target for producing coatings of four compositions: $Ti_{85}Nb_{15}$ (Ti-26 wt% Nb), $Ti_{80}Nb_{20}$ (Ti-33 wt% Nb), $Ti_{70}Nb_{30}$ (Ti-40 wt% Nb), and $Ti_{60}Nb_{40}$ (Ti-56 wt% Nb), respectively. The thicknesses for all coatings was estimated to be approximately 0.8 μm.

TEM and STEM analyses were carried out using a FEI Tecnai G^2 F20 200 kV microscope equipped with a field emission gun (FEG) and an EDS EDAX spectrometer. The samples were prepared by focused ion beam (FIB) using a FEI Helios NanoLab dual beam microscope. Crystallographic analyses were carried out with an acceleration voltage of 200 kV using an ASTA™ NanoMegas system; two TEM instruments were employed: the aforementioned FEI Tecnai G^2 F20 200 kV microscope (LaB_6) and a JEOL JEM 2100F microscope. The ACOM step size was 5 nm based on a rectangular grid (600×400 pixels) [7].

3. Results and Discussions

Fig. 1 displays the chemical mappings obtained by STEM-EDS showing a homogeneous distribution of Ti and Nb confirming the formation of a solid solution corresponding to the β-Ti (BCC) phase [5]. Figs. 2-4 display the crystallographic orientation mappings for the coatings showing the textures for the different *x*, *y*, and *z* axes. The *y*-axis corresponds to the film growth direction. The increase in the Nb content caused changes in the film texture. For 15 at% Nb, the growth mode corresponded to the zone I of the structure zone diagram (SZD) [8], with high rate of grain nucleation in the direction of the plasma flux and the formation of columnar structures with marked texture of {113} for the *x*-axis, {110} for the *y*-axis, and {111} for the *z*-axis. With the increase in the N amount (20 and 30 at% Nb), there was a change in the texture: {110} for the *x*-axis, {113} for the *y*-axis, and {110} for the *z*-axis, yielding a characteristic morphology of the zone II of the SZD, with larger grain sizes and columnar growth. For higher Nb amount (40 at% Nb), a competitive growth mechanism might occur: aleatory grains grow since the start of the process, but at some time latter

*Corresponding author:nascente@ufscar.br

this aleatory grain growth is suppressed by the formation of energetically more stable grains with the following orientations: {110 for the *x*-axis, mainly {111} and {113} for the *y*-axis, and {110} for the *z*-axis. This film growth can be attributed to a transition zone between zone II and zone III of the SZD.

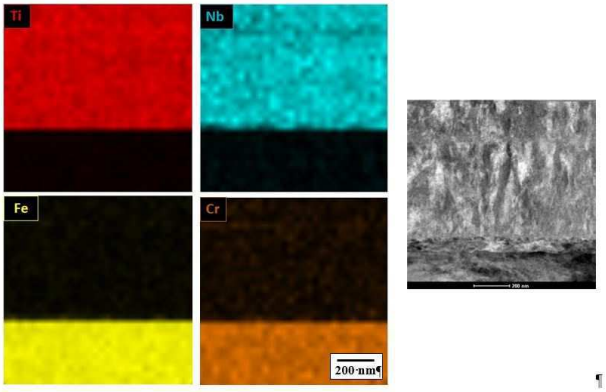

Fig. 1. *X-ray elemental mapping obtained by STEM-EDS for the $Ti_{85}Nb_{15}$ coating.*

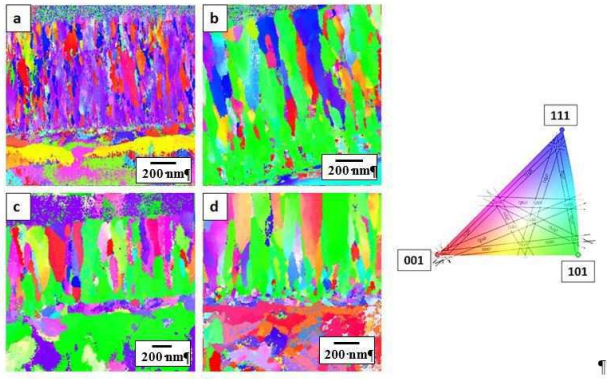

Fig. 2. *Crystallographic orientation mapping obtained by ACOM for the x-axis: (a) $Ti_{85}Nb_{15}$, (b) $Ti_{80}Nb_{20}$, (c) $Ti_{70}Nb_{30}$, and (d) $Ti_{60}Nb_{40}$.*

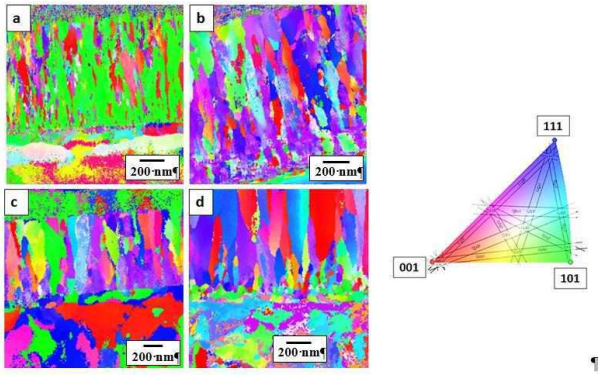

Fig. 3. *Crystallographic orientation mapping obtained by ACOM for the y-axis: (a) $Ti_{85}Nb_{15}$, (b) $Ti_{80}Nb_{20}$, (c) $Ti_{70}Nb_{30}$, and (d) $Ti_{60}Nb_{40}$.*

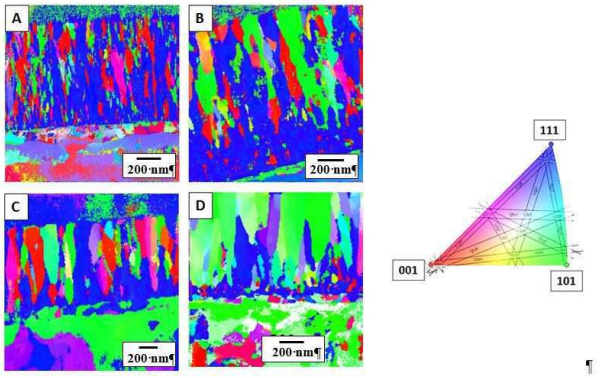

Fig. 4. *Crystallographic orientation mapping obtained by ACOM for the z-axis: (a) $Ti_{85}Nb_{15}$, (b) $Ti_{80}Nb_{20}$, (c) $Ti_{70}Nb_{30}$, and (d) $Ti_{60}Nb_{40}$.*

4. References

[1] B.D. Ratner, A.S. Hoffman, F.J. Schoen, J.E. Lemons (Editors), Biomaterials Science – An Introduction to Materials in Medicine, Third Edition, Academic Press, Oxford, 2012.
[2] M. Niinomi, Mater. Trans. 49 (2008) 2170-2178.
[3] D.A. Tallarico *et al.*, J. Vac. Sci. Technol. A 30 (2012) 051505.
[4] D.A. Tallarico *et al.*, Mater. Sci. Eng. C 43 (2014) 45-49.
[5] E.D. Gonzalez *et al.*, J. Vac. Sci. Technol. A 34 (2016) 021511.
[6] E.D. Gonzalez *et al.*, Sur. Coat. Technol. 326 (2017) 424-428.
[7] C.R.M. Afonso *et al.*, Sci. Rep. 7 (2017) 13618.
[8] A. Anders, Thin Solid Films 518 (2010) 4087-4090.

Acknowledgments

Part of the TEM-ACOM analysis was performed at the SME (Electron Microscopy Service) of the Universitat Politecnica de Valencia, Spain, with financial support of FAPESP-BPE (grant 2015/19978-6). This work was supported by CNPq (processes 30455/2013-4 and 302450/2017-2), CAPES (fellowship for E.D.G.), FAPESP (process 2017/25983-8), LNNano-CNPEM/MCTIC (proposals LMF-19204, LMF-20579, LMF-21683, and DualBeam-21800). The authors thank the Laboratory of Structural Characterization (LCE/DEMa/UFSCar) for the use of electron microscopes (TEM and STEM).

*Corresponding author:nascente@ufscar.br

EFFECT OF PLASMA PARAMETERS ON CARBON NANOTUBE FUNCTIONALIZATION BY MALEIC ANHYDRIDE

Teresa Tromm Steffen[1]* and Luis César Fontana[2] and Daniela Becker[3]
[1,2,3]*Center for Technological Sciences, UDESC, Joinville, Santa Catarina, Brazil*

1. Introduction

Carbon nanotubes (CNT) have been functionalized by plasma in order to prevent agglomerate and improve their bonding with polymeric matrices in nanocomposite's synthesis [1]. A monomer that can be used as an activating on nanotube wall is maleic anhydride (MA), which can provide both functional groups, like carboxyl, and the anhydride group itself to be attached to nanotubes walls and tips [2]. In this paper, CNT and MA in solid form were premixed by two different ways before the plasma treatment. So the aim of this work is to analyze the effect of both premix and plasma parameters on CNT functionalization.

2. Experimental

Multi-walled carbon nanotubes used in this work were purchased from Chengdu Organic Chemicals Co. Ltd (TNIM4), with purity higher than 95%, an external diameter range of 10-30 nm. Maleic anhydride, with purity higher than 98,5%, were purchased from Sigma-Aldrich. CNT and MA were mixture by two methods. The first one took place in a planetary mill by 10 minutes at 300 rpm. The second one was manually made with mortar and pestle assistance. Both the mixture were done with 90:10 (CNT:AM) mass proportion. After that, the samples were positioned in the way to occupy all the cylindrical volume of 1.5 cm length in the reactor tube. The samples were treated through inductively coupled radio frequency plasma (RF) (Fig. 1) at 35 W power input, 1 Torr gas pressure, by 15, 30 and 60 minutes, with and without nitrogen (1.2 sccm) in the working gas. Argon flow was utilized to clean the reactor volume by 15 minutes before the plasma discharge. Argon (11.0 sccm) and nitrogen (1.2 sccm) and pure argon (12.2 sccm) were utilized as working gas in the plasma. Samples treated were washed three times with methanol before characterization. Table 1 shows the experimental layout used in this paper.

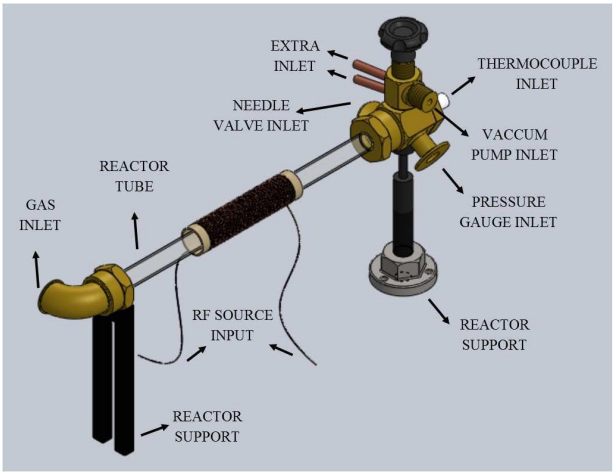

Fig. 1. *Schematic representation of RF plasma reactor used to functionalize the CNT.*

Table 1. *Samples conditions.*

SAMPLE	Moisture	Time	N_2 gas
CNT/pristine	-	-	-
CNT.p.15	planetary mill	15 min	no
CNT.p.30		30 min	no
CNT.p.60		60 min	no
CNT.p.15.N		15 min	yes
CNT.p.30.N		30 min	yes
CNT.p.60.N		60 min	yes
CNT.15	mortar	15 min	no
CNT.30		30 min	no
CNT.60		60 min	no
CNT.15.N		15 min	yes
CNT.30.N		30 min	yes
CNT.60.N		60 min	yes

3. Results and Discussions

FTIR spectra for CNT/pristine and all samples treated in RF plasma are shown in Fig. 2. It is observed that the treated samples shows new peaks referent to C=O vibration mode of carboxyl groups at 1740 cm^{-1}, 1725 cm^{-1} and 1704 cm^{-1}, indicating the ring opening of maleic anhydride and CNT functionalization [3,4]. Raman results (Fig. 3) shows that there is no significant difference on I_D/I_G ratio between the samples, which indicates that there is no high damage on CNT walls by plasma reactive species. Nevertheless, the TEM image in Fig. 4 shows an amorphous region, indicated by the arrow, which could be associated with defects produced on CNT walls by plasma treatment [3]. Fig. 5 show XPS measurements of oxygen (atomic percent) on CNT, for CNT/pristine (2.4 ± 0.1) and for all the other samples. For samples mixed in the planetary mill, the atomic percent of oxygen inserted on CNT was lower than for those samples mixed in the mortar. It indicates that the hand mortar method can be a better premix. Regarding to the nitrogen, when this gas is utilized in the plasma treatment, it is observed a decreasing in the oxygen content

*Corresponding author: teretromm@hotmail.com

inserted on CNT, which is in accordance to the fact that the nitrogen may cold the plasma, therefore it reduces the plasma reactivity [3]. About the treatment time, 30 minutes is a good option for samples mixed at the mortar, once, after that, the plasma seems to starts to remove the oxygen already inserted, by means of chemical attack [5]. Besides the differences noticed, the increasing in oxygen on the CNTs is not so high, which leads to believe that the plasma produced through inductively coupled radio frequency into a CNT volume is not strong sufficiently to produces significant changes on the CNTs walls.

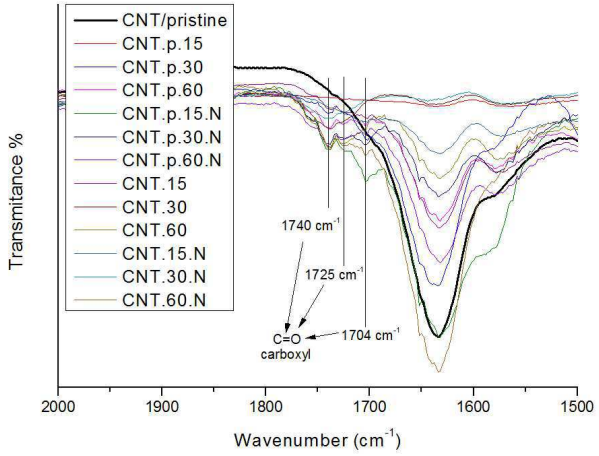

Fig. 2. *FTIR spectra showing new peaks at 1740, 1725 and 1704 cm^{-1}, related to C=O vibration mode of carboxyl groups.*

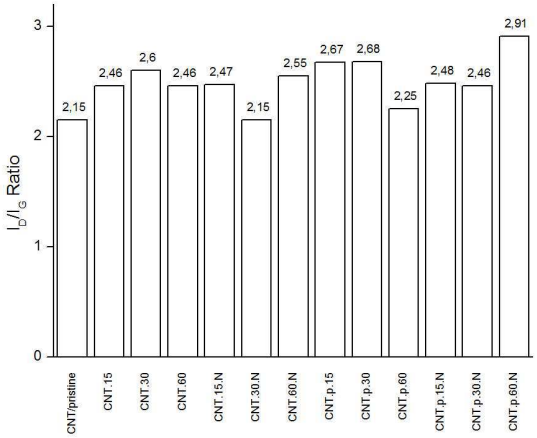

Fig. 3. *Raman I_D/I_G showing that there is no significant difference in defect increase after plasma treatment.*

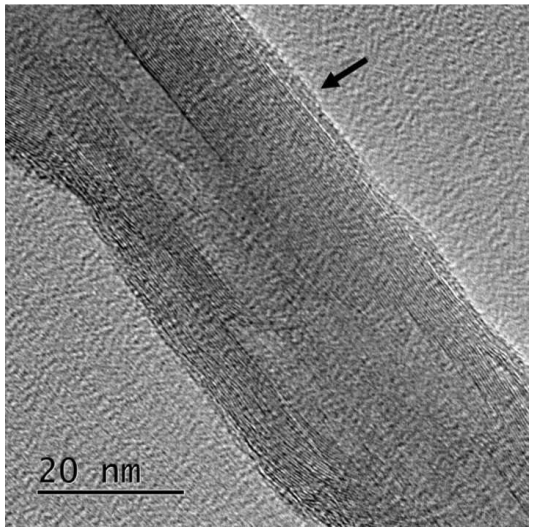

Fig. 4 *TEM image of CNT.15 sample showing a layer that could be an amorphous region associated to defects caused by plasma treatment.*

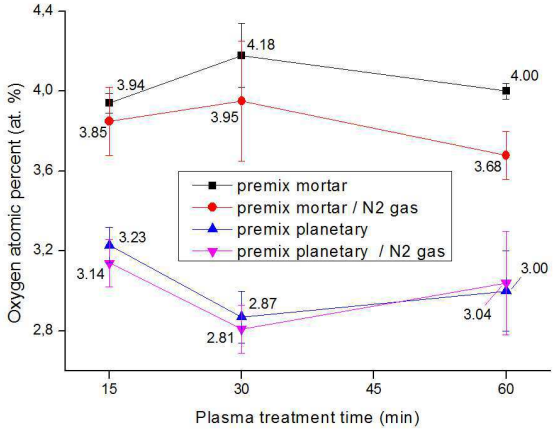

Fig. 5 *Oxygen atomic percent, obtained by XPS, for different premix samples treated by plasma with and without nitrogen.*

4. References

[1] C. Saka, Analytical Chemistry, (2017). doi 10.1080/10408347.2017.1356699
[2] Y. Lu, H. Li, H. Liu, Phys E, **43**, 510-514, (2010).
[3] T. T. Steffen, L. C. Fontana, J. Nahorny, D. Becker, Polim. Compos, doi 10.1002/pc (2018).
[4] G. Mishra, S. L. McArthur, Langmuir, **26**, 9654-9658, (2010).
[5] C. A. Ávila-Orta, P. González-Moronez. S. Suzuki, Eds. IntechOPen, Rijeka, 167–192 (2013).

Acknowledgments

The authors would like to thank the financial resources provided by CAPES by means of scholarships and CNPq by project Universal/445242/2014-0. Also thank to Claudia Correia from Univille, and Dr. Evaldo José Corat from INPE, by collaboration in samples characterizations.

*Corresponding author: teretromm@hotmail.com

MAGNETIC PROPERTIES OF Gd/GdN SUPERLATTICES

Francisco Alfaro*, Julio César Sagás and Luís César Fontana
Laboratory of Plasmas, Films and Surfaces, Santa Catarina State University (UDESC), Joinville -SC

1. Introduction

Multiphase materials can be designed to have very wide isothermal magnetic entropy change (ΔS) peaks by combining materials with different critical temperatures [1]. Gd is a standard material to study magnetic entropy changes. On the other hand, the Curie temperature of GdN can change from 70 K to 200 K depending on the nitrogen deficiency [2]. So that, it may be expected that Gd/GdN superlattices present a ΔS broadening. The present work reports the deposition of different Gd/GdN superlattices by DC grid-assisted magnetron sputtering. Sample magnetization was measured to investigate the role of GdN layers in the ΔS.

2. Experimental

Gd/GdN superlattices were grown on Si (111) p-type substrates by DC grid-assisted magnetron sputtering with constant current (0.40 A) and working gas pressure (~0.40 Pa). No external heating was used. For multilayer deposition, the N_2 flow was switched, while the Ar flow was maintained constant. Total film thickness is around 200 nm. Three samples with different multilayer structure were deposited: $[Gd(20nm)/GdN(20nm)]_4$, $[GdN(10nm)/Gd(10nm)]_8$ and $[GdN(5nm)/Gd(5nm)]_{16}$. For comparison, a pure Gd film was also deposited. The samples were analyzed by X-ray diffraction (XRD), X-ray photoelectron spectroscopy (XPS) and a physical property measurement system (PPMS) for magnetization measurements as a function of temperature in constant magnetic fields.

3. Results and Discussions

The chemical composition of $[Gd(20nm)/GdN(20nm)]_4$ along film thickness is shown in Fig. 1. Four layers of GdN are well defined. In the regions with the highest N concentration (~ 45% at.), the Gd/N ratio is close to 1. From magnetization curves, the isothermal magnetic entropy change (ΔS) was obtained using Maxwell Relations. Figure 2 shows ΔS for ΔH = 5T. The Gd film presents its characteristic behavior with a maximum around 270 K. The other samples show broadening of this ΔS peak, with samples $[Gd(20nm)/GdN(20nm)]_4$ and $[Gd(10nm)/GdN(10nm)]_8$ showing also a pronounced peak around 70K i.e. around the GdN Curie temperature.

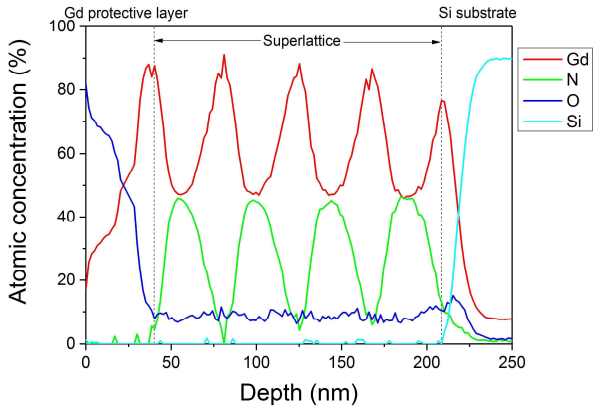

Fig. 1. *Atomic concentration of Gd, N, O and Si along the depth of the film relative to $Gd(20nm)/GdN(20nm)]_4$.*

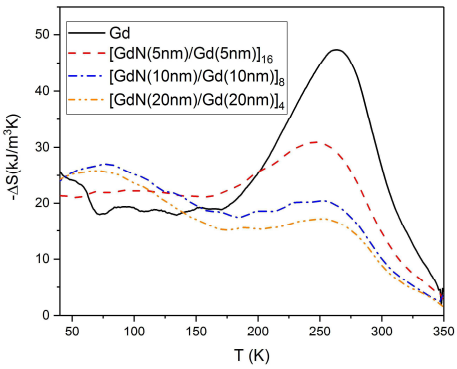

Fig. 2. *The isothermal magnetic entropy change per volume for ΔH = 5 T.*

The Gd/GdN films present a broader ΔS peak around 250-270 K when compared to Gd film. The GdN layers generate a second ΔS peak around 70 K, showing that its origin is the paramagnetic-ferromagnetic transition of GdN. Thus, multilayered structures of Gd/GdN broadens the temperature range of high ΔS.

4. References

[1] C. W. Miller, D. D. Belyea, and B. J. Kirby, J. Vac. Sci. Technol. A, **32**, 040802, 2014.
[2] B. J. Ruck *et al.*, Physica B: Condensed Matter, **407**, 2954-2956, 2012.

Acknowledgments

The authors thank LabCAM of UFSC and PAP-FAPESC. This project has been funded by the National Council for Scientific and Technological Development (UNIVERSAL/CNPq 455896/2014-3).

*Corresponding author: francisco@alfaro.com.br

SYNTHESIS AND CHARACTERIZATION OF NICKEL/ALUMINA CATALYTIC MONOLITH

Maíra O. Palm[1], Mauro E. S. Júnior[2], Leonardo Cardoso[1], Diego A. Duarte[1], Rafael de C. Catapan[1]*
[1]*Technological Center of Joinville, Federal University of Santa Catarina, Joinville, Brazi.l*
[2] *Chemical Engineering Department, University of Joinville Region, Joinville, Brazil.*

1. Introduction

Supported catalysts are largely used for synthesis synthesis of chemicals in flow reactors. The support aims at improving the dispersion of the catalyst and prevent aggregation [1]. Alumina (Al_2O_3) is usually used as support because of its thermal stability at high temperatures, good interaction with the metal and low cost [2-3]. Different metals can be used as the active phase of the catalyst. Nickel is widely used as active phase because of its low cost and high availability [3]. A coating layer on the support has the purpose of increasing the surface area and improving the dispersion of the active phase of the catalyst [2]. Since these characteristics are fundamental to obtain an optimized monolith and promote high H_2 production. The objective of this work was to investigate the production of a catalytic monolith of Ni supported over Al_2O_3, with coating layer, for application in H_2 production from ethanol. Scanning electron spectroscopy (SEM), energy dispersive spectroscopy (EDS) and X-ray photoelectron spectroscopy (XPS) techniques were used to analyze the characteristics of the coating layer, the homogeneity of the metal dispersion and interaction with the support.

2. Experimental

Commercial foams of Al_2O_3 (supplied by Goodfellow), with 26 pores/cm, 12.7 mm thick and 15 mm in diameter, were used as support for the monolith. In the coating step the foam was immersed for 1min in a slurry with Al_2O_3 particles. Then, it was dried at 110 ^oC for 1h30min and calcined at 600 ^oC for 2hr. The slurry was composed by 2 µm alumina (supplied by Almatis), sodium silicate (1%), nitric acid (1%) and distilled water. The pH of the slurry was controlled between 4 and 4.5 due to it influences the viscosity, hence the thickness of the coating [2]. Slurries with mass concentrations of 30 and 40 % alumina were prepared. Nickel (Ni) was impregnated using an aqueous solution of $Ni(NO_2)_3.6H_2O$. Monoliths were dried at 150 ºC overnight under 50 cm^3/min of air flow and then calcinated at 600 ºC under air during 2 h. Monoliths were characterized using SEM, EDS and XPS.

3. Results and Discussions

Figure 1 shows the coating thicknesses according to the production conditions. The thickness was measured in pores near the edge of the foam (external pores) and in the center of the foam (internal pores). It was noted that the foam immersed once in the 40% slurry obtained similar thicknesses of foam immersed 3 times in the 30% slurry. The followed tests were using 1 immersion in the 40% slurry.

Figure 2 presents SEM images of the foam immersed once in the 40% slurry with magnification of 2,500x. Figure 2-a shows the coating thickness obtained in external pores, which were between 10 and 12 µm. Figure 2-b shows the coating thickness obtained in internal pores, which were approximately 4 µm. Coating layers greater than 50 µm provide internal diffusion limitations [4]. The coating layer obtained with 1 immersion in the 40% slurry, besides not providing control by internal diffusion, did not show regions without coating.

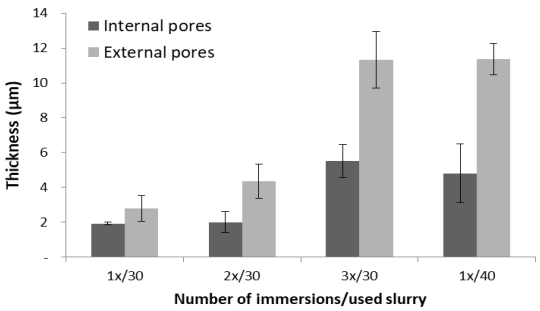

Fig. 1. *Coating thicknesses according to the methodology used.*

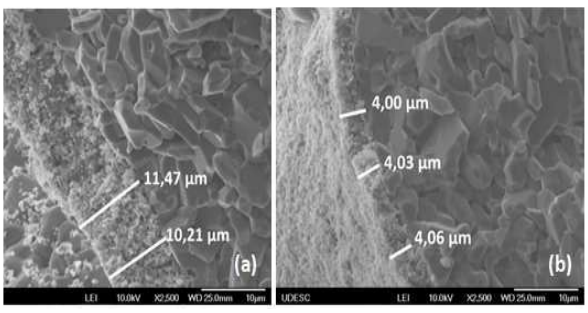

Fig. 2. *SEM showing the thickness of foam coating: a) external pores; b) internal pores.*

Ni particles were impregnated onto support after production of the coating layer. The content of the adhered metal was 7.33% by mass. Figure 3 shows SEM images of produced monolith from Ni impregnation in coated foam, with magnification of 50,000x. It is observed that Ni particles, with approximately 50nm diameter, are dispersed on the alumina particles, with approximately 0.5 µm diameter. Figure 4 shows SEM

*Corresponding author: rafael.catapan@ufsc.br

and EDS analysis of the coated foam with Ni. Using EDS analysis the high incidence of Ni particles in the analyzed region could be verified.

Figure 5-a shows the spectrum of the Al2p orbital of the coated Al_2O_3 foam without Ni. It is observed a deconvoluted peak in 74.48 eV, referring to the aluminum connected in the oxygen present in the Al_2O_3 structure [5]. Figure 5-b shows the spectrum of the Al_2O_3 with Ni, with a more complex profile and presence of seven peaks. The peaks with bonding energy of 66.51, 67.61 e 68.69 eV are related to the Ni3p orbital [6]. The first state represents the metallic nickel and the following two are oxidized states. The third peak may also be related to inelastic electrons of the Ni3p orbital. The metallic peak is more intense than the others, indicating that the surface is catalytically active [7].

Figure 6 shows the spectrum of the valence band for the samples with and without Ni. The results corroborate with the literature and show a reduction of the electron bonding energy in the valence band in the sample with Ni [8]. This reduction in the bonding energy in the valence band contributes to the increase of catalytic activity on the foam surface as the electrons become more accessible to participate in the catalysis.

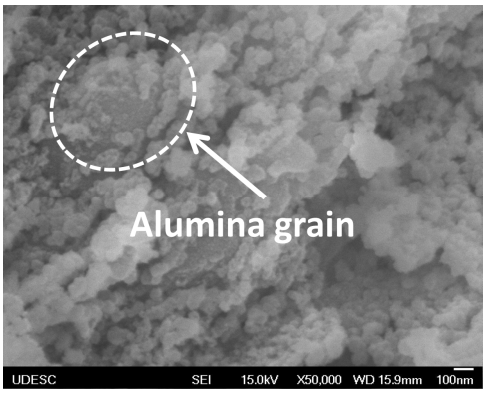

Fig. 3. *SEM showing Ni particles dispersed in alumina grain.*

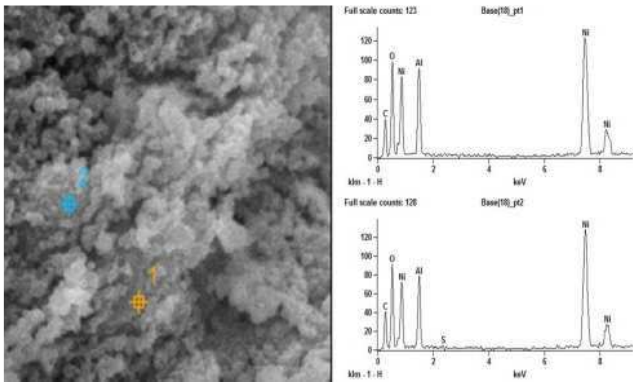

Fig. 4. *SEM with EDS showing the presence of Ni particles after impregnation process.*

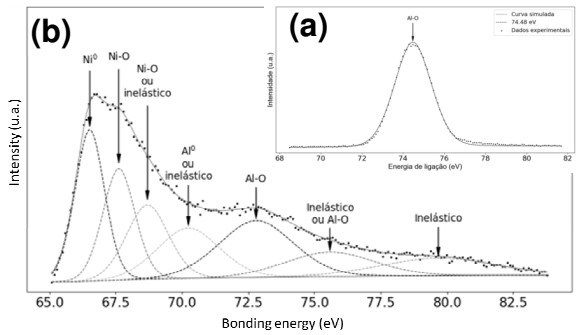

Fig. 5. *Spectrum of the Al2p orbital: a) sample without Ni; b) sample with Ni.*

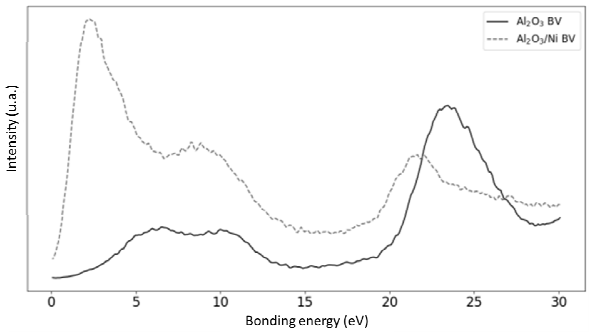

Fig. 6. *Valence band spectrum for samples with and without Ni.*

4. References

[1] D.K. Liguras; K. Goundani and X.E.Verykios, *J. of Pow. Sour.* **2004**, 130, 30-37.
[2] C. Agrafiotis; A. Tsetsekou. *J. of Mat. Sci*. **2000**, 35, 951-960.
[3] R. Faure, *et al*., *J. of Europ. Cer. Soc*. **2011**, 31, 303-312.
[4] S.Y. Joshi; M.P.Harold; V. Balakotaiah. *Chem. Eng*. Sci. **2010**, 65, 1729-1747.
[5] K. Djebaili, *et al., J. of Spec.* **2015**, 2015.
[6] T. Sarapatka. *Che. Phy. Letters.* **1993**, 212, 37-42.
[7] A. Venezia and C. Loxton. *Surf. Science.* **1988**, 194, 136-148.
[8] M. Konyushenko. *Tech. Phy.* **Letters**, 2015, 41, 922-925.

Acknowledgments

This work was funded by BMW do Brasil under project 2016/0110 UFSC.

*Corresponding author: rafael.catapan@ufsc.br

TRIGGERING VARIATIONS IN PHASE STABILITY BY TUNING THE PULSE FREQUENCY IN PULSED-DC MAGNETRON SPUTTERING OF A STAINLESS STEEL TARGET

Marcus V. F. Schroeder[1], Abel A. C. Recco[1]* and Carlos M. Garzón[2]
[1] *Santa Catarina State University – UDESC, Joinville, SC, Brazil*
[2] *National University of Colombia – UNal, Bogotá D.C., Colombia*

1. Introduction

Stainless steel (SS) protective coatings have been developed in pursuit of superior electrochemical corrosion resistance, oxidation resistance, tribological performance, and mechanical strength [1-3]. Functional coatings and interlayers of SS have been used in: biomedical materials, solar energy systems, electrical and magnetic systems, WC tribological powders, buffer layers for growth of nanotubes, amorphous FeCrNi/a-C:H coatings with self-organized nanotubular structure, and nanocomposite SS-Ag structures [3,5]. Experiments have demonstrated the role of both substrate heating and target chemical composition in phase fractions in SS sputtered coatings [5]. Predominance of BCC (body-centered cubic) and FCC (face-centered cubic) phases has been reported [3,5]. When 18-8 austenitic targets are sputtered at low substrate heating, fully BCC structures are obtained [3,5], which has been termed as a "metastable" structure due to not accounting for the austenitic structure of the target [5]. The effects of pulsed-DC sputtering on relative phase stability in metallic coatings have not been reported in the literature. In this contribution, we show that the relative phase stability between BCC and FCC structures can be varied by tuning the frequency in pulsed-DC magnetron sputtering. We also shown that, indeed, the lattice with the higher thermodynamic stability at low temperature is the BCC as opposed to the FCC (which is arbitrarily assumed as being more stable in the literature [5]). The aim of this research is to assess the effect of variations in the pulse frequency in the phase fractions in SS coatings sputtered from a 316L target. Both experimental results on phase fractions as a function of pulse frequency and theoretical thermodynamic equilibrium phase proportions as a function of temperature are reported and compared. As traditional thermodynamic equilibrium is not adequate for depicting far from equilibrium structures in metallic sputtered coatings [3], a new equilibrium with restrained atomic partition (due to kinetic constrains to atomic diffusion in magnetron sputtering) is proposed here.

2. Experimental

SS coatings were grown onto both AISI 1045 plain carbon steel and AISI 316L austenitic SS by sputtering a 316L target via pulsed-DC magnetron sputtering in an Ar atmosphere at 673 K external substrate heating. Steel's chemical composition were as follow:
1045 carbon steel (wt%): 0.04 P, 0.05 S, 0.8 Mn, 0.45 C, and balance Fe.
316 ASS (wt%): 16.9 Cr, 9.5 Ni, 1.8 Mn, 0.4 Si, 2.1 Mo, 0.03 C, and balance Fe.
For enhancing the ionization rate, a triode configuration was used, which has been presented elsewhere [6].
This contribution reports the relative BCC and FCC phase fractions as a function of the pulse frequency for samples obtained at non-pulses (conventional DC), and 50, 150, 250, and 350 kHz. Phase characterization was carried out via X-ray diffraction (XRD) in the Bragg-Brentano configuration.
The theoretical effect of temperature on the fraction of phases at the equilibrium was numerically simulated via the Calphad thermodynamic framework for the metastable equilibria where only FCC and BCC lattices were allowed in a Fe16.9Cr9.5Ni alloy (wt%) using Thermocalc® software. A detailed description of this numerical method is presented elsewhere [3,4,7]. *A posteriori*, we observed that neither equilibrium with full atomic partition between phases nor equilibrium with negligible atomic partitioning compressible depict experimental results. Thus, we proposed an unreported equilibrium where the atomic partitioning among phases is kinetically constrained, which we called equilibrium with incomplete atomic partitioning.

3. Results and Discussions

At non-pulsed (conventional DC) depositions, films were mainly composed of the BCC phase (20 % FCC + 80 % BCC). Pulsing the electrical power triggered stabilization of the FCC phase against the BCC one. Maximum FCC fraction (around 98 %) was obtained at 150 kHz. Figure 1 shows the proportion of FCC phase in the films as a function of pulse frequency.
Thermodynamic simulations showed stability of the BCC phase at low thermal energies and stabilization of the FCC phase at high thermal energies, disregarding the extend of atomic partitioning assumed in the simulation. However, equilibrium with incomplete atomic partitioning was the best suited for depicting stability of duplex BCC + FCC structures in a narrow temperature interval, which is typically reported in the literature [5].

*Corresponding author: abel.recco@udesc.br

Contrasting experimental results on the stabilization of the FCC phase in pulsed DC with theoretical stabilization of the FCC lattice when the thermal energy is increased, we suggest that adatom energy is increased in pulsed-DC in comparison to conventional DC. A maximum adatom energy is foreseen for 150 kHz pulse-frequency.

In pulsed-DC, the flux of ions towards the substrate is accompanied by an increased flux of energy, in comparison to conventional DC sputtering [8]. Although no experimental evidence has been reported in this realm, we suggest, with results in this contribution as a basis, that more energetic adatoms could be associated to pulsed-DC regarding to conventional DC sputtering. It has been shown that the higher the ion energy distribution the higher the energy transferred to film surface regions [9].

It has been reported that monomodal ion energy distribution in conventional DC is split into a bimodal energy distribution, where the fraction of ions in the new range of energies is varied as the pulse frequency is tuned [8]. This is qualitatively in accordance with peak FCC fraction observed at 150 kHz.

As a conclusion, we state that pulsed-DC sputtering can be associated to an increased proportion of the FCC phase instead of the BCC one, when compared with conventional DC sputtering. A rather agreeably correlation between increased stability of FCC phase in pulsed-DC and increased average energy of adatoms was formulated in this contribution with theoretical simulations of the effect of thermal energy on phase stability as a basis.

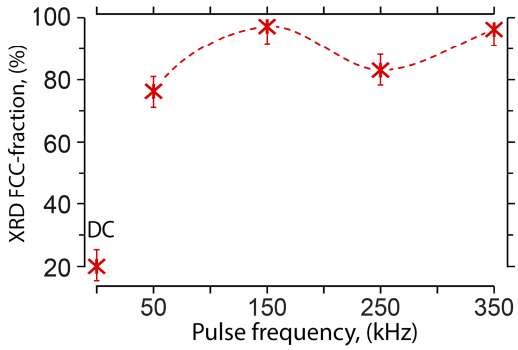

Fig. 1. *FCC phase fraction (assessed by X-ray diffraction) as a function of pulse frequency [7].*

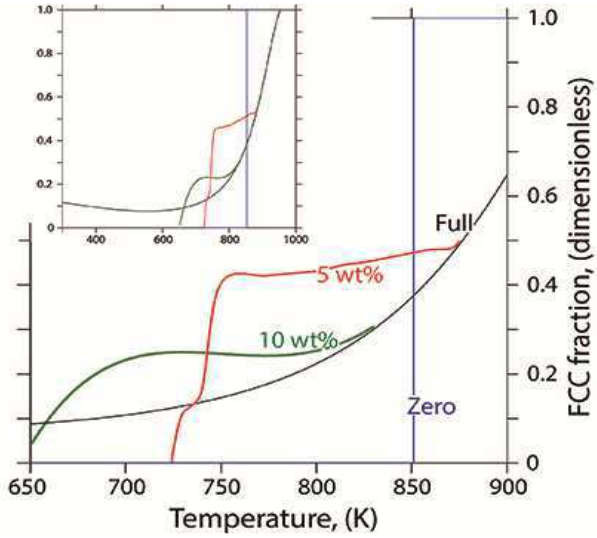

Fig. 2. *Numerical simulation on the equilibrium FCC phase fraction as a function of temperature assessed for diverse degrees of atomic partitioning among the microstructure components. 5 wt% and 10 wt%: the maximum solute depletion or enrichment allowed [7].*

4. References

[1] T. Li, L. Liu, B. Zhang, Y. Li and F. Wang, Corros. Sci., **124**, 46-55, (2017).
[2] C.G. Figueiredo and P.A. Dearnley, Surf. Eng., **28**, 683-692, (2012).
[3] C.M. Garzón and A.A.C Recco, Surf. & Coat. Tech., in press (2018).
[4] C.M. Garzón, G.A. Vergara and A.A.C. Recco, Mater. Lett. **206**, 34-38, (2017).
[5] X. Zhang, A. Misra, R.K. Schulze, C.J. Wetteland, H. Wang and M. Nastasi, J. Mater. Res. **19**, 1696-1702, (2004).
[6] L.C. Fontana and J.L.R. Muzart, Surf. Coat. Tech. **107**, 24-30, (1998).
[7] M.V.F.Schroeder, A.A.C. Recco and C.M. Garzón, Mater. Lett., **230**, 20-23, (2018).
[8] J.W. Bradley, H. Bäcker, Y. Aranda, P.J. Kelly and R.D. Arnell, Plasma Sources Sci. Technol. **11**, 165-174, (2002).
[9] H. Kersten, H. Deutsch, H. Steffen, G.M. Kroesen and R. Hippler, Vacuum **63**, 385-431, (2001).

Acknowledgments

The authors knowledge the financial and structural support provided by Santa Catarina State University (UDESC), Brazil, National University of Colombia (UNAL), Colombia, Thin Films, Surface Science, and Plasma Lab Facility (LPFS), Brazil and the Brazilian funding agency CAPES.

*Corresponding author: abel.recco@udesc.br

ALL-OPTICAL ELECTRICAL CONDUCTOR TEMPERATURE CHARACTERIZATION USING A FIBER BRAGG GRATING

Milton José Cinelli[1]*, Gabriel Bolacell[2], Stenio Aristilde[3], Cristiano M. B. Cordeiro[3] and Mauro Rosa[2]
[1]*State University of Santa Catarina (UDESC)*
[2]*Federal University of Santa Catarina (UFSC)*
[3] *State University of Campinas (Unicamp)*

1. Introduction

Fiber Bragg Grating (FBG) sensors may present different reflectivity characteristics whereas sensor sensitivity relies on germanium- or silica-doped fiber parameters as thermal expansion and thermo-optical coefficients. Conductor temperature is an important parameter to measure since it depends on many factors as Joule effect, ambient temperature, wind, radiation, and so on [1]. Furthermore, whether the conductor temperature exceeds the material maximum allowable temperature its life cycle is reduced due to early ageing and permanent elongations which may cause loss in strength. An FBG, first developed in 1978, is a periodic perturbation of the fiber core refractive index originated from launching an intense interference pattern in a photosensitivity single mode fiber core, usually doped by germanium [2]. Therefore, FBG technology has been applied as temperature and strain sensor recently in many research fields. These sensors are created based on the Bragg wavelength (λ_B) shift with temperature and strain as the effective refractive index (n_{eff}) and the grating period (Λ) are sensitive to such parameters. This relation is given by (1).

$$\lambda_B = 2 \cdot \Lambda \cdot n_{eff} \tag{1}$$

Thus, this paper aims to evaluate the conductor temperature when subjected to a constant power dissipation (P = 19.2 W) using an all-dielectrical optical fiber solution based on an FBG. The temporal evolution of temperature around the conductor and at 5mm away from it was characterized. The temperature in function of the distance from the conductor (Δh), from 3.0 to 25.0 mm, was also measured.

2. Experimental

The experimental setup includes a variable electrical current source (0 – 1000 A), an FBG with high reflectivity produced at Unicamp with a 266 nm UV laser and an appropriate phase mask, a wood rod with a slot to accommodate the FBG close to the conductor and a multimeter with a thermocouple in direct contact with the electrical cable to measure the temperature around the conductor. Fig. 1a and Fig. 1b illustrate the experimental setup in which the FBG wavelength is measured with the FS22 – BraggMeter optical interrogator. Also, it can be noted at Fig. 2 that the Bragg wavelength has the central peak at 1550.29 nm at room temperature (24 ºC).

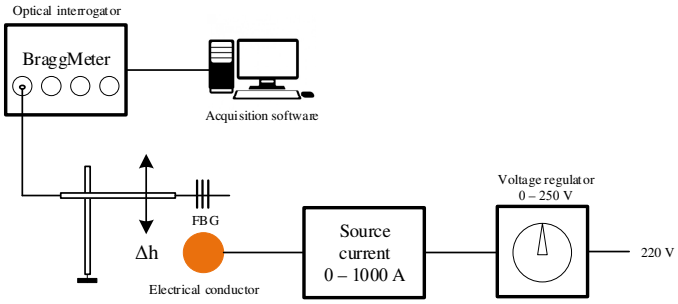

Fig. 1a. *Mounting scheme for temperature measurements of the electrical conductor.*

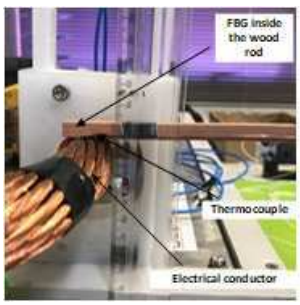

Fig. 1b. *Details of the experimental setup.*

*milton.cinelli@udesc.br

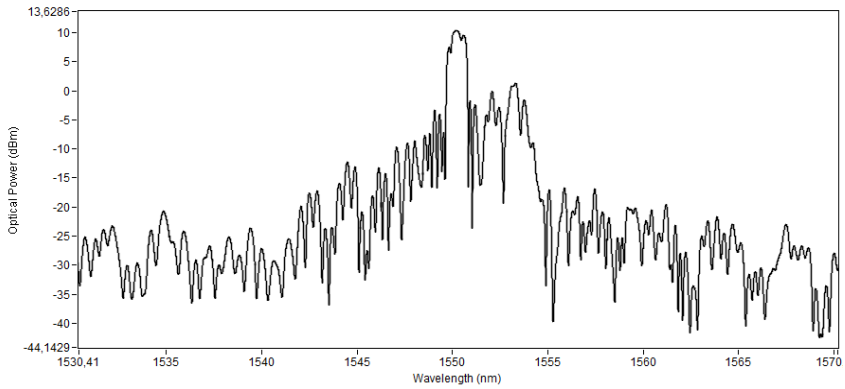

Fig. 2. *Spectral response of the high reflectivity FBG light reflection used on the experiment (logarithm scale).*

3. Results and Discussions

The FBG temperature sensor has an expected sensitivity of 12 pm/ºC and this information is used on the experiment. Some measures, exposed in Fig. 3a and Fig. 3b, were realized by varying the distance from the FBG to the conductor surface, ranging from 3.0 to 25.0 mm. It is important to highlight that on these experimental tests the electrical current carried by the conductor is equal to 800.0 amperes (starting point) and at each 1.0 minute was achieved a measure point, completing 10.0 minutes of experiment where the conductor remains increasing its temperature since the ambient temperature is constant and there is no forced cooling effect. The results, in Fig. 3a, show the temporal evolution of the FBG wavelength with the temperature measured directly over the conductor surface (circles) and 5.0 mm from it (triangles) using a standard thermocouple.

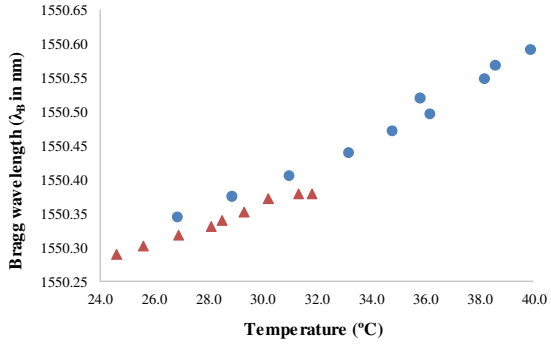

Fig. 3a. *Measurements with FBG with thermal contact with the conductor (circles) and with 5.0 mm of distance from it (triangles).*

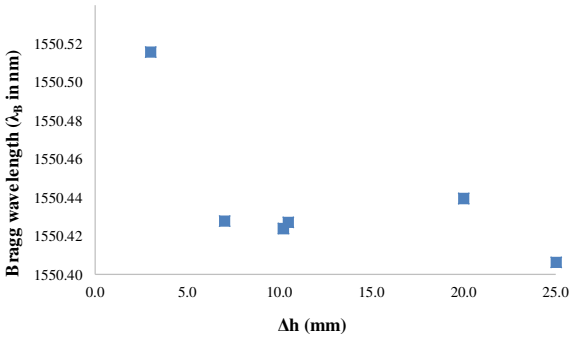

Fig. 3b. *Assessment of Bragg wavelength behavior with distance variation with constant power dissipated.*

It can be analyzed that the first experiment with the FBG with thermal contact with the conductor has a higher sensibility than the experiment with the FBG distanced from the conductor by 5.0 mm. Finally, from Fig. 3b, it is possible to identify that there is a temperature decrease relation with the distance of 0.4 ºC/mm (that can be obtained using the sensor sensitivity of 12.0 pm/ºC). Evaluating the set of results is evident that the position of the FBG impacts directly on the temperature measurement of the conductor. Clearly, even if the power dissipated (P = 19.2 W) remains the same, the act of distancing the FBG from the conductor takes the system to unreal conductor temperature measurement acquisition, jeopardizing the application. Accordingly, it can be concluded that the thermal contact of the FBG with the conductor provides much more reliable measurements and has a better sensitivity for the sensor application.

4. References

[1] F. E. Barón, G. Álvarez-Botero, F. Amortegui, D. Pastor and M. Varón. "*Temperature measurements on overhead lines using Fiber Bragg Grating sensors*", 2017 IEEE International Instrumentation and Measurement Technology Conference (I2MTC), May 2017.

[2] K. O. Hill and G. Meltz. "*Fiber Bragg Grating Technology Fundamentals and Overview*", IEEE Journal of Lightwave Technology, no. 8, August 1997.

*milton.cinelli@udesc.br

Acknowledgments

The work was developed under the framework of project TECCON II with Transmissoras Brasileiras de Energia (TBE). The authors would like to acknowledge CNPq and INESC P&D Brasil for supporting this research activity.

*milton.cinelli@udesc.br

INCREASING THE PLASMA CURRENT THROUGH IMPROVEMENT OF SECONDARY ELECTRONS EMISSION IN CCP-PLASMAS BY USING A NEW ASYMETRIC BIPOLAR PLASMA POWER SUPPLY (ABiPPS)

Juliano Sadi Scholtz[1], Alessandro Luiz Batschauer[2], Marcello Mezaroba[2] and Luis César Fontana[3]
[2] *University of Santa Catarina State (UDESC), Electric Power Proc. Group (nPEE), Joinville, SC, Brazil.*
[3] *University of Santa Catarina State (UDESC), Plasma, Thin Films and Surfaces Lab. (LABPLASMA), Joinville, SC, Brazil*

1. Introduction

In the last two decades it has been developed many different power supplies including RF, stabilized DC voltage and pulsed ones. Among them, the HiPIMS (High Power Impulse Magnetron Sputtering) became popular for producing a high ionization rate of sputtered atoms from the target, in films deposition applications [1], [2], [3], [4]. There is a challenge for developing topologies involving high voltage and current as well high switching frequency which has been pursued over the years. Conventional power supplies do not have these characteristics due to technological difficulties, mainly due to the availability of switches that can handle high voltage and high current values concomitantly with short switching times.
This paper present a new power supply based on half bridge cascade topology, with a reduced number of switches, in a modular half-bridge converter configuration using cell submodules, similar to those observed in [5]. Beyond the reduced cost and simple design, its bipolar configuration, with short period of positive pulse and longer negative pulses, can produces high emission of secondary electrons from the cathode. It can greatly increase the plasma ionization rate. A prototype with voltage range from -2.5kV to +2.5kV and frequency up to 500kHz, was built for studies of plasma generation.

2. ABiPPS CONVERTER

Figure 1 shows an illustration of the converter configuration, with "n" levels on each leg. This configuration enables the use of single low voltage submodules, allowing the construction of high voltage and high frequency converter [6].

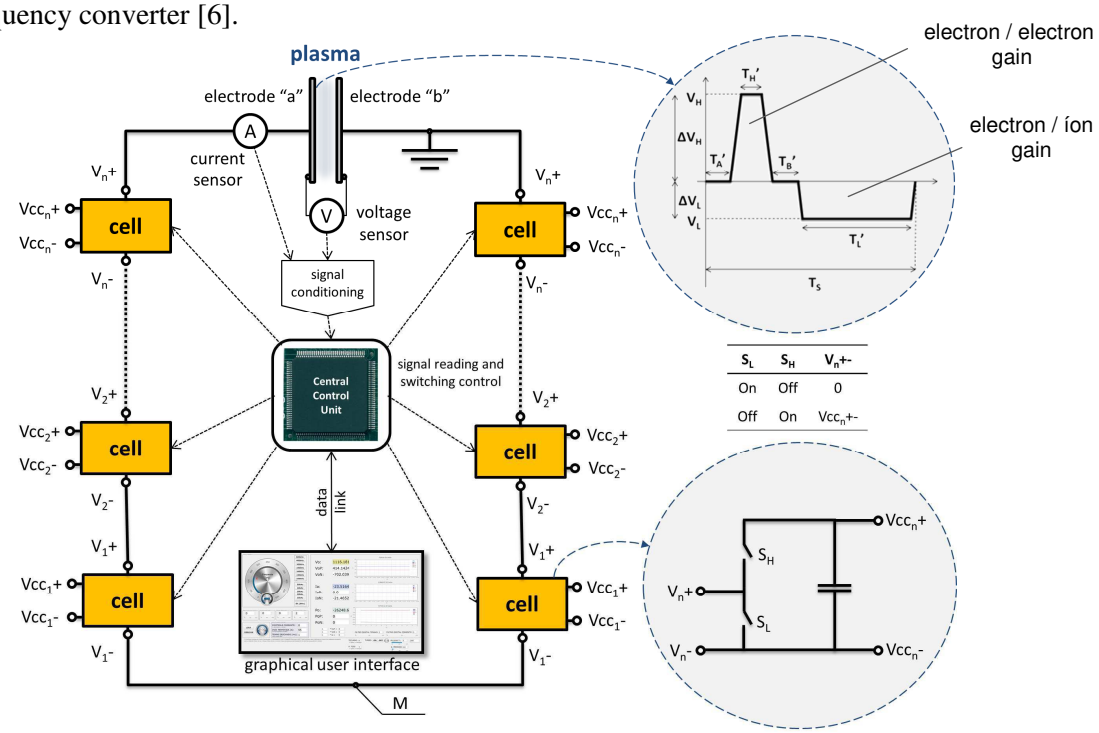

Fig. 1. Converter power circuit configuration (M: medium point that can be used for measurement).

3. Results and Discussions

In pulsed DC or DC plasmas, the secondary electrons are produced mainly by ion bombardment on the cathode. However, the yield of the secondary electrons produced by ions that collide with the cathode is very low (typically 0.1 or less for applied voltage potentials of the order of hundreds of Volts). On the other hand, the bombardment of the target (cathode) by electrons presents greater efficiency in the emission of secondary electrons.

*Corresponding author: luis.fontana@udesc.br

3.1 Comparison between the Converter Developed (ABiPPS) and a Comercial Power Supply

Fig. 2 shows the output current and voltage waveform for plasma produced through Argon working gas at pressure of 5.0 Torr, with the ABiPPS converter in comparison with a commercial pulsed power supply, in which the positive pulse voltage is fixed at 10% of the negative one.

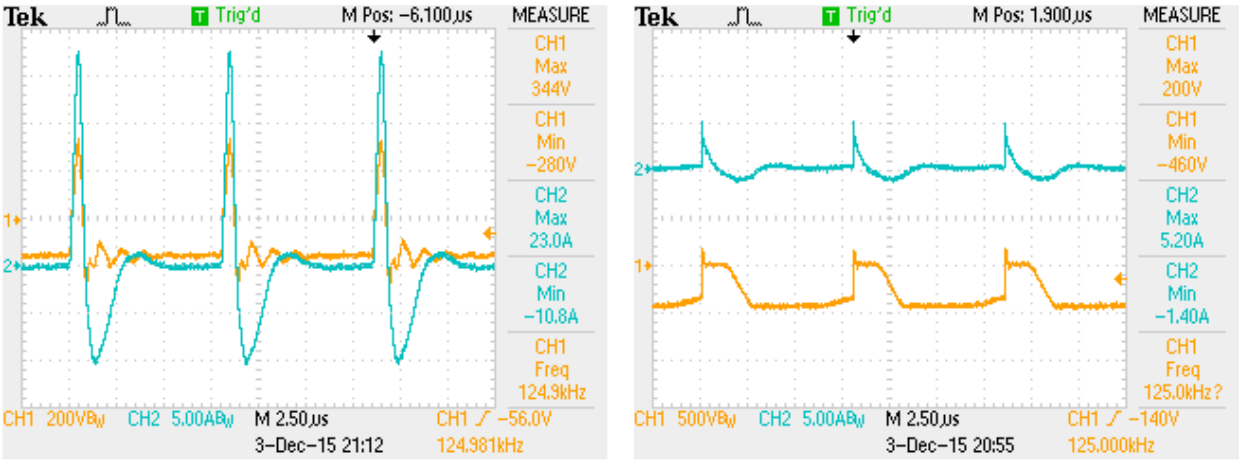

Fig. 2. Current and voltage waveform comparison between ABiPPS (a) and a commercial power supplies (b). During the negative voltage pulse, the current was 10.8A for ABiPPS and 1.4A for commercial power supply. Despite the voltage pulse being lower, it is observed much higher current for ABiPPS system. (plasma in argon at 5.0 Torr; measurements taken through TDS2024 oscilloscope, P5100A voltage and TCP312A current probes).

4. Conclusions

The ABiPPS power supply, applied to generation of non-equilibrium plasma, provides discharge in a wide range of current and voltage due to the flexibility to generation of short positive pulses and large negative pulses. The discharge is arcing free due to the periodic short period polarity inversion. It is possible to control the plasma density through different variables: pulsing rate; positive and negative pulses intensity; ratio between positive and negative period and rest time between the pulses. The short positive voltage pulses produce intense electronic bombardment on the electrode which increases the emission of secondary electrons from that surface. The noticeable result of this process is the far high current. High density plasma provide opportunity to new and superior applications in different fields as sputtering film deposition, surface treatment and chemical plasma.

4. References

[1] J. Laimer, M. Fink, T. A. Beer, H. Stori, "Plasma Dynamics as a Key to Successful Upscaling of Pulsed Plasma Processes," Surface and Coatings Technology, vol. 174-175, pp. 118-123, 2003.

[2] A. Anders, "High Power Impulse Magnetron Sputtering and Related Discharges: Scalable Plasma Sources for Plasma-Based Ion Implantation and Deposition," Surface & Coatings Technology, vol. 204, pp. 2864-2868, 2010.

[3] M. Mezaroba, L.C. Fontana, J.D. Sperb, R.L. Klein, "CC-CC FB-ZVS-PWM-OS Converter for Plasma Generation," VII International Conference of Industrial Applications, 7pp, 2006.

[4] A.L. Batschauer, M. Mezaroba, L.C. Fontana, J.A. Heerdt, J.D. Sperb e R.L. Klein, "Automatized Integrated System for Plasma Sputtering," Brazilian Congress of Power Electronics, 6pp, 2007.

[5] A. Lesnicar and R. Marquardt, "An Innovative Modular Multilevel Converter Topology Suitable for a Wide Power Range," IEEE Power Tech Conference Proceedings, 6pp, Bologna, Italy, Jun. 2004.

[6] Juliano Sadi Scholtz, Luis César Fontana, and Marcello Mezaroba Asymmetric Bipolar Plasma Power Supply to Increase the Secondary Electrons Emission in Capacitive Coupling Plasmas, IEEE TRANSACTIONS ON PLASMA SCIENCE, Vol. 46, Issue 8, Aug. 2018, DOI:10.1109/TPS.2018.2851071

Acknowledgments

The authors would like to thank the University of The State of Santa Catarina (UDESC) for the infrastructure and resources provided.

*Corresponding author: luis.fontana@udesc.br

BIODIESEL PRODUCTION THROUGH THE PLASMA TECHNOLOGY

Marina de Medeiros Machado[1*], Cátia Regina Silva de Carvalho Pinto[1,2], Anelise Leal Vieira Cubas[3], Roberth Andrés Villazón Montalván[1], Elisa Helena Siegel Moecke[3], Carlos Roberto de Oliveira Junior[3], João Marco Kretzer Gelsleichter[3], Kauan Santos Barcelos[3], Jonathan Alexsander Bork[4]

[1]*Federal University of Santa Catarina – UFSC. Department of Sanitary and Environmental Engineering. Florianópolis, Santa Catarina, Brazil.*
[2]*Federal University of Santa Catarina – UFSC. Engineering Mobility Center. Joinville, Santa Catarina.*
[3]*Environmental Engineering, University of Southern Santa Catarina (Unisul), Palhoça, SC, Brazil.*
[4]*Chemistry Engineering and petroleum Engineering. Civil Engineering laboratory, University of Southern Santa Catarina (Unisul), Tubarão. SC. Brazil.*

1. Introduction

The use of residues oils for biodiesel production represents a new step towards sustainability; since it allows the generation of energy from potentially polluting waste which is usually not properly discarded in the environment [1]. However, what is known about the production of biofuels from the waste cooking oil is based on the conventional process, where the transesterification reaction occurs through chemical catalysis [2]. The production of biodiesel by plasma is a new process that has been studied by some researchers [3,4,5] and it has presented superior results to the conventional technology, because it has advantages such as less reaction time, less amount of water in the production, ease in product separation, decrease of glycerine formation [2]. Regarding the state of the art of biodiesel produced by plasma Istadi et al. [3,5] research assumes that plasma-generated biodiesel can release 10 times less particulate matter than that produced by conventional processes. In this article is presented a different biodiesel production processes and verify the conversion rates of the triglycerides into esters, and to identify the main by-products formed and their quantities, to obtain a catalytic process type guideline.

2. Experimental

The raw material used was waste cooking oil originated from the food frying process from local restaurants, in Palhoça, Santa Catarina/Brazil. The waste cooking oils initially underwent a pretreatment step with heating to 50°C and filtering for the removal of impurities. The raw material was characterized by determining the acidity number by titration (AOAC n. 940.28, 2005), moisture content by using the Karl-Fischer method (ISO 12937, 2000), saponification by the AOAC official method 920.160, insaponificable matter by Ca 6a-40, and density by Cc 10a-25.

A quantity of 32 ml of waste cooking oil was heated until boiling for removal of water. It was added 0.15 to 0.5 g of basic catalyst (KOH) dissolved in 6.4 ml of methanol. The raw material was used in plasma technology in times to 15 and 30 minutes. The oil-alcohol sample (1:6) was introduced into the reactor, under mechanical stirring (2.0 rpm) and temperature (60°C), until complete conversion to esters, through the transesterification reaction, while a voltage of 7.7kV was perfoming.

The plasma reactor is cylindrical of the hybrid type gas-liquid at atmospheric pressure, the geometry used of the metallic electrodes was tip-plane. A high voltage DC - direct current (max. ± 17 kV) and current 30 mA was used to generate the plasma. The space between two electrodes, approximately 3 cm. To characterize the biodiesel the following parameters were determined: peroxide and acid number according to AOAC (2005) and saponificable determined by AOCS Cd 3-25. The determination of methyl esters was performed according to the European Standard Test Method of EN 14103 [7] using a Shimatzu (Kyoto, Japan) GC-2010AF gas chromatograph equipped with a flame ionization detector (FID) and a capillary column (RTX-5, 60 m long x 0.25 mm ID x 0.25 μm thick).

3. Results and Discussions

Table 1 shows the quantity of biodiesel and glycerol formed and the conversion rates of each sample produced.

*Corresponding author: marina.machado@hotmail.com

Samples	Reaction time (min)	Catalyst added (g)	Biodiesel formed (ml)	Glycerol formed (ml)	Conversion rate (%)
1	15	0.25	28	2.7	**64.63**
2	15	0.5	30	4.2	**76.48**
3	30	0.15	26	2.0	**25.00**
4	30	0.25	29	2.0	**54.23**
5	30	0.5	22	2.4	**88.58**

Table 1 Conversion of waste cooking oil samples into methyl esters.

According to Table 1, it's perceptible that longer reaction times, in general, provide smaller amounts of glycerin formed and higher yield of biodiesel, while the reaction time of 15 minutes presents lower yield rates, proportionally higher amounts of glycerin formed. It is also observed that the amount of catalyst used is proportional to the amount of glycerin formed, the higher the amount of catalyst, the greater the amount of glycerin produced. Moreover, samples with lower catalyst additions (KOH) present low conversion rates into methyl esters. Regarding time, variations were found ranging from 54.23 to 64.63%, and 76.48 to 88.58% in the conversion rates, using the same amount of catalyst at different times. Furthermore, when using 0.25g of KOH decrease of 16.09% in the conversion to esters is observed, increasing the reaction time from 15 to 30 min. However, with a higher amount of catalyst - 0.5g KOH - there is an increase of 13.66%, increasing the time from 15 to 30 min.

It is considered the fact that the plasma inserts a large amount of energy in the system and that the oil used is waste cooking oil that has instaurations, secondary reactions such as chain breakage or even the saponification of the fatty acids with the catalyst may have happened. This oscillation can also be attributed to the fact that transesterification is a reversible reaction and that its behavior and its constants in a plasma reactor are unknown. Thus, the oscillation in the conversions, although within a good range of general conversions, is a factor to be investigated in kinetic studies considering also the structure of the fatty acid to be transesterified in this reaction proposal.

According to Table 2 and Fig 1, the sample that presented the highest conversion percentage into methyl ester (biodiesel) was sample which had an exposure to the plasma reactor for 30 min and an addition of 0.5 g of catalyst (KOH) resulting in an ester conversion rate of 88.58%.

Properties	***Value***
Acid value (mg KOH/g)	0,378
Peroxide value (meq/kg)	19.95
Saponification value (mg KOH/g)	177.04

Table 2 Properties of the methyl esters produced using plasma technology.

There are also a few minor peaks referring to methyl components produced from primary fatty acids, but which represent only traces in the main composition of the biodiesel produced. According to Istadi et al. [5], using plasma technology to produce biodiesel provides the interference of the electrochemical reaction at carbon-carbon (C-C) bonds, while chemical catalysis presents carbon-oxygen (C-O) bond breakage processes. High electrochemical energy attacks the double bonds of unsaturated triglycerides through oxygenation. Oxygen molecules can be supplied by methanol during the reaction, where they replace each C-C double bond by a saturated molecule containing higher thermal stability [5]. Thus, with the use of waste cooking oil as a raw material and the application of the innovative technology of cold plasma it was possible to produce an environmentally and socially-friendly product. Biodiesel produced by plasma presents environmental advantages and potential use to improve human-being quality of life as for energy generation, especially in small, remote and difficult access communities.

4. References

[1] J. Yan, A. Li, Y. Xu, TPN Ngo, S. Phua, Z. Li, Bioresour. Technol., **123**, 332–733, (2012).
[2] EHS Moecke, R. Feller, HA Santos, MM Machado, ALV Cubas, ARA Dutra, LLV Santos, SS Soares, J. Clean. Prod., **135**(1), 679-688, (2016).
[3] NASA Istadi, DA Didi, MS Puput, TN Bambang, B. Chem. React. Eng. Catal., **4**(1), 23–31, (2009).
*Corresponding author: marina.machado@hotmail.com

[4] Y. Hyun, Y. Mok, D. Jang, J. Korean Oil. Chem. Soc., **29**(1), 81-87, (2012).
[5] I. Istadi, AD Yudhistira, DD Anggoro, L. Buchori, B. Chem. React. Eng. Catal., **9**(2), 111-120, (2014).
[6] ALV Cubas, MM Machado, CRSC Pinto, EHS Moecke, ARA Dutra, Waste manage., **47**, 149-154, (2016).
[7] European Standard Test Method. *EN 14103: fat and oil derivatives – fatty acid methyl esters (FAME) – determination of ester and Linolenic acid methyl ester contents*. Germany, (2003).

Acknowledgments
The authors acknowledge UNISUL, UFSC and financial support from Foundation for Research and Innovation of Santa Catarina State - FAPESC 3896/2013 (Brazil).

*Corresponding author: marina.machado@hotmail.com

EFFECTS OF PARTIAL SUBSTITUTION OF CARBON BY NITROGEN ON MICROSTRUCTURE AND HARDNESS OF AISI 420 STEEL

Felipe Augusto de Aguiar Possoli[1]*, Euclides Alexandre Bernardelli[1], Julio Cesar Klein das Neves[1], Paulo César Borges[1]
[1]*Universidade Tecnológica Federal do Paraná, DAMEC, PR, Brazil*

1. Introduction

Martensitic stainless steels (MSS) that have nitrogen (N) as interstitial element show advantages compared to those ones carbon (C) alloyed, because its atomic ordination's physical characteristics [1] which implies on electronic distribution and solid solution stability. In addition, studies have shown that might be synergic effects if both interstitials are present [1-2]. Among the benefits of MSS containing C+N are better resistance to corrosion [2] and to softening by tempering [1]. Although, some C+N MSS could show hardness decrease after low temperature tempering [1], indicating that either substitutional alloys and different relations of N and C might take an important role. The aim of this work is to study the effects of partial substitution of C by N on microstructure and hardness by the SHTPN process on AISI 420 (12 %Cr).

2. Experimental

Samples of 33x33x2.95 mm were cut from an AISI 420 sheet which was supplied in annealed form. The chemical composition is presented in Table1. It was analyzed by optical emission spectroscopy (OEM) through a Shimadzu OES-5500 ii spectrometer.

Alloy	C	Cr	Ni	Si	Mn	P	S	Mo
Analyzed*	0,336	12,110	0,243	0,358	0,256	0,031	0,000	0,037
AISI 420B	0,26-0,35	12,0-14,0	1,0	1,0	1,0	0,04	0,03	

Table 1. Results of chemical composition, showing the main elements of AISI 420 stainless steel used in this work and the AISI 420B alloy composition according to ASTM F899-09 standard
* percentage of Co, Nb, W, V e Ti are lower that 0.0025 %p.

The experimental procedure is presented in Fig. 1. Two set of samples were decarburized in muffle furnace (O_2 exposure) at 1050 ºC, one for 12 h and other for 24 h. Then, the samples were quenched in brine solution (5 %wt.) at room temperature. Posteriorly, they underwent the SHTPN treatment, which consisted in: plasma nitriding at 510 ºC for two hours (N_2:H_2=4:1) at 3 Torr pressure; followed by solubilization at 1100 °C (in a neutral salt bath) during one hour and then it was quenched in brine solution. Additional quench was employed to refine the microstructure. In this last treatment, soaking temperature and time were 1050 ºC and 30 min., respectively. A third set was just double quenched from the 1050 °C (15 and 10 min.) to keep nominal carbon content and then the set underwent the same process described before.

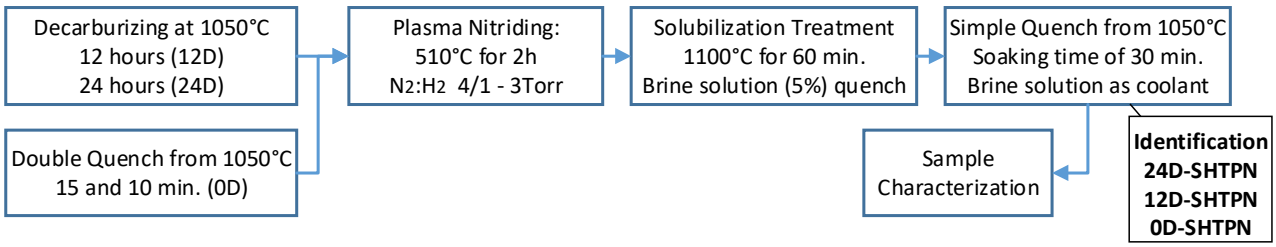

Fig. 1. *Flowchart of the experimental procedure.*

Samples were prepared to metallographic analyses after each process to ensure consistency of the results. By means of optical microscope compound layers were measured. Scanning Electron Microscope (Zeiss EVO MA 15) was used to analyze samples microstructure. Phase's analyses were executed on nitrided and SHTPN samples using a Schimadzu XRD 7000 x-rays diffractometer. The hardness profiles were taken using a microhardness tester, Schimadzu HMV-2T, configured to 25 gf load and holding time of 15 seconds.

3. Results and Discussions

The decarburized and plasma nitrided samples showed layer thickness as follows: 0D-(43.6 ± 1.2 μm); 12D-(43.1 ± 1.5 μm); and 24D-(46.3 ± 1.2 μm). The compound layer of the condition 24D is slightly larger, probably due to the low carbon content, improving nitrogen diffusion [3]. Phase's analyses showed the presence of ε, CrN e γ'nitrides for all of them.

*Corresponding author: felipepossoli@gmail.com

Fig. 2 shows SEM images from quenched samples after SHTPN treatment. It is possible to note that 0D-SHTPN condition has fine structured martensite packets and with lower carbon content, as represented by 12D-SHTPN and 24D-SHTPN conditions, the martensite packets turn coarser. The diffusion layer thickness is about 630 µm, except to 0D-SHTPN where was not possible to define a frontier with the core by the microstructure changes. Underneath the martensite layer of the 24D-SHTPN condition was possible to observe the presence of ferrite grains, showing that the decarburizing process was effective.

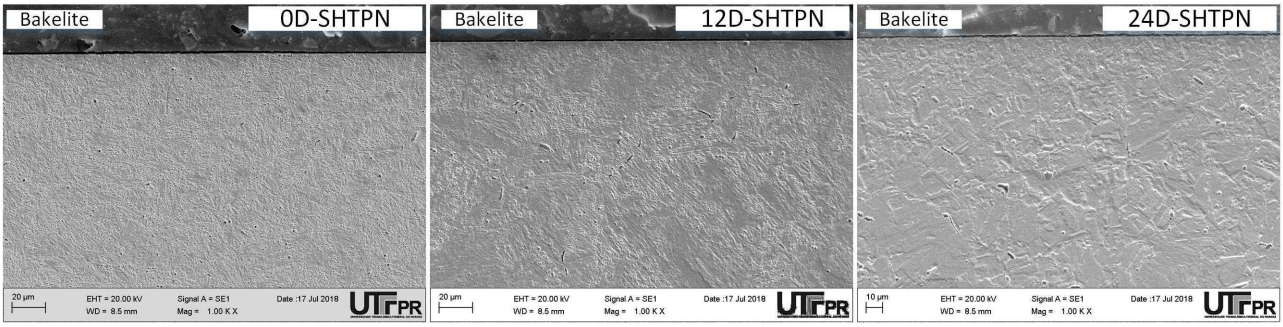

Fig. 2. *Microstructure of the samples treated by (SHTPN) process. Etchant: Villela.*

The x-ray diffraction pattern (35° to 75°) is shown in Fig. 3(a). In all conditions, martensite peaks were detected but not nitrides peaks, showing great solubilization of the N of the previous compound layer. The austenite peaks were related to retained austenite, which was formed due to high concentrations of carbon and nitrogen. Fig. 2 (b) shows the microhardness profile. It can be seen that the layer hardness is lower as the carbon content is decreased and as the carbon content increases, lower is the microhardness gradient. For example, the sample 0D-SHTPN profile does not show much difference in microhardness values between the diffusion layer and the core. It also indicates that the increase of N content in this condition lead to an imbalance between the microhardness gain and the effectiveness of martensitic transformation. Closer to surface (higher N concentration) there is a slight drop in microhardness too.

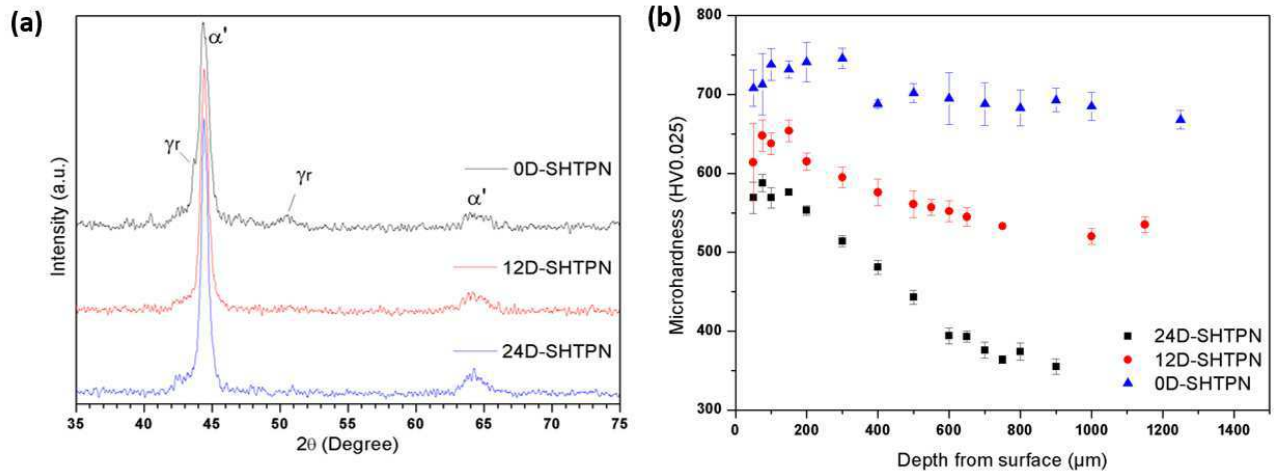

Fig. 3. *(a) X-ray diffraction pattern showing the austenite (retained) and martensite peaks and (b) Microhardness profile showing the influence of partial substitution of C by N on hardness using SHTPN treatment.*

4. Conclusions

Higher amounts of N and C leaded to high hardness value, both at surface and within the diffusion layer. However the highest C content of 0D-SHTPN (0.33 %C wt.), among the samples, incurred the lowest hardness gain by the SHTPN treatment. The lower hardness value of 12D-SHTPN and 24D-SHTPN conditions might be associated to lower C and N concentration where coarser martensite packs were present.

5. References

[1] V. G. Gavriljuk, H. Berns "*High Nitrogen Steels*", 1 st edition, Springer-Verlag Berlin Heidelberg, USA, (1999).
[2] X. Qi, H. Mao, Y. Yang, Corrosion Science, **120**, 90-98, (2017).
[3] C. E. Pinedo, W. A. Monteiro, Surface and Coating Technology, **179 (2-3)**, 119-123, (2004).

Acknowledgments

The authors are grateful to CNPQ for the financial support.

*Corresponding author: felipepossoli@gmail.com

AISI 420 PATTERNING BY LOW-TEMPERATURE PLASMA NITRIDING

F. I. Zanetti*, I. G. Zanella, W. L. Alexandre, R. P. Cardoso, S. F. Brunatto
Plasma Assisted Manufacturing Technology & Powder Metallurgy Group
Mechanical Engineering Department, Federal University of Paraná, PR, Brazil

1. Introduction

Low-temperature nitriding of stainless steel is an outstanding technology due the possibility of obtaining mechanical properties improvement without corrosion resistance loss [1]. Properties enhancement is achieved mainly by nitrogen supersaturation, which also increase the lattice parameter and promotes the development of residual stress. However, at the surface, where there is no restriction to perpendicular expansion, the material can freely expand [2]. Quenched AISI 420 stainless steel samples were low-temperature plasma treated at the temperature of 350 °C by 2 h with a TEM grid pattern placed on the surface. The treatments were carried out using a nitriding and an inert gas mixture. Development of a pattern matching the grid in both samples was achieved, for the sample treated in the inert gas mixture the sputtering effect causes small valleys on the regions exposed to the plasma while for the samples treated in nitriding gas mixture a plateau, caused by the surface expansion, was observed in the open spaces of the grid with surface hardness increase even in covered places by the grid.

2. Experimental

AISI 420 samples with 9,5 mm diameter and 10 mm height were air cooled from 1050 °C to obtain martensitic microstructure, the samples were grinded, mirror polished and then a TEM grid were positioned on the samples surface, these grids present hexagonal open spaces of 50 µm and 32 µm of covered places (mesh). Plasma treatments were carried out by 2 h and 0.5 h in a nitriding gas mixture, composed of 70 % N_2, 10 % Ar and 20 % H_2, and in the inert gas mixture by 2 h, composed by 80 % Ar and 20 % H_2, both at a flow rate of 200 SCCM, 400 Pa and at 350 °C with DC pulsed plasma peak voltage of 700 V, duty cycle of 8 % and auxiliary heating. Surfaces were analyzed by Vickers hardness measurements with a 25 gf load, in places exposed to plasma and covered by the grid mesh, and the surface expansion was evaluated by confocal microscopy equipped with Differential Interference Contrast.

3. Results and Discussions

The low-temperature plasma nitriding of quenched AISI 420 allows to create surface patterns by martensitic expansion, this pattern matching the TEM grid, can be observed in Fig. 1. a) as a higher plateau, formed in the sample surface exposed to plasma through the open spaces of the grid, moreover, the effect of expansion is more accentuated than the effect of sputtering, since the valleys are observed in the samples treated in inert gas mixture. The sample treated by 0.5 h in the nitriding flow also presents a higher plateau, demonstrating that the expansion occurs since the begin of nitriding.

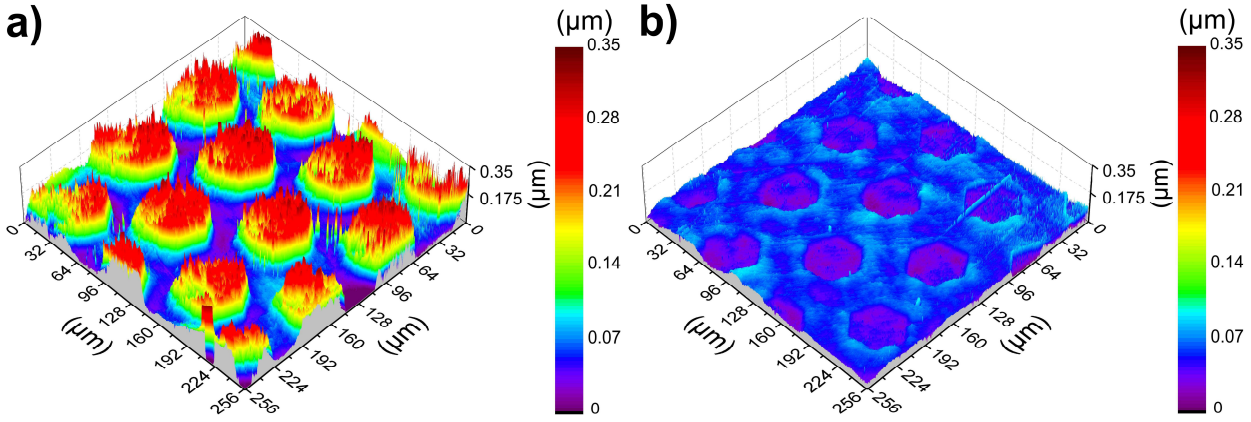

Fig. 1. *Surface height maps of samples after plasma treatment at 350 °C by 2 h. a) nitriding gas mixture b) inert gas mixture (80 % Ar + 20 % H_2).*

Surface hardness of the plasma nitrided sample increased from 560 ± 31 $HV_{0.025}$ to 908 ± 43 $HV_{0.025}$ in the plateau, this is well-established due the nitrogen diffusion and hard phases formation, however, even in places covered by the grid mesh, not exposed to plasma, the hardness increased by 172 ± 60 $HV_{0.025}$, indicating the nitrogen lateral diffusion and/or compressive residual stress. Surface hardness of the samples plasma treated in inert gas mixture also increased of 59 $HV_{0.025}$ (619 ± 30 $HV_{0.025}$) in open spaces of grid

*Corresponding author: fernando.iz@ufpr.br

without surface hardness increase in places covered by the grid mesh. Surface hardness for the sample 0.5 h were 776 ± 53 $HV_{0.025}$ and 582 ± 28 $HV_{0.025}$ for open and covered spaces respectively, and 530 ± 27 $HV_{0.025}$ for non-treated surface.

4. References

[1] Y. Xi, D. Li, D. Han, Surf. & Coat. Tech., **202**, 2577-2583, (2008).
[2] T. Czerwiec, G. Marcos, T. Thiriet, Y. Guo, T. Belmonte, 5th International EIGM/AMASE/FORGEMAT Conference on Advanced Materials Research, Nancy, France (2009)

Acknowledgments

The CAPES and CNPq which supported this work. The authors also are thanks to the Surface Engineering – LaMaTs for providing many of devices used in this research

*Corresponding author: fernando.iz@ufpr.br

USING A THREE-ELECTRODE DC REACTOR FOR AMOSPHERIC PRESSURE PLASMA-ASSISTED NITRIDING: INITIAL RESULTS

Guilherme Seiti Kobayashi[1]*, Felipe Augusto Zaias[1], Rodrigo Perito Cardoso[1]
[1]*Universidade Federal do Paraná*

1. Introduction

Plasma-assisted thermochemical treatments comply with stringent environmental and safety laws and regulations, while providing improvements of the surface mechanical properties of components. However these treatments usually occur in low pressure environments [1], which use high cost vacuum equipment, and imposes batch treatments . To overcome these limiting factors, it is interesting to study plasma-assisted thermochemical treatments at atmospheric pressure [2]. So, in this work a three-electrode DC reactor was used for nitriding treatment of AISI 1020 steel samples and the first results are presented here.

2. Experimental

A three-electrode reactor, as seen in Fig.1, under the influence of a potential difference, performs a micro-discharge between two electrodes – within a distance of tens of micrometers. This micro-discharge is thus expanded toward a third electrode – that is few millimeters from the micro-discharge –, which is the sample, due to its potential difference in relation to the micro-discharge. This setup is depicted on Fig. 2. To supply the energy necessary to the sample to achieve the treatment temperature a resistance was used. Using this apparatus, AISI 1020 steel cylindrical samples of 9mm of diameter and 11mm height, mirror polished, were nitrided at 450°C for 2h, using gas mixture of 95% N_2 + 5% H_2, with 99.999% purity, and a flow rate of 500 SCCM. After the treatment the samples were analyzed with by X-ray diffractometry (XRD), using a Shimadzu XRD 7000 diffractometer with a Cu Kα X-ray tube in the Bragg-Brentano configuration. For microstructural analysis, the samples were cross sectioned, grinded, mirror polished, and etched with Nital 3% reagent to reveal the microstructure and micrographs were obtained using an Olympus BX51M optical microscope. Finally, microhardness tests were performed using a Shimadzu Micro Hardness Tester HMV-2T applying a load of 50 gf and a peak-load contact of 15 s, the data presented are the mean of five measurements.

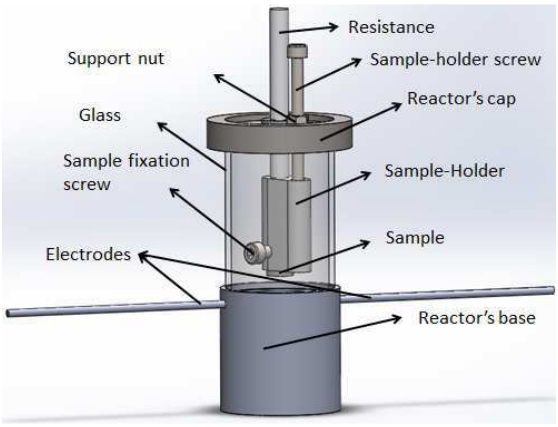

Fig. 1. *Scheme of the DC triode reactor applied in this work.*

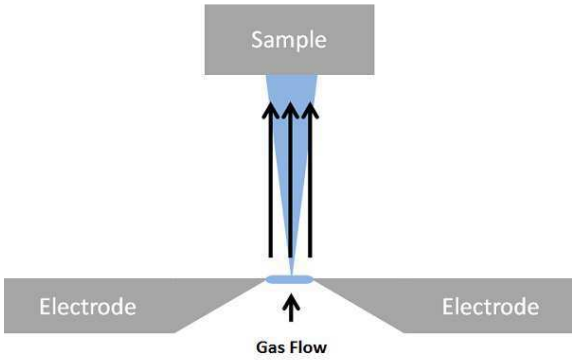

Fig. 2. *Scheme of the three electrodes disposition, micro discharge and expanded plasma.*

3. Results and Discussions

Although the micro-discharge was probably in arc regime, the expanded discharge was in a "glow discharge regime", thus corroborating to a successful nitriding. Due the arc regime on the micro-discharge (or instabilities leading to arcing), tungsten atoms of the electrodes responsible for the micro-discharge were deposited on the sample surface. This was seen on the surface micrograph and XRD analysis, as seen in Fig.3.

Through XRD, micrograph and hardness analysis it is shown that the treatment was relatively successful. An increase in hardness, from 216.7±7.2 to 339.6±8.4 HV0.05 was obtained after the treatment. But as seen on XRD analysis, as seen in Fig.3, the detected nitrides were $Fe_{16}N_2$, this could be due to the treatment temperature or a low Nitrogen potential on the expanded discharge. This was corroborated as seen in Fig.4, due the plate-like shapes seen near the treated surface on the cross section micrograph.

Corresponding author: *seiti.kobayashi@ufpr.br

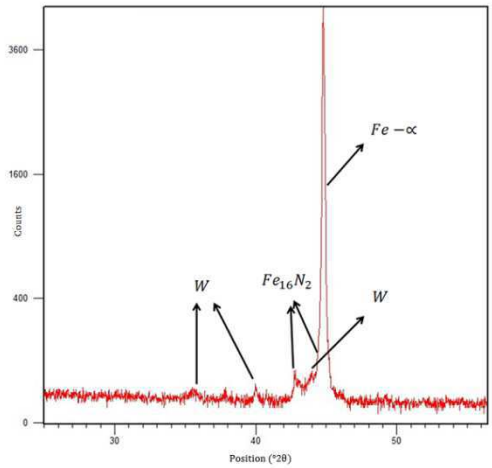

Fig. 3. *X ray difratometry analysis of the nitride sample for 2h at 450°C.*

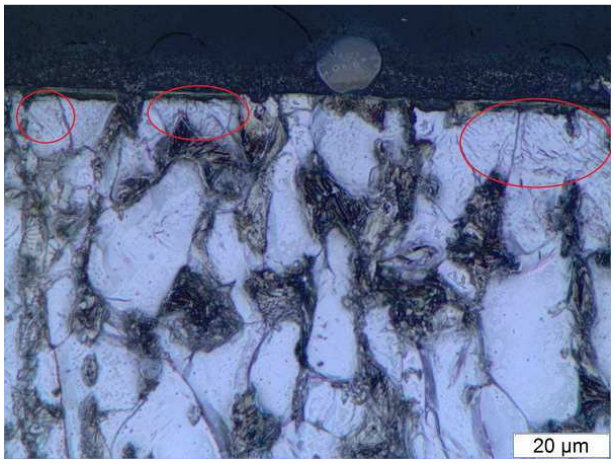

Fig. 4. *Cross section micrograph where plate-like structures of $Fe_{16}N_2$ are highlighted by circles near the treated surface.*

4. References

[1] Y. Sun, T. Bell, Mater Sci Eng A, **140**,419–434 (1991).
[2] P. Bruggeman, R. Brandenburg J. Phys. D: Appl. Phys., **46**, 464001 (2013).

Acknowledgments

We are greateful to Dr. Irineu Mazzaro from Laboratório de óptica de Raios-X e Instrumentação (LORXI), and Dr. Ana Sofia Clímaco Monteiro D'Oliveira from Laboratório de Engenharia de Superfícies, for offering laboratorial infrastructure.

Corresponding author: *seiti.kobayashi@ufpr.br

XXXIX Congresso Brasileiro de Aplicações de Vácuo na Indústria e na Ciência

08 a 11 de outubro de 2018 - Joinville - SC

SESSÃO DE PÔSTER
TERÇA - 9/10
XXXIX CBrAVIC

Apresentações em pôster do XXXIX CBrAVIC (Terça-feira – 09/10)

ID	TÍTULO
#1	**MICROSTRUCTURE AND TRIBOLOGICAL PROPERTIES OF THE PLASMA NITROCARBURIZED DIN 100CR6 STEEL** *M.A. Fontes, V.H.B. Scheid, D.S. Machado, L.C. Casteletti, P.A.P. Nascente*
#9	**EFFECT OF PROCESS TIME ON CORROSION RESPONSE OF 5052 ALUMINIUM ALLOY TREATED BY PLASMA ANODIZATION** *D. C. R.Santos,|G.S. Reis, R.R. Lucas, L.L.G. Silva.*
#10	**MODIFIED BATCH REACTOR FOR FURFURYL RESIN SYNTHESIS** *Ana C. M. Gaspar, Carla S. Bordim, Alvaro J. Damião*
#13	**COMPARATIVE STUDIES OF NITROGEN PIII AND PIII&D EXPERIMENTS USING TUBES OF SS304 AND TI6-AL4-V WITH 1.1 CM DIAMETER** *M.Ueda, C. Silva, L. Pichon, G.B. Souza*
#16	**EFFECT OF THE GAS PRESSURE ON THE DISCHARGE POWER OF A HYBRID CORONA-DBD REACTOR** *Alonso H. Ricci Castr, Gilberto Petraconi Filho*
#19	**APPLICATION OF OXYGEN PLASMA IN THE CLEANING PROCESS OF TIO_2 NANOTUBES SYNTHESIZED BY ANODIZATION TECHNIQUE** *R. C. Gonçalves, J. S. B. de Lima, A. S. S. Sobrinho, D. M. G. Leite, H. S. Maciel, R. S. Pessoa*
#20	**SUBSTRATE HEATING FOR SPUTTERING DEPOSITION SYSTEM** *Angel Fidel Vilche Peña, Gleyson Tadeu de Almeida Santos, Silvio Rainho Teixeira, Agda Eunice de Souza Albas*
#22	**SIMULATION AND ELECTRICAL CHARACTERIZATION OF SAW DEVICE** *Júlio C. Faria da Silva, Newton A. S. Gomes, G. Osvaldo Dias, Douglas M. G. Leite, Marcos Massi, Argemiro S. da S. Sobrinho*
#26	**AN ANALYTICAL APPROACH TO THE ELECTRIC POTENTIAL OF A CLEAVED SPHEROIDAL CONDUCTIVE DROPLET ON A DIELECTRIC SUBSTRATE** *Luis H. F. C. de Mello, Cesar J. B. Pagan*
#27	**Ti6Al4V SURFACE'S ROUGHNESS AND AREA CHANGES BY CONTROLLING CHEMICAL ETCHING TEMPERATURE** *Charles Jourdan Alberti, Danieli Aparecida Pereira Reis, Adriano Gonçalves dos Reis*
#28	**ISOTHERMAL OXIDATION BEHAVIOR OF THERMAL BARRIER COATING IN Ti-6Al-4V** *Filipe Estevão de Freitas, Adriano Gonçalves dos Reis, Danieli Aparecida Pereira Reis*
#29	**LOW COST ACESSORY FOR ELECTROSPINNING FIBER ALIGNMENT** *Armando Iwao Shimahara, Walter Pichi Jr., Ana Neilde Rodrigues da Silva, Maria Lúcia Pereira da Silva*
#30	**MICROFLUIDIC SETUP USEFUL FOR RESEARCH AND TEACHING** *Luiz Fernando Pinto, Armando Iwao Shimahara, Maria Lúcia Pereira da Silva*
#31	**CORNBREAD TREATMENT USING DIELECTRIC BARRIER DISCHARGE TO IMPROVE THE WETTABILITY** *Rogério Pinto Mota, Denise Katharina Schlößer, Alonso Hernan Ricci Castro*
#32	**ANISOTROPIC OPTICAL PROPERTIES OF HIGHLY TEXTURED GAN AND ALN FILMS ELUCIDATED BY SPECTROSCOPIC ELLIPSOMETRY** *D.M.G. Leite, C. Stegemann, A.S. da Silva Sobrinho, A.L.J. Pereira, M. Massi*
#33	**EFFECT OF PRESSURE ABOUT FACTOR B (P) FOR PLASMA GENERATED IN OPEN MICROHOLLOW CATHODE** *M. P. Gomes, B. N. Sismanoglu, I. M. Martin, E. C. Aragão, M. A. Okamura, L. M. S. Costa*

#34	**WEARING RESISTANCE IMPROVEMENT OF STEEL ALLOY AISI 4140 BY PLASMA NITRIDING** *F.C.Monção, A.Oliveira, G.V.Martins, A.S.da Silva Sobrinho[3], D.M.G.Leite[3], M.Massi*
#35	**DYNAMIC FRICTION COEFFICIENT MEASUREMENT TO POLYESTER RESIN COMPOSITES WHIT HOLLOW GLASS MICROSPHERES** *Carlos Alberto Fonzar Pintão, Airton Baggio, Edgar Borali, Lucas Pereira Piedade*
#36	**LASER WELDED DUAL PHASE STEELS: MICROSTRUCTURE AND MECHANICAL BEHAVIOR** *Monalisa Bandeira Valentim, Rafael Humberto de Mota Siqueira, Milton Sergio Fernandes de Lima*
#37	**MICROSTRUCTURAL EVOLUTION IN DISSMILAR CU(Cr) – STAINLESS STEEL LASER WELDS** *Sheila Medeiros de Carvalho, Rafael Humberto de Mota Siqueira, Milton Sergio Fernandes de Lima*
#38	**DLC COATINGS DEPOSITED ON GUITAR STRINGS** *E.D. Santos, R.S. Pessoa,N.K.A.M. Galvão, H.S. Maciel*
#39	**BETTER ADHESION OF PDMS SAMPLES TREATED USING A PLASMA JET FROM A FOUR-ELECTRODES DBD DEVICE** *Fellype do Nascimento, Munemasa Machida, Stanislav Moshkalev, Konstantin Kostov*
#40	**THE GEOMETRY RATIO EFFECT OF PTFE SAMPLE ON THE TORSION MODULUS (G)** *Lucas Pereira Piedade, Cesar Renato Foschini, Carlos Alberto Fonzar Pintão*
#42	**DEVELOPMENT, CHARACTERIZATION AND EVALUATION OF MECHANICAL PROPERTIES OF ALLOY AL-4CU-0.9SI-0.6MG-0.5MN-0.1FE FOR APPLICATIONS IN TURBOCHARGERS** *Gilberto Vicente Prandi, Renato Chaves Souza, Roberto Nunes Duarte*
#43	**ELECTRICAL STABILITY OF TiO_x THIN FILMS FOR APPLICATION AS TRANSPARENT AND CONDUCTIVE OXIDE** *L. C. D. Silva, R. S. Santiago, F. D. Origo, I. L. Graff, D. A. Duarte*
#44	**PRODUCTION OF Fe/Al_2O_3 SUPPORTED CATALYSTS BY PLASMA-ASSISTED PROCESS** *A. M. Santos, R. C. Catapan, D. A. Duarte*
#45	**TIO_2 COATINGS PRODUCED FROM OXIDATION OF METALLIC Ti FILMS PREVIOUSLY DEPOSITED ON GLASS SUBSTRATES** *Maria Elisa Philippsen Missner, Masahiro Tomiyama, Joel Stryhalskic, Luis Cesar Fontana*
#46	**EXPERIMENTAL VERIFICATION OF A NUMERICAL MODEL FOR TRANSIENT FLOWS OF RAREFIED GASES THROUGH LONG CHANNELS** *Ernane Silva, Cesar J. Deschamps*
#47	**INFLUENCE OF TIO_2 COATING COMPOSITION IN THE ADHESION OF MARINE MICROORGANISMS** *Moisés Luiz Parucker, Viviane Lilian Soethe Parucker, Rafael Galina Delatorre, João Victor Germano Pedrosa, Thayrine Bráz Taveira*
#48	**TIO_2 COATINGS FOR NATURAL BIOFOULING PROTECTION ON MARITME STRUCTURES: CONTACT ANGLE ANALYSIS** *Rafael Gallina Delatorre, Eder Marlon Ramos, Moisés Luiz Parucker, Viviane Lilian Soethe Parucker*
#49	**SPECTROCOPY OF AN ATMOSPHERIC NEEDLE PLASMA DISCHARGES** *Mauricio Antonio Algatti, Gustavo G. Vasques, Marcelo H. Mello e Milton E. Kayama*
#50	**REVALIDATION OF THE METALLIC LEAGUE CO-28CR-6ME (ASTM F75) - ABNT NBR ISO 7206-8 OF 2004 FOR NEW NORM ABNT NBR 7206-6 OF 2013 BY MEANS OF FATIGUE ASSAY AND ANALYZES FOR EXTENSOMETRY** *Sebastião Garcia Junior, Wilson Carlos Junior, João Roberto Moro*

#52	**SUBSTRATE HEATING EFFECTS ON HYSTERESIS CURVES OF REACTIVE MAGNETRON SPUTTER DEPOSITION** *Júlia Karnopp, Julio César Sagás*
#53	**OPTICAL AND ELECTRICAL PROPERTIES OF Ti SUBOXIDES GROWN BY REACTIVE GRID-ASSISTED MAGNETRON SPUTTERING** *Heitor Wilker Silva Barros, Diego Alexandre Duarte, Julio César Sagás*
#54	**RENEWABLE ENERGY: MICROBIAL FUEL CELLS** *Gabriel Neto, Elizabeth C. A. Trindade, Daniel V. F. Vanin, Ana L. Tavares, Claudimir A. Carminatti, Regina V. Antônio, Derce O. S. Recouvreux*
#55	**NANOCOMPOSITE STARCH/ BACTERIAL CELLULOSE NANOFIBERS FOR THE REMOVAL OF POLLUTANTS FROM AQUEOUS SOLUTIONS** *Gabriel Teodoro, Ricardo Brandes, Claudimir Carminatti, Regina Antônio, Derce Recouvreux*
#56	**CARBON FIBERS FUNCTIONALIZATION THROUGH N_2-H_2 RADIOFREQUENCY PLASMA** *Thayara Ceregatti, Carla Dalmolin, Luis César Fontana*
#59	**ONE-POT SYNTHESIS OF SILVER NANOWIRES/POLYPYRROLE NANOCOMPOSITES AT ROOM TEMPERATURE** *Rodolfo A. Baratto, Sergio H. Pezzin*
#60	**PULSED REACTIVE SPUTTER DEPOSITION: INSIGHTS FROM BERG MODEL** *Júlia Karnopp, Julio César Sagás*
#61	**ENERGY FLUX TO THE SUBSTRATE IN PULSED AND GRID-ASSISTED MAGNETRON SPUTTERING** *Thais Macedo Vieira, Julio César Sagás*
#64	**CHARACTERIZATION OF A PLATINUM/ALUMINA CATALYTIC MONOLITH FOR ETHANOL REFORMING** *Mauro E. Silva Júnior, Maíra O. Palm, Diego A. Duarte, Rafael de C. Catapan*
#65	**DEVELOPMENT OF SOFTWARE FOR XPS SPECTRA ANALYSIS** *L. R. Cardoso, M. O. Palm, T. P. de Carvalho, D. A. Duarte, R. C. Catapan*
#66	**ANODE EFFECTS ON A MAGNETRON SPUTTERING DISCHARGE: CHANGES IN HYSTERESIS CURVES AND SUBSTRATE FLOATING POTENTIAL** *Kleber Alexandre Petroski, Julio César Sagás*
#67	**X-RAY DIFFRACTION EVIDENCE IN GRAPHENE OXIDE FILMS OBTAINED BY VACUUM FILTRATION** *J. L. S. Gascho, S. F. Costa, S. H. Pezzin*
#68	**INFLUENCE OF THE MOLECULAR WEIGHT OF POLY(VINYLPYRROLIDONE) IN THE PRODUCTION OF SILVER NANOWIRES BY THE POLYOL METHOD** *J. L. S. Gascho, S. F. Costa, P. S. Tessaro, S. H. Pezzin*
#69	**HYSTERESIS OF THE SUBSTRATE FLOATING POTENTIAL IN MAGNETRON SPUTTERING SYSTEM** *Rafael Fróis da Silva, Julio César Sagás*
#70	**KINETICS ANALYSIS ON SILK AND COTTON WITH NATURAL DYEING** *Maria Elisa Philippsen Missner, Grazyella Cristina Oliveira de Aguiar, Catia Rosana Lange de Aguiar*
#71	**COLD-FORMED STEEL NITRIDING THROUGH ASYMMETRIC BIPOLAR PULSED PLASMA (ABIPPS)** *Renan Augusto da Cunha, Bruna Bianchi, Juliano Sadi Scholtz, Luis Cesar Fontana*
#91	**A MORPHOLOGICAL ASSESSMENT OF MICROCRYSTALLINE CELLULOSE TREATED WITH ACID HYDROLYSIS** *Daniel V.F.Vanin, Viviane Dias Andrade, Ana Letícia Tavares, Dayane Cristine Rodrigues, Claudimir A. Carminatti, Derce O. S. Recouvreux*

MICROSTRUCTURE AND TRIBOLOGICAL PROPERTIES OF THE PLASMA NITROCARBURIZED DIN 100CR6 STEEL

M.A. Fontes[1, 2*], V.H.B. Scheid[3], D.S. Machado[4], L.C. Casteletti[5], P.A.P. Nascente[1, 6]
[1]Universidade Federal de São Carlos, Programa de Pós-Graduação em Ciência e Engenharia de Materiais, 13565-905, São Carlos, SP, Brasil.
[2]Instituto Federal de Educação, Ciência e Tecnologia de São Paulo, Departamento da Mecânica, 14169-263, Sertãozinho, SP, Brasil.
[3]Centro Técnico Aeroespacial, Instituto de Estudos Avançados,12228-001, São José dos Campos, SP, Brasil.
[4]Tecumseh Products Company, CEP 13570-820, São Carlos, SP, Brasil
[5]Universidade de São Paulo, Escola de Engenharia de São Carlos, Departamento de Engenharia de Materiais, 13563-120, São Carlos, SP, Brasil.
[6]Universidade Federal de São Carlos, Departamento de Engenharia de Materiais, 13565-905, São Carlos, SP, Brasil.

1. Introduction

Plasma nitrocarburizing is a thermochemical process of surface hardening, which uses the luminescent discharge technology to introduce simultaneously nitrogen and carbon into samples surface [1]. The process can be carried out at a temperature below the eutectoid temperature of the Fe-N diagram, called ferritic nitrocarburizing, or above eutectoid temperature, being called in this case austenitic nitrocarburizing [2]. Both processes modify the surface properties of the samples due to the formation of crystalline phases on the surface, called nitrides and/or iron carbonitrides [3], considerably improving wear and corrosion resistance [2]. A layer consisting only ε-$Fe_{2-3}N$ phase is desirable for optimum wear resistance, but there is a greater probability of developing a compound layer consisting of a heterogeneous mixture of ε-$Fe_{2-3}N$ and γ'-Fe_4N [2]. The composition of the compound layer is very sensitive to the carbon amount in the treatment atmosphere; according to the phase diagram of the Fe-C-N system, the presence of carbon contributes considerably to the formation of the ε phase [4]. The nitriding process, which does not have carbon in its treatment atmosphere, produces a microstructure with no ε phase, or with only a very small quantity of it [5]. The stabilization of the ε phase is possible with the use of a carbon source, such as methane, on the nitrocarburizing atmosphere [6]. The objective of this study is to investigate the influence of temperature (ferritic and austenitic nitrocarburizing) and methane concentration on the wear resistance and surface hardness, as well the morphology, of DIN 100 Cr6 steel samples. This steel is used as raw material in the manufacture of a mechanical component applied in hermetic compressors for refrigeration.

2. Experimental

The pulsed dc luminescent discharge plasma nitrocarburizing process was carried out using a MP-250 equipment. The variables were the treatment temperature (550 and 600°C) and methane concentration in the gas mixture composition (0, 1.0, 1.5, and 2.0%), whereas the treatment time was fixed at 2 h. X-ray diffraction (XRD), scanning electron microscopy (SEM), and energy dispersive spectroscopy (EDS) analyses, as well as wear resistance and micro-hardness tests were used to characterize the samples. The chemical composition of the samples was: C in the range of 0.98 to 1.10; Cr in the range of 1.30 to 1.60; Mn in the range of 0.25 to 0.45; Si in the range of 0.15 to 0.35; balance Fe.

3. Results and Discussions

The results show that the modifications on the material surface considerably improve the mechanical properties such as hardness and wear resistance, due to the formation of nitrites. The compound layer composition and morphology are quite sensitive to the temperature and chemical composition of the treatment atmosphere.

Increasing the CH_4 concentration on the gas mixture contributes to the formation of the ε-Fe_{2-3} (C,N) phase, as can be observed at figure 1 (XRD for samples treated at 550°C), considerably enhancing the wear resistance and surface microhardness.

Ferritic nitrocarburizing promotes a thinner micro-porosity and compound layers, as shown respectively in figure 2 and figure 3, with a predominance of the ε phase, and with higher surface microhardness, as shown in figure 4. The austenitic nitrocarburizing produces a thicker micro-porosity and compound layers, and this compound layer comprises predominantly of the ε and γ'-Fe_4N phases.

*fontesma@hotmail.com

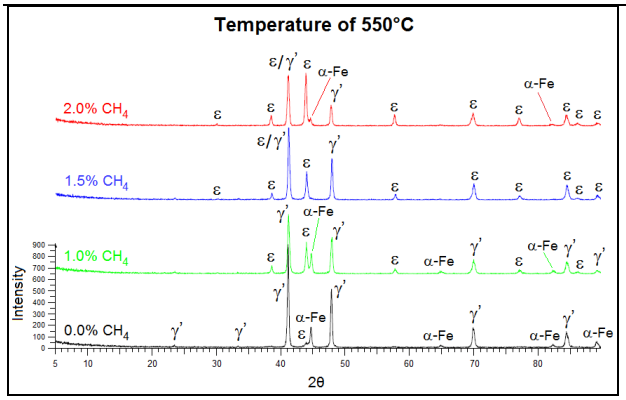

Fig. 1. *XRD for samples treated at 550°C at four different CH_4 concentrations.*

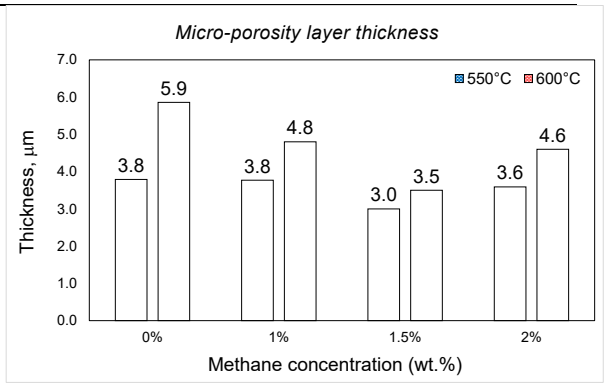

Fig. 2. *Micro-porosity layer comparison for all nitrocarburized samples.*

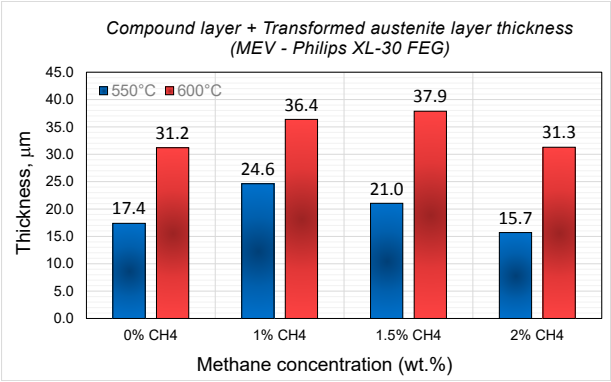

Fig. 3. *Compound layer and transformed austenite layer for all samples.*

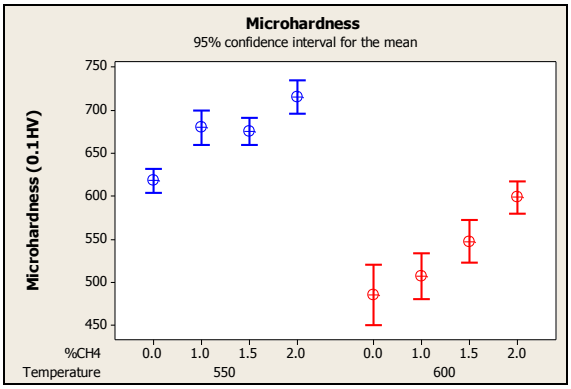

Fig. 4. *Superficial microhardness for samples treated in all conditions.*

4. References

[1] E. J. Mittemeijer and M. A. J. Somers. *"Thermochemical surface engineering of steels"*, Woodhead Publishing Series in Metals and Surface Engineering, USA, (2015).
[2] M. H. Sohi et al. Surf. Coat. Tech. **205**, 84-89 (2010).
[3] K. H. Jack. Acta Crystallogr. **3**, 392-394 (1950).
[4] R. L. O. Basso. *"Efeito do Carbono no Processo de Nitrocarburização com Plasma Pulsado da Liga Metálica AISI H13"*, Tese de Doutorado, Instituto de Física Gleb Wataghin, Universidade Estadual de Campinas, SP, (2007).
[5] K. T. Rie and F. Schnatbaum. Mat. Sci. Eng. A **140**, 448-453 (1991).
[6] J. R. Davis. *"Surface hardening of steels: understanding the basics"*, ASM International, USA, (2002).

Acknowledgments

The authors would like to thank Fernando Nawate from UFSCar/DEMa, for his assistance in the SEM/EDS measurements. CNPq is acknowledged for support.

*fontesma@hotmail.com

EFFECT OF PROCESS TIME ON CORROSION RESPONSE OF 5052 ALUMINIUM ALLOY TREATED BY PLASMA ANODIZATION

Santos, D. C., R.*, Reis, G. S., Lucas, R. R. and Silva, L.L.G.
Laboratório de Plasma Eletrolítico (LaPE), Fatec de Pindamonhangaba, CEETEPS/SP.

1. Introduction

Among several methods for surface treatment/modification of light metals and its alloys, plasma anodization or Plasma Electrolytic Oxidation (PEO) is an attractive technology to prevent their corrosion [1]. Technically, plasma anodization involves the combination of electrolytic process and plasma discharges, which promotes the growing of an oxide film from the oxidation of the metallic substrate under high polarization potential (hundreds of volts). Film properties are dependent on process parameters, mainly voltage, current density, time, temperature, electrolyte composition/concentration, and alloy composition [1]. This work shows the effect of process time on corrosion resistance of 5052 aluminium alloy treated by plasma anodization in a borate electrolyte.

2. Experimental

Small substrates of 5052 aluminium (Al) alloy were submitted to plasma anodization in an electrolytic solution prepared with distilled water and 10 g/l of borax ($Na_2B_4O_7$). The current density was kept around 20 Adm^{-2}, during the anodizations performed at 2, 4 and 8 min. Deposition rate was calculated by substrate masses measured before and right after each process. X-ray diffraction (XRD) was used to evaluate the chemical composition of the oxide films, and their corrosion resistance was determined from potentiodynamic polarization curves and electrochemical assays performed in a three-electrodes cell containing NaCl solution (3.5% weight).

3. Results and Discussions

Deposition rate was the same for processes of 2 and 4 min (0.15 mg/min), but it was the double that the previous one for 8 min-process. XRD spectra shows that oxide films are alumina (Al_2O_3), composed by α and γ phases. Process time looks important to development of the α-Al_2O_3, which is the predominant phase at 8 min-process. But, this phase seems no responsible by corrosion resistance of the samples. Better corrosion response was verified to substrate treated at 4 min. Probably, longer time of process induces defects in the oxide film structure, such as cracks that favor the substrate oxidation.

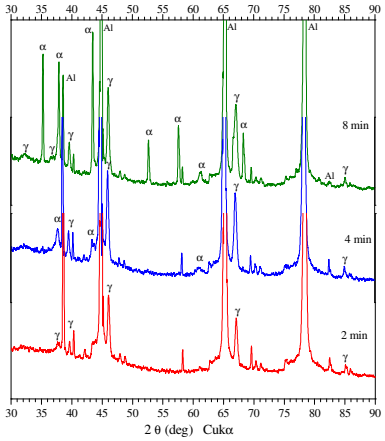

Fig. 1 – *XRD spectra of PEO films*

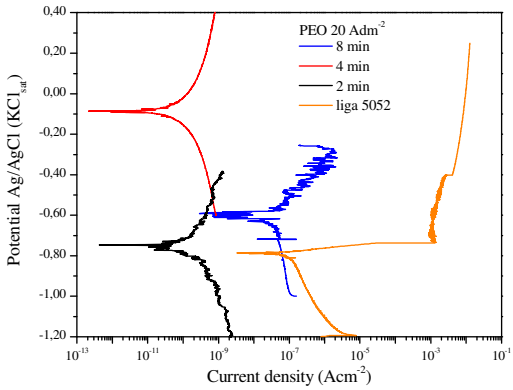

Fig. 2 – *Polarization curve of the PEO films.*

4. References

[1] Hussein, R.O.; Northwood, D.O. **Production of Anti-Corrosion Coatings on Light Alloys (Al, Mg, Ti) by Plasma-Electrolytic Oxidation (PEO). In** Developments in Corrosion Protection. Edited by Mahmood Aliofkhazraei. IntechOpen, February 20th 2014. DOI: 10.5772/57010. Available at https://www.intechopen.com/books/developments-in-corrosion-protection

Acknowledgments
The authors thank to FAPESP for financial support, UNESP-Sorocaba for MEV images, and INPE – S. J. Campos for XRD analysis.

*Corresponding author: deborah.santos@fatec.sp.gov.br

MODIFIED BATCH REACTOR FOR FURFURYL RESIN SYNTHESIS

Ana C. M. Gaspar[1], Carla S. Bordim[2] and Alvaro J. Damião[2]*
[1]*EEL-USP, Lorena, Brazil*
[2]*IEAv-DCTA, São José dos Campo, Brazil*

1. Introduction

Furfurilic resin is a thermoset polymer whose synthesis is made by the acid catalysis of furfurylic alcohol. This material is used as a polymeric precursor of monolithic glassy carbon (MGC). The MGC is obtained by vacuum carbonization of polymerized furfurylic resin [1,2]. Due to the existing difficulty in the synthesis reaction control (polycondensation), this work shows the implantation and evaluation of the new stainless steel reactor process, and also analyzes the process and product obtained by this new reactor. The reactor enabled more control of synthesis reaction and it brought more safety and easiness to the process. The viscosity depends on the final reaction temperature; the batch reactor allows stopping the reaction at the programmed temperature. Two temperature controllers were used in the control system. One controls the double jacket temperature, acting on the heating/cooling system; and the other measures the reactants temperature. The synthesis process starts with the double jacket cooling, when the programmed temperature is obtained. It finishes when the programmed final temperature is reached. As the synthesis reaction is extremely exothermic, water from an emergency tank is added to the inner part of the tank, by the control system in order to stop the reaction, if the reaction goes above 100 ºC. The final target is to produce MGC roughness patterns [3].

2. Experimental

The batch reactor operates in a non-continuous manner, with no inlet or outlet flow during the process. The reagents are charged to the top and withdrawn from the bottom of the reactor. A schematic view is presented in Figure 1. The reactor has double heating/cooling jackets. The process starts when the internal temperature reaches 32 ºC. The sulfuric acid is added to the furfurylic alcohol. Then, an exothermic reaction starts and itt stops when the temperature is diminished by introducing cooled water in the double jacket. The resin viscosity depends on the reaction's final temperature. Resins having final temperatures of 64 ºC, 65 ºC, 72 ºC and 100 ºC were produced. The viscosity was measured with a Brookfield DV-III + Pro viscometer. The reins were polymerized and carbonized at 1,000 ºC. Samples of MGC obtained after carbonization were characterized by the Archimedes test.

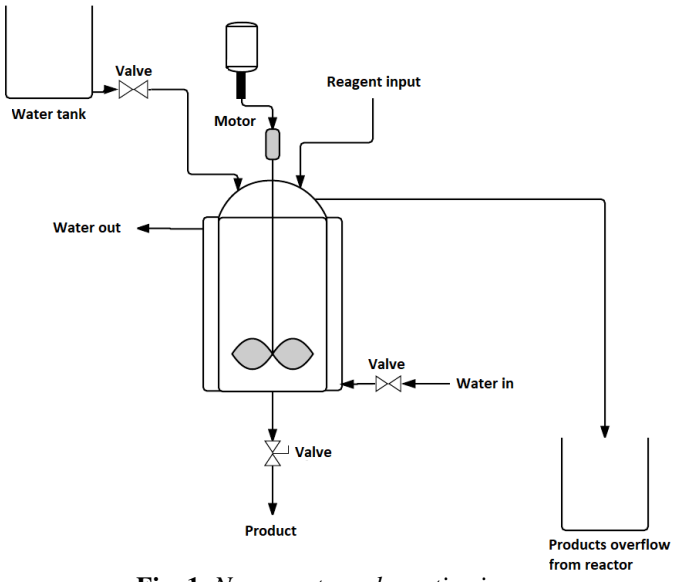

Fig. 1. *New reactor schematic view.*

3. Results and Discussions

The initial tests were done using water instead of alcohol. All the controls were tested. The viscosity showed a minimum between 65 ºC and 72 ºC. Lower viscosity is important in the next step, the polymerization, which depends on the catalyzer dispersion (p-toluenesulfonic, PTSA). The 65 ºC resin produced the lowest MGC porosity.

*Corresponding author: alvdamiao@terra.com.br

4. Conclusion

A metallic reactor was developed for the furfurylic resin synthesis. Resins having final temperatures of 64 ºC, 65 ºC, 72 ºC and 100 ºC were produced. The best resin viscosity and MGC porosity were obtained for the final synthesis temperature of 65 ºC.

5. References

[1] GAMA S., et al, PI 0403714-6 A. 2006.

[2] Nascimento, F., Carbono vítreo para aplicações em isolamento térmico. 2016. 113 p. Dissertação de mestrado em Física e Matemática Aplicadas – Instituto Tecnológico de Aeronáutica, São José dos Campos, São Paulo, 2016.

[3] Damião, et al, PI 0705155-7 A2, 2018.

*Corresponding author: alvdamiao@terra.com.br

COMPARATIVE STUDIES OF NITROGEN PIII AND PIII&D EXPERIMENTS USING TUBES OF SS304 AND TI6-AL4-V WITH 1.1 CM DIAMETER

M.Ueda[1], C. Silva[1], L. Pichon[2] and G.B. Souza[3]
[1]*Laboratório Associado de Plasma e Materiais, INPE, S.J.Campos, SP*
[2]*Université de Poitiers, Poitiers, France*
[3]*Universidade Estadual de Ponta Grossa, Ponta Grossa, PR*

1. Introduction

Surface modifications of the interior of metallic tubes using depositions of DLC and other films or ion implantations of different species, have become the subjects of much interest for research and developments, in recent years [1, 2]. Plasma Immersion Ion Implantation (PIII) and Deposition (PIII&D) treatments are the best options for those purposes when compared to the techniques of ion nitriding or ion beam implantation. These facts are impacting positively some parts of modern industries using tubes, as the pre-salt petroleum extraction sector, where more than 50 km of DLC coated segmented steel tubes are already being used in the explorations in the pre-salt fields of different countries. On the other hand, nitrogen PIII (N-PIII) has been shown to improve the mechanical, chemical, as well as tribological properties of the inside walls of SS304 and Ti6-Al4-V tubes [3]. Hence, a broad range of applications of PIII and PIII&D treatments in tubes are envisaged in pharmaceutical, chemical, defense, aerospace, medical and food industries. Therefore, researches on nitrogen implantation and film deposition inside metallic tubes are under way in our laboratory for some years, looking for high performance tubes to be used in such industries as well as for space use [4].

2. Experimental

In this work, comparative studies of two cases of N-PIII were made: one, inside an SS304 tube, and other inside Ti6-Al4-V tube. Both tubes were closed with a lid in one side and had a small internal diameter of 1.1 cm, a thickness of 2 mm and were 15 cm long. They were driven by a high power RUP-6 pulser (maximum nominal power of 12 kW), under similar optimized conditions of operations and pressures of 4 – $6x10^{-2}$ mbar.

3. Results and Discussions

For SS304 tube, the N-PIII treatment produced a reasonably thick (more than 1.5 µm) nitrogen rich layer consisting of Ti_2N and TiN, below FeO and CO depositions (Fig.1). On the other hand, for Ti6-Al4-V tube, a similar thickness nitrogen rich layer was obtained but a much thinner film deposition of Fe and C oxides was seen (Fig.2). Both the measurements of the elemental profiles by GDOES and the method of 2D – deposition on Si wafer targets detecting the plasma and sputtered materials expelled from the tube confirm this tendency. The resultant mechanical and tribological properties for these two cases will also be discussed in the presentation.

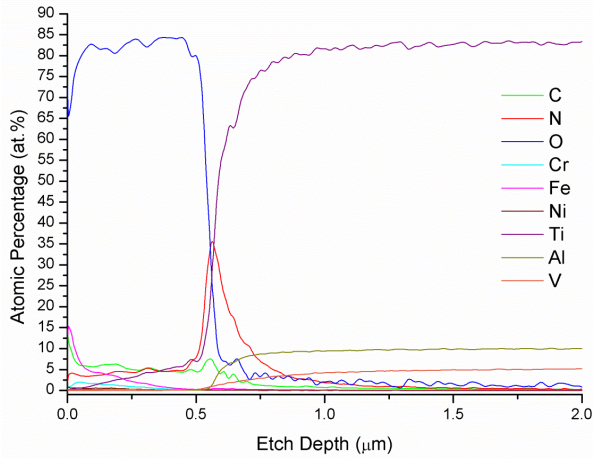

Fig. 1. *GDOES elemental profiles of TAV samples treated by PIII and PIII&D inside the SS304 tube of 1.1 cmØ, for 2h.*

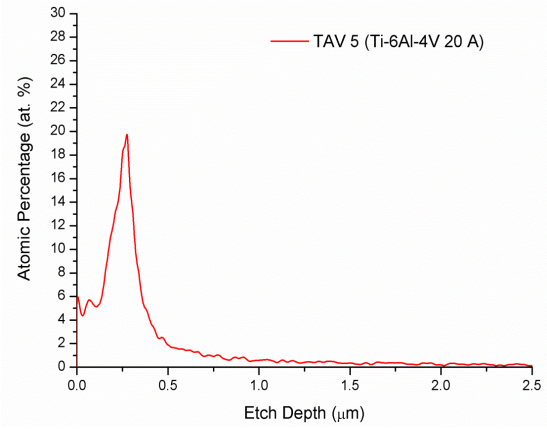

Fig. 2. *GDOES profiles of nitrogen implanted on the TAV sample treated by Nitrogen-PIII inside TAV tube of 1.1 cmØ, for 2h.*

*Corresponding author: mario.ueda@inpe.br

4. References

[1] R. Wei, C. Rincon, T.L. Booker, J.H. Arps, Surf. Coat. Technol. **188-189** (2004) 691.
[2] M. Ueda, C. Silva, N.M. Santos, G.B. Souza, Nuclear Instrum. Meth. B, **409** (2017) 202.
[3] M. Ueda, C. Silva, A.R. Marcondes, H. Reuther, G.B. Souza, accepted for publication in Surface and Coatings Technology, 2018.
[4] M. Ueda, A.R. Silva, E.J.D.M. Pillaca,S.F.M. Mariano, R.M. Oliveira, J.O. Rossi, C.M.Lepienski and L.Pichon, Rev. Sci. Instrum. **87** (2016) 013902.

Acknowledgments
Work supported by MCTIC, CNPq and CAPES.

*Corresponding author: mario.ueda@inpe.br

EFFECT OF THE GAS PRESSURE ON THE DISCHARGE POWER OF A HYBRID CORONA-DBD REACTOR

Alonso H. Ricci Castro* and Gilberto Petraconi Filho.
Technological Institute of Aeronautics, ITA,São Jose dos campos, SP-Brazil.

1. Introduction

The non-thermal cold plasma can be generated under different pressures and gas compositions. The choice of pressure and type of gas depend to the required applications and change the properties of plasma. The pressure influences the properties of plasma. Typically in a low pressure (0.01 mbar) glow discharge is observed ions energies around to 14.5 eV, but when the pressure was increase (0.07 mbar) that energies decrease to 3 eV [1]. However, the properties of plasma change when small drops of liquids are introduced. The plasma can break and ionize the molecular bonds on the surface and vaporize some droops [2]. The effect of introduce small drops of water on plasma can be enhance the production of activate radicals, which are capable of altering the surfaces of polymeric materials. The chemical reaction between the particulate of the gas phase and the area of the contact surface may have a reduced lifetime due to successive collisions of the gas particles that are acting on the surface.

2. Experimental Setup

The atmospheric pressure cold plasma is generated using a hybrid corona-dielectric barrier discharge. The reactor consists in two cylindrical electrodes with variable gap. The high voltage electrode is made from a metallic tube with 6.5 mm of external diameter and has a hole for entrance to different gases and liquids. The second electrode is grounded made from metallic tube with 140 mm of external diameter and covered by dielectric layer from alumina with 5.5 mm of thickness. This system can work with different pressure or gas nature. The power supply can operate with different voltage amplitude (1-35 kV), frequencies (1- 40 kHz) and wave signals. On this work, the voltage was fixed on 23 kV_{p-p} and the frequency on 23 kHz. The gap between two electrodes was fixed on 2 mm. The water vapor is generated using a commercial ultrasonic nebulizer. The size of atomized water have 5μm at a flow rate about 0,7 mL/min.

3. Results and Discussions

Figure 1 shows the variation of the discharge power as a function of pressure using air and steam as working gas. The discharge power evaluated by Lissajous method was lightly highest when the discharge operates with water vapor. This effect is related with the ionization of the surface of water drops increasing the conductivity of the gap.

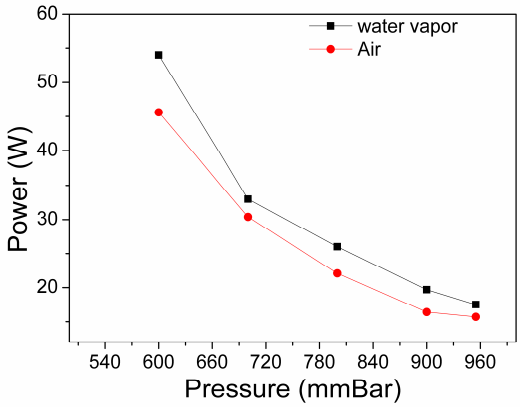

Fig. 1. *Variation of power on different pressure fixing voltage 23 kV, frequency: 23kHz and gap: 2mm.*

4. References

[1] Saboohi, Solmaz, et al. *"Comparison of plasma polymerization under collisional and collision-less pressure regimes."* The Journal of Physical Chemistry B 119.49 (2015): 15359-15369.

[2] Fanelli, Fiorenza, et al. *"Insights into the Atmospheric Pressure Plasma-Enhanced Chemical Vapor Deposition of Thin Films from Methyldisiloxane Precursors."* Plasma Processes and Polymers 9.11-12 (2012): 1132-1143.

Acknowledgments

The authors acknowledgement CNPq and FAPESP by the financial support.

*Corresponding author: Alonso_elfisico@yahoo.com

APPLICATION OF OXYGEN PLASMA IN THE CLEANING PROCESS OF TIO_2 NANOTUBES SYNTHESIZED BY ANODIZATION TECHNIQUE

R. C. Gonçalves[1], J. S. B. de Lima[2], A. S. S. Sobrinho[3], D. M. G. Leite[3], H. S. Maciel[2,3] and R. S. Pessoa[2,3]*
[1]*Universidade do Vale do Paraíba/Laboratório de Nanotecnologia e Processos a Plasma, 12244-000, São José dos Campos, Brazil.*
[2] *Instituto Científico e Tecnológico, Universidade Brasil, 08230-030, São Paulo, Brazil*
[3] *Centro de Ciência e Tecnologia de Plasmas e Materiais – PlasMat, Instituto Tecnológico de Aeronáutica, 12228-900, São José dos Campos, SP, Brazil.*

1. Introduction

Titanium dioxide (TiO_2) nanotubes have advantageous properties when compared to thin or bulk material due to their high surface area and high number of hydroxyl groups, opening a wide range of applications mainly in photocatalysis and biomedicine [1]. TiO_2 nanotubes are often synthesized on titanium foils by the anodizing technique. However, the chemicals used in the anodizing process generate impurities on the nanotubes which require a subsequent cleaning step [2].

2. Experimental

In this work, two cleaning processes were investigated: (1) using isopropanol, followed by acetone, and again of isopropanol in an ultrasonic bath for 10 min for each step; (2) using an oxygen plasma in continuous exposure, aiming to verify the efficiency of the plasma in cleaning of the contaminants after the anodizing process. TiO_2 nanotubes were grown by anodization process from Ti foil using aqueous and organic electrolytes containing fluorides (ethyleneglycol and NH_4F) at a voltage of 50V. For the study of the plasma cleaning process, a capacitive parallel plate reactor for the generation of an oxygen plasma was used. During the process the samples were placed on the electrode biased by a pulsed DC source. The treatments were performed in a discharge power of 400 W. For chemical and morphological characterization of the samples, FT-IR and SEM techniques were used.

3. Results and Discussion

Investigations were carried out on the effect of the type of cleaning process. It was observed from SEM micrographs (Figs 1 and 2) that the oxygen plasma cleaning process more efficiently removed the impurities of TiO_2 nanotubes although the chemical analysis showed close results for both processes.

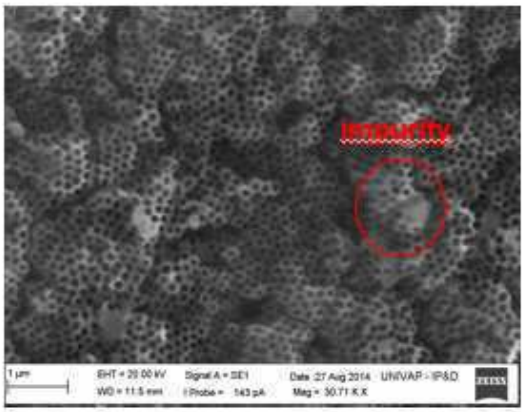

Fig. 1. *Micrograph of the TiO_2 nanotubes cleaned by chemical process.*

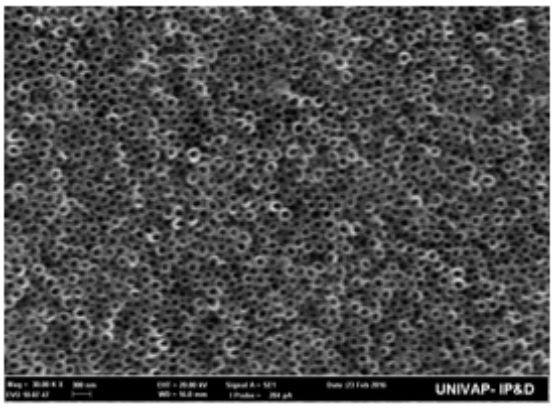

Fig. 2. *Micrograph of the TiO_2 nanotubes cleaned by oxygen plasma process.*

4. References

[1] R. S. Pessoa, M. A. Fraga, L. V. Santos, M. Massi, H. S. Maciel. Nanostructured thin films based on TiO_2 and/or SiC for use in photoelectrochemical cells: A review of the material characteristics, synthesis and recent applications. Materials Science in Semiconductor Processing, v. 29, p. 56-68, 2015.
[2] D. Regonini, C. R. Bowen, A. Jaroenworaluck, R. Stevens, A review of growth mechanism, structure and crystallinity of anodized TiO_2 nanotubes, Materials Science and Engineering: R: Reports v. 74, issue 12, p. 377–406, 2013.

Acknowledgments

R.S. Pessoa would like to acknowledge the financial support of FAPESP (grant nº 2018/01265-1).

*Corresponding author: rspessoa@ita.br

SUBSTRATE HEATING FOR SPUTTERING DEPOSITION SYSTEM

Angel Fidel Vilche Peña[1]*, Gleyson Tadeu de Almeida Santos, Silvio Rainho Teixeira and Agda Eunice de Souza Albas

Departamento de Física, Faculdade de Ciências e Tecnologia
Universidade Estadual Paulista UNESP

1. Introduction

The temperature of the substrate is of great importance parameter in the growth of thin films, whether for crystallization of deposited material, promotion of chemical reactions or simply giving the minimum heating necessary to promote the formation of the film, are some of the applications resulting from the heating of the substrate. Depending of the deposition system, a heater element normally utilized in thermal evaporation such as W, Ta or Mo is used [1]. Quartz lamps are also used when there is substrate rotation. The temperature control is done using a thermocouple or one optical pyrometer.

The older depositions system or the modern sputtering deposition systems with a simpler configuration do not incorporate a substrate heating system and this is the purpose of this work: to provide a minimum configuration in order to obtain a substrate heating necessary to obtain films of strontium titatane at temperatures greater than 300ºC needed to obtain a crystalline film.

2. Experimental

The sputtering deposition system Orion 5, has four windows available: two for observation, one for interfacing with a substrate exchange system in vacuum (with removable cover) and one available for other uses (with blind cover). For this work, the removable cover was replaced by a similar containing two water feedthroughs connected internally with a W spiral filament and a K-type thermocouple placed on a level above the filament in order to measure the temperature (Figure 1) under the following conditions : substrate without rotation and in contact with the tip of the thermocouple by touching the substrate (in this case the substrate movement is used). To obtain the film, the filament was heated by a high current transformer to heat the substrate-containing plate; this plate was thermally insulated from the original drive system by four ceramic insulators (with the substrate rotating to ensure uniformity in substrate heating.) From time to time, the rotation stops and the temperature is measured by lowering the substrate to the temperature where the current was decreased to just maintain the temperature in the desired range.

3. Results and Discussions

One strontium titanate film was prepared heating the substrate at a temperature slightly above 300 ° C. The substrate had a Ti deposition (200W DC, 20min) followed by a deposition of strontium Titanate (200W RF, 30min). The diffractogram is shown in figure 2.

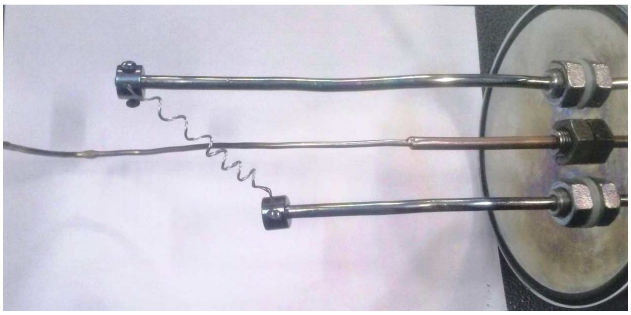

Fig. 1. *Cover of the deposition system of the sputtering deposition system showing the type K thermocouple and the two water cooled feedthroughs, connected to the W spiral filament.*

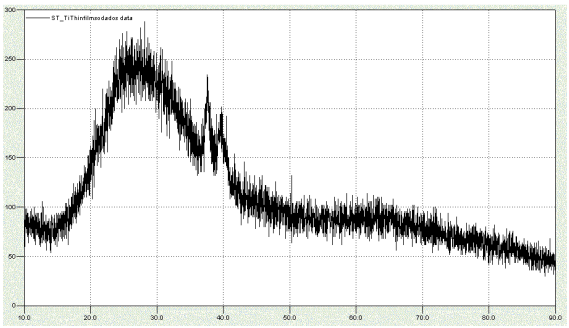

Fig. 2. *Diffractogram obtained from the strontium titanate film with the substrate heated at temperatures greater than 300 C, showing the two crystallization peaks.*

Films prepared with and without substrate heating are clearly different not only in crystallinity as shown in Figure 2, but in external appearance, yellow, when the substrate is heated and almost transparent when the substrate is at room temperature.

Using a previous calibration we can monitor the temperature of the substrate in a small temperature range. Fine adjustments in this system will come from the installation of an optical pyrometer in addition to a computerized controller to operate on the current transformer. The low cost of this proposal and the initial good results are the main attraction.

*Corresponding author: angel.pena@unesp.br

4. References

[1] F. Paulo Rouxinol; B. Cláudio Trasferetti; Richard Landers; Mário A. Bica de Moraes, J. Braz. Chem. Soc. vol.15 no.2 São Paulo Mar./Apr. 2004.

Acknowledgments

FAPESP 2013/07296-2 - CEPID - Centros de Pesquisa, Inovação e Difusão

*Corresponding author: angel.pena@unesp.br

SIMULATION AND ELECTRICAL CHARACTERIZATION OF SAW DEVICE

Júlio C. Faria da Silva[1], Newton A. S. Gomes[1], G. Osvaldo Dias[1], Douglas M. G. Leite[1], Marcos Massi[2] and Argemiro S. da S. Sobrinho[1]*

[1]*Technological Institute of Aeronautics-ITA, São Jose dos Campos, SP, Brazil*
[2]*Universidade Presbiteriana Mackenzie, São Paulo, SP, Brazil*

1. Introduction

SAW sensors are widely used in various applications such as telecommunication systems (mobile phones and various wireless devices), chemical sensors, biochemical sensors, gas sensors and biosensors [1, 2]. These devices can operate in dry or humid environments [2] covering a wide range of operating frequencies ranging from hundredths of hertz to hundreds of terahertz [3, 4]. These characteristics render SAW sensors applicable in various sectors of the economy, from home applications to the most sophisticated technological devices used in the automotive, aerospace and communication sectors.

The basic structure of a SAW device consists of a thin piezoelectric film deposited on a substrate and metallic contacts composing the so called interdigital transducers (IDT's) deposited on the piezoelectric film. An AC voltage applied on the film by the IDT's induce mechanical (acoustic) waves in the film (indirect piezoelectric effect) which, in turn, induces electrical current on the IDT's (direct piezoelectric effect). Both effects results in an electromechanical coupling creating mechanical waves, mainly on the surface of the piezoelectric film, which consists in the main property for the operation of the device.

In this work we have developed a model to simulate the wave propagation in a piezoelectric material (AlN) to evaluate the surface and bulk propagation of the wave along the film. We have also carried out the electrical characterizations of a first SAW device prototype consisting of AlN film with electrical contacts and IDT's obtained by Cr deposition.

2. Results and Discussions

The simulation model used to validate all the geometrical and physical parameters for the fabrication of the a SAW device was performed choosing the geometry of the IDT's sets, the definition of the piezoelectric material and the physical properties of the material represented by the electrical and mechanical matrices' coefficients. All these parameter was included in the COMSOL simulation program to obtain the acoustic wave propagation simulation on the surface of the SAW device. The simulated devices was performed considering a substrate of AlN films with thicknesses of 0.6 µm. Figure 1 shows COMSOL simulation for the time evolution of the wave propagation of the SAW device.

As expected, the results show that the waves have stronger intensity on the surface of the device and falls exponentially along the bulk. This decay is a very important condition for the good operation of this king of device.

Due to technical limitation in the confection of a photolithography mask the SAW device prototype was confectioned using a silkscreen mask limiting the width of IDTs in 55µm. The build device was then electrically characterized by measurement of the return loss (RL) and insertion loss (IL). Figure 2 shows the result for the intensity response of these signals as function of frequency.

The non-symmetrical value for the resonance frequency in each case is related to the difference in the impedance matching for each gate. Nevertheless, we could achieve a good level of electromechanical coupling (RL value around -27 dB) and we can see that device can operate as band pass filter with resonance frequency around 10 MHz.

It was developed a physical model to simulate the electromechanical properties of a SAW device. The model takes account of the geometrical (photolithographic patterns), mechanical and fundamental physical properties of the materials to clearly understand the operation of the device and validate the fabrication process. It was also characterized a first device prototype, the results showing a good level of electromechanical coupling and allowed to foresee an application as band pass filter.

For this first device prototype the photolithographic masks didn't have the resolution required and the patterns are larger than those we have simulated. Nevertheless, this problem is already surpassed by the fabrication of a high resolution masks and new devices are going to be fabricated in accordance with our simulations. Considering that we have already achieved good electromechanical results for our first low resolution device we can glimpse, promising high operation performance SAW devices to be applied as sensors and high resolution filters.

*Corresponding author: argemirosss@gmail.com

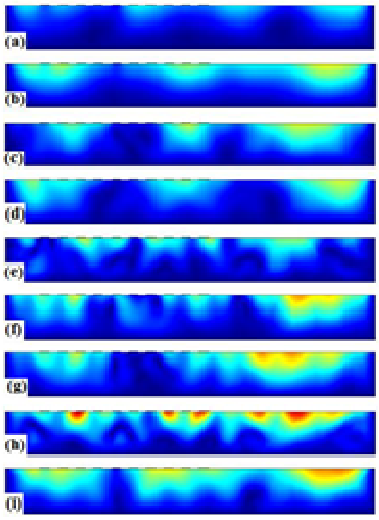

Fig. 2: *Cross section of a SAW device showing the time evolution of the wave propagation in an AlN film of 5 μm thickness. (a) t_i = 0 s, (i) t_f = 200 ns.*

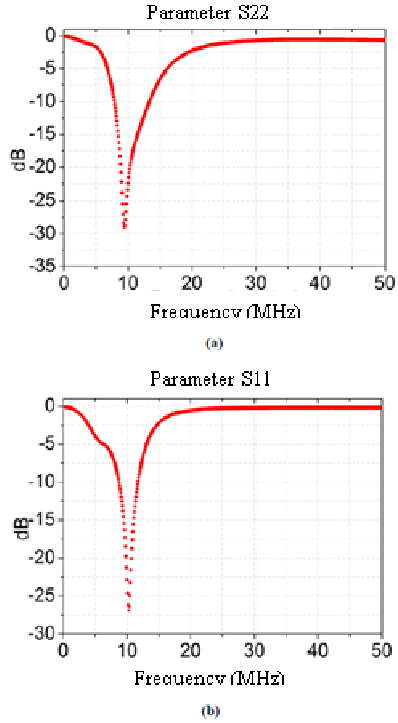

Fig. 3: *Return parameter for the input signal from the gate 2 on the gate 2 (a), f = 9.41 MHz; and the return parameter for input signal from the gate 1 reflected on the gate 1 (b), f = 10.24 MHz.*

References

[1] H. Pang et al., Phys. Status Solidi, 210(8) (2013) 1575.
[2] N. J. R. Muniraj and K. Sathesh, Elixir International Journal, (2011) 5138.
[3] R. M. White, International Frequency Control Symposium, Berkely: IEEE.,(1998) 587.
[4] D. S. Ballantine, Acoustic wave sensors: theory, desing and physico-chemical applications. London: Academic Press limited, (1997).

Acknowledgements

The authors acknowledge the CNPq and CAPES and FAPESP for the financial support.

*Corresponding author: argemirosss@gmail.com

AN ANALYTICAL APPROACH TO THE ELECTRIC POTENTIAL OF A CLEAVED SPHEROIDAL CONDUCTIVE DROPLET ON A DIELECTRIC SUBSTRATE

Luis H. F. C. de Mello[1] and Cesar J. B. Pagan[1]*
[1] *School of Electrical and Computer Engineering of UNICAMP, Campinas SP, Brazil*

1. Introduction

For many systems, film growth depends on how the electric field attracts or repels the chemical components in the vicinity of condensed particles, although much of what happens in the process is still unknown [1]. To contribute with this analysis, we propose a simplified analytic model for the electric potential of a charged conductive droplet on a dielectric substrate, picturing the droplet as an oblate spheroid horizontally cleaved at a certain distance from the substrate plane. We begin with the solution of the Laplace equation in spheroidal coordinates for the problem of an oblate spheroid in free space, summed with its dielectric image. Although at first glance, this method could not be used, given the cleavage of the spheroid and the superposition with its image, we treat such construction as an approximation, compensating the error by adding a monopole and dipole terms of a multipolar expansion, whose values are adjusted from a least-squares fitting of the results of the same problem when solved with a finite element method software simulation. The result is a parametric relationship that can be readily used to represent the droplet's electric potential.

2. Theory

We are interested in the electric field produced by a conductive droplet on a substrate during the process of growing a thin film as occurs in chemical vapour deposition technique. In the absence of external field sources, a charge q is supposed to be lying in the droplet, as a consequence of the chemical reactions preceding its formation.

The problem of a conductive spheroid in free space is solved with proper spheroidal coordinate system applied to Laplace equation with given boundary conditions [2]. In the presence of the dielectric substrate, the system loses the symmetry and the new geometry should be considered. If the spheroid did not touch the substrate, the method of electrostatic images should be enough to solve the problem, but this is not the case in a film growth reactor: we should consider a droplet that is deposited on the substrate. In this work, we have done this by picturing a cleaved spheroid to represent the droplet, that is, a spheroid where the intersection with the semi-infinite space that represents the substrate is excluded from its body (figure 1). We are interested in the vacuum region.

Our approach to solving this system is to use the image method as if there wasn't an intersection between the spheroid and the surface and the spheroid did not penetrate in the substrate. To mitigate the difference from this model with the exact solution, we add a correction as the sum of a monopole and a dipole terms, placed in the symmetry axis at the surface of the substrate. The values of such terms are found by least-squares fitting of a numerical solution obtained by the COMSOL® finite element method software. The final solution is then the sum of the field produced by the spheroid with its electrostatic image in the substrate plus the adjusted monopole and dipole terms. Once calculated for a usable range of values (the spheroid's flattening f and its normalized height h from the substrate), a semi-empirical numerical relationship is produced that can avoid considerable computational time in numerical simulations.

3. Results and Discussions

The problem depends on the aspect ratio of the spheroid, that means that is linear with q and depends only on the ratios a/b and h/a (or h/b). It also depends on the dielectric constant ε_r. Instead of consider a charge q in the droplet, we started with the equivalent (and more manageable) problem of a droplet with a fixed potential on its surface. Once we suppose that the problem is linear, we choose the value of 1 volt for the surface of the droplet. In our simulations with COMSOL®, we obtained the values for monopole q_k and dipole p_k terms for a number of combinations of f, h and ε_r. One example is shown in figure 2, where we have a comparison for a potential plot from our model (continuous lines) and the COMSOL® simulation. The proximity of the curves is better in the vicinity of the spheroid and, in general, the agreement for electric potential values are better than 0.1 V in all points except in a small region in the z axis, slightly above the droplet.

From a practical point of view, our model should be tested to evaluate if it is good enough for most requirements in film-growth simulations in CVD reactors. The work is still being done and we hope to find better results with the inclusion of higher-order multipolar correction terms and also through other approaches under consideration.

*cesarpagan@fee.unicamp.br

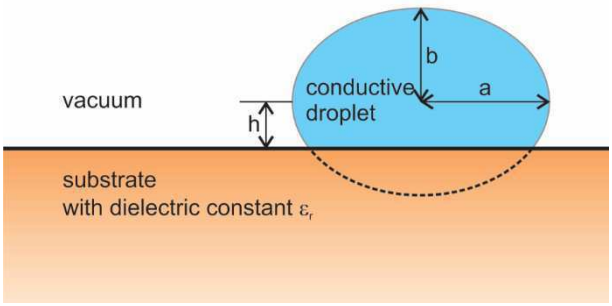

Fig. 1. *A cleaved droplet on a dielectric substrate. The droplet is a spheroid with semi-axes a and b. The distance from the center to the substrate is h. In our model, the substrate is a semi-infinite space. The origin of the coordinate system coincides with the center of the original spheroid.*

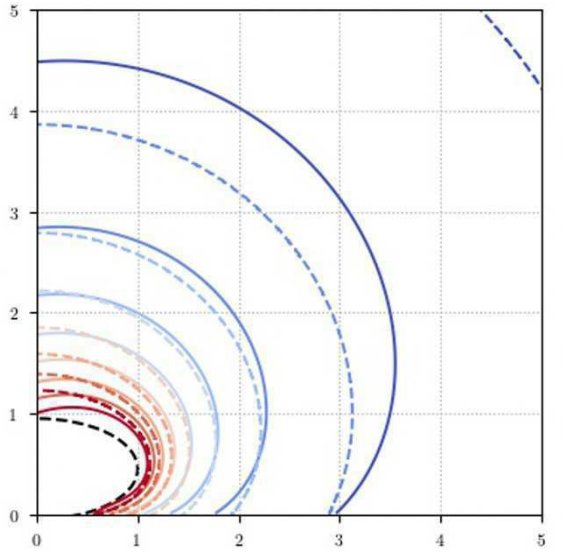

Fig. 2. *Comparison of potential between our model (continuous lines) and simulated by COMSOL® (dashed lines). In this system* $f = 0.5$ *and* $\bar{h} = 0.9$ *and* $\varepsilon_r = 4.2$. *The potential for the surface is 1 V and lines are plotted in steps of 0.1 V.*

4. References

[1] M.E.A. Warwick, L.-M. Romero-Nunez, A.J.T. Naik and R. Binions, 7.08 - Electric Field–Assisted Chemical Vapor Deposition for Nanostructured Thin Films, In Comprehensive Materials Processing, edited by Saleem Hashmi, Gilmar Ferreira Batalha, Chester J. Van Tyne and Bekir Yilbas, Elsevier, Oxford, 2014, Pages 171-190, doi.org/10.1016/b978-0-08-096532-1.00704-4.

[2] See, for example, Stratton, J. A., Electromagnetic Theory. New York: John Wiley & Sons, 2007.

Acknowledgements

We wish to acknowledge the financial support received for this work from Coordenação de Aperfeiçoamento de Pessoal de Nível Superior (CAPES), Brazil.

*cesarpagan@fee.unicamp.br

Ti6Al4V SURFACE'S ROUGHNESS AND AREA CHANGES BY CONTROLLING CHEMICAL ETCHING TEMPERATURE

Charles Jourdan Alberti[1], Danieli Aparecida Pereira Reis[2,3] and Adriano Gonçalves dos Reis[1*]
[1]*Universidade Estadual Paulista (Unesp), Instituto de Ciência e Tecnologia, São José dos Campos-SP Brazil*
[2]*Universidade Federal de São Paulo (UNIFESP), São José dos Campos-SP, Brazil*
[3]*Instituto Tecnológico de Aeronáutica, São José dos Campos-SP, Brazil*

1. Introduction

Titanium and its alloys have been widely used as implants in dental and orthophedic area due to their mechanical properties and biocompatibility. Many methods have been used to modify surfaces to enhance tissue repair events, such as chemical etching. Nanopits can be created on commercially pure Ti and Ti6Al4V by etching with an aqueous mixture of H_2SO_4 and H_2O_2 and has been showed beneficial effects on both short-term and long-term osteogenic events in vitro [1-4]. Treatment time can affect the morphological and physicochemical characteristics of the nanoporous surface created by this chemical oxidative patterning [1]. Otherwise, it is still not known if treatment temperature can also affect these properties, and the objective of this work is to evaluate if the treatment temperature can be used to control the surface's roughness and area changes of Ti6Al4V.

2. Experimental

Ti6Al4V samples of 20x20x2 mm were mechanically polished to a mirror finish by using SiC grinding paper, then diamond past, and finally a suspension of SiO_2. The polished samples were then cleaned with acetone in an ultrasonic bath for 20 min and finally dried in air. The piranha solution used for etching was prepared by carefully adding pure (95-98%, equivalent to 36N) H_2SO_4 to an equal volume of 30% aqueous H_2O_2. Polished Ti6Al4V samples were immersed in freshly prepared solutions and etched during 30 minutes at three different temperatures: 25 °C, 40 °C and 60 °C, thereby defining three different conditions for physicochemical analysis (plus the original untreated polished samples as controls). After etching was stopped, the samples were rinsed with distilled water, cleaned further with acetone in an ultrasonic bath for 20 min, and subsequently dried in air. Surfaces of etched samples and untreated controls were examined by using an optical profilometer Veeco Wyko NT1100 to evaluate the surface's roughness and area changes in an area of 229.2 x 301.3 µm.

3. Results and Discussions

A quantitative analysis of surface's root mean square (RMS) roughness and area changes, based on the profilometer topographies, are shown in the Figures 1 and 2, respectively.

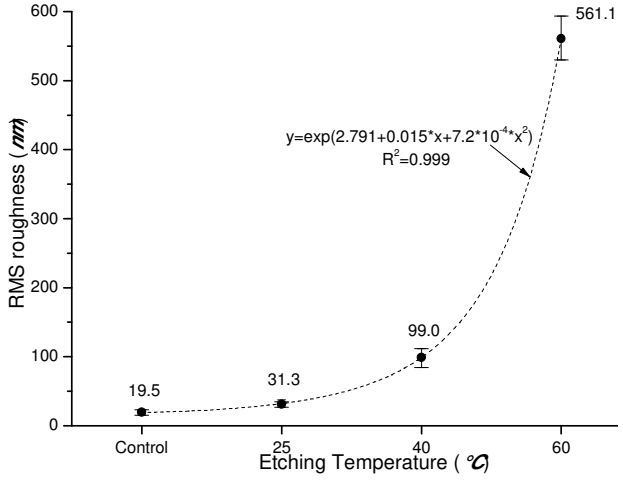

Fig. 1. *Ti6Al4V RMS surface's roughness changes as a function of etching temperature.*

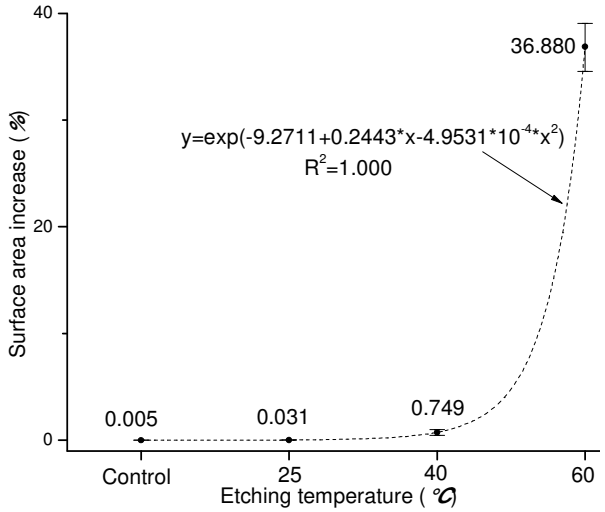

Fig. 2. *Ti6Al4V surface's area changes as a function of etching temperature.*

From Figures 1 and 2 it can be noted that increasing the etching temperature led to an exponential increase in the surface's roughness and area, respectively. The peaks and valleys generated due to increased roughness provided a larger surface area than a completely flat surface. Increasing the surface area increased the area of contact between the metal and bone cells, improving the conditions for osseointegration [5-6].

*adriano.reis@ict.unesp.br

Therefore, surface's roughness and area can be tailored by modifying the temperature of the chemical etching.

4. References

[1] J-H. Yi; C. Bernard; F. Variola; S.F. Zalzal; J.D. Wuest; F. Rosei, Surf. Sci., **600**, 4613-4621, (2006).
[2] F. Variola; J-H. Yi; L. Richert; D. Wuest, F. Rosei; A. Nanci, Biom., **29**,1285-98, (2008).
[3] P.T. de Oliveira; S.F. Zalzal; M.M. Beloti; A.L. Rosa; A. Nancy, J. Biomed. Mater. Res. A, **80A-3**, 554-564, (2007).
[4] A.L. Rosa; R.B. Kato; L.M. Castro Raucci; L.N. Teixeira; F.S. de Oliveira; L.S. Bellesini; P.T. de Oliveira; M.Q. Hassan; M.M. Beloti, J. Cell. Biochem., **115**, 540-548, (2014).
[5] A. Wennerberg; C. Hallgren; C. Johansson; S. Danelli, Clin. Oral Implants Res., **9**, 11-19, (1998).
[6] P.M. Brett; J. Harle; V. Salih; R. Mihoc; I. Olsen; F.H. Jones, Bone, **35**, 124-133, (2004).

Acknowledgments

This work was supported by CNPq (Proc.nº 403070/2016-3) and FAPESP.

*adriano.reis@ict.unesp.br

ISOTHERMAL OXIDATION BEHAVIOR OF THERMAL BARRIER COATING IN Ti-6Al-4V

Filipe Estevão de Freitas[1*], Adriano Gonçalves dos Reis[2] and Danieli Aparecida Pereira Reis[1,3]
[1]*Universidade Federal de São Paulo (UNIFESP), São José dos Campos-SP, Brazil*
[2]*Universidade Estadual Paulista (Unesp), Instituto de Ciência e Tecnologia, São José dos Campos-SP Brazil*
[3]*Instituto Tecnológico de Aeronáutica, São José dos Campos-SP, Brazil*

1. Introduction

Ti-6Al-4V alloy have wide use in aeronautical components due to high specific strength and relative high temperature resistance [1]. Air plasma spray (APS) yttria-stabilized zirconia (YSZ) of thermal barrier coating systems (TBC) increases the operational lifetime of turbine blades and allows higher operating temperatures [2], which it is related to the oxidation resistance provided by the coating [3]. In this work, isothermal oxidation of plasma sprayed YSZ thermal barrier coating in equiaxed Ti-6Al-4V was evaluated by thermogravimetric analysis at 600 ºC.

2. Experimental

Ti-6Al-4V specimens were commercially acquired and cut into disks of diameter 5 mm and thickness 3 mm. Firstly, NiCrAlY (Bond Coat Amdry 962) metal powder with a particle size of 106 ± 53 μm was applied by APS on the substrate surface. Then, stabilized zirconia with 8% yttria (Top Coat Metco 204NS-G) powder with a particle size range of 125 ± 11 μm was applied by APS on the metallic bond coat. This processes were conducted using a commercial plasma spray system (Sulzer Metco 9M pistol, Sulzer Metco 9MP powder feeder and Praxair PC-100 gas controller). Metallography and optical microscopy characterization (Zeiss, Axioscope A1) was used to analyze the TBC cross section.
Using thermogravimetric analysis (NETZSCH, TG 209 F1), isothermal oxidation at 600 ºC was performed in synthetic air (20% O_2 and 80% N_2) with flow and purge of 20 mL/min for about 7 hours.

3. Results and Discussions

Figure 1 shows the cross-sectional morphology of TBC as-sprayed sample. The achieved thickness of NiCrAlY bond coat was 140 ± 40 μm, whereas the thickness of YSZ ceramic top coat was 290 ± 40 μm. Figure 2 shows weight gain as a function of oxidation time of equiaxed Ti-6Al-4V with and without TBC. After 7 hours of isothermal oxidation, it is observed that the weight gain of coated sample was about 46% lower than the uncoated one. It is known that a thermally grown oxide (TGO) is formed along the interface between top coat and bond coat, which grows with longer oxidation times [4]. As the TGO layer grows, the stress profile changes in the top coat, leading to crack propagation and thus failure [5]. No visual failures were observed in the coating, probably because of the relatively short oxidation time. It was concluded that TBC was efficient to protect against oxidation.

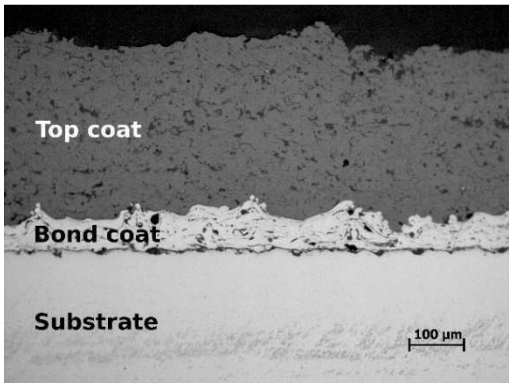

Fig. 1. *Cross-sectional morphology of TBC as-sprayed sample.*

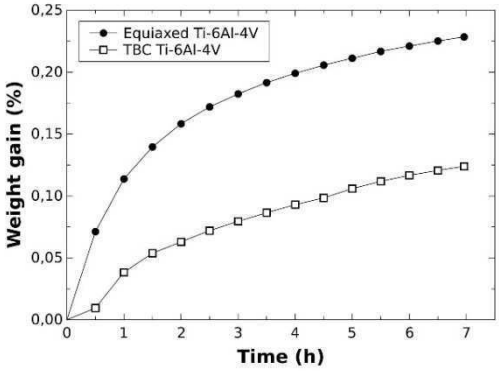

Fig. 2. *Weight gain as a function of oxidation time of equiaxed Ti-6Al-4V with and without TBC.*

4. References

[1] R. Sahoo, B. B. Jha, and T. K. Sahoo, Trans. Indian Inst. Met., **71**, 1573-1582, (2018).
[2] M. S. Sahith, G. Giridhara, and R. S. Kumar, Mater. Today Proc., **5**, 2746-2751, (2018).
[3] J. L. Smialek, B. J. Harder, and A. Garg, Surf. Coatings Technol., **285**, 77-86, (2016).
[4] S. Nath, I. Manna, and J. D. Majumdar, Corros. Sci., **88**, 10-22, (2014).
[5] M. Gupta, R. Eriksson, U. Sand, and P. Nylén, Surf. Coatings Technol., **271**, 181-191, (2015).

*Corresponding author: filipe.estevao@gmail.com

Acknowledgments
The author is grateful to the CAPES [grant numbers 1636393/2016] for the financial support and GE Celma (Petrópolis, Brazil) for plasma spray deposition.

*Corresponding author: filipe.estevao@gmail.com

LOW COST ACESSORY FOR ELECTROSPINNING FIBER ALIGNMENT

Armando Iwao Shimahara[1], Walter Pichi Jr.[1], Ana Neilde Rodrigues da Silva*[1,2] and Maria Lúcia Pereira da Silva[1,2]

[1]*Faculty of Technology of Sao Paulo, CPS, Brazil*
[2]*Polythecnic School, University of Sao Paulo, Brazil*

1. Introduction

More and more earlier, due to the complexity of the modern world, undergraduate students are exposed to complex concepts, such as nanotechnology. However, this knowledge rarely is obtained by experimental route since the required experiments, as a rule, use research equipment [1]. Thus, the development of low cost devices should be a primary concern not only on research but also on education. Furthermore, small devices add portability to setups and should also be a target.

Electrospinning is a simple way of producing, among others, nanofibers, for using from medical purposes to environmental protection, nanowires for sensing developing, fiber mats etc. For sensors improvement, in special on detection limit, fibers alignment is a crucial issue and can be done using moving parts on the electrodes [2]. Therefore, it was the aim of this work to project, manufacture and test a small device for fiber alignment.

2. Experimental

This work uses the common rules for project and manufacturing of electronic and mechanical devices. The boundary conditions were the use of parts and pieces: 1) commercially off-the-shelf, i.e. easily purchased and 2) although reliable, of low cost. After the manufacturing of the prototype, tests were carried out using tachometer, to determine radial velocity of the electrode, and nanofibers were deposited, to evaluate alignment, using a setup described elsewhere [2]. Main results were checked upon simulation of the electromagnetic fields using FemLab® program. Reagents were purchased from Sigma Aldrich®. A 6% w/w solution of polyacrylonitrile (PAN) dissolved in dimethylformamide (DMF) was used in the electrospinning process in order to evaluate the prototype performance and fibers alignment. Optical microscopy was carried out to evaluate fiber alignment and morphology.

3. Results and Discussions

The prototype consisted of two separated elements, mechanical and electrical pieces, respectively, as can be seen in Figure 1. The mechanical part is composed by one aluminum cylindrical electrode with 140mm high and external diameter of 25 mm. This electrode is attached to a fan cooler (GC®; dimensions: 40x40x10; 12 V; 5500 rpm) that had its encapsulation removed. The electrical connection is provided by a metallic brush and this set is packed in a plastic box (120X80X55 mm) in order to keep electrical isolation and to guarantee that only the aluminum cylindrical electrode is grounded during the electrospinning whereas the box is in a floating potential. Figure 2 shows the simulations; since the electrical field orients the fiber formation, a grounded electrode that shows a more density of parallel streamlines probably will also tend to orient the mat formation, although acute edges create small disturbance (Figure 2A). Furthermore, there are meaningful differences among a bare electrode (Figure 2A) and the one that shows the beginning of the mat formation (Figure 2B); on such case, the density of streamlines is unbalanced, which could hinder fiber orientation.

The electrical part consists on controller and power source (Figure 3). The power source is a commercial device (Showa®, 7 DC outputs, from 1.5 to 12 V, 1 A current) that was used at 12 V. The controller is composed of a potentiometer that split the voltage in two ways: a) powered the fan cooler and b) powered a voltmeter that is connected to a voltage divider that provide the voltage decay proportional to the powered fan cooler, in other words, the divider calibrates the measurement, which means the display result is actually the rotation (in rpm) obtained on the fan.

The estimated costs are approximately US$ 20.00 (R$80.00) for each element, not considering work man-hours, especially because is a do yourself project. Nonetheless, graduate persons can manufacture the prototype in less than 40 hours (excluding purchase).

Although the prototype has a nominal rotational velocity range of 0 to 7000 rpm, the system stability is better above 1000 rpm; thus the nominal range of 4000-7000 rpm was measured using tachometer and showed accuracy better than 20%.

*Corresponding author: neilde@lsi.usp.br

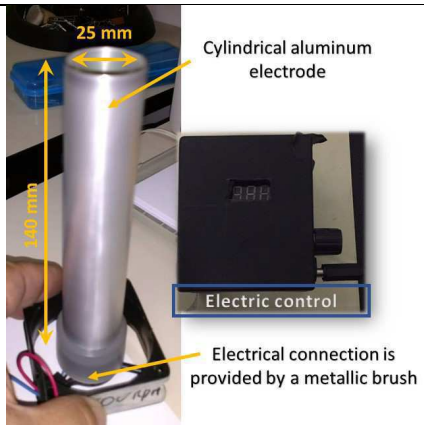

Fig. 1. *Disassembled prototype*

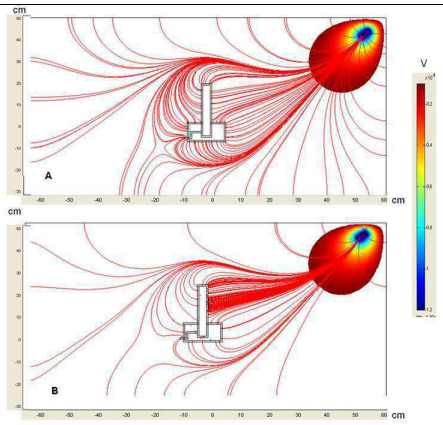

Fig. 2. *FemLab® simulations of a 115 mm exposed electrode to the environment: A – bare electrode and B- after the beginning of mat formation*

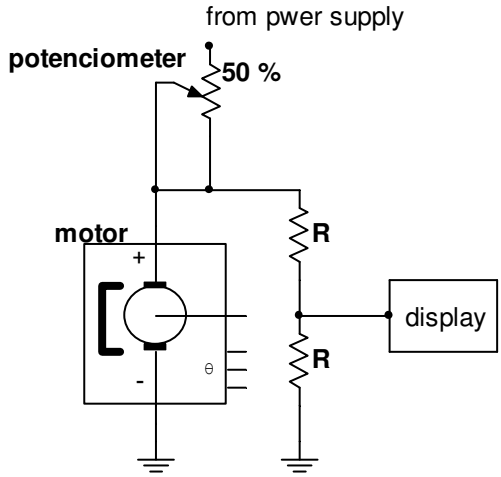

Fig. 3. *Electrical scheme*

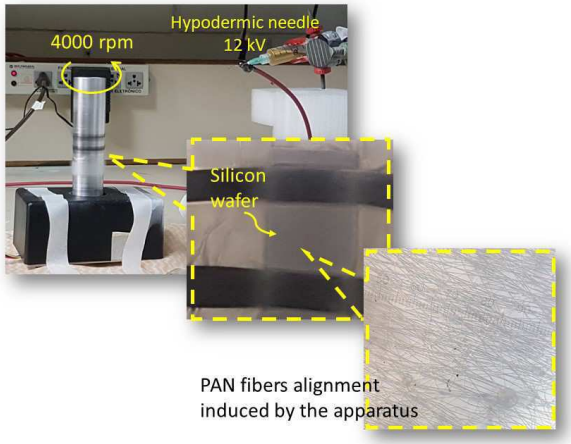

Fig. 4. *Alignment of the electrospun PAN fiber induced by the prototype.*

The nanofibers were electrospun using the prototype and different velocities were tested. The Figure 4 shows an optical image of the fibers electrospun with 12 kV and 4000 rpm. A preferential alignment is observed. More experiments should be done in order determine the best relation between the applied tension and the prototype rotation.

4. References

[1] M. Agarwal *et al.*, *2015 IEEE Frontiers in Education Conference (FIE)*, El Paso, TX, 1-5 (2015).
[2] R. Furlan et al. *32nd Symposium on Microelectronics Tech. and Devices (SBMicro)*, IEEE, 1-4 (2017)

Acknowledgments

FAPESP and CNPq for financial support.

*Corresponding author: neilde@lsi.usp.br

MICROFLUIDIC SETUP USEFUL FOR RESEARCH AND TEACHING

Luiz Fernando Pinto[1], Armando Iwao Shimahara[1] and Maria Lúcia Pereira da Silva[1,2]*
[1]*Faculty of Technology of SãoPaulo, CPS, Brazil*
[2]*School of Engineering, University of São Paulo, Brazil*

1. Introduction

Among the astonishing changes provoked by the microelectronic development on the last few decades some are really unsuspected, such as the appearance of new equipment and processes on Chemical Engineering and Chemistry. These new devices on processing required new setups, which led to the important role of microfluidic tools on the research today. On the other hand, one of this rising areas that is not well perceived is the Process Intensification (PI) of Chemical Engineering processes [1]; moreover, the actual dimensions of microfluidic setups/tools do not considering the needs of PI optimization, since the devices on this area are considered "big" (hundreds of microns or even a few centimeters) if compared to the conventional microfluidic dispositive. Another important issue is the price of such commercial microfluidic devices that, above all, tend to hinder undergraduate students to interact with these new concepts, equipment and tendencies [2]. Thus, the aim of this work was the development of a low cost microfluidic setup useful for research and teaching, especially on PI area.

2. Experimental

This work is based on project and manufacturing rules of mechanical devices. As a general rule, the work considered for al parts and pieces: 1) the purchase of only commercially off-the-shelf products, 2) easiness of assembly and disassembly parts and pieces; 3) reliability with low cost, 4) ability to carry out experiments on continuous flow using gas (air) or liquid (water) as fluids and 5) the use not only on undergraduate teaching but also as a research device, which means versatility and manipulation of small prototypes (mesostructures) mainly for surface analysis, respectively. These mesostructures were manufactured on acrylics, which allows the use of optical microscopy and tracers (mainly aqueous solution of aniline) to provide a better fluid analysis. Moreover, the mesostructures were also previously tested and represents the most common unit operations [3]. Reactants were PA grade and environmentally correct.

3. Results and Discussions

The manufactured dispositive is mainly composed of three different parts: a) base – where all parts and pieces of a modular setup can be assembled, b) the modular pieces and c) the diagnosis devices, which in this case are two optical digital microscopes, which means the photos are directly collected on a computer, with amplification up to 200X or 500X (VC68U, Akkord, USA). Whereas the 200X microscope is useful on contact angle measurements the 500X amplification one is more appropriate for microfluidic analysis of the mesostructures.

The base is composed of two parts: an aluminum recipient (approximately 1.0m length X 0.5m width X 5 cm height) and two drilled plastic pallets (0.5m length X 0.5m width X 2.5 cm height) disposed inside the aluminum container. Whereas the plastics pallets work as the holder for microfluidic setup, the aluminum device avoids that any leak of liquids during tests hits researcher or other equipment. Furthermore, the aluminum choice for the external container favors to ground any electric equipment used on the setup. Since the pallets are regularly potholed [4], it is possible to machine fastening pins (in this case PVC was used as material, just for economic considerations) for fixing the modular pieces.

The modular pieces are mainly: a) air compressor (for instance, Vigo Ar 300, Brazil) and water pump (for instance, Sarlo S300, Brazil) for carrying on the fluids; b) plastic recipients, for water and reactants storage; c) flow meters for air control and d) general connections, such as valves, usually used on medical care (Hartmann, Brazil). Aside these conventional pieces, two identical modules were machined for: a) support planar – as silicon wafers, or three-dimensional – for instance rough plastic material, samples and to allow changes on focus during the use of the microscope; b) support three-dimensional mesostructures; on that situation, the structures are attached to the module by the use of two flexible hooks, i.e., in a similar way of the "third hand" on a soldering electrical setup. On the other hand, on such conditions, the microscope will be held by its own support or the correct focus will not be achieved. Figures 1 and 2 show the assembly of both configurations; however, it worth noticing that, due to the need of stiffness, the modules are not interchangeable (i.e., the second module is not designed to be disassemble), but the microscopes can be.

The main achieved results are shown in Figures 3 and 4. Measurements of contact angle can be done with water or any reactant, even volatile ones, if a fume hood is used. Due to the area that the microscope can analyze, the sample thickness also is not a concern. The accuracy on this technique is quite dependent of the amount of liquid used to produce the drop; 1 μL drops can be recorded by the microscope on the maximum

*Corresponding author: malu@lsi.usp.br

amplification. Furthermore, several distinct drops size or reactants can be recorded simultaneously and as a function of time (video record), which favors the study of surface changes such as due to chemical reactions. The evaluation of fluidic behavior on microchannels as narrow as 100 µm can be easily done, even in three-dimensional structures; thus, several unit operations can be simulated on this setup. By the controlling of depth of focus, it is also possible to infer differences on fluidic behavior inside these channels.

In summary, considering that the whole set costs less than US$ 300.00 (R$1,000.00), not including labor costs, and also the shown capabilities, this setup is an useful way of carry out experiments on microfluidics and/or PI process not only on research but also on teaching.

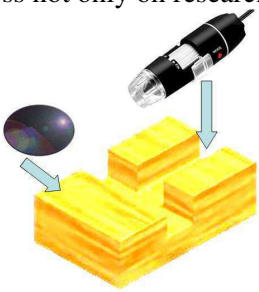

Fig. 1. *Module for contact angle measurement*

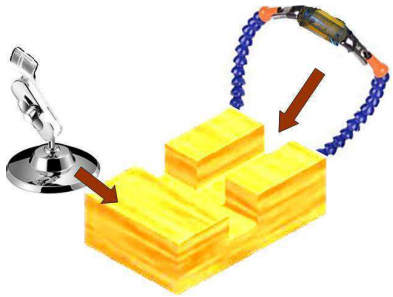

Fig. 2. *Module for microfluidic analysis*

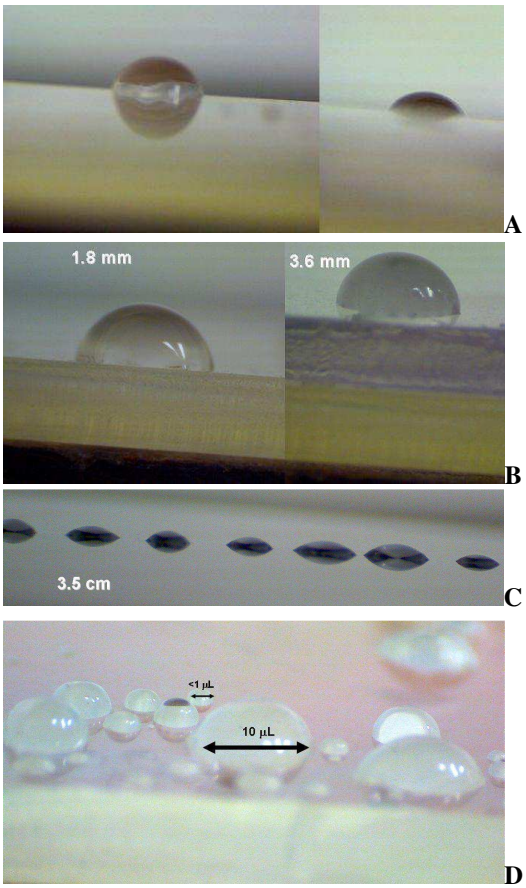

Fig. 3. *Contact angle measurement: A – drop nearest and farthest of the microscope; B – smooth and thin, rough and thick substrates; C - 10 drops reacting on the silicon surface and far from the microscope; D – different volumes of drop over a PVC substrate*

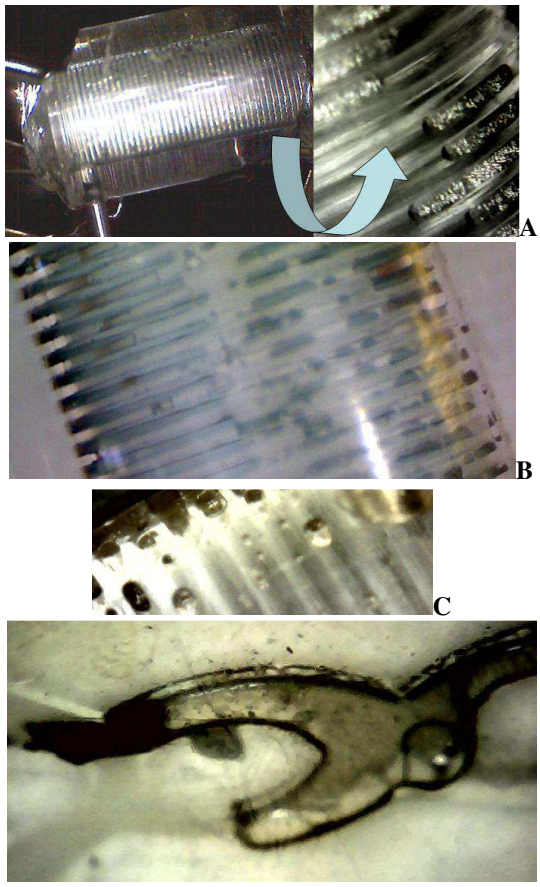

Fig. 4. *Microfluidic analysis: A – microstructure composed of 100 µm 3D-channel and detail of the it; B – glycerol tainted with dye on the microchannel; C – small drops of oil tainted with dye exiting the structure; D - planar structure filled with drops of tainted oil*

4. References

[1] N. M. Nikačević et al., Chem. Eng. and Processing: Process Intensification, **52**, 1-15 (2012).
[2] M. Agarwal et al., 2015 IEEE Frontiers in Education Conference (FIE), El Paso, TX, 1-5 (2015).
[3] M. L. P. Silva et al., 9th Int. Conference on Eng. Education, San Juan, 1-5 (2006).
[4] E.G., https://impallets.com.br/produtos/palete-de-plastico-modular-25x50x2-5cm-azul. Access July/2018

Acknowledgments

FAPESP and CNPq for financial support.

*Corresponding author: malu@lsi.usp.br

CORNBREAD TREATMENT USING DIELECTRIC BARRIER DISCHARGE TO IMPROVE THE WETTABILITY

Rogério Pinto Mota*[1], Denise Katharina Schlößer[2] and Alonso Hernan Ricci Castro[3].
*[1]*Faculty of Engineering, Campus Guaratinguetá (FEG), Sao Paulo State University (UNESP), Guaratinguetá, SP-Brazil,* [2]*Technical University Darmstadt, TUDa, Darmstadt, Germany,* [3]*Technological Institute of Aeronautics, ITA, São Jose dos Campos, SP-Brazil.*

1. Introduction

The atmospheric pressure plasma (APP) is a prominent technique to modify surface properties of different materials. The APP can be used on treatment of thermosensitive materials like polymers or cellular tissues [1]. Actually, it is possible generate APP using Corona Discharge, Plasma Jet and Dielectric Barrier Discharge (DBD). The DBD can treat samples homogeneously, operate with different types of gas, voltage amplitude and frequency [2]. The effect of plasma on polymers can change the surface wettability and this effect can improve the adhesion of cell, dyes and different types of glues. On this work we study the change on the wettability of cornbread after DBD plasma treatment.

2. Experimental Setup

The plasma was generated using a DBD and the reactor consists in two aluminum parallel electrodes, with 200 mm of diameter and 2 mm of thickness. The electrodes were coated by dielectric barrier (Mylar) with 1 mm of thickness. The space between dielectrics (Gap) was 3 mm. The DBD operated with sine signal voltage of 30 kV peak to peak and 60 kHz of frequency. The electrical characterization was made using capacitor (68 nF) and resistor (10 Ω), connected in series with the grounded electrode. The signal of charge and current on the resistor and capacitor was collected using oscilloscope TDS 3032 and prove Tektronix P2220. The high voltage signal was measure using a high voltage prove Tecktronix P6015A.

3. Results and Discussions

The effect of plasma on cornbread was measured using a water contact angle (WCA). The cornbread before treatment showed hydrophobic behavior with WCA close to 102°. Figure 1 shows the change on the wettability after treatment. It was possible to observe that after 1 minute of treatment with plasma the wettability of cornbread did not change too much and the WCA is stable close to 60°. The changes on the wettability of surface can be related with changes on the surface topography that was result of interaction plasma – surface. The interaction with plasma can be incorporate polar groups like O-H, C-O C-OH.

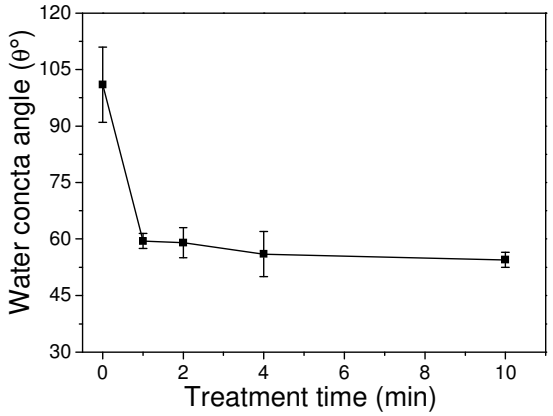

Fig. 1. *Water contact angle of corn leaves samples treated with plasma.*

4. References

[1] Penkov, O. V., Khadem, M., Lim, W. S., & Kim, D. E. *Journal of Coatings Technology and Research*, *12*(2), 225-235, 2015.
[2] Pankaj, S. K., Bueno-Ferrer, C., Misra, N. N., O'Neill, L., Jiménez, A., Bourke, P., & Cullen, P. J. *Innovative Food Science & Emerging Technologies*, *21*, 107-113, 2014.

Acknowledgments

The authors acknowledgement CAPES by the financial support.

*Corresponding author: rmota@feg.unesp.br

ANISOTROPIC OPTICAL PROPERTIES OF HIGHLY TEXTURED GAN AND ALN FILMS ELUCIDATED BY SPECTROSCOPIC ELLIPSOMETRY

D.M.G. Leite[1*], C. Stegemann[1], A.S. da Silva Sobrinho[1], A.L.J. Pereira[2] and M. Massi[3]
[1]*Technological Institute of Aeronautics, Plasmas and Processes Laboratory, São José dos Campos, SP, Brazil.*
[2]*Universidade Federal da Grande Dourados, Grupo de Pesquisa em Materiais Fotônicos e Energia Renovável (MaFER), Dourados, MS, Brazil.*
[3]*Mackenzie Presbyterian University, School of Engineering-PPGEMN, São Paulo, SP, Brazil.*

1. Introduction

Low temperature reactive sputtering is known to produce amorphous or nanocrystalline films with columnar microstructure aligned with the growth direction [1,2]. In the special case of wurtzite AlN and GaN, it is common to observe the coincidence of the crystallographic c-axis with the columns direction [3,4]. In this scenario, sputtered AlN and GaN films is likely to show interesting anisotropic behaviors, mainly those related to mechanical, electronic and optical properties. In this work, the anisotropic optical properties of highly textured sputtered GaN and AlN films are studied by Spectroscopic Ellipsometry (SE). By varying the incident angles from 30° to 80° it is expected to separate the in plane and out of plane contributions from the refractive index, Tauc gap and other optical constants.

2. Experimental

Representative GaN and AlN films were grown by planar reactive sputtering technique onto Si (100) substrates. Both films have wurtzite nanostructure highly textured with c-axis perpendicular to substrate surface as demonstrated by XRD experiments. The GaN films have been also characterized by high resolution TEM [3], which revealed its columnar nanostructure. These films were then submitted to ES experiments in a HORIBA Uvisel II ellipsometer. The spectra were obtained in the spectroscopic mode in the 0.6 to 6.0 eV energy range with fixed incident (and detection) angle at 35, 40, 50, 60, 70 and 80°. The outputs were then modeled by the DeltaPsi® software in order to calculate the refractive index dispersion and the optical gap in each situation.

3. Results and Discussions

As preliminary results, Fig. 1 and Fig. 2 show, respectively, the θ-2θ XRD pattern and the dispersions of the refractive index for different incident angles for an AlN sample. These and further results are discussed in terms of the intrinsic and extrinsic anisotropic responses of the wurtzite nanocolumns.

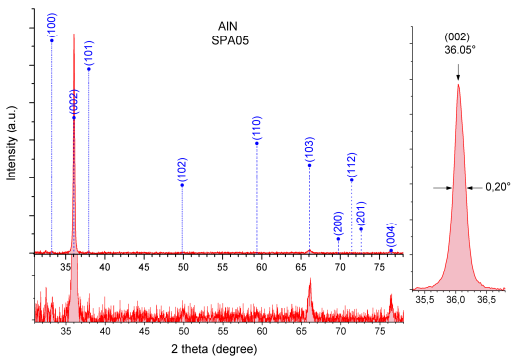

Fig. 1. *XRD patters of AlN sample (red curve) compared to the powder diffraction pattern (blue marking). The low intensity peaks (bottom) and the (002) peak (right) are shown in details.*

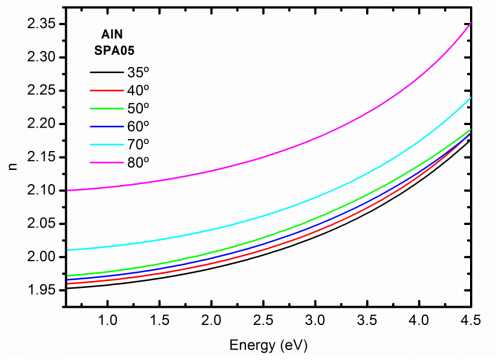

Fig. 2. *Refractive index dispersions obtained by SE at different incident angles.*

4. References

[1] D. L. Smith, *Thin Film Deposition: Principles and Practice*. Boston: McGraw-Hill Inc., 1995.
[2] D. Depla, *Magnetrons, reactive gases and sputtering*. Diederik Depla, 2013.
[3] D. M. G. Leite, et. al., *J. Cryst. Growth*, vol. 327, no. 1, pp. 209–214, 2011.
[4] V. Brien, et. al., *J. Cryst. Growth*, vol. 307, no. 1, pp. 245–252, 2007.

*Corresponding author: leite@ita.br

Acknowledgments
The authors thank the financial support of FAPESP (2015/06241-5), CAPES (88881.122156/2016-01), and FINEP (01.12.0485.00).

*Corresponding author: leite@ita.br

EFFECT OF PRESSURE ABOUT FACTOR B (P) FOR PLASMA GENERATED IN OPEN MICROHOLLOW CATHODE

Marcelo P. Gomes[1]*, Bogos N. Sismanoglu[1], Inácio M. Martin[1], Eduardo C. Aragão[1], Marcos A. Okamura[1] and Luis M. S. Costa[1]

[1]*Instituto Tecnológico de Aeronáutica* (*ITA*), *Departamento de Física, São José dos Campos, Brasil*

1. Introduction

In this work are presented the results obtained for the parameter $b(p)$ for argon plasma generated in open microhollow cathode (OMHC) and show what the effect of the pressure about it. This parameter is often used to describe the equilibrium state a plasma [1-3]. It indicates how the population of each excited state of the atomic state distribution function (ASDF) deviates from the local thermodynamic equilibrium (LTE), Being defined by: $b(p) = n(p) / n^s(p)$, Where $n(p)$ is the population of the excited level p and $n^s(p)$ is the population of the level p in Saha equilibrium. Through the values presented by parameter $b(p)$ it is possible to obtain information about the transport mechanisms of particles of the active region of the plasma. When, for example, $b(p) > 1$, the plasma is classified as ionization plasma, there will be a flow of particles out of the system. While for $b(p) < 1$ the plasma is classified as recombination plasma, there is a flow of particles into the system [4].

2. Experimental

The configurations of micro plasmas generators found in the literature, as well as the materials used in its fabrication are as different as possible. In the case of this work, the configuration chosen for the study of microplasmas was open microhollow cathode (OMHC), which is formed by a capacitor of plane-parallel plates with a dielectric (mica) between them and a hole diameter (diameter chosen: 250μm, 500μm and 1000μm), perforating the center of the plates along with the dielectric [5-6]. This device was powered by a high voltage source of direct current (DC). As electrodes, we used copper, molybdenum and tantalum to produce OMHC discharges. In relation to the experimental conditions, our microplasmas were generated in a gas mixture, Ar-H_2, for pressure range 90-800Torr. To perform the spectroscopic analysis we used a high-resolution optical spectrometer with a focal length of 1 m. Figure 1 show the reactor used to generate our micro discharges. Through relation 1 shown below, were determined population densities of the argon atom excited state, where was considered that the microplasma was at steady state. Intensities (I_k) of the spectral lines emitted by the argon plasma were measured with the aid of the spectroscope previously described.

$$n(p) = \frac{1}{hc} \sum_{k=1\ldots} \frac{I_k \lambda_k}{g_k A_k} \qquad 1$$

where, The summation indicates that the population of one excited level may be due to the contribution of several others. The index k in the summation indicates the levels that contribute to the population of the state $n(p)$. In our case, about 40 states were identified in the spectra of ArI, for the wavelength range of 4000Å to 8120Å. To determine the values of the factor $b(p)$ took the results of the distribution functions of the atomic states (ASDF) of ArI obtained in equation 1 and the values of $n^s(p)$ estimated by Saha distribution law.

3. Results and Discussions (bold face Times New Roman 11 pt)

From the results obtained for $b(p)$ it was concluded that the microplasmas generated in our open microhollow cathode are of the ionization type, mainly, for low pressure values. In ionization plasmas, the transport of charged particles occurs outside the system and the electron density is relatively low. The dominant improper balances in an ionization plasma are the corona balance (CB) and the excitation saturation balance (ESB). The first is related to process of producing a state via electronic collision with its respective destruction by radioactive decay. In relation to second balance, have that the production of a state is due to excitation of the lower level and its destruction with the excitation to the adjacent upper level. Taking into account the diameters of the holes and the pressure values, we have that the larger the hole diameter and the gas pressure inside the reactor, the faster the microplasma tends to local thermodynamic equilibrium. For the MHC with the 250μm hole only a few states reached the partial local Saha equilibrium when the gas pressure was 800Torr. In relation to the open MHC of 500μm, we verify that for the pressure value of 800Torr, Figure 2, practically all states belonging to tail of the ASDF of ArI presents the partial local Saha equilibrium (pLSE). Was for the microhollow cathode with the 1000μm hole diameter that the

*Corresponding author: gomesmpfis@yahoo.com.br

discharge evolved more quickly to the pLSE when the pressure was increased. For pressure of 400Torr several levels are on the eminency of reaching the pLSE

Fig. 1 *Discharge chamber and electrical measurements equipment's* [7].

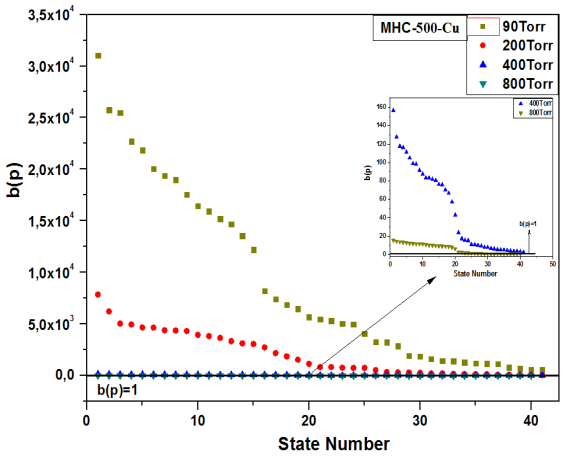

Fig. 2. *Factor $b(p)$ for generated plasmas open MHC of 500μm for different pressure values. For each excited state of the argon atom was assigned a number* (*State Number – see table 1*).

Table 1. *Partial list of energy levels of ArI.* ***S. N.*** *refers to the state number;* ***E*** *and* ***g*** *are the energy and statistical weight of the level respectively* [7].

S. N.	Paschen notation	E (eV)	g
1	1p0	0	1
2	1s5	11,548	5
3	1s4	11,624	3
4	1s3	11,723	1
5	1s2	11,828	3
6	2p10	12,907	3
7	2p9	13,076	7
8	2p8	13,095	5
⋮	⋮	⋮	⋮

4. References

[1] J. M. A. Mullen. Excitation equilibria in plasmas: A classification. Physics Reports, **191**, 109-220, (1990).

[2] K. T. A. L. Burn. Deviations from thermal equilibrium in plasmas. Physics Letters A, **328**, 489-492, (2004).

[3] M. D. Calzada, M. C. García, J. M. Luque and I. Santiago. Influence of the thermodynamic equilibrium state in the excitation of samples by a plasma at atmospheric pressure. Journal Applied Physics, **92**, 2269-2275, (2002).

[4] J. M. A. Mullen. Excitation equilibria in plasmas: a classification. 1986. 221f. Thesis (PhD in Engineering) – Technische Universiteit Eindhoven, Eindhoven.

[5] M. P. Gomes, B. N. Sismanoglu, J. Amorim. Characterization of microhollow cathode discharges. Brazilian Journal Physics, **39**, 25-30, (2009).

[6] B. N. Sismanoglu. Caracterização de microplasmas anulares e tubulares. Aplicação em microjatos de plasma. 2005. 163f. Tese (Mestrado em Física) – Instituto Tecnológico de Aeronáutica. São José dos Campos.

[7] M. P. Gomes. Microplasmas em equilíbrio de excitação. 2011. 214f. Tese (Doutorado em Física) – Instituto Tecnológico de Aeronáutica. São José dos Campos.

Acknowledgments

Thanks FAPESP, CNPq and CAPES by the fellowships grants support to the group's researchers. The ITA Division of Fundamental Sciences for supporting this research.

*Corresponding author: gomesmpfis@yahoo.com.br

WEARING RESISTANCE IMPROVEMENT OF STEEL ALLOY AISI 4140 BY PLASMA NITRIDING

F.C.Monção[1], A.Oliveira[2], G.V.Martins[3], A.S.da Silva Sobrinho[3], D.M.G.Leite[3] and M.Massi[1]
[1]*Mackenzie Presbyterian University, School of Engineering-PPGEMN, São Paulo, Brazil*
[2] *Federal University of São Paulo, ICT/UNIFESP, Brazil*
[3] *Technological Institute of Aeronautics, ITA/DCTA, Brazil*

1. Introduction

The wear fatigue of machines parts is always a challenge in the industrial sector, due to the demands of replacing parts of machines in a premature way. The main impacts of this are unscheduled machine downtime, productivity losses, delays in the shipment of products to customers and consequently, financial losses. According to Jost [1], between 1.0 and 1.4% of gross domestic product in an industrialized country can be saved by the introduction of best practices in tribology and for that, investments in research and development in tribology should be made. Surface Technology or Surface Engineering which is a subfield of Materials Engineering and Nanotechnology, has been placed in prominent position and has been attracted the interest of researchers in searching of a solution to the problem of low performance in tribological properties of materials. According to Bell [2], in Surface Engineering both traditional and innovative technologies can be used for the purpose of modifying properties of materials and according to Strafford and Subramanian [3] Surface Engineering encompasses all the techniques and processes used to induce, modify and improve the surface performance of materials. In this improvement, it is expected the increase in wearing resistance which can be presented in several ways, however in this study will be discussed wearing by the friction of sliding or rolling contacts that happen due to the fatigue of the contact between two parts. According to Ahmed [4], this phenomenon can be defined as a form of propagation of cracks caused by alternation.
In this context, plasma nitriding emerges as a feasible and efficient solution for steels surface hardening. This thermochemical treatment consists basically of the introduction of elemental nitrogen to the surface of the part and subsequently diffused into the metal in the core direction. This work aims to verify the influence of plasma nitriding on the surface of AISI 4140 steel parts, checking by appropriate characterization tests the changes occurred in the samples.

2. Experimental

Samples with 25 mm of diameter and 5 mm of thickness were machined from a drawn steel bar of AISI 4140 steel and the flat faces were sandpaper ground in a sequence with increasing mesh (#240, #320, #400, #600 and #1000) and then polished with diamond paste with abrasive size of 3 μm. From the same drawn steel bar of AISI 4140 steel, was taken a specimen in order to perform the test of chemical composition. For the plasma nitriding processes were defined the following fixed parameters: gas mixture 25%N_2 and 75%H_2, working pressure around 3Torr, pulsed voltage 300 to 450V and treatment time 3h. The variable parameter was the temperature which was set in three levels as follows: 500°C, 550°C and 600°C. Before start the plasma nitriding process was carry out the sputtering process on the samples for 45 minutes, with 40 sccm of argon gas and 40 sccm of hydrogen in order to clean up their surface removing all possible oxide layers. After the experiments of plasma nitriding, it was used appropriated characterization tests in order to identify the effects of plasma nitriding on the samples especially with respect to wear resistance.

3. Results and Discussions

The results of chemical composition test is under the specification as presented in Table 1.

Table 1. *Chemical Composition of the AISI 4140 steel*

Composição Química (%) (Chemical Analisys %)											
C	Mn	Si	P	S	Cr	Ni	Mo	Al	Cu	V	N
0.420	0.860	0.300	0.008	0.003	1.030	0.040	0.220		0.020	0.010	

Table 2 presents the roughness results and show clearly that the nitriding process increases the roughness.

*Corresponding author: massi.marcos@gmail.com

***Table 2**. Roughness test of samples surfaces before and after plasma nitriding*

Roughness test by Mitutoyo Roughness Digital Tester			
Before Plasma Nitriding		After Plasma Nitriding	
Ra	Rz	Ra	Rz
0,02==> 0,05	0,09 ==>0,29	0,14==> 0,25	0,71==>1,27

The sample surface roughness Ra measured by AFM in contact mode shows similar results in comparison to the Standard Digital Roughness (see Fig.1 and Table 3).

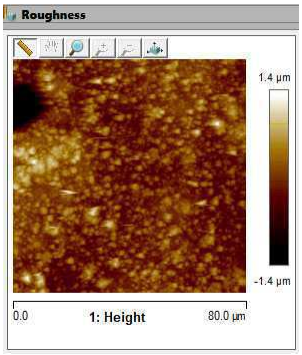

Fig. 1. *Sample surface*

Results	
Image Raw Mean	308 nm
Image Mean	0.0260 nm
Image Z Range	4183 nm
Image Surface Area	7102 µm²
Image Projected Surface Area	6400 µm²
Image Surface Area Difference	11.0 %
Image Rq	355 nm
Image Ra	240 nm

***Table 3**. Rughness Ra by AFM*

Microhardness samples surfaces comparing the hardness before and after the treatment of plasma nitriding it can be notice a significant increasing in the microhardness of samples after plasma nitriding. The increasing factor is between 2 and 2.5 times.

***Table 4.** Comparison of microhardness before and after plasma nitriding Microhardness load of 50g*

Microhardness (Core X Surface)		
Nitriding Temperature	Microhardness (HV)	
	Core	Surface
500 °C	308	649
550 °C	299	667
600 °C	305	759

4. References

[1] Jost, H.P.: Tribology micro & macro economics: A road to economic savings, Tribology and Lubrication -Technology, Vol. 61, No. 10, pp. 18-23, 2005.
[2] Bell, T., Surface engineering: past, present and future. Surface Engineering, 1990. 6(1): p. 31-40.).
[3] Strafford, K.N. and C. Subramanian, Surface engineering: an enabling technology for manufacturing industry. Journal of Materials Processing Technology, 1995. 53: p. 393-403.
[4] R.Ahmed: Rolling Contact Fatigue: Heriot-Watt University - United Kingdom, 2002.

Acknowledgments

The authors acknowledge the financial support of FAPESP (Grants 2011/50773-0) and CAPES (Grant 23038.005807/2014-11).

*Corresponding author: massi.marcos@gmail.com

DYNAMIC FRICTION COEFFICIENT MEASUREMENT TO POLYESTER RESIN COMPOSITES WHIT HOLLOW GLASS MICROSPHERES

[1]*Carlos Alberto Fonzar Pintão**, [2]*Airton Baggio*, [3]*Edgar Borali and* [4]*Lucas Pereira Piedade*
[1 2,3,4] *Physics Departament – FC – UNESP - 17033-360, SP, Brazil*

1. Introduction

Nowadays, the studies of tribology bring together knowledge acquired in physics, chemistry, mechanics, and material science to explain and predict the behavior of mechanical systems. These studies can be applied in several areas such as automotive, aerospace, electronics, biomedical and optics. The discovery and existence of new materials, with surfaces previously prepared for a specific function, has required that efforts have to be made in characterizing them physically [1]. Thus, in this work a tribometer rotary with spherical body against was constructed (Fig. 1) to determine the coefficient of dynamic friction (COF) and to characterize the effect of the inclusion of hollow glass microspheres in composites based on unsaturated polyester resin. This study of the COF will serve as a basis to compare what effect will have the addition of the microspheres in relation to the composites obtained in the traditional way.

2. Experimental

To measure the coefficient of dynamic friction, we use a tribometer rotary with spherical body against (diameter of 10 mm). The system for measuring tangential or friction force is a force sensor (*FS*) Pasco, which will be in contact with a rod. Because of the relative motion between the sample and body against, there will be the dynamic frictional force ($F_{FRICTION}$) that is transmitted to this rod in contact with the *FS*. Through an interface, a *FS* and a specific program from PASCO, one can register this force (F_S) in function of time (t). The measurement of this force can be accomplished within a time interval of 30 minutes. Distinct normal forces (N) are applied by the body against on the surface of the sample by gravity by changing the weights respective. For each pair of material (stainless steel 304 with hollow glass microspheres in composites of polyester) the curve of the coefficient of dynamic friction (COF or μ) as a function of time is determined. In this case it is possible to define the relation: $\mu = F_{FRICTION} / N = F_S \ f_C / N$. The parameter f_C is the calibration factor.

3. Results and Discussions

In the initial measurements of COF versus time it is observed that, for a Normal force of 2,04N, the effect of the glass hollow microspheres is present as we increase their amount. The value of the coefficient of dynamic friction changes from the value of the pure Resin to another of four times greater. The greater the amount of microspheres in the composite, the greater the wear effect of the composite and its COF.

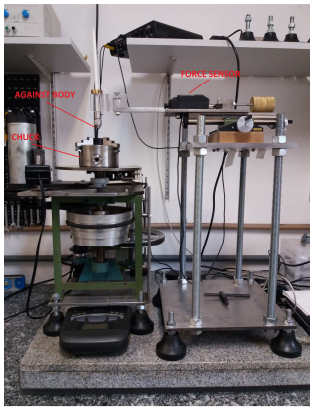

Fig. 1. *Rotary tribometer with spherical body*

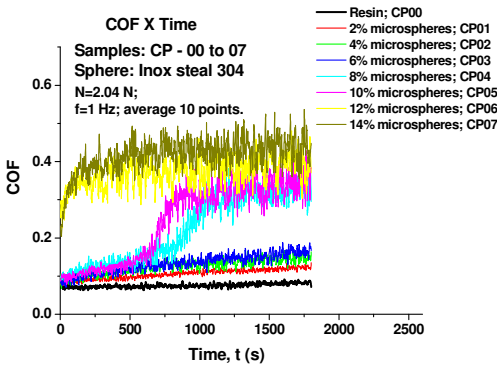

Fig. 2. *Results of COF versus time (stainless steel 304 and hollow glass microspheres in resin)*

4. References

[1] BROSTOW, W. et al. Tribology with enphasis on polymers: Friction, Scratch resistance and wear. Journal of Materials Education. v. 24 (4-6): 119-132, 2003.

Acknowledgments

The authors thank the Brazilian funding agencies, FAPESP, process number: 2007/04094-9, and Capes, process number: BEX 6571/14-0.

* Corresponding author: fonzar@fc.unesp.br

LASER WELDED DUAL PHASE STEELS: MICROSTRUCTURE AND MECHANICAL BEHAVIOR

Monalisa Bandeira Valentim[1], Rafael Humberto de Mota Siqueira[2] and Milton Sergio Fernandes de Lima[1]*
[1]*Photonics Division, Instituto de Estudos Avançados, São José dos Campos, SP, Brazil.*

1. Introduction

Automotive industries have been continuously substituting low C Mn steel with advanced high strength steels (AHSS) in order to fulfill the stringent demands for reducing fuel consummation and increase security of users. Among the possible steel classes, dual phase (DP) steels are extensively used in Brazilian industries, in particular in the security shell of the cars, including roof and pillars. The present contribution aims to investigate the laser weldabilty of DP 600 steels in terms of microstructural changes and mechanical behavior in order to provide a possible route for the mobility engineering projects.

2. Experimental

The studied alloy was a DP 600 steel in the form of 1.6 mm thick sheets and with composition Fe-0.010C-0.46Si-1.87Mn-0.0040N-0.017P-0.0031S. The compositions and tensile strength results were obtained from the Brazilian steelmaker Usiminas, as $\sigma_y = 420$ MPa, σ_{max}=630 and ε_{max} = 25% are the yield strength at 0.2% offset, tensile strength and maximum strain, respectively. The laser was an ytterbium-doped glass fiber laser (IPG, YLR-2000) with maximum power of 2000W. The beam delivery is carried out by a 100 µm internal diameter fiber. The laser beam focal position of 138 mm was fixed at the bottom of the sheets. A lateral tube delivered the gas shielding using pure argon at 8.5 l/min flux. The other parameters were welding speed 50 mm/s and power 1300W. The obtained welds were characterized by optical and scanning electron microscopy, microhardness and tensile strength.

3. Results and Discussion

Full penetration welds without pores or cracks had been obtained. The fusion zones (FZ) of DP600 steels were complex because of the rapid cooling. Bainite and martensite were the microconstituents of the welds. The heat affected zone (HAZ) presented refined microstructure compared to the fusion zone, because of the solid state diffusion kinetics. Martensite and ferrite were observed in different regions of the HAZ. In the partially transformed region, the microstructure was not so refined as the HAZ, but the amount of martensite is higher than HAZ because the temperature allowed full austenitization.

The hardness of the fusion zone was substantially higher than the base material, 360 HV compared to 200 HV due to the martensite transformation. Therefore, one possible issue of the coupons may be related to the local brittleness of the FZ. The tensile results shown that the tensile properties are similar for base material (BM) or Welded (W) coupons, as can be seen in Fig. 1 and Table 1.

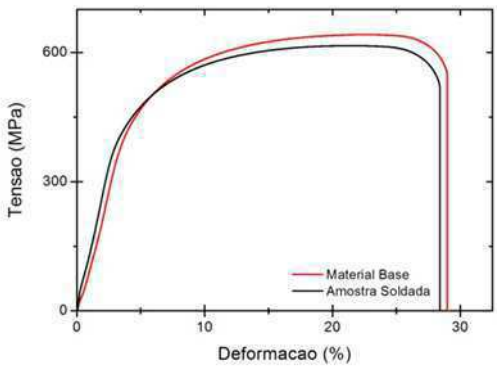

Fig. 1. *Tensile deformation curve comparing the base material (red) with the welded coupon (black).*

	σ_y (MPa)	σ_{max} (MPa)	ε_u (%)
BM	426 ± 57	642 ± 3	30 ± 1
W	360 ± 21	630 ± 12	26 ± 2

Table 1. *Comparison of mechanical behavior between BM and W conditions.*

In conclusion, the laser welded coupons could be classified as a DP 600, similarly to the bas material, since the maximum strain was kept above 600 MPa.

Acknowledgments

The authors acknowledge the financial support of the Usiminas company. Thanks are also due to Conselho Nacional de Desenvolvimento Científico e Tecnológico-CNPq (PIBIC 2017-2018) and Fundação de Amparo à Pesquisa do Estado de São Paulo-FAPESP (grant 2016/16683-8).

*Corresponding author: Miltonsflima@gmail.com

MICROSTRUCTURAL EVOLUTION IN DISSMILAR CU(CR) – STAINLESS STEEL LASER WELDS

Sheila Medeiros de Carvalho[1]*, Rafael Humberto de Mota Siqueira[2] and Milton Sergio Fernandes de Lima[1]
[1]*Photonics Division, Instituto de Estudos Avançados, São José dos Campos, SP, Brazil.*

1. Introduction

Stainless steel and copper alloys joints are often applied in aerospace, marine and power industries where both high thermal and electrical conductivity (Cu) and corrosion resistance (steel) are required. Although the evident advantages, the weldability of these very dissimilar metals is a challenge due to differences in their physical properties, as well as the solutes heterogeneity [1, 2]. A given method to avoid the solidification cracks requires particular attention as well [3,4]. Usually, these cracks result from the combined effect of segregation of copper to the grain boundaries of steel and to the presence of residual stresses [5].

Magnabosco et al. [6] investigated three different welded joints produced by electron beam welding. The first joint was obtained between plates of copper C11000 and AISI 304L steel. The second joint was obtained between a plate of C11000 and AISI 304. The last one was obtained between a plate of copper C 18100 and AISI 316L. Due to the high thickness of the specimen 2 and 3, a two pass was chosen in order to solve the limited heat input issue. The first specimen did not reveal defects, but the other two showed porosity in the copper-rich phase and intergranular cracks at the interface between the fusion zone and the base stainless steel. This investigation demonstrated that this kind of welding can be very dependent on the strict control of process variables such as weld power, number of runs and weld speed.

The aim of this study is to investigate laser beam weld of copper C18200 and steel AISI 304 in the lap joint configuration for possible application in the space industry considering both microstructure and mechanical behavior.

2. Experimental

Sheets of copper class C18200 previously solution and aging heat treated (90 mm x 50 mm x 2.05 mm) and stainless steel AISI 304L (90 mm x 50 mm x 0.75 mm) were used as the start materials. Table 1 summarizes their measured chemical compositions.

Table 1. Chemical compositions of the starting materials (wt. %).

Material	Fe	C	Mn	Si	Cr	Ni
AISI 304	Bal.	0.07	2.00	0.75	17.5 - 19.5	8.0 - 10.5
Material	Cu	Cr	Fe	Zr	Zn	Ni
C18200	Bal.	0.704	0.02	0.072	0.032	0.005

An ytterbium fiber laser with 2kW power (IPG, Model YLR-2000) was used with a head focal distance of 160 mm and a tilt angle of 2°. The plates were polished with SiC paper grade 600. After. The samples were clamped in a lap-joint weld geometry. The focal spot with a diameter of 200 µm. All welded condition was obtained by a single-run 1 m/min speed. Pure Argon with 8.0 l/min flow were used as a protective gas for all the experiments using a rounded nozzle 3 mm behind the fusion zone.

The microstructures of the joints were observed using a light optical microscope ZEISS model Imager2m and a scanning electron microscope (SEM) modelMIRA3-TESCAN equipped with an energy-dispersive X-ray spectrometry (EDS) after standard grinding, polishing, and etching using a solution of iron chloride (5 vol.%. FeCl3 + 50 vol.%. HCl + 45 vol.%. H2O) for 10 seconds. A thermodynamics database FEDAT of ThermoCalc Software (Andersson et al. , 2002) was used to study the phase balance of the welds.

The tensile strengths of the joints were evaluated at room temperature using an Instron EMIC DL10000 machine at a cross-head speed of 1.0 mm/min. The Vickers hardness profiles with a load of 50 gf and indentation time of 10 s were generated across the transversal section of the weld bead.

3. Results and Discussions

Figure 3 shows macrographies of the welds cross sections for the conditions listed in Table 3. The keyhole, characterized by a vapor channel into the melt pool, could be clearly seen in all conditions. The aspect ratios, as the depth per the top diameter, did not change appreciably within the heat input range and are situated around 1.8. The melt depth situated between 0.6 and 0.7 mm.

As can be seen in Figure 3 the weld could be divided in two regions after etching, one light gray representing Fe-rich zone and a dark gray zone near to the Cu phase. Therefore, it could be foreseen a partial dissolution

*Corresponding author: Sheila_mcarvalho@yahoo.com.br

between the materials, but with limited chemical homogeneity in the fusion zone. The chemical heterogeneity has been expected since the welding speed (1 m/min) together with different liquid densities allow low dilution between Fe and Cu melts. In addition, as previously discussed, the Fe-Cu phase diagram presents a miscibility gap (Figure 1).

The time involved in homogenization is quite short due to the rapid solidification. Considering an average liquid bath of about 0.6 mm and the welding speed of 1 m/min, the laser interaction time was about 0.036 seconds. The homogenization will thus be incomplete, although Marangoni convection may occur, and the weld presents two distinctive regions, Cu-rich and Fe-rich. Those regions are clearly seen in Figure 1. During the miscibility gap period, a large range of possible micro-constituents may occur. After a period of an almost homogeneous liquid in a given region, a phase separation followed by secondary precipitation gave rise to second-phase decorated globules.

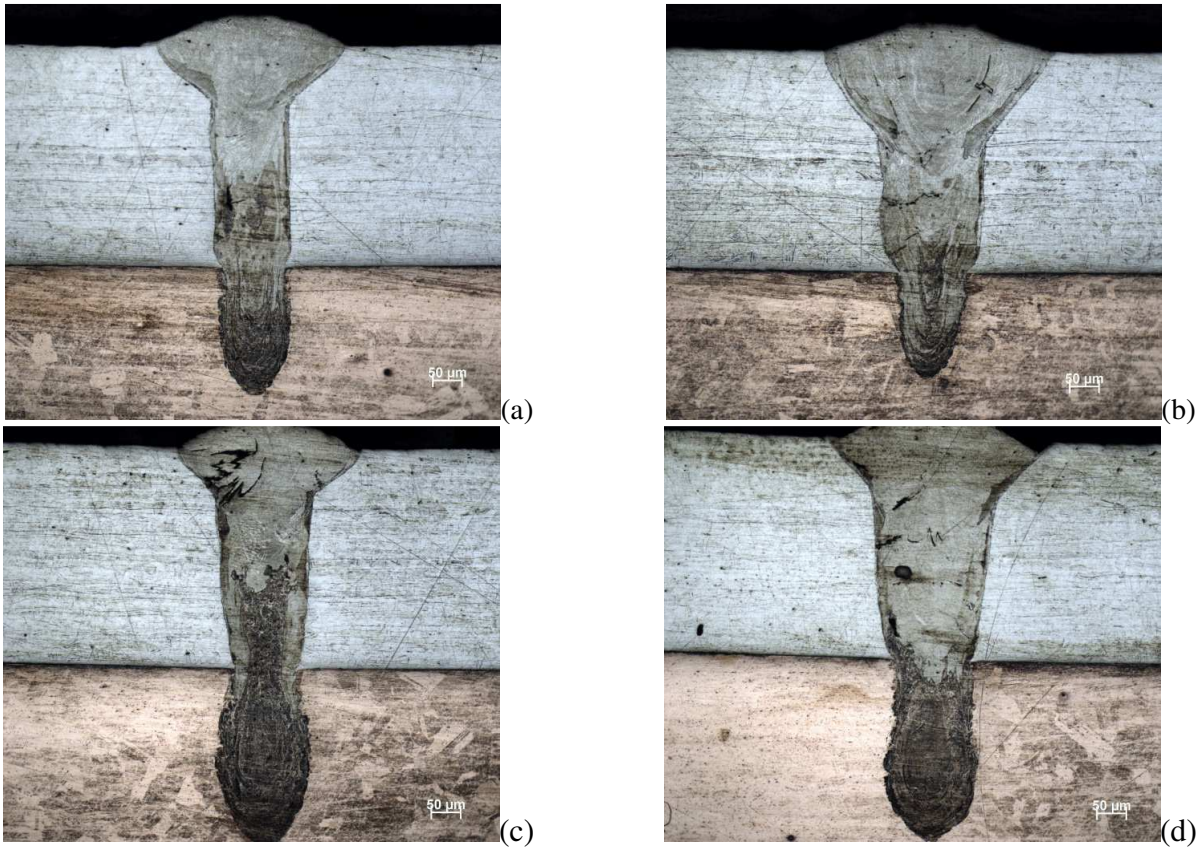

Fig. 1. *Copper –steel welded macrostructure by using laser focused on the steel surface with differents laser powers: (a) laser power of 1200 W; (b) laser power of 1400 W; (c) laser power of 1600 W and ; (d) laser power of 1800 W.*

In conclusion: A 0.75 mm thick 304 stainless steel sheet was successfully joined to a 2.05 mm thick C18200 copper bar using a fiber laser. The welds were produced with an intensity between 3.8×104 and 5.7×104 W/mm2 and a heat input between 72 and 108 J/mm, giving a aspect ratio of 1.8 and a melt depth between 0.6 and 0.7 mm. The microstructure of the weld beads is marked by chemical heterogeneities due to the phase separation between Cu and Fe in the liquid state. The phase separation gave rise to globular precipitates which further transforms due to a secondary precipitation.

4. References

[1] Z. Sun and J.C. Ion J. Materials Science **30**, 4205-4214, (1995).
[2] E.F. Nippes and D.J. Ball Welding J. **61**, 75s-81s, (1982).
[3] W.F. Savage at al. Welding Journal **57**,145s-152s, (1978).
[4] F.F. Noecker and J.N. DuPont, J. Mat. Sci. **42**, 510-521, (2007).
[5] S.J. Matthews and W.F. Savage Welding Journal **50**, 174s-182s, (1971).
[6] I. Magnabosco et al. Mater. Sci.Eng. A **424**, 163–173, (2006).

Acknowledgments

The authors thank Instituto de Aeronautica e Espaco (IAE) for providing the materials and the funding from Financiadora de Estudos e Projetos grant number 01.09.0546.05 – Strategic Materials Network.

*Corresponding author: Sheila_mcarvalho@yahoo.com.br

DLC COATINGS DEPOSITED ON GUITAR STRINGS

Santos, E.D.[1], Pessoa, R.S.[2], Galvão, N.K.A.M.[2] and Maciel, H.S.[2]
[1] *Centro Universitário de Volta Redonda (UNIFOA), Volta Redonda - RJ, Brazil*
[2] *Instituto de Tecnologia da Aeronáutica (ITA), São José dos Campos - SP, Brazil*

1. Introduction

Although Brazil presents well in the market of musical instruments, its position is not yet consolidated because the country was inserted late in this niche, which is led by the United States and Japan, countries that offer products of the highest quality [1]. Emerging countries such as China and India also represent a risk to the position achieved by Brazil, since they manufacture instruments at low costs and reasonable quality. Considering that Brazilian industry cannot compete in quality with market leaders, nor in price with emerging countries, the search for technologies capable of assigning innovative properties to national products has intensified, since this is the main elements to changing the dynamics of this market in favor of Brazil. Many of these researches focus on problems in guitar strings, such as the rust [2], the increased friction with the musician's fingers, and acute dermatitis due to injuries caused by rusted string [3]. The present research aims to solve these problems through the application of diamond-like carbon (DLC) coatings. Once coated, the surface of the string presents protective properties against oxidation process. In addition, it presents lubricant and antimicrobial properties that favor comfort during the use of the instrument. Moreover the ongoing deposition of piezoelectric thin film will be reported.

2. Experimental

The DLC coatings were prepared by methane plasma in a system Plasma Enhance Chemical Vapor Deposition (PECVD) in three steps: (I) guitar string was cleaned by argon plasma; (II) a silicon film was deposited on the samples; (III) subsequently, the DLC coating was deposited. The silicon interlayer was characterized by SEM-EDX and the DLC coating was characterized by Raman spectroscopy.

3. Results and Discussions

The EDX analyzes evidenced the peaks corresponding to the silicon interlayer (Fig. 1). The Raman spectrum showed a shift of the D band of 38 cm^{-1} for the left and of the G band of 46 cm^{-1} also for the left, demonstrating a graphitic phase hydrogenation ordering of about 20% (Fig. 2). In comparison with bare samples, the DLC coated sample showed a black color, that is typical of a film with more than 1 µm (Fig. 3).

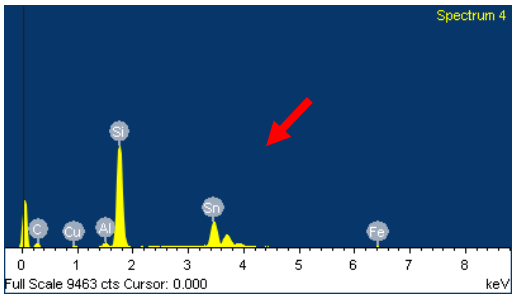

Fig. 1. *EDX spectrum of silicon (red arrow), and some elements that make up the substrate.*

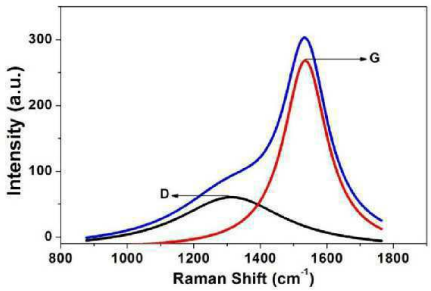

Fig. 2. *Raman spectrum of the DLC film.*

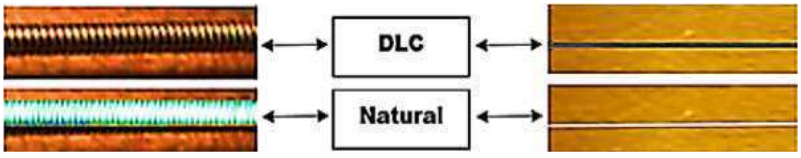

Fig. 3. *Observation of the samples, coated and uncoated, by naked eye.*

4. References

[1] Bezerra, D.R.P. Estratégias de marketing na entrada de empresas brasileiras no mercado internacional. 2009. Dissertação (Mestrado) — Pontifícia Universidade Católica de São Paulo.
[2] QUORA. My strings rust REALLY fast, anyone have the same problem? 2016. Available in: https://www.quora.com/How-do-you-stop-your-guitar-strings-from-rusting>. Access date: 07/2018.

*Corresponding author: odairtur@gmail.com

[3] Sheehan, M.P. Avocational Contact Dermatitis—Pearls for Recognition and Management. Current Treatment Options in Allergy, v. 2, n. 4, p. 322 – 332, Dec 2015. ISSN 2196-3053.

*Corresponding author: odairtur@gmail.com

BETTER ADHESION OF PDMS SAMPLES TREATED USING A PLASMA JET FROM A FOUR-ELECTRODES DBD DEVICE

Fellype do Nascimento[1]*, Munemasa Machida[2], Stanislav Moshkalev[1] and Konstantin Kostov[3]
[1]*Center for Semiconductor Components and Nanotechnologies, State University of Campinas, Campinas, SP, Brazil*
[2]*Institute of Physics "Gleb Wataghin", State University of Campinas, Campinas, SP, Brazil*
[3]*Faculty of Engineering, Sao Paulo State University, Guaratinguetá, Sao Paulo, Brazil*

1. Introduction

Atmospheric Pressure Plasmas (APP) have received considerable attention in recent years due to their versatility, easiness of operation and low cost of implementation compared to plasmas in vacuum environment, and Dielectric Barrier Discharge (DBD) is a kind of configuration commonly used to produce APP jets [1,2]. The use of APP jets to treat surfaces of a wide range of materials has been growing along the latest years, mainly due to the low temperatures of that kind of plasmas, which is important to avoid damages to the treated samples [3].

In a recent work, it was shown that a DBD device using a four-electrodes configuration is able to enhance the energy transfer when compared to a one-electrode configuration [4]. Then in this work we compared adhesion results of poly (dimethylsiloxane) (PDMS) treated with plasma jets from three different configurations: using a single-electrode DBD device and a multi-electrodes DBD device in one- and four-electrodes configuration. The results showed that the adhesion is practically the same when only one electrode is used. But there is a significative improvement in adhesion in the four-electrodes case.

2. Experimental set up

To allow a comparison of adhesion results between single- and multi-electrodes devices, the last one was mounted in two different configurations: in the first, only one electrode was kept in the device, placed at its center and, in the second, four electrodes were used, arranged at the vertices of a square. Fig. 1 shows the upper views of the arrangements used.

The production of plasma jets, in any configuration, is as follows: a continuous gas flow is injected inside the DBD devices and high-voltage pulses are applied to the electrode(s) inside the closed glass tube(s). Thus a primary discharge is formed in the region between the glass tube(s) and the device wall, producing a plasma jet that leaves the device through a gas outlet. It is important to note that in the four-electrodes configuration all the electrodes are connected in parallel, that is, the same high-voltage pulses are applied to all of them. Argon gas (4.8 purity) was used as the working gas in all cases.

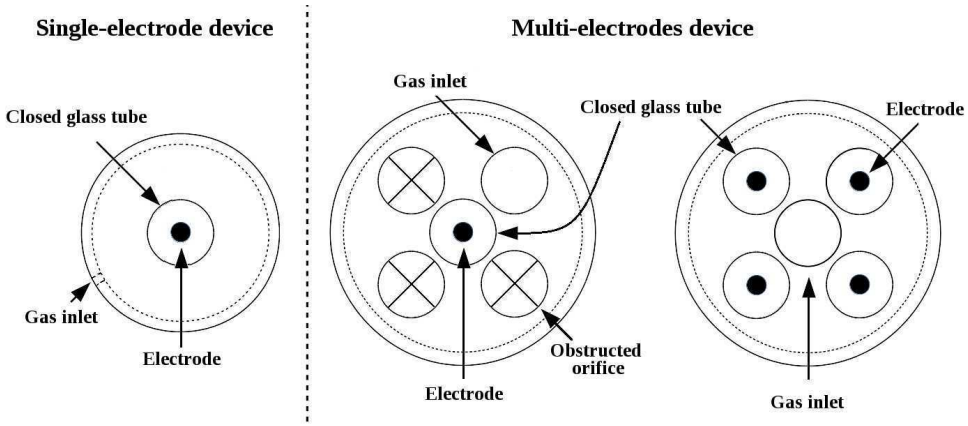

Fig. 1. *Upper views of the arrangements of the DBD devices used: Single-electrode (left), Multi-electrodes in one-electrode configuration (center) and four-electrodes configuration (right). Elements are out of scale.*

For the adhesion procedure between two similar PDMS samples, the surfaces of one side of both samples were exposed to plasma treatment for the same time interval. Then the treated surfaces were put in touch and pressed against each other immediately and, after this, they are allowed to cure for two days at room temperature. After this period, tests were conducted to measure the tensile strength supported by the adhesion between samples. The back sides of samples (that were not treated by plasma) were glued with an epoxy-based commercial adhesive to the heads of stainless steel screws of 15mm in diameter. Finally, the

*Corresponding author: fellype@gmail.com

adhesion was tested through the application of an increasing tensile force to the screws until samples detachment, indicating the adhesion failure.

3. Results and Discussion

Figure 2 shows the results obtained in the tests for measurements of adhesion quality in each of the configurations used for treatment of PDMS surfaces. The values of the tensile strengths shown if the figure are averaged values of five tests.

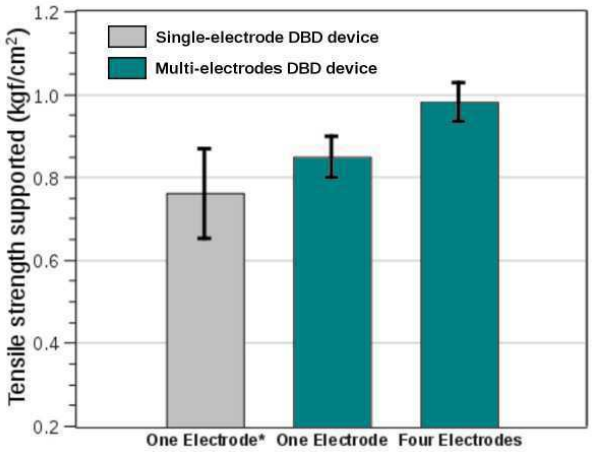

Fig. 2. *Averaged tensile strengths supported in adhesion tests between PDMS samples treated with DBD plasma jets in different configurations.*

As can be seen in Fig. 2, the tensile strengths supported by adhered samples are almost the same (within the uncertainties) when the treatment of PDMS samples were performed using plasma jets from the single-electrode device and the multi-electrodes device with only one electrode. But when the four-electrodes configuration is used, the tensile strength supported by adhered samples is increased by ~15%. The most likely reasons for the improvement in adhesion are the increases in both the power and the vibrational temperature of the plasma when in the four-electrodes configuration [4].

We can conclude that the enhancement in energy transfer obtained using the multi-electrodes device in a four-electrodes configuration also benefits the processing of materials.

Additional studies are being conducted in order to know the modifications in the PDMS surface morphology and chemistry using the multi-electrodes DBD device. There are also studies in progress to optimize the multi-electrodes device.

4. References

[1] X. Lu, G. V. Naidis, M. Laroussi, K. Ostrikov, Phys. Rep., **540**, 123, (2014)
[2] R. Brandenburg, Plasma Sources Sci. Technol., **26**, 053001, (2017)
[3] M. Bashir, J. M. Rees, S. Bashir, W. B. Zimmerman, Phys. Lett. A, **378**, 2395, (2014)
[4] F. Nascimento, M. Machida, K. Kostov, S. Moshkalev *et al*, Eur. Phys. J. D, **71**, 274, (2017)

Acknowledgments

This work was supported by CNPq and FAPESP.

*Corresponding author: fellype@gmail.com

THE GEOMETRY RATIO EFFECT OF PTFE SAMPLE ON THE TORSION MODULUS (G)

[1]Lucas Pereira Piedade, [2]Cesar Renato Foschini and [3]Carlos Alberto Fonzar Pintão*
[1 2,3] *Physics Departament – FC – UNESP - 17033-360, SP, Brazil*

1. Introduction

The modulus of elasticity is a measure of the rigidity of a material. It is an important parameter that is connected with the description of other mechanical properties, being the object of attention in Engineering. Traditionally, it is obtained by quasi-static methods, usually destructive (stress-strain curves), and dynamic methods in non-destructive techniques (ultrasound and vibrations). Measurements with alternative methods are appreciated because they are dynamic and non-destructive, and do not alter the physical and chemical properties of the sample, making it of great practical interest [1].

This research was carried out with the purpose of measuring the torsion modulus (G) of Polytetrafluoroethylene (PTFE), a versatile and highly requested engineering plastic on the market. Because it performs a specific structural function and is subject to mechanical stresses, it is important to know its torsion modulus. The main objective was to test the effects on modulus G by maintaining an L/D≥10 ratio for the equation that was derived from the study of mechanical spectroscopy and material resistance [2].

2. Experimental

Three PTFE samples with different circular sections D (5.10mm, 6.30mm and 8.20mm), and length L (53.55mm, 66.15mm and 86.1mm, respectively) were submitted to torsion. For this purpose, a measurement system with a rotational motion sensor coupled to a torsion pendulum, built in the Laboratory of Physical and Rheological Characterization - Department of Physics – Campus Bauru was used.

A torsion of 1.78 ° is applied at the end of the specimen attached to the pendulum and with the other fixed to a static base by means of an electromagnet. For four different inertias, the sample should oscillate freely until stops its movement. For a solid sample of circular section of radius R and length L, the equation of G is:

$$G = \frac{2}{\pi}\frac{L}{R^4} I\omega_0^2 \left(1-\frac{\delta^2}{4\pi^2}\right) \qquad (1)$$

Where, R, L, I, ω_0 and δ are the radius, length, moment of inertia, angular frequency and friction, respectively.

3. Results and Discussions

The values of the parameters δ and ω_0 are obtained from the relaxation curve, angular position (θ) versus time (t) (Figure 1), using the app Origin 7.0. It can be seen in Figure 2 that G is independent of the values of I. Keeping the L/D ratio ≥ 10 the values of G are practically the same considering the associated error. In literature [3], G values for PTFE are found within a range of 137 MPa to 616 MPa. The results obtained by this technique showed values of G within this range (mean value 335 MPa) for PTFE samples. Based on the presented results, maintaining a L/D≥10 ratio makes samples of different geometries present the same torsion rigidity values G, considering the associated error.

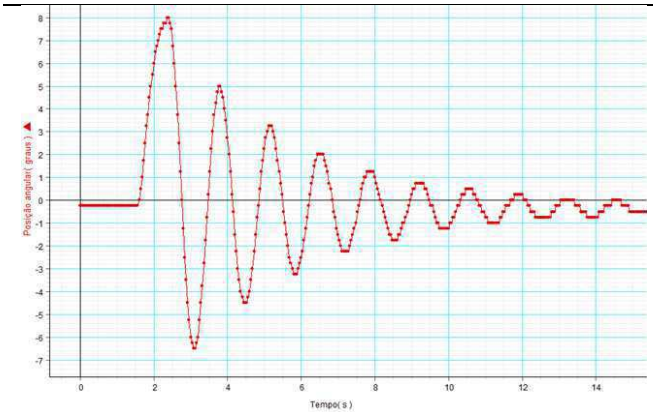

Fig. 1. *PTFE Relaxation Curve angular position (θ) versus time (t). The sample oscillates freely until stops its movement.*

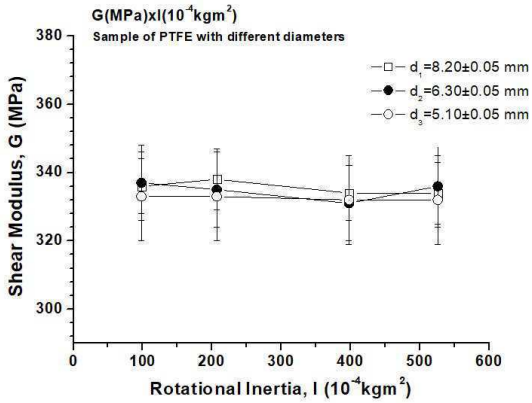

Fig. 2. *Experimental values of G as a function of I for PTFE samples.*

4. References

[1] C. A. F. Pintão et. al, Torsion modulus using the technique of mechanical spectroscopy in biomaterials, J. Mech. Sci. Tech. (Seoul. Print), 31 (5) (2017) 2203-2211

[2] A. S. Nowick and B. S. Berry, Anelastic relaxation in crystalline solids, Academic Press, New York (1972).

[3] W. D. Callister Jr, Materials Science and Engineering, 7th Edition, John Wiley & Sons Inc., USA (2007).

Acknowledgments

This work was supported by CAPES and FAPESP.

DEVELOPMENT, CHARACTERIZATION AND EVALUATION OF MECHANICAL PROPERTIES OF ALLOY AL-4CU-0.9SI-0.6MG-0.5MN-0.1FE FOR APPLICATIONS IN TURBOCHARGERS

Gilberto Vicente Prandi*, Renato Chaves Souza and Roberto Nunes Duarte
Federal Institute of Education, Science and Technology of São Paulo– Campus São João da Boa Vista

1. Introduction

One of the ways to get more power in combustion engines is to increase the amount of air and fuel in the combustion cameras by adding extra cylinders, or increasing the size of existing ones, both techniques would disqualify the popular cars, since this technique increases the fuel consumption and its weight, an alternative solution for this problem is the use of turbochargers. [2].

Turbochargers have been widely used in popular cars in order to provide greater power to the engine. However, this device was originally developed for aircraft, which used turbocharging to compensate the rarefaction of air at high altitudes, but it was noted, however that power increased, which popularized chargers in racecars in the years following the 1930s [1].

The turbocharger is composed of a centrifugal air compressor, directly connected to a centripetal turbine. A shaft supported by floating bearings placed in a central frame connects the compressor rotor and the turbine rotor. The centrifugal compressor consists of an aluminum frame and a rotor (cold part). A frame of different material, which must withstand very high temperatures, forms the centripetal turbine (hot part). Among the materials used for hot part are, Titanium, Inconel and steel. The central frame incorporates the diffuser plate, thrust bearing, collar, oil centrifuge, oil deflector, sealing rings, as well as axle and thrust bearings, see Fig.1. [3].

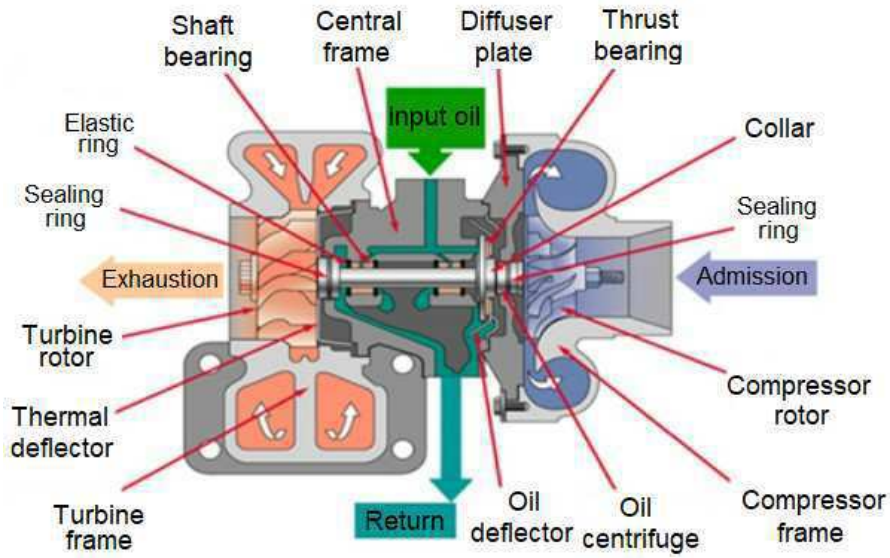

Fig.1 - *Face view of a turbocharger [4].*

Based on the above considerations, this work aims to determine, through laboratory tests and literary research, the physical, chemical and mechanical characteristics of aluminum alloy Al-4Cu-0.9Si-0.6Mg-0.5Mn-0.1Fe vacuum cast and thermally treated according to a previously raised aging curve.

2. Experimental

The elements of alloys and materials popularly used in the turbochargers industry were studied and the elemental alloy of study was produced, the composition was then melted by the partner company, it was used a method of vacuum casting, popularly used in this application. It generated through the foundry specimens similar to the final format to be experimented. Samples were also made for lifting the aging curve. Specimens with a final format similar to the ones tested were generated by vacuum casting, however, they were passed through a 100, 220, 320, 420, 600, and 1200 Grit sanding process on a lathe Ferrari, model RDMM 7045W, in order to remove imperfections that would hinder the traction test.

*Corresponding author: gilbertovprandi13@gmail.com

At first, the samples were treated in an oven of the INTI brand and model FE-1700 with a solubilization time parameter of five hours at a temperature of 500 °C; therefore, the samples were submitted to the artificial aging treatment with a temperature of 350 °C from one to twenty-two hours in increments of one hour.
The samples were subjected to hardness tests in order to raise the aging curve of the material, from that, with the time that the hardness was given to the material, the traction specimens were treated.
Finally, the specimens with and without heat treatment were subjected to the tensile test in a dynamic mechanical testing machine of the brand Instron and model 8801.

3. Results and Discussions

In Fig. 2, one of the tensile tests performed, it is possible to analyze the maximum values and the yield stress of the material before the heat treatment in the same. Also in this figure, it is possible to analyze the significant increase of the properties of the material when treated at the point of greatest hardness of the aging curve.
Thus, with the analysis of the best point to treat the developed alloy in order to improve its characteristics, it was possible to develop an alloy that best fits the turbocharger industry, allowing an advance in their development, since the alloy is a possible substitute for the currently used 2000 series alloys.
Future steps for the research, in order to characterize it as a substitute for the 2000 series, involve analyzes of fatigue, optical microscopy and fracture mechanics in the alloy in question.

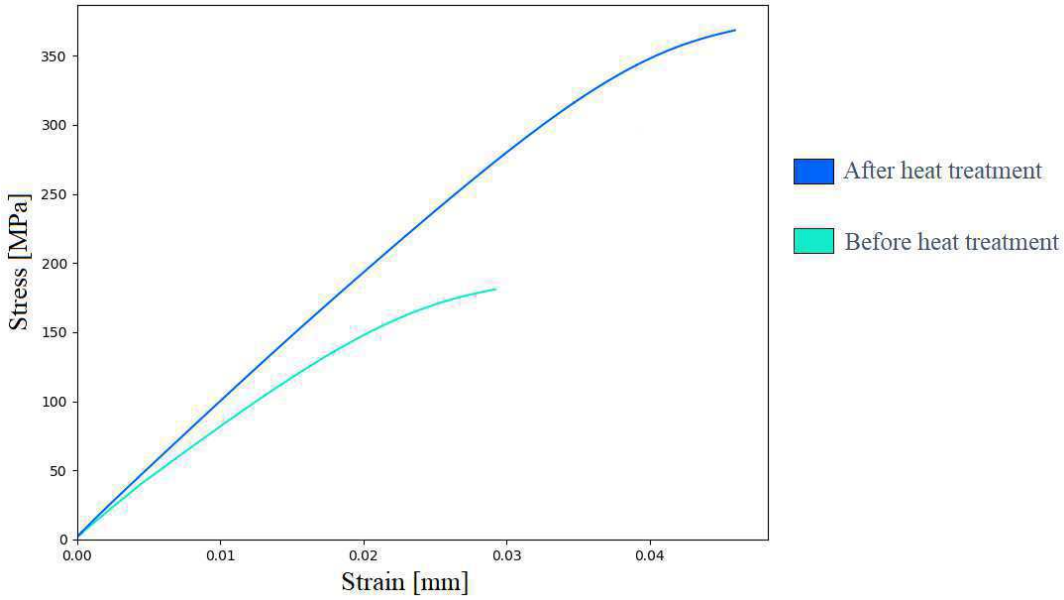

Fig.2 - *Traction analysis performed on molten samples.*

4. References

[1] BIAGIO TURBOS - TECNOLOGIA, INOVAÇÃO E EVOLUÇÃO, Available at: <http://biagioturbos.com/br/>. Accessed on: 8 Aug. 2018, (2016).
[2] F. Brunetti, Motores de Combustão Interna, 1st edition, Blucher, (2012).
[3] D. Q. LUZ, F.A. TORRES, and J. P. L. SANTOS, Avaliação De Projetos De Máquinas Pelo Enfoque Da Manutenibilidade: O Caso Do Sistema De Turbo Compressores. Salvador: Universidade Federal Da Bahia - Escola Politécnica, (2008).
[4] Mega Turbos Minas Gerais - Turbinas de Minas - Products. Available at: <http://www.megaturbos.com.br/produtos.html>. Accessed on: 8 Aug. 2018, (2015).

Acknowledgments

To CNPq for the financial assistance through the scholarship PIBITI. To the Research Group on Materials and Projects (GPMP) and its members for the assistance provided. To the IFSP - Campus São João da Boa Vista, for the equipment and laboratories use. To Biagio Turbos, for the aid with the foundry and preparation of the alloy.

*Corresponding author: gilbertovprandi13@gmail.com

ELECTRICAL STABILITY OF TiO_x THIN FILMS FOR APPLICATION AS TRANSPARENT AND CONDUCTIVE OXIDE

L. C. D. Silva[1], R. S. Santiago[1], F. D. Origo[2], I. L. Graff[3] and D. A. Duarte[1]
[1]*Federal University of Santa Catarina, Laboratory of Surface Treatments, Joinville, SC, Brazil.*
[2]*Institute of Advanced Studies, Laboratory of Surface and Optical Measurements, São José dos Campos, SP, Brazil.*
[3]*Federal University of Parana, Laboratório de Superfícies e Interfaces (LSI), Curitiba, PR, Brazil.*

1. Introduction

The development of transparent and conductive oxides (TCO) allowed rewriting the optoelectronic scenario from fabrication of flat panel monitors, touch panels and light emitting diodes. These materials in industry have improved the general characteristics of silicon solar cells and development of new technologies, such as, dye-sensitized solar cells [1,2]. Indium tin oxide ($Sn:In_2O_3$) and fluorine doped tin oxide ($F:SnO_2$), also called as ITO and FTO, respectively, are the best TCOs commercially available [3]. However, the expensive price of indium has increased researches about cheaper materials, which includes titanium dioxide (TiO_2) [4,5]. Thin coatings of anatase or rutile TiO_2 present the transparency of common glass, but its insulating nature, with electrical resistivities higher than 10^2 Ω.cm at room temperature in both structures, has challenged many researchers for application of this material as TCO. The increase of the electrical conductivity may be performed from two ways: (i) extrinsic and (ii) intrinsic doping. The first method includes doping with elements from VA and VB groups of the periodic table, such as, Nb, Ta and P [6,7]. This procedure may conserve the optical transparency, surface chemical stability and increase the electrical conductivity with the fifth electron of the extrinsic atom injected into conduction band. The second method is self-doping, which increases the electrical conductivity, but decreases both transparency and surface chemical stability due to the oxygen vacancies. This paper conducted studies about the electrical resistivity over time of TiO_x coatings deposited by reactive sputtering in order to evaluate the stability of the electrical properties of the films and application of this material as TCO.

2. Experimental

Films were deposited on grounded sodalime glass substrates (25×75 mm^2) by reactive grid-assisted magnetron sputtering. Samples were evacuated until 1×10^{-4} Torr (~1.3×10^{-2} Pa) base pressure with a mechanic (Edwards E2M5) and turbomolecular (Pfeiffer HICUBE 80 eco) pumps ensemble. Films were deposited with a DC Pinnacle Plus power supply at several powers (340, 370, 400, 430 and 460 W). The titanium target, used as sputtering source, has 99% purity. Hysteresis curves were acquired before each deposition in order to define the transition region during the reactive deposition. All films deposited were darkened (blue/green) and semitransparent. The deposition time were fixed at 10 minutes with the working pressure kept between 3.0 (~0.4 Pa) and 3.5 mTorr (~0.47 Pa) with the argon flow rate at 1.7 sccm. The oxygen flow rate was kept between 3.4 and 4.8 sccm, according to the power applied in target (to keep the working pressure constant due to different target gas consumption for a given target power). The substrate temperature was about 50°C. Coatings were investigated by profilometry, optical spectrophotometry, four-point probe and XPS. The electrical resistivity was measured twice, with the second measurement performed one year apart.

3. Results and Discussions

Profilometry results indicate the increase of the film thickness as the target power increases, as shown in Fig. 1. This effect is caused by the increased target sputtering, which, as consequence, decreased the optical transmittance (Fig. 2). Figure 3 presents the electrical resistivity as function of the power supply for measurements conducted after deposition and one year later. Results, for measurements conducted after deposition, show a slightly decrease of the resistivity with the increasing target power, with values lower than 0.02 Ohm.cm. The decreasing resistivity is caused by the increased film thickness. One year later, same measures revealed resistivities one order higher. All films present oxygen vacancies on surface due to the suboxide nature of the coatings (depositions were done in the metallic mode). Daily exposition to the atmosphere and humidity led to adsorption of oxygen-based compounds on surface vacancies, including OH radicals coming from water splitting. Figure 4 show the XPS of the sample deposited at 400 W, one year after deposition, and data suggests a high signal of adsorbed oxygen. This effect has changed the chemical composition of the surface in all samples over time, increasing the electrical resistivity and indicating the non-stability for applications as TCO.

*Corresponding author: diego.duarte@ufsc.br

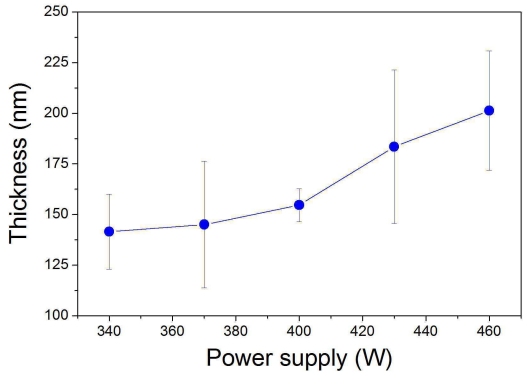

Fig. 1. *Film thicknesses as function of the power supply.*

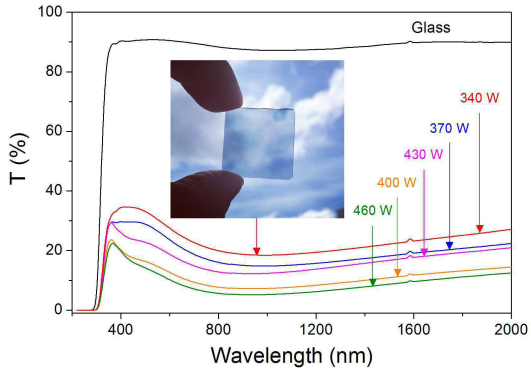

Fig. 2. *Transmittance of the films between 220 and 2000 nm.*

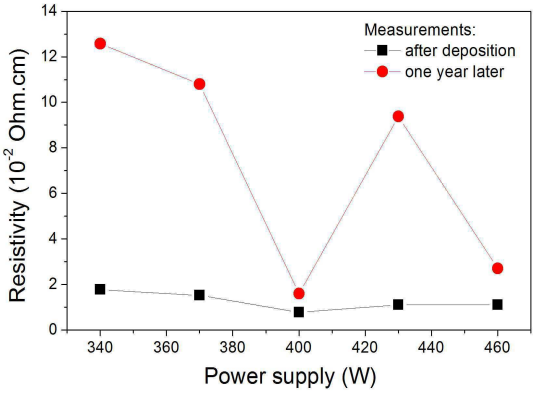

Fig. 3. *Electrical resistivity as function of the power supply.*

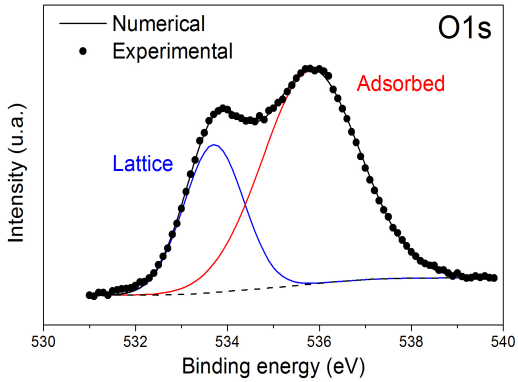

Fig. 4. *Spectrum of the O1s orbital for sample deposited at 400 W.*

4. References

[1] Müller, B. Rech, J. Springer and M. Vanecek, "TCO and light trapping in silicon thin film solar cells", Solar Energy, vol. 77, 2004, pp. 917-930.

[2] B. O'Regan and M. Grätzel, "A low-cost, high-efficiency solar cell based on dye-sensitized colloidal TiO_2 films", Nature, vol. 353, 1991, pp. 737-740.

[3] C. G. Granqvist, "Transparent conductors as solar energy materials: A panoramic review", Sol. Energy Mater. Sol. Cells, vol. 91, 2007, pp. 1529-1598.

[4] T. Minami, "Transparent conducting oxide semiconductors for transparent electrodes", Semicond. Sci. Technol., vol. 20, 2005, pp. S35-S44.

[5] Diebold, "The surface science of titanium dioxide",Surf. Sci. Rep, vol. 48, 2003, pp. 53-229.

[6] C. S.-Vazquez, N. Noor, A. Kafizas, R. Q.-Cabrera, D. O. Scanlon, A. Taylor, J. R. Durrant and I. P. Parkin, "Multifunctional P-doped TiO_2 films: a new approach to self-cleaning, transparent conducting oxide materials", Chem. Mater., vol. 27, 2005, pp 3234-3242.

[7] Y. Furubayashi, T. Hitosugi, Y. Yamamoto, K. Inaba, G. Kinoda, Y. Hirose, T. Shimada and T. Hasegawa, "A transparent metal: Nb-doped anatase TiO_2", Appl. Phys. Lett., vol. 86, 2005, pp. 252101.

Acknowledgments

Authors thank to PIBIC/CNPq for financial support, LPFS/UDESC for films deposition and LOFF/UDESC, LSI/UFPR and LMSO/IEAv for profilometry, XPS and optical measurements, respectively.

*Corresponding author: diego.duarte@ufsc.br

PRODUCTION OF Fe/Al_2O_3 SUPPORTED CATALYSTS BY PLASMA-ASSISTED PROCESS

A. M. Santos*, R. C. Catapan and D. A. Duarte
Federal University of Santa Catarina, Technological Center of Joinville, Department of Mobility Engineering, Joinville, SC, Brazil.

1. Introduction

The combination of plasma and catalysis processes to produce hydrogen is an innovative next-generation green technology that satisfies needs for energy and materials conservation, and environmental protection [1]. This combination results in synergic effects, providing unique fuel conversion outcomes, such as, greater selectivity and lower activation temperature [2-3]. Although there are several studies in literature about simultaneous use of plasma and catalysis (also known as plasma-assisted catalysis – PAC) to convert fossil fuels into H_2, few have been studied about the effect of plasma as a pretreatment of catalysts. Among several plasma processes, sputtering stands out as an interesting technique to be used for this purpose. The sputtering process changes the surface stoichiometry, *i.e.*, it becomes richer in the less volatile material. For example, the bombardment of ions on alumina (Al_2O_3) produces a surface that is rich in Al, since O is more volatile [4]. Alumina is commonly used as catalyst or catalyst support in industry reforming [5].
Previous investigations have shown that noble metals such as Pt and Rh have remarkable activity in the catalytic conversion of methane (CH_4), ethanol (C_2H_6O), propane (C_3H_8) and carbon dioxide (CO_2) to syngas (H_2 and CO) [6-8]. However, high cost and the restricted availability of these metals are major barriers for their use in industrial catalytic applications. Thus, significant attention has been placed on the use of some non-noble transition metal catalysts, especially, Ni and Co supported catalysts, due to their availability and lower cost [9]. Based on this, the present study aims to investigate surface modifications in catalysts supports induced by plasma pretreatment and evaluate the capability of sputtering as a possible technique to be used in the production of heterogeneous supported catalysts. For this, owing to the higher cost of nickel and cobalt compared to other more common metals, Fe was selected as testing material due to its similar sputtering yield [10]. Although its characteristics are not the best for the desired application, it is also possible to find in literature some studies about Fe/Al_2O_3 catalysts [11-12].

2. Experimental

Alumina foams with 26 pores/cm, 12.7 mm of thickness and 15 mm of diameter (purchased from Goodfellow) were sputtered over an iron-based substrate in a reactor using 43.4 sccm Ar for 2 hours with temperature of 450 °C, pressure of 0.98 Torr and 650 ± 12 V DC. These samples were previously fractured and cleaned using an Ultrasonic Cleaner model VR Ultrasonic by 600 seconds. After treatment, it was observed that the samples (originally white) presented a dark layer on the surface. Samples with and without plasma treatment were analyzed by X-Ray Diffraction (XRD) using an PANalytical Empyrean with incident Cu K_α radiation (λ=1.5406 Å), scan position 2θ from 20 to 90°, step size 2θ of 0.01° and scan step time of 29s. These same samples were also morphologically characterized by Field Emission Gun Scanning Electron Microscope (FEG-SEM) using an JSM-6701F with voltage of 15.0 kV and magnification of 40x to 30.000x. For this, samples were previously covered by a thin gold layer to secure the electrical conductivity needed. Finally, X-Ray Photoelectron Spectroscopy (XPS) analyses using an SCIENTA OMICRON ESCA+ with Al K_α excitation source (hν=1486.7 eV) and energy step of 0.5 eV were conducted to evaluate chemical properties of the surface, such as, oxidation states of elements and chemical interactions.

3. Results and Discussions

Results from XRD in Fig. 1 indicate the α-Al_2O_3 phase for sample without treatment [13-14]. Although it is not the best alumina phase for catalysis applications, this is highly used due to its good correlation between catalytic and mechanical properties. The XRD spectrum present in Fig. 2, which is related to the treated sample, shows that almost all the peaks had an intensity increase, except the peak located at 80°. However, this increase in peaks intensity is probably related to the greater mask diameter used in the analysis of plasma treated samples. Furthermore, it was noticed that the intensity increasing of each peak was not the same, which makes it possible to affirm that some cryptographic modifications have occurred. In summary, new peaks did not appeared after the plasma treatment, and the width of the original sample peaks were not significantly affected. By Scherrer equation evaluations and FEG-SEM analyses, it was noticed that plasma treatment tends to increase smoothly the mean grain size.

*Corresponding author: santos.andrey@posgrad.ufsc.br

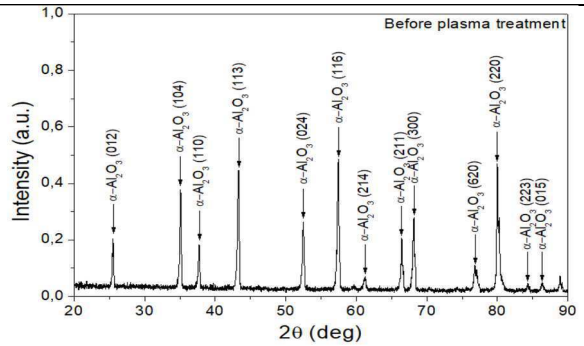

Fig. 1. *XRD spectrum of alumina foam sample without plasma treatment.*

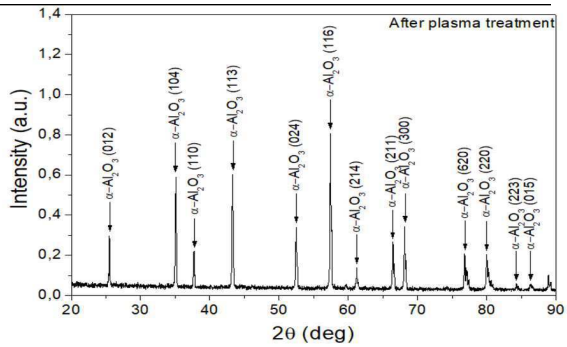

Fig. 2. *XRD spectrum of alumina foam sample with plasma treatment.*

XPS spectra from samples without and with plasma treatment, Fig. 3 and 4 respectively, shows that after sputtering a large inelastic peak appears for greater binding energy values from 705.3 eV. This phenomenon indicates a high number of collisions of the photoelectron detected and is a characteristic of metallic materials. Moreover, binding energy of this magnitude is characteristic of Fe2p, which means that iron, from substrate holder, was deposited on the sample. Furthermore, in the non-treated sample is observed a threshold of 2.5 eV to start the photoelectron emission. On the other hand, in the plasma treated alumina sample this threshold is almost zero because of its electrical conduction. This observation, in addition to the XRD results discussed above and the fact that plasma treatment was conducted in a mean temperature of 450 °C, suggest that iron sputtered from the substrate is only deposited over the alumina fragment surface, creating an amorphous layer of dispersed particles.

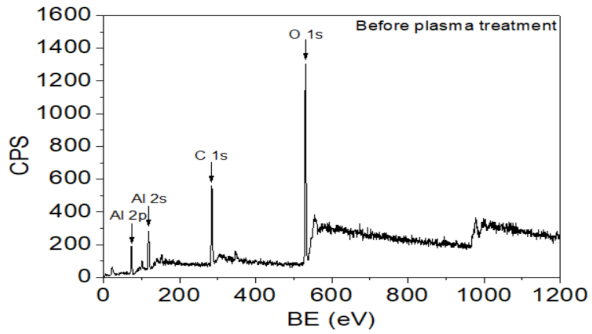

Fig. 3. *XPS spectrum of alumina foam sample without plasma treatment.*

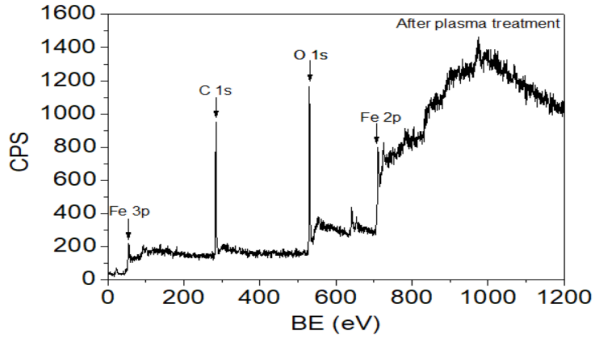

Fig. 4. *XPS spectrum of alumina foam sample with plasma treatment.*

4. References

[1] T. Nozaki and K. Okazaki, Catalysis Today, **211**, 29– 38, (2013).
[2] H.L. Chen *et al.*, Applied Catalysis B: Environmental, **85**, 1–9, (2008).
[3] L. Liu *et al.*, Catal. Sci. Technol., **7**, 4216-4231, (2017).
[4] F.F. Chen and J. P. Chang *"Lecture Notes on Principles of Plasma Processing"*, 1st edition, Kluwer Academic, USA, (2003).
[5] J. Lee, E. J. Jang and J. H. Kwak, Journal of Catalysis, **345**, 135–148, (2017).
[6] S. Ayabe *et al.*, Applied Catalysis A: General, **241**, 261–269, (2003).
[7] B. Silberova, H. J. Venvik, A. Holmen, Catalysis Today, **99**, 69–76, (2005).
[8] S. Corthals *et al.*, Catalysis Today, **159**, 12–24, (2011).
[9] A. W. Budiman *et al.*, Catal. Surv. Asia, **16**, 183–197, (2012).
[10] Sputtering Yield Rates, http://www.semicore.com/reference/sputtering-yields-reference.
[11] A.S. Al-Fatesh *et al.*, Journal of Saudi Chemical Society, **22**, 239–247, (2018).
[12] A. Boubnov *et al.*, J. Phys.: Conf. Ser., **430**, 012054, (2013).
[13] Powder Diffraction and Cell Refinement of Al_2O_3, https://bit.ly/2Mjmfhi.
[14] B. Yazdani1 *et al.*, Scientific Reports, **5**, 11579, (2015).

Acknowledgments

The authors acknowledge the support of BMW do Brasil under the project UFSC/2016/0110, LPFS/UDESC for plasma treatments and PlasMat/ITA for XRD measurements.

*Corresponding author: santos.andrey@posgrad.ufsc.br

TiO_2 COATINGS PRODUCED FROM OXIDATION OF METALLIC TI FILMS PREVIOUSLY DEPOSITED ON GLASS SUBSTRATES.

Maria Elisa Philippsen Missner[1]*, Masahiro Tomiyama[2], Joel Stryhalskic[3] and Luis Cesar Fontana[2]
[1] *Department of Enginnering, Federal University of Santa Catarina - UFSC, Campos Blumenau, Brazil*
[2]*Plasma Physics Laboratory, University of the State of Santa Catarina - UDESC, Santa Catarina, Brazil*
[3]*Federal Institute of Santa Catarina - IFSC, Jaraguá do Sul, Brazil*

1. Introduction

Titanium dioxide TiO_2 is a well know semiconductor material which has promising chemical and physical properties such as high refractive index, photoinduced hydrophilicity, wide band gap, high physical and chemical stability and it is a nontoxic material [1]. TiO_2 thin film has been used in a wide application range, as photocatalyst, gas sensing and optical coating, water and air purification, corrosion barrier, solar cells, electrical devices, and self-cleaning surfaces [2, 3].

Taking into account the drawback associated to Reactive Magnetron Sputtering TiO_2 films deposition on glass substrates, the present paper aims to prepare TiO_2 films in two steps: 1- Metallic Ti films deposition on glass substrates through pulsed Magnetron Sputtering, and 2- oxidation of Ti films by heat treatment in atmospheric air, with thermodynamic parameters similar to that used in the toughening glass process. Metallic deposition of Ti through Magnetron-Sputtering is a very simple process that provides dense films with good adhesion and easy control in the thickness of the layer. It could make possible the deposition of nanometric thickness films on large area glass substrates. The oxidation of the Ti films can be done simultaneously to the glass quenching process, producing transparent, photocatalyst and self-cleaning TiO_2 films.

2. Experimental

Metallic Ti films deposition was performed through a pulsed DC triode magnetron sputtering system (TMS). The sputtering from a Ti target (99.5% purity) was done during 3.0 minutes, in argon atmosphere. The argon plasma was generated through a DC pulsed power supply (Pinnacle Plus 5kW). The deposition chamber is a stainless steel cylindrical geometry, with diameter of 28.0 cm and height of 24.0 cm. The magnetron was cooled by water and the vacuum was performed with turbo molecular pump system. The soda-lime glass substrates were 30x10x4 mm^3 samples.

The film depositions were carried out with samples heated at 300 °C through a resistive heater. The chamber was pumped down until reach a base pressure of 10^{-5} Torr (0.4 Pa). The work pressure, during the film depositions, was maintained at 10^{-3} Torr ($1.3x10^{-3}$).

A set of the samples with Ti films were conducted to a oxidation at 650 °C, during one hour. The oven heating rate was 20 °C/min and the cooling rate was 10.3 °C/min.

3. Results and Discussions

Figure 1 shows the Tauc linear extrapolation result for indirect transition to obtain the band gap energy of the glass substrate for the film 650 °C. It is observed a double gap. The results indicate that it decreases the band gap energy in relation of TiO_2 in the rutile phase. For the soda-lime glass used in this article band gap values were also estimated, with Eg = 3.5 eV. As $Eg_{glass} > Eg_{film}$ indicates that the absorption of the radiation is being made mostly by the film.

Figure 2, show XPS analysis of 650 °C sample. It is verified that the proportion of oxygen and titanium, near to the surface, corresponds to TiO_2 stoichiometry. The depth profile through the film, highlight that near the TiO_2 / glass interface, occurs diffusion of atoms from the glass substrate (Si, Na, Ca) to the film. However, these atoms are next to the interface region and do not reach the surface of the film, so that the hydrophilic properties correspond to the TiO_2 compound and are not affected by the substrate atoms.

It has been observed also, through visual inspection and optical microscopy, that the films do not present any displacement, indicating good adherence to the substrate. The inter-diffusion at the interface between the substrate and film atoms provides a match between the film and substrate structure.

*Corresponding author: elisa.p.missner@ufsc.br

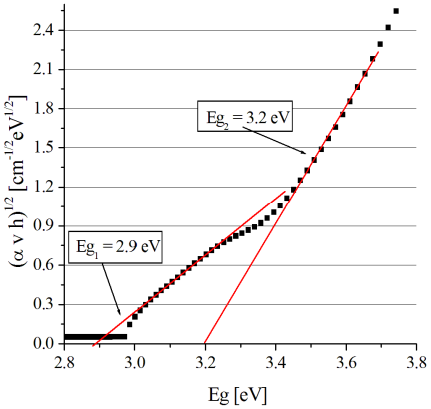

Fig. 1. *Scheme resulting from the linear extrapolation of Tauc to obtain the band gap energy of the glass substrate with Ti film (650 °C).*

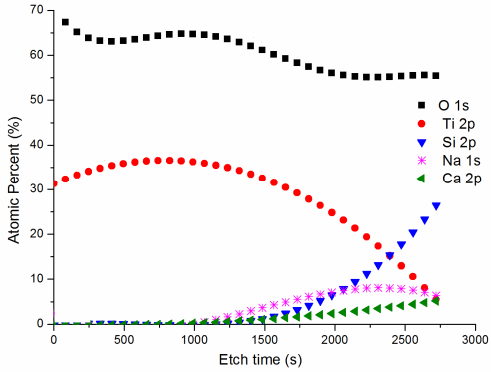

Fig. 2. *XPS measurements showing the depth profile composition of the film, showing that there are diffusion of atoms from the substrate (Si, Na, Ca) to the TiO_2 film.*

Ti metal films with thicknesses up to 130 nm deposited on glass substrates become transparent when oxidized under the same thermodynamic conditions as glass temper, ie at 650 °C in atmospheric air for 1.0 h. This means that the oxidation of the film can be done concomitantly to the temper process.

Through the technique XPS we see the diffusion of atoms of the substrate (Si, Ca, Na) for the film. However, the concentration of these atoms is restricted in the region of the interface and does not reach the surface of the TiO_2 film, maintaining it is hydrophilic properties. This diffusion effect can also contribute to the good adherence of the film due to the creation of a gradual transition in the chemical composition of the film / substrate.

The band gap energy, obtained by the Tauc method, indicates the existence of two values: 2.9 eV and 3.2 eV. These band gap energy values are in agreement with the literature for rutile (3.06 eV). The origin of the second band gap may be related to the formation of a layer contaminated with substrate atoms, however larger investigations are necessary to conclude about this. This indicates that the TiO_2 films obtained by the technique used in this work have the potential to become active when irradiated UV near.

4. References

[1] M. Pelaez, N.T. Nolan, S.C. Pillai, M.K. Serry, P. Falaras, A.G. Kontos, P.S.M. Dunlop, J.W.J. Hamilton, J.A. Byrne, K.O. Shea, M.H. Entezari, D.D. Dionysiou, Applied Catalysis B: Environmental 125 (2012), pp. 331–349.

[2] U. Diebold, The surface science of titanium dioxide, Surface Science Reports, 48 (2003), pp. 53-229.

[3] B. Wang, S. Wei, L. Guo, Y. Wang, Y. Liang, B. Xu, F. Pan, A. Tang, X. ChenEffect of deposition parameters on properties of TiO2films deposited by reactive magnetron sputtering. Ceram. Int., 43 (2017), pp. 10991-10998, 10.1016/j.ceramint.2017.05.139.

Acknowledgments

The authors thanks: FINEP, FAPESC and CAPES.

*Corresponding author: elisa.p.missner@ufsc.br

EXPERIMENTAL VERIFICATION OF A NUMERICAL MODEL FOR TRANSIENT FLOWS OF RAREFIED GASES THROUGH LONG CHANNELS

Ernane Silva* and Cesar J. Deschamps
Federal University of Santa Catarina

1. Introduction

Numerical simulations of rarefied gas flows are usually based on the kinetic theory or Direct Simulation Monte Carlo Method (DSMC). Many numerical results are available in the literature for steady flow in a variety of geometries [1]. However, few studies were conducted considering transient flow since the associated computational costs are generally high [2-4]. In order to overcome this difficulty, Sharipov and Graur [5] argue that transient flows in many practical situations can be modeled applying numerical results obtained from the linearized stationary kinetic equation, reducing significantly the computational costs. Experimental studies involving transient flows of rarefied gases are also scarce in the literature. Recently, Silva *et al.* [6] presented a series of measurements obtained from rarefied transient flows of N_2 through a channel of circular cross-section connecting two reservoirs. The aim of the present study is to compare such measurements with numerical results obtained with the model proposed by Sharipov and Graur [5].

2. Theory

Consider the isothermal flow of gas through a long channel connecting two reservoirs with constant volumes. The numerical model proposed by Sharipov and Graur [5] assumes that the channel length L is much larger than its characteristic transversal size a. Under this assumption end effects can be neglected and the time to establish a steady flow at each cross-section is much smaller than that required to establish a steady flow in the whole channel. Hence, a steady solution for the mass flow rate can be applied for each cross-section and the dimensionless pressure distribution $p'(t', x')$ along the channel can be expressed as

$$\frac{\partial p'}{\partial t'} = \frac{\partial}{\partial x'}\left(G_P \frac{\partial p'}{\partial x'} \right), \tag{1}$$

where $G_P = G_P(\delta)$ is the Poiseuille coefficient, which depends on the rarefaction parameter given by $\delta = ap/(\mu v_m)$. The variables μ and v_m are the gas viscosity and the most probable molecular speed. The dimensionless quantities in Eq. (1) are defined as $p' = p/p_A(t=0)$, $x' = x/L$ and $t' = t/\tau$, where $\tau = 2L^2/(av_m)$ is the characteristic time to establish a steady flow in the channel. The boundary conditions are $p(t,0) = p_A(t)$ and $p(t,L) = p_B(t)$, where $p_A(t)$ and $p_B(t)$ are the pressures in the reservoirs. The initial condition $p(0,x)$ is also necessary. The values of $p_A(t)$ and $p_B(t)$ are obtained from the mass balance in the reservoirs, which can be written in the following dimensionless forms:

$$\frac{\partial p'_A}{\partial t'} = \frac{V_C}{V_A}\left(G_P \frac{\partial p'}{\partial x'} \right)\Bigg|_{x'=0}, \tag{2}$$

$$\frac{\partial p'_B}{\partial t'} = -\frac{V_C}{V_B}\left(G_P \frac{\partial p'}{\partial x'} \right)\Bigg|_{x'=1} . \tag{3}$$

Eqs. (1)-(3) are solved employing the finite difference method with an implicit time discretization scheme. In this case, $x'_{i+1} = x'_i + \Delta x'$, $x'_0 = 0$ and $\Delta x' = 1/N$, where N is an integer. Also, $t'_{k+1} = t'_k + \Delta t'$ and $t'_0 = 0$. This procedure results in the following system of equations:

$$\left[\frac{\Delta x'^2}{\Delta t} + G_{P_{k+1,i-1/2}} + G_{P_{k+1,i+1/2}} \right] p_{k+1,i} = G_{P_{k+1,i-1/2}} p_{k+1,i-1} + G_{P_{k+1,i+1/2}} p_{k+1,i+1} + \frac{\Delta x'^2}{\Delta t} p_{k,i} , \tag{4}$$

$$\left[\frac{\Delta x'}{\Delta t} + G_{P_{k+1,0}} \right] p_{k+1,i} = G_{P_{k+1,0}} p_{k+1,1} + \frac{\Delta x'}{\Delta t} p_{k,0}, \tag{5}$$

$$\left[\frac{\Delta x'}{\Delta t} + G_{P_{k+1,N}} \right] p_{k+1,i} = G_{P_{k+1,N}} p_{k+1,N-1} + \frac{\Delta x'}{\Delta t} p_{k,N} . \tag{6}$$

The Poiseuille coefficient $G_P(\delta)$ was calculated using the expression proposed by Sharipov and Graur [5], which was obtained by interpolating numerical data available in the literature for diffuse gas-surface interaction. The Gauss-Siedel method was adopted to solve the system of equations.

*Corresponding author: ernane.silva@ufsc.br

3. Results and Discussions

All the experiments performed by Silva *et al.* [6] adopted a channel of circular cross-section with length $L = 92.22 \pm 0.01$ mm and diameter $D = 435.5 \pm 3.5$ μm. Therefore, it is assumed $a = D/2$. Results of $p_A(t)$ and $p_B(t)$ are presented in Fig. 1 for an experiment in which $V_A = 173.3$ ml and $V_B = 174.5$ ml and the equilibrium pressure is $p_{eq} = 5775.22$ Pa. The numerical predictions were obtained considering $N = 500$ and $\Delta t' = 1$. The adopted convergence tolerance of the iterative procedure for pressure solution was equal to 10^{-7}. As can be seen in Fig. 1, the numerical model is capable of capturing the transient behavior of the pressure in the system with accurately considering the low computational cost involved in this solution. Fig. 2 shows that the deviations between numerical predictions and measurements are smaller than 1% for p_A and 10% for p_B. The greatest deviations for p_B were observed in the beginning of the experiment, when the experimental uncertainty is greater. In this sense, it is possible to conclude that the model proposed by Graur and Sharipov [5] is a valuable modeling approach for transient rarefied gas flows through long channels. Similar conclusions are obtained for other rarefaction conditions and system volume configurations, as shown in Fig.3 and Fig. 4 for an experiment with $V_A = 181.1$ ml, $V_B = 28.5$ ml, and $p_{eq} = 117.14$ Pa.

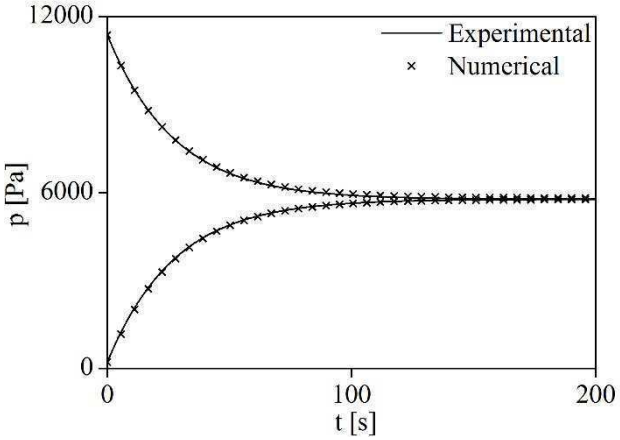

Fig. 1. *Pressure variation for experiment with $V_A = 173.3$ ml and $V_B = 174.5$ ml with $p_{eq} = 5775.22$ Pa.*

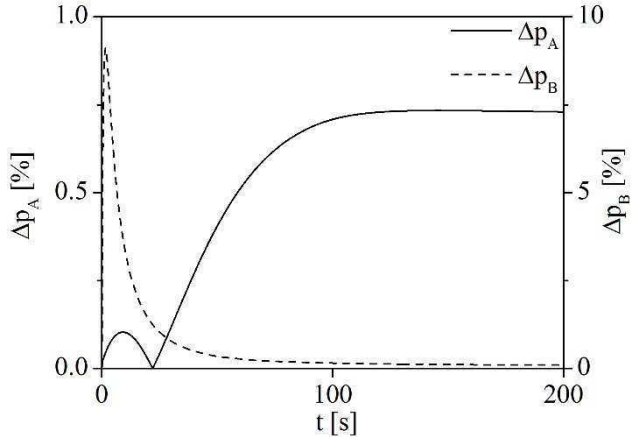

Fig. 2. *Pressure deviation for experiment with $V_A = 173.3$ ml and $V_B = 174.5$ ml with $p_{eq} = 5775.22$ Pa.*

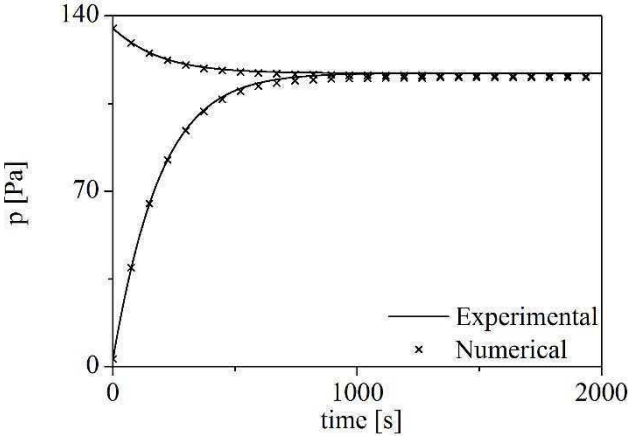

Fig. 3. *Pressure variation for experiment with $V_A = 181.1$ ml and $V_B = 28.5$ ml with $p_{eq} = 117.14$ Pa.*

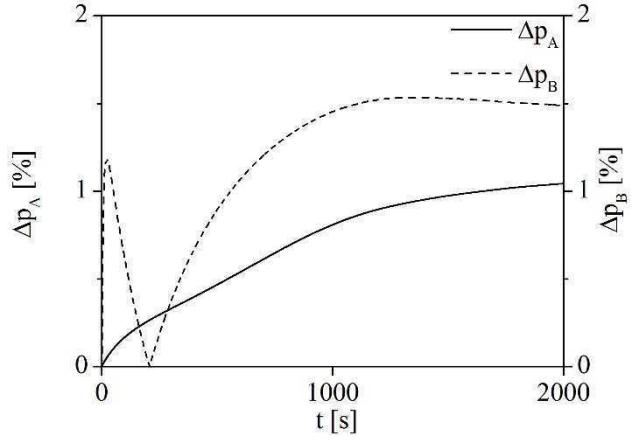

Fig. 4. *Pressure deviation for experiment with $V_A = 181.1$ ml and $V_B = 28.5$ ml with $p_{eq} = 117.14$ Pa.*

4. References

[1] F. Sharipov and V. Seleznev, J. Phys. Chem. Ref. Data, **27**(3), 657-706, (1998).
[2] J. Lihnaropoulos and D. Valougeorgis, Fusion Eng. Des., 86, 2139-2142, (2011).
[3] F. Sharipov, J. Vac. Sci. Technol., A, **30**(2), 021602 (2012).
[4] F. Sharipov, Vacuum, **90**, 25-30, (2013).
[5] F. Sharipov and I. Graur, Vacuum, **100**, 22-25, (2014).
[6] E. Silva, C. J. Deschamps, M. Rojas-Cárdenas, C. Barrot-Lattes, L. Baldas and S. Colin, Int. J. Heat Mass Transfer, **120**, 422-434, (2018).

*Corresponding author: ernane.silva@ufsc.br

INFLUENCE OF TIO_2 COATING COMPOSITION IN THE ADHESION OF MARINE MICROORGANISMS

Moisés Luiz Parucker[1*], Viviane Lilian Soethe Parucker[2], Rafael Galina Delatorre[2], João Victor Germano Pedrosa[1] and Thayrine Bráz Taveira[1].

[1]*Universidade Federal de Itajubá – Campus Itabira, Rua Irmã Ivone Drumond, 200, Distrito Industrial, Itabira-MG, Brasil, CEP: 35.903-087, Fone: (55 31) 3839-0800*

[2]*Universidade Federal de Santa Catarina – Campus Joinville, Rua Dr. João Colin, 2700, Bairro Santo Antônio, Joinville –SC, Brasil, CEP: 89.218-035, Fone: (55 47) 3204-7400*

1. Introduction

Controlling the problem of marine biofouling without simultaneously creating unacceptable environmental impacts on non-target species is a considerable challenge. In order not to damage the environment and respect existing legislation, the search for "green" technologies free of biocides is urgently sought out by the marine coatings industry [1].

The most problematic biofouling arises from the colonization of macroorganisms such as macroalgae spores, barnacle larvae, bryozoans, molluscs, polychaetes, tunicates and coelenterates [2]. The barnacles are the most well-known arthropods found in submerged structures in the marine environment that also generate the greatest problems.

In this study, the efficiency of thin films of titanium dioxide was evaluated for its ability to minimize the biofouling process in steels commonly used in the naval sector, in order to reduce aggression to the marine environment.

Studies have been developed which demonstrate the efficiency of TiO_2 in relation to its antimicrobial property due to its photocatalytic action, which encouraged the use of this material in the development of the present work [3].

2. Experimental

AISI 1020 steel samples were used as a substrate for deposition of thin films of TiO_2 using a Magnetron Sputtering equipment. A high purity (99.9%) titanium target and partial O_2 pressures of PO_2/Pt = 0.4 were used for deposition 1, PO_2/Pt = 0.6 for deposition 2 and PO_2/Pt = 0.0 for deposition 3. The material was characterized by XRD using a Panalytical X'pert PRO X-ray diffractometer in the θ-2θ configuration and grazing incidence X-ray diffraction (GIDRX). The chemical analysis of the thin films was performed by the Tescan®-SEM dispersive energy spectroscopy technique, which was also used to analyze the surface of the thin films before and after insertion in the marine environment, in periods of 1 day and 1 to 5 weeks, to identify the products that would lead to biofouling.

3. Results and Discussions

The chemical composition of the thin film was evaluated by Energy Dispersive Spectroscopy (EDS) analysis and showed the presence of Ti and O_2 in the proportions of 43.5% +/- 0.80 (PO_2/Pt 0.4), 62.4 +/- 0.93 (PO_2/Pt 0.6) and 51.2 +/- 0.86 (PO_2/Pt0.0).

The XRD diffractograms of samples PO_2/Pt 0,4 and PO_2/Pt 0,6 presented crystalline structures and peaks characteristic of TiO_2 in the anatase (A) and rutile (R) phases. The sample PO_2/Pt 0.4 presents TiO_2 with characteristics of the anatase phase while the samples with PO_2/Pt 0.6 shows peaks corresponding to the anatase phase in the same planes of the sample PO_2/Pt 0.4, but the rutile phase can be found in two planes. For the diffractogram of the thin film of the sample with PO_2/Pt 0,0, an amorphous structure was formed.

With the SEM, images of the surfaces of the thin films were obtained, showing that the coating of the substrates were practically homogeneous, with no significant differences in the chemical composition as a function of the PO_2/Pt deposition ratios. Fig. 1 to 4 shows the SEM images on the surfaces of films without exposure in the marine environment and after 1 day, 2 weeks and 5 weeks of exposure.

As observed in Fig. 2, the thin film obtained in the PO_2/Pt 0.4 condition showed adhesion of materials. In Fig. 2 (A) the fixation of materials with 1 day of immersion in the marine environment did not take place. Fig. 2 (B) shows the adhesion of several types of organisms to the surface of the film. Comparing these organisms with the literature, it has been possible to identify that they are diatoms [4, 5, 6, 7, 8, 9, 10]. With 5 weeks of immersion at sea (Fig. 2 (C)), it is possible to verify an intensification in the adhesion of these organisms.

*Corresponding author: moises.parucker@unifei.edu.br

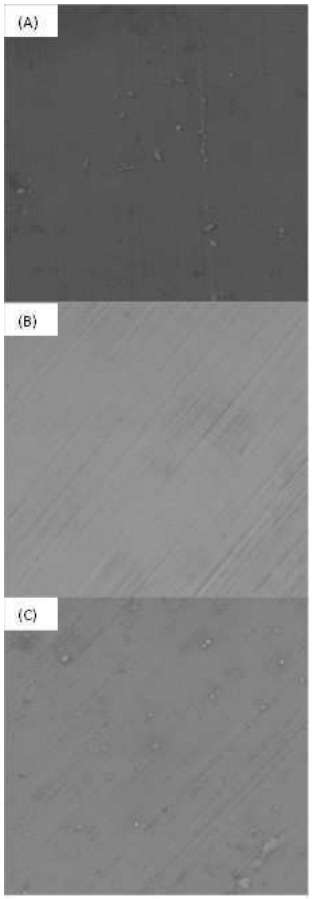

Fig. 1. *Thin Films (A) PO_2/Pt04 (B) PO_2/Pt06 (C) PO_2/Pt0,0.*

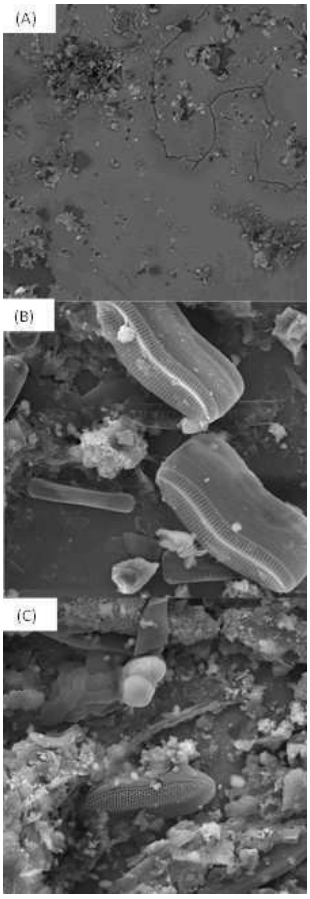

Fig. 2. *PO_2/Pt0,4 (A) 1 day (B) 2 weeks (C) 5 weeks.*

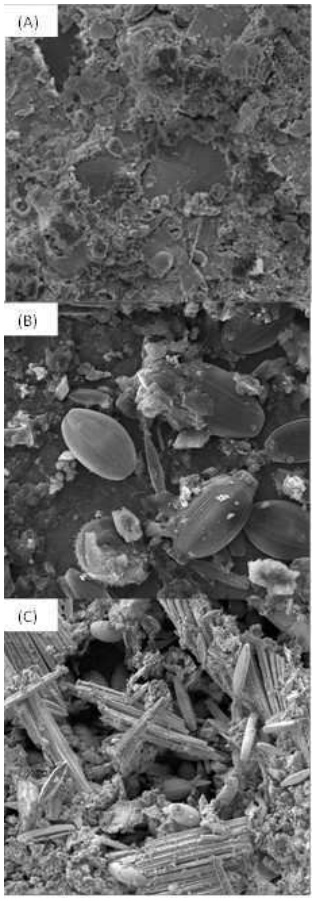

Fig. 3. *PO_2/Pt0,6 (A) 1 day (B) 2 weeks (C) 5 weeks.*

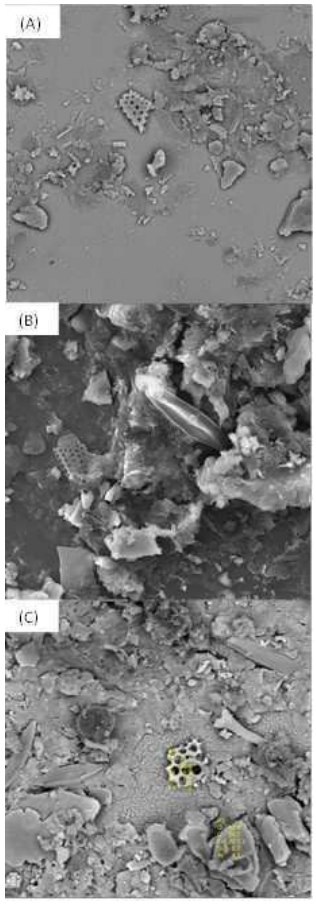

Fig. 4. *PO_2/Pt0,0 (A) 1 day (B) 2 weeks (C) 5 weeks.*

For the PO_2/Pt 0.6 film (Fig. 3) a similar behavior is observed for the film obtained in the PO_2/Pt 0.4 condition. The longer immersion time caused an increase in the adhesion of materials. The PO_2/Pt 0.0 film showed adhesion of materials after 1 day of immersion (Fig. 4 (A)).

The PO_2/Pt 0.4 and PO_2/Pt 0.6 samples showed lower adhesion of marine microorganisms than the PO_2/Pt 0,0 sample, due to the crystalline phases of anatase and rutile, which contribute in a significant way in the fight against biofouling when compared to the amorphous structure, which has the diatom as the predominant microorganism adhered, in which the barnacle larvae were not found, the main microorganism responsible for marine biofouling.

4. References

[1] J. A. Callow, M. E. Callow. Nat. Commun., (2011).
[2] S. Abarzua and S. Jakubowski. Mar. Ecol. Prog. Ser., **123**, 301-312, (1995).
[3] S. Bonetta. AMB Express, **3**, (2013).
[4] L. F. Fernandes, R. M. Souza-Mosimann, G. F. Fernandes. Insula Florianópolis, **20**, 11-112, (1990).
[5] M. Landucci and T. A. Ludwig. Acta Botânica Brasileira, **19**, 345-357, (2005).
[6] I. M. V. Moreira. Acta Biol. Parana., **4**, 135-198, (1975).
[7] C. Moresco. Brasil Botânica, **34**, 359-373, (2011).
[8] F. C. P. Ribeiro, C. do S. F. Senna, L. Torgan. Rodriguesia, **59**, 209-324, (2008).
[9] A. M. Silva et al. Acta Bot. Bras., **24**, 997-1016, (2010).
[10] L. C. Torgan; R. N. Carvalho. Iheringia. Sér. Bot., **66**, 139-146, (2011).

*Corresponding author: moises.parucker@unifei.edu.br

TiO_2 COATINGS FOR NATURAL BIOFOULING PROTECTION ON MARITME STRUCTURES: CONTACT ANGLE ANALYSIS

Rafael Gallina Delatorre[1]*, Eder Marlon Ramos[1], Moisés Luiz Parucker[2] and Viviane Lilian Soethe Parucker[1]

[1] *Universidade Federal de Santa Catarina – Campus Joinville, Rua Dona Francisca, 8300, Bloco U, Joinville –SC, Brasil, CEP: 89.219-600, Fone: (55 47) 3204-7400*

[2] *Universidade Federal de Itajubá – Campus Itabira, Rua Irmã Ivone Drumond, 200, Distrito Industrial, Itabira-MG, Brasil, CEP: 35.903-087, Fone: (55 31) 3839-0800*

1. Introduction

Biofouling is characterized as the accumulation of living matter on the surface of solid structures. For technological applications, specially for naval industry, it is a problem to solve as old as the big navigations, leading to losses of power in ships. Nowadays it still remains a problem to deal with, especially now when most of transport of products is performed by maritime ways. The usual solution is to use special paints with antifouling and toxic components, making it harmful for the environment and submitted to strong control by the authorities, where the most effective ones are currently prohibited of using. This fact enables the search for environmental friendly solutions for naval surface treatments. This work explores the photocatalytic properties of TiO_2 for the use as natural biocide and antiadherent surface, as a nontoxic solution for biofouling. TiO_2 exhibit photocatalytic properties when exposed to ultraviolet radiation, that higher wave lengths (UV-A) reaches the surface of the Earth coming from the Sun, while the lower ones (UV-C) are absorbed by atmosphere.

2. Experimental

Thin films of titanium oxide were prepared by magnetrom sputtering on the surface of naval steel discs and microscope glass. Two different preparation conditions leads to the formation of crystalline TiO_2 with different amounts of anatase and rutile phases, aswell as an amorphous phase of titanium oxide. The thickness of films and roughness of surface stays at 520 – 580 nm and 40 – 90 nm, respectively [1]. Electrical measurements were performed using four points in line technique, using a homemade apparatus connected to a Keithley 2400 Source Meter Unit. Photocatalytic activity of surface was tested by contact angle measurements. Contact angle were measured using a Ramé-Hart Instrument Co goniometer and deionized water as liquid. The radiation for photocatalytic activation was applied by a 5 W lamp at 253,8 nm UV-C region or a 9 W lamp at 365,3 nm UV-A region, both sources tested positioned at 2,0 and 20 cm from surface. The UV activation was performed with and without a water column interlayer between the radiation source and the sample surface, for water absorption tests, that was adjusted with heights of 1,0 cm and 10 cm. When used the water interlayer, samples passed through a drying process with acetone and hot air during 1 minute, for after contact angle measurements.

3. Results and Discussions

The electrical measurements evidenced different electrical behavior for each material, were the mixed phases TiO_2 crystal exhibited very high resistance, higher than 10^6 Ω, that was attributed to an almost insulator material, while the amorphous phase exhibited ohmic behavior with low resistance, with a value of 2.62×10^{-2} Ω.m for resistivity.

Contact angle measurements evidenced no appreciable difference between two materials, showing very similar behavior. For UV-C incidence and no water column, contact angle values shown a strong variation to hydrophilic values after around 100 minutes exposition, with a higher variation when the source is closer to the surface (2,0 cm distance). This behavior was already observed by several authors, attributed to the activation of photocatalytic reactions producing H_2O_2 and OH^- [2]. The difference observed for higher distances evidences the notorious differences on intensity that reaches the surface. Running the experiment with a water column, results exhibited a lower variation on contact angle in comparison to the results without water, meaning a decrease in radiation intensity that reaches the surface, but steel with photocatalytic activity.

For UV-A incidence, a very little change to more hydrophilic behavior is observed only after 1400 minutes of exposition, for the more closer source-surface geometry. This result shows that the amount of photocatalytic reaction was considerably lower for this radiation frequency, meaning that the radiation is below the band gap of materials.

The results makes promisor the use of titanium oxides for biofouling protection of naval surfaces, since promotes the formation of biocide agents like H_2O_2 and OH^- very localized on that regions, and with very

*Corresponding author: Rafael.delatorre@ufsc.br

low toxicity for humans and most species, being relevant only for microorganisms. Since the protective properties for biofouling on ships needs activation by UV incidence under the water, the use of UV-C is very effective but needs to be applied very near the surface, requiring some practical developments. The use of UV-A has not such needs, since it is notorious that these frequencies reaches the surface of Earth and are not absorbed by water, where the source can be the Sun properly, that emits UV in all frequencies. However, the very low intensity makes a low quantity biocide production, reducing the potential for effective biofouling prevention. Nevertheless, other works evidence no need of high intensity reaction formation for effectively action of TiO_2 as biocide for microorganisms, the base food of any more complex living being [3].

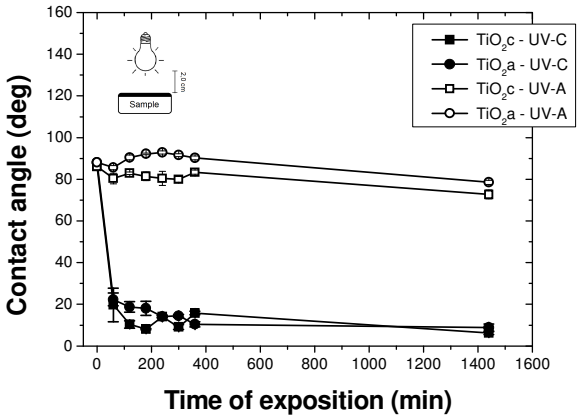

Fig. 1. *Contact angle for water drop on TiO_2 surface, as a function of time of exposition under UV-C radiation and UV-A radiation. Crystal – c; Amorphous – a.*

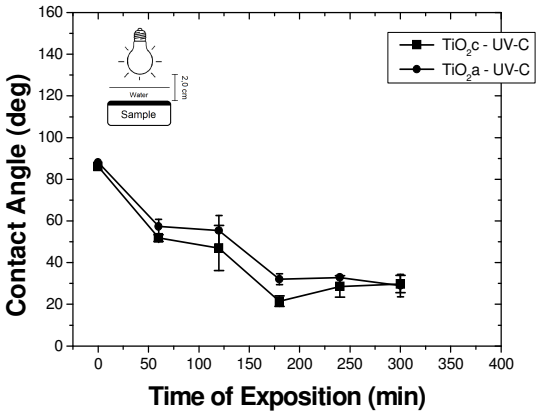

Fig. 2. *Contact angle for water drop on TiO_2 surface, as a function of time of exposition under UV-C radiation through a water column above the surface. Crystal – c; Amorphous – a.*

4. References

[1] R. G. Delatorre, E. M. Ramos, K. F. Souza, M. L. Parucker and V.L.S.Parucker, XVI Meeting of the Brazilian Materials Research Society, Gramado, 2017.
[2] R.M Pasquarelli, D.S. Ginley and R. O'Haire, Chem. Soc. Rev., **40** (2011).
[3] A. Fujishima, T.N. Rao and D.A. Tryk, J. Photochem. Photobiol. C: Photochem Rev., **1** 1 (2000)

Acknowledgments

Authors would like to acknowledge the Laboratory of Plasma, at UDESC University, for the support for contact angle measurements and thin film preparation.

*Corresponding author: Rafael.delatorre@ufsc.br

SPECTROCOPY OF AN ATMOSPHERIC NEEDLE PLASMA DISCHARGES

Mauricio Antonio Algatti, Gustavo G. Vasques, Marcelo H. Mello and Milton E. Kayama
FEG-DFQ-UNESP – Campus de Guaratinguetá-Av. Ariberto Pereira da Cunha 333, 12516-410 Guaratinguetá, SP, Brazil

1. Introduction

Plasma micro-discharges at atmospheric pressure have been applied in a broad band of medical and environment science and technology in order to improve the health and life quality. The plasma characterization by spectroscopy methods is of paramount importance for processes customization as well for its use in industrial applications. In this paper one has performed plasma spectroscopy of Ar for characterization of the plasma environment. The final goal is to improve the plasma parameters for using these micro-plasmas for materials processing in order to improve the materials biocompatibility.

2. Experimental

The plasma plume is generated from the tip of a surgical needle with 0.7 mm o.d.. The applied voltage had sinusoidal waveform with 5.8 kV peak-to-peak and frequency of 37 kHz. The voltage is applied between the needle and an external brass ring. The borosilicate capillary is located between them and a filamentary discharge type evolves at the site [1]. The device had two independent entrances for the gas with flow controlled by needle valves. The Fig.1 shows the schematic view of the experiment. The light was collected by a large numerical aperture lens with collimator to reduce the stray light. An optical cable with wide spectral band leads the light to a spectrometer. The light was collected in longitudinal and transversal direction in relation to the plume.

3. Results and Discussions

A typical spectrum of discharges with argon is shown in the figure 2. It shows the generation excited neutral and ionized species with the spectral lines separated in bands, the ArI in the range of 680-750 nm and ArII between 300-400 nm. The side-on measurements indicates the presence of ionized species close to the tip of the needle and excited neutral species at border and end of the plume. No spectral emission from the ambient gas was observed due to the shielding effect in this two gas flow arrangement.

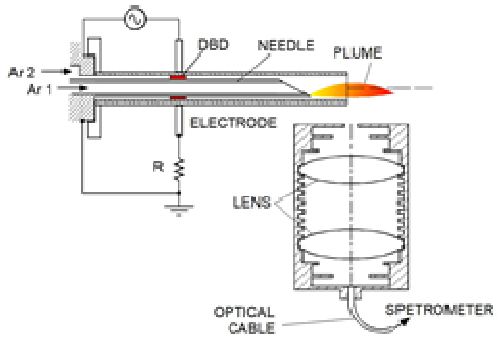

Fig. 1. *Schematic view of the experiment.*

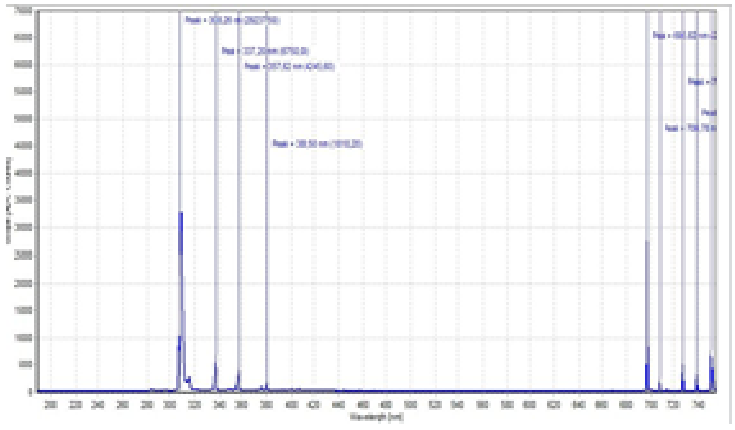

Fig. 2. *Spectral lines of the Ar plasma plume.*

4. References

[1] Kayama, M.E., Silva L.J., Prysiazhnyi. V, Kostov, K.G, and Algatti M.A., Characteristics of Needle-Disk Electrodes Atmospheric Pressure Discharges Applied to Modify Wettalility. *IEEE Trans. Plasma Sci.* 0093-3813, (2017).

Acknowledgements
Authors would like to thank FAPESP and CNPq for financial support.

EFFECT OF PLASMA PARAMETERS ON CARBON NANOTUBE FUNCTIONALIZATION BY MALEIC ANHYDRIDE

Teresa Tromm Steffen[1]* and Luis César Fontana[2] and Daniela Becker[3]
[1,2,3]*Center for Technological Sciences, UDESC, Joinville, Santa Catarina, Brazil*

1. Introduction

Carbon nanotubes (CNT) have been functionalized by plasma in order to prevent agglomerate and improve their bonding with polymeric matrices in nanocomposite's synthesis [1]. A monomer that can be used as an activating on nanotube wall is maleic anhydride (MA), which can provide both functional groups, like carboxyl, and the anhydride group itself to be attached to nanotubes walls and tips [2]. In this paper, CNT and MA in solid form were premixed by two different ways before the plasma treatment. So the aim of this work is to analyze the effect of both premix and plasma parameters on CNT functionalization.

2. Experimental

Multi-walled carbon nanotubes used in this work were purchased from Chengdu Organic Chemicals Co. Ltd (TNIM4), with purity higher than 95%, an external diameter range of 10-30 nm. Maleic anhydride, with purity higher than 98,5%, were purchased from Sigma-Aldrich. CNT and MA were mixture by two methods. The first one took place in a planetary mill by 10 minutes at 300 rpm. The second one was manually made with mortar and pestle assistance. Both the mixture were done with 90:10 (CNT:AM) mass proportion. After that, the samples were positioned in the way to occupy all the cylindrical volume of 1.5 cm length in the reactor tube. The samples were treated through inductively coupled radio frequency plasma (RF) (Fig. 1) at 35 W power input, 1 Torr gas pressure, by 15, 30 and 60 minutes, with and without nitrogen (1.2 sccm) in the working gas. Argon flow was utilized to clean the reactor volume by 15 minutes before the plasma discharge. Argon (11.0 sccm) and nitrogen (1.2 sccm) and pure argon (12.2 sccm) were utilized as working gas in the plasma. Samples treated were washed three times with ethanol before characterization. Table 1 shows the experimental layout used in this paper.

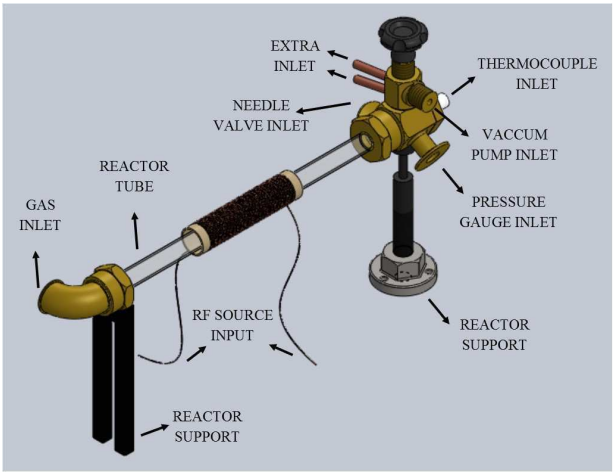

Fig. 1. *Schematic representation of RF plasma reactor used to functionalize the CNT.*

Table 1. *Samples conditions.*

SAMPLE	Moisture	Time	N_2 gas
CNT/pristine	-	-	-
CNT.p.15	planetary mill	15 min	no
CNT.p.30		30 min	no
CNT.p.60		60 min	no
CNT.p.15.N		15 min	yes
CNT.p.30.N		30 min	yes
CNT.p.60.N		60 min	yes
CNT.15	mortar	15 min	no
CNT.30		30 min	no
CNT.60		60 min	no
CNT.15.N		15 min	yes
CNT.30.N		30 min	yes
CNT.60.N		60 min	yes

3. Results and Discussions

FTIR spectra for CNT/pristine and all samples treated in RF plasma are shown in Fig. 2. It is observed that the treated samples shows new peaks referent to C=O vibration mode of carboxyl groups at 1740 cm^{-1}, 1725 cm^{-1} and 1704 cm^{-1}, indicating the ring opening of maleic anhydride and CNT functionalization [3,4]. Raman results (Fig. 3) shows that there is no significant difference on I_D/I_G ratio between the samples, which indicates that there is no high damage on CNT walls by plasma reactive species. Nevertheless, the MET image in Fig. 4 shows an amorphous region, indicated by the arrow, which could be associated with defects produced on CNT walls by plasma treatment [3]. Fig. 5 show XPS measurements of oxygen (atomic percent) on CNT, for CNT/pristine (2.4 ± 0.1) and for all the other samples. For samples mixed in the planetary mill, the atomic percent of oxygen inserted on CNT was lower than for those samples mixed in the mortar. It indicates that the hand mortar method can be a better premix. Regarding to the nitrogen, when this gas is utilized in the plasma treatment, it is observed a decreasing in the oxygen content

*Corresponding author: teretromm@hotmail.com

inserted on NCT, which is in accordance to the fact that the nitrogen may cold the plasma, therefore it reduces the plasma reactivity [3]. About the treatment time, 30 minutes is a good option for samples mixed at the mortar, once, after that, the plasma seems to starts to remove the oxygen already inserted, by means of chemical attack [5]. Besides the differences noticed, the increasing in oxygen on the CNTs is not so high, which leads to believe that the plasma produced through inductively coupled radio frequency into a CNT volume is not strong sufficiently to produces significant changes on the CNTs walls.

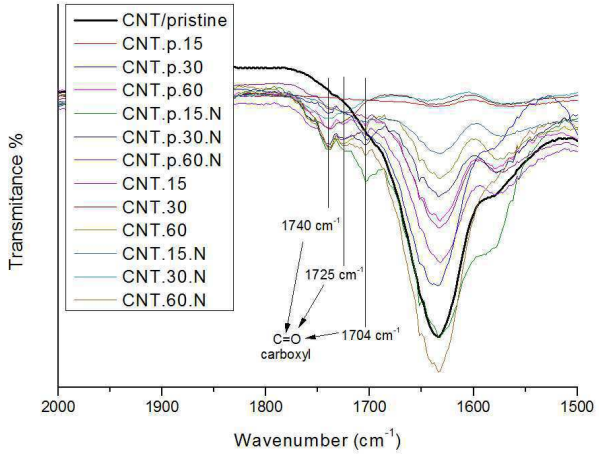

Fig. 2. *FTIR spectra showing new peaks at 1740, 1725 and 1704 cm^{-1}, related to C=O vibration mode of carboxyl groups.*

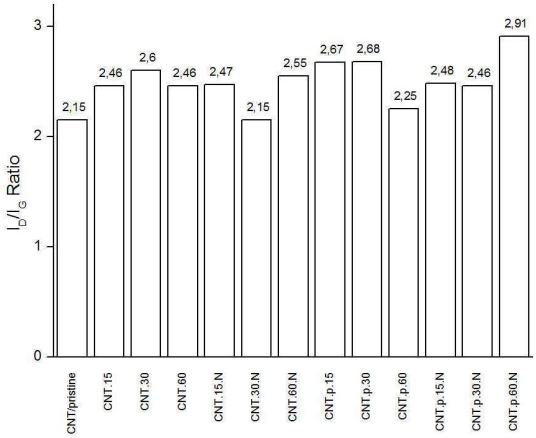

Fig. 3. *Raman I_D/I_G showing that there is no significant difference in defect increase after plasma treatment.*

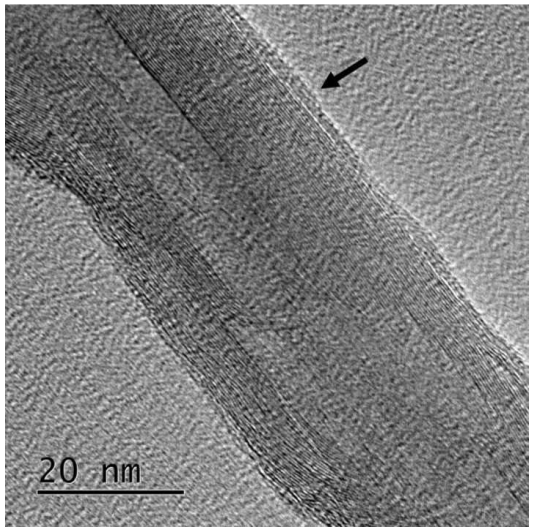

Fig. 4 *MET image of CNT.15 sample showing a layer that could be an amorphous region associated to defects caused by plasma treatment.*

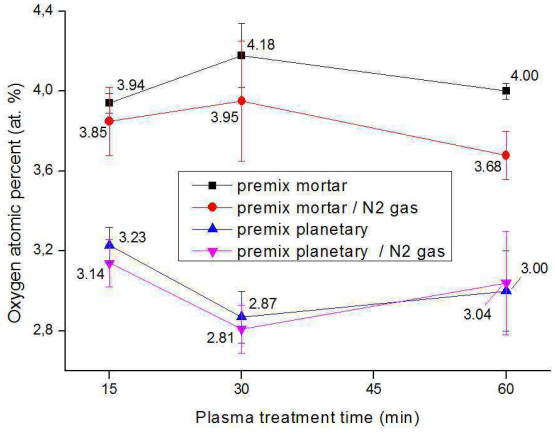

Fig. 5 *Oxygen atomic percent, obtained by XPS, for different premix samples treated by plasma with and without nitrogen.*

4. References

[1] C. Saka, Analytical Chemistry, (2017). doi 10.1080/10408347.2017.1356699
[2] Y. Lu, H. Li, H. Liu, Phys E, **43**, 510-514, (2010).
[3] T. T. Steffen, L. C. Fontana, J. Nahorny, D. Becker, Polim. Compos, doi 10.1002/pc (2018).
[4] G. Mishra, S. L. McArthur, Langmuir, **26**, 9654-9658, (2010).
[5] C. A. Ávila-Orta, P. González-Moronez. S. Suzuki, Eds. IntechOPen, Rijeka, 167–192 (2013).

Acknowledgments

The authors would like to thank the financial resources provided by CAPES by means of scholarships and CNPq by project Universal/445242/2014-0. Also thank to Claudia Correia from Univille, and Dr. Evaldo José Corat from INPE, by collaboration in samples characterizations.

*Corresponding author: teretromm@hotmail.com

SUBSTRATE HEATING EFFECTS ON HYSTERESIS CURVES OF REACTIVE MAGNETRON SPUTTER DEPOSITION

Júlia Karnopp* and Julio César Sagás

Laboratory of Plasmas, Films and Surfaces, Santa Catarina State University (UDESC), Joinville -SC

1. Introduction

In magnetron sputtering deposition, atoms are sputtered from a target by ions generated in magnetically confined plasma. The insertion of a reactive gas into the chamber allows the formation of compound films. However, the reactive gas is also gettered on target surface, causing the phenomenon of target poisoning. The compound formation on surfaces provokes the hysteresis on the process curves (pressure, voltage, etc.) as a function of reactive gas flow. It makes the process unstable around critical points: the first critical point (1st CP) corresponds to target poisoning (increasing the gas flow) and the second critical point (2nd CP) to target depoisoning (decreasing the gas flow).

Berg et al. [1] developed a qualitative model to simulate reactive sputter deposition. From the model, the hysteresis curves can be obtained using balance equations for the number of reactive gas atoms on substrate and target. However, it does not include explicitly the substrate temperature, one parameter often varied in sputter deposition. The substrate heating can also have some effect on gas density near the substrate. Gas temperature is related to the flux of particles arriving at surfaces and the substrate temperature defines the probabilities of adsorption and desorption, which is described by the sticking coefficient. The process of gas adsorption can be described by the Langmuir [2] or Kisliuk [2,3] model. The first considers only molecular chemisorption on surface, while Kisliuk model takes into account the physisorption of molecules in a precursor state. In this state, the atoms can move on surface before chemisorption or desorption. In this work, the substrate heating effects on hysteresis curves were evaluated both theoretically and experimentally.

2. Methodology

To include explicitly the substrate temperature in Berg model, the rate of gas adsorption was rewritten using Kisliuk and Langmuir models. For the Langmuir model, the chemisorption rate is

$$r^L = F\alpha_0 exp\left(\frac{-E_{chem}}{kT_s}\right)(1-\theta_c) \quad (1)$$

where F is the flux of reactive molecules, α_0 is the pre-exponential factor, E_{chem} is the activation energy of chemisorption, T_s the substrate temperature and θ_c is the compound fraction on film surface. For the Kisliuk model,

$$r^K = F\,\frac{1}{1+\frac{K_{des}}{K_{chem}}exp\left(\frac{E_{chem}-E_{des}}{kT_s}\right)}\,\frac{1}{\left(1+\frac{\theta_c}{1-\theta_c}K\right)} \quad (2)$$

where K_{des} and K_{chem} are the frequency factors of desorption and chemisorption respectively and E_{des} is the desorption activation energy. The parameter K is the ratio between the probability of desorption from precursor state and the sum of probabilities of chemisorption and desorption from an empty site.

Hysteresis curves were simulated varying the substrate temperature (323 K, 373 K, 473 K, 573 K and 673 K). Another set of simulations were carried out changing the gas temperature near to substrate (400 K and 600 K) for a fixed substrate temperature, using Kisliuk model. The parameter K was fixed at 1. The simulations results were compared with experimental hysteresis curves obtained in a magnetron sputtering system at different target/reactive gas combinations: (i) Ti/N_2, (ii) Ti/O_2, (iii) Al/N_2 and (iv) Al/O_2. Both targets have 100 mm in diameter. The argon partial pressure was kept at 0.40 Pa and the discharge current was fixed at 1.0 A. The hysteresis curves of pressure and voltage were obtained with the substrate at room temperature and heated at 373 K, 473 K, 573 K and 673K. The reactive gas flow rate was varied from 0.0 sccm to 7.5 sccm for O_2 and up to 4.5 sccm for N_2. The resolution of mass flow controllers is 0.01 sccm and the flow rate steps utilized were around 0.2 sccm.

3. Results and Discussions

The simulated curves show different behaviors for each adsorption model (Fig. 1). According to the Langmuir model the 1° CP shifts to larger reactive gas flow rates when the substrate temperature increases

*Corresponding author: julia_karnopp@outlook.com

(about 0.5 sccm for a raise in temperature of 350 K). However, the trend is opposite using the Kisliuk model, i.e. the 1° CP is shifted to lower reactive gas flow rates, and the shift is higher than using Langmuir model (about 1.5 sccm for the same range of substrate temperature). In the Langmuir model, the sticking coefficient increases with temperature (equation 1), therefore the gas consumption on substrate is higher and the critical point is dislocated for bigger gas flow rates. On the other hand, for Kisliuk model, the sticking coefficient decreases with surface temperature (equation 2), and consequently the 1° CP shifts to smaller gas flow rates with substrate heating.

The hysteresis curves simulated for different gas temperatures close to substrate (Fig.1) show the same effect observed for substrate temperature using Kisliuk model, but with lower magnitude. The gas heating causes a decreasing in the flux of reactive gas molecules to substrate and, consequently, decreases the chemisorption rate (equation 2). The 2° CP is practically unaffected in all simulations, once that it depends mainly on the sputtering yields.

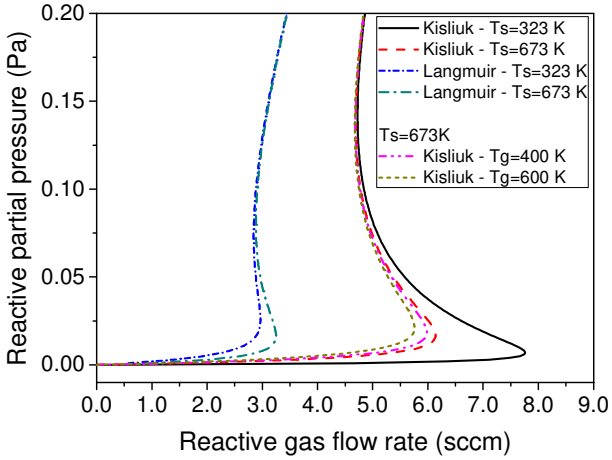

Fig. 1. *Hysteresis curves of reactive gas pressure for substrate temperature at 400 K and 600 K.*

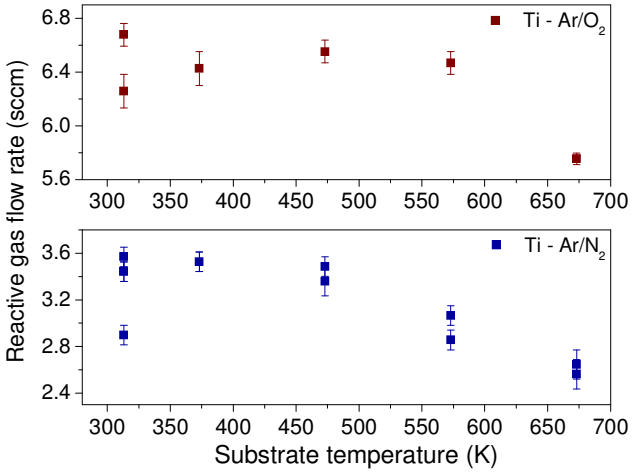

Fig. 2. *The experimental gas flow rates of first critical points for different substrates temperatures using a Ti target on Ar/N_2 and Ar/O_2 atmospheres.*

The figure 2 shows the reactive gas flow rate corresponding to first critical point as a function of substrate temperatures for Ti target on different atmospheres. Using oxygen, the 1° CP remains almost constant between 300 K and 573 K and decrease about 0.7 sccm at 673 K. Thus, the behavior of simulated results is not observed experimentally. For nitrogen, it is possible to observe a variation in the critical point similar to Kisliuk model, i.e. it is reduced with substrate temperature. Between 323 K and 673 K, the reactive gas flow rate decreases by 1.0 sccm, approximately. The 2°CP remains constant with substrate temperature in all experiments. For Al target, there are no significantly changes in the critical points. Therefore, in hysteresis curves, the effects of substrate heating are negligible.

As the 1° CP is affected by many parameters, only the hysteresis curves are insufficient to check the effects of this isolated parameter (substrate temperature). Consequently, it is not possible, from this study, to affirm which adsorption model is more adequate to describe the reactive sputtering deposition. Furthermore, additional studies are necessary.

4. References

[1] S. Berg, E. Särhammar, Thin Solid Films, 565, **186–192**, (2014)
[2] W. Ranke, Y. Joseph. Phys. Chem. Chem. Phys, 4, **2483–2498**, (2002)
[3] P. Kisliuk, J. Phys. Chem. Solids, 3, **95-101,** (1957)

Acknowledgments

The authors thank to PROBIC-UDESC and to FAPESC by the financial support.

*Corresponding author: julia_karnopp@outlook.com

OPTICAL AND ELECTRICAL PROPERTIES OF Ti SUBOXIDES GROWN BY REACTIVE GRID-ASSISTED MAGNETRON SPUTTERING

Heitor Wilker Silva Barros[1]*, Diego Alexandre Duarte[2] and Julio César Sagás[1]
[1] *Laboratory of Plasmas, Films and Surfaces, Santa Catarina State University (UDESC), Joinville, Brazil*
[2] *Laboratory of Surface Treatments, Technological Center of Joinville, Federal University of Santa Catarina (UFSC), Joinville, Brazil.*

1. Introduction

Titanium dioxide (TiO_2) is a chemically stable semiconductor transparent to visible light. TiO_2 thin films have been extensively investigated due to its applications in photocatalysis, gas sensors, smart windows, antireflection coatings, optical filters and other electronic devices [1-5]. Each one of these applications requires specific optoelectronic properties that depend on the material structure. For applications as transparent conductive oxide (TCO), for example, a low resistivity (10^{-4} Ω.cm) and a high visible light transmittance (above 80%) are required [2]. On the other hand, for applications in solar cells, there is interest in expanding the wavelength range of light absorption to the visible range.

To tune the optoelectronic properties, several works doped TiO_2 with different metals like niobium (Nb), and non-metals like nitrogen (N) [3, 4]. However, non stoichiometric oxygen also strongly affects the characteristics of the films. So, there is a growing interest in the formation of Ti suboxides (TiO_x), especially due to their lower resistivity [6]. Therefore, in this work, TiO_x films were grown by reactive grid-assisted magnetron sputtering (GAMS) from a Ti target at different oxygen concentrations in flow gas. The effect of the different titanium oxide phases on the optical and electrical properties of the thin films was evaluated.

2. Experimental

The films were deposited onto glass and silicon (substrates) by grid-assisted magnetron sputtering in an atmosphere of Ar and O_2, without substrate heating. The substrates were kept at floating potential. The silicon substrate was used only for film thickness measurements. The Ti target (purity 99.5%) used had 100 mm in diameter. Before each deposition, the chamber was evacuated to a base pressure less than 10^{-5} Torr (1.3 Pa) and the target was pre-sputtered in an Ar discharge for 2 min. The current was fixed at 1.00 A during depositions. The grid-target distance was kept at 2.0 cm and the Ar flow rate was around 2.4 sccm. The concentration of O_2 in the working gas flow rate (Γ) was varied in the range 0-70 %. The working pressure was 3.0 mTorr (0.40 Pa) for TiO_x depositions and 8.0 mTorr (1.1 Pa) for TiO_2 deposition (poisoned target), corresponding to Γ = 70 %. The films were analyzed by profilometry, optical spectrophotometry, X-ray diffraction (XRD) and X-ray photoelectron spectroscopy (XPS). The electrical properties were measured using the van der Pauw method.

3. Results and Discussions

The films thicknesses were about 150 nm for TiO_x and 80 nm for TiO_2. The formation of Ti suboxides is confirmed by XRD analysis, with most of the structures close to TiO. A possible factor for this small variety of suboxides is the low deposition temperature, as discussed by Hashimoto et al. [7] and Feil [5]. Different oxidation states were observed in XPS spectra. The contribution of Ti^{3+} and Ti^{2+} states falls with increased O_2 concentration, while the presence of Ti^{4+} states grows, showing the increase in the degree of oxidation of the films. It raises the resistivity (Fig. 1) and results in the formation of TiO_2. The high non stoichiometric oxygen decreases the resistivity of the films in more than two orders of magnitude when compared to TiO_2 (with resistivity in the order of 10^2 Ω.cm). The values of TiO_x films resistivity are very close to those found in TCOs.

The optical properties were also affected, with significant changes in reflectance and absorbance, as can be noted by the visual aspect of the films (Fig. 2). The presence of a second optical gap was identified for samples with Γ = 64% and Γ = 69%, shifting the absorbance to the region of visible and near infrared radiation. The transmittance of all TiO_x films is very small when compared to TiO_2, which forbid their use as TCO. It indicates that the current structure is not suitable for this purpose, so other mechanisms must be used to achieve the properties demanded by this application (such as Nb doping).

*Corresponding author: heitorwillker@hotmail.com

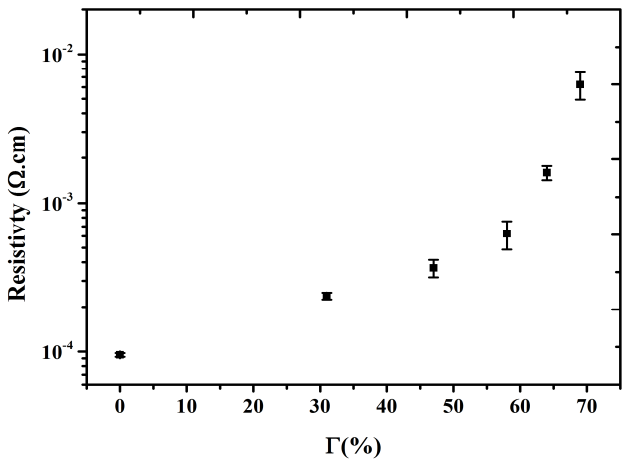

Fig. 1. *Resistivity as a function of O_2 concentration in working gas flow rate.*

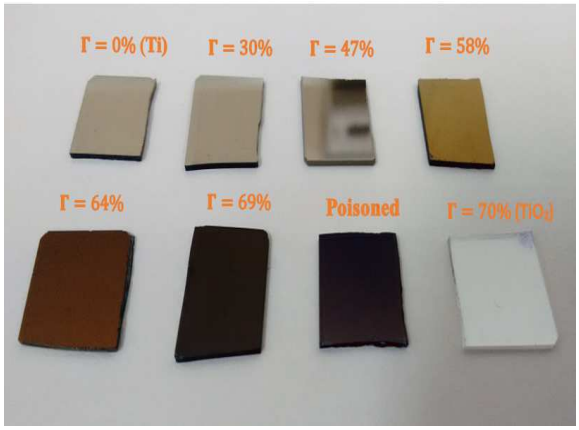

Fig. 2. *Changes in the color of the samples with O_2 concentration in gas flow.*

The results show that the optical properties of the films can be controlled through the insertion of oxygen, ranging from a specular appearance to films of yellow and blue coloration, and then to transparent films. In view of all these characteristics, there is the possibility of using the films as catalysts, since the active states (Ti^{3+} and Ti^{2+}) are responsible for performing, for example, the breakdown of the H_2O molecule; effect needed to produce self-cleaning windows.

4. References

[1] Diebold, U. Surface Science Reports, **48**, n. 5-8, 53-229 (2003).
[2] Hitosugi, T. et al. Physica Status Solidi (a), **207**, n. 7, 1529-1537, (2010).
[3] Furubayashi, Y., et al. Applied Physics Letters **86**, n. 25, 252101, (2005).
[4] Duarte, D. A.; Massi, M.; da Silva Sobrinho, A. S. International Journal of Photoenergy, **2014**, (2014).
[5] Feil, A. F. Deposição e caracterização de filmes finos de TiO_x formados por DC Magnetron Sputtering reativo: estudo de transição estrutural. Dissertação (Mestrado em Engenharia e Tecnologia de Materiais) - Pontifícia Universidade Católica do Rio Grande do Sul, Porto Alegre, (2006).
[6] Arif, A. F. et al. Scientific Reports, **7**, 3646, (2017)
[7] Hashimoto, S. et al. Surface Science, **556**, n. 1, 22-32, (2004).

Acknowledgments

The authors thank to PROMOP/UDESC by the financial support, and the Thin Film Laboratory (LOFF/UDESC); Synthesis and Catalysis Laboratory (SINCA) and the Technological Institute of the Aeronautics (ITA) for cooperation in the characterization of the samples.

*Corresponding author: heitorwillker@hotmail.com

RENEWABLE ENERGY: MICROBIAL FUEL CELLS

Gabriel Neto[1], Elizabeth C. A. Trindade[3], Daniel V. F. Vanin[3], Ana L. Tavares[2], Claudimir A. Carminatti[3], Regina V. Antônio[4] and Derce O. S. Recouvreux[3]*

[1]*Undergradute in Aerospace Engineering, UFSC, Joinville, SC, Brazil*

[2]*Undergraduate in Naval Engineering, UFSC, Joinville, SC, Brazil*

[3]*Graduate Program in Engineering and Mechanical Sciences, UFSC, Joinville, SC, Brazil*

[4]*Graduate Program in Energy and Sustainability, UFSC, Araranguá, SC, Brazil*

1. Introduction

Microbial fuel cells (MFC) have recently emerged as a promising and sustainable technology meeting the growing energy needs and sustainability, especially when wastewater is used as a substrate as a form of treatment. It can extract chemical energy from complex organic substrates and convert it into useful electricity, thereby proving to be an efficient manner of sustainable energy production [1].

MFC are systems capable of oxidize organic compounds and harvest free electrons, which are then transferred from the anode to the cathode via a conductive material connected by a resistor. This biological catalysis process, done by exoelectrogenic organism, produces electric current that can be further used to generate electrical energy [2].

There are different types of MFC; however, basic designs used in laboratories include double-chamber MFC, single-chamber MFC, upflow MFC and stacked MFC. A double-chamber MFC basically consists of a device with two compartments, an anodic and a cathodic chamber, a proton or cation exchange membrane and an electrical circuit. In the anodic region there are microorganisms that transfer electrons, resulted from the metabolism of organic compounds, to a negative electrode (anode) immersed in the culture medium. The electrons then flow through an electric circuit to the cathode, where protons along with electrons and oxygen can combine to form water. In addition, CO_2 and H_2 also are produced in the anodic chamber [3]. Anaerobic digestion of organic substrate by the microorganisms is essential for electrons release, because of their metabolism mechanism [3]. Industrial and domestic residues such as sewage, cattle, swine and brewery wastewaters have been employed as potential substrates in MFC technology achieving exceptional results [4]. Better bacteria adhesion on the anode electrode will positively influence electron transfer to the other chamber, as well as the electrode material plays an important role in the MFC system [5]. Schematic diagram of MFC is shown in Fig. 1.

Several studies have been carried out evaluating the anode performance with respect to its structural and chemical properties, which can be enhanced by using different types of electrodes. In this context, the aim of this work was to assemble a double-chamber H-shaped MFC with carbon fiber (CF) as an anodic electrode to produce electrical energy.

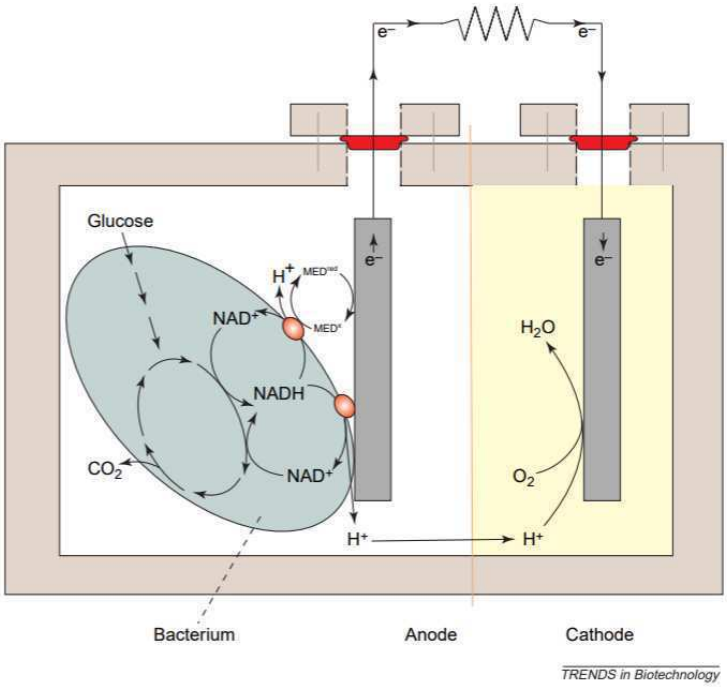

Fig. 1. *Schematic diagram of a double-chamber microbial fuel cell [6].*

*Corresponding author: derce.recouvreux@ufsc.br

2. Experimental

A fuel cell apparatus with two chambers and lateral outlets, H-shaped, containing electrodes for the cathode and anode, separated by a Nafion® 115 membrane, selective to H+ was constructed. Cathodic and anodic electrodes were fixed in titanium wire and connected by a 1000 Ω resistor. In the sterile anaerobic chamber (225 ml), which contains the CF electrode, cultures of the Escherichia coli bacteria cells (ATCC 25992) were inoculated (10% inoculum) in a Luria-Bertani medium (LB), along with glucose as electron donor, for the formation of a microbial biofilm and electricity generation. In the cathode chamber, a carbon cloth electrode was immerse in a potassium ferricyanide (III) ($K_3Fe(CN)_6$) and phosphate buffer solution, continuously bubbled with air. Daily measurements of the electric potential difference were obtained by a digital multimeter (Minipa ET1002) in order to monitor the MFC performance.

3. Results and Discussion

A double-chamber MFC containing CF electrode in the anode chamber was constructed in this study. In this fuel cell it was used a pure *E. coli* bacterial culture, glucose as the carbon source, and as electron donor. The performance of the MFC was monitored for 11 days. When electrical current production became stable the electric potential differences were measured daily with a digital multimeter and the data was recorded to determine the voltage production (Fig. 2). The greatest value observed for electric potential difference was 23.4 mV in the ninth day of operation (Fig. 3).

There are several factors involved in the efficiency of MFC, such as internal resistance, electrode potential and oxygen availability, which can increase the potential of MFC. Also, continuous electric power generation by MFCs is largely dependent on its reliance on biofilm formation by the microorganisms to facilitate electron transfer from the biofilm to the anode [7].

The results of this study, despite of presenting low electric power, it demonstrate that glucose can be used for electric power generation in MFC for practical applications. In particular, this study's parameters can be used as reference for other MFC configurations, as well as for testing electrodes and proton exchange membranes under development in our laboratory.

Fig. 2. *Set-up of H-shaped microbial fuel cells, constructed to evaluate the performance of a carbon fiber electrode.*

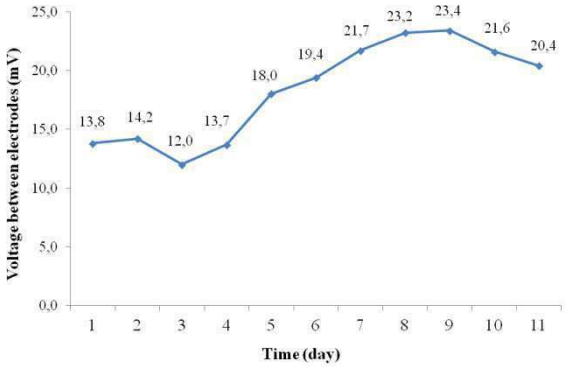

Fig. 3. *Electric potential (millivolts) for microbial fuel cells containing E. coli* bacteria *and carbon fiber anode electrode.*

4. References

[1] A. M. Moqsud, K. Omine, N. Yasufuku, M. Hyodo, Y. Nakata, Waste Manage. **33**, 2465-2469, (2013).
[2] D. R. Lovley, Nat Rev Microbiol **4**, 497-508, (2006).
[3] A. D. Tharali, N. Sain, W. J. Osborne, Frontiers in Life Science, **9**, 252–266, (2016).
[4] G. Zhao, F. Maa, L. Wei, H. Chua, C. C. Chang, X. J. Zhang, Waste Manage, **32**, 1651-1658, (2012).
[5] A. Terada, A. Yuasa, T. Kushimoto, S. Tsuneda, A. Katakai, M. Tamada, Microbiology, **152**, 3575-3583, (2006).
[6] K. Rabaey; W. Verstraete. Trends in Biotechnology, **23**, 291-298, (2005).
[7] B. E. Logan. Nat Rev Microbiol., **7**, 375-381, (2009).

Acknowledgments

The authors gratefully acknowledge the financial support of the Federal University of Santa Catarina, the Brazilian National Council for Scientific and Technological Development (CNPq) and Coordination for the Improvement of High Education Personnel (CAPES).

*Corresponding author: derce.recouvreux@ufsc.br

NANOCOMPOSITE STARCH/ BACTERIAL CELLULOSE NANOFIBERS FOR THE REMOVAL OF POLLUTANTS FROM AQUEOUS SOLUTIONS

Gabriel Teodoro[1], Ricardo Brandes[1], Claudimir Carminatti[1], Regina Antônio[2] and Derce Recouvreux[1]*
[1]*Graduate Program in Engineering and Mechanical Sciences, UFSC, Joinville, SC, Brazil*
[2]*Graduate Program in Energy and Sustainability, UFSC, Araranguá, SC, Brazil*

1. Introduction

Water pollution by chemicals is increasing and has become a major problem for public health and the environment. Wastewater originated from manufacturing and chemical processes in industries contributes to water pollution. Industrial wastewater usually contains chemical compounds in the form of toxic wastes and organic pollutants [1]. Various methods for water purification and recycling have been developed and used. Of these methods, adsorption presents itself as one of the most promising ways to treat water, due to its high efficiency, easy handling and availability in the form of a wide array of adsorbents. At an industrial level, pollutants are removed from water by using columns and contactors filled with suitable adsorbents [2].

Cellulose is the cheapest, most abundant and readily available polysaccharide on Earth, synthesized by plants and some microorganisms, such as fungi, algae and bacteria [3]. Bacterial cellulose (BC) has a unique nanostructure characterized by high purity due to the absence of lignin, hemicellulose, pectin and other compounds related to plant cellulose; high crystallinity (60-90%), high mechanical strength and a network structure constituted of nanofibers are also characteristics of BC [4].

Starch is a natural and biodegradable adsorbent, which has extensive applications on food, pharmaceuticals, tissue engineering, agriculture, cosmetics, pulp and paper, and other industrial applications [5]. Starch granules can be converted into thermoplastic starch (TPS) through the disruption of the molecular chain interactions under specific conditions and in the presence of plasticizers, such glycerol [6]. Starch is a sustainable biopolymer and a low cost alternative for the production of adsorbents. In spite of the aforementioned advantages of the use of starch-based plastics for a sustainable development, the applications of such materials are still restricted by their low mechanical properties [7]. The approach that has been used to overcome these drawbacks is the combination of BC with other polysaccharides, aiming to obtain biobased materials with distinct functionalities and enhanced properties. The combination with cellulose fibers is a way to improve the mechanical performance of starch-based materials. In particular, nanocellulose like BC has gained growing attention in the last decade because of its unique mechanical properties [8]. In this context, this work had as main objective the production of a nanocomposite constituted by starch and bacterial cellulose nanofibers for adsorption applications.

2. Experimental

The *Komagataeibacter hansenii* bacterium ATCC 23769, obtained from the collection of tropical culture (CCT) (André Tosello Foundation), Campinas - SP, was utilized for the production of BC. *K. hansenii* was cultivated in Erlenmeyer's flasks of 125 ml and the composition of the culture medium used was 25 $g \cdot l^{-1}$ glycerol of carbon source, 3 $g \cdot l^{-1}$ of peptone and 5 $g \cdot l^{-1}$ of yeast extract. The culture medium was prepared by dissolving the ingredients in distilled water and then autoclaving the mixture at 121 °C for 20 minutes. After the growing period of the BC was complete, the supernatant was collected, washed out with filtered water and submitted to purification in a 0.1 M NaOH solution at 60 °C for 24 hours to remove cell debris and contaminants of the culture medium. Once the purification process was completed, the BC membranes were disintegrated in water using a mixer and filtered in order remove the excess of water.

To prepare the nanocomposite, cassava starch (Yoki, Brazil) was gelatinized by suspending starch granules in distilled water (3% w/v) at 90 °C and continuously stirring the compost with a stirring rod. Glycerol (Nuclear-PA) (5% of dry weight of starch) was added and dispersed in the starch suspension. Subsequently, disintegrated BC (10 w/w, in relation to dry starch mass) was added, mechanically stirred and homogenized in an ultrasonic bath (USC-1880A) for 15 min. Finally, the nanocomposites were freeze-dried (L101, LioTop, Liobras) to obtain a porous structure.

The microstructure and morphology of the samples, freeze-dried under vacuum (-55 °C), were characterized with scanning electron microscopy (SEM) at LCME/UFSC microscope JEOL JSM-6390 LV. For observation in SEM, samples were placed in an aluminum slide and coated with gold. The surface of the samples was covered with a 30 nm layer of gold using a Leica EM SCD 500.

Adsorption analysis was developed by mechanically stirring the starch/BC nanocomposites (1 g) in a solution containing 50 ml of methylene blue (10 ppm) at pH 5.5. Samples of methylene blue solution were collected in amounts of 1 ml at different times and the absorbance was measured at 664 nm in a visible

*Corresponding author: derce.recouvreux@ufsc.br

spectrophotometer (Bel - Photonics, model 1105). The removal efficiency (%) of methylene blue by the starch/BC nanocomposites was defined according to Eq.

$$Removal\ efficiency\ (\%) = \frac{(C_o - C_f)}{C_o} \times 100 \quad (1)$$

where C_o and C_f are the initial and final concentrations of methylene blue solution (mg·l^{-1}), respectively.

3. Results and Discussion

The porous structure of starch-BC nanocomposites was obtained through freeze-drying and can be observed in the SEM micrographs as shown in Fig. 1. These images provided indication of the good dispersion of BC nanofibers on the starch matrix since no significant agglomerates of nanofibers are observed. This demonstrates the excellent compatibility between the starch and BC nanofibers. Fig. 1(a) shows the bacterial cellulose hydrogel produced. The hydrogel was disintegrated in order to be used on nanocomposites. Fig. 1(b) shows freeze-dried starch/BC nanocomposite. In the micrograph shown in Fig. 1(c) a dense layer coating the nanocomposite can be observed. The fractured surface shown on the SEM micrograph in Fig. 1(d) indicates the presence of a porous microstructure of starch/BC nanocomposite and an interconnected network of BC nanofibers inserted on the starch matrix.

Starch/BC nanocomposites were then submitted to adsorption test. The adsorption evaluation was based on the removal percentage of methylene blue by the nanocomposite, starting from an initial solution with a known concentration of methylene blue and measuring its subsequent concentrations after given time spans. The graph presented in Fig. 2 shows that the starch-BC nanocomposites reached a removal by adsorption efficiency of 70 (%) after 170 minutes. These results demonstrate that the nanocomposite's high capacity to remove methylene blue could be used to treat water contaminated by wastewater pollutants.

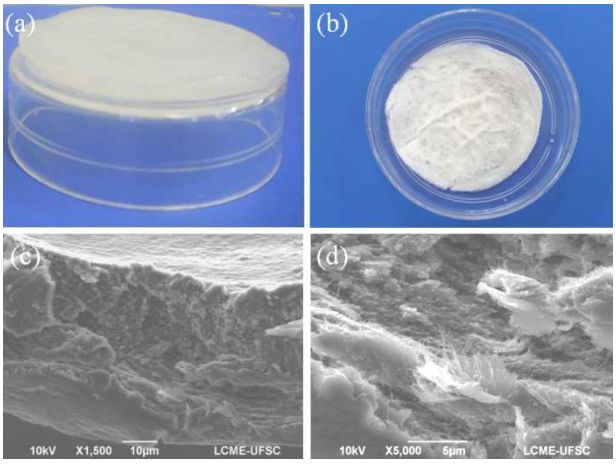

Fig. 1. *(a) Bacterial cellulose hidrogel, (b) Starch/BC nanocomposite freeze dried, (c) SEM micrographs of the fractured surface, (d) SEM micrographs of the porous microstructure observed in starch/BC nanocomposite.*

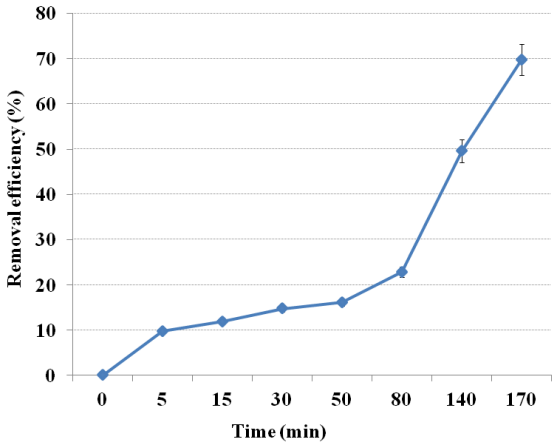

Fig. 2. *Removal efficiency of blue methylene by the starch/BC nanocomposite.*

4. References

[1] M. S. Abdel-Raouf, A. R. M. Abdul-Raheim, J. Pollut. Eff. Cont. **5**, 180-193, (2017).
[2] I. Ali1, V. K. Gupta, Nature Protocols, **1**, 2661-2668, (2006).
[3] R. J. Moon, A. Martini, J. Nairn, J. Simonsen, J. Youngblood, Cellulose nanomaterials review: structure, properties and nanocomposites, Chem. Soc. Rev., **40**, 3941-3994, (2011).
[4] R. Brandes, C. Carminatti, A. Mikowski, H. Al-Qureshi, D. Recouvreux, J. Nano Res., **45**, 142-154 (2017).
[5] P. R. Chang, J. G. Yu, X. F. Ma, Preparation of porous starch and its use as a structure-directing agent for production of porous zinc oxide. Carbohydrate Polymers, **83**, 1016-1019, (2011).
[6] A. Córdoba, N. Cuéllar, M. González, J. Medina, Carbohyd Polym, **73**, 409-416, (2008).
[7] A. K. Mohanty, M. Mirsa, T. Drzal, Journal of Polymers and the Environment, **10**, 19-26, (2002).
[8] L. C. Tomé, S. C. M. Fernandes, D. S. Perez, P. Sadocco, A. J. D. Silvestre, C. Pascoal Neto, I. M. Marrucho, C, S. R. Freire, Cellulose, **20**, 1807-1818, (2013).

Acknowledgments

The authors gratefully acknowledge the financial support of the Federal University of Santa Catarina and The Central Laboratory of Electronic Microscopy (LCME-UFSC) for microscopic analysis.

*Corresponding author: derce.recouvreux@ufsc.br

CARBON FIBERS FUNCTIONALIZATION THROUGH N_2-H_2 RADIOFREQUENCY PLASMA

Thayara Ceregatti[1]*, Carla Dalmolin[1] and Luis César Fontana[1]
[1] *Universidade do Estado de Santa Catarina, Centro de Ciências Tecnológicas, UDESC, Joinville-SC*

1. Introduction

Carbon fibers (CFs) are used for reinforcements in polymer matrix composites. It exhibits thermal stability and corrosion resistance [1]. Among various current collectors, carbon materials show good performance on supercapacitor or secondary battery electrodes. As the structure is malleable, carbon fiber is suitable to accommodate structural changes of conducting polymers such as polyaniline during electrochemical tests [2-4]. In addition, carbon fiber combines a large surface area, has low electrical resistance, and is a light and flexible material [1]. However, fabrics based on synthetic carbon fibers are often hydrophobic , due to the lack of polar functional groups [2]. The hydrophobic nature of these tissues limits their applications and therefore the plasma treatment has been studied to improve the wettability and to promote the formation of active sites for the growth of conductive polymers. [1,3,5].

2. Experimental

The clean and dry carbon fibers mesh (Panex 30 – USA) were cut into short segments (2 x 2 centimeters) and used as received. The plasma treatments were conducted inside of a plasma reactor, which consists of a glass chamber supported by two stainless steel brackets. The samples were fixed to a support made of ceramic and the chamber was evacuated to a base pressure of less than 0,01 Torr. When the pressure was stabilized, a gas mixture consisting of 20% N_2 and 80% H_2 was introduced into the chamber so that the working pressure was close to 1.0 Torr. The electric energy of the plasma was supplied by induction of electric field through a coil connected to an electric source operating in frequency of 13.56 MH. The power supplied to the plasma was 100 W and the treatment time ranged from 2 to 30 min.

Table 1. *Nomenclature used for each carbon fiber sample and its treatment parameters.*

Sample	Gases	Pressure/Torr	Power/W	Time/min
FC	--	--	--	--
FC02	$N_2 + H_2$	1,0	100	02
FC05	$N_2 + H_2$	1,0	100	05
FC10	$N_2 + H_2$	1,0	100	10
FC30	$N_2 + H_2$	1,0	100	30

3. Results and Discussions

The Plasma RF produced in N_2 / H_2 atmosphere was characterized by optical emission spectroscopy. The optical emission spectrum acquired during the treatment is shown in Figure 1. The emission lines / bands correspond mainly to H (atomic hydrogen) at 656.4 nm, to H_2 (molecular hydrogen), to N_2 (molecular nitrogen) at 337 nm, N_2^+ (391.4 nm), followed by N_2^* (315.8 nm) and NH (336 nm) excited species [1]. The presence of ions, excited species and atomic hydrogen indicates that reactivity of the plasma is high.

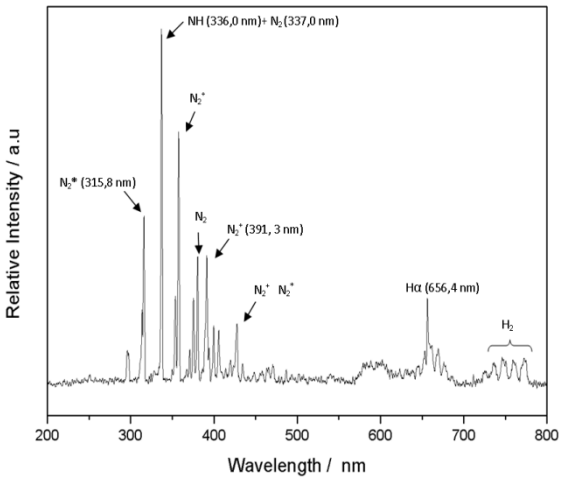

Fig. 1. *Optical emission spectra obtained in N2 / H2 RF plasma, used in carbon fiber treatments.*

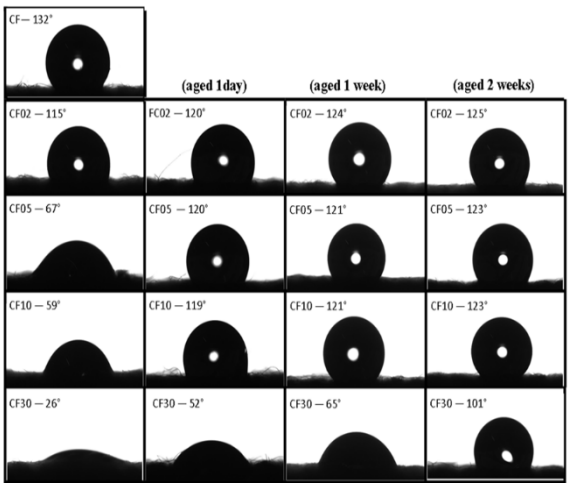

Fig. 2. *Droplets on Carbon Fiber fabric after treatments and the evolution of the contact angle over time.*

*Corresponding author: thay.ceregatti@gmail.com

The ability to modify the surface of the carbon fibers by plasma was verified by performing measurements of static contact angle with deionized water in the samples. Figure 2 shows the water droplets in the CF tissues treated at different times, followed by the evolution of the contact angle value over time. After treatment with plasma, the wettability increased in all cases, indicating that a large number of radicals were generated on the surface of the fiber by breaking the C-C bonds, and to the introduction of several N and N-H groups in the surface, which turned the samples more hydrophilic. The evolution of the contact angle over time had significant changes. On the first day, the measured angles increased rapidly, but this progression became slower and the angle stabilized at approximately 120 °, which somewhat less than the value is observed prior to treatment. That is, there is a tendency for fiber to recover the value of contact angle to restore the state of lower free energy.

For the determination of the groups that may be present on fiber surface, samples were studied by XPS, 48 hours after plasma treatment. Typical XPS spectra of the untreated (CF) and plasma treated FCs for 5 minutes (CF05) and 10 minutes (CF10) are shown in Figure 3. The quantitative values are shown in Table 2. The major peaks shown in the spectra were characterized as C (1s), O (1s), N (1s). Oxygen is present in all samples, but its intensity after plasma treatment has increased. It is believed that CF surfaces became highly reactive after plasma treatment and it may have occurred oxidation of the surface through the reaction with the oxygen present in the air. The static contact angle measurements have indeed shown that the angle tends to stabilize after a few hours in contact with atmospheric air. As intended, Nitrogen is present in samples treated by plasma. Optical spectroscopy inside the plasma showed an abundance of N2* and NH reactive species that can collide with CF surface, breaking C-C bonds, and inserting N into the carbon structure. However, longer plasma treatments reduced the N content in the samples, indicating that a higher exposure of the CF to the plasma may reduce the nitrogen adsorption due to an increase in the temperature of the samples.

Table 2. *XPS results obtained from carbon fibers untreated and treated by plasma (at. %).*

Condition	O (1s)	N (1s)	C (1s)
CF Untreated	1,56	N/A	98,26
CF 05 min plasma	10,0	1,57	83,82
CF 10 min plasma	9,94	0,63	85,96

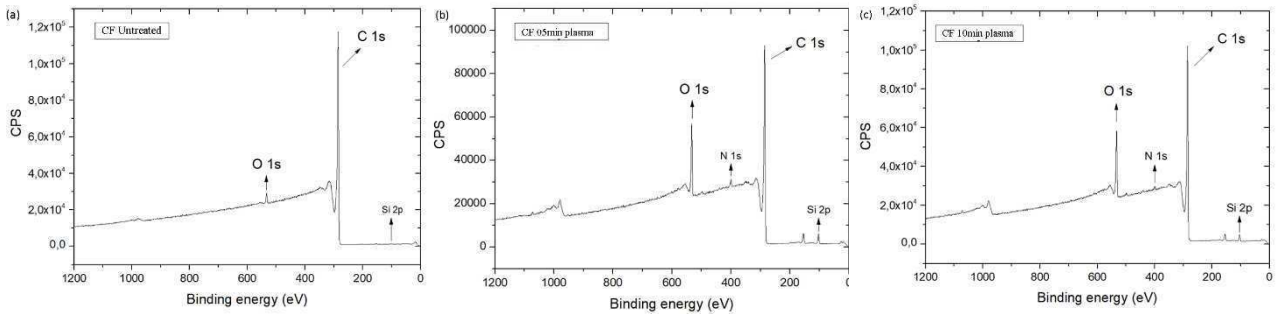

Fig. 3. *X-ray photoelectron spectra corresponding to (a) CF untreated and (b) RF plasma treated carbon fiber (5 min) and (c) RF plasma treated carbon fiber (10 min).*

Functionalization of carbon fibers with plasma technology is promising since the plasma is reactive. The plasma treatment reduced the contact angle of the carbon surfaces and the analyzes of the XPS indicated the presence of functional groups in the surface carbon fiber but the time of the treatment, the temperature of the plasma and the exposure of the samples in the air must be controlled.

4. References (bold face Times New Roman 11 pt)

[1] CORUJEIRA, S.; CHARITIDISHANSHAN, G. Vacuum, Surfaces, and Films, 35, 021404, (2017).
[2] CANOBRE, S. C. Doctoral Thesis – UFSCar, (2004).
[3] CHANG, W. M.; WANG, C. C.; CHEN, C. Y. Electrochimica Acta, **212**, 130–140, (2016).
[4]KOTAL, M. et al. Applied Materials and Interfaces, **5**, 17, 8374–8386, (2013).
[5] TIWARI, S.; BIJWE, J. Procedia Technology, **14**, 505–512, (2014).

Acknowledgments
Authors would like to thank UDESC, FAPESC, CAPES and CNPq for scholarships and grants that made this work possible.

*Corresponding author: thay.ceregatti@gmail.com

ONE-POT SYNTHESIS OF SILVER NANOWIRES/POLYPYRROLE NANOCOMPOSITES AT ROOM TEMPERATURE

Rodolfo A. Baratto[1] and Sergio H. Pezzin[1]*
[1]*Santa Catarina State University, Center of Technological Sciences, Chemistry Department, Joinville-SC, Brazil*

1. Introduction

One-dimensional (1D) silver nanomaterials and its composites have applications in transparent and conductive electrodes, solar cells, electrochemical capacitors, ion lithium/lithium-oxygen batteries, electrochemical sensors and catalysis [1,2]. A composite of silver nanowires (AgNW`s) and polypyrrole (PPy), in a core-shell nanostructure (coaxial nanocables) where a silver nanowire is the core and a layer of polypyrrole is the shell, can enhance the electrochemical properties and the durability of both the materials simultaneously. In order to avoid the use of organic solvents and high temperatures during the synthesis process, as well as to avoid purification and separation processes, a one-pot method was developed to synthesize AgNW-Ppy nanocables in aqueous media and room temperature.

2. Experimental

The silver nanostructures and the polypyrrole layer that covers them are produced simultaneously by the redox reaction between silver nitrate and pyrrole monomer in the presence of the capping agent polyvinylpyrrolidone (PVP). Pyrrole (≥98%), polyvinylpyrrolidone (PVP, Mn ~ 40,000 g mol^{-1}), and $AgNO_3$ (≥99.5%) were purchased from Sigma-Aldrich. Pyrrole was purified by distillation before use, while all other chemicals were used without further purification.

The Ag/PPy nanocables and other nanoparticles were synthesized through the redox reaction between $AgNO_3$ and the pyrrole monomer in aqueous medium and in the presence of PVP, yielding a composite of polypyrrole and silver. Nitric acid is a by-product [3]. All experiments were performed under constant stirring, at room temperature and using deionized water. $AgNO_3$ solutions have been added to the system at a constant rate by means of a syringe pump.

3. Results and Discussions

Fourier transform infrared and ultraviolet-visible spectroscopies confirm the formation of doped (conductive) PPy. Scanning electron microscopy (SEM) images show that, initially, there is the formation of small hexagonal silver crystals, then, some of these crystals evolve to Ag/PPy nanocables, while others give rise to a series of different nanostructures caped with PPy. The relative amounts of these nanostructures depend on the reaction conditions, which govern faceting and branching crystal growth mechanisms.

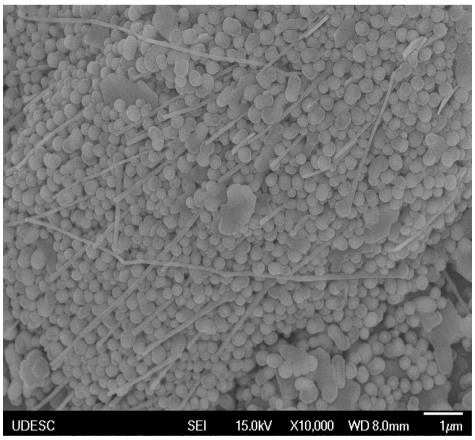

Fig. 1. *SEM image showing high aspect ratio Ag/PPy nanocables along with nanospheres that consist mostly of smaller PPy coated silver nanohexagons.*

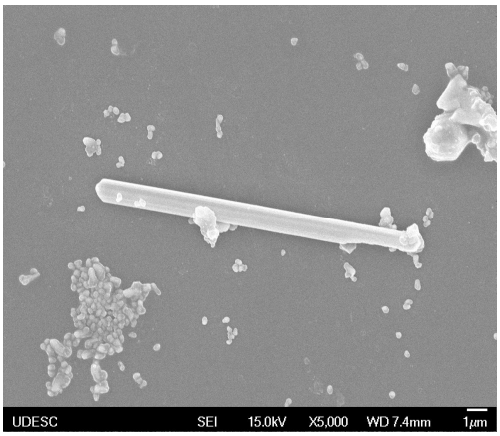

Fig. 2. *SEM image showing a Ag/PPy columnar crystal, after 72h of reaction.*

The results indicate that Ag/PPy nanocables evolve from silver nanohexagons, which form in the beginning of the reaction, by branching. It occurs more likely in faster growing crystals within a medium size range. If branching conditions are not achieved, faceting prevails and silver nanohexagons became small PPy caped nanospheres or larger smooth faceted sheets. Under some certain conditions silver nanohexagons can evolve to columnar crystals (hexagonal prisms), however, this mechanism is yet not well understood.

The variations of this method proved to have potential to the production of a series of PPy coated nanoparticles: high aspect ratio nanocables, nanorods, nanohexagons, faceted sheets and nanospheres. Also, if desired, the PPy layer could be easily removed if there is interest only in the silver nanoparticle. Reaction rate and temperature are both factors that influence crystal growth velocity and final morphology, both still need to be better understood in future studies.

Moreover, UV/VIS/NIR and FTIR spectroscopies confirm the formation of polypyrrole in its conductive state (doped with NO_3^-), while thermogravimetric analysis (TGA) shows an increase in thermal stability with the increase in the mass% of silver nanoparticles in the material, which may be related to the increase in orderliness of PPy chains.

4. References

[1] L. Botian, W. Xing, T. Liming, Progress in Chemistry, **30**, 338-348, (2018).
[2] K. M. Coakley, M. D. McGehee, Chem. Mater., **16**, 4533–4542, (2004).
[3] J. Stejskal, Chem. Papers, **67**, 814–848, (2013).

Acknowledgments

CAPES, FAPESC (484/2017, 2017TR867), Prof. Dr. Marcio Vidotti (UFPR).

PULSED REACTIVE SPUTTER DEPOSITION: INSIGHTS FROM BERG MODEL

Júlia Karnopp* and Julio César Sagás
Laboratory of Plasmas, Films and Surfaces, Santa Catarina State University (UDESC), Joinville -SC

1. Introduction

In magnetron sputtering deposition, ions generated in magnetically confined plasma collide with a metal target and remove atoms from its surface. The insertion of a reactive gas into the chamber allows the formation of compound films on substrate and also on target surface, causing the phenomenon of poisoning. The compound formation on surfaces become the discharge unstable and causes the hysteresis on the process curves (pressure, voltage, etc.) as a function of reactive gas flow rate. The reaction between reactive gas and metal atoms can form a dielectric compound film on target, leading to arcing [1]. To avoid this, it is common the use of pulsed magnetrons [1]. During the pulse off, the target bias goes close to ground (unipolar pulse) or to slightly positive values (bipolar pulse). By this procedure, the positive charge accumulated on compound surface can be neutralized.

The pulsed magnetron discharge can exhibit a different dynamic than in DC mode. In plasma, the gettering of reactive gas is increased by dissociation and formation of excited species. In the pulsed discharge, if the current is switched off, the electron generation decreases and, consequently, the creation of other species. This can change the chemisorption rate of reactive gas on surfaces, as well as, the sputtering rate.

The dynamic of pulsed reactive sputtering has already been studied using an earlier version of Berg model [3], but the processes of direct implantation and knock-on of reactive gas in target were not included and the sticking coefficient was considered constant during all the pulse. These effects can be included using the upgraded Berg model [4]. In the present work, the pulsed reactive sputtering was simulated considering the processes of implantation of reactive gas and variation of the sticking coefficient in phase with the current, in order to analyze the dynamics of compound formation.

2. Methodology

The dynamic of pulsed reactive sputtering deposition was simulated using the Berg model with two layers in the target [4]. It must be pointed out that the use of only two layers: surface (where occurs chemisorption) and sub-surface (where occurs implantation) cannot reproduce correctly the time scale, but it allows to investigate the overall mechanisms. The simulations were made for constant current (0.5 A) and square pulsed current between 0.0 A and 1.0 A. The duty cycle was fixed at 50% and the frequency was varied (10 Hz, 100 Hz and 1000 Hz). In $t = 0$ the pulse is on. The sticking coefficients for substrate and target were pulsed in phase with current to simulate the effect of modification in gas composition during pulse on and off. A more reactive environment is expected during pulse on, which reflects in a higher adsorption probability. Three different situations were simulated, with sticking coefficients of 0.02, 0.08 and 0.10 during pulse off and 0.10 during pulse on. The gas flow rate used is 1.5 sccm. This value corresponds to target poisoning for constant current constant of 0.5 A and sticking coefficient equal to 0.10.

3. Results and Discussions

When the current is pulsed, all processes that contribute to increase or decrease the compound fraction on surfaces (and partial pressure) vary in time, as can be seen in figures 1 and 2. During the pulse on, the current and sticking coefficient are maximum, consequently the rates of chemisorption, implantation and sputtering are high. The compound fractions on substrate and target surfaces reduce due to the high sputtering and deposition rates, and the reactive gas partial pressure decreases due to the higher gas consumption, as can be seen in between 0.1 s e 0.15 s for 10 Hz (figure 1). On the other hand, when the pulse is off, the sputtering and implantation rates are null and the partial pressure of reactive gas increase due to reduction on gas consumption by surfaces after compound formation.

Increasing sticking coefficient during the pulse off, from 0.02 to 0.08, the amplitude of the variations and the average value of compound fractions on substrate and target increase. It is caused by the raise in the compound formation rate during pulse off. In fact, for 0.08, the compound fraction in target became 1.0 when the pulse is off, for 10 Hz and 100 Hz. For 0.02, it occurs only for 10 Hz.

*Corresponding author: julia_karnopp@outlook.com

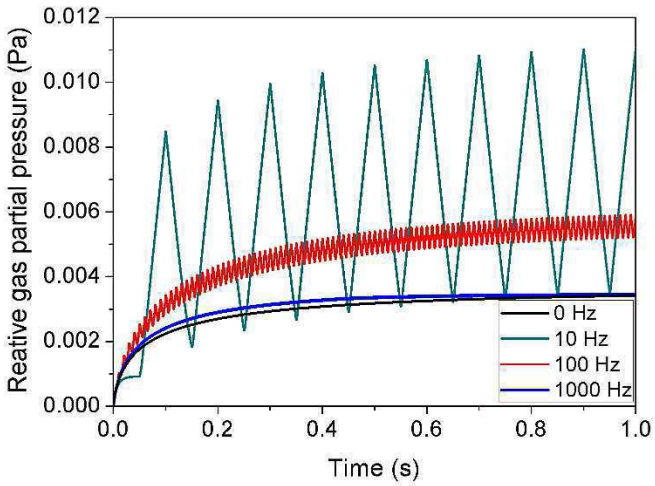

Fig. 1. *Reactive gas partial pressure for different frequencies and sticking coefficient pulsing between 0.08 and 0.1.*

With the increase in pulse frequency, the amplitude of variations in compound fractions and pressure decreases. In addition, the average value of these parameters reduces and approximates to the value for constant current (Fig. 1 and 2). When the frequency increases the system response to oscillations is reduced. For very high values the system cannot respond to variations in current.

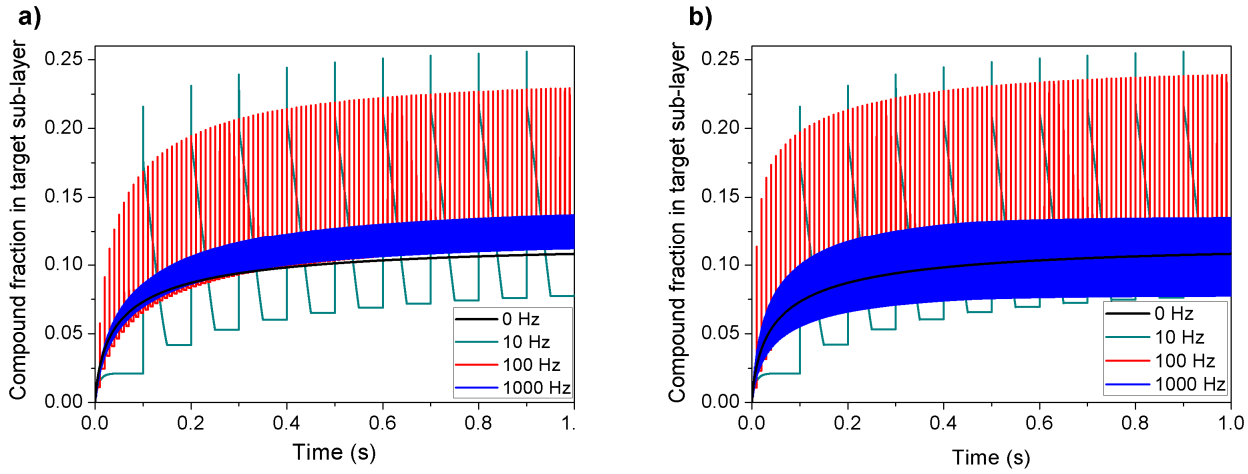

Fig 2. *Compound fraction in target sub-layer for different pulse frequencies and sticking coefficient pulsing between 0.02 e 0.10 (a) and between 0.08 and 0.10 (b).*

The figures 1 and 2 show the compound fraction on target sub-layer. This fraction increases by direct implantation and knock-on and decreases when the reactive gas atoms are transferred to surface layer after sputtering. When the pulse is on (as in 0.1 s for 10 Hz) the implantation rate is high, and the compound fraction increases until a peak. After, the current is constant and the compound fraction on sub-layer declines towards a minimum value when the pulse is turned off, remaining constant until the next pulse. All process in sub-layer are interrupted during pulse off, while the chemisorption still going on at surface. Thus, the behavior of sub-layer can be slightly different from target surface.

4. References

[1] A. Anders, J. Appl. Phys. 121, 171101 (2017)
[2] B. Chapman “Glow Discharge Process: Sputtering and Plasma Etching”, John Wiley e Sons (1980)
[3] L. B. Jonsson, T. Nyberg, and S. Berg. J. Vac. Sci. Technol. A, 18, 503 (2000)
[4] S. Berg, E. Särhammar, Thin Solid Films, 565, 186–192, (2014)

Acknowledgments

The authors thank to PROBIC-UDESC and to FAPESC by the financial support.

*Corresponding author: julia_karnopp@outlook.com

ENERGY FLUX TO THE SUBSTRATE IN PULSED AND GRID-ASSISTED MAGNETRON SPUTTERING

Thais Macedo Vieira* and Julio César Sagás
Laboratory of Plasmas, Films and Surfaces, Santa Catarina State University (UDESC), Joinville -SC

1. Introduction

Among the several film deposition processes, magnetron sputtering stands out. The process consists of a magnetically confined discharge in front of a cathode (target). The ions generated in the plasma are accelerated towards the target, leading to the sputtering phenomenon. The ejected atoms condense on a surface (substrate) forming the film. Different configurations of magnetron sputtering system were developed, as the pulsed magnetron sputtering [1] and the grid-assisted magnetron sputtering [2].
The structure and properties of films are strongly dependent of parameters involved in deposition. The bombardment of substrate by energetic particles (ions, metastable, electrons, etc) provides energy to the film during its growth. This energy transfer affects the density, morphology and crystalline phase of the film. So, the energy flux to the substrate must be monitored to control the properties of deposited material [3].

2. Experimental

A calorimetric probe [4] was designed and constructed to measure the energy flux during film deposition. The probe consists of a copper disk with 20 mm in diameter and 2.0 mm in thickness. The choice for copper is due to its high thermal conductivity. The reduced dimensions also ensure the measurement time can be fast, since the time to stabilize the temperature will be small. The probe is placed in a cylindrical Macor ceramic base. The probe temperature is monitored by a type K thermocouple inserted in the probe. Measurement time was about ten minutes for each condition.
The experiments were made with a stainless steel target (100 mm in diameter) in a pure argon discharge. The working pressure used was around 0.40 Pa. The probe-to-target distance was fixed at 6.0 cm. Initially, with the probe at potential floating, measurements were made for different plasma power (20, 50, 100, 200, 400, 600, 800 and 1000 W), in order to verify the proper operation of the probe. Subsequently, the power supply was used in asymmetrical pulsed mode with pulse time off and power set at 1.1 μs and 400 W, respectively. These measurements were made for frequencies of 0, 50, 100, 150, 150 and 200 kHz. To compare the grid-assisted magnetron sputtering to the conventional magnetron sputtering, the probe was also grounded, negatively (-90 V) and positively biased (20 V) using a DC power of 400 W in target. For measurements in the grid-assisted magnetron sputtering, the grid-to-target distance was fixed at 2.0 cm.

3. Results and Discussions

It is observed that increasing the discharge power, the energy flux to the substrate rises, as expected. On the other hand, increasing the discharge frequency, there is a reduction in energy flux (Fig. 1). Once that the pulse off time is fixed, the increase in frequency implies in a reduction of pulse on time. This can be a possible explanation to the observed behavior. However, a detailed analysis of voltage and current waveforms are needed. It is noted that from 0 to 200 kHz, the energy flux reduction is around 100 W/m^2.

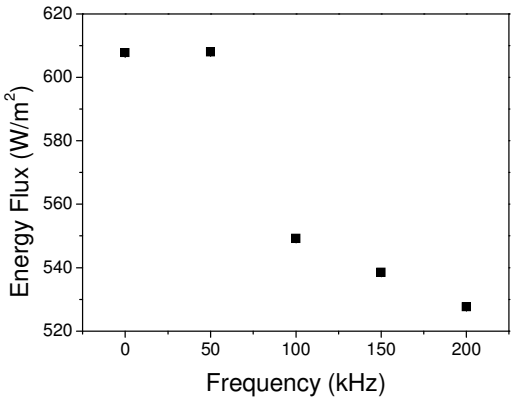

Fig. 1. *Energy flux to the substrate as function of pulse frequency for conventional magnetron.*

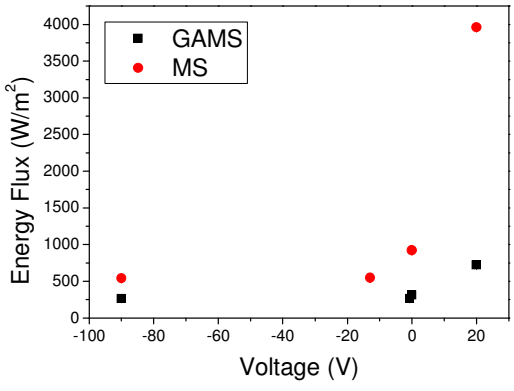

Fig. 2. *Energy flux at different bias conditions for conventional (MS) and grid-assisted (GAMS) magnetron sputtering*.

*Corresponding author: vieira.thaism@gmail.com

When the probe is biased, a much higher energy flux is observed for positive bias, as a result of much larger substrate current (around 100 mA for 20 V), when compared to negative bias (around 11,5 mA for -90V). The large difference in substrate current is caused by the change in majority charge carrier with bias. For positive bias, the current is predominantly electronic, while it is predominantly ionic for negative bias. The energy flux to the substrate during deposition with the presence of the grid between the target and the substrate is small when compared to conventional magnetron. The difference is greater when the probe is biased at 20 V (Fig. 2).

The lower energy flux measured in grid assisted magnetron sputtering is consequence of plasma confinement between the target and the grid. The presence of the grid reduces ion and electron bombardment, once that the plasma is kept away from the substrate. These results show that grid-assisted magnetron sputtering is more suitable for deposition onto thermally sensitive substrates, even for positive bias.

4. References

[1] C. Yang, et al.. Surface and Coatings Technology, 304, 51-56, (2016).
[2] L. C. Fontana, J. R. L. Muzart. Surface and Coatings Technology, 107, 24-30, (1998).
[3] Cormier, P.-A. et al.. Surface and Coatings Technology**,** 254, 291-297, (2014).
[4] Kersten, H., Deutsch, H., Steffen, H., Kroesen, G. M. W., Hippler, R., Vacuum, *63*, 385–431, (2001).

Acknowledgments

T.M. Vieira thanks UDESC by the financial support through PROBIC grant.

*Corresponding author: vieira.thaism@gmail.com

CHARACTERIZATION OF A PLATINUM/ALUMINA CATALYTIC MONOLITH FOR ETHANOL REFORMING

Mauro E. Silva Júnior[1,2], Maíra O. Palm[2], Diego A. Duarte[2] and Rafael de C. Catapan[2]*
[1]*University of Joinville Region, Chemical Engineering Department, Joinville, Brazil*
[2]*Federal University of Santa Catarina, Joinville Center of Technology, Joinville, Brazil*

1. Introduction

Supported catalysts are widely used in reforming reactions for H_2 production. The support has the role of providing an extensive surface area for deposition of the active phase, preventing metal agglomerations [1]. Alumina (Al_2O_3) is usually used as support because of its thermal stability at high temperatures, good interaction with the metal and low cost [2,3]. Several metals are used as active phase. Platinum (Pt) is used because its higher selectivity for H_2 at low temperature reaction, good stability in reactions conditions and activity for water gas shift reaction, which favors H_2 production when compared to others non-noble metals [4,5]. The objective of this work was to investigate the morphological characteristics of the Pt/Al_2O_3 catalyst. Scanning electron microscopy (SEM), energy dispersive spectroscopy (EDS) and X-ray diffraction (XRD) techniques were used to analyze the morphological characteristics, metal dispersion and interaction metal-support.

2. Experimental

Commercial foams of Al_2O_3 (supplied by Goodfellow), with 26 pores/cm, 12.7 mm thick and 15 mm in diameter, were used as support for the monolith. Platinum was impregnated using an aqueous solution of $H_2PtCl_6 \bullet 6H_2O$ with concentration of 0,0257 M for 16 h. Monoliths were dried at 150 ºC overnight under 50 cm^3/min of air flow and then calcinated at 600 ºC under air during 2 h. Monoliths were characterized using SEM, EDS and XRD.

3. Results and Discussions

Figure 1 shows the support after impregnation step. Visually there was a change in the color of the support. The shade of gray was proportional to the concentration of platinum in the support. In the external pores of the support, the impregnation was more effective, due to easier diffusion of the precursor solution onto the surface. When analyzing through the inner region of the monolithic structure, the capillary pressure provides resistance to the diffusion of the precursor solution to the internal pores [6].

Fig.1. *Monolith used for support.*

Figure 2 shows the external surface of the catalyst. It was observed that the active phase was distributed throughout the surface of the monolith. Figure 3 shows XRD spectrum for the non-impregnated support and impregnated support. Peaks relative to platinum (ICDD 01-087-0636) were detected at 2θ equal 39.7º relative to plane (111) and 46.2º relative to plane (200) [7]. Platinum particle size was estimated using Scherrer equation, resulting in average size of 38.4 nm. Between 2θ values of 75º and 85º there was a widening of the peaks, possibly due to the interaction of the Pt with the support.

Figure 4 shows the comparison between Al_2O_3 surface without the impregnation step and after the impregnation step. After the impregnation of the foam, small particles appeared on the surface of support, associated with the platinum particles. Figure 5 shows different regions of the external surface of catalyst. Figure 5a shows regions where the active phase was agglomerated. Figure 4b shows the region where active phase was highly dispersed on the surface of Al_2O_3. The agglomeration of the active phase occurred in the drying and calcination step [8].

*Corresponding author: rafael.catapan@ufsc.br

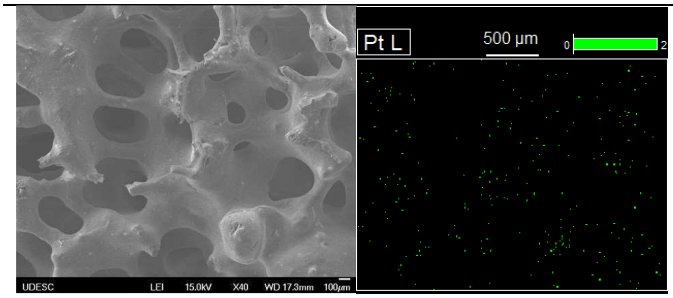

Fig. 2. *SEM showing the surface of catalyst.*

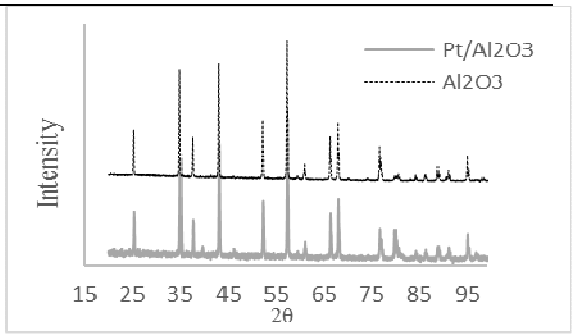

Fig. 3. *XRD spectrum of catalyst.*

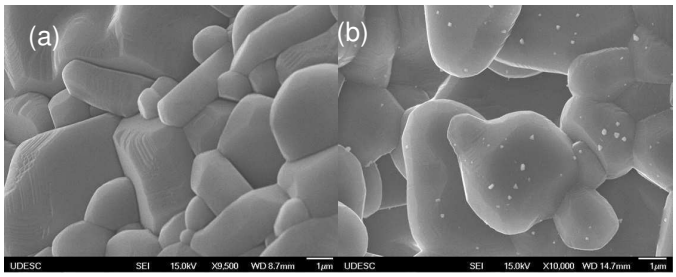

Fig. 4. *(a) non – impregnated support; (b) impregnated support.*

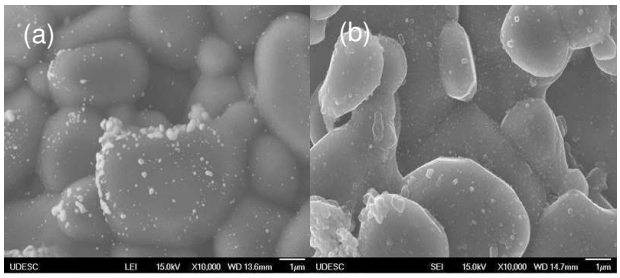

Fig.5. *(a) Agglomeration regions; (b) Disperse regions.*

Figure 7 shows a comparative between external and internal surface of the catalyst. Figure 7a, the image of the external surface, the presence of Pt sites is observed, while on the internal surface, Figure 7b, the site concentration is much lower. This indicates non-uniform impregnation, with a concentration gradient in the monolith. Non-uniform impregnation can occur by several factors, being influenced by the drying and calcination step, concentration and temperature of the precursor solution, impregnation time and support structure [6,8].

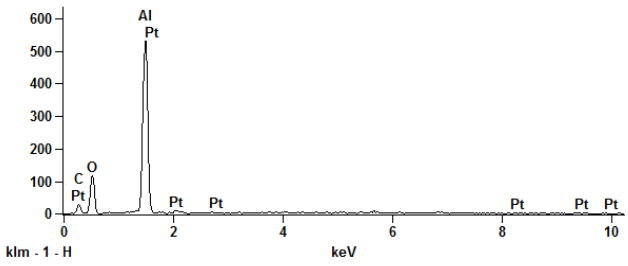

Fig. 6. *EDS showing the presence of Pt particles in disperse region of Fig. 5b.*

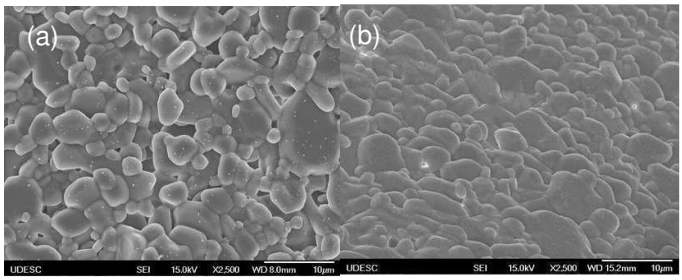

Fig.7. *(a) External surface, (b) Internal surface of the catalyst.*

New techniques for impregnation of the active phase should be investigated to improve the distribution of the active phase on the support, maximizing the use of the monolithic structure, without changing the total metal content desired.

4. References

[1] D.K. Liguras; K. Goundani and X.E.Verykios, *J. of Pow. Sour.* **2004**, 130, 30-37.
[2] C. Agrafiotis; A. Tsetsekou. *J. of Mat. Sci.* **2000**, 35, 951-960.
[3] R. Faure, *et al.*, *J. of Europ. Cer. Soc.* **2011**, 31, 303-312.
[4] T. Hou, *et al.*, *J. Renew. Sustain. Ener.* **2015**, 44, 132-148.
[5] M. Schmal, *et al.*, *Can. J. Che. Eng.* **2011**, 89, 1166-1175.
[6] C. Perego; P. Villa. *Catal. Today*. **1997**, 34, 281-305.
[7] A. Fernández, *et al.*, *Appl. Catal. B-Environ.* **2016**, 180, 336-343.
[8] T. Vergunst; F. Kapteijin; J. A. Moulijn, *Appl. Catal. A-Gen.* **2001**, 213, 179-187.

Acknowledgments

This work was funded by BMW do Brasil under 2016/0110 UFSC's project.

*Corresponding author: rafael.catapan@ufsc.br

DEVELOPMENT OF SOFTWARE FOR XPS SPECTRA ANALYSIS

L. R. Cardoso*, M. O. Palm, T. P. de Carvalho, D. A. Duarte* and R. C. Catapan
Federal University of Santa Catarina, Technological Center of Joinville, Joinville, 89219-600, SC, Brazil.

1. Introduction

X-ray Photoelectron Spectroscopy (XPS) or Electron Spectroscopy for Chemical Analysis (ESCA) is a technique widely used in materials science for surface analysis [1, 2]. This method was proposed by the Siegbahn's team in the late 50s [3, 4] and is based in the principle of the photoelectric effect, first observed by Heinrich Hertz and outlined by Albert Einstein. The experiment provides ample information about the chemical nature of the material and consists in the emission of photoelectrons from solid surfaces due to the incidence of high energy photons (soft X-ray). These lines penetrate around 10 atomic layers (10 nm) below surface, which makes XPS a suitable technique for investigation of solid surfaces and solid-gas boundaries [5, 6]. The kinetic energy *K* of the photoelectrons is measured by energy analyzers and the binding energy *U* is calculated from the conservation principle, where the amount of collected photoelectrons (counts per second – CPS) is graphically presented, by the equipment, as function of *K* or *U*. The result is a spectrum with several lines (peaks) where each one represents the element and orbital from which electrons are coming from. Despite providing a large amount of data, specific techniques are needed to extract hidden information from spectrum, such as, the chemical concentration and intensity of oxidized states, located around a given peak assigned to a metallic atom. This paper presents an analysis of Ni catalysts supported on Al_2O_3, performed using an original software produced by our research group and written in Python that was developed to conduct fast calculations using optimization techniques.

2. Materials and methods

This study applies the Trust-Region method for spectrum deconvolution in Gaussian-Lorentzian peaks with the L/G ratio optimized, where the background may be subtracted by Shirley [8] or Tougaard algorithm [9]. The program (called XPS Peak Finder) was written in Python language and presents a simple graphic user interface (GUI), where either students or professional researchers can use it. The software calculates the peak intensity, position, L/G ratio and the full width at half maximum (FWHM) of each deconvoluted peak. The present analysis was applied for investigation of Ni catalysts supported on Al_2O_3 foams and a TiO_2 film with deconvolution of the Ni2p and Ti2p orbitals, respectively.

3. Results and Discussions

Figure 1 and 2 present the Ni2p and Ti2p signals. Background of the Ni2p orbital was removed by Shirley method [8]. The subtracted data were used for deconvolution. Figure 1 shows a complex spectrum deconvoluted in twelve (12) peaks. In this case is observed spin-orbit coupling. The six first peaks, in the lower BE side, are assigned to spin 3/2. The last ones, to spin 1/2. The $2p_{3/2}$ signal shows three peaks located at 853.58, 855.07 and 856.08 eV. The first one is assigned to metallic Ni (Ni^0). The other ones are related to oxidized states. The same behavior is observed to the $2p_{1/2}$ signal. Peaks are located at 870.78, 872.06 and 873.61 eV. The modeled spectrum presents 0.56% arithmetic error.

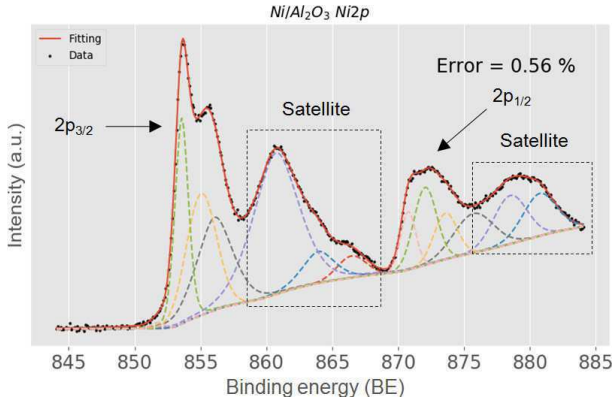

Fig. 1. *Deconvolution of the Ni2p orbital for Ni-covered Al_2O_3 ceramic foam. Signal is presented as function of the binding energy (option selected by user).*

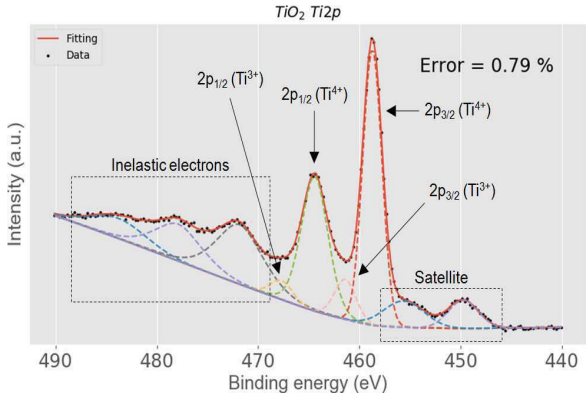

Fig. 2. *Deconvolution of the Ti2p orbital for TiO_2 deposited by reactive sputtering. Signal is presented as function of the binding energy (option selected by user).*

*Corresponding authors: leonardorudolfocardoso@gmail.com or diego.duarte@ufsc.br

The background of the Ti2p orbital was removed by Tougaard method [9]. The subtracted data were used for deconvolution. Figure 2 shows data deconvoluted in nine (9) peaks, where the two first ones are satellite electrons. The three last peaks, in the higher BE side, are signals related to inelastic electrons. Two main peaks in figure 2 are related to the spin-orbit coupling of the orbital 2p. Both signals are related to oxidized states Ti^{4+}. Each peak also presents Ti^{3+} signals, assigned to oxygen deficiency on the film surface. Oxidized states are fundamental for catalysis [7]. The simulated spectrum presents 0.79% arithmetic error. Even though the arithmetic errors are low, the code solves only the mathematical problem. The user must have a certain degree of knowledge regarding the nature of the material under investigation to provide the software a reliable initial guesses for the number of peaks and their respective positions, ensuring an accurate peak deconvolution and avoiding spectra misinterpretation. The correct application of these conditions makes the XPS Peak Finder a trustworthy tool for XPS spectra analysis.

4. References

[1] E. Bubert, H. Jennet, Surface and thin film analysis, Wiley-VCH (2002).
[2] D. Briggs, J. T. Grant, Surface analysis by Auger and X-ray photoelectron spectroscopy, IM Publications and Surface Spectra, Manchester, 2003.
[3] C. Nordling, E. Sokolowski, K. Siegbahn, Precision Method for Obtaining Absolute Values of Atomic Binding Energies, Phys. Rev., 105 (1957) 1676.
[4] E. Sokolowski, C. Nordling, K. Siegbahn, Chemical shift effect in inner electronic levels of Cu due to oxidation, Phys. Rev., 110 (1958) 776.
[5] H. Bubert, J. Rivière, in Surface and Thin Film Analysis, ed. By H. Bubert and H. Jenett (Wiley-VCH, Weinheim, 2002), p. 6.
[6] C. C. Chusuei, D. W. Goodman, X-ray photoelectron spectroscopy: Encyclopedia of Physical Sciences and Technology, 3rd ed., Academic Press, v. 17 (2002).
[7] I. Y Pakharukov, I. P. Prosvirin, I. A. Chetyrin, V. I. Bukhtiyarov, V. N. Parmon, In situ XPS studies of kinetic hysteresis in methane oxidation over Pt/Al_2O_3 catalysts, Catalysis Today, 278 (2016) 135.
[8] D. A. Shirley, Phys. Rev. B, 5 (1972) 4709.
[9] S. Tougaard, Surf. Inter. Anal., 11 (1988) 453.

Acknowledgments

This project was supported by BMW Brazil under project UFSC/2016/0110.

*Corresponding authors: leonardorudolfocardoso@gmail.com or diego.duarte@ufsc.br

ANODE EFFECTS ON A MAGNETRON SPUTTERING DISCHARGE: CHANGES IN HYSTERESIS CURVES AND SUBSTRATE FLOATING POTENTIAL

Kleber Alexandre Petroski* and Julio César Sagás
Laboratory of Plasmas, Films and Surfaces, Santa Catarina State University (UDESC), Joinville -SC

1. Introduction

The grid-assisted magnetron sputtering (GAMS) is a film deposition system derived from conventional magnetron sputtering [1]. In such system, a grounded grid is inserted between the target and the substrate. This system was developed aiming to suppress the hysteresis observed on process curves as a function of reactive gas flow rate. In fact, it was demonstrated both experimentally [1] and theoretically [2] that the grid can reduce and even eliminate the hysteresis. It is a consequence of a reduction in the effective gettering area due to metal deposition on the grid. At the same time, the grid can change the current-voltage relations of magnetron discharges, increasing magnetron efficiency [3]. When grounded, the grid becomes the main discharge anode, being a sink of electrons [4]. On the other hand, there is a reduction of the deposition rate because part of the sputtered atoms is deposited on the grid. In this work, it is proposed to change the grid commonly used in GAMS by ring anodes with external diameter of 110 mm and internal diameters of 20, 40, 60, 80 and 100 mm.

2. Experimental

Measurements were carried out in a homemade magnetron sputtering chamber. Two different targets were used: Ti and Al. Both with a diameter of 100 mm and positioned at 60 mm from the substrate. The substrate floating potential was measured at pure Ar discharges (0.40 Pa), while hysteresis curves were obtained in Ar/O_2 and Ar/N_2 atmospheres, maintaining the Ar partial pressure in 0.40 Pa. The discharge current was fixed at 1.00 A in constant current mode. The anode was 20 mm away from the target. The different anode internal diameters correspond to the following ratio between anode internal diameter and target diameter (β): 0.20, 0.40, 0.60, 0.80 and 1.00. The experiments were not made in order of increasing or decreasing β, to avoid superposition with the effects of target erosion.

3. Results and Discussions

Figure 1 shows the hysteresis widths for the Al/O_2 and Al/N_2 combinations of target/reactive gas. In the first case, results indicate that the smaller the diameter of the anode the smaller the hysteresis width. However, in the equivalent case using N_2 as reactive gas, the results seem to indicate the opposite behaviour, but the error bars do not allow further conclusions. The changes in hysteresis widths are very small, which difficult the precise measurement. Despite that, another effects as target erosion can also contribute to such changes.

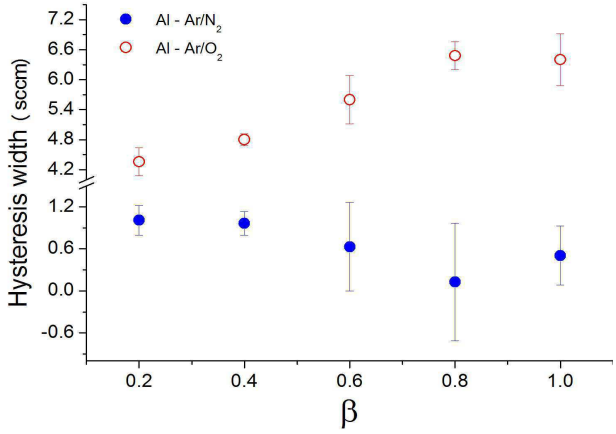

Fig. 1. *The hysteresis widths for Al/O_2 and Al/N_2.*

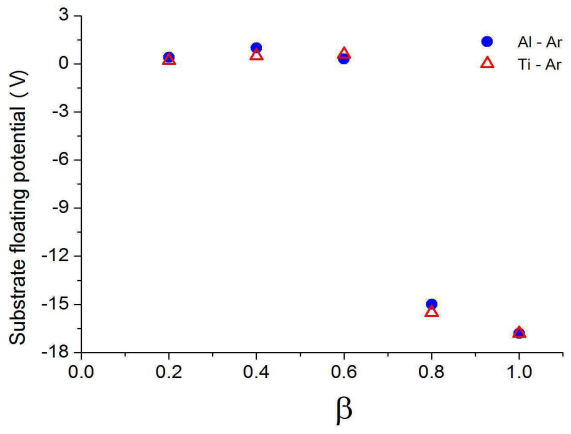

Fig. 2. *The substrate potential floating for different targets.*

From figure 2, a significant change in substrate floating potential can be observed with increased β. For small values (small internal anode diameters), the plasma is efficiently confined between cathode and anode, avoiding plasma bombardment of substrate. It results in a low substrate floating potential. For large values for β, however, the plasma can escape from the confinement, reaching the substrate. As consequence, the substrate floating potential reaches the typical values for glow discharges. So, the substrate bombardment

*Corresponding author: kleber.a.petroski@gmail.com

can be controlled by the anode internal diameter. One drawback of this strategy is the modification of deposition profile.

4. References

[1] L.C. Fontana, J.L.R. Muzart, Volume 114, Issue 1, 7-12 (1999).
[2] J.C. Sagás, D.A. Duarte, D.R. Irala, L.C. Fontana, T.R. Rosa, Surface & Coatings Technology, v. 206, 1765-1770 (2011).
[3] J.C. Sagás, L.C. Fontana, H.S. Maciel. Vacuum; 85, 705-710 (2011).
[4] J.C. Sagás, R.S. Pessoa, H.S. Maciel, Brazilian Journal of Physics, v.48(1), 61-66 (2018).

Acknowledgments

The authors would like to thank Brazilian agency CAPES for their financial support.

*Corresponding author: kleber.a.petroski@gmail.com

X-RAY DIFFRACTION EVIDENCE IN GRAPHENE OXIDE FILMS OBTAINED BY VACUUM FILTRATION

J. L. S. Gascho[*1], S. F. Costa[1] and S. H. Pezzin[1].
[1]*Graduate Program in Materials Science and Engineering, UDESC – Joinville.*

1. Introduction

Graphene can be obtained by various methods, one of the most used methods is the oxidation of graphite, which is abundant and has low cost [1]. Graphene oxide (GO) consists of two dimensional (2D) sheets of covalently linked carbon atoms, i.e., graphene sheets, presenting oxygenated functional groups such as hydroxyl, carbonyl, and epoxy, in its basal planes and edges [2], generating substantial insulating domains, due to the presence of carbon atoms with sp^3 hybridization which interrupts the passage of electrons between the planar carbons (sp^2). These groups can be further eliminated by reduction reactions, producing reduced graphene oxide (RGO) or graphene, in the case of a single nanoplatelet [3].
This study aimed to produce graphene oxide films (GOF) and reduced graphene oxide films by chemical and thermal reductions (CGOF and TGOF), checking the X-ray diffraction (XRD) analysis.

2. Experimental

Graphene oxide (GO) was produced from natural graphite provided by *Graphite of Brasil* by the Hummers method. Process times and proportions of the reagents were modified as suggested by Hirata et al. (2004) [3,4]
About 50 mg of GO were dispersed in 50 mL of deionized water by sonication (Sonics VCX 750) and the GO films were prepared by its vacuum filtration of 10 mL, on cellulose membrane (0.45 μm). This films were treated in a AN1031/Eurotherm 2416 tubular oven under argon atmosphere (with gas flow of one bubble by second). Were heated at 5°C/minute, from 20°C to 800°C, producing thermally reduced GO films, TGOF. For the produced of chemical reduced graphene oxide films, a solution of GO was heated to 80°C under magnetic stirring, using $NaBH_4$ as the reducing agent. From this RGO solution a 0,1 mg/mL was made, of which 10 mL were filtered on cellulose membrane (0.45 μm) forming the chemically reduced GO film, CGOF.
In order to determine the interplanar spacing of the atomic planes present in the material, the X-ray diffraction (XRD) technique (XRD 6000) was used, with a 2θ angle ranging from 5 to 70°, wavelength of 1 , 5406 A, 40 kV voltage and 30 mA current.

3. Results and Discussions

The X-ray diffractogram for graphite provided 2 characteristic peaks of this material at 2θ = 26° (d_{002} = 0.34 nm) and 2θ = 55° (d_{004} = 0.17 nm), corresponding to planes (002), and (004), respectively [5]
After oxidation, these peaks are shifted to smaller angles. In the X-ray diffractogram of the GO, Figure 1, only a 002 peak at 2θ = 10° (d_{002} = 0.84 nm) is found, confirming the efficiency of the oxidation reaction, with an increase in the interplanar distance of the graphene nanoplatelets due to the insertion of oxygen groups [6]. However, after the formation of GO films, other peaks are observed at 2θ = 14° (d_{002} = 0.63 nm), 2θ = 17° (d_{002} = 0.52 nm), 2θ = 19° (d_{002} = 0.48 nm), this structure not yet reported in the literature for this type of material. In addition to a peak with low intensity at 2θ = 26° (d_{002} = 0.34 nm), referring to graphite.
After the reductions, both chemical and thermal, the GO films presented X-ray diffractograms without the presence of the peak at 2θ = 10° (Figure 1), indicating that no part of the reduced GO films has graphene nanoplatelets with interplanar spacing of 0.84 nm, confirming the reduction of part of the oxygenated groups, with the reduction of the interplanar spacing. Already the peaks at 2θ = 14° (d_{002} = 0.63 nm), 2θ = 17° (d_{002} = 0.52 nm) and 2θ = 19° (d_{002} = 0.48 nm) continue to appear even after reduction. This indicates a partial reduction of the GO.
Brahmayya et al., in 2017, find a peak close to it, in 2θ = 12,8° (d = 0,69 nm), for GO, and after the chemical reduction of exfoliated graphene oxide with sodium borohydride and subsequent grafting of sulfonic acid containing aromatic radicals, this peak had been shifted to 2θ = 26.5° (d = 0,34 nm), and they explained this suggesting that the GO nanosheets were re-stacked by л-л interaction upon sulfonation24. The peak close to 19° was also observed by Arbuzov et al., in 2013, for the GO reduced with hydrazine and thermally, but they were not so sharp and defined peaks like those obtained in this work [7].
Kim et al., 2013, affirmed that when the peak at 26° can be observed, it is because π-π re-stacked occurred, and this happens quite frequently in the formation of GO films, especially if a vacuum filtration method is used for their production, as the used in this work, but if the peak at 26º don't appear, can't be say that the pi-pi re-stacking occurred. Therefore, the processing of GO films is difficult due to the agglomeration and

*Corresponding author: juliagascho@hotmail.com

rearrangement of the graphene sheets resulting from the pi-pi interplanar interaction and the van der waals forces [8].

Lu et al., in 2017, obtained graphene films with GO through a vacuum filtration method similar to the one used in this work. They also obtained an XRD peak close to 17º, which, according to them, suggests that the GO sheets are uniformly dispersed between the sheets of graphene, that is, it is a film with graphene and GO sheets intercalated, which can also to explain the appearance of the XRD peak in 17º of the films produced in this work [9].

Nevertheless, materials with the same crystalline structure to the films produced in this work have not yet been reported in the literature. Based on the references cited in the XRD analysis, it is possible to state that the GO and RGO films produced in this work have a different crystalline structure, which has regions with different interplanar distances. That is, it deals with films that have the combination of crystalline regions with different interplanar distances, where there may also be the presence of graphene sheets intercaled with GO sheets.

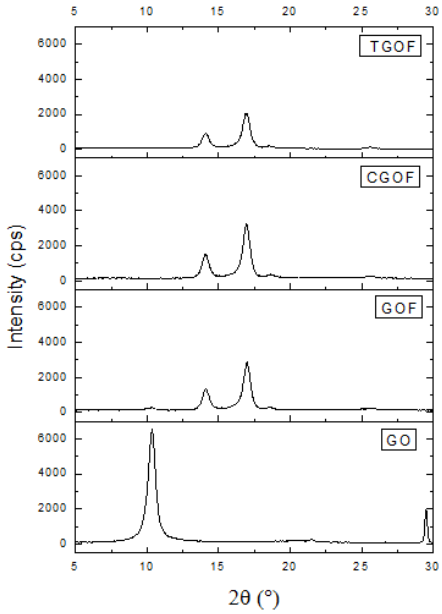

Fig. 1. *X-ray diffraction to the GO, GOF, CGOF e TGOF.*

4. References

[1] W. S. Hummers and R. E. Offeman. Preparation of graphitic oxide. JACS, 80, 1339, (1958).

[2] S. Rapino, et al. Playing peekaboo with graphene oxide: a scanning electrochemical microscopy investigation. Chem. Comm., 50, 13117-13120, (2014).

[3] A. Nikolakopouloua, et al. Study of the thermal reduction of graphene oxide and of its application as electrocatalyst in quasi-solid state dye-sensitized solar cells in combination with PEDOT. Electrochim. Acta., 111, 698-706, (2013).

[4] M. Hirata, et al. Thin-film particles of graphite oxide 1: High-yield synthesis and flexibility of the particles. Carbon, 42, 2929–2937, (2004).

[5] S. Peng, X. Fan, S. Li, J. Zhang. Green Synthesis and Characterization of Graphite Oxide by Orthogonal Experiment. J. Chil. Chem. Soc., 58, (2013).

[6] A. Guimont, et al. Grafting of polyethylene onto graphite oxide sheets: acomparison of two routes. Polymer Chem., 4, 2828-2836, (2013).

[7] A. A. Arbuzov, V. E. Muradyan, B. P. Tarasov. Synthesis of graphenelike materials by graphite oxide reduction. Russ. Chem. B., International Edition (Rússia), 62, 1962-1966, (2013).

[8] K. H. Kim et al. High quality reduced graphene oxide through repairing with multi-layered graphene ball nanostructures. Sci. Rep., 3, 3251, (2013).

[9] Y. Lu, T. Wang, Z. Tian, Q. Ye. Preparation of Graphene Oxide Paper as an Electrode for Lithium-Ion Batteries Based on a Vacuum Filtration Method. Int. J. Electrochem. Sci., 12, 8944 – 8952, (2017).

Acknowledgments

This study was financed in part by CAPES, UDESC, CNPq, and FAPESC.

*Corresponding author: juliagascho@hotmail.com

INFLUENCE OF THE MOLECULAR WEIGHT OF POLY(VINYLPYRROLIDONE) IN THE PRODUCTION OF SILVER NANOWIRES BY THE POLYOL METHOD

J. L. S. Gascho[*1], S. F. Costa[1], P. S. Tessaro[1] and S. H. Pezzin[1].
[1]*Center of Technological Sciences, Santa Catarina State University - UDESC, Joinville, SC, Brazil.*

1. Introduction

Silver particles with small sizes have attracted scientific interest because of its unusual properties compared to bulk metal. Colloidal particles, because of the effects of quantum size and surface effects, show excellent electrical conductivity, catalytic activity, chemical stability and antimicrobial activity [1].

Due to the high electrical and thermal conductivity of silver, the synthesis of silver nanowires has been an active research area [2]. Various methods for synthesis of nanowires silver (Ag) have been developed. These methods include chemical synthesis, electrochemical technique, hydrothermal method, photodetection technique by ultraviolet irradiation, DNA template, template of porous material, and the Polyol Method [1]. As in a series of recent publications, metal nanowires of uniform size can be synthesized by various chemical methods, among which the most striking is the polyol process when these methods are compared in terms of cost, performance and simplicity [3].

The polyol process is based on reduction of an inorganic salt of a polyol at elevated temperature. In this method, each reagent performs a defined function, ethylene glycol (EG) is used as solvent and reducing agent, poly(vinylpyrrolidone) (PVP) is used as a stabilizing agent from the reaction system and has an important role in controlling the shape of the silver nanocrystals, and silver nitrate ($AgNO_3$) is the precursor which is used as a source of silver ions (Ag) [1]. Sodium chloride is used as a source of chloride ions in order to assist in the reduction of silver during the nucleation and growth [4].

In this work silver nanowires were produced from the Polyol Method, using a fixed temperature and modifying the molecular weight of PVP, using two types of PVP with different molar masses and observing the interference of this factor on the morphology of the produced nanowires.

2. Experimental

To obtain the silver nanowires was used the Polyol Method with reagents such as silver nitrate (AgNO3, 99%), poly(vinylpyrrolidone) (PVP) 40000 g/mol and 350,000 g/mol, sodium chloride (NaCl, 99.5%) purchased by Sigma-Aldrich® LTD, ethylene glycol (mono) ($C_2H_4(OH)_2$) (EG) (VETEC), acetone PA (Cinética Reagentes e Soluções) and absolute ethanol (Biotec® Especialidades Químicas).

With the aid of a syringe pump (SDAMed® - SDA1800), 5 mL of a solution 0.12 mol/L of $AgNO_3$ in ethylene glycol were added to the flask's solution at a rate of 5 ml/hr, maintained under heating (165 ° C) and magnetically stirred throughout the reaction process. At the end of the addition, the mixture continued under stirred for 30 min.

Then, the reaction product was centrifuged (Excelsa TI-FANEM® model 206) (7000 rpm) twice with acetone and once using ethyl alcohol. The supernatant from the centrifugation was discarded and the precipitate collected and dispersed into ethanol for storage.

To characterize the product, analysis by scanning electron microscopy with field emission gun (FE-SEM) (JEOL 6701F) have been carried out.

3. Results and Discussions

Figures 1 and 2 show FE-SEM images of silver nanowires obtained by the Polyol Method in this work. In Figure 1, concerning to synthesis with PVP with lower molecular weight, there was the formation of long silver nanowires and nanometric sizes, obtaining a high yield of the desired product. With a higher molecular weight PVP, there was also the formation of silver nanowires, but in a lower proportion, and nanoparticles with different morphologies (Figure 2).

PVP has as main function to guide the anisotropic growth of silver particles and stabilize the reaction system. Thus, the molecular weight of the PVP may interfere on the silver particle's size. For instance, Coskun *et al* (2011) reported that lower silver ions are reduced to Ag atoms, leading to the formation of active centers in the structure that varies depending on a size of the thermal energy available. In this step, structural defects can influence the shape of nanoparticles. The growth after the formation of the cores defines the morphology of the particles, yielding a distribution of monocrystalline seeds with single or multiple defects. Thus, one must regulate the crystallinity of the seed in a reaction for the production of a specific form [5].

According to Wiley *et al* (2007) the seeds with multiple defects, with decahedric pentagonal structures, are most abundant. This morphology of abundant seeds are the more reactive due to these defects, since germinated they grow in pentagonal nanorods, and the PVP will interact more strongly with the faces, {100},

*Corresponding author: juliagascho@hotmail.com

than with the faces in the nanowire ends, {111}, as seen in Figure 3 and 4. The side surfaces nanorods are thus passivated PVP, while the ends remain reactive with the silver atoms. As a result, nanorods grow rapidly in nanowires with tens of micrometers in length [6].

From the results of the syntheses it is observed that the size of the polymer chain of PVP interferes in the formation of silver nanowires with higher molecular weight. At the time of formation of the seed occurs the core's activation with various structures, having cores with multiple defects, others with only one defect, or even crystals that grow to form cubes or spheres. Thus, it can be concluded that the use of PVP with lower molecular weight, increases the tendency to form cores with multiple defects, and as a final product silver nanowires.

With the images obtained by FE-SEM and study of polyol synthesis, it can be concluded that by using PVP with molecular weight of 40000 g/mol silver nanowires formation is favored due to multiple defects of germinated seeds. Using a higher molecular weight PVP it was obtained, besides nanowires, silver nanoparticles with other morphologies.

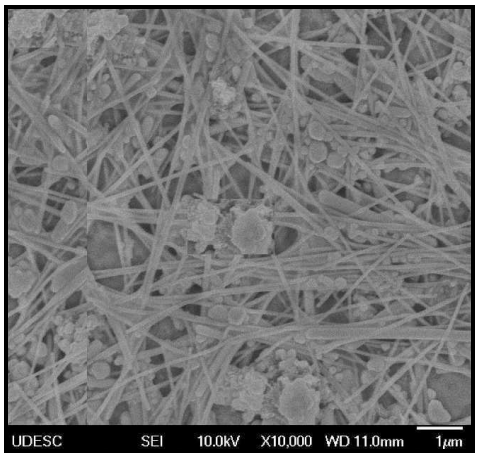

Fig. 1. *FE-SEM images of silver nanowires produced using PVP of 40,000 g/mol.*

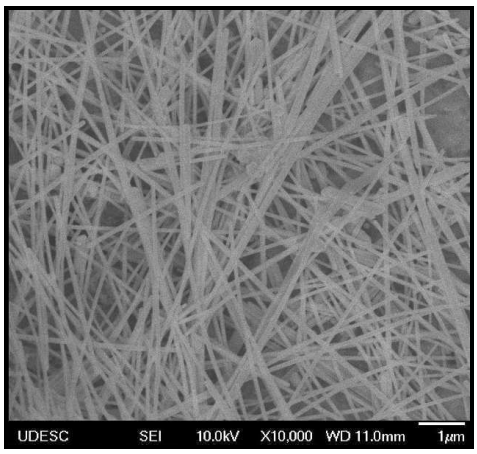

Fig. 2. *FE-SEM images of silver nanowires produced using PVP of 350,000 g/mol.*

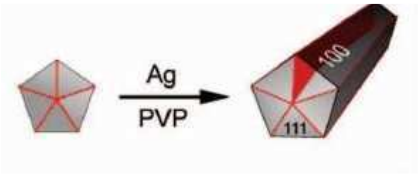

Fig. 3. *Anisotropic growth of Silver Nanowires in PVP. Font: Adapted from to Wiley et al (2007).*

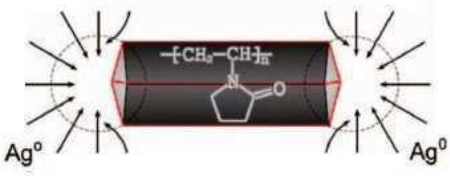

Fig. 4. *Anisotropic growth of Silver Nanowires in PVP. Font: Adapted from to Wiley et al (2007).*

4. References

[1] A. Zielinskaa, et al. Preparation of silver nanoparticles with controlled particle size. Proc. Chem., 1, 1560–1566, (2009).

[2] K. E. Korte, S. E. Skrabalak, Y. Xia. Rapid synthesis of silver nanowires through a CuCl- or $CuCl_2$-mediated polyol process. J. Mater. Chem., 18, 437–441, (2008).

[3] C. Chen, et al. Study on the synthesis of silver nanowires with adjustable diameters through the polyol process. IOP Publishing, Nanotech., 17, 3933–3938, (2006).

[4] Y. G. Sun and Y. N. Xia. Large-scale synthesis of uniform silver nanowires through a soft, self-seeding, polyol process. Adv. Mater., 14, 833–837, (2002).

[5] S. Coskun, B. Aksoy, H. E. Unalan. Polyol synthesis of silver nanowires: An extensive parametric study. Cryst. growth & design, 11, 4963-4969, (2011).

[6] B. Wiley, Y. Sun, Y. Xia. Synthesis of Silver Nanostructures with Controlled Shapes and Properties. Acc. Chem. Res., 40, 1067–1076, (2007).

Acknowledgments

This study was financed in part by CAPES, UDESC, CNPq, and FAPESC.

*Corresponding author: juliagascho@hotmail.com

HYSTERESIS OF THE SUBSTRATE FLOATING POTENTIAL IN MAGNETRON SPUTTERING SYSTEM

Rafael Fróis da Silva* and Julio César Sagás
Laboratory of Plasmas, Films and Surfaces, Santa Catarina State University (UDESC), Joinville - SC

1. Introduction

Film deposition by magnetron sputtering consists in the removal of atoms from a target by ion bombardment. The ions are generated in magnetically confined plasma in front of the target. Among a great number of different configurations, it can be highlighted the grid-assisted magnetron sputtering [1-4]. This system differs from magnetron sputtering by introducing a grounded grid (made of stainless steel) in front of the magnetron and positioned in the luminescent region of the plasma [4], in which it does not affect the magnetic field lines. The grid acts as the main discharge anode draining electrons from the plasma, and changing the spatial distribution of the discharge [3, 4].

The removed atoms are deposited on the inner surfaces of the chamber. In the presence of a reactive gas, chemical reactions occur in the film and on the target surface, forming a compound film. This process can lead to target poisoning and to hysteresis in the process curves as a function of reactive gas flow rate. Several investigations were made to understand the hysteresis in partial pressure, deposition rate, discharge voltage and other parameters [3, 5]. However, minor attention is paid to parameters related to the substrate, as its floating potential. The floating potential of a piece in contact with plasma is directly related to the electron temperature. However, in grid-assisted magnetron sputtering, the plasma is confined between the target and the grid. So, the substrate floating potential is related to the flow of charged species that "escapes" from the grid.

The main objective of this work is to investigate the substrate floating potential and the discharge voltage as a function of O_2 flow rate during deposition of stainless steel films. This material was chosen due to the technological interest in such films.

2. Experimental

The measurements were carried out in a grid assisted magnetron sputtering chamber described elsewhere [4]. A 316L stainless steel target with 100 mm in diameter was used. The grid is a rectangular mesh (11.8 cm x 16.0 cm) with spacing of 2.0 mm between the wires and it was kept grounded in all measurements. The substrate has a diameter of 100 mm and it is 6.0 cm away from the target. The base pressure was below 10^{-2} Pa. The gases flow rates were adjusted using thermal mass flow controllers. The Ar partial pressure was fixed to 0.40 Pa. The plasma was powered with a DC power supply operating in constant current mode (1.00 A). The grid-to-target distance was 2.0 cm. For comparison, measurements without the grid were made under the same conditions.

3. Results and Discussions

In figure 1, the hysteresis curves for discharge voltage with and without grid can be observed. Increasing the reactive gas flow rate, an increase in discharge voltage is observed for both cases, until an abrupt drop. The drop is caused by target poisoning and the abrupt reduction of secondary electron yield due to the compound formation. The previous rise can be attributed to the formation of some intermediary compounds on the target surface with a lower secondary electron yield than the metal. On the same figure, it can be seen that in the metallic mode (increasing flow), the discharge voltage is higher with grid than without. This indicates that, in this position, the grid is draining high energy electrons, decreasing the magnetron efficiency [5].

In figure 2, the behavior of substrate floating potential is shown. A large difference is observed with the introduction of the grid. The grid confines the plasma close to the target, i.e. the plasma is kept away from the substrate. It results in a reduced substrate bombardment and a lower magnitude of substrate floating potential. Removing the grid, the floating potential reaches the typical value of pieces inserted in a glow discharge. When target poisoning occurs, a drop in substrate floating potential is observed in both cases. After poisoning, the partial pressure of O_2 increases, which can lead to the formation of negative ions in plasma.

*Corresponding author: rfroisfisica@gmail.com

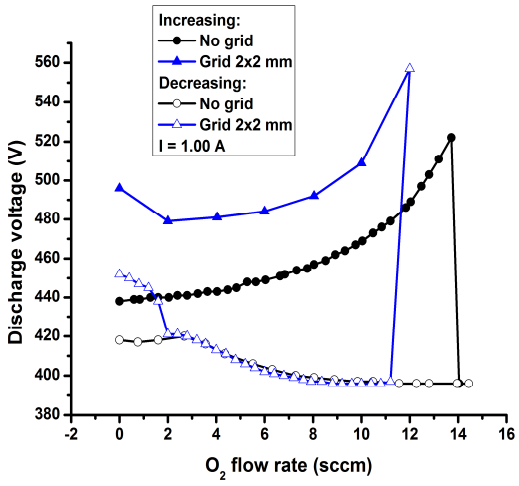

Fig. 1. *Discharge voltage as a function of the O_2 flow rate.*

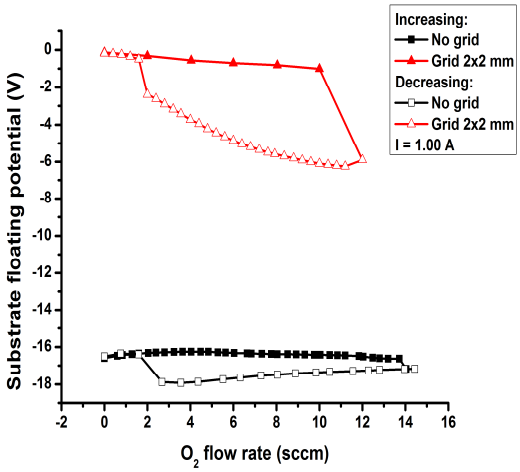

Fig. 2. *Substrate floating potential as a function of the O_2 flow rate.*

Typically, this elevates the electron temperature, causing a change in floating potential. Besides that, negative ions formed on target can also hit the substrate, affecting its charge. More studies are necessary to understand the mechanisms involved in this process.

4. References

[1] L. C. Fontana, J. L. R. Muzart. Surf. Coat. Technol., **107**, 24–30, (1998).
[2] L. C. Fontana, J. L. R. Muzart. Surf. Coat. Technol. **114**, 7–12, (1999).
[3] J. C. Sagás, D. A. Duarte, D. R. Irala, L. C. Fontana, T. R. Rosa. Surf. Coat. Technol. **206**, 1765–1770, (2011).
[4] J. C. Sagás, L. C. Fontana, H. S. Maciel. Vacuum **85**, 705–710, (2011).
[5] J. C. Sagás, D. A. Duarte, S.F. Fissmer. Vacuum **85**, 1042-1046, (2011).
[6] J. C. Sagás, D. A. Duarte, L. C. Fontana. J. Phy. D: Appl. Phys. **45**, 505204, (2012).
[7] D. A. Duarte, J. C. Sagás, L. C. Fontana, A. S. da Silva Sobrinho, M. J. Cinelli. Eur. Phys. J. Appl. Phys. 52, **31001** (2010).

*Corresponding author: rfroisfisica@gmail.com

KINETICS ANALYSIS ON SILK AND COTTON WITH NATURAL DYEING

Maria Elisa Philippsen Missner[1], Grazyella Cristina Oliveira de Aguiar[1] and Catia Rosana Lange de Aguiar[1]
[1] *Department of Enginnering, Federal University of Santa Catarina - UFSC, Campos Blumenau, Brazil*

1. Introduction

In the dyeing process there are three important steps: sample assembly, fixation form and final treatment [1].

Damascene [2] used some natural dyes to perform dyeing in tissues. In the research, verified that the pH of the water for dyeing does not change, concluding that it does not impact the environment when discarded. The study by Diniz et al. [3] obtained good results of dyeing of cotton fibers with saffron dissolved in boiling water, indicating even low residual concentration of dye at the end of dyeing.

The search for increasing the ability of the dye molecule to remain in the fiber could reduce the amount of dye needed in the dyeing process, thereby reducing cost and would certainly improve the human and environmental protection conditions [4].

According to the current market situation, which is increasingly searching for elements with lower environmental impact, the present study aims to evaluate the dyeing capacity of natural pigments by means of different dyeing techniques, analyzing their fixation after tests of solidity.

2. Experimental

For purposes of comparison of the results, samples of 100% cotton and 100% silk were also dyed by the exhaustion dyeing process. The natural dye used was saffron. The sample size was 15 cm x 9.0 cm.

Samples of cotton and silk fabrics were washed in water with neutral detergent and heated for two hours . The heating temperature was kept constant at 80 °C, avoiding boiling. After this process, the samples were rinsed and allowed to air dry at room temperature.

After the purging process, the samples were wet in running water, twisted and spread on a clothesline. Still wet, these samples were dipped in iron oxide mordant solution during one minute for better fixation of color dyes in the tissues.

To obtain the dyeing solution was used 20 g/L saffron with hot water. The dyeing for kinetics determination was performed at 100 °C for 60 minutes and the aliquots of bath were collected at times 10, 20, 30, 40, 55 and 80 minutes. The isotherms determination was done with dye contraction 100%, 75%, 50%, 25% and 10%. The aliquots of the bath were collected at the beginning and end of the dyeing process and its concentration determined by reading of spectrophotometer with 418 nm wavelength.

3. Results and Discussions

Figure 1 shows the kinetic behavior of the cotton fibers dyeing with the natural dye of saffron, where it is possible to observe that there is the exhaustion of the dye over time.

In figure 2, the kinetic behavior of the silk fibers shows that a peak of current exhaustion occurs in the time of 30 minutes. After this period, the phenomenon of migration between perceived dye/fiber occurs by increasing the concentration of dye in the solution over time.

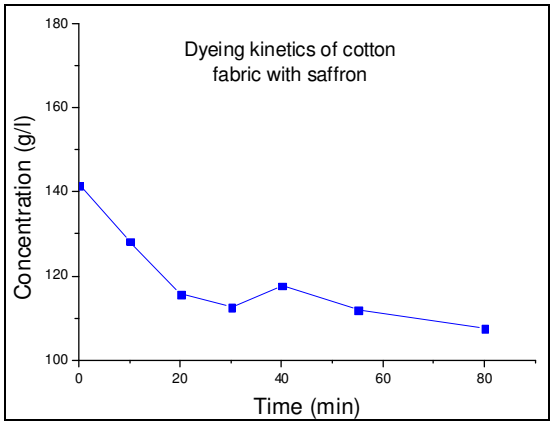

Fig. 1. *Kinectics of cotton dyeing with saffron.*

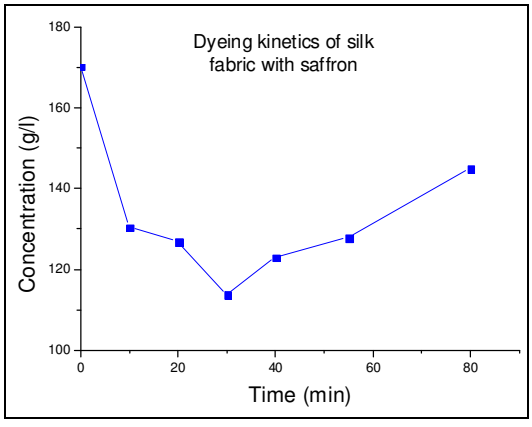

Fig. 2. *Kinectics of silk dyeing with saffron.*

The mechanism of dyeing for the cotton fibers was adjusted to the Freundlich's isothermal model as shown in figure 3. This mechanism indicates that the interaction between dye/fiber is weak and that they

*Corresponding author: elisa.p.missner@ufsc.br

have the same polarity. The dye/fiber bonds are by hydrogen bonding and by van der Walls forces. For the dyeing of the silk fibers there was no adjustment for the isotherm models used, figure 4.

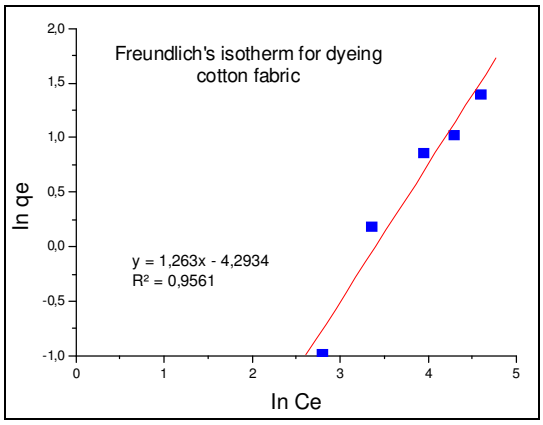

Fig. 3. *Freundlich's isotherm for dyeing of cotton fabric.*

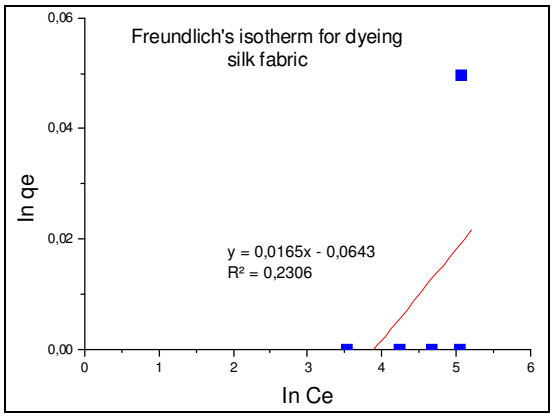

Fig. 4. *Freundlich's isotherm for dyeing of silk fabric.*

Figures 5 and 6 show that both dyeing are governed by the kinetic model of pseudo 2nd order, which considers that the limiting step of the process is the adsorption in the solid, involving electrostatic attractions from the exchange or sharing of electrons between the adsorbent and the adsorbate.

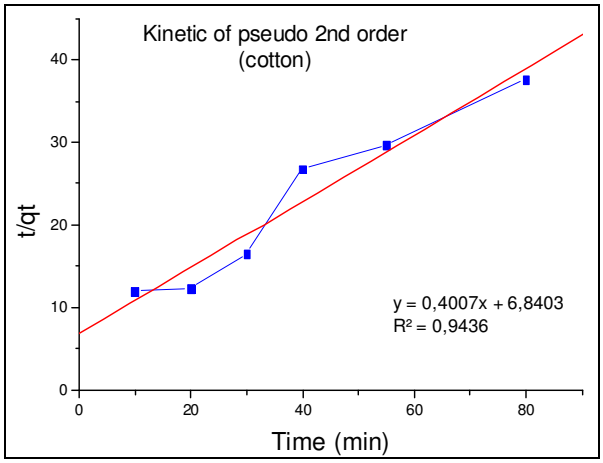

Fig. 5. *Kinect of pseudo 2nd order for cotton dyeing.*

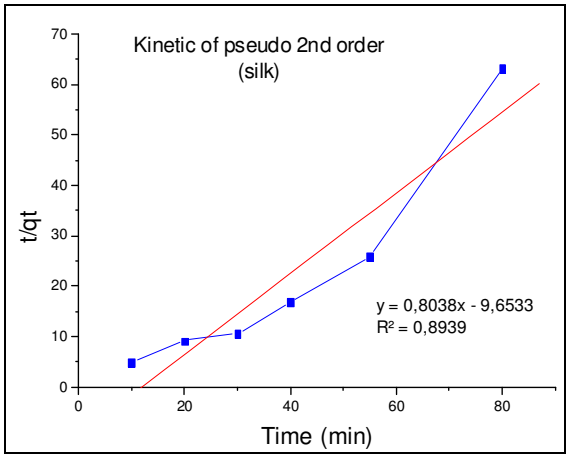

Fig. 6. *Kinect of pseudo 2nd order for silk dyeing.*

These results indicate that dyeing with saffron dye is possible, but it is still necessary to study mordants that promote stronger interactions between dye and fiber.

4. References

[1] Peters, R. H.; Textile Chemistry; Vol. 3; Elsevier; Amsterdam, 1975.
[2] DAMASCENO, Silvia MB; SILVA, Fernanda TF; FRANCISCO, Antonio C. Sustentabilidade do processo de tingimento do tecido de algodão orgânico. XXX Encontro Nacional de Engenharia de Produção, São Carlos, 2010.
[3] DINIZ, Juliana F., FRANCISCATTI, Patrícia, SILVA, Tais L. Tingimento de tecidos de algodão com corantes naturais açafrão e urucum. Revista de Iniciação Científica CESUMAR. 13, p. 53-62, 2011.
[4] GUARATINI, Cláudia CI; ZANONI, Maria Valnice Boldrin. Corantes têxteis. Química nova, p. 71-78, 2000.

*Corresponding author: elisa.p.missner@ufsc.br

COLD-FORMED STEEL NITRIDING THROUGH ASYMMETRIC BIPOLAR PULSED PLASMA (ABIPPS)

Renan Augusto da Cunha[1], Bruna , Bianchi[1], Juliano Sadi Scholtz[2] and Luis Cesar Fontana[3]
[1]*Academic of Mechanical Enginering – UDESC CCT – Scholarship PROBIC/UDESC*
[2]*Member of PowerPlasma – Joinville, SC*
[3]*Professor at Department of Physics, Santa Catarina State University*

1. Introduction

Plasma nitriding is one effective methods for increasing wear resistance, fatigue strength, surface hardness, and for protecting the surface of materials from corrosion. This method has been commonly used in industry for the last four decades [1, 2]. The objective of this work is to verify the feasibility of the plasma nitriding process of cold-formed low carbon steel with complex geometry. The work also seeks to analyze the variation of the properties and microstructures of the samples, based on the temperature and time of nitriding. The samples were screws made of low carbon steel and manufactured by the process of cold forming. The most usual application of those screws is in fixing shingles, because of this, should present high hardness and good corrosion resistance.

2. Experimental

Before performing the nitriding treatments, the process of hydrogen cleaning was carried out in the samples. The cleaning process occurred within the reactor with the plasma generated in an atmosphere composed entirely of hydrogen for a period of 20 minutes. The plasma nitriding treatment was carried in a vacuum chamber of stainless steel. The plasma was generated through a home-made power supplier named ABiPPS (Asymmetric Bipolar Plasma Power Supply) [3], which can generates alternating pulses of tension with short positive pulse (ns) and large negative pulses (μs). The Asymmetric pulses of voltage improve the ionization rate of the plasma. The atmosphere used in this work was composed by a mixture of $Ar/N_2/H_2$ and was based on previous work about bipolar nitriding of nodular cast iron austempered [4]. After the treatments the samples were characterized by metallographic techniques. These techniques are: cutting of the samples, inlay, marking, sanding, polishing, chemical attack and cleaning. After preparation the samples were analyzed using optical microscopy and Vickers microhardness tests with 10 grams load and 10-second penetration time.

3. Results and Discussions

Nitriding treatments were performed varying their parameters, as shown in Figure 1. In order to verify the diffusion of nitrogen atoms in the samples, hardness profiles were performed on treated samples in comparison with a sample without treatment (AST), as showed in Figure 2.

Naming	Atmosphe (%)	Pressure (torr)	Time (h)	Temperature (°C)
A339-4h	N_2 : H_2 : Ar 80 : 10 : 10	7,4 ± 8	4	339 ± 3
A320-8h	N_2 : H_2 : Ar 80 : 10 : 10	4,7 ± 3	8	320 ± 3
A576-2h	N_2 : H_2 : Ar 80 : 10 : 10	3,6 ± 0,4	2	576 ± 12

Fig. 1. *Parameters of plasma nitriding processes.*

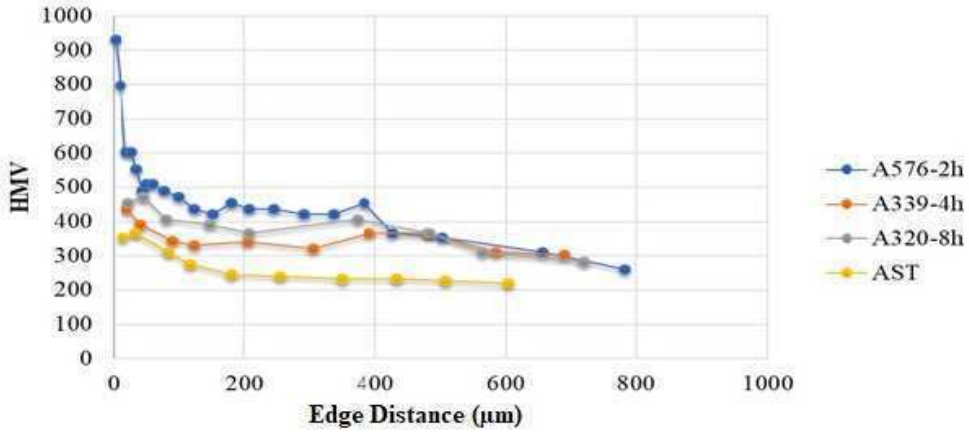

Fig. 2. *TheVickers hardness profile.*

The sample A339-4h and A320-8h when analyzed through optical microscope did not present composite layer (white layer). This result was attributed to the fact that the processes was carried out in low temperature and high energy ions bombardment. Figure 3 show micrographs of a sample (A576-2h) treated in high temperature, where it is observed the formation of the composite layer, with thickness of 6.0 ± 0.5 µm and hardness of 860 ± 74 HV.

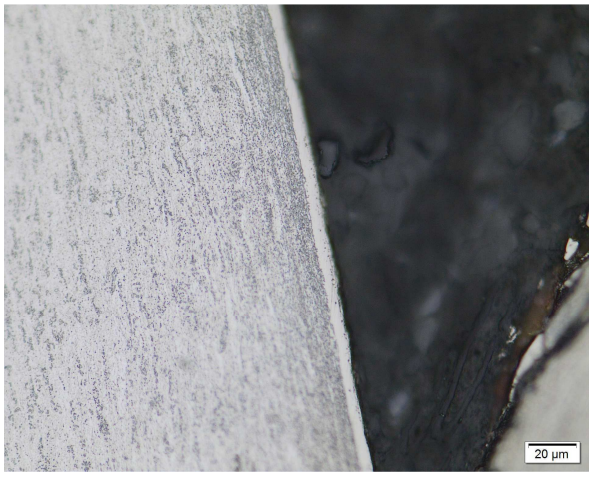

Fig. 3. *A576-2h sample compound layer.*

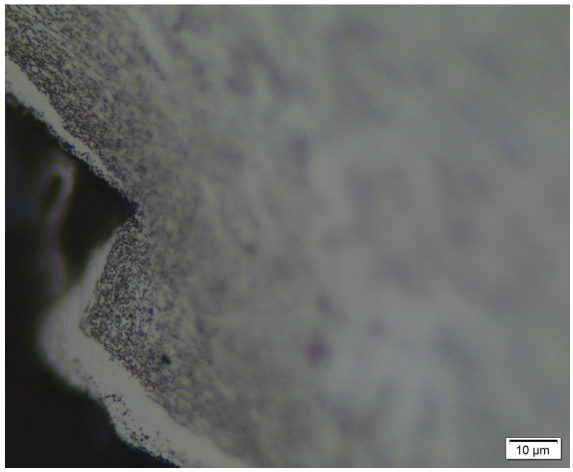

Fig. 4. *Region with depression of samples A576-2h.*

The main problem encountered in the A576-2h treatment was the presence of depressions defects on the surface of the samples. The plasma treatment don't reach these micrometer depressions during the treatment because the electric field is more intense at its upper extremity which hinder the formation of the composite layer at the lower end, as shown in Figure 4.

4. References

[1] CHIAVERINI, V. Aços e ferros fundidos. 6ª edition, São Paulo,2002.
[2] ASM HANDBOOK, Vol. 04 Heat Treating, ASM International The Materials Information Company, 1991.
[3] Juliano Sadi Scholtz, Luis César Fontana, and Marcello Mezaroba Asymmetric Bipolar Plasma Power Supply to Increase the Secondary Electrons Emission in Capacitive Coupling Plasmas, IEEE TRANSACTIONS ON PLASMA SCIENCE, Vol. 46, Issue 8, Aug. 2018, **DOI:**10.1109/TPS.2018.2851071
[4] BIANCHI, Bruna Trevizan. *Nitretação de ferro fundido nodular austemperado (ADI) em plasma gerado por fonte ABiPPS (Asymmetric Bipolar Plasma Power Supply)*. Relatório de Trabalho de conclusão de curso-Mechanical Engineering, University of the State of Santa Catarina – julho de 2018.

Acknowledgments

The authors are grateful to the University of the State of Santa Catarina for structural and financial support.

A MORPHOLOGICAL ASSESSMENT OF MICROCRYSTALLINE CELLULOSE TREATED WITH ACID HYDROLYSIS

Daniel V.F.Vanin[1], Viviane Dias Andrade[1], Ana Letícia Tavares[2], Dayane Cristine Rodrigues[3], Claudimir A. Carminatti[1], Derce O. S. Recouvreux[1]*

[1]*Graduate Program in Engineering and Mechanical Sciences, UFSC, Joinville, SC, Brazil*

[2]*Undergraduate in Naval Engineering, UFSC, Joinville, SC, Brazil*

[3]*Undergradute in Logistics and Transport Engineering, UFSC, Joinville, SC, Brazil*

1. Introduction

Cellulose is the most abundant biopolymer available in nature and has been known since 1838. Firstly described as a fibrous material resultant from chemical treatment of plant tissues, it's molecular formula was readily determined by elemental analysis as $C_6H_{10}O_5$ [1].

This natural polymer is formed by glucose units, linked together by a $\beta\,(1 \rightarrow 4)$ glycosidic bond. Each glucose block is twisted 180° from each other to form cellobiose, the cellulose monomer [2]. Figure 1 shows the cellulose chemical structure, as well as the cellobiose unit.

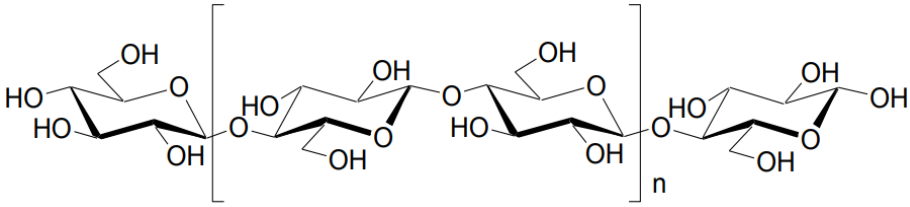

Fig. 1. *Basic chemical structure of cellulose. In Square brackets is a cellobiose* [3].

The majority of cellulose is found in the plant kingdom; however, it can be produced by bacteria, algae and fungi [1], [4] and also tunicates, from the subphylum Tunicata in the animal kingdom [5].

In any plant, cellulose is used as the structural building block, as it is encountered in vegetable cell walls to form a well oriented fibrillated matrix along with other substances such as hemicellulose, to achieve higher hierarchical structures. Figure 2 schematically shows the hierarchical structure of cellulose and the microfibril structure.

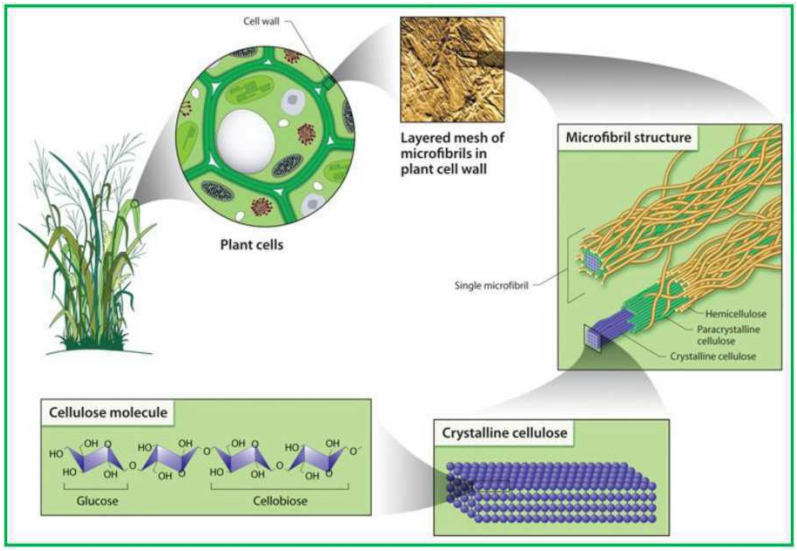

Fig. 2. *Scheme of the hierarchical structure of cellulose* [3].

By hydrochloric acid-assisted degradation of cellulose fibers and subsequent sonification, Battista have isolated microcrystalline cellulose (MCC), which presented itself as chemically stable, physiologically inert, micrometer-sized block-like particles [1], [6]. This low aspect ratio particle is commonly used in cosmetics, dairy, food, and pharmaceuticals [6].

*Corresponding author: derce.recouvreux@ufsc.br

Acid hydrolysis, especially sulfuric acid, have been used to hydrolyze disordered or paracrystalline domains of cellulose. Therefore, this study aimed to break MCC down into smaller pieces, increasing the materials aspect ratio by treating with acid hydrolysis.

2. Experimental

Microcrystalline cellulose (purchased at local market) was subjected to sulfuric acid (Synth) hydrolysis in order to break it down into smaller pieces. Thus, 2.5 g of MCC was mixed with 80 ml sulfuric acid solution (50% wt.) under magnetic stirring and constant temperature of 40 °C for 45 min. To stop the hydrolysis process, approximately 800 ml ice was added to the solution. Next, a centrifugation process (Centurium Scientific) was used to remove the acid and neutralize the system. Hence, six centrifuge cycles were performed at 6000 rpm, adding distilled water between each cycle and discarding the supernatant, which was further neutralized for appropriate disposal. The final decanted material reached a pH 6 after the centrifugation process. As an attempt to further break down the hydrolyzed material, an ultrasonic bath (Unique) was performed at full power and room temperature for 25 min.

3. Results and Discussion

Scanning electron microscopy (SEM) was performed to evaluate the effects of acid hydrolysis treatment in MCC. Figure 3 illustrates the morphological aspects of *Avicel ©,* a MCC provided by Sigma Aldrich. The *Avicel* © PH-101 is commercialized with a 50 μm particle size. In contrast, Figure 4 shows a SEM image of MCC after treatment. It can be observed that the MCC granule was totally fragmented, resulting in rod-like units of approximately 5-15 μm in diameter. However, due to sulfate grafting of cellulose, negatively charged regions around sulfate ions further intensify interchain bonds, tightly packing together the smaller pieces.

Moreover, the attempt to further breaking down the treated material with ultrasonic bath do not demonstrated to be so efficient, as "big" agglomerates tended to form, but it may have contributed to avoid larger agglomerates. Furthermore, isolated MCC can be observed in Figure 3 background in a variety of sizes.

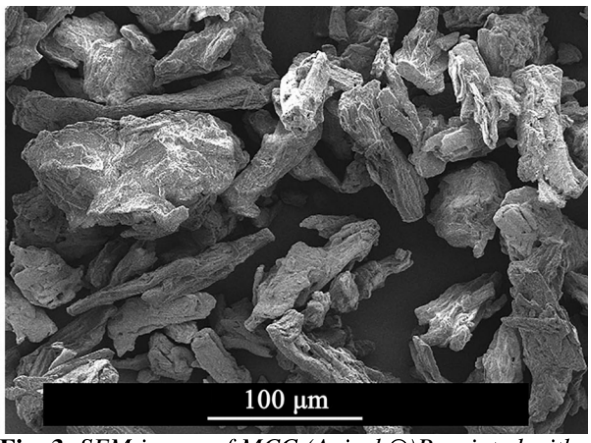

Fig. 3. *SEM image of MCC (Avicel ©)Reprinted with permission* [6].

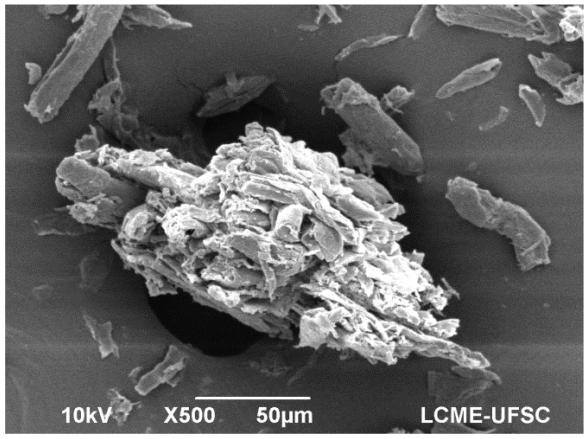

Fig. 4. SEM image of MCC after treatment.

4. References

[1] D. Klemm, B. Heublein, H. P. Fink, and A. Bohn, "Cellulose: Fascinating biopolymer and sustainable raw material," *Angew. Chemie - Int. Ed.*, vol. 44, no. 22, pp. 3358–3393, 2005.

[2] Y. Habibi, L. A. Lucia, and O. J. Rojas, "Cellulose Nanocrystals : Chemistry, Self-Assembly , and Applications," *Chem. Rev.*, vol. 110, no. 6, pp. 3479–3500, 2010.

[3] G. Siqueira, J. Bras, and A. Dufresne, "Cellulosic bionanocomposites: A review of preparation, properties and applications," *Polymers (Basel).*, vol. 2, no. 4, pp. 728–765, 2010.

[4] R. Brandes *et al.*, "Influence of the Processing Parameters on the Characteristics of Spherical Bacterial Cellulose," *Fibers Polym.*, vol. 19, no. 2, 2018.

[5] Y. Zhao and J. Li, "Excellent chemical and material cellulose from tunicates: Diversity in cellulose production yield and chemical and morphological structures from different tunicate species," *Cellulose*, vol. 21, no. 5, pp. 3427–3441, 2014.

[6] K. Vanhatalo, T. Lundin, A. Koskimäki, M. Lillandt, and O. Dahl, "Microcrystalline cellulose property–structure effects in high-pressure fluidization: microfibril characteristics," *J. Mater. Sci.*, vol. 51, no. 12, pp. 6019–6034, 2016.

*Corresponding author: derce.recouvreux@ufsc.br

Acknowledgments

The authors gratefully acknowledge the financial support of the Federal University of Santa Catarina, the Brazilian National Council for Scientific and Technological Development (CNPq) and Coordination for the Improvement of High Education Personnel (CAPES). This research was supported by LCME-UFSC.

*Corresponding author: derce.recouvreux@ufsc.br

XXXIX Congresso Brasileiro de Aplicações de Vácuo na Indústria e na Ciência

08 a 11 de outubro de 2018 - Joinville - SC

SESSÃO DE PÔSTER
QUARTA - 10/10
XXXIX CBrAVIC

Apresentações em pôster do XXXIX CBrAVIC (Quarta-feira – 10/10)

ID	TÍTULO
#23	**PONTUAL DEFECTS STUDY OF TERNARY TITANIUM ALLOYS FOR BIOMEDICAL APLICATIONS USING DYNAMICAL MECHANICAL ANALYSIS** *Marcos Ribeiro da Silva, Pedro Kuroda, Raul Araújo, Carlos Roberto Grandini*
#72	**BEHAVIOR OF GLIDING ARC DISCHARGE REPETITION FREQUENCY IN PLASMA ASSISTED FUEL RICH COMBUSTION OF NATURAL GAS** *Armando José Pinto, Julio César Sagás, Pedro Teixeira Lacava*
#74	**SURFACE MODIFICATION OF CELLULOSE PULP WITH FLUORINATED COMPOUND BY PLASMA ENHANCED CHEMICAL VAPOR DEPOSITION (PECVD)** *L. S. Oliveira, A.O. Delgado-Silva, E.C. Rangel, R.F. Mendes, L.E.V. Vaz*
#75	**MODIFIED BATCH REACTOR FOR FURFURYL RESIN SYNTHESIS** *Sara Aparecida Alexandre, Lara Campideli Santos, Rafael Farinassi Mendes, Lívia Elisabeth Vasconcellos de Siqueira Brandão Vaz*
#76	**SUN TRACKING MECHANISM EFFECTS ON A PHOTOVOLTAIC SYSTEM** *Erick S. Nunes, Alexandre W. Arins*
#77	**STUDY OF PLASMA PROCESS FOR TREATMENT OF CUTTING TOOLS MANUFACTURED IN HIGH-SPEED STEEL** *P. Egert, H.R.T. Silva, A. Seeber, H.C.M. Zanella, J.V.J. Hoffmann*
#78	**PLASMA OXIDATION OF LOW CARBON STEEL IN CATHODIC POTENTIAL AND FLOATING POTENTIAL** *Paula Fin, Juliano Sadi Scholtz, Luis C. Fontana*
#79	**BEHAVIOR OF TI-30NB-5MO ALLOY AFTER COLD ROLLING FOLLOWED BY ANNEALING AND AGING** *Magna Bibiano de Oliveira, Rubens Coutinho Toledo, Thailler Machado Nunes da Silva, Alexandra de Oliveira França Hayama*
#81	**SPECIMEN SIMULATION SUBJECT TO FATIGUE IN AL-X%NI ALLOY** *Mateus de Oliveira Silva, Gilberto Vicente Prandi, Roberto Nunes Duarte, Renato Chaves Souza*
#82	**LASER BEAM WELDING OF DUAL PHASE DP600 STEEL FOR APPLICATIONS IN AUTOMOTIVE STRUCTURES** *Jimes de Lima Percy Júnior, Ana Maria do Espírito Santo, Rafael Humberto Mota de Siqueira, Milton Sergio Fernandes de Lima*
#83	**SURFACE TREATMENT OF CARBON FIBER BY ARGON AND UREA VAPOR PLASMA** *Camila Presendo Pinto, Abel A. C. Recco, Carla Dalmolin, Daniela Becker, Luis César Fontana*
#84	**GRAPHITE EXFOLIATION VIA PULSED UNDERWATER DISCHARGE** *Elisa Héllen Segundo, Marco Aurelio Nespolo Vomstein, Daniela Becker, Luis Cesar Fontana*
#85	**EVALUATION OF THE CHEMICAL COMPOSITION OF RICE HUSK ASH (RHA) AND WOOD ASH (WA) FOR GLASS APPLICATION** *Eduardo Coveseviski, Rudinei Malinovki*
#87	**DEVELOPMENT OF CVD MICRO / NANOCRYSTALLINE DIAMOND TOOLS FOR ALUMINUM ALLOY MILLING** *Argemiro Pentian Junior, José Vieira, Vladimir J. Trava Airoldi, João Roberto Moro*
#89	**EFFECT OF THE PLASMA PROCESS ON THE MORPHOLOGY OF CELLULOSE ACETATE MEMBRANES**

	H.R.T. Silva, J.V.J. Hoffmann, P. Egert, A. Seeber, A., Magnago, W. Stieven
#90	**NUMERICAL CALCULATION OF POWER IN DBD-LIKE DEVICES** *Milton E. Kayama, Gustavo G. Vasques, Marcelo H. Mello and Mauricio Antonio Algatti*
#92	**EFFECT OF NIOBIUM PERCENTAGE ON THE WETTABILITY AND OPTICAL TRANSPARENCY OF TiO2:Nb FILMS** *Aline Medeiros Morais, Joel Stryhalski , Julio C. Sagás , Luís C. Fontana*
#93	**USE OF PLASMA TREATMENT TO IMPROVE FLAT FABRIC WETTABILITY** *Camila Thais Mamani, Teresa Tromm Steffen, Luis César Fontana, Daniela Becker*
#94	**DESIGN AND MANUFACTURE A HIGH EFFICIENCY UNIBODY CAR IN COMPOSITE MATERIALS** *Augusto Ricci Ferreira and Gabriel Benedet Dutra*
#95	**ANALYSIS OF GRANITE POWDER USING LASER DIFFRACTION, FTIR AND XRD** *S. C. S. M. Santos, P. A. Suzuki, A. R Bigansolli, B. B. Lima-Kühn*
#96	**ABLATIVE PROPERTIES OF CERAMIC MATERIALS TESTED IN A SUPERSONIC PLASMAS WIND TUNNEL** *Cristian Cley Paterniani Rita, Gilberto Petraconi Filho, Alexei Mikhailovich Essiptchouk, Tiago Moreira Bastos Campos, Felipe Rocha Caliare, Felipe de Sousa Miranda*
#98	**EFFECT OF THE GAS PRESSURE ON THE DISCHARGE POWER OF A HYBRID CORONA-DBD REACTOR** *Alonso H. Ricci Castro, Gilberto Petraconi Filho*
#101	**EVOLUTION OF THE HARDNESS PROFILE WITH APPLIED DUTY CYCLE IN PLASMA NITRIDING OF THE AISI 420 STAINLESS STEEL** *Zanella, I. G, Zanetti, F. I; Brunatto, S. F; Cardoso, R. P.*
#102	**NITRIDING OF AUSTEMPERATED DUCTILE IRON (ADI) IN PLASMA GENERATED BY ABIPPS (ASYMMETRIC BIPOLAR PLASMA POWER SUPPLY)** *Bruna T. Bianchi*, Wilson L. Guesser, Juliano S. Scholtz, Luis C. Fontana*
#103	**RIETVELD REFINING: ELUCIDATION OF PEROVSKITES LNF STRUCTURE***L. C. D. Douglas Washington da Silva, Leticia Trezecik Silvano, Marilena Valadares Folgueras*
#105	**DEPOSITION AND CHARACTERIZATION OF TITANIUM NITRIDE FILMS INTERLAYERED WITH FILM OF TITANIUM DOPED OR NOT WITH ALUMINUM OR COPPER, FORMED BY DISCHARGE IN DUAL CATHODIC CAGE** *T.M. Gonçalves, A.A. Margon, B.P. Pimentel, G.P. Donatti, L.C. Gontijo*
#106	**PERMETHRIN POLYMERIZATION ON POLYAMIDE FABRIC BY HYBRID CORONA-DIELECTRIC BARRIER DISCHARGE OPERATING AT ATMOSPHERIC PRESSURE** *A. Petraconi, F. Gasi, E. Bittencourt, A.H.R. Castro, F.S. Miranda, A.M. Essiptchouk, L. Nascimento, R.S. Pessoa, G. Petraconi, H.S. Maciel*
#107	**USE OF GLASS WASTE AS A PARTIAL SUBSTITUTE FOR CEMENT TO OBTAIN MORTAR** *A.C. Martin, L.M. Scolaro, B.F. Zappelino, M.V. Folgueras*
#108	**POWER CURVES OF SMALL WIND TURBINES INSIDE A LABORATORY WITH CONTROLLED EXHAUST FAN** *Gustavo M. Franco, Joel Luiz da Rosa, Samuel Strelow, Henrique de Souza Medeiros*
#109	**MICROSTRUCTURAL CHARACTERIZATION OF BORIDE LAYERS ON VANADIS 10 TOOL STEEL – PRELIMINARY RESULTS** *Anael Preman Krelling, Alexcier Krawczuk Capitani, Gabrielli Zavatini, Bruna de Freitas Zappelino,*

	Elisangela Aparecida dos Santos de Almeida, Julio Cesar Giubilei Milan, César Edil da Costa
#110	**ELECTROCHEMICAL CHARACTERIZATION IN SOLUTION OF A FERTILIZER MIXTURE FOR PLASMA DEPOSITED TITANIUM OXIDE FILMS IN ASTM A36 STRUCTURAL STEELS WITH THE USE OF CATHODIC CAGE** *G.P. Donatti, A.A. Margon, B.P. Pimentel, T.M. Gonçalves, L.C. Gontijo*
#111	**INFLUENCE OF THE ADDITION OF BY-PRODUCTS OF THE VINYL INDUSTRY IN THE PROPERTIES OF THE BIODEGRADABLE POLYMER POLY (LACTIC ACID)** *Laísa Cristina Klemann, Paula Sacchelli Pacheco, Wagner Mauricio Pachekoski, Derce de Oliveira Souza Recouvreux, Daniela Becker*
#112	**SYNTHESIS AND CHARACTERIZATION OF COMPOUNDS NIO-BACE0.2ZR0.7Y0.1O3-Δ IN ANODE FOR SOLID OXIDE COMBUSTIBLE CELL** *Paula Sacchelli Pacheco, Adilson Luiz Chinelatto, Wagner Mauricio Pachekoski*
#113	**EFFECTS OF NITRIDING AND DEPOSITION OF TITANIUM NITRIDE FILM THROUGH CATHODIC CAGE IN THE RESISTANCE TO STEEL TYPE API 5L X70 CORROSION** *A.A. Margon, B.P. Pimentel, T.M. Gonçalves, G.P. Donatti, C.S. Carvalho, L.C. Gontijo*
#114	**USE OF DIFFERENT PROPORTIONS OF HYDROGEN AND ACETYLENE FOR PRODUCTION OF THIN FILMS BY PECVD** *L. G. Heinig, J. Rodrigo da Costa, R. A. de Simone Zanon, J. M. Pureza*
#116	**ANALYSIS OF GLASS AND CLAY POWDER USING LASER DIFFRACTION** *Gabriel A. R. Bigansolli, L. A. Franco, B. B. Lima-Kuhn1 and T.Y.A. Souza*
#117	**CHARACTERIZATION OF TI-AL FILMS OBTAINED BY ASYMMETRIC PULSED MAGNETRON SPUTTERING** *Deivison Daros Paim, Abel André Cândido Recco, Luiz Cesar Fontana*
#118	**INFLUENCE OF THE TREATMENT TEMPERATURE ON THE EDGE EFFECT OF NITIDEDUNS 32750 SUPER DUPLEX STAINLESS STEEL** *J.F. Vieira, S.F. Brunatto, R.P. Cardoso*
#119	**SYNTHESIS AND CHARACTERIZATION OF NANOCOMPOSITE OF POLY (VINYL BUTIRAL) REINFORCED WITH ZINC OXIDE NANOWIRES** *R.C.T. Porto, P.Z. Uchôa, S. H. Pezzin, J.C. Hoepfner, A.L. Nogueira*
#120	**PLASMA NITRIDING OF MARAGING STEEL C300 OBTAINED BY SELECTIVE LASER MELTING FOR FABRICATION OF INJECTION MOLDS** *I. F. Ostrovski1, A. M. Zanatta, A. Rabelo, S. Bodziak, V. L. Soethe Parucker, D. A. Duarte*
#121	**DEVELOPMENT OF RADIATION-ABSORBENT MATERIALS** *Isabelle de Geus Quintiliano, Viviane L. Soethe, Vinícius Martins Freire, Rafael G. Delatorre, Moisés L. Parucker*
#122	**EFFECT OF SOLUBILITY TREATMENT IN PLASMA NITRIDING WITH PULSED FLOW OF NITROGEN OF STAINLESS STEEL ISO 5832-1** *Heitor Augusto Pinto Cavalli, Anna Carolina Sphair, Paulo Cesar Borges, Marcio Mafra, Ricardo Fernando dos Reis, Euclides Alexandre Bernardelli*
#123	**TRANSFORMATION OF AUSTENITE AND FERRITE DURING LOW TEMPERATURE PLASMA NITRIDING OF DUPLEX STAINLESS STEEL** *Lucas Tomazi Durand, Lucas de Souza Gonçalves, Felipe de A. Possoli, Carlos Maurício Lepienski, Euclides Alexandre Bernardelli, Julio Cesar Klein das Neves, Márcio Mafra*
#124	**SCRATCH RESISTANCE OF THE NITRIDED LAYER OF DUPLEX STAINLESS**

	STEEL SAF 2205 *Luis E. A. dos Santos Rosa, Yamid E. Nuñez de la Rosa, Ane C. Rovani, Felipe de A. Possoli, Márcio Mafra, Paulo C. Borges and Giuseppe Pintaude*
#125	**IMPLANTATION ENERGY EFFECTS ON THE NITRIDING AND CARBURIZING OF SUPERAUSTENITIC STAINLESS STEEL** *Rafael F. Chuproski, Willian R. de Oliveira, Francisco C. Serbena, Rodrigo P. Cardoso, Silvio F. Brunatto, Paulo Soares and Gelson B. de Souza*
#126	**EFFECT OF INTERMITTENT FLOW OF NITROGEN GAS IN THE PRECIPITATION OF CHROMIUM NITRIDE DURING PLASMA NITRIDING OF STAINLESS STEEL ISO 5832-1** *Camila Gonçalves Marques, Alfredo Rubega Neto, Heitor Augusto Cavalli, Carlos Maurício Lepienski, Marcio Mafra, Euclides Alexandre Bernardelli*
#129	**MICROSTRUCTURE OF Ti-Al-N THIN FILMS OBTAINED BY REACTIVE PULSED MAGNETRON SPUTTER DEPOSITION** *Arthur A. Lenzi, Alessandra C. S. Dias1, Abel A. C. Recco, Deivison D. Paim*
#130	**PROJECT AND CONSTRUCTION OF REACTOR FOR THERMOCHEMICAL PLASMA NITRIDING** *Priscila Eduarda Kraft Lopes, Gil Magno Portal Chagas, Gustavo Jamir da Silva, Marcelo Malewschik, Joel Stryhalski, Luis César Fontana*
#131	**SURFACE TREATMENT OF ARTIFICIAL SKINS WITH ARGON PLASMA FOR DERMAL REGENERATION IN BURNS** *M. F. Gonçalves, M. W. Gonçalve[1], M. A. T. Duarte, V. L. Soethe Parucker, D. A. Duarte*
#132	**REACTIVE DYEING OF COTTON FABRICS FUNCTIONALIZED BY THE PLASMA TECHNIQUE** *Laura Palermo Gomes, Fernando Ribeiro Oliveira, Catia Rosana Lange de Aguiar, Camila Thais Mamani, Teresa Tromm Steffen, Luis Cesar Fontana, Daniela Becker, Maria Elisa Philippsen Missner*

PONTUAL DEFECTS STUDY OF TERNARY TITANIUM ALLOYS FOR BIOMEDICAL APLICATIONS USING DYNAMICAL MECHANICAL ANALYSIS

Marcos Ribeiro da Silva*, Pedro Kuroda[2], Raul Araújo[2] and Carlos Roberto Grandini[2]
[1]*Instituto Federal de São Paulo (IFSP)*
[2]*Universidade Estadual Paulista Júlio de Mesquita Filho (UNESP – Bauru)*

1. Introduction

Titanium alloys with presence of β stabilizers (Mo, Zr,Ta, V,Nb) are using in different areas of engineering, from aerospace to biomedical applications. Ti-6Al-4V is the most widely used titanium alloy biomaterial [1], but vanadium and aluminum cause cytotoxic effects in the human body. To circumvent such effects, these elements could be replaced by other beta-stabilizer elements, such as zirconium, niobium, molybdenum, and tantalum, which decrease the beta-transus temperature and improve the elastic modulus of the alloy [2,3,4]. Ti-20Zr-xMo and Ti-10Zr-yMo alloys system are promising alloys for biomedical applications because they have no cytotoxic elements.

2. Experimental

Ti-10Mo-XZr alloys (X=5 and 10 wt) were prepared using an arc-melting furnace with a water-cooled crucible in an argon-controlled atmosphere, and hot-rolled to obtain the samples for dynamical mechanical testes. Commercially pure metals were used as precursors, in the shape of cylindrical titanium bars, zirconium sheets and molybdenum wires, previously pickled and washed in an ultrasonic washer, aiming to eliminate impurities in these materials.

A homogenization heat treatment at 1273 K for 24 h , with heating rate of 10^0C, were subjected in the samples, in a vacuum better than 10^{-6} Torr. After this step the samples were slowly cooling in air and the same steps were repeated , to ensure that the samples were free of residual stresses . After annealing the samples were submitted to a solubilization heat treatment, with heating rate of 10^0C/min, vacuum in magnitude of 10^{-5} Torr until 1273 K for 2 hours, after that the samples were faster cooling in water.

The samples were characterized by: density measurements using an Explorer-Ohaus analytical balance, the method used to obtain measurements was the Archimedes principle, using water as reference samples; x-ray diffraction (XRD) using a Rigaku/Dmax 2100 PC diffractometer, the powder method was used with Cu; Kα radiation, scan range from 20 to 80 0 in a fixed time mode; (SEM) using Carl Zeiss EVO-LS15 equipment; OM using Olympus BX 51 M ; dynamical Mechanical Analysis using an Areva Metravib DMA-25, in the temperature range of 300 to 720 K, heating rate of 1.0 K/min and frequency range of 1 to 40 Hz. All samples were measured in the tension mode.

3. Results and Discussions

The results of XRD and SEM micrographs showed that in the prepared alloys has the coexistence of alpha and beta phases, showing the beta stabilizing character of the added elements in alloys. For the elastic modulus, it can be observed that the addition of the solute in the two systems decreases the Young modulus as confirmed by thermoactivated process in Anelastic Spectrum. Fig1 shows a the internal friction spectra measurements for Ti-10Mo-10Zr measured with frequency range of 1 to 40 Hz before background extraction. One single process was observed, and the peak shifts slightly to higher temperatures, with higher work frequencies, characteristic inherent to thermally activated processes. The peak height and FWHM differences characterizes a multi process peak, and the thermally activated process indicates stress induced order of point defects.

*Corresponding author: marcosrs@ifsp.edu.br

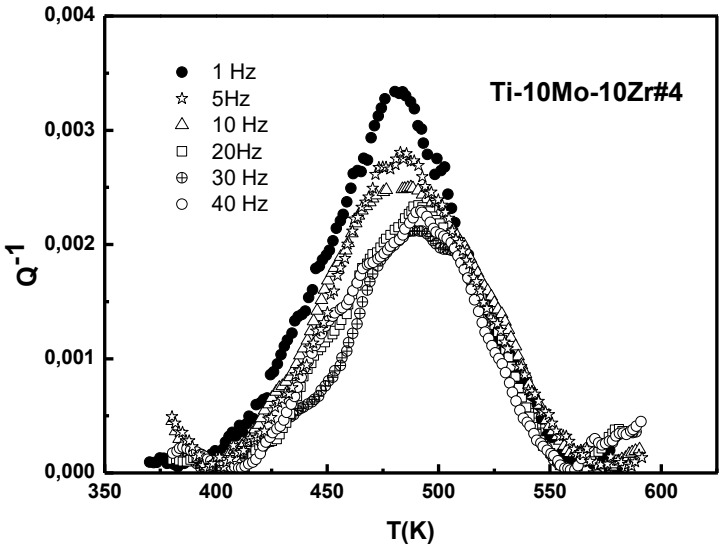

Fig.1 – *Mechanical Spectrosopy for Ti-10Mo-10Zr.*

4. References

[1] M. S. Blanter, I. S. Golovin, H. Neuhäuser and H.-R. Sinning: *Internal Friction in Metallic Materials: A Handbook* (Springer-Verlag, Heidelberg 2007).
[2] F. B. Vicente and C. R. Grandini: Defect and Diffusion Forum Vol. 354 (2014), p. 159-165.
[3] D. R. N. Correa, P. A. B. Kuroda and C. R. Grandini: Advanced Materials Research Vol. 922 (2014), p. 75- 80.
[4] W.-F. Ho, S.-C. Wu, S.-K. Hsu, Y.-C. Li and H.-C. Hsu: Materials Science and Engineering: C Vol. 32 (2012), p. 517-522.

Acknowledgments

Financial support: CNPq and FAPESP

*Corresponding author: marcosrs@ifsp.edu.br

BEHAVIOR OF GLIDING ARC DISCHARGE REPETITION FREQUENCY IN PLASMA ASSISTED FUEL RICH COMBUSTION OF NATURAL GAS

Armando José Pinto[1]*, Julio César Sagás[2] and Pedro Teixeira Lacava[1]
[1]*Laboratory of Combustion, Propulsion and Energy, Technological Institute of Aeronautics (ITA), São José dos Campos, Brazil.*
[2]*Laboratory of Plasmas, Films and Surfaces, Santa Catarina State University (UDESC), Joinville, Brazil.*

1. Introduction

Different non-thermal plasmas at atmospheric pressure have been applied in combustion process to emission control [1–3] and increase of flammability limits [4–6]. Among then it can be highlighted the gliding arc discharge (GA). It has the simplest design, can operate with DC or AC power supplies and can be constructed in different geometries [1,7]. The GA discharge is a non-steady state discharge, operating in repetitive cycles of breakdown, evolution and extinction. Recent studies show an increase in flammable range using an AC gliding arc discharge in a fuel rich combustion of natural gas. However, high speed camera measurements showed that the flame generated occurs in cycles, as the discharge [1,4]. The ignition happens at the breakdowns and the flame is ceased a few instants after the discharge. Such pulsation can affect the combustion stability. So, the study of repetition frequency is necessary for applications like plasma assisted combustion.

Although many works deal with electrical characterization of gliding arc discharges [8 ,9], little attention is given to the effect of gas mixture in the discharge repetition frequency [10,11]. In this work, the relationship between the discharge repetition frequency and the process parameters was evaluated in a DC reverse vortex flow gliding arc. The main goal is to determine how the gas mixture composition and mass flow rate can affect the repetition frequency, and so the breakdown occurrence.

2. Experimental

The plasma reactor is coupled to a fuel lean swirl stabilized burner system. However, in this work only the plasma reactor was used. The reactor is composed of a hollow stainless steel cylinder with 50 mm of length and 26 mm of inner diameter. A convergent-divergent nozzle at the exit of the reactor acts as the ground electrode while the reactor wall acts as the negative one.

The discharge was generated in a fuel rich premixed mixture of natural gas and air. A BRC 10 kV - 1 A Unipower 10kW DC power supply was used to generate and sustain the discharge. A 50 kΩ - 2 kW ballast resistor was installed in series with the power supply in order to limit the maximum discharge current to 200 mA. Voltage and current waveforms were recorded using a Tektronix TDS2024C oscilloscope and two Tektronix P6015A 1000:1 voltage probes. The discharge frequency was determined by applying a Fast Fourier Transform to the voltage waveforms.

In the first series of experiments, the discharge was generated in two fixed fuel flow rate 0.25 g/s and 0.49 g/s. For each one, the air mass flow rate was varied to achieve equivalence ratios from 3.0 to 5.2. A set of additional experiments was performed with fixed total mass flow rate (1.85 g/s and 2.10 g/s) i.e. the air flow rate was reduced proportionally to the fuel flow rate increase, in order to change only the equivalence ratio.

3. Results and Discussions

The results show that the mean voltage and current remains almost constant for the range of equivalence ratios and total mass flow rates used in this work. On the other hand, the discharge repetition frequency can increase up to 2.6 times. Both the raise in equivalence ratio (with constant total mass flow rate) and the increase in total mass flow rate (for constant equivalence ratio) cause a growth of the discharge repetition frequency as showed in figure 1. In the first case, this is caused by the higher methane content in the gas. Methane has a lower ionization potential leading to a lower breakdown voltage. Consequently, the repetition frequency increases. In the second case, the rise in discharge repetition frequency is caused by the increased arc velocity.

*Corresponding author: armando.jpinto@yahoo.com.br

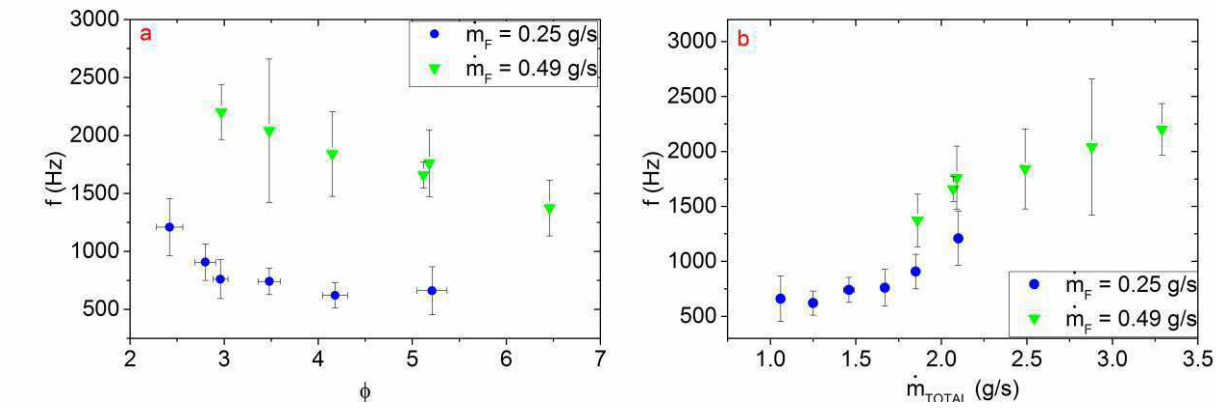

Fig. 1. *Discharge frequency as a function of the equivalence ratio (a) and total mass flow rate (b) of the plasma.*

The reduction in discharge repetition frequency as a function of equivalence ratio (with constant fuel mass flow rate) increases the probability of failure in flame ignition. This can make the system unstable in high equivalence ratios. On the other hand, the increase in total mass flow rate can lead to a flame blow off. Both phenomena must be considered to choose an optimum operational condition for plasma assisted burners.

4. References

[1] Varella R. A., Sagás J. C. and Martins C. A., *Fuel* **184** 269–76 (2016).
[2] Lee D. H. et al., Kim K.-T, Kang H. S., Song Y.-H. and Park J. E., *Environ. Sci. Technol.* **47** 10964–10970 (2013).
[3] Song Y. H., Kim K. T., Lee J. O., Lee D. H. and Hwang N. K., *Int. J. Plasma Environ. Sci. Technol.* **7** 97–103 (2013).
[4] Sagás J. C., Maciel H. S. and Lacava P. T., *Fuel* **182** 118–23 (2016).
[5] Kim W., Do H., Mungal M. G. and Cappelli M. A., *Combust. Flame* **153** 603–15 (2008).
[6] Bak M. S., Do H., Mungal M. G. and Cappelli M. A.,*Combust. Flame* **159** 3128–37(2012).
[7] Zhu F., Zhang H., Li X., Wu A., Yan J., Ni M. and Tu X., *J. Phys. D. Appl. Phys.* **51** 105202 (2018)**.**
[8] Zhu J., Sun Z., Li Z., Ehn A., Aldén M., Salewski M., Leipold F. and Kusano Y., *Phys. D. Appl. Phys.* **47** 295203 (2014).
[9] Zhang H., Du C., Wu A., Bo Z., Yan J. and Li X., *Int. J. Hydrogen Energy* **39** 12620–35 (2014).
[10] Yu L., Yan J. H., Tu X., Li X. D., Lu S. Y. and Cen K. F., *EPL (Europhysics Lett.)* **83** 45001 (2008).
[11] Rusu I. and Cormier J.-M., *Int. J. Hydrogen Energy* **28** 1039–43 (2003).

Acknowledgments

The authors would like to thanks to the Brazilian Coordination for the Improvement of Higher Education Personnel (CAPES) for the financial support.

*Corresponding author: armando.jpinto@yahoo.com.br

SURFACE MODIFICATION OF CELLULOSE PULP WITH FLUORINATED COMPOUND BY PLASMA ENHANCED CHEMICAL VAPOR DEPOSITION (PECVD)

Oliveira, L. S.[1]*, Delgado-Silva, A. O.[2], Rangel, E. C.[3], Mendes, R. F.[4] and Vaz, L. E. V. De S. B.[5]
[1]*Department of Forestry Sciences; Federal University of Lavras; Lavras/MG*
[2]*Department of Physics, Chemistry and Mathematics; Federal University of São Carlos; Sorocaba/SP*
[3]*Paulista State University "Júlio de Mesquita Filho"; Sorocaba/SP*
[4]*Engineering Department; Federal University of Lavras; Lavras/MG*
[5]*Engineering Department; Federal University of Lavras; Lavras/MG*

1. Introduction

Cellulose is a linear polymer composed of β-1-4-glycosidic bonds which has several free hydroxyl groups making it quite hydrophilic [ref number 1, ref number 2]. In cementitious matrix composites, the hydrophilic character of this polymer is a major problem. Into alkaline medium, cellulose fibers mineralize and consequently degrade the composites reducing their life time [ref number 3, ref number4]. Plasma treatment of cellulose with fluorinated compounds is efficient for modifying its surface, enabling an increase of the hydrophobicity by incorporating fluorine at the active sites of such polymer [ref number 5, ref number 6]. In this context, the objective of this work was to superficially modify the cellulose pulp by Plasma Enhanced Chemical Vapor Deposition (PECVD) using fluorinated compound. After the treatment, the pulps are going to be introduced into cementitious composites for improvement of its durability as a final product.

2. Experimental

The surface treatment of cellulose by PECVD was carried out at the Laboratory of Technological Plasmas (LaPTec) of the Paulista State University "Júlio de Mesquita Filho" (UNESP) at the Sorocaba / SP. The characterization of the materials was carried out at the Federal University of Lavras (UFLA) in Lavras / MG. The cellulose pulp was bleached by Kraft process from *Eucalyptus urophylla x Eucalyptus grandis* and obtained from Suzano Papel e Celulose de Suzano / SP. For the treatment of the pulp with fluorine compound was used a glass cylinder reactor containing two parallel electrodes connected to an Edwards E2M18 rotary pump of vacuum brand and a radiofrequency source model RF-300 of Tokyo Hy-Power brand (13 , 56 MHz, 1-300 W) coupled to an MB-300 impedance setter of the Tokyo Hy-Power brand. The applied power and the deposition time were kept fixed at 120 watts and 10 minutes, respectively. The gas pressure of the fluorinated compound used was $3x10^{-1}$ Torr, $5x10^{-1}$ Torr and $7x10^{-1}$ Torr and the background pressure, the pressure required for the plasma to be formed, was 10% with respect to the pressure of the fluoride compound used. The upper electrode received the radiofrequency (RF) while the lower electrode (sample port) was grounded. The untreated cellulose pulp (control) and cellulose pulp treated with fluorinated compound at pressures of $3x10^{-1}$ Torr (CMS-F1), $5x10^{-1}$ Torr (CMS-F2) and $7x10^{-1}$ Torr (CMS-F3) were sampled, "glued" on double-face tape attached to glass slides and analyzed in a Krüss goniometer coupled to the computer with Advance Software at UEPAM's Nanotechnology Laboratory. For moisture absorption analysis, the ASTM standard E-104-85 (1996) was used [ref number 7].

3. Results and Discussions

The moisture absorption of all the treated samples decreased when compared to the control. In addition, the contact angle of CMS-F1, CMS-F2 and CMS-F3 was above 90° and below 120° which characterizes them as hydrophobic surfaces. Camargo et. al. (2017) and Santos et al. (2012) [ref number 1, ref number 6] found similar results to this work when they modified the surface of the cellulose and corn starch films, respectively, making them more hydrophobic when compared to the control. Therefore, the surface treatment of cellulose pulp by PECVD using fluorinated compound proves to be efficient to increase the hydrophobicity of the cellulose pulp and therefore could be used in the production of cementitious composites.

4. References

[1] CAMARGO, J. S. G. de et. al. Materials Research, **20**, 842 – 850, (2017).
[2] DONINI, I. A. N. et. al. Eclética Química, **35**, 165 – 178, (2010).
[3] TEIXEIRA, R. S. et. al. Cement and Concrete Composites, **85**, 1- 8, (2018).
[4] TONOLI, G. H. D. et al. Construction and Building Materials, **24**, 193–201, (2010).
[5] KARBOWIAK, T. et. al. Journal of Colloid and Interface Science, **294**, 400–410, (2006).
[6] SANTOS, A. E. F. et. al. Carbohydrate Polymers, **87**, 2217– 2222, (2012).

*Corresponding author: laissalviano@yahoo.com.br

[7] AMERICAN SOCIETY FOR TESTING AND MATERIALS. **ASTM E-104-85**,3p., (1996).

Acknowledgments

The authors would like to thank the Coordination of Improvement of Higher Education Personnel - CAPES and Foundation for Research Support of the State of Minas Gerais - FAPEMIG for the financing of this work, UFSCar campus Sorocaba / SP, LaPTec at UNESP campus Sorocaba / SP and the laboratory complex of the UEPAM in the Department of Forestry Sciences of UFLA where the work was carried out.

*Corresponding author: laissalviano@yahoo.com.br

PHYSICAL AND MECHANICAL BEHAVIOR OF CEMENT COMPOSITES EXTRUDED WITH SILANE FUNCTIONALIZED CELLULOSIC PULP AT DIFFERENT CONCENTRATIONS

Sara Aparecida Alexandre[1]*, Lara Campideli Santos[2], Rafael Farinassi Mendes[3] and Lívia Elisabeth Vasconcellos de Siqueira Brandão Vaz[3]

[1]*Master's Degree (MSc) in Biomaterial Enginnering from the Federal University of Lavras (UFLA), Brazil*

[2]*Graduation Student of ABI at Federal University of Lavras (UFLA), Brazil*

[3]*Teacher and Researcher of the Engineering Department (DEG) of the Federal University of Lavras (UFLA), Brazil*

1. Introduction

Cement composites are ceramic and exhibit brittleness when subjected to tensile tests at static bending [1]. Thus, reinforcing agents may be inserted to increase their ductility and toughness and to prevent a sudden fracture. Asbestos is a material that has satisfactory physical and mechanical properties, low cost, good matrix adhesion and high availability [2]. However, it may be associated with some respiratory diseases, a fact that led to its limitation of use in Brazil and prohibition in some countries of the world, such as Japan and Belgium. Synthetic fibers, such as polyvinylpyrrolidone (PVA), have been tested and, although satisfactory, have a high cost for composite production compared to asbestos fibers and vegetable fibers [3]. Vegetable fibers present low cost, high availability, are renewable and exhibit resistance comparable to inorganic fibers [4, 5, 6]. For application in cement, Kraft pulp can be used, in which the extractives and the lignin are removed from the vegetal fiber, for example, as they negatively affect its cure and hinder the superficial modification of the lignocellulosic material [7]. The cellulose pulp is hydrophilic and, when inserted in the cement matrix, presents problems such as mineralization causing the fiber to stiffen, carrying to rupture without adequate elongation, degradation due to the alkalinity of the cement and dimensional instability due to the absorption and release of moisture, damaging the fiber-matrix relation. It is possible to modify the cellulosic pulp through the insertion of hydrophobic groups in its structure, in order to minimize such events. Among the compounds used for surface coating of cellulose are silanes, such as triethoxyoctylsilane (OTES) [8].

2. Experimental

For the production of fiber-cement, the experimental proposal was based on the superficial modification of the cellulose pulp, obtained by the Kraft pulping process, with triethoxyoctylsilane, via hydrolysis, in concentrations of 0, 5, 10, 15, 20 and 25% in relation to dry mass of cellulose pulp. The formulation for extrusion composites was 5% cellulose pulp, 60% CPV-ARI Portland cement, 33% ground agricultural limestone, 1% hydroxypropylene methylcellulose (HPMC) and 1% polyether carboxylic additive (ADVA), with final water / cement ratio of 0.4. The mechanical and physical properties were evaluated with 28 days of curing of the composites. In order to make it possible to verify the effect of the surface chemical modification of cellulose pulps on the physical and mechanical properties of the fiber cement produced, tests have been developed that provide information about the physical properties such as water absorption, apparent density and apparent porosity, as well as the mechanical properties of modulus of elasticity (MOE), modulus of rupture (MOR) to static flexion, limit of proportionality (LOP) and toughness.

3. Results and Discussions

The most satisfactory results regarding the physical and mechanical properties of the composites were obtained for the treatment of 5% of hydrolyzed triethoxyoctylsilane on the dry mass of the Kraft pulp before the aging of the cements. This fact is due, among the applied concentrations, to the chemical interactions between the composite used to modify the surface and the cement, increasing the ductility and the tenacity of the composite, improving the fiber-matrix interaction. Its durability can also be analyzed after accelerated aging cycles in a climate simulation machine with high temperature, rainfall and ultraviolet radiation. It was observed a decrease in the values of the physical and mechanical properties of the fibrocement after 10 and 20 cycles of accelerated aging. However, these values were higher than the control composites, meeting the norm NBR 15498 (ABNT, 2007), remaining the concentration of 5% silane with the best results. All treatments comply with the NBR 12800 standard (ABNT, 1993), which establishes a maximum water absorption value of 37% for fiber cement.

*Corresponding author: salexandre.eng.amb@gmail.com

4. References

[1] C. Lopes, A. Nolasco, M. Tomazello Filho, T. Dias and A. Pansini, Ciência Florestal, **21**, 315-322, (2011).
[2] J. Winkler, Environment International, **80**,72-78, (2015).
[3] Instituto Brasileiro do Crisotila. Utilização do amianto no Brasil.Disponível em <http://www.ibcbrasil.org.br/pesquisas>. Acesso: jun. 2017.
[4] S. R. Albinante, E. B. A. V. Pacheco and L. L. Y Visconte, Química Nova, **36**,114-122, (2013).
[5] A. M. Ferreira and A. J. F. Carvalho, Materials Research, **17**, 807-810, (2014).
[6] N. Quiévy, M. Jacquet, M. Sclavons, C. Deroanne, M. Paquot and J. Devaux, Polymer Degradation and Stability, **95**, 306-314, (2010).
[7] U. Klock, A. S. Andrade, J. A. Hernandez, FUPEF. Série Didática, n. 4/98, (2013).
[8] R. F. Mendes, L. M. Mendes, J. E. Oliveira, H. Savastano Júnior, G. Glenn, G. H. D. Tonoli, Polymer Engineering & Science, **55**, 1273-1280, (2015).

Acknowledgments

The authors would like to thank Universidade Federal de Lavras (UFLA), Programa de Pós-Graduação em Engenharia de Biomateriais (UFLA) and Coordenação de Aperfeiçoamento de Pessoal de Nível Superior (CAPES).

*Corresponding author: salexandre.eng.amb@gmail.com

SUN TRACKING MECHANISM EFFECTS ON A PHOTOVOLTAIC SYSTEM

Erick S. Nunes[1*] and Alexandre W. Arins[1]
[1]*Instituto Federal de Santa Catarina – IFSC – Joinville – SC*

1. Introduction

The most part of the energy used on our planet comes from sources with finite resources and harmful to our ecosystem. Starting from this premise, scientists from all around the world are searching for new forms of energy production that are less polluting and more efficient.

Solar energy is an efficient source of virtually inexhaustible energy that will serve us for a long time. The need to take advantage of this energy has motivated researchers to make photovoltaic cells economically efficient, enabling their use on a large scale. Photovoltaic cells use solar radiation and convert it directly into electricity. In addition to being used in power generation, photovoltaic cells find other applications. One example is the use of solar cells to help produce hydrogen, which can be used as a fuel source for electric cars.

When the photovoltaic panels are installed it is very important to determine the best position to set them, because their efficiency depends directly on the angle of incidence of solar radiation. To improve the efficiency of photovoltaic cells it is possible to use a mobile system to trace the maximum power point (MPP). The best capture of the solar rays occurs when the plates are positioned perpendicular to the solar rays.

In the last decade, several methods for maintaining MPP systems have been proposed [1-5]. The solar tracking can be performed through a block of light resistive sensors (LDRs), which provide the control signals for independent tracking of solar coordinates [4,5].

2. Experimental

For this research, a solar tracking system based on LDR sensors was constructed, whose arrangement is capable of continuously positioning a photovoltaic plate at its MPP point. The tracker has two axes of rotation, each axis is controlled by a servo motor controlled by an Arduino UNO that receives signals from the LDR sensors, one for each axis.

For the tests, the MPP control system and a fixed photovoltaic plate were initially positioned facing towards the geographic north, and the set plate was oriented for a 30º angle of inclination related to the horizontal plane. In this experiment two solar panels of the Star Solar brand model CNC85x115-18 (12 V / 1,5 W), made with polycrystalline silicon.

3. Results and Discussions

Voltage measurements were performed between 8 h and 16 h. The data are shown in the graph of Figure 1 where it is possible to verify that the board coupled to the solar tracking system registered power values, on average, higher than the fixed system.

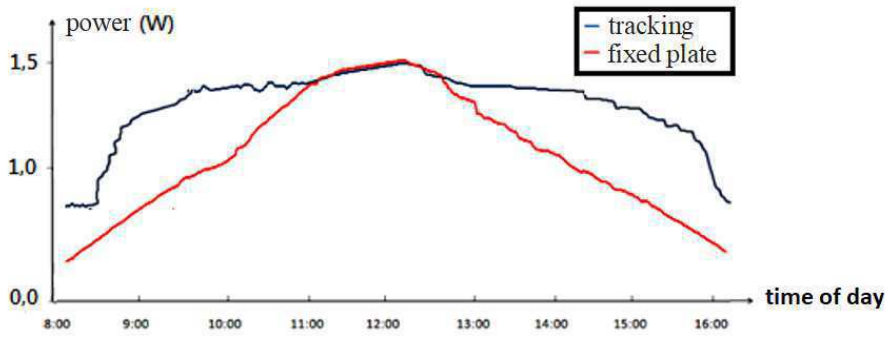

Fig. 1. *Graph of the maximum power obtained using the systems with fixed plate and with tracking system.*

The developed tracker simply and efficiently repositions the photovoltaic plate. An analysis of the results shows that the use of solar trackers in photovoltaic panels increases the yield of the system. It has been found that the use of the tracking system generates an increase in power and, consequently, an energy around a 34% gain in relation to the static module.

*Corresponding author: erick.szns@hotmail.com

4. References

[1] W. Xiao, M. G. J. Lind, W. G. Dunford, and A. Chapel, Real-time identification of optimal operating points in photovoltaic power systems, IEEE Trans. Ind. Electron., vol. 53, no. 4, pp. 1017–1026, Jun. 2006.
[2] W. Xiao, W. G. Dunford, P. R. Palmer, and A. Capel, Application of centered differentiation and steepest descent to maximum power point tracking, IEEE Trans. Ind. Electron., vol. 54, no. 5, pp. 2539–2549, Oct. 2007.
[3] N. Mutoh, M. Ohno, and T. Inoue, A method for MPPT control while searching for parameters corresponding to weather conditions for PV generation systems, IEEE Trans. Ind. Electron., vol. 53, no. 4, pp. 1055–1065, Jun. 2006.
[4] R. Gules, J. De Pellegrin Pacheco, H. L. Hey, and J. Imhoff, A maximum power point tracking system with parallel connection for PV stand-alone applications, IEEE Trans. Ind. Electron., vol. 55, no. 7, pp. 2674–2683, Jul. 2008.
[5] T. Esram, Comparison of photovoltaic array maximum power point tracking techniques, IEEE Trans. Energy Convers., vol. 22, no. 2, pp. 439–449, Jun. 2007.

Acknowledgment

We thank the financial support of IFSC's Institutional Program for Incentive to Scientific Production and Technological Innovation.

*Corresponding author: erick.szns@hotmail.com

STUDY OF PLASMA PROCESS FOR TREATMENT OF CUTTING TOOLS MANUFACTURED IN HIGH-SPEED STEEL

Egert, P. [1*], Silva, H.R.T.[1], Seeber, A.[2], Zanella, H.C.M.[1] and Hoffmann, J.V.J.[1]
[1]*Universidade do Sul de Santa Catarina/UNISUL, SC, Brazil*
[2]*Universidade Federal do Pampa/UNIPAMPA, RS, Brazil*

1. Introduction

High-speed steel is used in tools manufacturing for usage in processes of metallurgical industry. When produced, these materials require a great control in their chemical composition and physical properties, in order to meet requirements in services. There are several processes to treat surface and can be used in these materials as plasma nitriding that is a process that allows change properties of metallic materials through nitrogen atoms diffusion in the its surface [1]. With variation of parameters used in electric discharge that generates plasma is possible obtain only the diffusion layer, or diffusion layer and the compound layer. The result is improvements in its mechanical performance as the increase in hardness, by the formation of the thicknesses of the layers formed in the process of plasma nitriding, in samples of fast steel [2]. In addition to this, surface enrichment with transition metals, such as niobium (Nb), is another possible technique to improve the performance of these surfaces. In this study we present the validation of an experimental system used to alter the high-speed steel surface through plasma process. The system was technically feasible for the niobium surface enrichment process associated with plasma nitriding, that is, Nb atoms were removed from a target via "Active Sputtering" and deposited on the high-speed steel forming an Nb_4N_3 phase.

2. Experimental

For plasma nitriding treatments and Niobium “Active Sputtering", a pulsed direct current (DC) reactor was used (Fig. 1) where an electric discharge was produced in a single cycle in the mixtures of nitrogen (N2) and hydrogen (H2) and argon (Ar) and hydrogen (H2), respectively.

Fig.1. *Detalhamento dos eletrodos internos do sistema experimental a plasma.*

Plasma nitriding is carried out in a reactor of electric current continues (dc), in a gas mixture of 75% N_2 + 25%H_2. Variables investigated are time (30, 60, 120 and 180 minutes); and temperature (400˚C and 500ºC). Tension and chain were adjusted to achieve the values of temperature wanted. In this step, the chemical species of the plasma are ionized and react with the metallic surface, positioned as cathode in the electric discharge. Subsequently, a niobium enrichment step was performed (temperature of 400 ° C and 500 ° C, duration of 30 min, pressure of 2 Torr in a gas mixture of 75% Ar + 25% H_2, with voltage and current adjusted for the reach of the temperature value). In this second step, we replace the N_2 of the gaseous atmosphere with the Air, and the chemical species begin to react with a niobium metallic surface (target), positioned as cathode, where Nb atoms are plucked and deposited on the surface of the high-speed steel, floating potential.

Samples of cutting tools of industrial machine were used, provided by Indústria Catarinense de Maquinas Operatriz Têxtil. The samples treated were analyzed microscopically using a scanning electronic microscope in order to evaluate thickness of layers obtained in the nitriding process and Dispersive Energy Spectroscopy (SEM / EDS), seeking to identify the elemental presence of Nb on the surface of the material. Vickers Microhardness tests (HV) were also performed to know about surface microhardness resulting on the material. The phases formed with Nb were analyzed by X-ray diffraction (XRD).

*Corresponding author: *joaovictorhoffmann@gmail.com*

3. Results and Discussions

Performing the work allows an understanding on the surface changes in samples of high-speed steel obtained from plasma treatment. Surface analysis of samples from different techniques can be evidenced as follows.

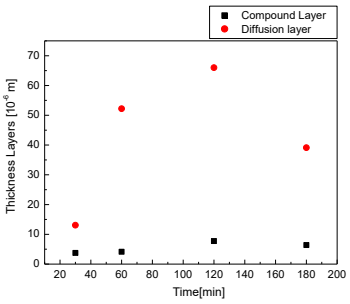

Fig.2. *Thickness by MEV of compound and diffusion layer formed in samples of plasma nitrated in gas mixture (75%N_2+25%H_2) and at 500°C.*

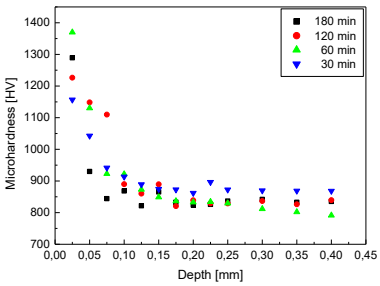

Fig.3. *SurfaceVickers microhardness in samples of plasma nitrated high-speed steel in gas mixture (75%N_2+25%H_2) and at 500°C.*

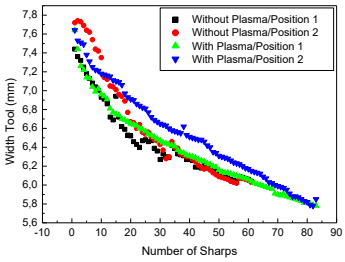

Fig.4. *Wear Operation test of plasma treated cutting tools and cutting tools without treatment.*

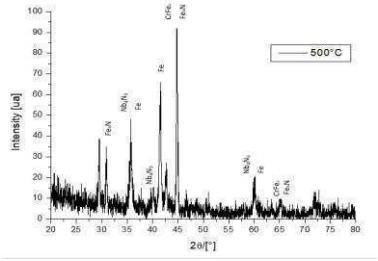

Fig.5. *Espectros by DRX sample surface plasma-treated in a 50% N_2+50%H_2, 2 Torr, 400°C and 30min, 75%Ar+25%H_2, at 2 Torr,30 min and* ***500°C.***

The study showed that treatment time above 2h do not contribute to increase the thickness of layer and studies on the surface microhardness profile corroborates this behavior on the surface diffusion of nitrogen in these metal components. Comparative results about the operation wear of plasma treated cutting tools, with those do not treated, we observe that cutting tools manufactured in high-speed steel presented higher operational durability when submitted the plasma treatment process, changing the properties of metalic material, when compared to the tools without any treatment. Through the XRD analyzes, we identified the presence of niobium nitride, on the surface of the samples treated at 500 ° C, which stabilized to the Nb_4N_3 phases, in addition to the iron containing phase, Fe_8N. The study carried out allows the conclusion that the experimental system used in the plasma nitriding process followed by active sputtering of niobium allowed a superficial enrichment of the Nb with high-speed steel. In addition, when the temperature employed in the process was 500 ° C, under the conditions employed, the niobium nitride phase, Nb_4N_3, was stabilized in the material. The study should now have its continuity seeking to form and elucidate the behavior of a possible layer containing N and Nb, in front of the operation of these tools.

4. References

[1] R. L. Paiva, R. B. Silva, R. V. Arencibia, R. S. Ruzzi, E. C. Bianch and P. R. Aguiar, Revista Matéria, **22** no.3, (2017).

[2] O. Belahssen, A. Chala, B. Djamel and C. H. Foued, International Journal of Engineering, **27**, 621-624 (2014).

Acknowledgments

The work received scholarship from the *Programa Institucional de Bolsas de Iniciação em Desenvolvimento Tecnológico e Inovação* (PIBITI), of the *Conselho Nacional de Desenvolvimento Científico e Tecnológico* (CNPq), also acoounted with support from the *Indústria Catarinense de Maquinas Operatriz Têxtil*.

*Corresponding author: *joaovictorhoffmann@gmail.com*

PLASMA OXIDATION OF LOW CARBON STEEL IN CATHODIC POTENTIAL AND FLOATING POTENTIAL

Paula Fin[1]*, Juliano Sadi Scholtz[2] and Luis C. Fontana[1]
[11]*Laboratory of Plasmas, Films and Superfaces – Universidade do Estado de Santa Catarina, Joinville, SC, Brazil*

1. Introduction

The steel sheets for electrical purposes usually pass through an annealing process, with the aim of improving the magnetic properties (Landgraf, 2016). During this process one superficial dielectric layer is formed, which is consisted of an iron oxide (Giroto, 2010). The plasma oxidation can be carried out with samples placed as the cathode of discharge or it can be maintained at floating potential. The plasma treatment in cathodic potential (CP) presents some difficulty if the geometry of the samples are complex, e. g., it can produces thermal gradient, and hollow cathode problems, which damage precision machined parts (Georges, 1999). An alternative process is the oxidation carried out in floating potential (FP). In this case the cathode consist in a grid surrounding the samples. The samples were treated in CP and FP modes, at three different temperatures.

2. Experimental

The experiments were performed in a 30cm diameter by 30cm height with grounded walls. The oxidation parameters of ABNT 1006 samples were: base pressure of $4x10^{-2}$ Torr; working gas: pure O_2; working pressure 0.5 Torr; treatment time: 2h, treatment temperatures: 300°C, 400°C e 500°C. In one arrangement, the sample was treated in a cathodic potential (CP) whereas in the other arrangement the sample was treated in a floating potential (FP). The power supply used for the plasma generation was a bipolar pulsed source that generates positive pulses of high intensity and short period (1µs), adjustable in intensity and frequency, named ABiPPS (Asymmetric Bipolar Plasma Power Supply, (Scholtz et al. 2018)). The source parameters used were: negative pulses with duration of 10µs interspersed by three positive pulses of 1µs. The negative pulses were adjusted between - 800V and -1000V and the positive pulses between + 400V and + 500V, in order to keep the temperature of the samples constant.

3. Results and Discussions

The surface oxides were characterized using the XPS in three different points of each sample, using a spot size of 400µm. In the XPS results (Fig.1), three distinct peaks are observed for the samples treated at 300°C ~~e~~ and 400°C. The peaks are at 709.9 eV, 715.9 eV and 723.4 eV, which may correspond to the FeO (Fe 2p1/ 2 peak located at ~723.1 eV and Fe 2p3/2 peak at ~709.5 eV and peak at ~715.5 eV). For the sample treated at 500°C (Fig.1) the peaks appear at 723.8 eV and 710.2 witch correspond to the Fe_3O_4 (Fe 2p1/2 peak at ~724.1 eV and a Fe 2p3/2 peak at ~710.6 eV) (Toru at all, 2008). Similar results are observed for samples treated in CP mode (Fig.2). However, when the sample was treated at 500°C in CP, a peeling on the surface oxides occurred, as observed on Fig. 3 (f). The region I of the Fig. 3 (f) shows a part of the sample where ~~that~~ the oxide layer had not been peeled and the region II where the film was peeled. This effect did not happen in the other samples (Fig. 3). In this case, the region that kept the film exhibit the phase Fe_3O_4 and the region that the film was removed present the phase FeO (Fig. 2).

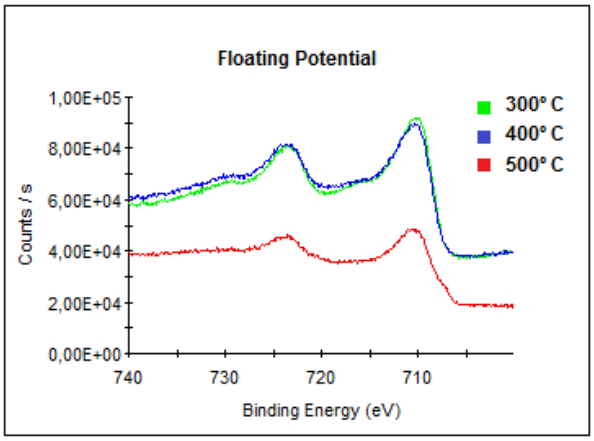

Figure 1. *XPS analyze of the samples treated in floating potential at 300ºC, 400ºC and 500ºC.*

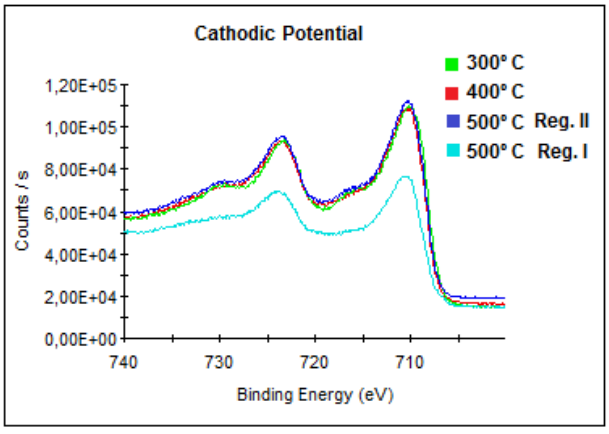

Figure 2. *XPS analyze of the samples treated in cathodic potential at 300ºC, 400ºC and 500ºC.*

*Corresponding author: paula.fin89@gmail.com

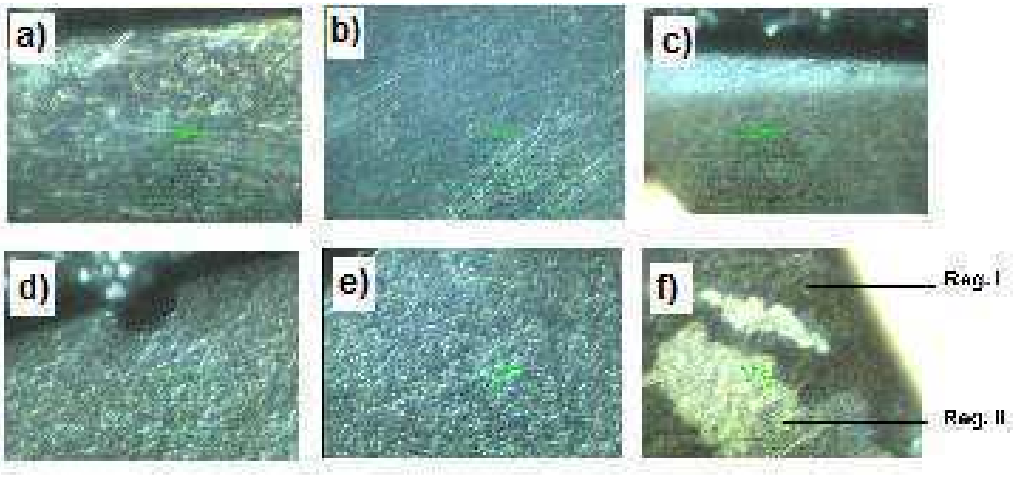

Figure 3. *Images of the samples treated at (a) 300ºC FP, (b) 400º FP, (c) 500 FP, (d) 300º C CP, (e) 400º CP (f) 500º CP –Reg. I with film, Reg. II without film.*

4. References

[1] LANDGRAF, F. G. **Propriedades Magnéticas de Aços para fins Elétricos.** Instituto de Pesquisas Tecnológicas do Estado de São Paulo, 2016; p. 121.

[2] Giroto, Ellen Regina. **O efeito do potencial de oxigênio na oxidação subsuperficial e suas influências nas propriedades magnéticas de aços elétricos após o recozimento final.** Masters dissertation – Universidade de São Paulo, São Paulo, 2010; p; 7-11. [Advisor: Doutor Fenando Gomes Landgraf].

[3] Georges, Jean. Inventor; Plasma Metal SA, Assignee. **Nitriding Process and Nitriding Furnace Therefor**. United States patent USOO.5989363A. 1999 Nov 23.

[4] Yamashita, Toru; Hayes, Peter. **Analysis of XPS Spectra of Fe2þ and Fe3þ Ions in Oxide Materials.** University of Queensland, Australia, 2008.

[5] Juliano Sadi Scholtz, Luis César Fontana, and Marcello Mezaroba Asymmetric Bipolar Plasma Power Supply to Increase the Secondary Electrons Emission in Capacitive Coupling Plasmas, IEEE TRANSACTIONS ON PLASMA SCIENCE, Vol. 46, Issue 8, Aug. 2018, DOI:10.1109/TPS.2018.2851071

Acknowledgments

We are grateful to FAPESC/UDESC (PAP TR655) and CAPES by supporting this work.

*Corresponding author: paula.fin89@gmail.com

BEHAVIOR OF Ti-30Nb-5Mo ALLOY AFTER COLD ROLLING FOLLOWED BY ANNEALING AND AGING

Magna Bibiano de Oliveira, Rubens Coutinho Toledo, Thailler Machado Nunes da Silva and Alexandra de Oliveira França Hayama*

Universidade Federal de Mato Grosso, Engenharia Mecânica /ICAT, Av. dos Estudantes, n° 5055, Cidade Universitária, Rondonópolis-MT, 78736-900

1. Introduction

Young's Modulus is an important mechanical property in the alloys that are used in biomedical applications. Beta-type titanium alloys, as Ti-30Nb-5Mo alloy, are composed of non-toxic and biocompatible materials such as Nb, presents a lower Young's Modulus, ranging from 55 to 85 GPa for some beta-type alloys [1], close to the human bone (20 to 40 GPa) [2]. Materials as the stainless steels and the Cr-Co-Mo alloys are also used in the production of orthopedic implant and may present Young's modulus close to 200 GPa and superior values to 240 GPa, respectively. When materials with Young's modulus higher than human bone are used, most tension is not transfer to the bone, as a result, the bone could be subjected to degradation and consequently osteoporosis [3].

One way to optimize the mechanical properties of the titanium alloys is to perform the aging thermal treatment which promotes the precipitation of reinforcement phases, causing an increase in the mechanical strength of the material. The focus of this study is beta titanium alloy which have applications in biomedical industry. In this context, this work presents the main results of the mechanical and microstructural characterization of the Ti-30Nb-5Mo alloy (wt%), annealed and then aged.

2. Experimental

Starting material consists of 50g ingots each and was obtained by electric arc melting furnace with controlled atmosphere. After melting, the ingots were encapsulated in quartz tubes under vacuum and then submitted to the solutioning heat treatment, which consists of heating the material at a temperature of 1,000°C for 8 hours, followed by quenching in water and simultaneously breaking the quartz. After this heat treatment, samples of Ti-30Nb-5Mo alloy (wt%) were deformed by cold rolling up to 86% of thickness reduction. After this, samples were sealed in quartz tubes under vacuum and annealed at 700 and 800°C for 1 hour. After annealing, the quartz tubes were broken inside of a container with water in room temperature. After this, sample were aged in temperature of 260ºC, the times considered were 1, 15, 30, 60 and 120 min. These samples also were sealed in quartz tubes under vacuum, but in this case, were cooled inside the quartz tubes in the air.

Microstructural analysis was performed using light optical microscopy. The mechanical behavior was evaluated by the Vickers hardness test and the resulting values represent the average of 10 measurements, using a 98gf applied for 20s, and measurements of Young's modulus using ultrasonic method.

3. Results and Discussions

After solutioning heat treatment it was verified that the material presented a grain size of 390 μm, and the elements, Nb and Mo, contributed to the stabilization of beta-phase which resulted in a ductile material and in a plastic deformation up to 86% of reduction in thickness by cold rolling, without intermediary annealing. Some cold-rolled sample presented shear bands that form approximately 40° with the rolling direction (Figure 1). These bands are a result of plastic instability during deformation [4].

Annealed samples were totally recrystallized with grain size near to 12 ± 2 μm for the annealed sample annealed at 700°C and 24 ± 5 μm for the annealed sample annealed at 800°C. The grain size in this condition decreased dramatically with respect to the grain size of the sample in the initial condition, as expected. Annealed samples did not present changes in the values of Young's modulus in relation to the deformed samples and Vickers hardness values decreased in this condition, due the elimination of defects, mainly dislocations, in the microstructure of the material.

Annealed and then aged samples presented microstructure similar to the annealed samples. Higher values of Young's modulus and Vickers hardness were obtained in the aged samples in relation to the annealed samples. Stabilization was observed in the values of Young's modulus after approximately 30 min of aging heat treatment, as observed in the Figure 2. The increase in the Young's modulus can be related to omega and alpha phases which precipitate in the material during the aging heat treatment.

*Corresponding author: alexandra_hayama@ufmt.br

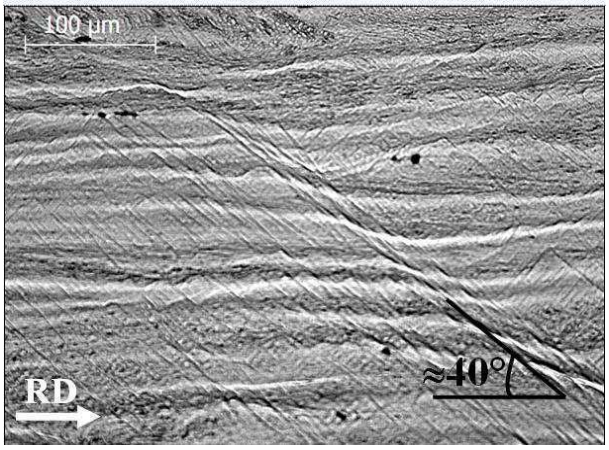

Fig. 1. *Microstructure of the Ti-30Nb-5Mo alloy cold-rolled showing shear bands with approximate angle of 40° with the rolling direction (RD) indicates by the arrow.*

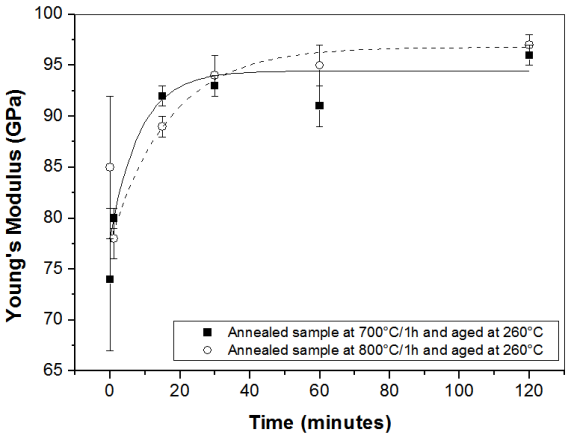

Fig. 2. *Variation of Young's modulus in the aged condition of the Ti-30Nb-5Mo alloy.*

4. References

[1] M. Niinomi, Mechanical properties of biomedical titanium alloys. Materials Science and Engineering A, 243, 231-236, (1998).

[2] M. Tane, S. Akita, T. Nakano, K. Hagihara, Y. Umakoshi, M. Niinomi, M. and H. Nakajima, Peculiar elástica behavior of Ti-Nb-Ta-Zr single crystals. Acta Materialia, 56,2856-2863, (2008).

[3] R. R. Tarr, I. C. Clarke, T. A. Gruen, and A. Sarmento, A., 1983, Comparison of loading behavior of femoral stems of Ti-6Al-4V and cobalt-chromium alloys: A Three-Dimensional Finite Element Analysis. Titanium Alloys in Surgical Implants. American Society of Testing Materials, 88-101, (1983).

[4] F. J. Humphreys and M. Hatherly, M. "*Recrystallization and related annealing phenomena",* 2nd edition. Elsevier, U.K., (2004).

Acknowledgments

The authors are thankful to FAPEMAT – Fundação de Amparo à Pesquisa do Estado de Mato Grosso (Process N° 154536/2014 and process N° 169548/2015) for the financial supporting, to CBMM – Companhia Brasileira de Metalurgia e Mineração for the niobium samples and to Prof. Dr. Rubens Caram for the technical supporting.

*Corresponding author: alexandra_hayama@ufmt.br

SPECIMEN SIMULATION SUBJECT TO FATIGUE IN AL-X%NI ALLOY

Mateus de Oliveira Silva*, Gilberto Vicente Prandi, Roberto Nunes Duarte and Renato Chaves Souza
Federal Institute of Education, Science and Technology of São Paulo – Campus São João da Boa Vista

1. Introduction

The use of software to perform simulations is a method that has been widely used to contribute to the development and characterization of a model that helps to determine possible results for a given subject, obtaining a qualitative analysis on the behavior of the same during its application , and can be compared with actual data obtained in laboratory tests and analyzes. We emphasize the simulations focused on the electrical and mechanical areas, being fundamental for the execution and development of a product design. To perform a characterization of a material, it aims to establish a collection of initial data on its properties, such as mechanical strength, eutectic point, among other characteristics. In order to perform the same, the use of CAD and CAE concepts to describe and develop the virtual model is substantial for the operation of the software that plays the role of performing the simulations.

It is observed that aluminum has the ability to bind to other materials when cast, forming aluminum alloys in the dissolution of other metallic materials or metalloid substances capable to alter the atomic structure of the material, modifying their characteristics [1]. Thus, to identify the mechanical strength properties is crucial to determine the maximum stresses of the material, therefore, when subjecting the same under dynamic load during cyclical period is characterized as fatigue [2].

To validate the developed model, it is necessary to compare it with real data, so the preparation of specimens for fatigue analysis is necessary, since the existing unidirectional solidification-oriented studies in stationary regime in alloys with low content of such elements as Nickel are few known [3].

The development of this project aims to contribute to the analysis of fatigue tests and dendritic growth on Al-Ni alloys (aluminum-nickel), with the main objective to build a virtual model for the representation of a real test having a margin of acceptable error, where the software is the Salome-Meca, of the company Code-Aster.

2. Experimental

The material was produced in the unidirectional solidification laboratory of the Solidification Research Group of Unicamp, where after the manufacture of the Al-Ni alloy ingots used the unidirectional solidification method in steady state, it was prepared for the specimens for the axial fatigue test.

The preparation of the specimens involves cuts in different sections because the ingot material presents different dendritic growth with the length variation. The raw material goes through machining processes to fit the designed model and then sanding to remove imperfections that interfere with the test.

The axial fatigue test uses dynamic test machine, the Instron 8001, with a test frequency of approximately 30 Hz, with a voltage ratio of R = 0.1, until the fracture or 10^7 cycles. A data collection is performed before and after the test to analyze the behavior of the material.

It uses a virtual machine, since the Salome-Meca software is only available for the Linux platform. With the same in operation, it is possible to develop the geometry of the object, mesh development, virtual test and analysis of data obtained. The data obtained in the simulation are compared with the fatigue test data for model validation.

3. Results and Discussions

During the course of the project it was possible to note the capacity of the Salome-Meca to perform the processing of inserted information, being able to guarantee its functionality, although still it is not possible to guarantee that the models that are being developed have good reliability, because the research is still in progress.

During the execution of the tests and with the aid of materials for consultation, it was possible to notice a slight influence of the nickel in the alloy, even if the content in the composition is low, it is possible to notice some differences in relation to its fatigue behavior.

It is worth mentioning that certain results obtained show some distortions, in addition to a problem in the machinery, the material presented different behaviors, so it was necessary to readjust the specimen to improve its fixation, between other aspects. The specimens are dimensioned according to the dimensions of the ingot and the claw of the machine, so it does not follow a specific standard.

We have the curves obtained in sections 2 and 4 of the material, demonstrated the following result, since the research is still under development and certain aspects still can not be concluded.

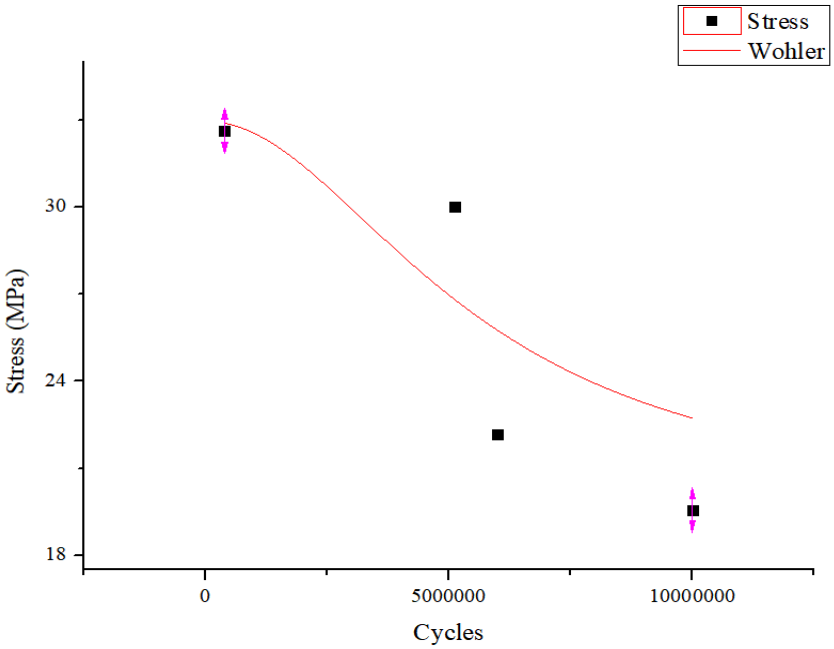

Fig. 1. *Fourth Section of Al-Ni.*

4. References

[1] ABAL. Associação Brasileira de Alumínio. **Alumínio: Características Químicas e Físicas,** 2017.

[2] BUDYNAS, R. G.; NISBET, J. K. **Elementos de Máquinas de Shigley: Projeto de Engenharia Mecânica.** 8. Ed [s.l.] AMGH, 2011.

[3] CANTÉ, M. V. **Solidificação Transitória, Microestrutura e Propriedades de Ligas Al-Ni.** p. 178, 28 jul. 2009.

Acknowledgments

To CNPq for the financial support provided through the scholarship PIBIFSP. To IFSP campus São João da Boa Vista for the opportunity to do an academic research and for the solidification research group at Unicamp for the supply of aluminum alloy.

LASER BEAM WELDING OF DUAL PHASE DP600 STEEL FOR APPLICATIONS IN AUTOMOTIVE STRUCTURES

Jimes de Lima Percy Júnior[1*], Ana Maria do Espírito Santo[1], Rafael Humberto Mota de Siqueira[2] and Milton Sergio Fernandes de Lima[2]

[1] *Universidade Federal de São Paulo, São José dos Campos, SP*

[2] *Instituto de Estudos Avançados, Divisão de Fotônica, São José dos Campos, SP*

1. Introduction

Advanced High Strength Steels (AHSS), such as Dual Phase (DP) steel, have being used in automotive bodies. Due to the relative high yield strength of these steels, it is possible to use thinner profiles compared to the conventional steels, thus reducing the automotive body weight . Laser beam welding (LBW) of AHSS blanks has become a mandatory process due to its characteristics and the possibility of welding dissimilar joints [1-3]. This work aims to study the weldability of the a Dual Phase DP600 steel by the laser welding process, without filler metal (autogenous), and obtain the microstructure and mechanical behavior.

2. Experimental

It was used a Dual Phase DP600 steel, with 0.010 wt% of carbon and additions of manganese (1.87 wt.%) and silicon (0.46 wt.%). The Dual Phase DP600 steel microstructure is composed of a ferritic matrix with martensite in the grain boundaries [4]. The dimensions of welded samples were 100 mm wide, 200 mm long by 1.8 thick.

The welding was carried out using an Yb:Fiber laser, IPG model YLR-2000, with power of 1500 W, welding speed of 50 mm/s and argon as shielding gas, with a flow rate of 8 l / min. For the microstructure examination the welded specimens were submitted to metallography to reveal the phases along the microstructure. The tensile strength and Vickers hardness tests were performed in order to determine the mechanical behavior.

3. Results and Discussions

In the fusion zone (FZ), Fig. 1, and in the heat affected zone (HAZ), Fig. 2, there is formation of martensite. The high cooling rate causes the formation of the matensite and restrains the formation of softer phases such as ferrite [5, 6]. The welding parameters that had been used in DP600 steel showed a weld bead with absence of defects, such as pores and cracks.

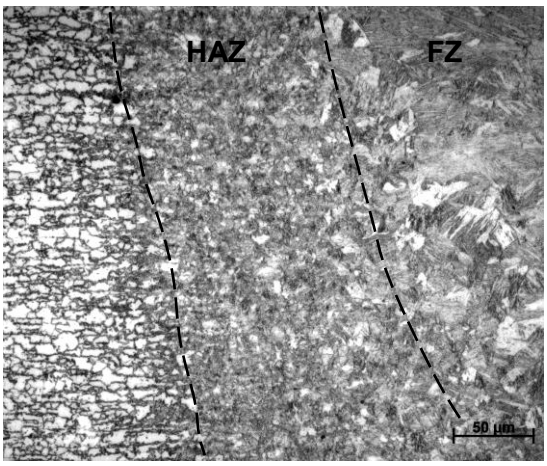

Fig. 1. *Heat affected zone (HAZ) microstructure.*

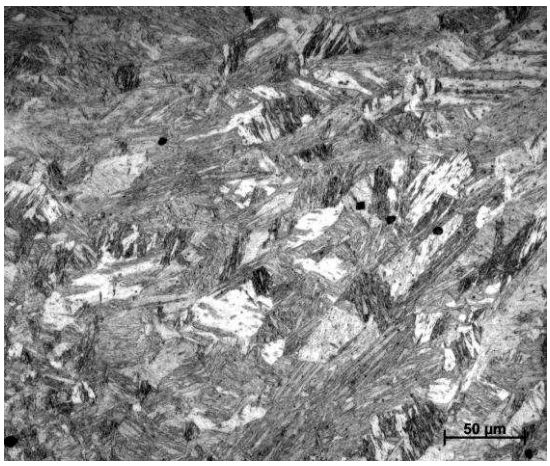

Fig. 2. *Fusion zone (FZ) microstructure.*

The Vickers test, Fig. 3, revealed an increase of 62% in the hardness of HAZ, compared to the base metal. The martensite formed due to transformation in the solid state is harder than the martensite coming from the solidification, because the time at the austenite locus, required for complete austenitization, is higher near to the fusion line

The tensile tests, Fig. 4, showed 630 ± 10 MPa of the tensile strength, 330 ± 10 MPa of the yield strength and 26 ± 2 % for the maximum deformation. All coupons were broken in the base material, therefore the weld presented the required toughness. The tensile test curves, for the three samples (01, 02 and 03), showed similar behavior, indicating good reproducibility of the process.

*Corresponding author: jimesjr@hotmail.com

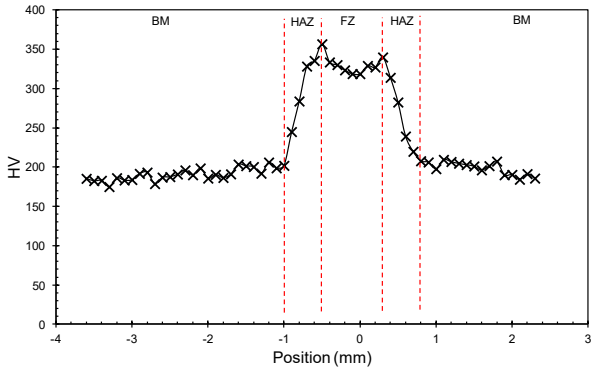

Fig. 3. *Vickers hardness across the weld bead.*

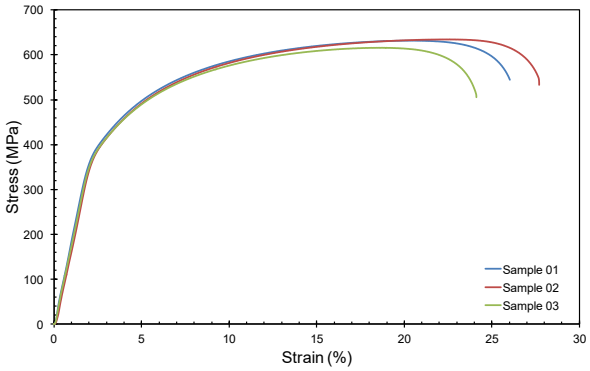

Fig. 4. *Graphic Stress versus Strain.*

Laser beam welding of the Dual Phase DP600 steel using a Yb:fiber laser for application in automotive structures looks promising, due to the low defects concentration and good mechanical properties of the weld bead. The LBW process, due to its high reproducibility, high welding speed and ease of automation, is promising as one chain in the industry 4.0.

4. References

[1] D. Maltock, 2011 AISTech Conf. Proceedings, **I**, (2011).
[2] S. Keeler, M. Kimchi, P. Mooney, *"Advanced High-Strength Steels Application Guidelines Version 6.0"*, WorldAutoSteel, USA, (2017).
[3] D. Dong, Y. Liu, et al., Mat. Sci. & Eng. A, **594**, 17-25, (2014).
[4] A. Tataru, V. Potemkin, et al., Jour. of Chem. Tech. and Metal., **58**, 617-623, (2015).
[5] V. Colla, M. Desanctis, et al., Metal. and Mat. Trans. A, **42A**, 2781-2793, (2011).
[6] S. Kou *"Welding Metallurgy"*, 2nd edition, Wiley, USA, (2016).

Acknowledgments

The authors thank the financial support of the following agencies, CAPES (Coordenação de Aperfeiçoamento de Pessoal de Nível Superior) and CNPq (Conselho Nacional de Desenvolvimento Científico e Tecnológico).

*Corresponding author: jimesjr@hotmail.com

SURFACE TREATMENT OF CARBON FIBER BY ARGON AND UREA VAPOR PLASMA

Camila Presendo Pinto*, Abel A. C. Recco, Carla Dalmolin, Daniela Becker and Luis César Fontana
Laboratory of Plasmas, Films and Surfaces, Universidade do Estado de Santa Catarina, Joinville – SC

1. Introduction

Properties such as good electrical conductivity, corrosion resistance, thermal stability and high mechanical strength combined with its low weight/performance ratio make the carbon fiber a great option to be used as reinforcement in polymeric composites. However, the chemical inertia and hydrophobicity of its surface may result in poor interfacial adhesion between matrix and fiber [1]. Plasma treatment promotes a better adhesion by promoting both physical and chemical changes through the insertion of reactive groups, enhancement of roughness and removal of impurities from the fiber surface without affecting the bulk properties [1].

In addition, functionalization with nitrogen may promote better adhesion between carbon fiber and polymers such as epoxy [2] and polyaniline [3]. Focusing in nitrogen compounds, one of the gases used in the plasma treatment is NH_3 but it is toxic and corrosive. On the other hand, the urea is a non-inflammable, low toxic and a cheap alternative source of nitrogen [4,5]. Plasma treatment of carbon fibers with gaseous urea has been little explored. In view of this, in this work, a new method of functionalization of carbon fiber with urea is proposed. A DC pulsed plasma was used in the cathodic cage configuration, so that the samples were treated at floating potential [6], with an atmosphere composed by argon and urea vapor, in order to promote the insertion of nitrogen functional groups in the fiber surface with minimum damage to its structure.

2. Experimental

The carbon fiber cloth used in this work was PANEX® 30 Fabric PW06 from Zoltek, exhibiting 99% carbon, thickness of 673 μm and density of 1.75 g/cc. The urea used was Ureia P.A - ACS, supplied by the company Dinâmica Química Contemporânea Ltda, with 99% purity, and a melting point between 132°C and 135°C.

A lab made plasma reactor, used in this work, consists of a glass vacuum chamber and a grounded stainless-steel base, in which are connected a vacuum pump model Adixen Pascal SD 2010, a gas mass flow controller and a pressure gauge model APG100-XM from Edwards and a power supply model Pinnacle Plus™ pulsed DC power supply from the company Advanced Energy Inc. As represented in Figure 1, the urea was heated and kept at 150°C and the resulting flow of gas controlled by a needle valve entered in the plasma chamber trough a tube towards the cathodic cage. The samples were maintened at floating potential during the treatment. The cathodic cage consists of a stainless-steel cylindrical grid with diameter ø = 11 cm and 42% of open area. The samples were placed inside of the cathodic cage in order to maintain it at floating potential and to prevent overheating and energetic ion bombardment, minimizing possible damages in the carbon fiber surface.

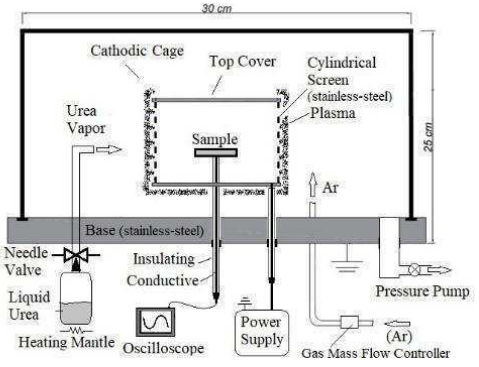

Fig. 1. *An illustrative description of the reactor plasma system created.*

For the fiber treatment, Argon gas was released at flow of 5.65 sccm, reaching a pressure of $5x10^{-1}$ Torr. Subsequently, the urea vapor was released as gas into the reactor until a final pressure of $5.5x10^{-1}$ Torr was reached. The samples were treated for 5 min in a pulsed DC plasma, at 300V and frequency of 100 kHz with a duty cycle of 60%, (t_{on} of 6 μs e t_{off} of 4 μs). Also, the samples were analyzed by Field Emission Gun Scanning Electron Microscopy (FEG-SEM) to detect changes in the fiber surface and static contact angle to evaluate changes in the hydrophobic behavior of the carbon fiber after plasma treatment.

*Corresponding author: camilapresendo@gmail.com

3. Results and Discussions

Through the SEM analysis it is possible to note that the plasma treatment was effective in promoting changes in the surface of the carbon fiber. In comparison with the surface of the untreated fiber, Figure 2(a), which is clean and grooved along the longitudinal axis, the treatment with Ar-urea, Figure 2(b), permitted the growth of a thin film on its surface. This may be due to the deposition of urea or nitrogen functional groups dissociated in the plasma. The roughness derived from the addition of functional groups on the fiber can improve interfacial adhesion between polymer and reinforcement by mechanical adhesion [1,7]. Moreover, according to work of CHENG et al. [8] the doping of the carbon fiber with nitrogen can promote the nucleation and uniform growth of catalytic nanoparticles superficially enabling the polymerization of polymers like polyaniline on its surface.

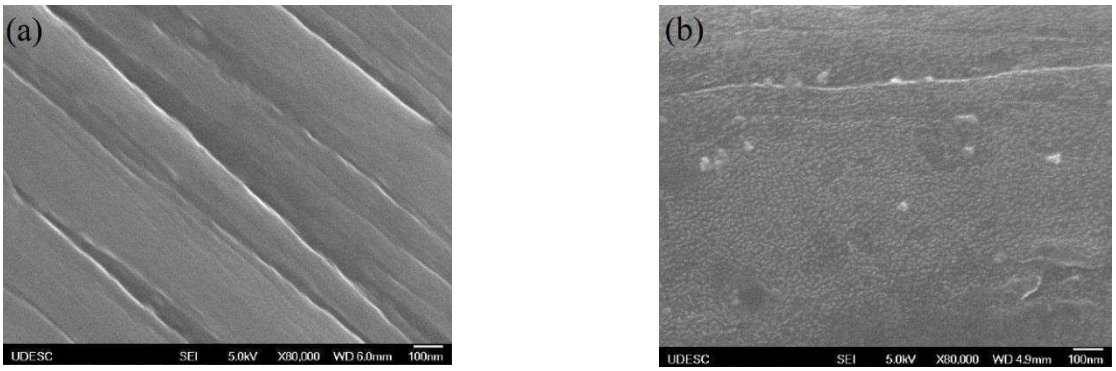

Fig. 2: *SEM micrographs of (a) untreated carbon fiber and (b) film nucleation on carbon fiber surface after Ar-urea plasma treatment.*

Through the static contact angle analysis, it was noted that the plasma treatment with Ar-urea changed the hydrophobic behavior of the carbon fiber surface. As it can be seen in Figure 3, after plasma treatment the static contact angle between a water droplet and carbon fiber surface decreased to 52°, when compared to the carbon fiber without treatment (142°), indicating a hydrophilic behavior. However, with the samples aging, the carbon fiber returned partially to its hydrophobic original state, due to the exposition to air, which may cause surface oxidation [3].

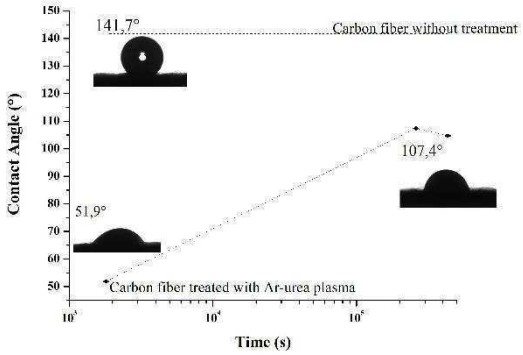

Fig. 4: *Evolution of the contact angle through sample aging.*

4. References

[1] M. Sharma, S. Gao, E. Mäder, H. Sharma, L.Y. Wei and J. Bijwe, Compos. Sci. Technol., **102**, 35-50, (2014).
[2] J. Moosburger-Will, E. Lachner, M. Löffler, C. Kunzmann, M. Greisel, K. Ruhland and S. Horn, Appl. Surf. Sci., **453**, 141-152, (2018).
[3] S. Corujeira Gallo, C. Charitidis and H. Dong, J. Vac. Sci. Technol. A, **35**, 021404-3, (2017).
[4] T. Nakamura, H. Hayashi and T. Ebina, J. Nanopart. Res., **16**, 2699-1, (2014).
[5] C. Giordano, C. Erpen, W. Yao, B. Milke and M. Antonietti, Chem. Mater., **21**, 5136-5144, (2009).
[6] F.H. Corrêa, D. Becker and L.C. Fontana, Rev. Bras. Apl. Vácuo, **37**, 59-64, (2018).
[7] J. Jang and H. Yang, J. Mater. Sci., **35**, 2297-2303, (2000).
[8] Q. Cheng, J. Tang, J. Ma, H. Zhang, N. Shinya and L.C. Qin, J. Phys. Chem. C., **115**, 23584-23590, (2011).

Acknowledgments

We would like to thank CAPES for the research grant and FAPESC/PAP (TR 655) for the financial support.

*Corresponding author: camilapresendo@gmail.com

GRAPHITE EXFOLIATION VIA PULSED UNDERWATER DISCHARGE

Elisa Héllen Segundo[1*], Marco Aurelio Nespolo Vomstein[1], Daniela Becker[1] and Luis Cesar Fontana [1].
[1]*Center for Technological Sciences, Santa Catarina State University– CCT/UDESC, Joinville, Santa Catarina, Brazil.*

1. Introduction

Graphite has been widely used as a dispersed phase in the manufacture of polymer composites because it is an abundant material on the earth's surface and cheap. Each sheet of graphene has high aspect ratio, large surface area and excellent electrical and thermal conductivity. By separating the layers to a nanometric thickness, they can effectively reinforce a matrix, as well as increase the thermal and electrical conduction of the material [1]. Graphene have attracted attention due to their properties and potential application in energy storage devices, catalysis, sensors, and polymeric nanocomposites [2,3]. Nevertheless, the method used to obtain these materials determines their structure and, thus, could influence their application. Different techniques have been developed to obtain graphene nanosheets, distinctive among them we find chemical vapor deposition and chemical exfoliation [4], graphite exfoliation in liquid phase by sonication [3, 5], by electrochemical exfoliation [6] and by pulsed underwater electrical discharge or underwater pulsed plasma [2, 7, 8, 9]. Pulsed underwater electrical discharge and underwater pulsed plasma can be carried out at atmospheric pressure and allows for a good level of control over chemical reactions, in addition to providing a short treatment time [7, 9]. This work presents graphite exfoliation with electric pulses of 1.5 kV in aqueous medium and the characterizations of the samples obtained through TEM, SEM-FEG and FMA.

2. Experimental

For the graphite exfoliation process, we used deionized water as solvent with 1% vol. of graphite that was used as started material from Grafite do Brasil with a density of 2,31g / cm^3. These solutions containing the graphite were placed in the handmade reactor built from a bench drill, the equipment contains a rod-shaped electrode for mixing and the solutions were mixing at 3000 rpm for 30 and 50 min. It was connected to the ground while the second electrode was positively biased in a pulsed mode with voltage of 1.5 kV at the peak. The power supply used consists of a multi-level converter that reaches up to 400 V in each of the ten levels, capable of generate 2 KV, positive and negative. Its wave form can be controlled by software, using a computer in the process to generate a pulsed voltage The applied voltage consist of sets of five short pulses (1.5 kV; 1 µs ton; 1 µs toff) with 200 µs off between the set pulses. We observed an exponentially damped sinusoid waveform immediately after the end of the pulses train, which is a characteristic of underwater pulsed plasma [10]. The current was measured indirectly using a shunt resistor of 10 ohms and the pulses are around 7A at peak, allowing us to maintain the temperature up to 343 K in the liquid.
After the treatment, the samples were sonicated for 5 min, and then centrifuged for 10 min at 400 rpm, finally centrifuged for further 90 min. at 2000 rpm. Then the samples of supernatant were analyzed by Transmission Electron Microscopy TEM, SEM-FEG and AFM.

3. Results and Discussions

Figure 1 shows MEV-FEG images of pristine graphite samples (Figure 1a), water-exfoliated supernatant samples (Figure 1b) for 50 minutes. In general, following the exfoliation process, the samples exhibited a thinner supernatant with smaller sizes which indicates onset of exfoliation. The images of supernatant displayed through TEM and AFM confirms this result, in which it is possible to observe fine sheets of graphene (figure 2), which shows samples with variations of up to eleven layers.

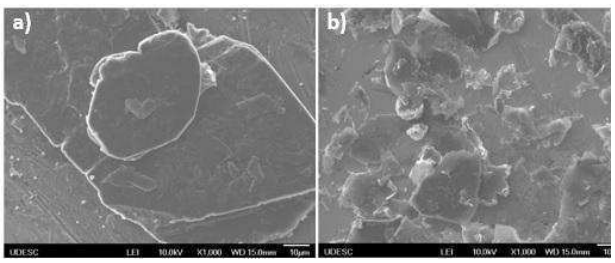

Fig. 1. *SEM-FEG micrographs a) pristine b) treated for 50 in water.*

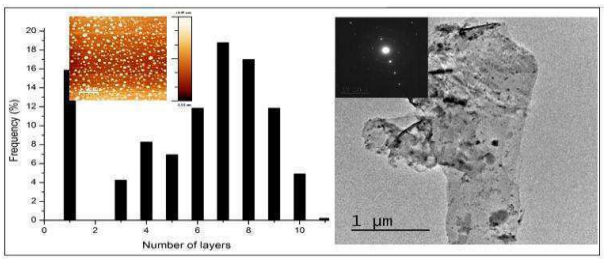

Fig. 2. a)*Number of graphene layers distribution treated with water for 50 minutes(TEM). b) TEM image with diffraction pattern*

*Corresponding author: lee.segundo@gmail.com

4. Conclusions

The SEM-FEG images have shown that the treated material of supernatant is finer than the pristine;
The AFM analysis of supernatant reveal that the samples was exfoliated and had few layers (1-11).
TEM images shows AFM shows sheets of graphene which indicates the effectiveness of the pulsed electric discharge method in aqueous medium for graphite exfoliation.

5. References

[1] D. A. Nguyen; Y. R. Lee; A.Y. Raghu; H. Jeong; C. M. Shin; B. K. Kimc. Morphological and physical properties of a thermoplastic polyurethane reinforced with functionalized graphene sheet. Society of Chemical Industry. 412- 417, (2009).
[2] D.V. Thanh, L. Li, C. Chu, P. Yen, K. Wei, Plasma-assisted electrochemical exfoliation of graphite for rapid production of graphene sheets, Roy. Soc. Chem. **4** (14), 6946–6949, (2014).
[3] Y. Arao, M. Kubouchi, High-rate production of few-layer graphene by high-power probe sonication, Carbon, **95**, (2015), 802–808.
[4] C. Lin, P.T.K. Loan, T. Chen, K. Liu, C. Chen, K. Wei, L. Li, Label-free electrical detection of DNA hybridization on graphene using Hall effect measurements: revisiting the sensing mechanism, Adv. Funct. Mater. **23**(18), 1–7, (2012).
[5] S. Wang, M. Yib, Z. Shen, The effect of surfactants and their concentration on the liquid exfoliation of graphene, RSC Adv. 656705–56710, (2016).
[6] R. Bakhshandeh, A. Shafiekhani, Ultrasonic waves and temperature effects on graphene structure fabricated by electrochemical exfoliation method, Mater. Chem. Phys. (2018).
[7] E. H. Segundo, L. C. Fontana, A. A.C. Recco, J. S. Scholtz, M. A. N. Vomstein, D. Becker. Graphene nanosheets obtained through graphite powder exfoliation in pulsed underwater electrical discharge. Materials Chemistry and Physics, **217**, 1–4, (2018).
[8] J. Shen, Y. He, J. Wu, C. Gao, K. Keyshar, X. Zhang, Y. Yang, M. Ye, R. Vajtai, J. Lou, P.M. Ajayan, Liquid phase exfoliation of two-dimensional materials by directly.
Probing and matching surface tension components, Nano Lett. **15** (8), 5449–5454, (2015).
[9] H. Lee, M.A. Bratescu, T. Uenoad, N. Saito, Solution plasma exfoliation of graphene flakes from graphite electrodes, RSC Adv, **4** (93), 51758–51765, (2014).
[10] P. Vanraes, A. Nikiforov, C. Leys, Electrical and spectroscopic characterization of underwater plasma discharge inside rising gas bubbles, J. Phys. D Appl. Phys. **45,** 1–10, (2012).

Acknowledgments

The authors would like to express gratitude for the financial support provided by CAPES by means of scholarships, CNPq and FAPESC/UDESC/PAP.

*Corresponding author: lee.segundo@gmail.com

EVALUATION OF THE CHEMICAL COMPOSITION OF RICE HUSK ASH (RHA) AND WOOD ASH (WA) FOR GLASS APPLICATION

Eduardo Coveseviski[1]* and Rudinei Malinovski[2]
[1,2]*Santa Catarina State University – UDESC, Postgraduate Program in Materials Science and Engineering - PGCEM*

1. Introduction

One of the energy sources for furnaces and/or boilers in industries is the burning of wood. In Brazil, in 2016, 74.5 million tons of fuelwood were produced for energy consumption, and the industry consumed about 23.3 million (31.28%) [1]. Of all the wood burned, 3% result in ash [2]. In the chemical composition of the Wood Ash (WA) the SiO_2 oxides (12.7 to 54.5%) and Al_2O_3 (8.8 to 25.9%) are present in greater quantity [3]. In Brazil, in the year 2015, about 12 million tons of rice were produced [4], with 20% of this production being in the form of ash [5]. Rice husk is an abundant residue of agricultural production and has been used efficiently as a source of energy through burning. However, combustion generates the ash disposal environmental problem [6]. But, the Rice Husk Ash (RHA) contains a high content of silica (SiO_2) in its chemical composition, which can be extracted and used, adding value to ash [7]. Both WA and RHA have a large amount of silica in their chemical composition and so several studies have being done to incorporate it into glass production. The common inorganic glasses used for cups, lenses, bottles, windows and so forth are silica glasses in which other oxides such as CaO and Na_2O are added [8]. The most common glass families are: Sodium-Calcium glasses (71-73% SiO_2, 12.5-16.5% Na_2O, 5-11% CaO), Borosilicate glasses (66-79% SiO_2, 3,5-13 B_2O_3), Alumino-borosilicate glasses (62-72% SiO_2, 6-17% Al_2O_3, 5-11% B_2O_3), Lead glasses (32-56% SiO_2, 24-65% PbO) and Aluminosilicate glasses (57- 64.5% SiO_2, 16-24.5% Al_2O_3, 8-10% CaO). The glass obtained using basic raw materials is colorless. Colors in glasses are generated by components that are dissolved in their mass during their elaboration, usually they are metals that interact with the light filtering some colors and letting pass others [9]. The main aim of this paper is to evaluate the chemical composition of Rice Husk Ash (RHA) and Wood Ash (WA) and to indicate the best application of ashes in substitution to natural silica in the main glass families.

2. Experimental

The rice husk used in the experiments to obtain the silica was supplied by a company placed in the region of Chapecó-SC. The sample contained fragments of rice and other organic materials and due to it the rice husk was sifted to eliminate the fragments by passing them through 1.17 mm and 2.36 mm mesh sizes. The rice husk was calcined in a muffle oven using a heating rate of 10°C/min at a temperature of 900°C set for 1 hour for CO_2 elimination. The Wood Ash was supplied by an industry of pine wood panels placed in the state of Paraná. First, WA was calcined using the same conditions as the rice husk. The calcined material was sifted and the one that pass through the 600μm mesh was used in the experiments. By x-ray fluorescence a chemical analysis of both ashes was developed where was obtained a quantitative analysis of the components of each ash.

3. Results and Discussions

The figure 1 (a) shows the rice husk as received. After calcination of the husk, the RHA (Figure 1 (b)) presented a light color indicating that a good part of the carbon was released during the calcination and the material is oxidized. The figure 1 (c) shows the Wood Ash as received presenting a black coloration, typical of a carbonized material. After calcination (figure 1 (d)) is verified that the coloring has changed to light brown due to CO_2 release.

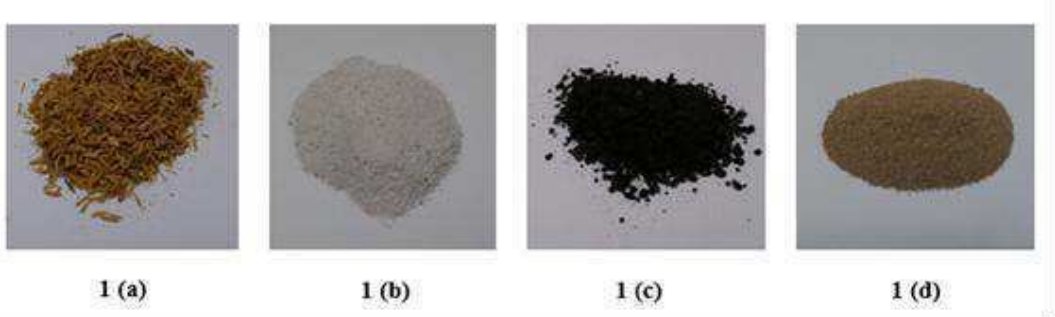

Fig. 1. *Material obtained before and after ash calcination process.*

*Corresponding author: coveseviski@gmail.com

The results of x-ray fluorescence chemical analysis of the Wood Ash and of the Rice Husk Ash can be viewed in table 1.

Table 1. *X-ray fluorescence results of chemical analysis of wood ash and rice husk ash.*

Calcined Wood Ash (WA)										
Components	SiO_2	Al_2O_3	CaO	Fe_2O_3	MgO	K_2O	SO_3	TiO_2	P_2O_5	ZrO_2
% (Percentage)	52.5	17.77	11.07	7.97	0.86	3.83	1.98	1.81	1.11	1.1
Rice Husk Ash (RHA)										
Components	SiO_2	K_2O	P_2O_5	CaO	Al_2O_3	SO_3	MnO	Fe_2O_3	ZnO	CuO
% (Percentage)	84.5	5.5	4.54	1.87	1.21	1.18	0.68	0.45	0.05	0.03

Evaluating the chemical composition of RHA can be analyzed that it has 84.50% of SiO_2 in its composition. This high amount of silica allows RHA to be applied in obtaining all glass families. However, Sodium-Calcium glasses are best indicated to the use of RHA due to the high quantity of SiO_2 in its composition (71-73% SiO_2). Thus, the residue will be better utilized, being possible to apply RHA in flat glass and cups, typical products of Sodium-Calcium glasses.

In the chemical composition of the calcined WA can be observed that is contained 52.5% of SiO_2, 17.77% of Al_2O_3 and 11.07% of CaO. These are the 3 main components of the Aluminosilicate glasses. In this way, the wood ash is indicated for application in this family of glasses where the 3 oxides of the composition of WA can be used to manufacture products from the electro-electronic and pharmaceutical areas.

Due to ash contains metal oxides in its composition, using a large percentage of ash in the glass dosage is not expected to provide a totally colorless glass.

4. References

[1] BEN – **Balanço Energético Nacional 2017 ano base 2016.** Ministério de Minas e Energia. Disponível em: HTTPS://ben.epe.gov.br/downloads/Relatorio_Final_BEN_2017.pdf. Acesso em Dezembro de 2017.

[2] BORLINI, M. C.; SALES, H. F.; VIEIRA, C. M. F.; CONTE, R. A.; PINATTI, D. G.; MONTEIRO, S. N. **Cinza da lenha para aplicação em cerâmica vermelha. Parte I: características da cinza.** Cerâmica, v.51, n. 319, p. 192-196, set. 2005.

[3] SIDDIQUE, R. **Utilization of Wood ash in concrete manufacturing. Resoucers, Conservation and Recycling,** v. 67, p. 27-33, jul. 2012.

[4] EMBRAPA ARROZ E FEIJÂO. **Dados de conjuntura da produção de arroz (Oryza sativa L.) no Brasil (1985-2015)**. Disponível em: HTTP://www.cnpaf.embrapa.br/socioeconomia/index.htm. Acesso em Agosto de 2017.

[5] FOLETTO, E. L.; HOFFMANN, R.; HOFFMNN, R. S.; PORTUGAL JR, U. L.; JAHN, S. L. **Aplicabilidade das cinzas da casca do arroz.** Química Nova, 28, (6), 1055-1060, 2005.

[6] CHANDRASEKHAR, S.; SATYNARAYANA, K. G.; PRAMADA, P. N.; RAGHAVAN, P.; GUPTA, T. N. **Processing, proprieties and applications of reactive silica from rice husk – an overview.** Journal of Materials Science, v. 38, p. 3159-3168, 2003.

[7] PRASAD, R.; PANDEY, M. **Rice husk ash as a renewable source for the production of value addes silica gel and its application: an overview.** BCRECB, v. 7(1), p. 1-25, 2012.

[8] CALLISTER, W. D.; RETHWISCH, D. G. **Ciência e Engenharia de Materiais: Uma Introdução.** 8 ed. Rio de Janeiro: LTC, 2012. 817p.

[9] AKERMAN, M. **Natureza, Estrutura e Propriedades do Vidro.** CETEV – Centro Técnico da Elaboração do Vidro, 2000.

Acknowledgments

This work has financial support from FAPESC and CAPES, as well as technical and scientific support from the UDESC-CCT multiuser laboratory.

*Corresponding author: coveseviski@gmail.com

DEVELOPMENT OF CVD MICRO / NANOCRYSTALLINE DIAMOND TOOLS FOR ALUMINUM ALLOY MILLING

Argemiro Pentian Junior[1]*, José Vieira[2], Vladimir J. Trava Airoldi[2] and João Roberto Moro[1]
[1]*Instituto Federal de Educação Ciência e Tecnologiade São Paulo – IFSP_ Bragança Paulista*
[2]*Instituto Nacional de Pesquisas Espaciais – INPE – São José dos Campos.*

1. Introduction

The need for better performance carbide tooling at a reasonable value in a short time, coupled with industrial competition boosted technological advances in the field of precision machining. The use of high-speed machining led to the search for new and advanced materials with improved wear characteristics [1].
The increase in cutting speed implies an increase in the removal rate, reducing the cost of material removed, but also implies an increase in the use of coolant and reduction of the life of the tool, raising labor costs. The replacement of the necessary tools and care with refrigerant maintenance is sometimes greater than the value of the tool [2,3].
CVD diamond-coated tungsten carbide cutting tools obtained by the HFCVD technique would be an excellent choice for machining, with an interesting cost-benefit ratio [4, 5, 6, 7]. However, the machining performance of diamond-coated tools is not robust due to the non-optimized adhesion between the carbide tool and the deposited diamond film [2].
Aiming to study the performance of 7075 aluminum alloy machining with WC-Co cutting tools with deposition of CVD diamond films, we set out to study and obtain such coated substrates.

2. Theory

The cobalt is a transition metal and during deposition of CVD diamond negatively influences the adhesion of the film [8]. One of the reasons is the catalytic effect that the cobalt exhibits during the initial phases of deposition promoting the nucleation and growth of the graphite phase with greater density of sp2 hybridizations.
Different authors have studied substrate surface preparation processes to improve the nucleation and growth of the diamond film. Surface preparation plays a key role in nucleation control and is important in obtaining high quality, high tack diamond films. The increase in nucleation density may improve the homogeneity of the films, increasing the adhesion between film and substrate [9].
Due to the deposition process of CVD diamond films on WC-Co substrates being dependent on critical factors preceding deposition, the experiments will be conducted in steps to ensure optimal growth parameters and conditions.
The surface preparation will be carried out by polishing with silicon carbide sandpaper in the granulations from 220 to 1200, and for finishing the cloth with diamond solution (6 - 0.25 μm) as an abrasive. The composition and surface evaluation studies will be through FEG-MEV, AFM, XRD and EDX. An evaluation of chemical methods of surface modification by selective removal of Cobalt using a two step chemical treatment of the first step in Murakami solution (K3 [Fe (CN) 6] + KOH + H2O), and in the second step using royal water (HNO 3 / HCl = 1: 3) [10].
The substrates are submerged in a polymer solution of cationic character, PDDA (Poly (DiallylDimethylAmmonium chloride)) for 30 minutes to ensure efficient functionalization and then immersed in the anionic solution nano diamond particles on PSS (Poly Sodium Styrenesulfonate) to occur on the surface, and were washed in D.I water after each step, so that the excess of polymer and particles were removed.
The study of CVD diamond nucleation on WC-Co substrates will be conducted by exposing the ready-made substrates to the growth conditions for short periods of time. The evaluation by FEG-MEV will aim to identify the growth morphology obtained and the correlation between nucleation density and growth parameters.
The depositions are performed in hot filament reactor (HFCVD) varying the following parameters: the diluted concentration of methane in hydrogen ([CH4]), the system pressure (P), the temperature of the tungsten filament and the temperature of (NCD), ultra-nano-crystalline (UNCD), mono-layer and multi-layer diamond films were used to obtain microcrystalline diamond (MCD) films. The results used for the tools will be with growth of two hours in atmosphere of 2% of CH4 in Hydrogen in the pressure of 50 torr at 850ºC.

3. Results and Discussions

Using the grown films will be carried out machining tests of the aluminum 7075 in various conditions, aiming to improve the cost benefit of these tools of important use in various branches of industry.

*Corresponding author: junior.pentian@outlook.com

4. References

[1].Dubar, M., A. Dubois, and L. Dubar, Wear analysis of tools in cold forging: PVD versus CVD TiN coatings. Wear, 2005. 259(7): p. 1109-1116.

[2] Gomez, H., et al., Adhesion analysis and dry machining performance of CVD diamond coatings deposited on surface modified WC–Co turning inserts. Journal of Materials Processing Technology, 2012. 212(2): p. 523-533.

[3] Derflinger, V., H. Brändle, and H. Zimmermann, New hard/lubricant coating for dry machining. Surface and Coatings Technology, 1999. 113(3): p. 286-292.

[4] Wei, Q.-p., et al., Synthesis of micro- or nano-crystalline diamond films on WC-Co substrates with various pretreatments by hot filament chemical vapor deposition. Applied Surface Science, 2010. 256(13): p. 4357-4364.

[5] Wang, T., et al., Deposition of diamond/β-SiC/cobalt silicide composite interlayers to improve adhesion of diamond coating on WC–Co substrates by DC-Plasma Assisted HFCVD. Surface and Coatings Technology, 2011. 205(8): p. 3027-3034.

[6] Braga, N.A., et al., Optimal parameters to produce high quality diamond films on 3D Porous Titanium substrates. Diamond and Related Materials, 2011. 20(1): p. 31-35.

[7] Haubner, R., A. Köpf, and B. Lux, Diamond deposition on hardmetal substrates after pre-treatment with boron or sulfur compounds. Diamond and Related Materials, 2002. 11(3): p. 555-561.

[8] Kim, G.-H., Transmission electron microscope observation of diamond/WC interface. Journal of Crystal Growth, 1997. 178(4): p. 634-638.

[9] Chatterjee, S., et al., Analysis of surface preparation treatments for coating tungsten carbide substrates with diamond thin films. Journal of Materials Science, 1997. 32(11): p. 2827-2833.

[10] Vieira, José, Growth Of High Adverse Diamond Films And Low Residual Tensions On Wc-Co Substrates, 2018, Instituto Nacional de Pesquisas Espaciais: São José dos Campos, p 20.

*Corresponding author: junior.pentian@outlook.com

EFFECT OF THE PLASMA PROCESS ON THE MORPHOLOGY OF CELLULOSE ACETATE MEMBRANES

Silva, H.R.T.[1*], Hoffmann, J.V.J.[1], Egert, P.[1], Seeber, A.[2], Magnago, R.[1] and Stieven, W.[1]
[1]*Universidade do Sul de Santa Catarina/UNISUL, SC, Brazil*
[2]*Universidade Federal do Pampa/UNIPAMPA, RS, Brazil*

1. Introduction

The interest in developing products polymer base in health area is due to the biocompatibility, low toxicity and favorable pharmacokinetics, highlighting pharmaceutical applying, as controlled release and encapsulation of drugs and wound dressings [1]. Although polymer applying is growing, performance improvements are achieved whether physical-chemical properties are controlled. When using as dressings matrix, in so far as characteristics as porosity, surface tension and absorbing capacity are controlled, the result could be a material with good performance in drug release. A way of control perform of polymer characteristics is submit them to plasma treatments [2, 3]. The study shows superficial changes of cellulose acetate membranes with and without incorporation of fruit peels of the *Citrus Reticulata* (EBET-CR) plant, treated in plasma N_2(75%)+H_2(25%). Different times were used (varying from 15 to 35 min) and temperatures (varying from 50 to 100°C) in membrane treatments, characterized by scanning electron microscopy (SEM), atomic force microscopy (AFM), contact angle measurements and zeta potential.

2. Experimental

The cellulose acetate membranes were prepared and then plasma-treated. The plasma process was ensured by an electric pulsed direct current (DC) discharge in an atmosphere composed of N_2(75%)+H_2(25%). Different conditions of time and temperature were used in the plasma treatment of membranes: varying temperature from 50°C to 100°C with a constant pressure of 1.4 Torr and a time of 15 min; varying time from 15 min to 35 min, with a constant pressure of 1.4 Torr and a temperature of 90°C; study of the modifications in the upper and lower surface of the membrane with treatment time of 15 minutes, constant pressure of 1.4 Torr and a temperature of 90°C.
After treatments, the membranes were studied on the surface modifications that occurred. These analyzes were performed by scanning electron microscopy (SEM), atomic force microscopy (AFM), contact angle measurements and zeta potential.

3. Results and Discussions

The realization of the study allows an understanding of surface changes in cellulose acetate membranes. The surface modification in the membranes, resulting from the plasma interaction, can be evidenced in the images below.

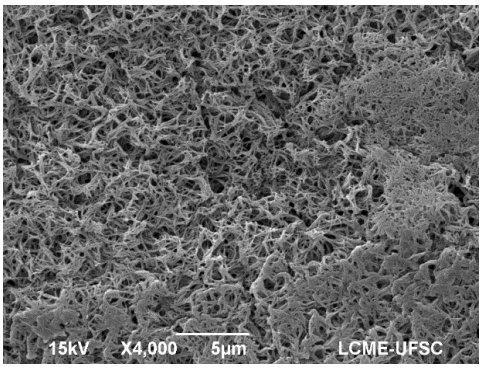

Fig. 1. Electronic m*icrograph of cellulose acetate membranes,4000x,* ***without treatment*** *. Top surface.*

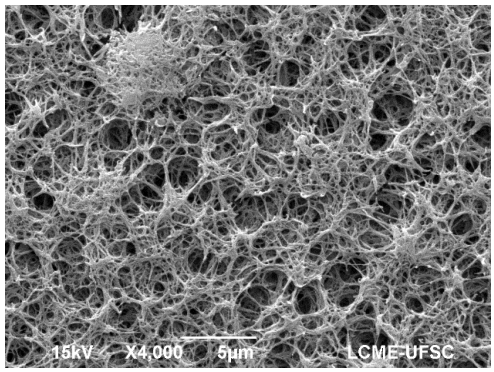

Fig. 2. Electronic m*icrograph of cellulose acetate membranes, 4000x. Plasma treated of N_2-H_2, 1.4 Torr,* ***15 min, 90°C****. Top surface.*

The results show that variations in time and temperature result in modifications in the surface morphology of the membranes. Increasing the treatment time, from 15 min to 25 min, keeping the temperature constant at 60 ° C, results in different characteristics on the membrane surface. The surface treated in the greater time presents a greater number of cavities than the treated membrane at 15min. When the treatment temperature is increased from 60 ° C to 80 ° C, keeping the time constant at 15 min, different characteristics are also

*Corresponding author: helofloripa2004@yahoo.com.br

evidenced therein. Lower temperatures result in less attacked surfaces.
The surface analyzes of the membranes, using the sessile drop method, are presented in the table 1:

Table 1: *Surface analyzes of the membranes by the sessile drop method.*

Treatment Time [min]	**Treatment Temperature [°C]**	**Temperature [°C]**	**Umid. Relat. Durante o Ensaio [%]**	**Angle t=0s [°]**	**Angle t=10s [°]**	**Angle t=20s [°]**
Without treatment	Without treatment	24	42	61.0	58.0	52.0
15	60	20	43	50.0	42.0	37.0
30	90	20	43	54.0	52.0	42.0
15	90	20	43	50.0	37.0	38.0
30	60	20	43	55.0	34.0	27.0

The results demonstrate that variations in the times and temperature of the plasma treatment result in modifications in the surface morphology of the membranes. These parameters generate a decrease in the contact angle between the membrane and the drop, when compared to the membrane without treatment.
It can be seen that the untreated membrane has an angle of contact with the drop, higher for the three instants under study, compared to the treated membrane, due to the increase in membrane hydrophilicity with plasma treatment.
Therefore, results indicate relationship between resulting morphology and material wettability, increased with time and temperature rise. Therefore, membranes hydrophilicity might be improved with the plasma treatment used.

4. References

[1] D.Puppi, F. Chiellini, A. M. Piras A and E. Chiellini, Progress in Polymer Science, **35**, 403–440, (2010).
[2] P.M.L. Perez et al., Journal of Materials Chemistry, **17**, 4064-4071, (2007).
[3] H.A. Gulec, A. Topadi, C. Topadi, N. Albayrak, M. Mutlu, Journal of Membrane Science, **350**, 310-321, (2010).

Acknowledgments

This work had scholarship by the Institutional Program of Scientific Initiation Grants (PIBIC), by National Council for Scientific and Technological Development (CNPq).

*Corresponding author: helofloripa2004@yahoo.com.br

NUMERICAL CALCULATION OF POWER IN DBD-LIKE DEVICES

Milton E. Kayama, Gustavo G. Vasques, Marcelo H. Mello and Mauricio Antonio Algatti
FEG-DFQ-UNESP – Av. Ariberto P. Cunha 333, 12516-410, Guaratinguetá, SP, Brazil

1. Introduction

The calculations of the power in dielectric barrier discharges (DBD) are usually performed through the drop of the voltage on capacitor or resistor connected in series with the discharge. The current signal has usually a waveform formed by a sequence of fast spikes each one associated to the filamentary discharge present in this type of discharge. A numerical program was developed in order to perform the calculations that allow this calculation even in case of low signal to noise ratio.

.

2. Experimental and numerical program

The DBD was generated using a surgical needle with 0.7 mm o.d. and a 1.0 mm thick brass cylinder with a borosilicate capillary between them. The applied voltage had sinusoidal waveform with 5.8 kV peak-to-peak and frequency of 37 kHz applied to the needle [1]. The gas used was argon. The current and the charge was measured respectively by a resistor and capacitor connected between the cylinder and the ground. The power is given by the average in one period of the instantaneous power or in equivalent form, by the charge produced by a infinitesimal variation of the applied voltage. The data acquire acquisition is generally performed by a previous setting of real time recording or the values given by the mean value of N cycles. A numerical program was developed in order to calculate the power in practical situation, the so-called POWERVI and LISSA for measurements with resistor and capacitor, respectively. The first calculates the average power over various points of the recorded data using signals of the applied voltage and the current. The latter uses the applied voltage and the charge on the capacitor. Intrinsic procedures are used to smooth in case of noisy signals. The diagrams of these programs are shown in the figure 1.

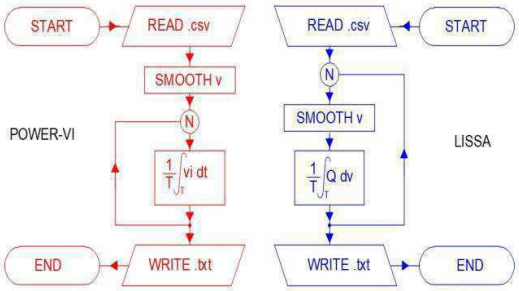

Fig. 1. *Diagram of the programs POWER-vi and LISSA to calculate power in DBD's.*

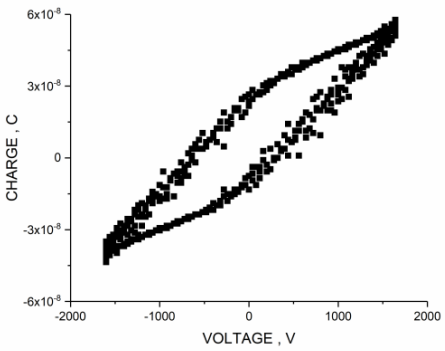

Fig. 2. *Charge of the capacitor during a cycle of the applied voltage.*

3. Results and Discussions

The figure 2 shows a typical Lissajous figure generated by the charge on the capacitor during the variation of the applied voltage in one cycle of the discharge. The analysis indicated reduction of the uncertainty on the power calculation when the data acquisition is set in the digitalizer using the mean value of a large number of cycles. In spite of different features of the load element used to obtain current and charge an approximate value of the power can be obtained according to the values of the resistance and the capacitance.

4. References

[1] Kayama, M.E., Silva L.J., Prysiazhnyi. V, Kostov, K.G, and Algatti M.A., "Characteristics of Needle-Disk Electrodes Atmospheric Pressure Discharges Applied to Modify Wettalility" *IEEE Trans. Plasma Sci.* 0093-3813, (2017). 3813, (2017).

Acknowledgments

The text of the acknowledgement must not be indented. It is also written using Times New Roman 11 pt.

EFFECT OF NIOBIUM PERCENTAGE ON THE WETTABILITY AND OPTICAL TRANSPARENCY OF TiO_2:Nb FILMS

Aline Medeiros Morais[1]*, Joel Stryhalski [2], Júlio C. Sagás [1], Luís C. Fontana [1]
[1]*Laboratory of Plasma, Films and Surfaces - Santa Catarina State University, Joinville, SC, Brazil*
[2] *Federal Institute of Santa Catarina, Jaraguá do Sul, SC, Brazil*

1. Introduction

Titanium dioxide (TiO_2) is a photocatalytic, transparent, low toxicity, with good chemical and thermal resistance material semiconductor [1]. TiO_2 films has been used in various applications such as photocatalysis, gas sensing, solar cells, electronic devices (such as variators) and self-cleaning coatings. TiO_2 films deposited on glass substrates can become superhydrophilic when activated by sunlight (in the UV range). It may provide properties to surface as self-cleaning and prevention of dust and pollutants damage by atmospheric air [2].

The photocatalytic and superhydrophilic properties of TiO_2 are derived from the formation of photogenerated charge carriers (electron and hole), that occurs after absorption of ultraviolet (UV) light. If the incident photons energy is higher than the band gap energy (it is 3.2 eV for anatase phase and 3.0 eV for rutile phase), the photons can be absorbed by the TiO_2 film, generating electron-hole pairs [3]. However, this band gap energy for TiO_2 corresponds to the energy of UV light and the activation through solar radiation becomes inefficient, because only 5-7% of the solar radiation is in the UV range. To modify this band gap energy and increase the hydrophilicity of TiO_2 films, the strategy of doping this material with other chemical elements, such as Nb, has been used. The incorporation of a transition metal (Nb) as solid solution in the TiO_2 structure can result in the formation of new energy levels between the valence band and the conduction band. In addition, the Ti atoms are arranged into the TiO_2 crystal lattice as Ti^{4+} ions while the niobium (substitutional) enters in the crystal lattice as Nb^{5+} ion. In this way, the additional electron of the Nb is injected into the conduction band and could increase the hydrophilicity of the TiO_2:Nb film [4]. The Nb doping can modifies the photocatalytic performance of transparent TiO_2 films and it can increase the electrical conductivity, providing properties of TCO (transparent conducting oxide) to TiO_2 [5].

2. Methodology

Titanium dioxide (TiO_2) thin films with variable quantities of Nb were deposited by magnetron sputtering triode technique, using a bimetallic titanium target (99.5% purity) and a Nb insert (99.9% purity). The plasma was powered by a pulsed power supply (Pinnacle-Plus / Advanced Energy). Before depositing of the films, the samples were washed with isopropyl alcohol, in ultrasound. The vacuum system reached a base pressure of 10^{-5} Torr ($1.33x10^{-3}$ Pa) before deposition. Films were deposited using argon (Ar) plasma at $3x10^{-3}$ Torr (0,40Pa) work pressure. The substrates used for films deposition were soda-lime glass samples, containing SiO_2 (72%), Na_2O (14%) and CaO (9%) [6].

After deposition, the films were oxidized in ambient atmosphere at 600 °C during 1.0 h, in a cycle similar to the glass annealing treatment. Surface roughness, chemical composition, crystalline phases, wettability and optical properties were measured by atomic force microscopy (AFM), X-ray fluorescence dispersive energy spectroscopy (EDX), X-ray diffraction (XRD), contact angle, and UV-Vis spectroscopy, respectively.

3. Results and Discussion

The Nb/(Nb + Ti) ratio into the films depends on the relative sample position to the target. The film thickness and composition, measured by EDX, are shown in Table I. The film thickness was 80 ± 10nm and the Nb/(Nb + Ti) ratio varied between 1.9 and 4,9% at.

Contact angles measurements were performed before and after irradiation with UVC (255 nm) for 24 h. After the irradiation it was measured the contact angles in different aging times: immediately after removal from the UV cabin (0 h); at 8 h and at 72 h, as showed in Fig.1. Between the measurements, the samples were kept in a dark container.

After expose the film to UV, at time 0 h, it was observed that the contact angle decreased for all samples, regardless of the niobium concentration present into the film, that is a well-known phenomenon for pure TiO_2 [7]. Sample with 1.9% Nb had a contact angle of 60° before UV exposure. After the UV radiation this angle got down to approximately 32°. The samples with 4.5% Nb and 4.9% Nb had a contact angle of approximately 62° before UV exposure, and exhibited 17 ° and 23° contact angle, respectively, after UV irradiation. Samples with higher concentration of Nb are more resistant to the aging, as shown the figure 1.

*Corresponding author: eng.aline2010@gmail.com

Nb (%at)	Thickness (nm)	Sa (nm)
1,9	88	3,39
2,1	76	4,15
4,5	92	5,77
4,9	89	4,86

Tab. 1. *Atomic percentage of niobium and film thickness measured through EDX.*

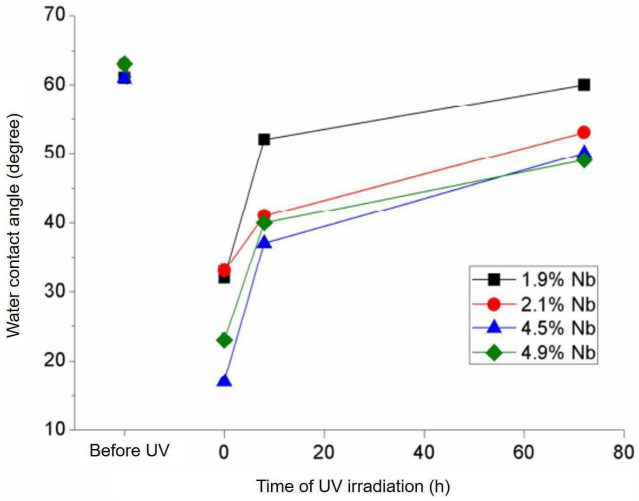

Fig. 1. *Temporal evolution of the TiO_2: Nb films contact angle, with different concentrations of Nb (%at) after UVC light (255 nm) irradiation over 24 hours.*

4. References

[1] U. Diebold, Surf. Sci. Rep. 48 (2003) 53–229.
[2] J. Deubener, G. Helsch, A. Moiseev, H. Bornhöft, J. Eur. Ceram. Soc. **29** (2009) 1203–1210.
[3] K. Nakata, A. Fujishima, J. Photochem. Photobiol. C Photochem. Rev. **13** (2012) 169–189.
[4] M. Mazur, D. Kaczmarek, E. Prociow, J. Domaradzki, D. Wojcieszak, J. Bocheński, Mater. Sci. **32** (2014).
[5] M. Murugan, R. Subasri, T.N. Rao, A.S. Gandhi, B.S. Murty, Prog. Org. Coatings **76** (2013) 1756–1760.
[6] F.C. Aleixo, T.J.S. Ballmann, M. V Folgueras, J.A. Junkes, V.P. Della, R.P. Malschitzki, Cerâmica **62** (2016) 358–364.
[7] M.E. Philippsen, M. Tomiyama, J. Stryhalski, F. De Tio, Rev. Bras. Apl. Vac. **35** (2016) 128–132.

Acknowledgments
We are grateful to FAPESC/UDESC (PAP TR 655 2017) for the financial support and CAPES for the scholarship awarded.

*Corresponding author: eng.aline2010@gmail.com

USE OF PLASMA TREATMENT TO IMPROVE FLAT FABRIC WETTABILITY

Camila Thais Mamani[1]*, Teresa Tromm Steffen[1], Luis César Fontana[1], Daniela Becker[1]
[1] *Center for Technological Sciences, UDESC, Joinville, Santa Catarina, Brazil*

1. Introduction

In textile's process, the finishing, which includes, beside others, degumming and dyeing, is one of the most water-consuming process steps. In the way to reduce the manufacturing resources at these steps, the plasma technique is pointed as a more economical, ecological and environmental friendly tool to chemically modify the fabric against the conventional chemical process [1]. The plasma treatment can activate the fabric surface improving their interaction to the dyes and increase the fabric wettability, increasing the dyeing yield. Therefore, the aim of this work is to treat flat fabric by to different types of O_2/N_2 plasma and evaluate the wettability and the surface chemical modifications.

2. Experimental

The textile sample used at this work is a 100% cotton flat fabric. Two different plasma treatments were carried out to promote chemical modifications on the fabric. The first one consists of inductively coupled radio frequency plasma (RF), at 100 W power input and 66.7 Pa gas pressure. The second one took place in active screen DC plasma at 200 V, 100 kHz frequency and 66.7 Pa gas pressure. For both plasma treatments it was utilized the proportion 20% oxygen and 80% nitrogen as reactive gases. The samples were treated by 1, 3 and 10 minutes in each plasma type. Tab. 1 shows the samples names and conditions used at this paper.

Sample	Plasma type	Treatment time
S0	-	-
RF-1	RF	1 minute
RF-3	RF	3 minutes
RF-10	RF	10 minutes
DC-1	DC	1 minute
DC-3	DC	3 minutes
DC-10	DC	10 minutes

Tab. 1. *Samples names and conditions.*

3. Results and Discussions

The samples treated by plasma and the S0 sample, which was not submitted to any treatment, were chemically analyzed by XPS. The oxygen and nitrogen atomic percent are respectively 17.4 and 2.0 for S0 sample, and for treated samples these values are present in Fig. 1 and Fig. 2. As shown in Fig. 1 the oxygen atomic percent was highly increased after plasma treatment, and that this value increase by increasing the treatment time, as also reported by [2]. Besides that, the RF plasma proves to be more efficient than the active screen DC plasma in the way to promote oxygen bonding at flat fabric surface. Regard to nitrogen presence, by RF plasma treatment it seems not to be possible to increase this atom content. In fact, Fig. 2 shows that it is even possible to induce the decrease of nitrogen atomic percent on flat fabric surface by means of chemical attack of RF plasma specimens. For DC plasma process just the 10 minutes treatment shows a significant change on nitrogen atomic percent, been the DC-10 sample the only one among all the others to show nitrogen atomic percent increase after plasma treatment. This behavior of so different degree of nitrogen and oxygen atoms attachment, underlies the fact that oxygen species is much more reactive than the nitrogen ones, despite the highest nitrogen presence [2].

*Corresponding author: camilathaismamani@gmail.com

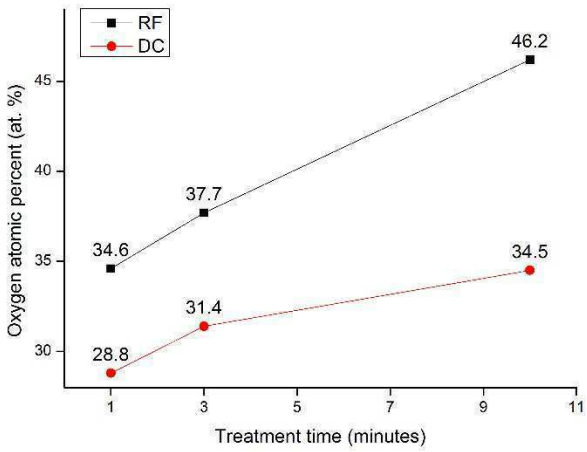

Fig. 1. *Oxygen atomic percent of samples treated by 1, 3 and 10 minutes in RF and DC plasma.*

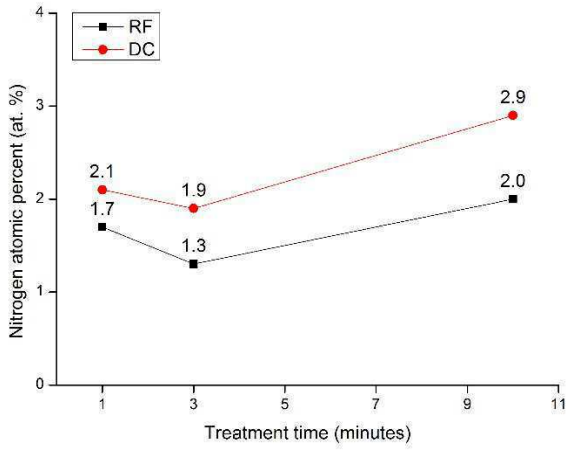

Fig. 2. *Nitrogen atomic percent of samples treated by 1, 3 and 10 minutes in RF and DC plasma.*

Once that XPS shows the flat fabric surface's chemical modification, the samples were submitted to water contact angle measurement. Fig. 3 shows that 1 hour after plasma treatment the DC-1 sample present a slightly decrease in contact angle, which is almost all recovered after 24 hours. However, the changes in wetting behavior for this sample are not so significant, and in comparison to S0 sample it remains hydrophobic. Otherwise, for sample DC-3, even after 24 hours the contact angle is below 90°, conferring to this sample a hydrophilic behavior. For DC-10 sample and for all others treated in RF plasma, it was not possible to obtain the contact angle, once the surface fabric present a super hydrophilic behavior with water drop instantaneous absorption. This behavior remains like that until 24 hours after plasma treatment. The wettability is related to oxygen atomic percent on flat fabric surface [3], as shows the Tab. 2, and seems to be a critical value of this atom presence, between 30 and 35 oxygen at%, from which the fabric surface presents a super hydrophilic behavior. Therefore, the DC plasma can be used as a tool to improve a flat fabric wettability with treatment time higher than 10 minutes, while the RF plasma shows to be a more efficient tool, reaching considerable results even for treatment times as short as 1 minute.

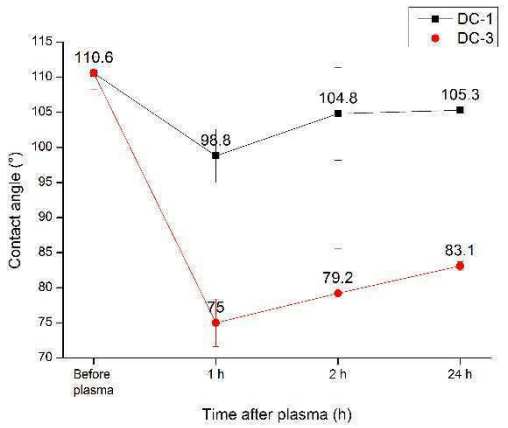

Fig. 3. *Contact angles for samples before and 1, 2 and 24 hours after plasma treatment*

Sample	O at %	Wettability
S0	17.4	hydrophobic
DC-1	28.8	hydrophobic
DC-3	31.4	hydrophilic
DC-10	34.5	super hydrophilic
RF-1	34.6	super hydrophilic
RF-3	37.7	super hydrophilic
RF-10	46.2	super hydrophilic

Tab. 2. *Oxygen atomic percent and wetting behavior for all the samples*

4. References

[1] R. Morent, et al., Surf. & Coat. Tech., **202**, 3427-3449, (2008).
[2] S. Inbakumar, et al., Cellulose, **17**, 417-426, (2010).
[3] B. Ghimire, D. P. Subedi, R. Khanal, AIP Advances, **7**, 085213, (2017).

Acknowledgments

The authors would like to thank the financial support provided by FAPESC/PAP, CAPES and CNPq.

*Corresponding author: camilathaismamani@gmail.com

DESIGN AND MANUFACTURE A HIGH EFFICIENCY UNIBODY CAR IN COMPOSITE MATERIALS

Augusto Ricci Ferreira[1] and Gabriel Benedet Dutra[1]
[1]*Federal University of Santa Catarina (UFSC) – Technological Center of Joinville*

1. Introduction

The demand for a sustainable economy and an increased priority of energy safety is increasing interests and investments at the field of electrical vehicular transports [1]. Following these ideas, the EFICEM team of Federal University of Santa Catarina is a group that has the objective to produce new prototypes that aimed to obtaining a better efficiency. The team competes annually at the Shell Eco Marathon Brazil and at Shell Eco Marathon Americas, the competition that has the most efficiency cars in the world [2]. The production of a new careen for the new prototype entire of composite materials as carbon fiber and epoxy resin aimed to fix the problems of the last prototype. The problems were structural rigidity, small intern surface, aerodynamics performance. Furthermore, the entire part must be in accordance with new rules of the competition. This manuscript reports all the conception and manufacturing steps of the unibody car.

2. Experimental

The manufacturing of the unibody structure started with a project in 3D software CAD/CAM (computer-aided design) Solid Works 2018. After this step, a high-density polyurethane block was machined using a precision CNC vector machining at Protville company to obtain the plug. From this plug, the mold was manufactured in composite via spray-up process. This manufacturing step was carried out at Lan Fibras Company, located in Joinville/SC. The materials used were roving fiberglass and ortho-polyester resin. Afterwards, this mold was used at the final lamination. In order to achieve the final part – unibody car - a vacuum bag process was performed. For structural performance a sandwich panel was used, where the materials were layers of carbon fiber cloth (200g/m²), core material of semi-rigid PVC foam (6mm width) D60 Divinicell and epoxy resin from Barracuda Composites company AR260 with AH260 cure agent. The steps are shown in Fig. 1.

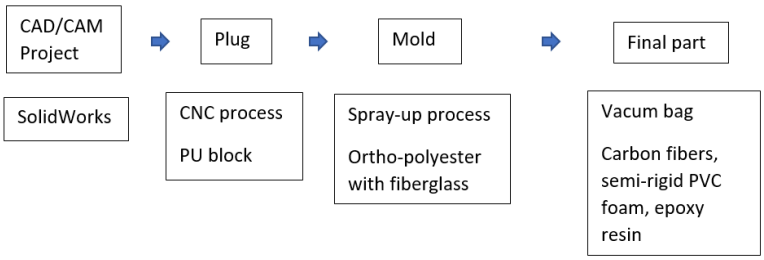

Fig. 1. *Summary of the manufacturing steps of the unibody.*

3. Results and Discussions

Hereby, the details about the process steps are described. Initially, the main dimensions of the unibody were projected considering the requirements of the Shell Eco Marathon 2018[2]. From the last version, an extra distance between the pilot and the front of the car was included, which also guarantees a wider visibility of the pilot. In addition, a larger internal space and better insulation of the pilot in relation to the steering system and wheels were also some of the requirements of the new project. Even with these modifications, the design needed to maintain the fundamental aspects of aerodynamics and droplet shape of the car. Fig 2 shows the project with all the requirements. The next step was to obtain the plug, which must replicate in three dimensions the project of the final part. For this, a polyurethane block was machined, see Fig. 3.

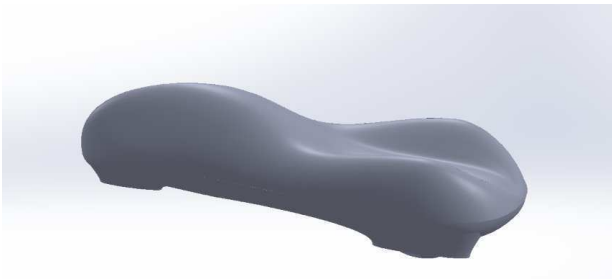

Fig. 2. *3D Solid Works project of the entire project*

Fig. 3. *Plug in polyurethane after machining.*

Corresponding author: augusto.rf@grad.ufsc.br

Afterwards the plug was prepared to the next step. Since the material of the block adheres with the polyester resin used in the spray-up process, it was necessary to use a water-based acrylic paste together with a water-based paint for the insulation of the plug. After finishing the plug, the mold got laminated using fiberglass and resin via spray up process. The process should provide a rigid and robust component, which will be used as a mold of the final part. **Fig 4** shows the mold after the process. The crucial point of the process was the final part. In order to achieve a high performance part, a vacuum bag process was used. The vacuum removes the excess of resin and removes any voids from the lamination [3-4]. First, resin was spread all over the mold and then positioned the first layer of carbon fiber. Then, the semi-rigid PVC foam, previously cut, were placed onto the entire mold. Sequentially, resin was once again passed through with other layer of carbon fibers, forming the sandwich structure. Finally, bag was used to seal the entire mold. The bag was sealed with sealing tape. The vacuum pump was used at a pressure of 500 mm Hg for approximately four hours. Finally, the unibody was demolded, see **Fig 5**.

Fig. 4. *Mold after spray up process, bottom view.*

Fig. 5. *Composite unibody demolded.*

Fig. 6. *EFICEM prototype competing at Shell Eco Marathon Americas 2018.*

4. References

[1] BNDES, *Veículos elétricos: história e perspectiva no Brasil.* Rio de Janeiro (2010). Available in: <https://www.bndes.gov.br/bibliotecadigital> Acessed in: 20 may 2018.
[2] SHELL. Shell Eco-marathon 2018 Global Rules Chapter I. 2018b. Available in: < http://www.shell.com/energy-and-innovation/shell-ecomarathon.html>. Acessed in: 10 jan 2018.
[3] WEST SYSTEM. Vacuum Bagging Techniques. 7 ed. Bay City: Gougeon Brothers (2010).
[4]GIBSON, R. F. Principles of composite material mechanics. 3rd Ed. Boca Raton: Taylor & Francis Group (2012).

Acknowledgments

We would like to express our gratitude for the EFICEM team for all support in this challenge.

Corresponding author: augusto.rf@grad.ufsc.br

ANALYSIS OF GRANITE POWDER USING LASER DIFFRACTION, FTIR AND XRD

S. C. S. M. Santos[1], P. A. Suzuki[2], A. R Bigansolli[1], B. B. Lima-Kühn[1,*]
[1]*UFRRJ – Universidade Federal Rural do Rio de Janeiro.*
Rodovia BR 465, Km 7, Seropédica, RJ, 23851-970, Brazil.
[2]*EEL/USP – Escola de Engenharia de Lorena, Universidade de São Paulo.*
Estrada Municipal do Campinho, s/n, Lorena, SP, 12600-000, Brazil.

1. Introduction

In the mineral sector, the granite beneficiation market is very promising, but tied to this, there are concerns about the generation of waste during the processing stages and with the possible inadequate destination of this waste generated [1]. The polymer industry, on the other hand, uses the incorporation of fillers to improve the thermo-mechanical properties, alter the surface appearance and, in particular, reduce the costs of the polymer composition. Thus, the knowledge of the load element characteristics and its influence on the polymer matrix is necessary [2].The present work has the objective of characterizing the granite powder using laser diffraction, FTIR and XRD, aiming at a future application as reinforcement in epoxy resin matrix [3].

2. The experiment

Initially the granite stone was fragmented to obtain pieces of reduced size. The pieces were then high-energy milled using a Retsch PM100 planetary ball mill. The milling was performed at the speed of 300 rpm for 8 minutes. Three samples were used for the powder characterization: sample 1 (collected after high energy milling), sample 2 (sieved to below 44 μm) and sample 3 (sieve's aggregate). The size distribution of powder was measured using a laser diffraction particle size analyzer (Mastersizer 2000. Malvern). The samples were analyzed by Fourier Transform Infrared (FTIR) spectroscopy. FTIR spectra were recorded with a BRUKER VERTEX 70 spectrometer by applying the ATR PLATINUM. Powdered samples were recorded for the 4000 cm^{-1} to 400 cm^{-1} region. For the XRD experiments, the measurements were carried out at room temperature using Ni-filtered Cu-Kα radiation in an diffractometer (Empyrean, Panalytical) and the measurement conditions were $10°<2\theta<90°$, 0.01° step. The phases were identified based on Villars and Calvert crystallographic data [4] and the Powder Cell software [5].

3. Results and Discussions

In high energy milling it was possible to obtain granite powder with micrometric particles. By laser diffraction analysis was observed that although the sieve (aperture size of 44 μm) used to segregate the samples, sample 2 has 10% of particles larger than 38.96 μm and sample 3 has 10% particles smaller than 39.187 μm. The quartz, albite (sodium feldspar) and microcline (potassium feldspar) were identified by XRD and the largest amount of albite in sample 3 indicates the albite is harder than the quartz and the microcline. According to FTIR analysis, the results show: feldspars (fine sharp bands in the spectral region (800–400 cm^{-1}), quartz (characteristic doublet 799 and 778 cm^{-1}) and biotite (1005 cm^{-1}) [6,7]. These results confirm the presence of quartz and feldspar in the granite and indicates the presence of biotite that was not identified by XRD.

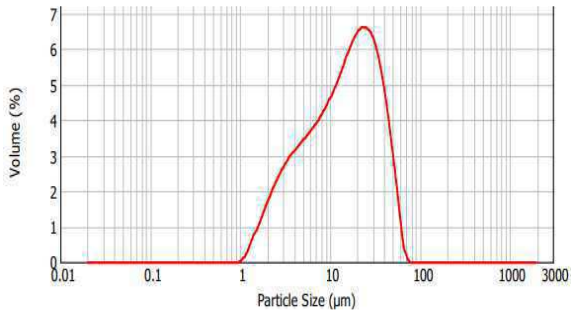

Fig. 1. *Particle size distribution of sample 2 (sieved to below 44 μm).*

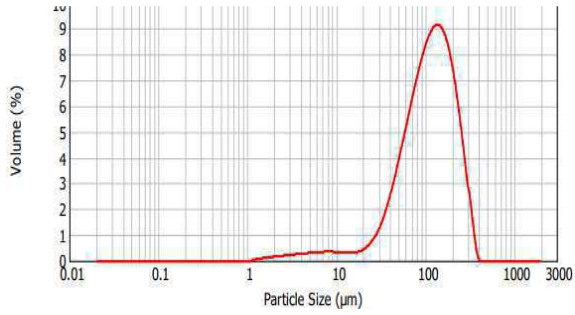

Fig. 2. *Particle size distribution of sample 3 (sieve's aggregate).*

*Corresponding author: belmiralima2@gmail.com

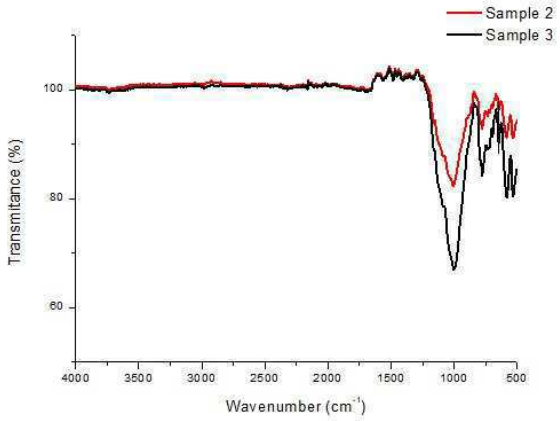

Fig. 3. *FTIR spectra for the granite (4000 cm^{-1} to 400 cm^{-1} region)*

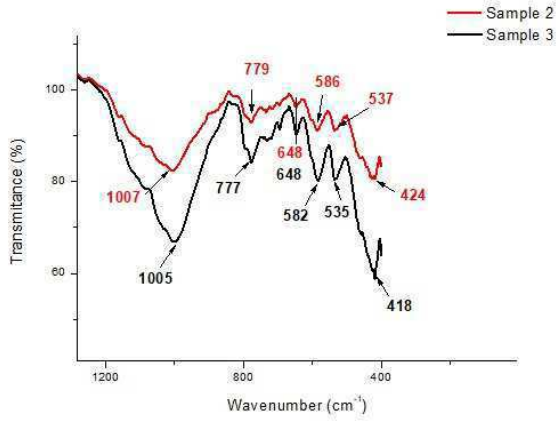

Fig. 4. *FTIR spectra for the granite (1300 cm^{-1} to 400 cm^{-1} region)*

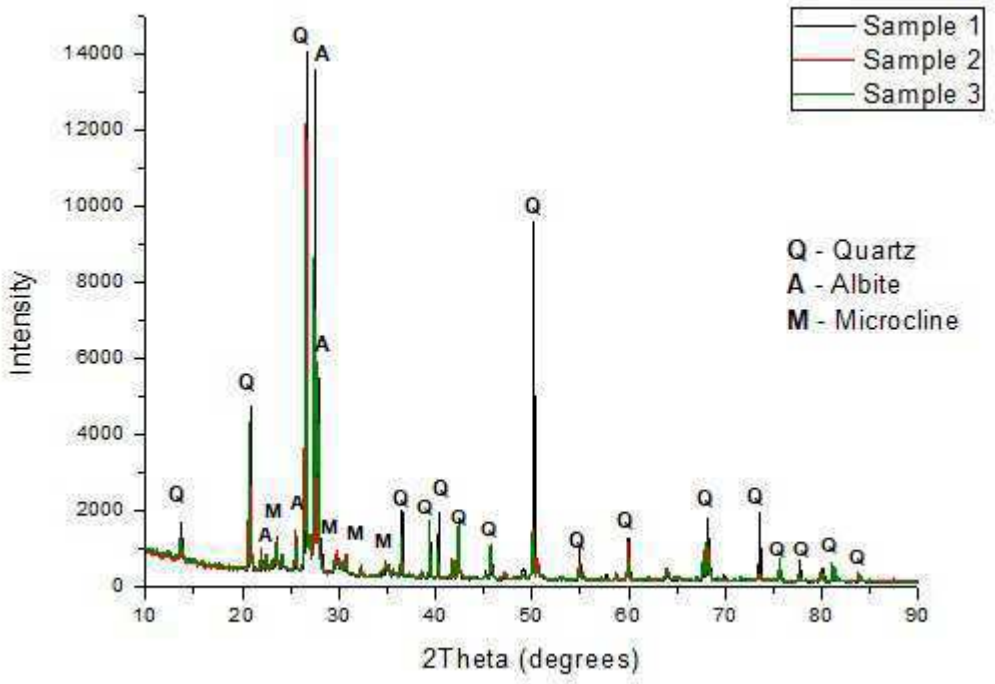

Fig. 5: *X-ray diffractogram of the granite samples.*

4. References

[1] Multimedia Writing ESHOJE. Brazilian exporters of ornamental stones exporters, 2017. http://eshoje.com.br/exportacoes-de-rochas-ornamentais-capixabas-crescem-mais-de-12-em-maio/.
[2] J. A. V. Gonçalves, D. T. Campos, G. J Oliveira, M. L. S. Rosa, M. A. Macedo, Materials Research, 17(4), 878-887, (2014).
[3] A. Piratelli-Filho, F. Levy-Neto. Materials Research, 13(4), 497-503, (2010).
[4] P. Villars, L.D. Calvert. *Pearson's Handbook of Crystallographic Data for Intermetallic Phases*. 2ª edition, Ed. Metals Park: ASM International, (1991).
[5] W. Kraus, G. Nolze. PowderCell (2.3). Berlim: Fed. I. Res. Test, 1999.
[6] V. C. Farmer. *The infrared spectra of minerals*. London: Mineralogical Society; (1974).
[7] Z. Kriva´csy, J. Hlavay. J Mol Struct, 4, 294-251, (1993).

Acknowledgments

The authors acknowledge Programa de Pós-Graduação de Engenharia de Materiais – PPGEM / EEL-USP and Universidade Federal Rural do Rio de Janeiro – UFRRJ.

*Corresponding author: belmiralima2@gmail.com

ABLATIVE PROPERTIES OF CERAMIC MATERIALS TESTED IN A SUPERSONIC PLASMAS WIND TUNNEL

Cristian Cley Paterniani Rita[1,2], Gilberto Petraconi Filho[1], Alexei Mikhailovich Essiptchouk[3], Tiago Moreira Bastos Campos[1], Felipe Rocha Caliare[1], Felipe de Sousa Miranda[1]

[1]ITA- Technological Institute of Aeronautics, LPP, S. J. Campos, SP, Brazil
[2]FATEC – Technology College – Pinda[ba], SP, Brazil
[3]UNESP – Paulista State University – S. J. Campos, SP, Brazil

1. Introduction

Mullite is a ceramic composed of silicon oxide and aluminum used in various technological applications due to its physical and chemical properties, such as: Low thermal expansion, high thermal stability, low density, low thermal conductivity, good mechanical resistance and creep resistance, good stability in severe chemical environments, among other properties [1,2]. The supersonic plasma wind tunnel was optimized to investigate the ablative properties of the ceramic composite – Mullite ($3Al_2O_3.2SiO_2$) deposited by the plasma spray process on Carbon - Carbon Substrate (C/C).

2. Experimental

The synthesis of the mullite is obtained from the mixture in sol-gel of materials that present in its composition (Al_2O_3) and (SiO_2) [1]. This solution was inserted in a Plasma Spray Reactor in order to process a nanostructured mullite coating on C/C. After the deposition process, the samples were exposed to a supersonic plasma jet with thermal flow of the order of 0.63MW/m^2. The ablation process analyzed in this experiment was characterized in relation to the specific mass loss as a function of the exposure time varying between 5s and 20s.

3. Results and discussions

The specific mass loss practically does not vary with the exposure time in the investigated range having a value of approximately 12.25 g/m^2. The SEM image shows that the coating has many cracks and suffers excessive degradation in the ablation process (see figure 1).

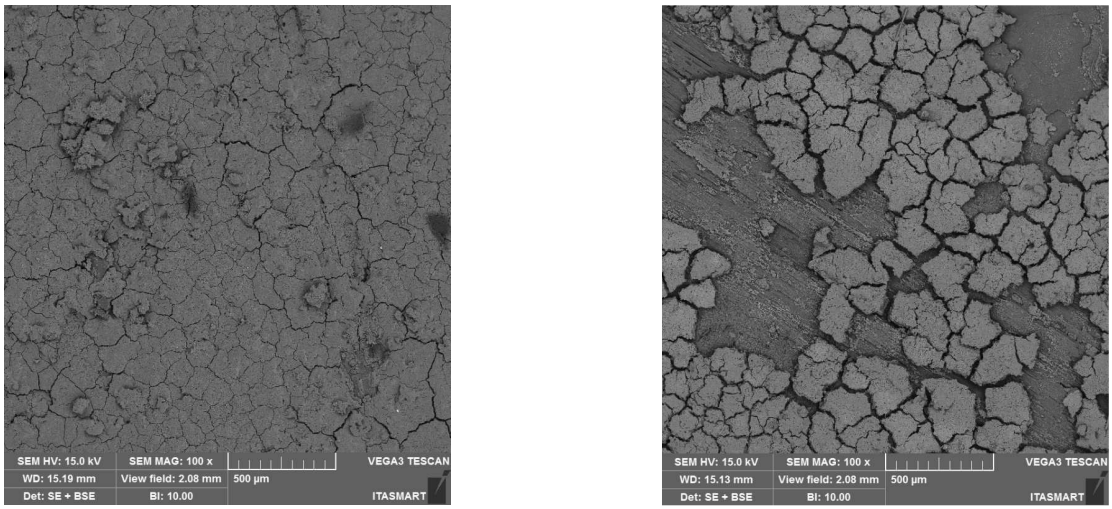

Fiure 1. SEM image: (a) Coating of Mullite on C/C. (b) Sample after the ablation process

4. References

[1] L. S. Cividanes, T. M. B. Campos, L. A. Rodrigues, D. D. Brunelli, G. P. Thin, J. Sol-Gel Sci Technol. **55**, 111-125, (2010).

[2] W. ZhongLiu, X. Peng, L. Zhuan, H. Wen, L. Heng, Y. XiaoYu, L. Yang, C. Wenbo, Journal of the European Ceramic Society, **35**, 3789-3796, (2015).

Acknowledgments

We acknowledge the financial support of FAPESP, CNPq and CAPES.

*Corresponding author: place the email of the corresponding author here (bookman old style 9 pt)

EFFECT OF THE GAS PRESSURE ON THE DISCHARGE POWER OF A HYBRID CORONA-DBD REACTOR

Alonso H. Ricci Castro[1]*, Gilberto Petraconi Filho[1].
[1]*Technological Institute of Aeronautics, ITA,São Jose dos campos, SP-Brazil.*

1. Introduction

Non-thermal plasmas can be generated under different pressures and gas compositions. The choice of pressure and type of gas depends of the required applications and changes the properties of plasma. The pressure influences the properties of plasma. Typically in a low pressure (0.01 mbar) glow discharge ions energies are around to 14.5 eV, but when the pressure is increased (0.07 mbar), their energies decrease to 3 eV [1]. However, the properties of plasma change when small drops of liquids are introduced. The plasma can break and ionize the molecular bonds on the surface and vaporize some drops [2]. The introduction of small drops of water on plasma can enhance the production of activate radicals, which are capable of altering the surfaces of polymeric materials. The chemical reaction between the particulate of the gas phase and the contact surface may have a reduced lifetime due to successive collisions of the gas particles that are acting on the surface.

2. Experimental Setup

The atmospheric pressure cold plasma is generated using a hybrid corona-dielectric barrier discharge. The reactor consists in two cylindrical electrodes with variable gap. The high voltage electrode is made from a metallic tube with 6.5 mm of external diameter and has a hole for entrance to different gases and liquids. The second electrode is grounded made from metallic tube (steel) with 140 mm of external diameter and covered by dielectric layer from alumina with 5.5 mm of thickness. This system can work with different pressure or gas type. The power supply can operate with different voltage amplitudes (1-35 kV), frequencies (1- 40 kHz) and wave signals. In this work, the voltage was fixed in 23 kV_{p-p} and the frequency on 23 kHz. The gap between the two electrodes was fixed in 2 mm. The water vapor is generated using a commercial ultrasonic nebulizer. The size of atomized water have 5μm at a flow rate about 0,7 ml/min.

3. Results and Discussions

Figure 1 shows the variation of the discharge power as a function of pressure using air and steam as working gas. The discharge power evaluated by Lissajous method was lightly highest when the discharge operates with water vapor. This effect is related with the ionization of the surface of water drops increasing the conductivity of the gap.

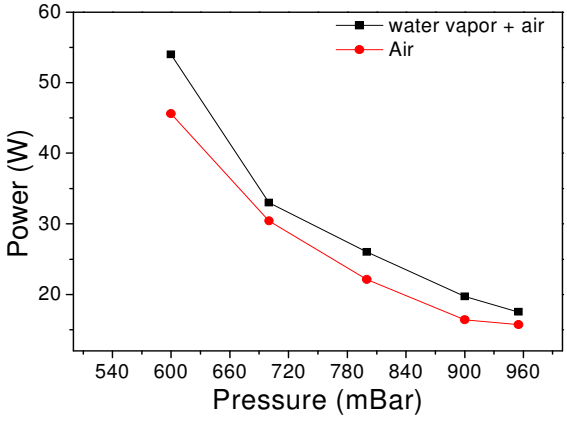

Fig. 1. *Variation of power on different pressure fixing voltage 23 kV, frequency: 23kHz and gap: 2mm.*

4. References

[1] Saboohi, Solmaz, et al. *"Comparison of plasma polymerization under collisional and collision-less pressure regimes."* The Journal of Physical Chemistry B 119.49 (2015): 15359-15369.
[2] Fanelli, Fiorenza, et al. *"Insights into the Atmospheric Pressure Plasma-Enhanced Chemical Vapor Deposition of Thin Films from Methyldisiloxane Precursors."* Plasma Processes and Polymers 9.11-12 (2012): 1132-1143.

Acknowledgments

The authors acknowledgement CNPq and FAPESP by the financial support.

*Corresponding author: Alonso_elfisico@yahoo.com

EVOLUTION OF THE HARDNESS PROFILE WITH APPLIED DUTY CYCLE IN PLASMA NITRIDING OF THE AISI 420 STAINLESS STEEL

Zanella, I. G*; Zanetti, F. I; Brunatto, S. F; Cardoso, R. P.
Plasma Assisted Manufacturing Technology & Powder Metallurgy Group
Mechanical Engineering Department, Federal University of Paraná, PR, Brazil

1. Introduction

Plasma-assisted thermochemical treatments are being increasingly applied in industry and academia for treating different types of materials. These treatments, like nitriding, cementation or nitrocement, provide changes in the material surface characteristics. Studies conducted by [1], show that applying the previous heat treatment can influence the nitriding treatment on the samples in the AISI 420 martensitic stainless steel, being the best results obtained for as-quenched samples. The plasma parameters are also expected to influence such treatment. Until now, studies that use plasma to alter the properties of the surface (corrosion resistance and wear resistance) of the martensitic stainless steels generally apply a treating system where the processing temperature is dependent only on the power. In this study, an apparatus permitting to control the processing temperature by an auxiliary heating system was applied to study the influence of duty cycle (mean power plasma, equivalent to the t_{ON}) in the low-temperature nitriding of the AISI 420 martensitic stainless steel.

2. Experimental Apparatus

The apparatus used in the present work is the same used by [2], however, for this study an auxiliary heating system , which allows to control the treatment temperature independently of the plasma power (duty cycle), was installed around the sample holder. Samples of AISI 420 martensitic stainless steels were heated and maintained at 1050 ° C for 1 hour and air-cooled. The pulsed power supply applied to generate the plasma has a frequency of 4.2 kHz and the mean power transferred to the plasma is controlled by adjusting the duty cycle (switched on time (t_{ON}) of the pulse). Plasma nitriding was performed at 350 ° C and pressure of 3 Torr, treatment time was fixed at 8 h and the gas mixture was composed of 70% N_2 + 20% H_2 + 10% Ar. To evaluate the role of duty cycle the switched on time (t_{ON}) of 10, 20 and 27□□s were applied for generating the plasma, being that the case where 27□□s represents the situation where the heating comes completely from the plasma (without auxiliary heating). The nitrided samples were characterized by X-ray diffraction (XRD), nanoindentaton (profile determination) and optical microscopy.

3. Results and Discussions

The analysis performed by XRD (figure 1) show that for the sample nitrided with t_{ON} 10μs, there was no displacement of the martensitic peak (α`) nor nitrides formation. However, for the condition with $t_{ON}$ 20μs and 27μs, the displacement of the peak to smaller angles occurred, indicating that the expansion of the martensitic phase by nitrogen, forming nitrogen-expanded martensite ($\alpha`_N$), was occurred. In this condition, it is possible to verify also that peaks of the ε-nitride are also detected.

In figure 2, the hardness profiles, obtained by nanoindentation, are presented. It can be observed that the surface is not hardened for the nitriding treatment with t_{ON} 10 μs, however, for the nitriding treatment with t_{ON} 20μs and 27 μs similar hardness profiles, with a relatively smooth hardness gradient, are observed, even if figure 1 suggest a more important fraction of ε-nitride for the sample treated with t_{ON} 27 μs. We can conclude that by controlling the duty cycle it is possible to control to some extent the obtained surface properties and fraction of phases. Moreover, it is possible to affirm that surfaces with interesting mechanical properties can be obtained applying a lower duty cycles, that produce a more stable plasma (especially important in industrial application).

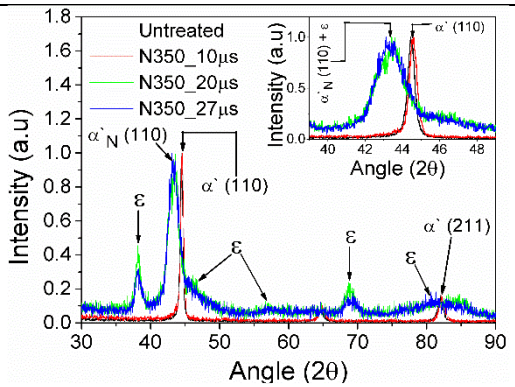

Fig. 1. *X-ray diffraction patterns for samples nitrides with different duty cycles.*

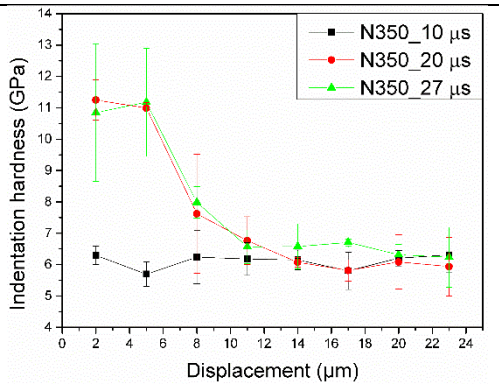

Fig. 2. *Hardness profile for nitrided samples produce with different duty cycles. Profiles obtained by nanoindentation applying a load of 20 mN.*

4. References

[1] R. P. Cardoso, C. J. Scheuer, and S. F. Brunatto, "Stainless Steel: Low-Temperature Nitriding Kinetics," *Encycl. Iron, Steel, Their Alloy.*, pp. 3283–3293, 2016.

[2] C. J. Scheuer, R. P. Cardoso, M. Mafra, and S. F. Brunatto, "AISI 420 martensitic stainless steel low-temperature plasma assisted carburizing kinetics," *Surf. Coatings Technol.*, vol. 214, pp. 30–37, 2013.

NITRIDING OF AUSTEMPERATED DUCTILE IRON (ADI) IN PLASMA GENERATED BY ABIPPS (ASYMMETRIC BIPOLAR PLASMA POWER SUPPLY)

Bruna T. Bianchi*, Wilson L. Guesser, Juliano S. Scholtz, Luis C. Fontana

Universidade do Estado de Santa Catarina, Centro de Ciências Tecnológicas, Departamentos de Física e de Engenharia Mecânica, Rua Paulo Malschitzki 200, Zona industrial Norte, 89219-710, SC, Brasil.

1. Introduction

This work consists in finding suitable parameters to perform a thermochemical treatment of nitriding in ADI at low temperature with an asymmetric bipolar plasma power supply, which makes possible the superficial hardening of the part without formation of white layer and without loss of properties of the base material.

The ADI (Austempered Ductile Iron) is the product resulting from the treatment of austempering in nodular cast iron, has a very fine microstructure of ferrite and stabilized austenite, the ausferrite. [1] – KOVACS, 1994. The nitriding is a thermochemical treatment of surface hardening, in which nitrogen is introduced on the surface of the material, in a nitrogenous atmosphere at a certain temperature. [2] – CHIAVERINI, 2002.

2. Experimental

The parameters evaluated were: time, temperature, initial microstructure of the sample (austempered or not) and constituent atmosphere, treatments were carried out at 300, 320, 340, 350, 365, 380 and 500° C, the atmospheres analyzed were N2:H2:Ar in ratio 80:10:10 and N2:Ar 90:10 and time 4 and 8 hours. The microhardness and metallography analyzes were performed.

3. Results and Discussions

It is possible to perform a nitriding treatment in ADI without loss of properties of the base material or formation of white layer, but there is a critical temperature for this to occur, in this work reached a temperature of 330 ± 10 [° C]. Above this temperature the base material begins to lose mechanical properties and below this temperature the formation of the hardened zone becomes very small.

As for the time of nitriding, it can be observed that its increase causes the increase of the hardened layer, and also a greater surface hardness. In relation to the atmosphere of plasma nitriding, it is concluded that the presence of hydrogen contributes positively to the treatment, and the best gas mixture found was 80:10:10.

Treatment		**01**	**02**	**03**	**04**	**05**	**06**	**07**
Time		4				8		4
Temperature		350	350	500	340	300	320	340
Atmosphere		$N_2:H_2:Ar$ 80:10:10	$N_2:Ar$ 90:10		$N_2:H_2:Ar$ 80:10:10			
Ductile Iron	Depth of hardened layer [μm]	25	25	75	50	20	70	30
	Surface hardness. [HV]	406	379	824	477	370	478	397
	Increase of surface hardness [%]	18	10	40	39	08	39	16
ADI	Depth of hardened layer [μm]	20	12	35	60	60	80	70
	Surface hardness [HMV]	723	682	810	966	810	868	883
	Increase of surface hardness [%]	10	04	23	47	23	32	34

Fig. 1. *Results table of all situations studied.*

*Corresponding author: brunatbianchi@gmail.com

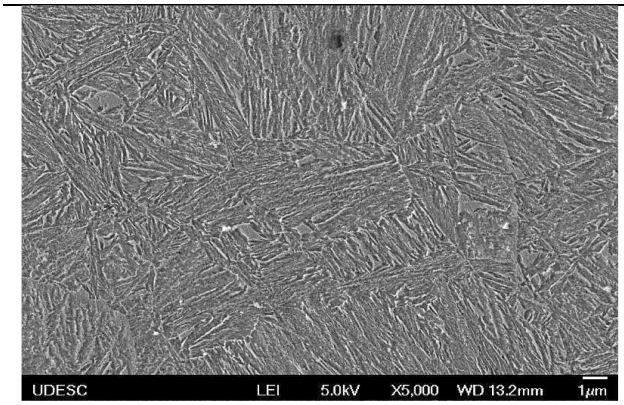

Fig. 2. *Nucleus of the best sample - MEV-FEG - 5000x.*

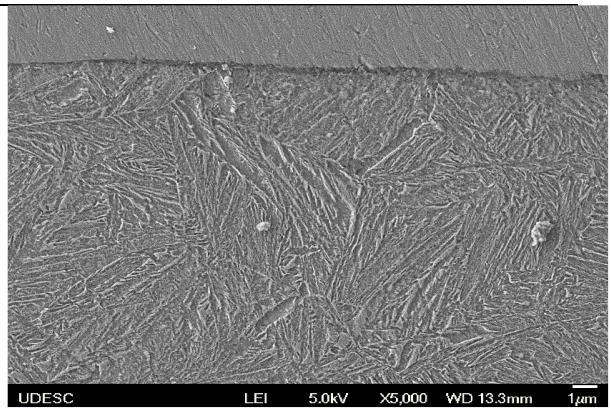

Fig. 3. *Periphery of the best sample - MEV-FEG - 5000x.*

.

4. References

[1] Kovacs, B., Keough, J.R., "*Physical Properties and Application of Austempered Gray Iron,"* AFS Transactions. (1994.)

[2] CHIAVERINI, V. *"Aços e ferros fundidos"*. 6 ed. São Paulo. (2002)

*Corresponding author: brunatbianchi@gmail.com

RIETVELD REFINING: ELUCIDATION OF PEROVSKITES LNF STRUCTURE

Douglas Washington da Silva[1]*, Leticia Trezecik Silvano[1], Marilena Valadares Folgueras[1]
[1]*Santa Catarina State University – CCT-UDESC*

1. Introduction

Perovskite are oxides with the general formula ABO_3, their composition can be varied due to substitutional solid solutions by substitution of cations in positions A and B [1]. Ionic size could produce distortion versions, since cubic ideal structure until orthorhombic, rhombohedral or tetragonal [2-3]. $LaNiO_3$ oxide belongs to the rhombohedral system with space group R-3c (n° 167), can be describe as hexagonal unit cell with parameters a=5,4573 e c=13,1601. Although $LaFeO_3$ show orthorhombic distortion with space group Pnma (n° 62) with parameters a=5,5647, b= 7,8551 e c=5,5560 A.

The first is a material that presents paramagnetic and metallic properties, while the second is an antiferromagnetic insulation material [3]. According Falcon [6] perovskites $LaNi_xFe_{1-x}O_3$ exhibit rhombohedral structure with $0<x<0,5$ and orthorhombic with $0,5<x<1$, all the solutions are single phase except that with the intermediate composition (x=0,5), where both phases are observed. Formation of the rhombohedral phase results in better performance of the material at high temperatures [4]. The Rietveld refining was used as a tool for structural analysis.

2. Experimental

$LaNi_{0,6}Fe_{0,4}O_3$ perovskites was synthesized by Pechini method with calcination at 700 and 900°C during 12 horas. Rietveld refining was applied to evaluate the influence of temperature in the formed material crystallinity. The X-ray diffraction data of the powder samples were recorded using a X SHIMADZU, X-RAY DIFFRACTOMETER LAB X XRD-6000 model, Cupper radiation, between 5 -80°, with steps of 0.02° and counting time of 5 s per step. The data were analyzed by means of the Rietveld method using the FullProf program.

3. Results and Discussions

The value obtained for factor S, Chi², R_{exp} R_B and R_{wp} was 1,69, 2,86, 5,12, 3,81 and 8,86 respectively to perovskites calcined at 900°C and 1,70, 3,26, 6,48, 5,81, 10,51 to perovskites calcined at 700°C. The quality of results obtained by refining is confirmed by the values of factor R_{wp} (weighted residual error), R_{exp} (expected error), and R_B (Bragg factor), S (adjustment quality given by the ratio between R_{wp} and R_{exp}, meaning the adequacy of the observed and calculated profiles) [5]. The S factor below 5, R_{wp} and R_{exp} close or below 10 and Chi² tending 1 (lowest value achieved for the structure) is indicative of good accuracy of the refinement values. In this way, it's possible observe that results obtained through rietveld refining have good quality and the similarity between the calculated values and the experimental data show that there was greater structural ordering for the sample calcined at 900°C for 12 hours, with lower residue and data values closer to the ideal ones. However, regardless of the heat treatment temperature, the only crystalline phase was the rhombohedral structure with symmetry R -3 C.

4. References

[1] Falcon, H.Goeta, A.E .Punte, G. Carbonio, R.E. Journal of solid state chemistry. v, **133** p, 379, 1997.
[2] Wanderley, J. B. M. Borges, F. M. M. Ribeiro, J. P. Pimentel, P. M. Melo, D. M. A. Cerâmica v, **59** p, 156, 2013.
[3] Niwa, E. Uematsub.C, Mizusaki, J. Hashimoto, T. Solid State Ionics. v,**274** p,119, 2015
[4]. Raigoza, C.F.V. Raigoza, Garcia,D Eiras, j.A. Kiminami, R.H.G.A. boletín de la sociedad española de cerámica y vidrio. v, **56** p,13, 2017.
[5] Panigrahi, M.R. Rietveld analysis of single phase $Ba_{0.99}Dy_{0.01}TiO_3$. Ceramic. Physica B. 2016.

Acknowledgments

The authors are grateful for Coordination for the Improvement of Higher Education Personnel (CAPES), Santa Catarina State Research Support Foundation (FAPESC), Ponta Grossa State University (UEPG) and the Multiuser Center of the State University of Santa Catarina (CCT-UDESC).

DEPOSITION AND CHARACTERIZATION OF TITANIUM NITRIDE FILMS INTERLAYERED WITH FILM OF TITANIUM DOPED OR NOT WITH ALUMINUM OR COPPER, FORMED BY DISCHARGE IN DUAL CATHODIC CAGE

Gonçalves T. M.[1], Margon A. A[1]., Pimentel B. P[2]., Donatti G. P.[1], Gontijo L. C.[1]
[1,2] *Instituto Federal do Espírito Santo,*
[1]*Propemm- Programa de Pós-Graduação em Engenharia Metalúrgica e de Materiais*

1. Introduction

Thin films, monolayers and / or heterostructures that are used as semiconductors and dielectrics must have certain optical, electrical, magnetic and electrochemical properties. Among these thin films we can evidence those of titanium nitride deposited by plasma using double cathodic cage that have been researched to be used in coatings of cutting tools, implants and other devices. In the present study, the effect of the deposition of an intermediate layer, without the presence of nitrogen, and the doping with aluminum or copper were investigated. The purpose was to observe the efficiency of the deposition technique with the use of double cathodic cage and potentialities on physical properties of these films and their possible applications including with the use in doping of the films.

2. Experimental

The cathodic cages used for the deposition of the titanium nitride films were cylindrical in shape. These cages were made of Ti grade II, with holes in the sides and caps. The inside cage has two caps of one millimeter each and the outside cage was used a cap with holes of 10 mm thickness. When the films were deposited with aluminum and copper doping, the cap of this element (sometimes aluminum, sometimes copper) was placed in each case only in the inside cage. This was done - between the two titanium caps of one millimeter each. The films were deposited on glass substrates located inside the cages. During the deposition, all other parameters were kept stable (temperature, time and gas mixture, etc.). Except for the presence or not of nitrogen in the third half hour of treatment. In the other times we had the presence of 90% H_2 and 10% N_2. Thus the parameters of study are the physical and electrochemical properties of the films with and without the presence of this inner layer and its doping or not by aluminum or copper. The temperature value was set at 260°C (± 10°C), the pressure at 0.9 Torr (~ 0.9 mm Hg), the deposition time used was 2 hours and 30 minutes and the gas concentration was maintained at 10 % N_2 and 90% H_2, except for the inner layer which was 100% H_2.

3. Results and discussion

We observed that the deposition rate was higher in the deposited film with three layers, but without the presence of Al. In relation of the resistivity we can observe that the presence of doping element, like aluminum, did not improve. It is certain that parameters can be varied to find the conditions that can reduce the low resistivity of these films. We can also observe that the magneto-resistance increases with the thickness of the film without the aluminum doping. Once the titanium nitride is not magnetic we need more studies to understand what is actually occurring. In view of these results, it can be concluded that this technique of deposition of films using plasma double cathodic cage can be used to deposit films in a very significant range, because we deposit thin semiconductor and dielectric films with small changes in the parameters. Futhermore, we can evidence the possibility of doping of films with the use of solid materials and / or powders. It is important emphasizing the need for research aiming to know the total potential of this technique concerning physical and electrochemical properties.

	Thickness (nm)	Deposition rate (nm/s)	Resistivity ($\Omega.cm^2$)	Mobility ($cm^2/V\ s$)	Charge carries (cm^3)	Magnetoresistance
GCd-Ti-1	43(6)	0,0048(4)	0,566	2,08E+0	7,383E+18	1,33E+2
GCd-Ti_xN/Ti/Ti_xN	286(8)	0,032(6)	3,327E+4	1,573E+2	6,117E+12	6,091E+7
GCd-Ti_xN/Ti/Ti_xN-Al	44(5)	0,0049(5)	4,50	2,04E+2	6,67E+14	2,62E+5

Table 1: It shows the resistivity, mobility, number of charge carriers and magnetoresistance of deposited films

References

[1]- L. C. Gontijo, A.G. Cunha, P.A.P. Nascentec, Materials Science and Engineering B 177 (2012) 1783.
[2]- Daudt, N. F.; Barbosa, J. C. P.; Braz, D. C.; Pereira, M. B.; Alves Jr., C. TiN thin film deposition by cathodic cage discharge: effect of cage configuration and active species. Journal of Physics: Conference Series 406 012021, 2012.

pleooog@gmail.com

PERMETHRIN POLYMERIZATION ON POLYAMIDE FABRIC BY HYBRID CORONA-DIELECTRIC BARRIER DISCHARGE OPERATING AT ATMOSPHERIC PRESSURE

Petraconi, A[1], Gasi, F[2], Bittencourt, E[1], Castro, AHR[1], Miranda, FS[1], Essiptchouk, AM[3], Nascimento, L[1], Pessoa, RS[1] , Petraconi, G[1], Maciel, HS[1]
[1]*Instituto Tecnológico de Aeronáutica-ITA*
[2]*Universidade Federal do ABC-UFABC*
[3]*Universidade Estadual Paulista-UNESP*

1. Introduction

Permethrin is a common synthetic chemical, widely used as an insect repellent. In this present work, plasma polymerization experiments using a hybrid corona-dielectric barrier discharge (DBD) were carried out using monomers based on permethrin (15%), aiming to potentiate functionalities of insect-parasite repellency in polyamide fabric[1,2].

2. Experimental

A knitted fabric composed of 92% polyamide 6 (PA 6.6) and 8% elastomer was used for this research. The electric characterization of the discharge was performed by measuring the transferred power using the Lissajous figure method. Before polymerizing process, the fabric was exposed to the DBD discharge operating in atmospheric pressure with a controlled environment using air as oxidant agent at a fixed discharge power of 29 W. Tests to determine static and dynamic contact angle was performed to check the moisture absorption. Structure of synthesized permethrin was evaluated Fourier transformed infrared (FT-IR).

3. Results and Discussions

Structure of synthesized permethrin evaluated Fourier transformed infrared (FT-IR) spectroscopy confirm the grafting of permethrin on fabric surface, mainly by the increment of cyclopropyl groups corresponding to 1048 cm^{-1} characteristic of the permethrin (Figure 2).

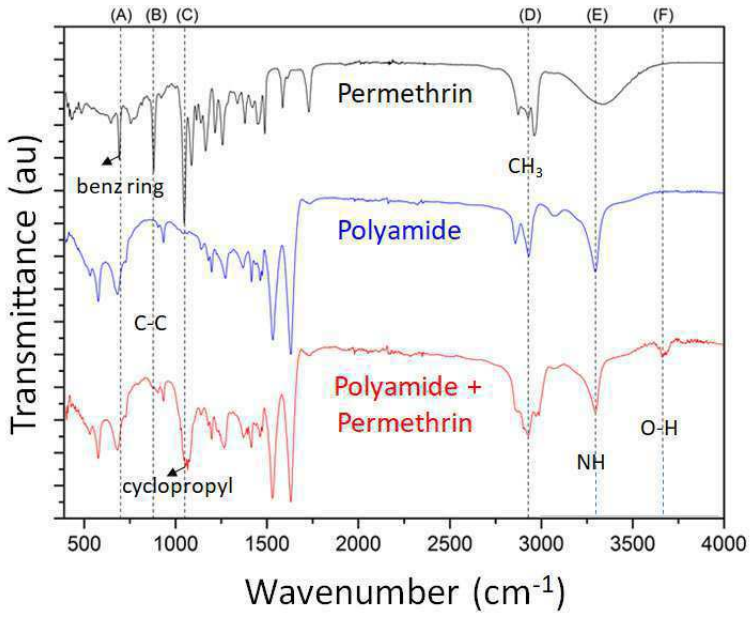

4. References

[1] Jerome A. Klun, Ashot Khrimian and Mustapha Debboun - Repellent and Deterrent Effects of SS220, Picaridin, and Deet Suppress Human Blood Feeding by Aedes aegypti, Anopheles stephensi, and Phlebotomus papatasi. J. Med. Entomol. 43(1): 34-39 (2006)
[2] R. Morent, N. De Geyter, J. Verschuren, K. De Clerck, P. Kiekens, C. Leys, Non-thermal plasma treatment of textiles, 3427–3449. doi:10.1016/j.surfcoat.2007.12.027.

Acknowledgments

We acknowledge the financial support of FAPESP, CNPq and CAPES.

*Corresponding author: place the email of the corresponding author here (bookman old style 9 pt)

USE OF GLASS WASTE AS A PARTIAL SUBSTITUTE FOR CEMENT TO OBTAIN MORTAR

Martin, A.C.[1*], Scolaro, L. M.[1], Zappelino, B. F.[1], Folgueras, M. V.[1]
[1]*Santa Catarina State University, Postgraduate Program in Materials Science and Engineering*

1. Introduction

Mortars are used in almost every stage of the construction. They are used to join materials such as blocks and coatings, and to level surfaces such as plaster and subfloor. [1]explain that the mortar is a mixture of cement, sand and water, that is like a concrete, but without a large aggregate.

The conscious destination of solid waste generated by man has been the subject of many researches that have as objective the use of these residues to generate alternative materials. It includes recycled products in engineering applications, not only involve environmental questions, but in many cases, it can modify or improve some properties and cost/benefit ratio. Hence, civil construction absorbs a range of recycled solid waste in building components [2].

Worldwide, waste glass is growing burden and new options are urgently needed for the large volumes of speciality, mixed, broken and contaminated glass that cannot currently be recycled. Conventional glass recycling technologies are limited by the need to separate waste glass into different glass types and the extreme sensitivity of the remelting process to any contamination [3]. Nowadays, there is an interest in using glass waste as a replacement of aggregates or cement in concrete or mortar [4]. In this study, we demonstrated that mixed broken glass could be used as primary input in the production of mortar. Glasses can be defined as amorphous or non-crystalline solids - that is, there is a structural disorder - and they have a glass transition temperature [5,6].

In this way, the objective of this work was to evaluate the possibility of partially replacing the Portland cement with the glass residue, which serves as pozzolanic material to obtain mortar.

2. Experimental

Glass bottle were broken and milled until pass trough mesh 325 (45µm). Glass composition was determined by x-ray fluorescence. Two mortar compositions were obtained: the first one, named sample A, was the pattern, without glass residue; the second one, named sample B, was the mortar with a partial replacement of cement by glass milled. Sample A considered 304,86g of Portland cement while sample B had 231,78g of cement and 57,94g of residue. Sand, lime and water was used too.

Fresh state mortars A and B were characterized by flow table the according NBR 13276 (2016), that establishes a scattering of 260 ± 5 mm. Hardened mortars were characterized by compressive strength in rectangular samples with dimensions of 4x4x16cm with 11, 32 and 60 days, carbonate content, differential thermal analysis and pozzolanic index according NBR 5752.

3. Results and Discussions

According to ASTM C618, the sum of SiO_2, Al_2O_3 and Fe_2O_3 must be higher than 70% for a pozzolanic material. Glass composition was determined by XRF and the major elements are SiO_2 (68.84%), CaO (23.54%), Al_2O_3 (3.60%) and Fe_2O_3 (1.28%), that is in accordance with establishes the ASTM. However the pozzolanic index must be determined.

In flow table, sample A scattering was 251,7mm, smaller than the desired, and sample B scattering was 257,3mm, according the NBR requirements. The first observation was the better scattering for sample with residue addition.

In the other hand, the most important property was the compressive strength. Sample A showed strength of 4.36MPa (11 days), 5.51MPa (32 days) and 5.33MPa (60 days) while sample B showed strength of 2.89MPa (11 days), 3.40MPa (32 days) and 3.53MPa (60 days). It´s possible to observe the lower strength for samples obtained with cement substitution by glass waste. [7] obtained a higher strength than presented in this work for samples with and without cement replacement by glass, although authors also observed a compressive strength decrease with addition of waste.

Thermal analyses present a similar behavior, but the $CaCO_3$ is higher for sample B. Carbonate content was evaluated in order to confirm the information. For sample A, the content was 0.45 while for sample B was 0.5. Thus thermal analysis is in accordance with carbonate content and higher $CaCO_3$ could explain the decrease of strength.

In pozzolanic test, maximum strength to pattern sample was 36.25MPa and for sample with glass was 21.63MPa. Relationship between these values indicates the material index as 59.67% and, as establishes ABNT , this index must be higher than 75% for a pozzolanic material. [8] performed a pozzolanic test according ASTM C311 with 20% of cement replacement by glass powder and obtained, for four different

*Corresponding author: amandacarolinemartin@gmail.com

glass samples, pozzolanic index around 70% to 74%, slightly lower than the minimum, but higher than what presented in this work.

Results presented indicate that glass milled used in this study isn´t a pozzolanic material, even with the composition according to ASTM, amorphous structure and small particle size, which could explain the small strength; as well the higher $CaCO_3$ content may adversely affect this result. So, in this work it wasn´t possible to use glass residue as a pozzolanic material to obtain mortar. In the other hand, further studies could be conducted in order to verify the possibility of use this waste as sand to obtain mortar.

4. References

[1] MEHTA, P. K.; MONTEIRO, P. J. M. **Concreto: microestrutura, propriedades e materiais.** São Paulo: Ibracon, 2 Ed., 2014. 751 p

[2] CINTRA, C. L. D.; PAIVA, A. E. M.; BALDO, J. B. Argamassas de revestimento para alvenaria contendo vermiculitaexpandida e agregados de borracha reciclada de pneus - Propriedades relevantes. **Cerâmica**, v. 60, p. 69-76, 2014.

[3] HERIYANTO;PAHLEVANI, F.; SAHAJWALLA, V. From waste glass to building materials e An innovative sustainable solution for waste glass. **Journal of Cleaner Production**, v. 191, p. 192-206, 2018.

[4] LU, J. X.; ZHAN, B. J.; DUAN, Z. H.; POON, C. S. Using glass powder to improve the durability of architectural mortar prepared with glass aggregates. **Materials and Design,** v. 135, p. 102-111, 2017.

[5] DOREMUS, R. H. **Glass Science**. John Wiley & Sons, 1994.

[6] GUTZOW, I.; SCHMELZER, J. **The Vitreous State: Thermodynamics, Structure, Rheology, and Crystallization.**Springer, 2013.

[7] TAN, K. H.; DU, H. Use of waste glass as sand in mortar: Part I – Fresh, mechanical and durability properties. **Cement & Concrete Composites.** v. 35, p. 109-117, 2013.

[8] SHI, C.; WU, Y., RIEFLER, C.; WANG, H. Characteristics and pozzolanic reactivity of glass powders. **Cement and Concrete Research.** v. 35, i. 5, p. 987-993, 2005.

Acknowledgments

The authors are grateful to CAPES and FAPESC for the financial support.

*Corresponding author: amandacarolinemartin@gmail.com

POWER CURVES OF SMALL WIND TURBINES INSIDE A LABORATORY WITH CONTROLLED EXHAUST FAN

Gustavo M. Franco[1]*, Joel Luiz da Rosa[1], Samuel Strelow[1], Henrique de Souza Medeiros[1]
[1]*Catholic University of Santa Catarina, Polytechnic School, Jaraguá do Sul, Brazil.*

1. Introduction

As the energy demand has been increased at the same time and proportion as the pollution, renewable energy sources has gained great attention, due their environmental friendly behavior, of the research groups and industries around the world. With the popularization of those sources, new wonderings about the performance's integrity and how to interpret the technical specifications came up. Based on that, wind energy appears as one of the most important of renewable sources. In Brazil, the wind farms, that produced only 0.2% of all the energy generated in 2007, reached 6.9% of the annual production in 2017, according to ONS (Operador Nacional do Sistema Elétrico). As reported by the organization, only wind and solar energy are increasing their participation on the national annual energy production. For that reasons, the comprehension and the search for improvements in the wind sector are needed, since in some cases, wind turbines can fail to reach the power specified by the manufacturers [1].

The Wind Turbines Tests Laboratory was created to explore and evaluate the power curves of small wind turbines. Those apparatus are mostly used on residential areas, therefore, it's important to create documents that are easy to non-expert people to understand. At the same time, all the data need to be well detailed, so the manufacturers can also have a good feedback of their product.

2. Experimental

At first, a laboratory arrangement was drawing in order to get the best position of the experiment (Fig. 1). The experimental apparatus (Fig. 2) is located at the Estudo e Desenvolvimento em Energias Renováveis Laboratory (EDER) at Catholic University of Santa Catarina. The experimental setup is composed by an exhaust fan (7.4 HP/six-pole) which is controlled by the CFW700 frequency inverter, both from WEG Company. The wind velocity is measured by two anemometer (Class 1 by NRG Systems) placed in front of and behind of the wind turbine (Notus 138 by Enersud).

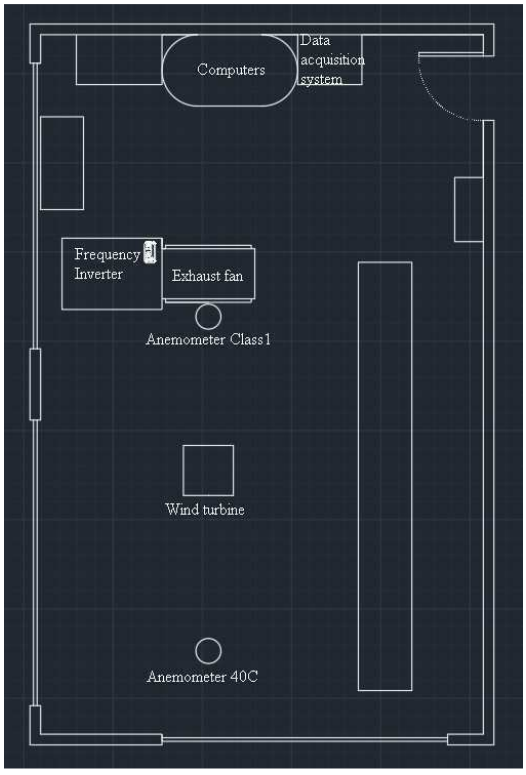

Fig. 1. *Design created for the laboratory of wind energy.*

Fig. 2. *Exhaust fan and the small wind turbine Notus 138.*

*Corresponding author: gustavo.franco@catolicasc.org.br

To collect the data and calculate the power generated, a small circuit was built, containing a current sensor (ACS712) and a voltage divider with three 560 ohms resistors, so the signal could be easier to read, since the data acquisition board used on the laboratory (NI USB-6008) tolerates the maximum of 10V, and the wind turbine has a nominal voltage of 12V. The voltage signals generated by the wind turbine and the current sensor are DC, and their both outputs were plugged in the analogical inputs of the USB-6008.

The data processing was made in the software LabVIEW, where the signals were filtered to eliminate the majority of the noise and were corrected with the offset and scale factor information given by the manufacturers. After that, all the samples were collected and placed in a table. Subsequently, this table was used to generate another table in the xlsx format, for the software Excel where the graphics were created.

For each power curve, a curve of power generated by available power on the wind (Fig. 4) was also generated using the KEF (kinetic energy flux) formula [2]:

$$KEF = \frac{A\rho V^3}{2} \ [W]$$

Where A is the swept area of the blades, ρ is the air density and V is the wind speed.

3. Results and Discussions

The wind turbine was placed in five different distances (1m, 1.5m, 2m, 2.5m and 3m) in front of the exhaust fan for the tests. Each test lasted 26 minutes, starting in 300 rpm up to 900 rpm. Every two minutes the speed was increased by 50 rpm, at the same time that the data acquisition system was collecting in the sample rate of 1sa/s. In total, each test had 1560 samples for each quantity and was done with a purely resistive load of 9.1Ω (will be reduced for future tests).

The results shown will be referring to the test of 2.5 m of distance between the exhaust fan and the small wind turbine. The first part is to analyze the power curve (Fig. 3):

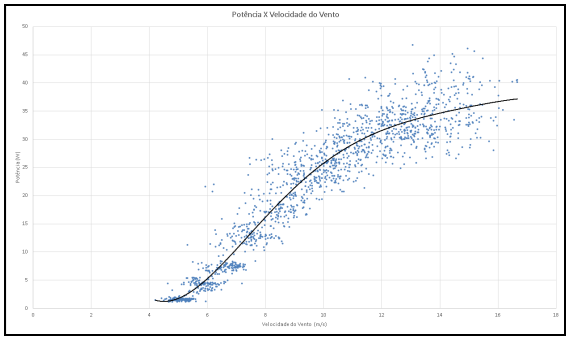

Fig. 3. *Power curve of the Enersud Notus138 small wind turbine.*

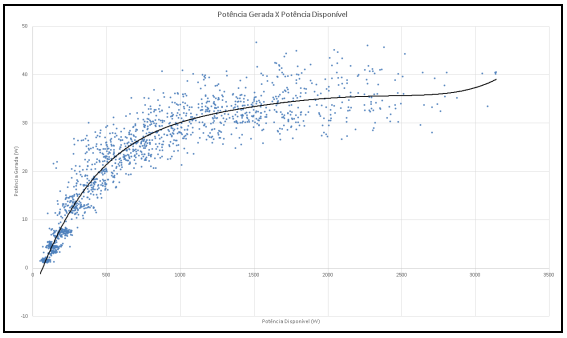

Fig. 4. *Curve of power generated by available power on the wind.*

The power curve of the distance of 2.5 m had the best distribution of data among all the others. After the speed of 10 m/s the power saturates, not having many more variations for higher speeds. It means that, it's not necessary to have a high wind speed for the wind turbine to approach its nominal power. Winds in the range of 5 m/s and 10 m/s cause intense variations in the power generated. In relation to the previous tests the generated power needed an available power higher, reaching 30 W of generated power having approximately 1000 W of available power.

The development of the laboratory is still progressing, as new equipment and structures are on the way, as a rail to improve the movement of the wind turbine and walls to be built around the exhaust fan-wind turbine system. The programming also had a big upgrade. Now the frequency inverter that controls the motor is connected to the computer, so the exhaust fan can be controlled in the software LabVIEW and the entire tests can be done automatically, without any human interaction from the beginning to the end.

4. References

[1] P. Gipe *"Testing the Power Curves of Small Wind Turbines"*, Wind-works, USA, (2000).
[2] R. W. Fox and A. T. McDonald, *"Introduction to Fluid Mechanics"*, 2th edition, John Wiley & Sons, Inc., USA, (2011).

Acknowledgments

*Corresponding author: gustavo.franco@catolicasc.org.br

The authors thank the University Center Católica de Santa Catarina, the professors involved and all the professionals that could help somehow.

*Corresponding author: gustavo.franco@catolicasc.org.br

MICROSTRUCTURAL CHARACTERIZATION OF BORIDE LAYERS ON VANADIS 10 TOOL STEEL – PRELIMINARY RESULTS

Anael Preman Krelling[1]*, Alexcier Krawczuk Capitani[1], Gabrielli Zavatini[1], Bruna de Freitas Zappelino[2], Elisangela Aparecida dos Santos de Almeida[2], Julio Cesar Giubilei Milan[2] and César Edil da Costa[2]
[1]*Instituto Federal de Ciência e Tecnologia de Santa Catarina – IFSC, Campus Joinville.*
[2]*Universidade do Estado de Santa Catarina – UDESC, Centro de Ciências Tecnológicas.*

1. Introduction

The use of surface treatment processes in engineering materials can improve their tribological properties, increase resistance to oxidation and corrosion, mechanical strength, among other factors [1]. In this sense, the boriding process is an alternative for the improvement of surface properties in ferrous and non-ferrous materials. Boriding is a thermochemical treatment in which boron atoms diffuse into the metal matrix. It is generally applied in the ferrous alloys to improve its surface hardness and wear resistance [2]. The boriding in steels typically occurs in the temperature range between 840 and 1050 ° C [3] and can be performed in a variety of media such as: powders, salts, fused oxides, gases and pastes [4]. The formation of a single-phase Fe_2B or biphasic layer, composed of Fe_2B (internal) + FeB (external) may occur. The Vanadis 10 tool steel is used in the manufacture of tools for cold forming processes and dies for powder metallurgy. This "family" of Cr-Mo-V cold work tool steel obtained by powder metallurgy was developed by Bohler-Uddeholm. As it is obtained through the technique of powder metallurgy, this steel has a more homogeneous microstructure compared to conventional steels [5]. The Vanadis 10 tool steel, despite its important application, has not been extensively studied by the scientific community. In recent years, some papers have been published on topics such as wear behavior [6], application of the Chemical Vapor Deposition (CVD) technique [7], wear behavior associated with Physical Vapor Deposition (PVD) [8], laser engraving [9] and influence of topography on the wear behavior [10]. However, it is not investigated the effect of the boriding treatment on the microstructure of the Vanadis 10 steel. Therefore, the aim of this work is to characterize the microstructure of borided layers formed on substrates of Vanadis 10 steel by powder-packed boriding treatment.

2. Experimental

Samples of Vanadis 10 tool steel, 20 mm in diameter and 15 mm in thickness, with a chemical composition of: 2.9 wt.% C, 0.5 wt.% Si, 0.5 wt.% Mn, 8.0 wt.% Cr, 1.5 wt.% Mo and 9.8 wt.% V, were sanded with SiC abrasive paper up to 600 grit, and polished with 1 μm alumina suspension before the boriding treatment. The powder-packed boriding treatments were carried out at 800 °C, 900 °C and 1000 °C for 6 hours. The samples were placed in a stainless steel container and covered with 15 mm of Ekabor 1-V2 boriding powder. After the treatment the samples were cooled in air. The morphology and stoichiometry of borides formed on steel surface were analyzed by Scanning Electron Microscopy (SEM) and X-ray Diffraction (XRD) analysis. The surface topography analysis was performed in a Leica DCM 3D confocal microscope at a magnification of 10x. Rockwell C indentation tests were used to evaluate the adhesion of the boride layers to the substrate according to VDI 3198 standard (see Fig. 1). The impression produced was analyzed by optical microscopy. HF1-HF4 represent sufficient adhesion whereas HF5 and HF6 show insufficient adhesion [11].

3. Results and Discussions

The XRD patterns for Vanadis 10 steel samples borided for 6 hours were shown in Fig. 2. Higher temperatures promote the formation of FeB phase. For an 800 °C temperature treatment there is a higher formation of Fe_2B boride phase. Despite the fact that there is no presence of Fe_2B in the diffractograms for 900 and 1000 °C it can be assumed that the formation of a dual layer (FeB + Fe_2B) takes place on Vanadis 10 tool steel [12]. The boride layers (Fig. 3) present a smooth morphology at the layer-substrate region. A high alloying element content typically leads to the formation of a thin and smooth interface of the boride layer with the substrate on ferrous alloys [13]. The boride layer thickness increase with an increase in the treatment temperature and reached 21.8 ± 1.8 μm for a 1000 °C boriding temperature. This result is in agreement with other works [3,14]. The boride layers adhesion to the substrate were classified from HF1 to HF5 for 800 °C and 900-1000 °C, respectively (Fig. 4). Only the presence of radial cracks was identified in Fig. 4(a). Figures 4(b) and 4(c) shows the presence of delamination areas, clear in (b) and dark in (c) owing to their small and high layer thicknesses, respectively. The adhesion of the boride layers decreased with the increase in boriding temperature due to the greater amount of FeB phase, which is more fragile than Fe_2B [14]. Finally, the surface roughness (*Ra* parameter) of the samples increased after the powder-packed

*Corresponding author: anael.krelling@ifsc.edu.br

boriding treatments up to 557%, for treatment temperature of 1000 °C, owing to the boride layer formation on the Vanadis 10 tool steel [15]. The increase in the roughness is associated with the formation of the initially disordered borided crystals formed over the steel surface that leads to a 16% increase in volume [12].

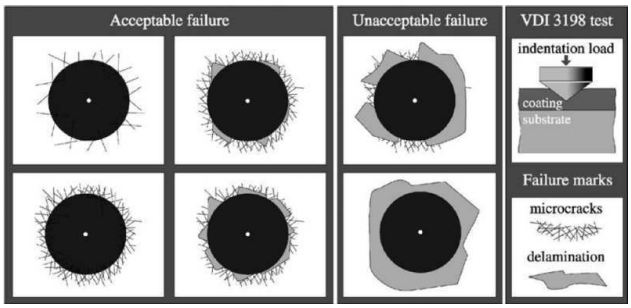

Fig. 1. *The principle of the VDI 3198indentation test* [11].

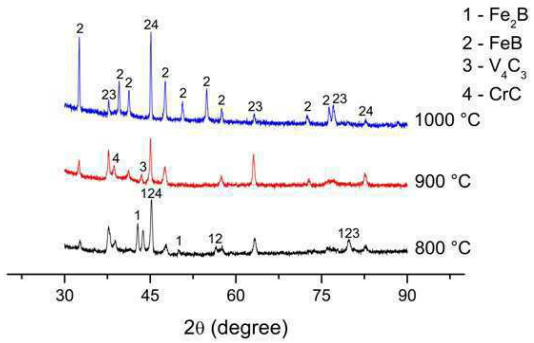

Fig. 2. *XRD patterns of Vanadis 10 steel samples borided for 6 hours.*

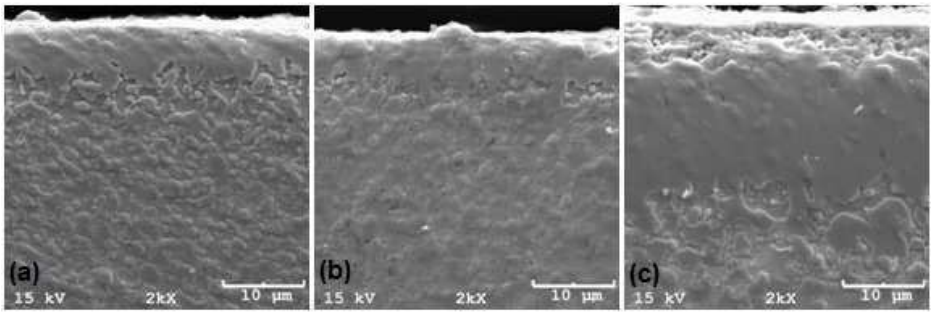

Fig. 3. *Boride layer thickness of 6 hours borided Vanadis 10 at: (a) 800 °C, (b) 900 °C and (c) 1000 °C.*

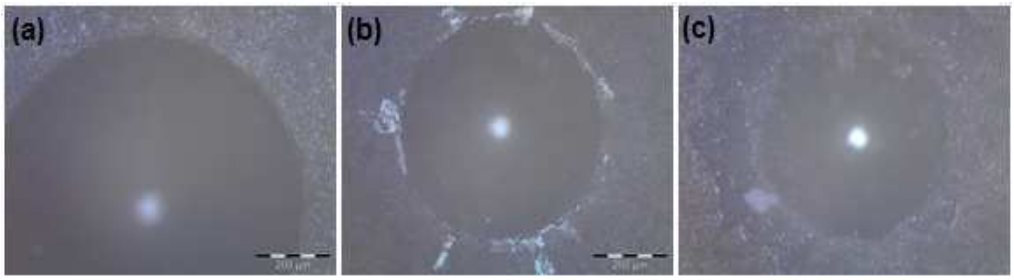

Fig. 4. *VDI test results of 6 hours borided Vanadis 10 at: (a) 800 °C, (b) 900 °C and (c) 1000 °C.*

4. References

[1] G. Kartal, et al., Surf. & Coat. Tech., **205**, 1578-1583, (2010).
[2] I. Campos, et al., Mat. Sci. Eng. A, **488**, 562-568, (2008).
[3] M. Béjar and E. Moreno, J. Mat. Proc. Tech., **173**, 352-358, (2006).
[4] S. Sahin, J. Mat. Proc. Tech., **209**, 1736-1741, (2009).
[5] J. Sobotová, P. Jurci and I. Dlouhy, Mat. Sci. Eng. A, **652**, 192-204, (2016).
[6] A. Määttä, P. Vuoristo and T. Mäntylä, Trib. Int., **34**, 779-786, (2001).
[7] F.J.G. Silva, et al., Diam. Relat. Mat., **11**, 1617-1622, (2002).
[8] M. Olsson and U. Bexell, Wear, **271**, 1903-1908, (2011).
[9] S. Kasman, Measur. **46**, 2577-2584, (2013).
[10] N.S. Nosar and M. Olsson, Wear **303**, 30-39, (2013).
[11] N. Vidakis, A. Antoniadis and N. Bilalis, J. Mat. Proc. Tech., **143-144**, 481-485, (2003).
[12] C. Martini, G. Palombarini and M. Carbucicchio, J. Mat. Sci., **39**, 933-937, (2004).
[13] R.S. Petrova, N. Suwattananont and V. Samardzic, J. Mat. Eng. Perform., **17**, 340-345, (2008).
[14] S. Taktak, Mat. & Des., **28**, 1836-1843, (2007).
[15] A.P. Krelling, et al., Trib. Int., **111**, 234-242, (2017).

Acknowledgments

*Corresponding author: anael.krelling@ifsc.edu.br

The authors would like to acknowledge financial support from CNPq, IFSC and UDESC.

*Corresponding author: anael.krelling@ifsc.edu.br

ELECTROCHEMICAL CHARACTERIZATION IN SOLUTION OF A FERTILIZER MIXTURE FOR PLASMA DEPOSITED TITANIUM OXIDE FILMS IN ASTM A36 STRUCTURAL STEELS WITH THE USE OF CATHODIC CAGE

Donatti G. P. [1] ; M,Margon A. A.[1], Pimentel B. P[1]; Gonçalves T.M.[1], Gontijo L. C.[!]
[1] *Instituto Federal do Espírito Santo*

1. Introducion

As grow the speed of technological development, many materials have been or are being developed to meet the needs of the various industrial sectors. Among these processes of continuous improvement, thin films applications have been tested in several researches as an alternative in the increase of resistance to corrosion and erosion due to the passivity of the elements deposited in austenitic stainless steels and in steels with low carbon content, both widely used in the chemical industry or for the production of various equipment.

2. Experimental

Test specimens of an ASTM A36 steel in the dimensions of 30x20 mm were made. These were sanded and polished until a mirrored surface was obtained. One of specimens did not undergo further treatments and was used as the standard sample to serve as a basis for comparison to the others. The samples were setted on the SDS-brand pulsed arc plasma reactor for treatment of Ti cation cathode deposition, grade II of purity, for deposition of the thin film of TixH. The deposition temperature was set at 260 ° C, the time in four hours and the gas mixture in 100% H2, and the pressure at 0.8 torr. Linear polarization tests were carried out in these samples, along with thickness measurements of these films in a confocal microscope and nanohardness measurements.

3. Results and Discussions

In the nanohardness tests, all measurements collected from the treated sample obtained an increase in their Vickers hardness, when compared to the untreated surface, with an average hardness of 254.6 Vickers in the deposited film and in the non-deposited matrix of 188.8 Vickers. In then Polarization Tafel Plots tests it is possible to identify that the deposited film presented a gain of passivation due to its oxide layer, suffering corrosion more slowly between -0.6V and -0.3V, due to the gains of less proportional variation of current density, being still It was possible to identify a uniform or generalized corrosion in the matrix in A36 and for the sample with deposition of thin film of titanium, a characteristic of corrosion in plates was observed. Using the confocal, it was posible to obtain the thickness of the film deposited in glass slide, average of 247.37 nm for the studied deposition process.

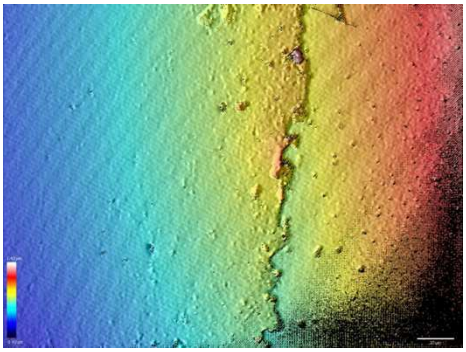

Fig. 1. *Step observed on the side of the deposited glass sample.*

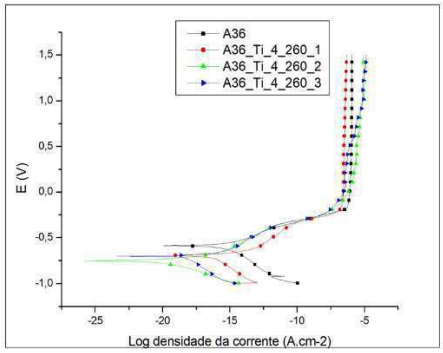

Fig. 2. *Experimental Tafel polarization plot of the matrix and the sample with titanium film. Potential (V) versus the logarithm of current density (A.cm^2).*

4. References

[1]- JONES, D.A. **Principles and Prevention of Corrosion**. Department of Chemical and Metallurgical Engineering, University of Nevada, Reno. Macmillan Publishing Company, New York, US, 1992.
[2] - QUINN Rod K; Armstrog Neal R., **Eletrochemical and surface analytical characterization of titanium and titanium hydride thin film electrode oxidation**. The Electrochemical Society, Nov. 1978.

*Corresponding author: pleooog@gmail.com

*Corresponding author: pleooog@gmail.com

INFLUENCE OF THE ADDITION OF BY-PRODUCTS OF THE VINYL INDUSTRY IN THE PROPERTIES OF THE BIODEGRADABLE POLYMER POLY (LACTIC ACID)

Laísa Cristina Klemann[1]*, Paula Sacchelli Pacheco[2]*, Wagner Mauricio Pachekoski[3], Derce de Oliveira Souza Recouvreux[4], Daniela Becker[5]

[1,2,3,4] *UFSC- Universidade Federal De Santa Catarina, Programa de Pós Graduação em Engenharia e Ciências Mecânicas . Joinville, Santa Catarina, Brazil.*

[5] *UDESC- Universidade Estadual De Santa Catarina, Programa de Pós Graduação em Ciências e Engenharia de Materiais- Joinville, Santa Catarina, Brazil.*

1. Introduction

Poly (lactic acid) (PLA) is a polymer that has great potential for applications in several areas, mainly due to its biodegradability. Despite its versatility, PLA presents some limitations such as its degradation during processing leading to a reduction in the mechanical properties of the material. During the processing of the material a rapid breaking of polymer chains and the consequent reduction of the molar mass can occur, directly affecting the properties of the polymer, reducing, for example, the mechanical resistance and causing the thermal degradation. Wine residue is an agroindustrial compound characterized by its high amount of polyphenols (natural antioxidant), adding value to the production of biomaterials. In this work, by-products of the wine industry such as waste and grape flour were added to the PLA in order to quantify the changes in property of the material when related to pure PLA. For this, thin films containing PLA with wine residue (WV) and grape flour (GF) in different compositions were prepared and analyzed.

2. Experimental

The grape flour and wine residue used were, respectively, the company "Cantinho da Saúde" in Gramado, Rio Grande and the wine industry in the city of Antônio Prado, also located in the same state. It is noteworthy that the residue of wine came from the Bordeaux grape. Both materials were oven dried at controlled temperature and then added to the PLA. The PLA was obtained by spinning the Ingeo 3251D from NatureWorks®. The mixture was made by an internal chamber mixer coupled to a torque rheometer (Thermo Scientific Haake Rheomix 600) equipped with roller type mixing rotors at UDESC (Santa Catarina State University).The conditions were 100 rpm, 6 minutes and 175 ° C. The dosage of wine residue and grape flour to PLA occurred in the proportions of 1, 2, 5 and 10% of residue and flour to the polymer. After rheometer processing, the material passed through the grinding process in a knife mill at the State University of Santa Catarina and pressed in the form of thin films. The pressing process took place under the following conditions, a pressing time of 30 seconds with an applied force of half a ton at a temperature of 180 ° C. After this process, the films were characterized.

3. Results and Discussions

The thermogravimetric curve of the pure PLA shows the occurrence of 3 thermal events, at 100ºC, 312ºC and 328ºC. The first event, at 100 ° C, the result showed occurred a mass loss of 0.4%; this loss may be associated with loss of moisture from the PLA. At 312 ° C, a 49% mass loss occurred due to the degradation of poly (lactic acid) chains with less molar mass resulting from thermal degradation during the above extrusion and pressing processes. In the third thermal event, the mass loss of 75% can be associated to the main thermal degradation event of poly (lactic acid), which continues until the temperature of 343ºC. After that temperature, 2% residual mass observed, which remains constant until the end temperature of the test at 600ºC [1]. In Figure 1, where thermal events associated to each sample reported, mixtures with 1% and 2% of WR and 1% of GF in PLA show an increase in the thermal degradation temperature of poly (lactic acid), suggesting an increase in the thermal stability of the biodegradable polymer. This process due to the phenomena that occur due to the phenolic compounds present in the wine residue, capable of improving the thermal stability of aliphatic polyesters during processing. Moreover, the addition of phenol-based compounds when applied to biodegradable polymers increases their thermal stability and their processing capacity [2, 3].

*Corresponding author: paula.sacchelli@gmail.com

	T_{onset} (ºC)	T_{endset} (ºC)	DTG (ºC)
PLA	277	343	328
1% WR	294	348	329
1% GF	322	346	347
2% WR	307	347	335
2% GF	311	350	338
5% WR	293	332	320
5% GF	308	349	337
10% WR	289	319	310
10% GF	289	324	308

Fig. 1. *Degradation Temperatures*

The evaluation of the morphology of the cryogenic fracture surface was performed using scanning electron microscopy analysis in the Jeol JSM 6701F (UDESC-CCT) equipment, with a maximum amperage of 10μA and varied increases. The determination of the dispersed phase diameter was performed by measuring approximately 200 domains of each sample using Image J. software. The scanning electron microscopy analyzes of the PLA mixture with WV containing 2% found some entanglements of particles that may have arisen by the mixing technique used. The rheometer may have not completely mixed the residue to the polymer. In this immiscibility (Fig. 2), it can be observed that approximate spherical domains are found in the PLA matrix (Fig. 3), in which found particles in the scale of 1μm referring to the wine residue. In addition, in the PLA sample with WV it is possible to verify that the particles had a good adhesion to the polymer obtaining no holes or gaps between the particles with the matrix. Pure PLA has a smooth and continuous fracture surface, indicating a brittle fracture behavior that corresponds to its low elongation value [4]. This surface shape was found during the micrographs and showed that there was no change the roughness of the polymer with the addition of wine residue. Regarding the sample, containing PLA with GF containing 1%, the analysis showed a continuous surface with no fractures (Fig. 4). It can be noticed the presence of spherical particles dispersed in the PLA matrix besides voids of plucking, characterizing a lack of adhesion between the phases (Fig. 5). Involvement of the particle with the polymer by extrusion without any chemical coupling may be the reason for these observations.

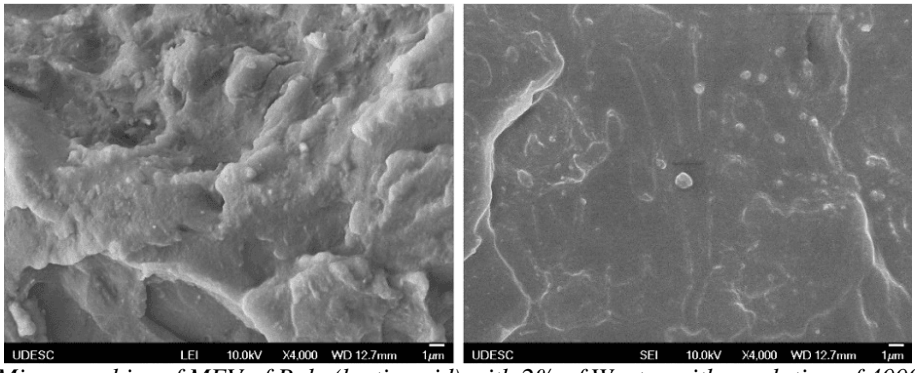

Fig.2. *Micrographies of MEV of Poly (lactic acid) with 2% of Wastes with resolution of 4000x.*

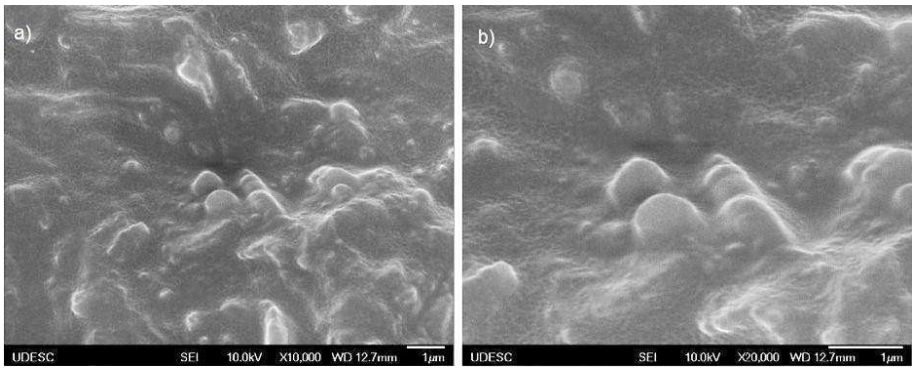

Fig.3. *MEV of Poly (lactic acid) with 2% of Winery Residue with a resolution of a) 10000x and b) 20000x.*

*Corresponding author: paula.sacchelli@gmail.com

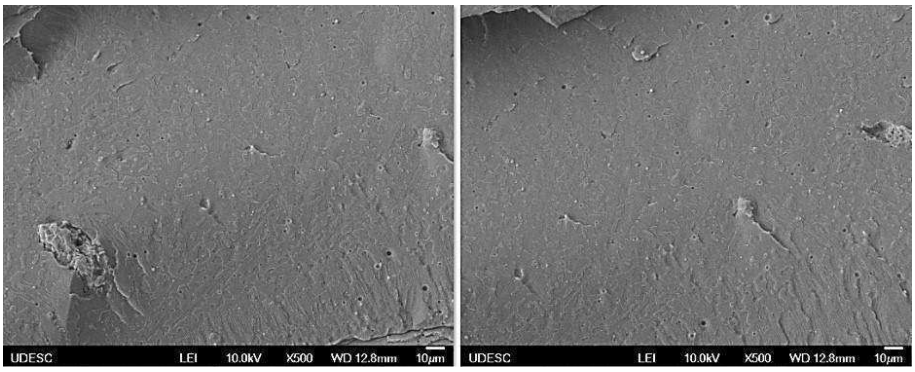

Fig.4. *MEV of the Poly (lactic acid) with 1% of Grape Flour with resolution of 500x.*

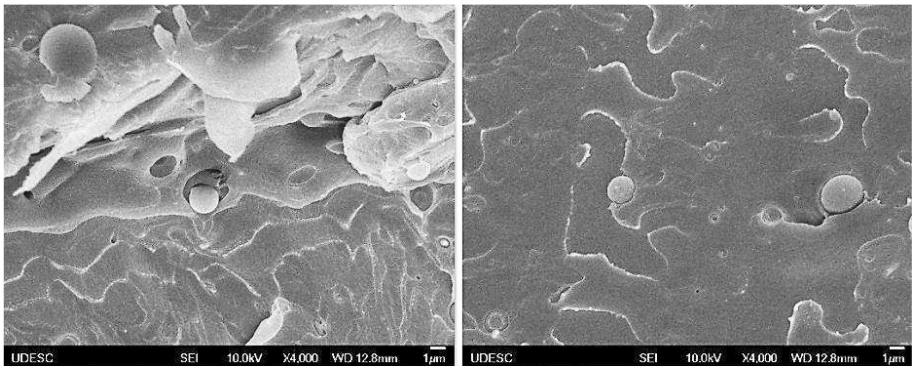

Fig.5. *MEV of the Poly (lactic acid) with 1% of Grape Flour with resolution of 4000x.*

4. References

[1] CHEN, C.; CHUEH, J.; TSENG, H.; HUANG, H.; LEE, S. **Preparation and characterization of biodergadable PLA polymeric blend.** Biomaterials, v. 24, n. 1, p. 1167-1173, 2003.

[2] MALINCONICO, M.; CERRUTI, P.; SANTAGATA, G.; IMMIRZI, B. **Natural polymers and additives in commodity and specialty applications: A challenge for the chemistry of future**. Macromol. Symp., v. 337, p. 124-133, 2014.

[3] MOUSAVIOUN, P.; GEORGE, G.; DOHERTY, W. **Environmental degration of lignina/poly(hydroxybutyrate) blends.** Queensland University of Technology, Australia, 2012.

[4] BUCKNALL, C. B.; PAUL, D.R. **Notched impact behavior of polymer blends: Part 1: New model for particle size dependence.** Elsevier, n. 50, p. 5539 – 5548, 2009.

*Corresponding author: paula.sacchelli@gmail.com

SYNTHESIS AND CHARACTERIZATION OF COMPOUNDS NiO-BaCe0.2Zr0.7Y0.1O3-δ IN ANODE FOR SOLID OXIDE COMBUSTIBLE CELL

Paula Sacchelli Pacheco [1]* Adilson Luiz Chinelatto[2], Wagner Mauricio Pachekoski[3]
[1,2]*UEPG- Universidade Estadual De Ponta Grossa, Departamento de Engenharia de Materiais.*
[1,3] *UFSC- Universidade Federal De Santa Catarina, Programa de Pós Graduação em Engenharia e Ciências Mecânicas*

1. Introduction

Proton fuel cells (PCFC) are electrochemical devices capable of converting chemical energy into electrical energy with high efficiency and low emission of pollutants. The structure of PCFC composed by the electrodes that divided in a cathode and an anode and an electrolyte. In this type of cell, the proton is the charge carrier causing the operating temperature to occur at intermediate temperatures (600 and 800ºC). The functioning of these cells is very similar to that of the Solid oxide full cell (SOFCs), the difference is that the conduction happens through protons and the formation of water occurs at the cathode, preventing the dilution of the fuel during the operation of the cell. For an efficient functioning of the PCFC, the anode plays a fundamental role since hydrogen oxidized at the anode; the materials for the anode composition of fuel cells based on a cermet, which consists of a metallic phase, and a ceramic matrix conducting ions. In this work, it was proposed made a compound BCZY doped whit a nickel oxide , in order to obtain a compound NiO-BaCe0.2Zr0.7Y0.1O3-δ and to investigate if its application in anode for proton fuel cells is viable. For this, the compositions was be done whit through the Pechini method.

2. Experimental

The resins that originated perovskite BaCe0.2Zr0.7Y0.1O3-δ (BCZY) were prepared based on the Pechini method. The calcination occurred at 350 ° C for 3h to eliminate part of the organic phases and again calcined at 900 ° C to form the desired phase. Doping with nickel oxide occurred in a ratio of 3 g of BCZY to 2g of Nickel Oxide, by mass in a ratio of 60% of BCZY to 40% of NiO. The samples where pressed and sintered.

3. Results and Discussions

The micrographs observed with secondary electrons and backscattered electrons (Fig. 1 and 2, respectively) for the fractured sample it presented him presence of porosity in the pastille. The larger grains with regular forms and smoother surfaces showed a lighter shade of gray while the smaller crystals with irregular surfaces have a darker shade of gray. This difference in the colors of the grains indicates that they have a morphological difference besides a difference in the composition, where one phase formed by BCZY and another by NiO, as indicated by the red arrows in the figure.

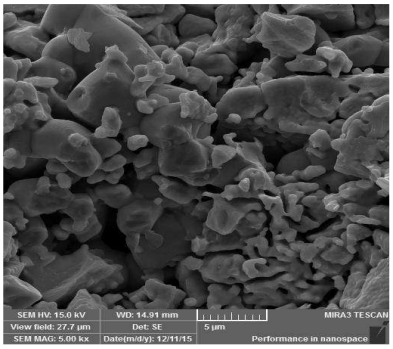

Fig. 1. *Micrographs of the fractured sample observed with secondary electrons.*

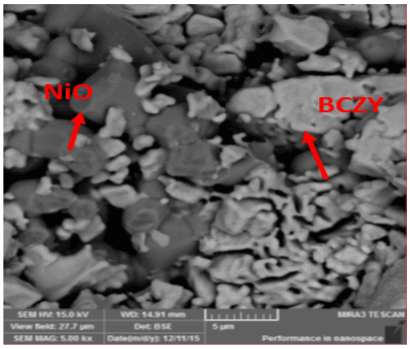

Fig. 2. *Micrographs of the fractured sample observed with backscattered electrons.*

For the polished sample (Fig. 3), the microscopy shows a porous material, a necessary condition to help diffusion of the gas at the anode [1, 2]. Beyond the light gray areas (BCZY ceramic phase) and the dark gray regions (nickel oxide phase) we can see that the nickel oxide phase was distributed to the occurred the percolation in the matrix phase (BY phase). Percolation is a necessary condition for an electronic conductivity to occur through this phase [3]. This percolation of the NiO phase is observe in figure 4. The presence of nickel in cermet is very important, the nickel phase increases both the electronic conductivity and the mechanical stability of this compound [1]. The microstructures show that formation of the desired compound occurred.

*Corresponding author: paula.sacchelli@gmail.com

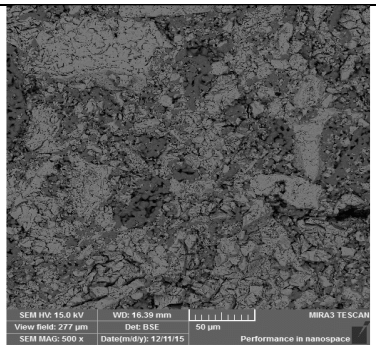

Fig. 3. *Micrographs of the fractured sample observed with secondary electrons.*

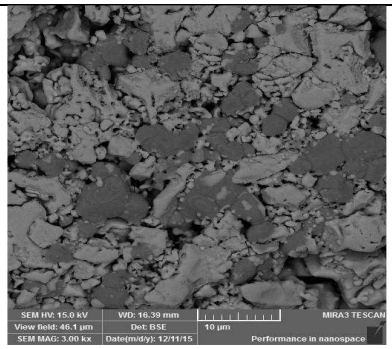

Fig.4. *Micrographs of the polished sample observed with backscattered electrons.*

The electrical characterization was performer by impedance spectroscopy. In this figure, we can observe the total conductivity measurements in function of the temperature for the two samples, to the compound NiO-BCZY (anode), and the compound BCZY doped with the ZnO (electrolyte) (Fig. 5). These samples of ZnO doped BCZY were not produced in this work and are represented in this analyze only as a counterpart between the material for the anode and the electrolyte material. At these results, the important aspects are the effects are the conductivity at 600ºC and the activation energy. These materials are studies to work in PCFC and must therefore have a conductivity in humid atmosphere greater than 10-2 (S.cm-1) at the operating temperature (600 ° C) The NiO-BCZY showed a conductivity of 1.43x10-3 (S.cm-1), even with Ni in the oxidized state and measured in air atmosphere. Although the value determined is below what is necessary, it is import to consider that the measurement occurred in atmospheric air and not in humid air. When compared to the conductivity of the electrolyte, the compound presented a lower conductivity, which explained by the presence of NiO, which is a phase less conductor than the BCZY [4]. The activation energy for the compound was 0.6 eV, while that observed for the electrolyte was 0.4 eV. These results show that these materials are promising for the applicability in fuel cells [4, 5].

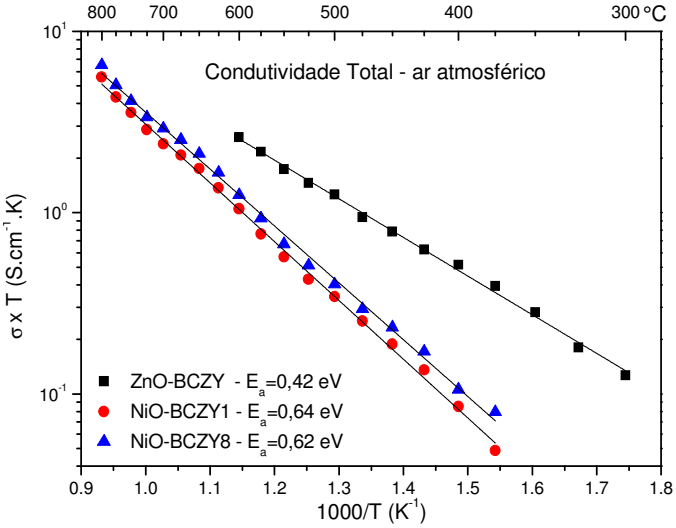

Fig. 5. *Temperature versus conductivity of ZnO-BCZY, NiO-BCZY1 and NiO-BCZY1 samples.*

4. References

[1] NASANI. N; RAMASAMY.D. et al. Fabrication and electrochemical performance of a stable, anode supported thin BaCe0.4Zr0.4Y0.2O3-d electrolyte PCFC. **Journal of Power Sources**. Vol, 278. Ano, 2015. P, 582-589, 2014.

[2] BARISON, S; DOUBOVA, L; SANSON, A. **Sputtering Deposition of BCZY Proton Conducting Electrolytes.** European Solid Oxide Fuell Cell Forum, Lucerna, july 2010.

[3] LEE. S; PARK. I; LEE. H; SHIN. D. Continuously Gradient Anode Functional Layer for BCZY Based Proton-Conduting Fuel Cells. **International Journal oh Hydrogen Energy.** vol,39. p.14342-14348., 2014.

[4] NASANI. N; RAMASAMY.D; ANTUNES. I; PEREZ. J; FAGG.D.P. Electrochemical behaviour of Ni-BZO and Ni-BZY cermeto anodes for Protonic Ceramic Fuel Cells (PCFCs) - A comparative study **Electrochimica ACTA**. December 2014.

[5] LUI, M; DING, D. SUN, W; LUI, M. High-performance NieBaZr0.1Ce0.7Y0.1Yb0.1O3-$_{\delta}$ (BZCYYb) membranes for hydrogen separation. **International Journal of Hydrogen Energy.** Year, 2013.

*Corresponding author: paula.sacchelli@gmail.com

EFFECTS OF NITRIDING AND DEPOSITION OF TITANIUM NITRIDE FILM THROUGH CATHODIC CAGE IN THE RESISTANCE TO STEEL TYPE API 5L X70 CORROSION

Margon A. A.[1] Pimentel B. P[1]; Gonçalves T.M.[1], Donatti G. P.[1], Carvalho C. S.[1], Gontijo L. C.[1]
[1] Instituto Federal do Espírito Santo

1. Introducion

The expansion of the pipeline network in Brazil demands improvement of the material properties of the pipelines to increase the transportation of resources at lower costs and with greater reliability. With increasing technological demand in the area of surface engineering, the use of thin film deposition and nitriding techniques can be seen as a solution to increase the useful life of components that are in conditions of mechanical stresses and environments susceptible to corrosion. In the present work will be studied the improvements that can be obtained in surface mechanical properties in API 5L X70 steel pipes, as well as the possible improvements in the resistance to corrosion and wear by techniques of nitriding and thin film deposition of titanium nitride with cathodic cage.

2. Experimental

The API 5L X70 pipeline steel was sectioned by waterjet cutter to remove 20 x 20 mm samples which were sanded and polished until a mirrored surface was obtained. Among these specimens obtained, one of them received no treatment and was used as standard pattern to serve as a basis of comparison for the others. Four samples were placed in the SDS-branded pulsed arc plasma reactor to nitriding treatment, two inside a cathodic cage of stainless steel, in suspended potential, to reduce edge effect and two were placed directly on the cathode. The nitriding temperature was set at 400ºC, the time at 4 hours and the gas mixture was maintained at 25% H_2 and 75% N_2 under a pressure of 2,5 torr. After nitriding, one sample was withdrawn of cathodic cage and another was withdrawn of the cathode (without insulation) to that samples could be analyzed. The two remaining speciemens were returned to the reactor with a third sample that received no treatment inside of cages of Ti, degree II of purity, so that there was a deposition of TixN Thin Film. The deposition temperature was set at 200 °C, the time at 3 hours, the gas mixture was fixed in 13% N_2 and 87% H_2, and the pressure at 0.8 torr.

3. Results and Discussions

By X-ray diffraction it has been observed a characteristic peak displacements of plasma nitrided samples and peak of FexNy formation, evidencing that there was modification of the surface with addition and possible saturation of the surface with nitrogen. Concerning to deposition, the dispersive energy testing of electrons made in a scanning electron microscope show the formation of titanium-containing compounds and measurements carried out on a 3- D confocal Microscope of the Leica brand show films of the order of 111 nanometers.

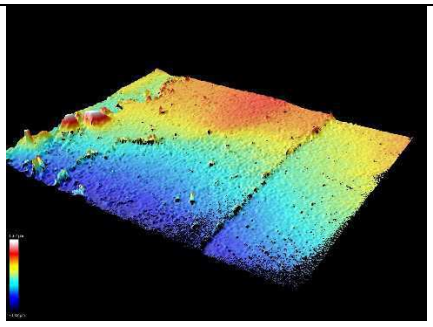

Fig. 1. *Picture showing the deposited thin film.*

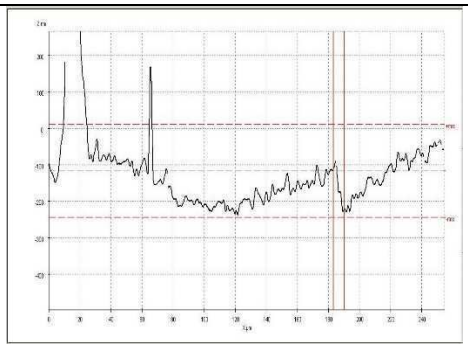

Fig. 2. *Picture of perfilometria showing the thin film step*

Referências

[1] - L. C. Gontijo, A.G. Cunha, P.A.P. Nascentec, Materials Science and Engineering B 177 (2012) 1783.
[2] - Daudt, N. F.; Barbosa, J. C. P.; Braz, D. C.; Pereira, M. B.; Alves Jr., C. TiN thin film deposition by cathodic cage discharge: effect of cage configuration and active species. Journal of Physics: Conference Series 406 012021, 2012.
[3] - Spies, H. J. Et Al. Adhesion And Wear-Resistance Of Nitrided And Tin-Coated Low-Alloy Steels. Surface & Coatings Technology, V. 74-5, N. 1-3, P. 178-182, Sep 1995.
[4] - Meriem-Benziane, M.; Bou-Said, B.; Boudouani, N. The effect of crude oil in the pipeline corrosion by the naphthenic acid and the sulfur: A numerical approach. **Journal of Petroleum Science and Engineering,** v. 158, p. 672-679, Sep 2017. ISSN 0920-4105.

USE OF DIFFERENT PROPORTIONS OF HYDROGEN AND ACETYLENE FOR PRODUCTION OF THIN FILMS BY PECVD

L. G. Heinig[1]*, J. Rodrigo da Costa[2], R. A. de Simone Zanon[3], J. M. Pureza[4]
[1]*Centro Universitário Leonardo da Vinci - UNIASSELVI*
[2]*EEM Deputado Nagib Zattar*
[3]*Universidade do Estado de Santa Catarina – UDESC, Departamento de Física*
[3]*Universidade do Estado de Santa Catarina – UDESC, Departamento de Engenharia Mecânica*

1. Introduction

Thin films are commonly deposited on materials surface to enhance or add properties, allowing use in different applications. However, the film characteristics are very sensitive to changes in parameters such as deposition pressure, substrate temperature, proportion of the gases. So, the main objective of our research is to produce films under different conditions and evaluate the changes in terms of structure, surface characteristics, mechanical and optical properties.

In this work, thin carbon films were grown in a PECVD – plasma enhanced chemical vapor deposition chamber under different acetylene and hydrogen proportions, while other parameters such as total pressure, deposition time, temperature and applied voltage materials were kept fixed. The analysis of the spectra generated by Raman spectroscopy showed intensity and position of D and G bands indicated specific degrees of structural and topological disorder. The contact angle data allowed to observe wetting dependence with the proportion of acetylene, resulting in films with hydrophilic characteristics. From the confocal microscopy data, roughness results were obtained, whereas the scanning electron microscopy analysis indicated the formation of granules and agglomerates on the surface of the film.

2. Experimental

The equipment used for deposition of the films by the PECVD technique [1] allows to grow films of hydrogenated amorphous carbon from the ionization of precursor gases in the reactor, through the electric discharge between two electrodes positioned parallel in the horizontal. The samples were fixed to the substrate holder, the chamber sealed, the system was evacuated by the mechanical pump, reaching a pressure of 2.4 x 10^{-2} Torr (3.20 Pa), and then the diffuser pump was turned on reducing the pressure to 1.6×10^{-5} Torr (2.1×10^{-3}Pa). The heating system was connected using a spiral resistor inside the substrate holder. The power supply to generate electric current of 1.6 Ampère, so that the sample port reached a temperature of approximately 200°C. After these procedures for evacuation and heating, it is necessary to wait about 4 hours for the system to stabilize, allowing the beginning of the deposition process.

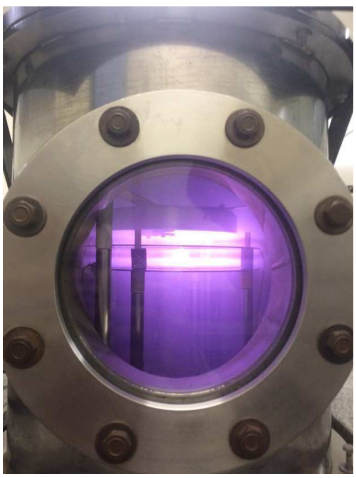

Fig. 1. *Deposition via PECVD using argon, hydrogen and acetylene. Source: Authors.*

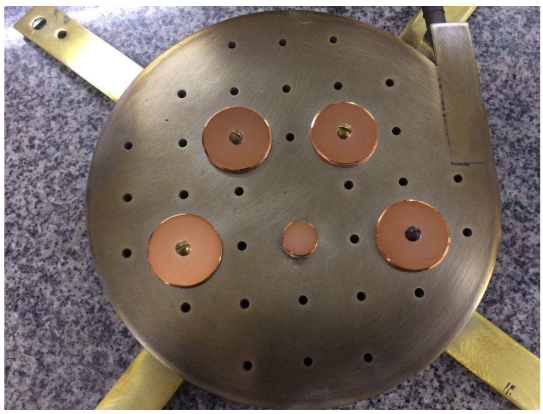

Fig. 2. *Condition of the fixed substrates in the sample port after deposition. Source: Authors.*

The gases, argon and hydrogen, are released under a 600V potential difference between the electrodes, to generate and maintain the plasma. After 10 minutes cleaning is done and the acetylene flow is opened until the desired total pressure is reached, so deposition occurs for 5 minutes. Figure 1 shows the

*Corresponding author: lianagh@gmail.com jaison.rodrigo@hotmail.com

appearance of plasma in a deposition with the carbonaceous precursor acetylene and Figure 2 shows the substrates after deposition.

3. Results and Discussions

The investigation of the structure of the films was fundamentally based on the Raman spectra, in which four samples were selected, deposited under different proportions of the hydrogen and acetylene gases. Table 1 shows the difference between the films that were deposited in an atmosphere of 40% Argon with different proportions of acetylene and hydrogen.

Sample	1	2	3	4
Argon	40%	40%	40%	40%
Acetylene	30%	35%	40%	50%
Hydrogen	30%	25%	20%	10%

From the results obtained by Raman spectroscopy for samples 1, 2, 3 and 4, regardless of the acetylene ratio, the shape of the material was not altered. The results point to a general behavior in which the carbon films formed have graphitic characteristics. Figure 1 and 3 shows two different spectra of samples 1 and 3.

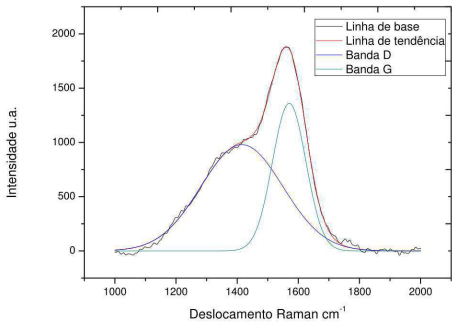

Fig. 3. *Adjustment of sample 01, with a ratio of 40% Ar, 30% C_2H_2 and 30% H_2. Source: Authors.*

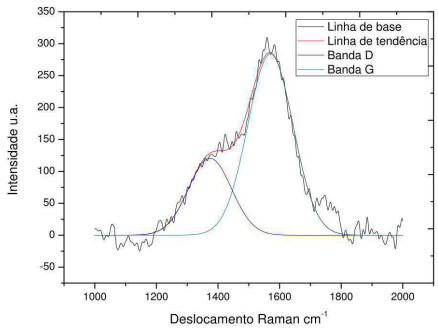

Fig. 4. *Adjustment of sample 03, with a proportion of 40% Ar, 50% C_2H_2 and 10% H_2. Source: Authors.*

G-band peaks around 1580 cm^{-1} have a more graphitic character and the D-band peaks are related to the system disorder [2]. The disorder related to the D-band corresponds to the vibrations of the "breathing" mode of the rings. Most of the cluttered carbons remain dominated by the graphite G and D modes, although they do not present graphitic ordering to derive the structural information from the DLC and the respective sp^3 fractions [3].

4. References

[1] J. F. Fragalli "*Produção e Caracterização de Filmes Finos de Silício Amorfo Hidrogenado Por Descarga Luminescente a 60Hz*" Doctorate Thesis, Institute of Physics - Universidade de São Paulo, 1994.
[2] M.S. Dresselhaus et al, Physics Reports **409**, 47-99 (2005).
[3] C. Casiraghi, A. C. Ferrari, J. Robertson. Physical Review B, **72**, 385 (2005).

Acknowledgments

Thanks to Professor Mônica de Mesquita Lacerda for the contributions in the work.

*Corresponding author: lianagh@gmail.com jaison.rodrigo@hotmail.com

ANALYSIS OF GLASS AND CLAY POWDER USING LASER DIFFRACTION

A. R. Bigansolli[1]*, L. A. Franco[1], B. B. Lima-Kuhn[1] and T.Y.A. Souza[2]
[1]*Departamento de Engenharia Química, Instituto de Tecnologia, UFRRJ, Seropédica, RJ.*
[2]*Departamento de Artes, Instituto de Ciências Humanas e Sociais, UFRRJ, Seropédica, RJ.*

1. Introduction

The red ceramics is a product of prominence in the civil construction being a material where can be incorporated several types of residues, among these, the glass has been used [1-2]. The glass has a good chemical compatibility with clay, the incorporation helps in the sintering by liquid phase and consequently reduces the energy cost [3]. The present work has the objective of characterizing the glass and the yellow clay by laser diffraction particle sizer analyzer, boths will be used as raw material in the future to obtain a ceramic mass.

2. Experimental

The glass samples were from Ambev and the yellow clay was provided by Curso de Belas Artes / UFRRJ. The clay after submitted to the drying process for 3 hours in the electric oven stove laboratory was grinded in the hammer mill and then comminuted in a porcelain mortar, then all material sieved to below 250 mesh screen. The glass bottle was washed for removal of the labels end then the glass bottle was fragmented to obtain pieces of reduced size. The pieces was then high-energy milled using a Retsch PM100 planetary ball mill. The milling was performed at the speed of 300 rpm for 8 minutes with inversion for 4 minutes. The size distribution of powder was measured using a laser diffraction particle sizer analyzer (Mastersizer 2000. Malvern).

3. Results and Discussions

Fig. 1 and Fig 2 show the particle size distribution for clay and glass, respectively. The Sauter diameter of 3,614 μm for clay and 8,388 μm for the glass were measured.

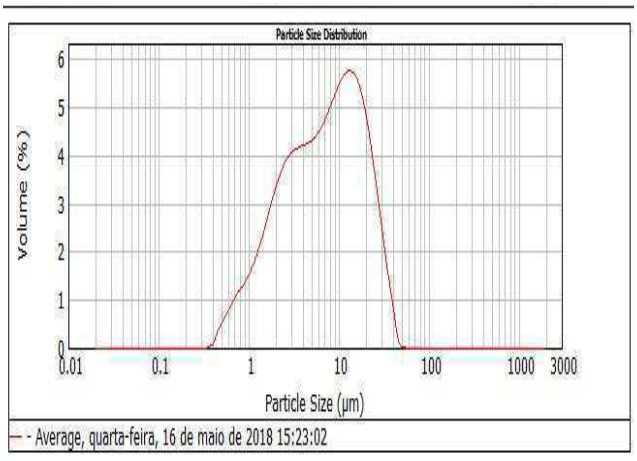

Fig. 1. *Particle size distribution of yellow clay sample.*

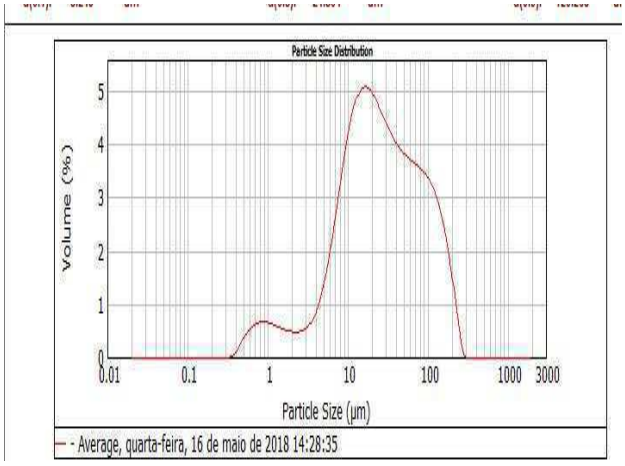

Fig. 2. *Particle size distribution of class sample.*

4. References

[1] K. O. Godinho, J. N. F. Holanda, A. G. P da Silva, Cerâmica, 51, 419-427, (2005).
[2] A. Zaccaron, G A. Benedet, F. Rosso, V. S. Nandi, P. Fernandes, A. M. Bernardin, R. Piccoli, Incorporação de vidro na composição da massa de cerâmica vermelha como valoração de resíduo, In: 7º Fórum Internacional de Resíduos Sólidos, 2016, Porto Alegre, RS. Anais do 7FIRS - Fórum Internacional de Resíduos Sólidos, 1-7, (2016).
[3] G. M. DIAS, Produção e caracterização de espuma de vidro para isolante térmico. Congresso Brasileiro de Engenharia e Ciência dos Materiais, Cuiabá. 1553-1560, (2014).

*Corresponding author: bigansolli.arb@gmail.com

CHARACTERIZATION OF Ti-Al FILMS OBTAINED BY ASYMMETRIC PULSED MAGNETRON SPUTTERING

Deivison Daros Paim [1]*, Abel André Cândido Recco[1], Luiz Cesar Fontana[1]
[1]*Laboratory of Plasmas, Films, and Surfaces – Santa Catarina State University, Joinville, SC, Brazil*

1. Introduction

The pulsed magnetron sputtering deployment it was an important tool in a sputtering deposition [1]. Whereas in the DC magnetron sputtering processes where there are a low deposition rate and target arcing events, the use of the pulsed source during the sputtering steady the plasma discharge and prevents the arcing formation. A pulse frequency range of 20 to 350 KHz is an alternative to modify the microstructure of the films as well as its physical properties [2]. In this contribution, we report the pulsed magnetron sputtering treatment using an asymmetric pulsed source. Thus, the films were obtained in different values of pulse frequency.

This contribution deals with the pulsed magnetron sputtering treatment using an asymmetric pulsed source and a $Ti_{0.33}Al_{0.67}$ target (with 78%at. of aluminum). The aim of this research was to characterize the effects of pulsed frequency on films deposited in metallic mode.

2. Experimental

The magnetron system type used in this research was a diode magnetron (one anode and one cathode), flat surface, cylindrical and type II. The $Ti_{0.33}Al_{0.67}$ target has 22% at titanium and 78% at aluminum its a chemical composition. The source used for the plasma discharge was a DC Pinnacle Plus® commercial source and the depositions were carried out in direct current and asymmetric pulsed mode, without the presence of reactive gas in the plasma atmosphere (metallic mode using only argon gas). Two different materials were used for the substrate; silicon and steel. Samples were identified according to the value of the pulse frequency used in the deposition. The process parameters are shown as depicted in Table 1

Samples	Polarization Current (mA)	Cathode Average Voltage (V)		Samples	Polarization Current (mA)	Cathode Average Voltage (V)
DC	22	490		200 KHz	23	371
50 KHz	20	461		300 KHz	20	332
100 KHz	25	430				

Tab. 1 *Deposition parameters. The temperature and time deposition, current, bias, argon flux and reverse time for pulsed treatments were kept constant in all depositions, 300°C; 20 minutes; 1,00A; -20V; 2,7sccm e 1,1μs, respectively.*

3. Results and Discussions

It was possible to verify through of X-Ray Photoelectron Spectroscopy (XPS) analysis that the increase in pulse frequency didn't present significant changes in the chemical composition between the films. The Al/Ti ratio remained approximately 2:1 (60% at Al and 30% at Ti).

The X-ray diffraction results (figure 1) showed that regardless of the pulse frequency used in the process, the phase formed in the films was TiAl. Films with approximately 60% at Al it can promote TiAl phase formation, with a tetragonal type structure [3].

As the pulse frequency increases, the time on (sputtering) has become each time smaller, decreasing the deposition rate and consequently decreasing the thickness of the films, as shown in Figure 2. The mean voltage required to maintain the plasma discharge decreased during the process due to the source operation mode, because the current was maintained constant. The mean voltage reduction is related owing to the change in the plasma kinetics (secondary electron emission and electron energy distribution) [4].

The Figures 3 to 7 shows the appearance of the microstructure and surface observed in the scanning electron microscope (SEM) and atomic force microscope (AFM). The transversal section of all films is similar to the Thornton model Zone T. The column-shaped morphology is the result of TiAl phase formation, with the tetragonal structure [3]. These columns are composed of grains and grain boundary and their morphology suggests that the growth of the films was obtained by the island growth mechanism.

No significant changes in hardness and reduced elastic modulus were observed with the increase in pulse frequency. The mean values were 8.8GPa and 162 GPa respectively.

*Corresponding author: deivisonpaim@gmail.com

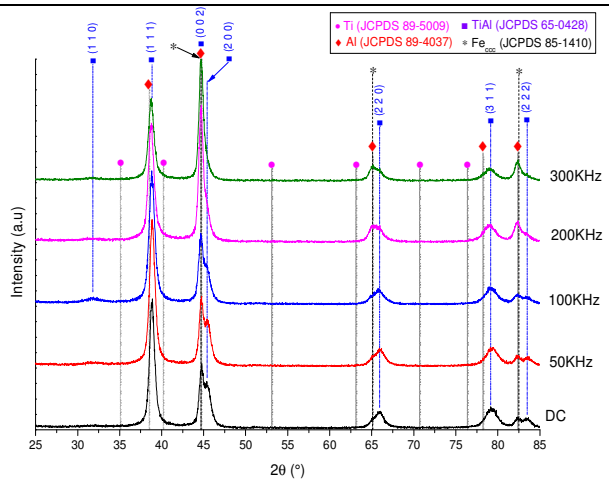

Fig. 1 *X-ray diffraction results of films. Copper target (Kα =1,5406 Å). Steel substrate.*

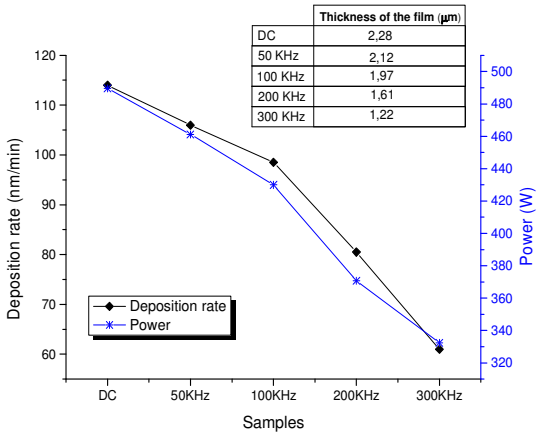

Fig. 2 *Deposition rate. The thicknesses of the films are shown in the table on the right, above the graph.*

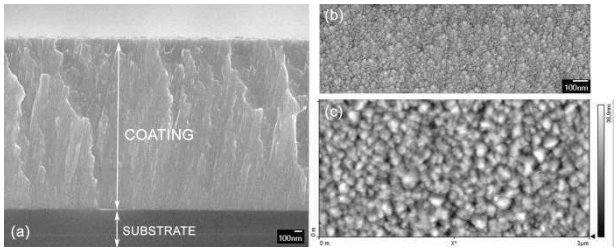

Fig. 3. *Sample DC. SEM of films deposited on silicon substrate: (a) cross section and (b) surface. (c) AFM of the film deposited on steel substrate.*

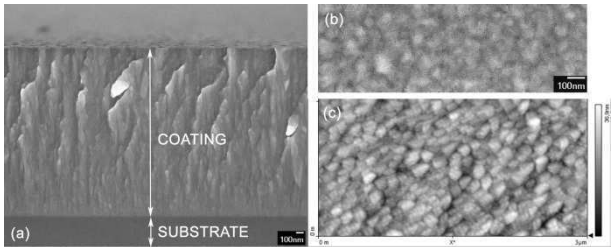

Fig. 4. *Sample 50KHz. SEM of films deposited on silicon substrate: (a) cross section and (b) surface. (c) AFM of the film deposited on steel substrate.*

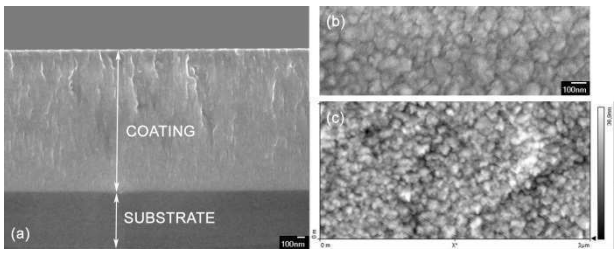

Fig. 5. *Sample 100KHz. SEM of films deposited on silicon substrate: (a) cross section and (b) surface. (c) AFM of the film deposited on steel substrate.*

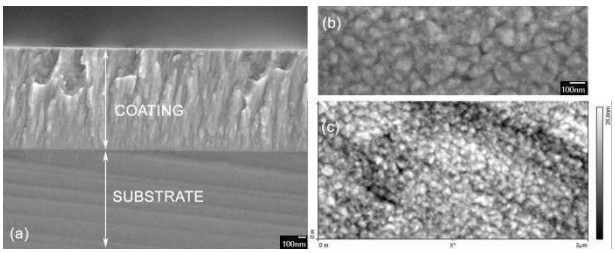

Fig. 6. *Sample 200KHz. SEM of films deposited on silicon substrate: (a) cross section and (b) surface. (c) AFM of the film deposited on steel substrate.*

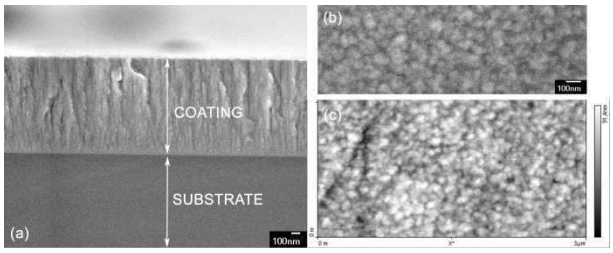

Fig. 7. *Sample 300KHz. SEM of films deposited on silicon substrate: (a) cross section and (b) surface. (c) AFM of the film deposited on steel substrate.*

4. References

[1] SCHILLER, S, K GOEDICKE, J RESCHKE, V KIRCHHOFF, S SCHNEIDER, E F MILDE. "*Pulsed magnetron sputter technology*." Surf. & Coat. Tech, **61**, 331-337, (1993).

[2] KELLY, P, J. J., ARNELL, R, D, D. "*Magnetron sputtering: a review of recent developments and applications.*" Vacuum, v. 56, n. 3, pp.159-172, (2000).

[3] IRUDAYARAJ, A A, P KUPPUSAMI, R THIRUMURUGESAN, E MOHANDAS, S KALAINATHAN, E V S RAGHUNATHAN. "*Influence of nitrogen flow rate on growth of TiAlN films prepared by DC magnetron sputtering.*" Surface Engineering, 7-11, (2007).

[4] BELKIND, A., FREILICH, A., LOPEZ, J., ZHAO, Z., ZHU, W., BECKER, K, E. "*Characterization of pulsed dc magnetron sputtering plasmas*." New Journal of Physics, **7**, 1-16, (2005).

*Corresponding author: deivisonpaim@gmail.com

Acknowledgments
The Santa Catarina State University and Santa Catarina Federal Institute for the financial support.

*Corresponding author: deivisonpaim@gmail.com

INFLUENCE OF THE TREATMENT TEMPERATURE ON THE EDGE EFFECT OF NITIDEDUNS 32750 SUPER DUPLEX STAINLESS STEEL.

Vieira, J. F; Brunatto, S. F; Cardoso, R. P.
Plasma Assisted Manufacturing Technology & Powder Metallurgy Group
Mechanical Engineering Department, Federal University of Paraná, PR, Brazil

1. Introduction

The development of new materials and processes is currently motivated by the industrial demand. In this context, the research for new treatment techniques, in order to adapt the properties of existing materials to new applications and / or to more severe operating conditions, is constantly growing. Among the materials the stainless steels stand out. These steels have excellent corrosion resistance, due to their native passive layer. Among stainless steels, duplex or super-duplex steels have superior properties when compared to other stainless steels, however, their low wear resistance makes these materials unattractive for some applications. Thus, to provide an increase in surface wear resistance, thermochemical treatments as plasma-assisted nitriding becomes alternative, but, for temperatures above 400 °C, the increase in surface hardness is tipically accompanied by a loss of corrosion resistance [1-2]. So, the potential of plasma-assisted thermochemical treatments is in the excellent surface properties obtained through their application at low temperature. However, even with these advantages there are some drawbacks such as the phenomenon known as edge effect, which produces a non-uniform treated surface when the sample (or component) present edges. The edge effect occurs because the samples are subjected to a high cathodic potential to produce plasma directly on their surface. According to Olzon-Dionysio et al. [3] this effect is a result of distortions in the electric field around the corners and edges, the shape of the plasma sheath, which is associated with the shape of the samples, and determines the distribution of the ion flux, creating non-treated regions characterized by different colors (or roughness) and hardness heterogeneity. This effect occurs mainly in the treatment of materials containing a high alloying elements content [3] like super duplex stainless steels. Thus, the objective of this research is to analyze the characteristics of the edge effect formed in duplex stainless steel, such as hardness and dimension, when suggested to low-temperature plasma nitriding.

2. Experimental

SAF 2507duplex stainless steel (UNS 32750), which is considered a super duplex, was used to produce the samples with 20x20x2 mm. The material was purchased in the form of rods having a diameter of 50.8 mm and samples were cut by electrical discharge machining. The chemical composition of the material, measured by X-ray fluorescence, was Cr (25.66%), Ni (6.88%) and Mo (4.10%), evidencing that the elements present in the alloy are in agreement with that established by the UNS standard. Finally, the samples were ground, mirror-polished, and cleaned in an ultrasonic bath with alcohol before the nitriding treatments. For ultimate cleaning purposes, before the nitriding step, the samples were plasma cleaned in a gas mixture of 80% H_2 + 20% Ar, under a pressure of 3 Torr, at 300 ° C for 0.5 h. Plasma nitriding was performed using a gas mixture composition of 70% N_2 + 20% H_2 + 10% Ar. The total gas flow and pressure were set at 3.33 x 10^{-6} Nm^3s^{-1} (200 sccm) and 3 Torr, with peak voltage of 700V. The samples were nitrided at 300, 350, 400 and 450C for 4h. The plasma apparatus consisted of a 4.16 kHz square wave pulsed DC power supply and a stainless-steel cylindrical vacuum chamber with 350 mm diameter and 380 mm high, attached to steel plates sealed with silicone rings at both ends.

3. Results and Discussions

Each sample had a unique surface characteristic; it has been found that as the treatment temperature is increased the edge effect is more evident because there is a higher effective time of applied cathodic potential to achieve higher temperatures. The edge effect of the samples appeared as a bright contrast under an optical microscope, corresponding to a smooth surface where little or no nitrided layer was formed. The top surface of the sample nitrided at 400 ° C for 4 hours, including the sample edge, is shown in Figure 1. It is possible to infer that the edge effect is present on the treated surface and this fact was confirmed by cross-sectional microstructural examination and microhardness tests.

In figure 2, the hardness of the surface, from the edge to the center of the sample (up to 10 mm), is shown. In the region where the edge effect is present there is a variation in the surface hardness, with these results it can be concluded that the edge effect, is actually characterized by a microstructural difference in the treated surface (Figure 1), is actually present, indications a poorly treated region. In all the samples there was region of lower surface hardness going from the edge until the center of the sample where the hardness remained

constant; however, for lower temperatures the edge effect was lower, consequently the hardness difference was lower.

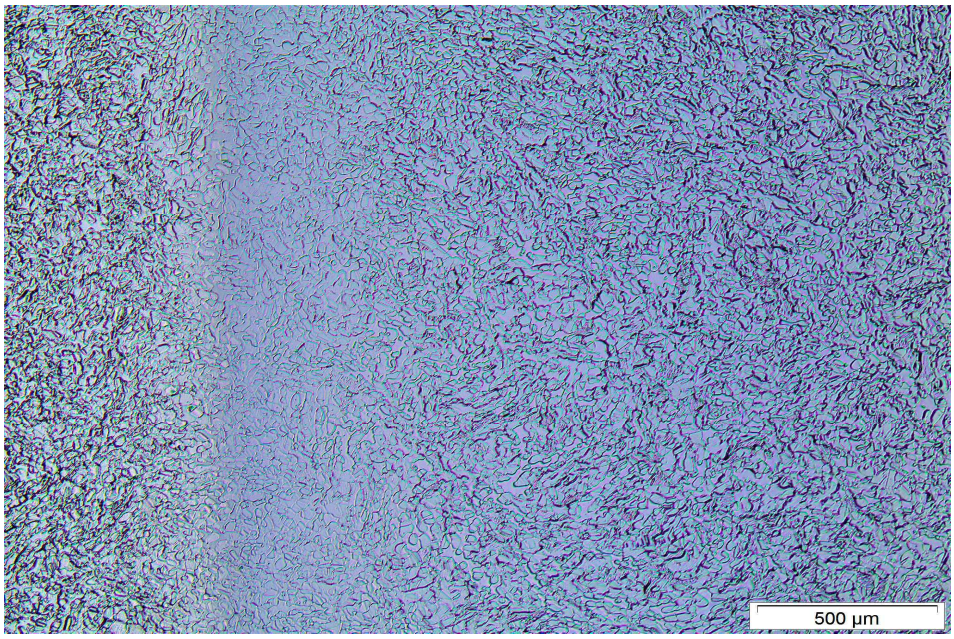

Figure 1 - *Treated sample surface - nitrided at 400 °C for 4h.*

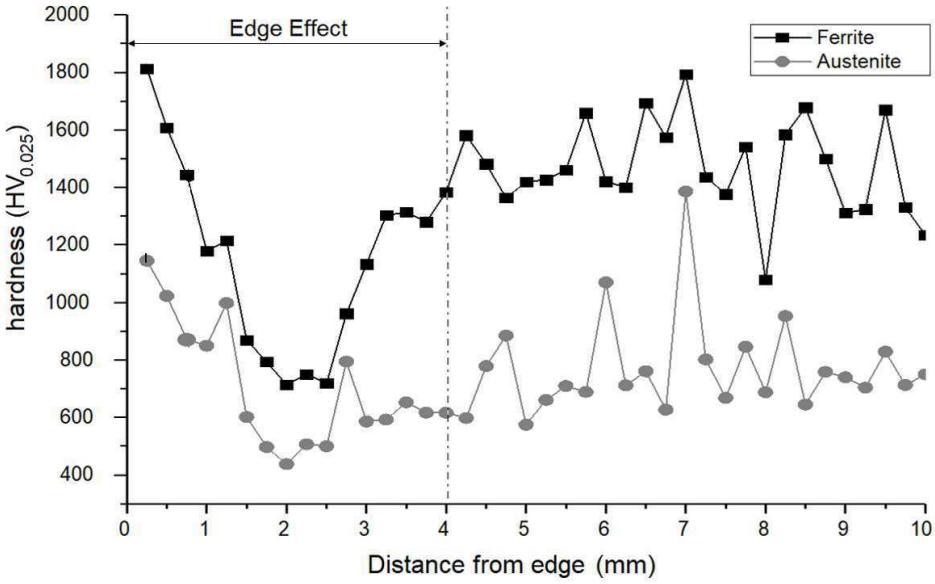

Figure 2 - *Hardness of the sample nitrided at 400 ° C for 4h.*

4. References

[1] Z.L. Zhang, T. Bell, Surf. Eng. 1 (2) (1985) 131–136.
[2] J.-P. Lebrun, H. Michel, M. Gantois, Memoires Scientifiques Ver. Metallurg. LXIX (10) (1972) 727738.
[3] OLZON-DIONYSIO, M. et al. Influences of plasma nitriding edge effect on properties of 316L stainlessteel. Surface and Coatings Technology, v. 204, n. 21–22, p. 3623–3628, 2010.

SYNTHESIS AND CHARACTERIZATION OF NANOCOMPOSITE OF POLY (VINYL BUTIRAL) REINFORCED WITH ZINC OXIDE NANOWIRES

Porto, R. C. T.[2*], Uchôa, P. Z.[1], Pezzin, S. H.[2], Hoepfner, J. C.[3], Nogueira, A. L.[1]

[1] *Masters in Process Engineering,, University of the Region of Joinville, Joinville, Santa Catarina, Brazil*
[2] *Center of Technological Sciences, Santa Catarina State University, Joinville, Santa Catarina, Brazil*
[3]*Department of Materials Engineering, State University of Ponta Grossa, Ponta Grossa, Paraná, Brazil*

1. Introduction

Nanocomposites of polymer matrix have great industrial applicability due to the ease of processing and variety of products used as phase matrix and phase reinforcement. Poly (vinyl butyral) (PVB) is a thermoplastic widely used as a matrix for the incorporation of various nanostructures [1], such as carbon nanotubes (NTC) and nanoparticles of titanium dioxide (TiO_2) and zinc oxide (ZnO), searching for electronic and antibacterial applications [2]. The characteristics of PVB undergo change according to the degree of acetalization resulting from the conversion of polyvinyl alcohol (PVA) into PVB.

2. Experimental

In this study, PVB was synthesized through the condensation reaction of PVA in acid medium and used as a matrix for the casting production of nanocomposites with zinc oxide nanowires (Nf_ZnO) in concentrations from 1 to 5% by mass. The degree of acetalization of the synthesized films was calculated by 1H nuclear magnetic resonance spectroscopy (^{1}H NMR), analyzes were performed Fourier transform infrared spectroscopy (FTIR) to investigate the interaction between matrix and reinforcement phases.

3. Results and Discussions

The degree of acetalization of the synthesized films was calculated by ^{1}H nuclear magnetic resonance (^{1}H NMR), resulting in 50 mol%. Fourier transform infrared spectrometry (FTIR) spectra showed the appearance of a band at 1560 cm^{-1} only in the samples containing Nf_ZnO, noting that the increase in the prominence of this band is directly related to the increase in the amount of Nf_ZnO present in the nanocomposite film. It is believed that this band may indicate the binding of the Zn to the oxygen atoms of the remaining hydroxyls from the conversion of PVA to PVB. Thus, the increase in Tg and the change in some bands in the FTIR spectrum for the nanocomposites suggest that the added Nf_ZnO presented good interaction with the PVB matrix.

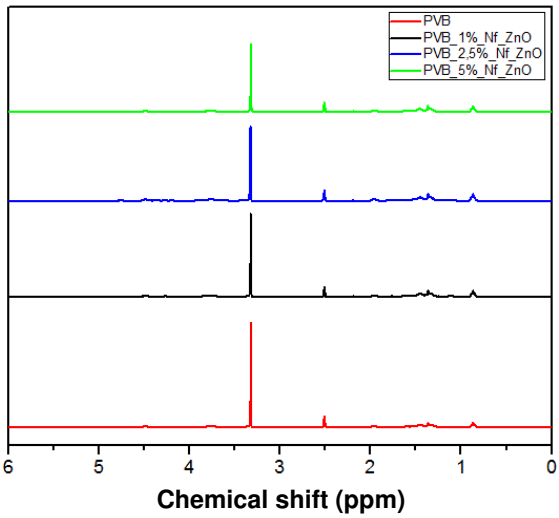

Fig. 1. *^{1}H NMR spectra for PVB and nanocomposites*

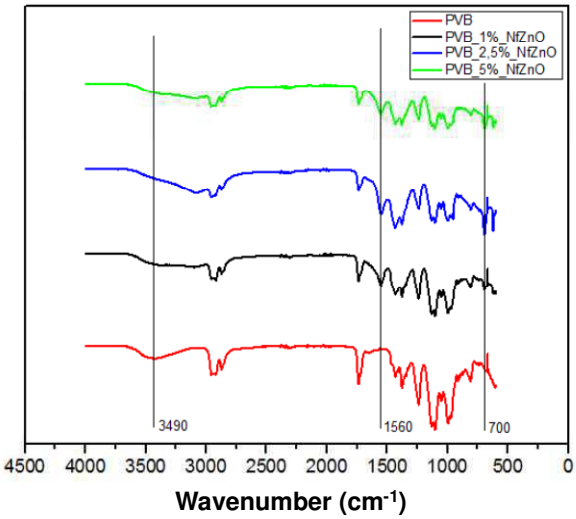

Fig. 2. *FTIR spectra for PVB and nanocomposites*

4. References

[1] HOEPFNER, J. C.; LOSS, M. R.; PEZZIN, S. H. Journal. Applied. Polymer. Science, **135**, 1-10, (2018).
[2] PORTO, R. C. T.; UCHÔA, P. Z.; NOGUEIRA, A. L.; PESCHEL, L. T.; JUSTI, B.; KOSLOWSKI, L. A. D, Revista Matéria, **22**, 1-8 (2018).

Acknowledgments

The authors are grateful to CAPES by financial support.

*Correesponding author: rctporto@hotmail.com

PLASMA NITRIDING OF MARAGING STEEL C300 OBTAINED BY SELECTIVE LASER MELTING FOR FABRICATION OF INJECTION MOLDS

I. F. Ostrovski[1,2]*, A. M. Zanatta[2], A. Rabelo[2] , S. Bodziak[3], V. L. Soethe Parucker[1], D. A. Duarte[1]
[1]*Federal University of Santa Catarina, Technological Center of Joinville, Laboratory of Surface Treatments, Joinville, SC, Brazil.*
[2]*National Service for Industrial Training, Institute for Innovation in Manufacturing Systems, Joinville, SC, Brazil.*
[3]*Faculty of Technology SENAI, Joinville, SC, Brazil.*

1. Introduction

Maraging steels are widely used in manufacture of inserts for injection molds and single cavity dies, both by traditional processes and selective laser melting (SLM), where SLM is most suitable for development of polymer or aluminum injection molds with complex cooling channels. The process often used to build cooling channels in such devices is by drilling process, which accounts circular section with linear axis or given by segments of surface line [1]. SLM is a rapid prototyping technology for additive manufacturing that allows fabricating metal components layer by layer according to a given CAD volume model, where, in each micrometric layer, the three-dimensional solid is obtained by a high power-density laser that melts and fuses the metallic powder together [2]. Among several applications, the main goal of this technique in injection molds is to improve the cooling process of complex geometries in mold cavities from cooling channels, known as conformal cooling, reducing distortions of the injected part and time required for manufacturing. However, the manufactured solid requires post thermal treatments for application in injection molds due to its low surface hardness and wear/corrosion resistance [1], where plasma nitriding may offer such improvements with a reliable control of the mechanical properties according to the experimental setup used [3]. Thus, this paper investigates the effects of the plasma nitriding time in the structure, nitride layer and microhardness of maraging steels C300 aiming the application of this material for fabrication of injection molds.

2. Experimental

Maraging steel C300 samples were 30×10 mm size manufactured by SLM and mechanically sanded and polished before thermal treatments. Plasma nitriding were carried out for 1, 2 and 5 hours under (443± 8)°C with the reactive gas mixture composed by 30%Ar and 70%N_2 controlled by mass flow inlet. Samples were cooled under vacuum in order to avoid surface oxidation. Structural properties were investigated by XRD (Panalytical Empyream with Cr as anode material). Before microindentation (Wilson Instruments model 402MVD–MEC 012), samples were cut, hot mounted, sanded polished and etched with 3.5% nital with the nitride layer measured by optical microscopy (Zeiss Imager.M2m with Axio Vision SE64 V4.9 software). Microhardness analyses were performed with 25 g load for 10 seconds under 24°C, in agreement to ASTM E384–17 pattern, where each measurement, along the nitride depth, was given by the average of three partial measurements. FEG (Zeiss model SUPRA 55-VP) analyses were also conducted in order to evaluate formation of precipitates.

3. Results and Discussions

Figure 1 shows XRD spectra of the nitrided samples in comparison with a pristine. The non-treated sample presents a martensitic structure (α–Fe) with a prominent decreasing after plasma nitriding with the main peaks assigned to the Fe_4N phase. In addition, a shift around 1.17° to lower 2θ values is observed to treated samples. This may be related to increasing of the volume density caused by nitrogen diffusion into steel lattice. Due to the higher signal of the peak assigned to the Fe_4N phase, spectrum of the sample treated for 2 hours was quantified by the Rietveld method in order to obtain the percentage structural concentration. Results are depicted in Fig. 2 and indicate 83.1% Fe_4N and 16.9% α–Fe. Figure 3 presents the thickness of the nitrided layer as function of the nitriding time. Results indicate that sample treated for 2 hours present the thickest layer. The longer plasma exposition decreases the nitriding layer and it may be caused by decreasing of nitrogen diffusion due to the formation of a thicker white layer. Typical microhardness profiles are shown in Fig. 4. The highest hardness values measured on the top of the samples are assigned to nitride layers, with formation of thin coherent precipitates according to FEG observations. These precipitates deform the lattice and increase the material hardness when the limit of nitrogen solubility is exceeded.

*Corresponding author: ivoneteostrovski@gmail.com

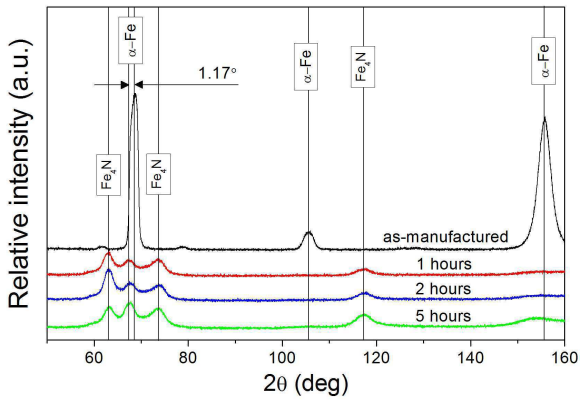

Fig.1. *XRD spectra of samples.*

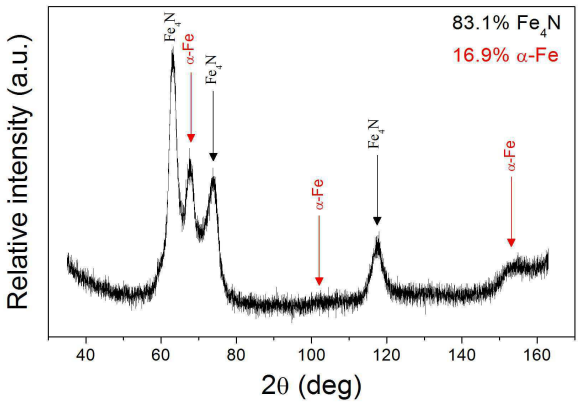

Fig.2. *Phase quantification of sample nitrided for 2 hours.*

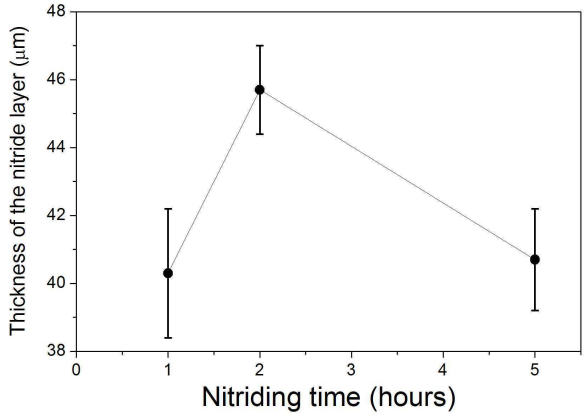

Fig.3. *Nitrided layer as function of the nitriding time.*

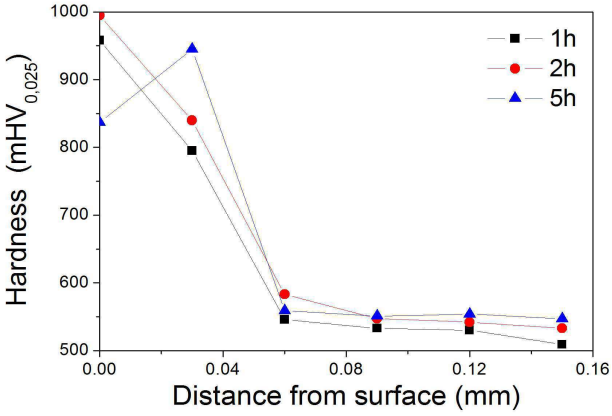

Fig.4. *Microhardness profiles of the nitrided layers for samples nitrided for 1, 2 and 5 hours.*

4. References

[1] A. Rabelo, Influência do tratamento térmico sobre a microestrutura e propriedades mecânicas do aço maraging C300 obtido por fusão seletiva a laser. Dissertação de Mestrado. Universidade Federal de Santa Catarina, Florianópolis, Brasil (2016).

[2] S. Marques *et al.*, Influência dos parâmetros do processo fusão seletiva a laser na microestrutura e densidade de peças fabricadas em aço maraging C300, 8º Congresso Brasileiro de Engenharia de Fabricação, (2015).

[3] R. M. M. Riofano, Efeitos das variáveis de nitretação por plasma na resistência à abrasão de um aço "maraging". Dissertação de Mestrado. Universidade de São Paulo, São Carlos, Brasil (1997).

Acknowledgments

Authors thank UDESC/LPFS, Mr. Tarcisio Boegershausen and Mr. Gabriel A. Rosa from SENAI.

*Corresponding author: ivoneteostrovski@gmail.com

DEVELOPMENT OF RADIATION-ABSORBENT MATERIALS

Isabelle de Geus Quintiliano[1]*, Viviane L. Soethe[1], Vinícius Martins Freire[1], Rafael G. Delatorre[1], Moisés L. Parucker[2]

[1]*Universidade Federal de Santa Catarina – UFSC- Joinville*
[2]*Universidade Federal de Itajubá – UNIFEI – Itajubá – MG*

1. Introduction

Ever since the development of radar, the desire to understand and create an element for absorber the waves produce in radar frequencies is required. The uses of radiation-absorbent materials (RAM) started mostly during World War II, Germany, concerned with radar camouflage for submarines, developed a carbonyl iron powder loaded rubber sheet about 0.3 inches thick and a resonant frequency at 3 GHz. [1] At the present time is also required for civilian uses such as in telecommunication and medicinal care. The World Health Organization (WHO) established the International EMF Project in 1996 to assess the scientific evidence of possible health effects of electromagnetic field (EMF) in the frequency range from 0 to 300 GHz [2].

Traditional absorption mechanism can be divided into three loss types: as electric, magnetic and dielectric. Absorptive layer can be made from either dielectric or soft magnetic materials with appropriate loss tangent. Usually the absorber layers are made from composite materials, mixtures of dielectric and/or soft-magnetic particles in some matrix; however, excellent absorbers can be made from ferrite for use at lower frequencies [3].

In this study was combined Fe_2O_3 and TiO_2 in a polymer matrix to study how a RAM, due the fact that Titanium dioxide (TiO_2) is a polymorphic material (anatase, brookite). It is commonly accepted that anatase is a more photocatalyst (compared to rutile and broo-kite), which is evident from the numerous studies that have highlighted the photocatalytic application of TiO_2 (with specific reference to the anatase crystalline phase) [4]. Ferrites are ceramic materials exhibit good electromagnetic loss performance as well magnetically and mechanically properties at elevated temperatures up to their Curie point [5].

2. Experimental

Were produced 12 samples with an exclusive proportion of the amount of additives. For all samples, are used 5,00g de polymer matrix and altered the percent of other two elements (Fe_2O_3 e TiO2), by varying the percentage by mass individually and together. Variations occurred at 0%, 6%, 8%, 15%, 20% and 24% thus ensuring a broad mass combination to expand the observation of energy absorption.

Figure presents an illustrative image of all samples produced and cutter process for waveguide characterization where the numbers for the samples relate to the concentrations of additives given in Table 1.

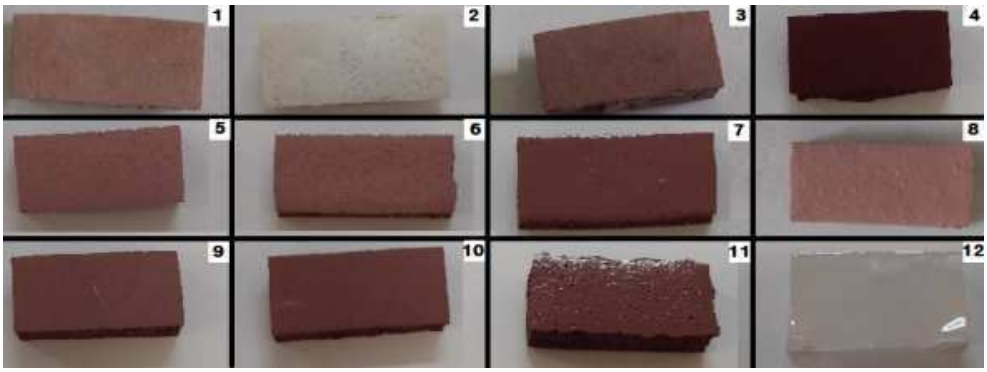

Figure 1. *Samples produced and cutter for evidence*

All the samples where analyses with waveguide in frequency range of 8.2 to 12.4 GHz and Scanning Electron Microscopy (SEM). The waveguide characterization reveals the properties of magnetic permeability and electrical permissivity, which are used to calculate parameters such as loss of electric and magnetic power. These dates allow to define a nature of the loss, that is, to enable the additive to a type of dielectric or magnetic debt. Scanning Electron Microscopy (SEM) was used to visualizing the microstructure of the material, the porosity and the agglomeration of the particulate in the composite.

3. Results and Discussions

*Corresponding author: isabelledgeus@gmail.com

With SEM analysis it was possible to observe a roughness in the structure which can contribute to the scattering of the incident electromagnetic radiation, aiding the phenomenon of reduction of the reflected energy. It is possible to observe also the occurrence of porosity, this is due to air bubbles formed during the process of manufacturing the samples. The figure 3 shows how this problem has affected the material.

Figure 2. *Side cut of sample 1, showing non-homogenization*

All these pores can act as spreading points of the incident electromagnetic radiation aiding the absorption phenomena.

The waveguide characterization evidence on absorption. The Figure 2 shows the results where the abscissa shows the electromagnetic wave frequency indicating [GHz] and in the ordered axis absorbed incident energy [%]

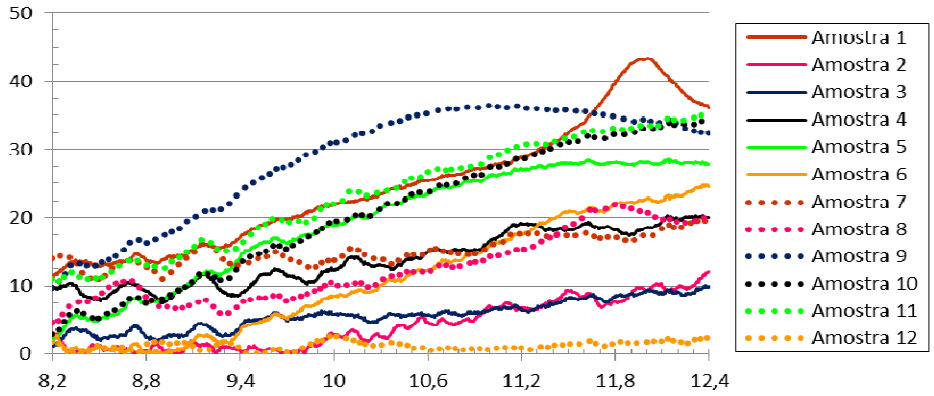

Figure 3. *Behavior of absorption as a function of frequency for samples with different contents of additives*

Analysing the data from the figure 3 is possible to conclude that the sample 1 (2,00g TiO_2 e 0,50g Fe_2O_3) exhibit the major attenuation energy incident (43.4 %) in the frequency range from 8.2 GHz to 12.4 GHz. Sample 1 has a higher TiO2 concentration, with a Narrow (N) band absorber character. Analyzing the other samples it is possible to realize that others models with more concentration TiO2 has also exhibit a great absorption. All the samples, expected the sample 1, presents a Wide (W) character, with absorptions above 10% for most compositions.

The samples did not obtain a complete homogenization and a series of discontinuities along the length, causing non-uniformity in the distribution of the particles generating changes in the behavior of the absorption. It is believed that the same properties can be obtained and improved with a better homogenization and standard.

4. References

[1] SAVILLE, P. Review of Radar Absorbing Materials. Defence Research & Development Atlantic Dartmouth, Canada. 2005.

[2] MICHELI, Davide; MARCHETTI, Mario. Mitigation of Human Exposure to Electromagnetic Fields Using Carbon Foam and Carbon Nanotubes. Engineering, [s.l.], v. 04, n. 12, p.928-943, 2012. Scientific Research Publishing, Inc,. http://dx.doi.org/10.4236/eng.2012.412a118.

[3] Mušič, Branka, Venturini, Peter, Žnidaršič, Andrej. "Electromagnetic absorbing materials." Informacije MIDEM volume 41. issue 2 (2011) str. 92-96. http://www.dlib.si/?URN=URN:NBN:SI:DOC-88GY3I1K

[4] Norman S. Allen, Noredine Mahdjoub, Vladimir Vishnyakov, Peter J. Kelly, Roelof J. Kriek,

*Corresponding author: isabelledgeus@gmail.com

The effect of crystalline phase (anatase, brookite and rutile) and size on the photocatalytic activity of calcined polymorphic titanium dioxide (TiO2), Polymer Degradation and Stability, Volume 150, 2018, Pages 31-36, ISSN 0141-3910, https://doi.org/10.1016/j.polymdegradstab.2018.02.008.

[5] K. Gaylor "*Radar Absorbing Materials – Mechanisms and Materials*", DSTO Materials Research Laboraty, Australia, (1989).

*Corresponding author: isabelledgeus@gmail.com

EFFECT OF SOLUBILITY TREATMENT IN PLASMA NITRIDING WITH PULSED FLOW OF NITROGEN OF STAINLESS STEEL ISO 5832-1

Heitor Augusto Pinto Cavalli[1]*, Anna Carolina Sphair[1], Paulo Cesar Borges[1], Marcio Mafra[1], Ricardo Fernando dos Reis[1], Euclides Alexandre Bernardelli[1]
[1]*Universidade Tecnológica Federal do Paraná, PPGEM, Curitiba-Pr*

1. Introduction

The nitriding of stainless steels with different mechanical treatment conditions results in different properties of the nitrided layer. The higher the degree of hardening, the greater the tendency to increase layer. In the work of Sphair [1] the author performed nitriding in stainless steel ISO 5832-1 cold drawn, with the objective of control the nitrogen potential in the nitriding atmosphere by means of intermittent nitrogen flow. The layers obtained had similar or even greater thicknesses than the samples treated with continuous gas flow. With this, the objective of the present work is to evaluate the influence of the material condition (drawn and solubilized) and the intermittent flow of gas in the thickness of the nitrided layer.

2. Experimental

The austenitic stainless steel ISO 5832-1 in the form of bar drawn with a diameter of 12.7 mm, was either solubilized at a temperature of 1100 °C for 18 minutes or used as received. Before performing the nitriding treatments, the faces and side of the samples were sanded up to 1200 mesh granulometry, polished in 1 μm aqueous alumina solution and cleaned in an ultrasonic bath with 98 GL ethyl alcohol for 15 minutes. In Tab. 1 the experimental conditions of nitriding are presented. Two modes of nitrogen flow were used, the first continuous flow (represented by the letter C in the code) and the second one of pulsed flow (represented by the letter P in the code), the latter performed with cycles of 10 minutes of bound nitrogen and 10 minutes off. Samples of the solubilized material were identified with the letter S in the code and the drawn samples were identified with the letter T in the code. After the nitriding, analyzes of Scanning Electron Microscopy (SEM), Optical Microscopy and nanoindentation were performed.

Temperature (°C)	t_{on} (μs)	t_{off} (μs)	T_{ap} (V)	Gas flow (cm³/min)	Pressure (torr)	Time (h)	N_2 flow condition (on/off) (min)	Code
400 ± 3	50 ± 10	200	500	200 (25%N_2 +25%H_2 +50%Ar)	4	0,5	Continuous	05CT, 05CS
							Pulsed (10/10)	05PT, 05PS
						2	Continuous	2CT, 2CS
							Pulsed (10/10)	2PT, 2PS
						8	Continuous	8CT, 8CS
							Pulsed (10/10)	8PT, 8PS

Table 1: *Parameters used in nitriding treatments.*

3. Results and discussion

Fig. 1 shows micrographs from all nitrated samples, where was observed the formation of the double layer (γ_N e γ_C) in all conditions. The γ_N layer is formed by nitrogen-rich expanded austenite and the γ_C layer is formed of carbon-rich expanded austenite. This effect occurs during the plasma cleaning phase, where the argon removes carbon from the walls of the reactor, which then diffuses into the material.

The measurements of the layers thickness in Fig. 1 indicate that the drawn samples present larger thicknesses for 0.5 hours of treatment, independently of the nitrogen potential. However, this behavior is reversed for 2 and 8 hours of treatment, probably due to recrystallization, which increases the diffusion of nitrogen when the treatment time is low. However, for long treatment times, due to the rapid formation of an expanded austenite layer, the drawn samples tend to have smaller nitrided layers than the solubilized samples. The use of an intermittent flow of nitrogen did not affect the growth of the nitrided layer, since the layers thickness is the same using either pulsed nitrogen flow or continuous flow.

Nanoindentation results, presented in Fig. 2, show that the nitrided layers have the same hardness, taking into account the standard deviation. Although, for 8 hours of treatment, at low depths of penetration of the nanoindentador the pulsed flow samples hardness is greater. This trend appears due to the formation of precipitates in the samples treated with continuous flow, resulting in increased roughness.

*Corresponding author: heitor.cavalli@gmail.com

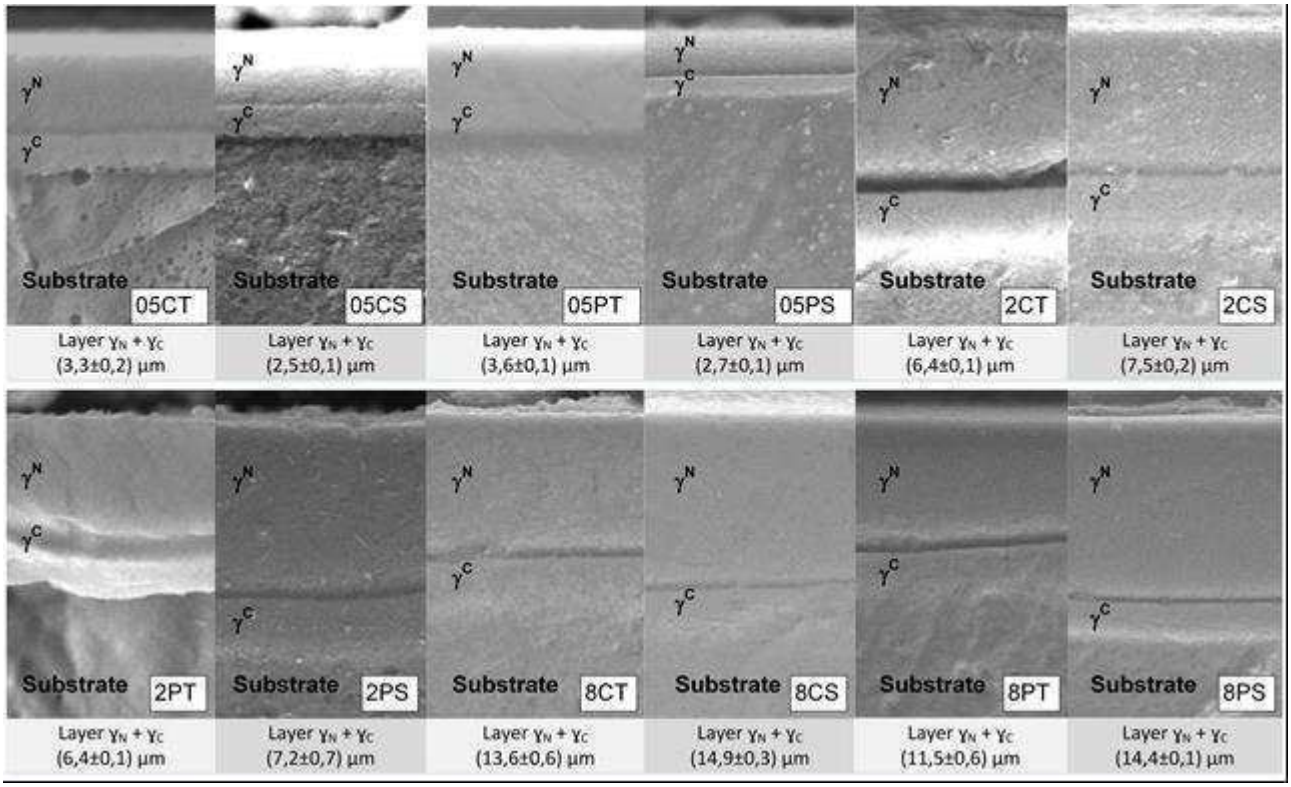

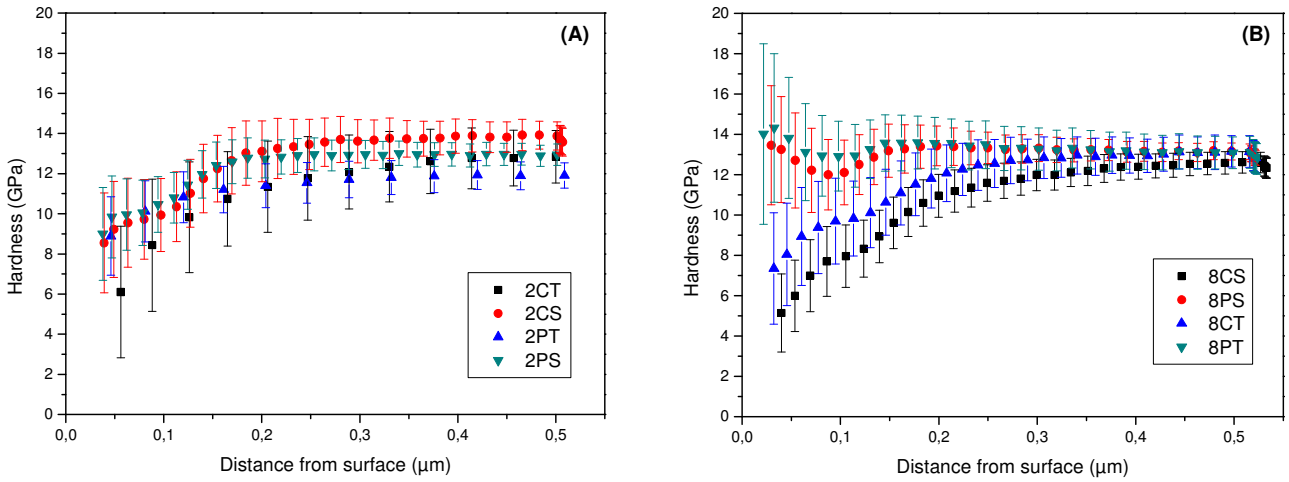

Fig. 2. *Results of the measurements of nanoindentation: (A) Nitriding time 2h; (B) Nitriding time 8 hours*

4. References

[1] A. C. Sphair, Dissertação (Mestrado em Engenharia de Materiais). Universidade Tecnológica Federal do Paraná, UTFPR, Paraná, Curitiba, (2017).

[2] A. F. Mendes, C. J. Scheuer, I. L. Joanidis, R. P. Cardoso, M. Mafra, A. N. Kleina, S. F. Brunatto, Materials Research, 17, 100-108, (2014).

[3] T. Czerwiec, H. He, S. Weber, C. Dong, H. Michel, Surface and Coating Technology, 200, 18-19, 5289-5295, (2006).

Acknowledgment

To the National Council for Scientific and Technological Development for financial support: Project 430088/2016-7.

*Corresponding author: heitor.cavalli@gmail.com

TRANSFORMATION OF AUSTENITE AND FERRITE DURING LOW TEMPERATURE PLASMA NITRIDING OF DUPLEX STAINLESS STEEL

Lucas Tomazi Durand[1]*, Lucas de Souza Gonçalves[1], Felipe de A. Possoli[1], Carlos Maurício Lepienski[1], Euclides Alexandre Bernardelli[1], Julio Cesar Klein das Neves[1], Márcio Mafra[1]
[1] *UTFPR -Federal University of Technology – Paraná State - Brazil*

1. Introduction

Duplex stainless steels are materials of industrial interest because they have a good combination of wear and corrosion resistances, being commonly applied in corrosive liquid tanks and petroleum refining equipment. In order to improve the tribological performance of these materials, plasma nitriding, a treatment that forms metastable phases such as expanded austenite [1,2], is applied. The present work studies the microstructure transformation of a duplex steel in phases expanded by nitrogen, aiming to better understand phenomena of the low temperature plasma nitriding and to extend of the applicability of this material.

2. Experimental

AISI 2507 duplex stainless steel samples (25 x 20 x 2 mm^3) were nitrided in a plasma reactor with auxiliary heating, in an atmosphere containing 20% H_2, 70% N_2 and 10% Ar at 3 Torr. As an attempt to evidence the beginning of phase transformations caused by nitrogen, treatment were carried out at low temperature (350°C), short time (2h), and low plasma power (15W). Treated samples were characterized by WDS (maps and amount of nitrogen), to identify nitrogen enrichment of ferrite and austenite. The of X-ray diffraction (XRD) analysis were conducted in the Brazilian Synchrotron Light Laboratory (LNLS).

3. Results and Discussions

Figure 1 shows a WDS nitrogen composition map of the sample surface. The dark phase, wich presents lower nitrogen content, was identified as ferrite. The lighter phase, which presents higher nitrogen content, was identified as expanded austenite. Quantitatively, nitrogen content is 3.6% and 8.6% (weight percentage) to ferrite and austenite, respectively. In Figure 2 XRD patterns compare untreated and plasma nitride samples. It is possible to observe the appearance of two groups of expanded austenite peaks: the broad peak at 48,7 and 56,5º refers to the previous austenite that was enriched by nitrogen and became expanded; the narrower peak at 49,2 and 58,0º requires further investigation to determine its origin.

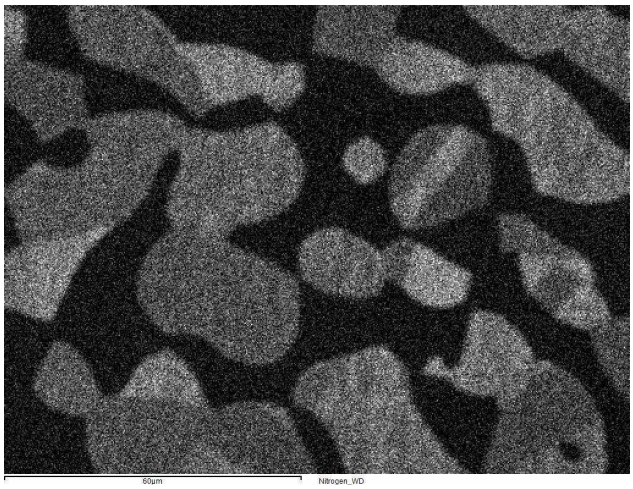

Fig. 1. *WDS nitrogen map of treated sample's surface.*

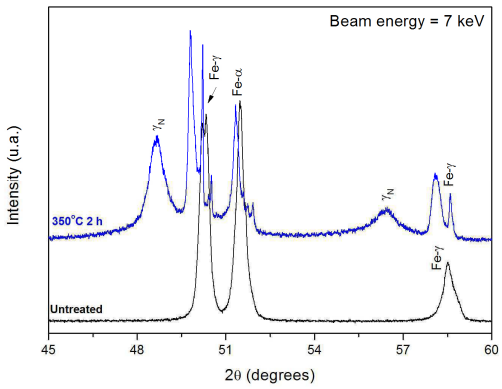

Fig. 2. *XRD pattern of untreated steel (black) and nitrided sample (blue).*

4. References

[1] M. Bobadilla and A. Tschiptschin, Material Research, **18(2)**, 390-394, (2015).
[2] C. Pinedo, L. Varela and A. Tschiptschin, Surf. & Coat. Tech., **232**, 839-843, (2013).

Acknowledgments

Authors are thankful to Brazilian National Scientific Council (CNPq) and Araucária Foundation for Support of Scientific and Technological Development in Paraná State, Brazil by financial support of NESAP project.

*Corresponding author: lucastdurand@gmail.com

SCRATCH RESISTANCE OF THE NITRIDED LAYER OF DUPLEX STAINLESS STEEL SAF 2205

Luis E. A. dos Santos Rosa[1]*, Yamid E. Nuñez de la Rosa[1], Ane C. Rovani[1], Felipe de A. Possoli[1], Márcio Mafra[1], Paulo C. Borges[1] and Giuseppe Pintaude[1]
[1]*Universidade Tecnológica Federal do Paraná*

1. Introduction

Duplex stainless steels have been successfully employed in the oil and gas industry [1]. However, in many situations, in addition to the corrosion resistance, the wear resistance is an important requirement for a proper component performance. Low-temperature plasma nitriding has been studied as a new process route to increase surface hardness of this class of material, without compromises its corrosion resistance [2]. The present work investigates the scratch resistance of the nitrided layer on duplex stainless steel SAF 2205.

2. Experimental

Samples of SAF 2205 (UNS S32205) duplex stainless steel (hardness of 368±36 $HV_{0.1}$) were prepared to a surface finish corresponded to a sanding #1200. Plasma nitriding was performed at 380°C for 10 hours, with 25% N_2 and 75% H_2, at 3 Torr, 600 Vdc. The nitrided surfaces were characterized by optical microscopy, X-ray diffraction and Vickers microhardness. The linear scratch test was conducted using 5 mm long tracks with applied loads of 2 and 5 N, using a Rockwell C diamond stylus. The scratched surfaces were analyzed in an optical interferometry. From these results, it is possible to estimate the abrasion factor (F_{ab}), which is the ratio between the formed groove area and the deformed lateral areas, besides the width of the scratches, that allows calculating the scratch hardness (H_S), as defined by the ASTM G171 Standard. For each test, 3 scratches were performed in order to obtain a significant mean value of the measurements. The coefficient of friction (COF) was obtained throughout the tests, by means of load cells configured for measuring the tangential and normal forces.

3. Resultats and Discussions

Plasma nitriding resulted in 3 μm thick layers. X-ray diffraction results showed that the layer formed consists predominantly of expanded austenite (S-phase). The top hardness was 1100 ± 175 $HV_{0.1}$. Table 1 presents the results obtained in the linear scratch test.

COF	2N	5N
Treated sample	0.068 ± 0.006	0.153 ± 0.005
Untreated sample	0.139 ± 0.007	0.158 ± 0.004
H_s [GPa]	2N	5N
Treated sample	4 ± 1	2 ± 1
Untreated sample	1.3 ± 0.2	1.6 ± 0.2
F_{ab}	2N	5N
Treated sample	0.68 ± 0.08	0.60 ± 0.08
Untreated sample	0.67 ± 0.05	0.60 ± 0.05

Tab. 1. *Results of the linear scratch test obtained for SAF 2205 untreated and after plasma nitriding.*

These results showed a much higher scratch hardness of the nitrided layer under 2 N load, implying a lower coefficient of friction, due to the minimized deformation effect. When the test was conducted under 5N load, the coefficients of friction determined for the nitrided surface and the substrate practically did not differ. This is related to the fact that this force was enough to crack the nitrided layer, exposing the substrate. The effect of the substrate is intense under higher applied force, so that the determined hardness for the nitrided layer falls to the point of being close to the value determined for the substrate. Regarding the abrasion factors, no significant difference was observed between the measured values, independent of the applied load and the presence of the nitrided layer.

4. References

[1] P. Craidy, L. Briottet, D. Santos, Int. J. Hydrogen Energy, **40**, 17084-90, (2015).
[2] J. Alphonsa, V.S., Raja, S. Mukherjee, Corrosion Sci., **100**, 121-32, (2015).

Acknowledgments

The authors thankful to the Brazilian National Scientific Council (CNPq) for the Scientific Initiation grant awarded to L.E.A.S. Rosa, and also for project Universal 443896/2014-3, and research grants of G. Pintaúde 308416/2017-1 and M. Mafra 309816/2015-7.

IMPLANTATION ENERGY EFFECTS ON THE NITRIDING AND CARBURIZING OF SUPERAUSTENITIC STAINLESS STEEL

Rafael F. Chuproski[1], Willian R. de Oliveira[1], Francisco C. Serbena[1], Rodrigo P. Cardoso[2], Silvio F. Brunatto[2], Paulo Soares[3] and Gelson B. de Souza[1]*

[1] *Department of Physics, Universidade Estadual de Ponta Grossa*

[2] *Department of Mechanical Engineering, Universidade Federal do Paraná*

[3] *Department of Mechanical Engineering, Pontifícia Universidade Católica do Paraná*

1. Introduction

Superaustenitic stainless steels (SASS) were developed for applications in severe environments. Thermochemical surface engineering treatments, such as nitriding and/or carburizing, can improve the wear and corrosion protection of the SASS surfaces to a higher degree [1]. Such treatments, when performed at relatively low temperatures (<400°C), result in a modified layer supersaturated either with nitrogen or carbon, free of precipitates, known as the expanded austenite or S-phase (γ_N or γ_C) [2]. In implantation-based or diffusion-based methods, the layer thickness depends mostly of the temperature-activated diffusion [3]. However, when carbon and nitrogen are implanted separately, or incorporated simultaneously in the hybrid nitrocarburizing treatment, a double layer is obtained, consisting in a high nitrogen concentration case at the top surface, followed by a layer with high carbon concentration. Such dual layer can be explained by the chromium affinity with nitrogen or carbon [2]. The lower affinity with carbon causes it to diffuse deeper in the material, while nitrogen is "trapped" in chromium sites, concentrating near the surface.

With the objective to analyze the effect of radiation-produced damages on the carbon and nitrogen diffusion through the expanded austenite, SASS surfaces were subjected to three different sets of nitriding/carburizing treatments, in which nitrogen was implanted under varied energies by plasma immersion ion implantation (PI3).

2. Materials and methods

UNS S31254 superaustenitic stainless steel samples were metallographically prepared to a mirror-like finishing.

Prior to PI3 treatments, the surfaces were sputter cleaned in a H_2 – Ar atmosphere for 20 minutes. Nitrogen implantation was performed in a chamber equipped with a r.f. remote plasma supply, under 1.8 Pa working pressure. Two voltages and frequencies were used, 6.5 kV and 10.5 kV. The temperature was kept constant by controlling duty cycles and, consequently, the ion fluences reaching the surfaces. Carburizing was carried out in a glow discharge system, using a H_2 – Ar – CH_4 atmosphere. The voltage applied was 700 V. Three sets of treatments were conducted: *(i)* N – nitriding only, *(ii)* N+C – nitriding with subsequent carburizing, and *(iii)* C+N – nitriding after carburizing. All treatments were carried out at 320 °C for 3 h. To equal all the heating times, the 6.5 kV and 10.5 kV only-nitrided surfaces were heat treated in a furnace with argon atmosphere for additional 3 h, under 320 ºC.

Treated samples were characterized by glancing angle X-ray diffraction, with incident angle of 2° and CuKα radiation. Hardness profiles were obtained by nanoindentation with 500 mN maximum load. Thicknesses of the produced layers were analyzed by scanning electron microscopy, after etching the cross-sectioned samples with Murakami´s reagent.

3. Results and Discussions

Analyses of the N (nitrided) batch revealed that changes in the implantation parameters clearly altered the structure of the modified layer, even at the same temperature. By assuming the S-phase as an expanded fcc austenite (though its real crystalline structure is not well understood yet [4]), we observed that lattice expansion was larger for the 6.5 kV treatment than for the 10.5 kV one. With less energy and ion fluences, the depth of implantation was shallower in the 6.5 kV case, resulting in higher nitrogen concentration at near surface and higher hardness profiles (13 GPa, as compared with 9 GPa for 10.5 kV). Figure 1 shows the diffractogram of the 6.5 kV sample.

In the N+C treatment, where carburizing was carried out on a previously nitrided surface, the N-produced layer underwent a second thermal treatment and diffused deeper in the material, causing the lattice parameters to reduce. The carbon addition to the layer did not produce significant changes in the peaks ascribed to the expanded phase, which now correspond to a mixed $\gamma_N + \gamma_C$ (see Figure 1). On the other hand, diffraction peaks were much broader for the C+N condition than for N or N+C, disclosing almost a splitting into two peaks, with maximums at $2\theta \sim 40.9º$ (γ_N) and ~ 42.1º (γ_C), a consequence of the different lattice expansions provided by nitrogen and carbon. Figure 2 shows the typical dual layer feature for the C+N condition. The hypothesis is that the γ_N growth pushed the γ_C boundary (produced first) deeper into the

*Corresponding author: gelsonbs@uepg.br

substrate [2]. Hardness profiles were lower for C+N than for N+C or N alone, reaching 12 GPa for the carburizing plus 6.5 kV nitriding layer. The N+C and C+N treatments whose nitriding voltage was 10.5 kV presented features similar to those described above and, at the same time, coherent with the trend expected for the increased implantation energy.

To summarize, ion implantation parameters such as fluence and energy can be effective variables to control, along with temperature, the nitrogen and carbon surface modification of SASS, with consequences not only in the microstructure but also in the surface mechanical properties.

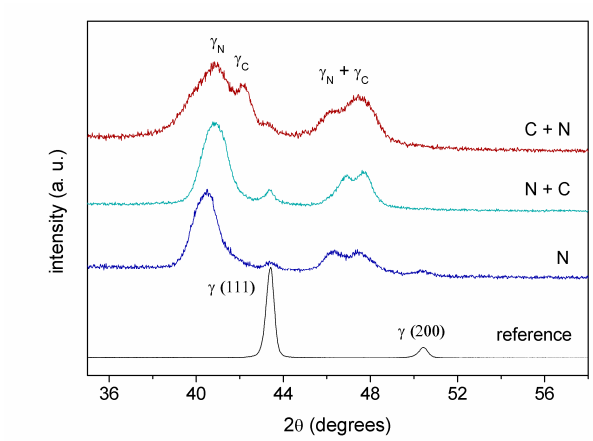

Fig. 1. *X-ray diffractograms of SASS submitted to nitriding (N), nitriding with subsequent carburizing (N+C) and nitriding after carburizing (C+N). In all the cases, nitriding was performed under 6.5 kV.*

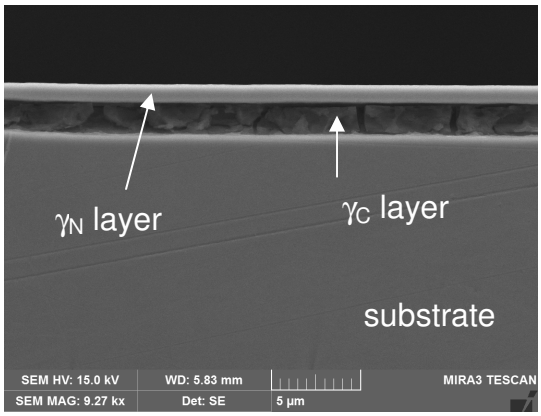

Fig. 2. *Secondary-electrons SEM micrograph of the cross-sectioned C+N sample, disclosing the dual layer feature. Nitriding was performed under 6.5 kV.*

4. References

[1] F. A. P. Fernandes, L. C. Castelletti, J. Gallego. J. Mater. Res. Tech., **2**, 158-164 (2013).
[2] H. Dong, Intern. Mat. Rev. 55(**2**), 65-98 (2010).
[3] A. Anders (ed.). Handbook of plasma immersion ion implantation. John Wiley & Sons Inc., (2000).
[4] M.P. Fewell, J.M. Priest, Surf. Coat. Technol., **202**, 1802–1815 (2008).

Acknowledgments

C-LABMU/UEPG, CNPq (grant nº 310819/2015-6) and Fundação Araucária / CNPq (PRONEX 15/2017 – NESAP).

*Corresponding author: gelsonbs@uepg.br

EFFECT OF INTERMITTENT FLOW OF NITROGEN GAS IN THE PRECIPITATION OF CHROMIUM NITRIDE DURING PLASMA NITRIDING OF STAINLESS STEEL ISO 5832-1

Camila Gonçalves Marques[1]*, Alfredo Rubega Neto[1], Heitor Augusto Cavalli[1], Carlos Maurício Lepienski[1], Marcio Mafra[1], Euclides Alexandre Bernardelli[1]
[1]*Universidade Tecnológica Federal do Paraná, PPGEM, Curitiba-Pr*

1. Introduction

The nitriding at low temperature of ISO 5831-1 stainless steel there are two important characteristics: the nitrided layer has high hardness, which increases the brittleness [1], being able to be verified the appearance of cracks and; the layer is thin [2], in a magnitude of 6 μm for 2 h of treatment and 8 μm for 4 h of treatment. In Sphair's work [2] the author performed nitriding with pulsed flow of nitrogen gas in order to control the nitrogen potential in the nitriding atmosphere and thus also to control the nitrogen concentration in the expanded austenite. That way, it was possible to reduce the nitrided layers brittleness. However, by pulsing the nitrogen flow the layer thickness tends to be smaller.

To increase the nitrided layer thickness using pulsed nitrogen flow, treatment time can be increased, which may result in brittle layers, or increasing the nitriding temperature. The downside of raising the temperature is that the temperature to initiate the sensitization of stainless steels is approximately 425 ° C [3]. Considering that the control of chromium nitride precipitation can be by temperature [4] and by nitrogen concentration [5], in this work it has been opted to control the chromium nitride precipitation by altering the nitrogen potential during the plasma nitriding of austenitic stainless steel ISO 5832-1 as a way to controlling the nitrogen concentration in the nitrided layer.

2. Experimental

The austenitic stainless steel ISO 5832-1 in the form of bar drawn with 12.7 mm of diameter, was solubilized at 1100°C temperature for 18 minutes. Before performing the nitriding treatments, the faces and sides of the samples were sanded up to 1200 mesh, polished in 1 μm aqueous solution of alumina and cleaned in an ultrasonic bath with 98 GL ethyl alcohol for 5 minutes. In Table 1 the experimental conditions of nitriding treatments are presented.

Temperature (°C)	t_{on} (μs)	t_{off} (μs)	T_{ap} (V)	Gas flow (cm³/min)	Pressure (torr)	Time (h)	N_2 flow condition (lig/des) (min)	Code
425 ± 3	50 ± 10	200	500	200 (25%N_2 +25%H_2 +50%Ar)	4	4	Contínuo	4C
							10/10	4P1010
							5/15	4P0515
							2/18	4P0218

Table 1: Parameters used in nitriding treatments.

3. Results and discussion

It is observed in Fig. 1 that for all the gas flow conditions, double layer was formed, where the outer layer is formed by austenite expanded to nitrogen (γ_N) and the inner layer formed by austenite expanded to carbon (γ_C). According to Czerwiec [6], the layer γ_C is formed during the cleaning stage process performed in situ with argon plasma, being the carbon derived from the reactor's walls.

The thickness of the expanded austenite layer (γ_N) is greater with the longer time under nitrogen flow, denoting that the stipulated times for the gas pulsing were efficient to control the nitrogen potential during plasma nitriding. Also, it is noticed the γ_C is barely affected by the different conditions of treatment, which it might be correlated with the formation of CN, that is pumped by the vacuum system or by the decrease of carbon concentration on the reactor's walls.

Fig. 2 shows the results obtained by Energy Dispersive Spectroscopy (EDS), which were performed in the adjacent region of the grain boundary. It is observed a smaller tendency to sensitization when using the pulsed nitrogen flow. This results are in agreement with Hereas [6], where the authors observed that the chromium nitride precipitation can be reduced when nitriding with a low nitrogen potential.

In Fig. 3 the X-ray diffraction results are shown, where it is observed that the formation of expanded austenite in all treatment conditions. The increase of austenite and the chromium nitride peaks is greater when using long nitrogen flow time, according to EDS results.

* Corresponding author: camilamarques@alunos.utfpr.edu.br

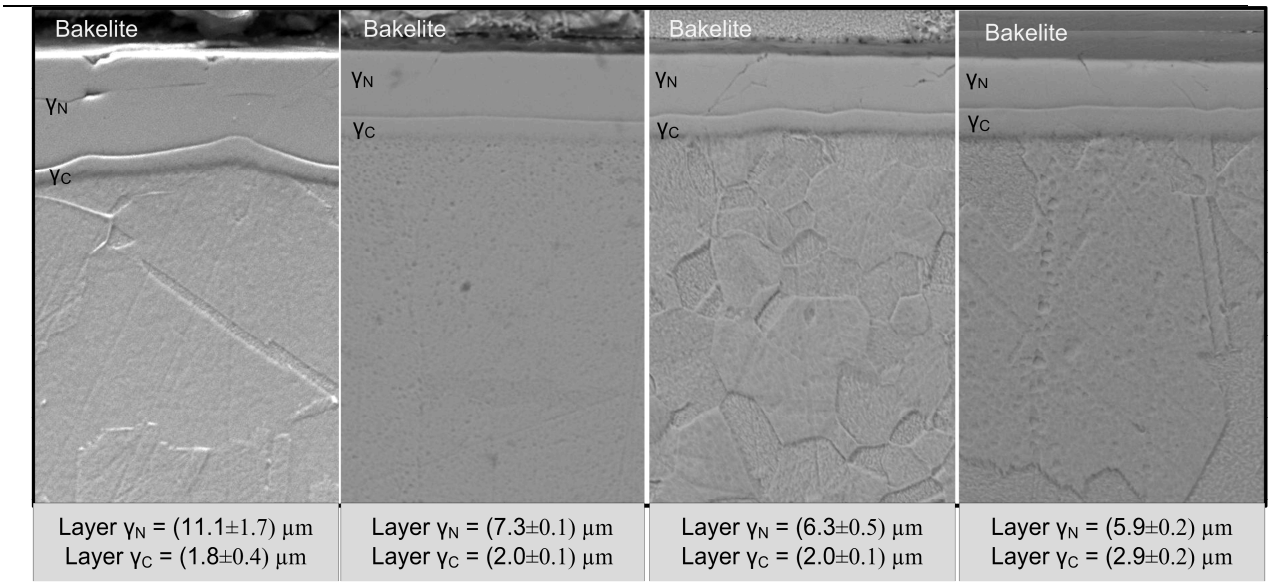

Fig. 1. Micrographs showing the double layers: expanded austenite by nitrogen (γ_N) and by carbon (γ_C). Magnification: 2000x.

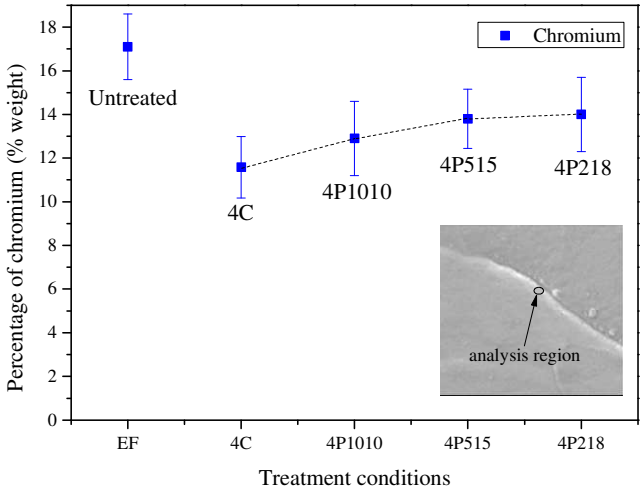

Fig. 2. EDS results showing the chromium percentage in the region adjacent to the grain boundary.

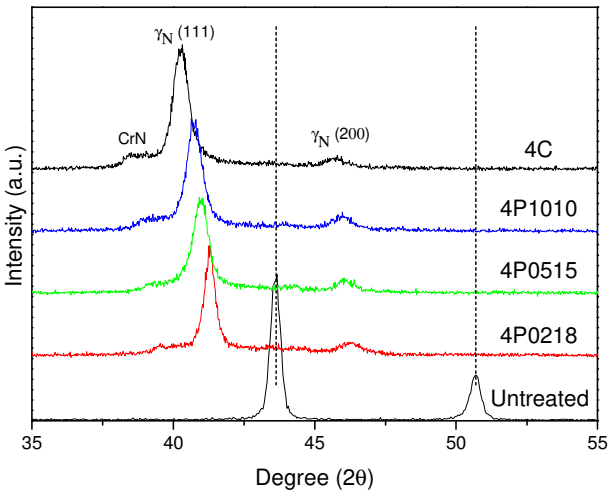

Fig. 3. X-ray diffraction showing the expanded austenite (γ_N) and chromium nitrides (CrN) peaks.

4. References

[1] A. F. Mendes, C. J. Scheuer, I. L. Joanidis, R. P. Cardoso, M. Mafra, A. N. Kleina, S. F. Brunatto, Materials Research, 17, 100-108, (2014).
[2] A. C. Sphair. Dissertação (Mestrado em Engenharia de Materiais). Universidade Tecnológica Federal do Paraná, UTFPR/Paraná, Curitiba, (2017).
[3] F. Borgioli; E. Galvanetto, T. Bacci, Vacuum, 127, 2016, 51 – 60, (2016).
[4] M. Yazici, O. Çomakli, T. Yetim, A. F. Yetim, A. Çelik, Surface and coatings technology, 261, 2015, 181 – 188, (2014).
[5] E. Heras, G. Ybarra; D. Lamas, A. Cabo; E. L. Dalibon, S. P. Brühlf, Surface and Coatings Technology, 13, 47-54, (2017).
[6] T. Czerwiec, H. He, S. Weber, C. Dong, H. Michel, Surface and Coating Technology, 200, 18-19, 5289-5295, (2006).

Acknowledgment

To the National Council for Scientific and Technological Development for financial support: Project 430088/2016-7.

* Corresponding author: camilamarques@alunos.utfpr.edu.br

MICROSTRUCTURE OF Ti-Al-N THIN FILMS OBTAINED BY REACTIVE PULSED MAGNETRON SPUTTER DEPOSITION

Arthur A. Lenzi[1*], Alessandra C. S. Dias[1], Abel A. C. Recco[1], Deivison D. Paim[1]
[1]*Laboratory of Plasmas, Films, and Surfaces – Santa Catarina State University, Joinville, SC, Brazil*

1. Introduction

Surface engineering has the objective of altering the surface properties of a material without changing the properties of its volume. Environmental degradation of the surface can be caused by friction, corrosion, work and strain, surface engineering research means to avoid this degradation. One of the solutions, it use a coating for improvement of the surface mechanical properties. Thin films are widely used as coatings, its main feature is the reduced thickness and complex atomic organization.

Titanium-aluminum-nitrogen films consist of a ternary, metastable and polycrystalline system. These thin films may present a crystalline structure or an amorphous phase, the characteristics of the film alter according to deposition parameters; different microstructural characteristics can be obtained by varying the aluminum concentration in the microstructure $Ti_{(1-X)}$ $Al_{(X)}$ N ($0 \leq x \leq 1$). The research revealed the influence of increasing the nitrogen flow in the deposition of $Ti_{0,33}Al_{0,67}N$ films, in the coating transversal section morphology.

2. Experimental

The experimental apparatus used in this work consists of a cylindrical reactor, made of stainless steel AISI 304, with a diameter of 280 mm and height of 240 mm connected to a vacuum system, which is formed by a mechanical pump of 5.0 m^3/h attached to a turbo molecular pump. Inside the reactor, there is a sample holder with a mask(Shutter). The power source used was asymmetric pulsed mode (Pinnacle Plus$^+$) at 100 kHz, with a duty cycle of 90 %. The distance between target and substrate was -78mm. To this process, some physicals parameters were held constant in all deposition like, the Ar flow in 1,48 sccm (standard centimeter cubic per minute), current of 1,0 A and a bias voltage of -20 VDC.

The nitrogen flow was the major parameter in this study, and all the values that are shown as depicted in Table 1, were deposited with a temperature of 300° C. The target has 67%wt of aluminum and 33%wt of titanium its a chemical composition. Two different materials were used for the substrate: Si (1 1 1) and steel. The cross-section image was obtained with the SEM (Scanning Electron Microscope-JEOL model 6701F). The topography surface image it's was a plot by an AFM (Atomic Force Microscope-NanoSurf-Nanite B).

3. Results and Discussions

The results as depicted in Table 1 indicates that the deposition rate and the power submit on the target decreases as the flow of the reactive gas increases. As the nitrogen flow increase, the Al and Ti atoms on the surface of the target can react s with N, and form the TiN and AlN [1]. The secondary electrons ejection rate of the AlN, it's higher than the Al atoms, and contributes to the ions formation on the plasma atmosphere. As the current was held constant, the biggest secondary electrons ejection contributes to decreases the Voltage applicate, which is directly proportional to the power used in the process.

Sample	$Power_{Target}$(W)	P(mTorr)	Deposition rate(nm/s)	$Flow_{N2}$(sccm)
0 sccm	430 ± 5	2,4 ± 0,2	1,58±0,02	0 ± 0,07
1,43 sccm	390 ± 5	2,4 ± 0,2	1,30 ± 0,04	1,43 ± 0,07
2,69 sccm	385 ± 5	2,4 ± 0,2	1,13 ± 0,01	2,69 ± 0,07
3,82 sccm	340 ± 5	5,0 ± 0,4	0,233 ± 0,006	3,82 ± 0,07
4,79 sccm	300 ± 5	6,0 ± 0,4	0,185 ± 0,002	4,79 ± 0,07
6,72 sccm	290 ± 5	7,5 ± 0,4	0,152 ± 0,007	6,72 ± 0,07

Table 1: Deposition condition

Figure 1 shows the appearance of the microstructure observed in the scanning electron microscope (SEM)The experimental result for a 0 sccm N_2 flow microstructure (figure 1-a), exhibited a columnar microstructure, similar to the Thornton model Zone T[3].

For low reactive gas flow until 2,69 sccm (figure 1-b), it was possible to note an undefined microstructure (not columnar), different from the Thornton model. This characteristic may be related with the microscope resolution, or the possible formation of the disordered AlN phase [4].

*Corresponding author: aa.lenzi@uol.com.br;

With a reactive gas flow range between 2,69 and 6,72sccm (figure 1-c), the columnar microstructure was observed again, however, with more thin columns. It may perhaps be related with the change in the atomic mobility of the atoms on the surface of the films [5].

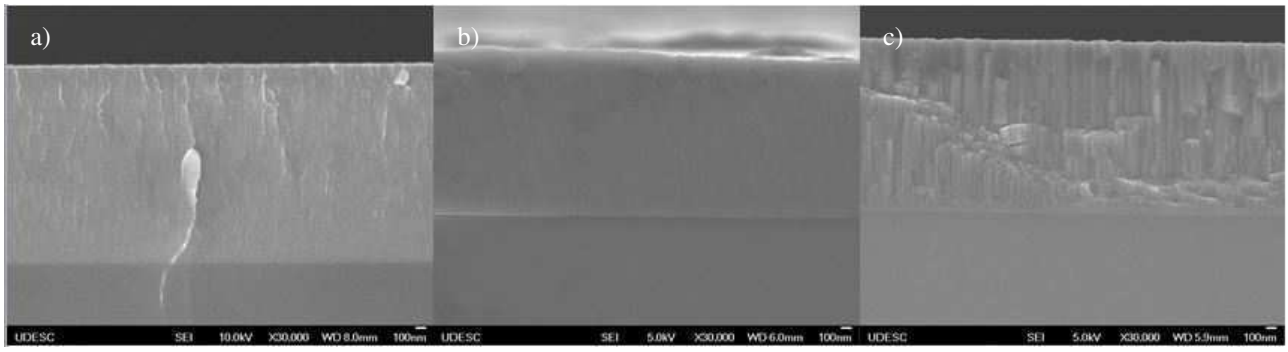

Figure 1: SEM cross section images for: a) 0 sccm; b) 2,69 sccm; and c) 4,79 sccm nitrogen flow.

It was possible to verify that for 0 sccm nitrogen flow, a well-defined columnar microstructure can be oberved with the SEM characterization. For low values 0 scccm < N2 flow ≤ 2,69 the microstructure was not well characterized, in other words, an undefined microstructure (not columnar). However, the columnar microstructure appears again on the microscope for high flows between 3,82 and 6,72 sccm.

4. References

[1]JEONG, J. J.; HWANG, S. K.; LEE, C. M. *Nitrogen flow rate dependence of the growth morphology of TiAlN films deposited by reactive sputtering*. Surf. & Coat. Tech, **151-152**, 82–85, (2002).

[2]PAIM, D. D. *Caracterização de filmes de Ti-AL e Ti-Al-N obtdos por diodo magnetron sputtering depositados sobre aço para trabalho a quente*. Joinville, SC: [s.n.].

[3] THORNTON, J, A. "Influence of apparatus geometry and deposition conditions on the structure and topography of thick sputtered coatings." Journal of Vacuum Science and Technology, **11**, 4, 666-670, (1974).

[4] LIU, Z, J., SHUM, W, P., LI, Y, K, SHEN, G, Y, E. "*Roughening kinetics of reactively sputter-deposited Ti-Al-N films on Si(100).*" Philosophical Magazine Letters, **83**, 10, 627-634, (2003).

[5] BELKIND, A., FREILICH, A., LOPEZ, J., ZHAO, Z., ZHU, W., BECKER, K, E. "*Characterization of pulsed dc magnetron sputtering plasmas*." New Journal of Physics, **7**, 1-16, (2005).

Acknowledgments

The authors knowledge the financial and structural support provided by Santa Catarina State University (UDESC), Brazil, and the Brazilian funding agency CAPES.

*Corresponding author: aa.lenzi@uol.com.br;

SURFACE TREATMENT OF ARTIFICIAL SKINS WITH ARGON PLASMA FOR DERMAL REGENERATION IN BURNS

M. F. Gonçalves[1*], M. W. Gonçalves[1], M. A. T. Duarte[2], V. L. Soethe Parucker[1], D. A. Duarte[1]

[1]*Federal University of Santa Catarina, Technological Center of Joinville, Laboratory of Surface Treatments, Joinville, SC, Brazil.*

[2]*Centro Universitário SOCIESC, Departamento de Engenharia Mecânica, Joinville, SC, Brazil*

1. Introduction

Official data from the Brazilian ministry of health indicates around one million burn incidents per year [1]. This fact evidences the need for studying methods to dermal regeneration aiming to improve the individual life quality or even lives, once 0.25% of these people dead directly or indirectly by burns caused [1]. Dermal regeneration matrices, or artificial skins, improve tissue regeneration due to biocompatibility with human skin. They are composed by type I collagen and glycosaminoglycans extracted from bovine tendons and shark cartilages, respectively, and a thin silicone layer to protect the alive structure that is applied on the burn tissue. The recovery from burns is often painful due to skin retraction that may limit the body movement, and aesthetic sequels [2]. The application of dermal matrices on the burn area increases the scar elasticity, and decrease aesthetic sequels and injury in the skin donor area once the graft removed may be thinner, improving the individual live quality. Besides treatments related to artificial skins, plasma-based processes have also been used to improve healing wounds due to ability generate chemical species capable to kill contaminants and catalyze reactions assigned to healing [3]. In this paper, the combination of both techniques aiming to increase the regeneration speed of dermal matrices is suggested with non-thermal Ar plasma.

2. Experimental

Dermal matrices (Integra®) were firstly frozen at –30°C and dried under vacuum at –50°C for 6 to 8 hours to remove water. Samples were treated for two different experimental setups. Samples named 1, 2 and 3 were treated for 120, 150 and 60 s, respectively, with argon plasma composed by 50 sccm mass flow rate and 3.4 torr working pressure, generated by 450 V DC and 0.32 A target current. Samples named 3, 4 and 6 were treated for 60, 120 and 180 s, respectively, with argon plasma composed by 20 sccm mass flow rate and 9.7 torr working pressure, generated by 400 V DC and 0.27 A target current. Characterizations were conducted by SEM (Jeol JSM-6390LV), XPS (Thermo Scientific K-Alpha) and DSC (TA *Instruments* Q20) in order to evaluate morphology, chemical properties [4, 5] and thermal stability [6], respectively. XPS spectra were deconvoluted with linear combination of Gaussian (80%) and Lorentzian (20%) profiles with a routine previously developed by our research group written in Octave [7].

3. Results and Discussions

XPS analyses of the O1s orbital are shown in Fig. 2. Each spectrum presents only one symmetrical peak related to lattice oxygen. The average peak position is located at 531.79 eV with the FWHM kept constant around to 1.8 eV for all spectra that indicates no chemical modifications in the samples structure. The symmetric spectra behavior also indicates no adsorption of oxygen from some oxygen-based compound, such as, water vapor and, then, no catalytic activity. The thermal stability curves obtained for the collagen are shown in Figure 2.

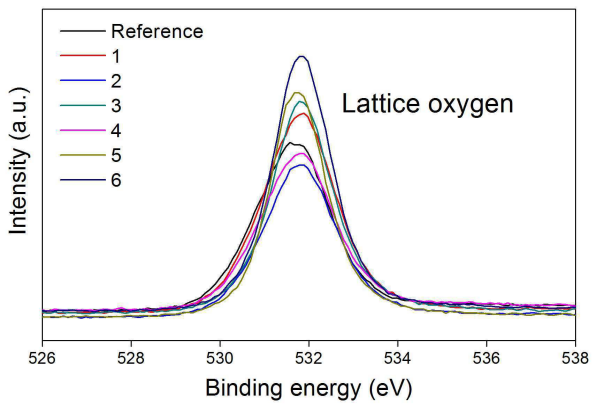

Fig. 1. XPS spectra of O1s orbital for samples 0-6.

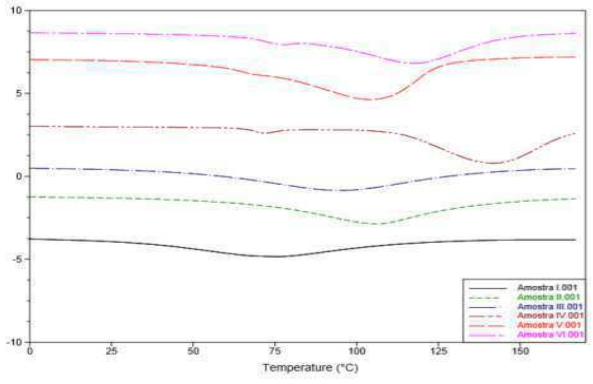

Fig. 2. DSC analyses for samples 1-6.

*Corresponding author: miriamfatimagoncalves@gmail.com

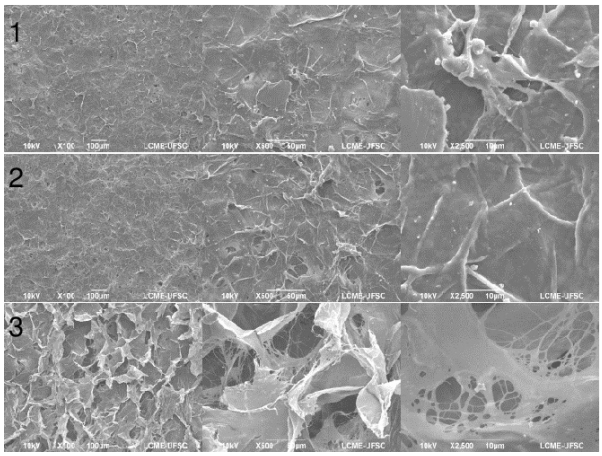

Fig. 3. SEM images for samples 1, 2 and 3 with 100, 500 and 2500 times magnification.

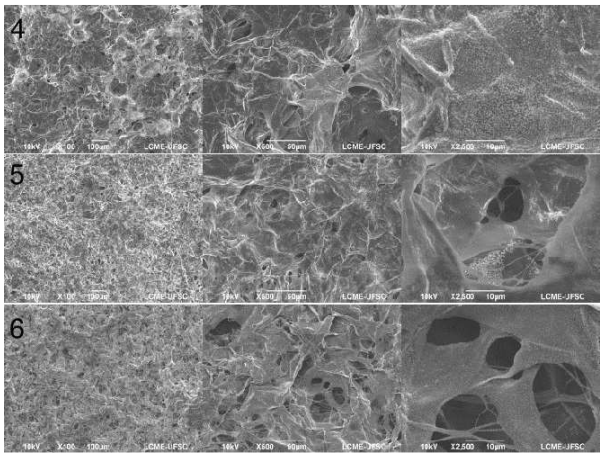

Fig. 4. SEM images for samples 4, 5 and 6 with 100, 500 and 2500 times magnification.

The curves of samples 1, 2 and 3 showed a transition that indicates fusion between 75 and 107°C, these samples have no transition indicating denaturation, one of the probable factors was the fact of plasma instability, providing insufficient temperature for transformation. Samples 4, 5 and 6 show a transition between 70 and 80°C relative to the denaturation temperature (Td) [8] showing that the stability of the plasma and consequent temperature increase altered the native structure of the collagen in triple helix. SEM images corroborate for such affirmation. These results show that argon plasma promotes structural modifications for cell growth but no chemical modifications for cellular growing, there was mobility of the chains closing the pores of the structure, therefore, other gases and conditions should be studied.

4. References

[1] Mistério da Saúde. Queimados. Available at http://portalms.saude.gov.br/component/content/article/842-queimados/40990-queimados. Last Access: 09/07/2018.
[2] R. Stella, Matriz dérmica regenera com melhor qualidade lesão por queimadura. Available at https://jornal.usp.br/ciencias/ciencias-da-saude/matriz-dermica-regenera-com-melhor-qualidade-lesao-por-queimadura/. Last access: 09/07/2018.
[3] P.-L. Shao *et al.*, PLOS ONE, 11, e0156699, (2016).
[4] P. Slepicka *et al.* Nuclear Instruments and Methods in Physics Research, Section B: Beam Interactions with Materials and Atoms, v. 332, p. 7–10, 2014.
[5] S. Rimpelovás *et al*. Plasma Processes and Polymers, 11, p. 1057-1067, 2014.
[6] M. G. Ionashiro, Fundamentos da termogravimetria, análise térmica diferencial e calorimetria exploratória diferencial. Editorial Giz, 2005.
[7] D. A. Duarte, PeakFinder. Available at http://diegoduarte.paginas.ufsc.br/codigos-em-octave/. Last acess: 07/11/2018.
[8] D. L. Nelson, M. M. Cox, Lehninger Principles of Biochemistry, 6th ed, New York: W. H. Freeman and Company, 2013.

Acknowledgments

Authors thank Promedon for kindly provide the dermal matrices and UDESC / LPFS by sample treatments and XPS analyzes.

*Corresponding author: miriamfatimagoncalves@gmail.com

REACTIVE DYEING OF COTTON FABRICS FUNCTIONALIZED BY THE PLASMA TECHNIQUE

Laura Palermo Gomes[1*], Fernando Ribeiro Oliveira[1], Catia Rosana Lange de Aguiar [1], Camila Thais Mamani[2], Teresa Tromm Steffen[2], Luis Cesar Fontana[2], Daniela Becker[2], Maria Elisa Philippsen Missner[1]

[1] *Department of Engineering, Federal University of Santa Catarina - UFSC, Campos Blumenau, Brazil*
[2] *Center for Technological Sciences, UDESC, Joinville, Santa Catarina, Brazil*

1. Introduction

Dyeing is a physical chemical process that modifies the textile substrate so that reflected light causes color perception through the application of dyes which are organic, soluble or dispersible compounds [1]. In the various types of dyes, the reactive dyes are widely used to dye cellulose and cotton because they obtain excellent brightness, equalization and solidity. The reactive dyes have an electrophilic group capable of forming a covalent bond with hydroxyl groups of the cellulosic fibers. Among the various types of reactive dyes, the main ones contain the azo and anthraquinone functions as chromophoric groups and the chlorotriazinyl and sulfatoethylsulfonyl groups as reactive groups [2]. In this dyeing, the dye also reacts with water to form the hydrolyzed dye, which is retained on the surface of the substrate and which must be removed through washing and soaping, so subsequent rinses must be made to avoid staining on the textile fabric [1].

One of the ways to remove impurities and improve the degree of whiteness is pre-bleaching, which aims to remove the waxes and greases, soluble substances and the yellowish coloration of the fibers, increasing to their white degree, in order to prepare the substrate for subsequent treatments [3]. Pre-bleaching is done in the presence of hydrogen peroxide, surfactant, silicates, alkalis, and complexing agents.

In the way to reduce the manufacturing resources at these steps of pre-bleaching is to treated with plasma. In this work, we compare two plasma different methods and pre-bleaching sample in the reactive dyeing process.

2. Experimental

The textile sample used at this work is a 100% cotton flat fabric with 0.08g. These samples were previously treated with plasma, by two different methods. One consists of inductively coupled radio frequency plasma (RF), at 100 W power input and 0.5 Torr gas pressure. The second one took place in active screen DC plasma at 200 V, 100 kHz frequency and 0.5 Torr gas pressure. Exposure time in each type of plasma were: 1, 3 and 10 minutes. The cotton standard sample with pre-bleaching represented with BL. Tab. 1 shows the samples names and conditions used at this paper.

Table 1. *Samples names and conditions.*

Sample	Plasma Type	Treatment time (minutes)
RF-1	RF	1
RF-3	RF	3
RF-10	RF	10
DC-1	DC	1
DC-3	DC	3
DC-10	DC	10
BL	-	-

These samples were exposed in the reactive dye process. In an infrared dyeing machine, the samples were placed to dye at 60 °C, with heating at 3 °C/min for 50 minutes, at 1:50 bath ratio, according to recipe in Tab 2.

Table 2. *Dyeing recipe with reactive dye.*

Concentration	Auxiliary
2 g/L	Dispersant and Sequestrant
3%	Reactive Dye
60 g/L	Sodium Chloride
15 g/L	Barrel

*Corresponding author: laura.palermo@grad.ufsc.br

After dyeing, the samples were washed in three steps. In the first one, only water was used, this remained for 10 minutes in the infrared dyeing machine at 40 ºC. The bath was removed and in the second stage was placed water and detergent with concentration of 2 g/L, where it remained in the machine for 10 minutes at 60 ºC. In the third washing step, the sample was washed again with water for 10 minutes at 40 °C. At the end of this process the samples were placed to dry in the oven at 60 °C.

3. Results and Discussions

Fig. 1 shows the concentration results after dyebaths 1, 2 and 3 taken to the DC and RF treated samples exposed at 1, 3 and 10 minutes and pre-bleaching samples (BL).
In dyebath 1, the DC-3 and RF-3 conditions showed a lower concentration of dye in the bath, which means that little dye reacted with water, and this had better interaction with textile fabric. In dyebath 2, the samples DC-3 and RF-1 presented better results. In the last dyebath process (dyebath 3), the RF-1 condition presented better results. However, the both plasma treatments left the textile fabric with a better affinity for the dye than BL, leaving less hydrolyzed dye in the washes.
In figure 2, shows the images of concentration at initial reactive dye process, after dyebaths 1, 2 and 3.

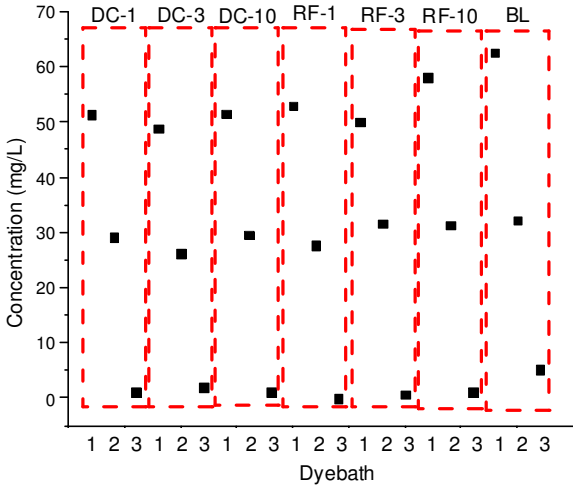

Fig. 1. *Concentration results after dyebaths 1, 2 and 3.*

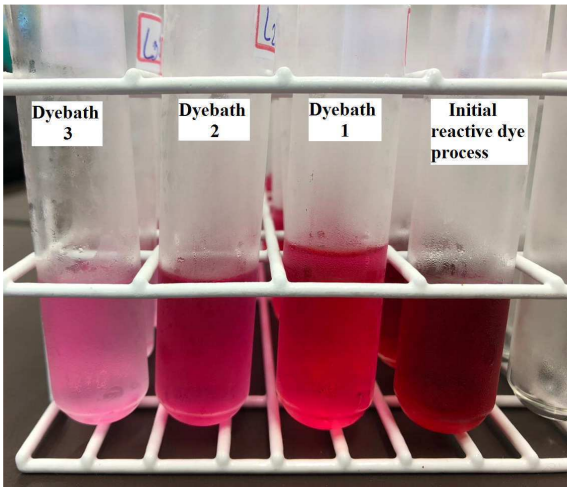

Fig. 2. *Images of concentration at initial reactive dye process, after dyebaths 1, 2 and 3.*

According to the three dyebath processes, the RF-1 sample showed a better dye impregnation, since in the third washing step it had a lower absorbance index at wavelength 518 nm. Although, all plasma treated samples had a better affinity for the dye than the pre-bleaching sample. This means that plasma treated samples could possibly be dyed with a lower concentration of dye than pre-bleaching to achieve the same color, however, further analysis would need to be done. Consequently, plasma treatment in addition to be more ecologically correct because it drastically reduces the use of water in the beneficiation process, it also gives a better interaction of the dye with the fiber, generating less hydrolyzed dye. Comparing the different plasma techniques, the RF samples had slightly more efficient because the second and the third dye baths concentration were a little smaller then de DC samples.

4. References

[1] SALEM, Vidal. **Tingimento têxtil**: fibras, conceitos e tecnologias. São Paulo. Blucher: Golden Tecnologia, 2010.
[2] GUARATINI, Cláudia CI; ZANONI, Maria Valnice Boldrin. Corantes têxteis. **Química nova**, p. 71-78, 2000.
[3] MALUF, Eraldo; KOLBE, Wolfgang. **Dados técnicos para a indústria têxtil**. São Paulo: IPT, 2003.

*Corresponding author: laura.palermo@grad.ufsc.br